PONTIFICIAE ACADEMIAE SCIENTIARVM SCRIPTA VARIA
69

STUDY WEEK

ON:

PERSISTENT METEO-OCEANOGRAPHIC ANOMALIES AND TELECONNECTIONS

September 23-27, 1986

EDITED BY
CARLOS CHAGAS and GIAMPIETRO PUPPI

PONTIFICIA
ACADEMIA
SCIENTIARVM

EX AEDIBVS ACADEMICIS IN CIVITATE VATICANA

MCMLXXXVIII

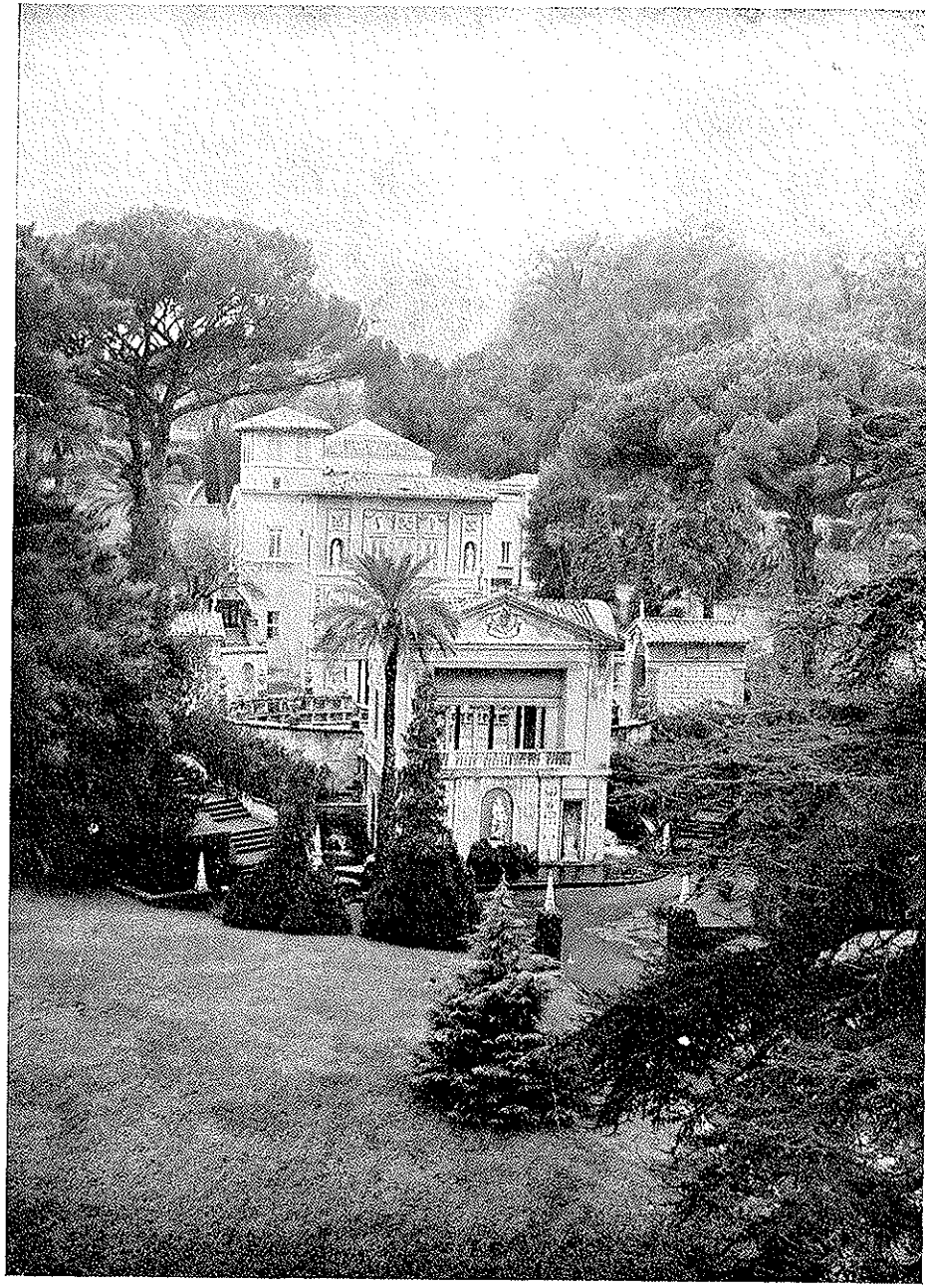

Casina Pio IV

The publication of this volume has been made possible by the generous contribution of the Società CARTIERE BURGO S.p.A., S. Mauro Torinese (Torino).

Il presente volume è stampato su carta « R 600 lucida » delle CARTIERE BURGO S.p.A.

The present volume is printed on paper « R 600 lucida » of the CARTIERE BURGO S.p.A.

PONTIFICIAE ACADEMIAE SCIENTIARVM SCRIPTA VARIA
69

STUDY WEEK

ON:

PERSISTENT METEO-OCEANOGRAPHIC ANOMALIES AND TELECONNECTIONS

September 23-27, 1986

EDITED BY
CARLOS CHAGAS and GIAMPIETRO PUPPI

PONTIFICIA
ACADEMIA
SCIENTIARVM

EX AEDIBVS ACADEMICIS IN CIVITATE VATICANA

MCMLXXXVIII

ISBN 88-7761-025-5

INDEX

SCIENTIFIC PAPERS

FOREWORD

From the 23rd to the 27th of September 1986, the Pontifical Academy of Sciences held a meeting on "Persistent Meteo-Oceanographic Anomalies and Teleconnections". During this Study Week some of the very important events which afflict many parts of the world were studied. Thus the El Niño Southern Oscillation, the monsoons and the causes of drought were scrutinized. Some of these events, as they seem episodic, attract the attention of governmental officers and the press only when they have happened or are happening. However, they must be studied in a multi-disciplinary way in order to prevent their consequences and, if possible, to preclude them. All of them have dire social and economic after-effects. They are a barrier to the steady and peaceful development of many countries and seem to lead vast regions to a subhuman perspective if important social, economic and technical measures are not taken urgently.

The approach to these problems needs an integrated research program, in which a vast collection of observational data could serve or be compared to the modelling approach. This is a field in which the atmosphere, the land and the oceans are interconnected in a way which unfortunately is quite unknown. Integrated research, using the best available methods for observation and data analysis, is needed to alleviate these problems.

The Study Week which met at the Pontifical Academy of Sciences has gone thoroughly through the meanders of the question and has presented data and suggestions which may lead to progress. Just by focussing on the question with their knowledge, the participants have already rendered a great service to humankind, greatly unaware, mostly in the rich countries, of the magnitude of the problem.

I want especially to thank my colleague, Pontifical Academician Giampietro Puppi for having organized this successful meeting. His perfect insight regarding the problems which challenge humanity has again been of very significant value to the work of the Pontifical Academy of Sciences. I extend my gratitude to all the participants, who brought to our working

table their experience gained in years of hard work, so often not fully appreciated by the academic corps. I wish also to express my thanks to all the staff of the Academy for their diligent help regarding the organization and execution of the meeting as well as its publication.

And finally my warmest thanks and appreciation go to the Società Cartiere BURGO S.p.A., for their generous support which made possible the publication of the present volume, and to Società TECNOMARE and I B M ITALIA for their collaboration in the organization and execution of the Study Week.

CARLOS CHAGAS

President of the Pontifical Academy of Sciences

LIST OF PARTICIPANTS

CARLOS CHAGAS, President of the *Pontifical Academy of Sciences*, Casina Pio IV, 00120 *Vatican City*, Italy.

LENNART BENGTSSON, Director, European Centre for Medium Range Weather Forecasts (ECMWF), Shinfield Park, *Reading*, Berkshire RG2 9AX, U.K.

ROBERTO BENZI, IBM Italia S.p.A., European Center for Scientific and Engineering Computing (ECSEC), Via Giorgione 159, 00147 *Rome*, Italy.

MARK A. CANE, Lamont-Doherty Geological Observatory of Columbia University, *Palisades*, N.Y. 10964, U.S.A.

R.K. DATTA, Director (NWP), Mausam Bhavan, India Meteorological Department, Lodi Road, *New Delhi* 110003, India.

CHRISTOPHER K. FOLLAND, Meteorological Office, Met013 Room R322, London Road, *Bracknell*, Berkshire RG12 2SZ, U.K.

B.J. HOSKINS, Department of Meteorology, University of Reading, 2 Early Gate, Whiteknights, P.O. Box 239, *Reading* RG6 2AU, U.K.

EUGENIA KALNAY, Head, Global Modelling Simulation Branch, Laboratory for Atmospheres, Goddard Space Flight Center, N.A.S.A., *Greenbelt*, Md. 20771, U.S.A.

BERNARD LEGRAS, Laboratoire de Météorologie Dinamique du CNRS, Ecole Normale Supérieure, 24 rue Lhomond, 75231 *Paris* Cedex 05, France.

KIKURO MIYAKODA, Geophysical Fluid Dynamics Laboratory, Princeton University, P.O. Box 308, *Princeton*, N.J. 08540, U.S.A.

T.N. PALMER, European Center for Medium Range Weather Forecasts (ECMWF), Shinfield Park, *Reading*, Berkshire RG2 9AX, U.K.

R.P. PEARCE, Head, Department of Meteorology, University of Reading, 2 Early Gate, Whiteknights, P.O. Box 239, *Reading*, Berkshire RG6 2AU, U.K.

GIAMPIETRO PUPPI, « A. Righi », Via Irnerio 46, 40126 *Bologna*, Italy.

EUGENE M. RASMUSSON, Department of Meteorology, University of Maryland, *College Park*, Md. 20742, U.S.A.

RICHARD J. REED, Department of Atmospheric Sciences, University of Washington, A.K.-40, *Seattle*, Wash. 98195, U.S.A.

J. SHUKLA, Director, Centre for Ocean-Land Atmosphere Interactions, Department of Meteorology, University of Maryland, *College Park*, Md. 20742, U.S.A.

ADRIAN J. SIMMONS, European Centre for Medium Range Weather Forecasts (ECMWF), Shinfield Park, *Reading*, Berkshire RG2 9AX, U.K.

A. SPERANZA, FISBAT C.N.R., c/o Dipartimento di Fisica, Via Irnerio 46, 40126 *Bologna*, Italy.

A. SUTERA, The Center for the Environment and Man Inc., McCauley Hall, 1678 Asylum Avenue, *West Hartford*, Ct. 06117, U.S.A.

S. TIBALDI, European Centre for Medium Range Weather Forecasts (ECMWF), Shinfield Park, *Reading*, Berkshire RG2 9AX, U.K.

JOSEPH J. TRIBBIA, Atmospheric Analysis and Prediction Division, National Center for Atmosphere Research, P.O. Box 3000, *Boulder*, Co. 80307, U.S.A.

A.C. WIIN-NIELSEN, Director, Danish Meteorological Institute, 100 Lyngbyvej, 2100 *Copenhagen*, Denmark.

AUDIENCE OF THE HOLY FATHER

On September 26, 1986, His Holiness John Paul II granted a Solemn Audience in the Apostolic Palace of the Vatican to the participants in the Study Week on "Persistent Meteo-Oceanographic Anomalies and Teleconnections".

The group, introduced by the President of the Pontifical Academy of Sciences, His Excellency Prof. Carlos Chagas, and accompanied by the Director of the Chancellery, Rev. Father Enrico di Rovasenda, and by the Co-Director, Ing. Don Renato Dardozzi, was paternally received by His Holiness, who at the end of the Audience wished to greet personally all the participants.

The President of the Academy, Prof. Carlos Chagas, delivered the following address:

Most Holy Father,

The meeting which is being held at Your Academy deals with an extremely important matter: Can science predict, and with what accuracy, the oncoming of some catastrophes like the flooding, of which the Indian monsoon is a prominent example, or the droughts which have devastated the region of the Sahel and the northeast of Brazil? The debate which is going on shows that some indication of such a possibility is emerging; although speaking about confidence and accuracy in the predictions is still premature.

This expectation is due to the renewal of meteorology and oceanography, brought about by the development of new techniques of observation, among them the use of satellites, and the supermachines able to simulate the complexities a climatic system presents with all the innumerable variables necessary to describe atmosphere, ocean and land and their mutual interactions.

The probability of success is also due to the efforts of the meteorologists and oceanographers, whose work, so many times frantic, has little visibility to the public, and in many countries does not receive from the governments the attention it merits. Their work, however, corresponds to the orientation You have so many times expressed.

Science should be directed solely for the benefit of humankind: to help women, men, and children to live in the absence of any hindrance which will not allow them to appreciate the beauty of our environment, the poetry of our lives, the best gift we have received from God.

Holiness, in the name of the group here present, and on behalf of the Pontifical Academy of Sciences, permit me to thank You for your generous reception, which will be always remembered. Your constant interest for the work of the Pontifical Academy of Sciences goes beyond the limits of our beautiful surroundings to reach the whole world scientific community.

Every one of the participants of the Study Week will go back to his work fortified by the certitude that Your deeds and pronouncement will help to make science and technology a more ethical instrument for the improvement of the dignity of the human condition.

The Holy Father replied with the following discourse:

Mr. President,
Ladies and Gentlemen,

1. *The present* Study Week on Persistent Meteo-Oceanographic Anomalies and Teleconnections *offers a fresh proof of the intention of the* Pontifical Academy of Sciences *to be of service to humanity, especially by its interest in the main scientific problems of the day. The theme of your Symposium is in fact one of the most urgent at the present time.*

I extend a most cordial greeting to the eminent specialists in the fundamental oceanographic and atmospheric problems that you are dealing with. I an pleased to see that you come from many different parts of the world: from North and South America, Europe and Asia. This is yet another demonstration of the harmonious collaboration that exists between scientists and that is of such benefit to world peace.

2. *Science does not merely have to study natural phenomena in themselves. It also has to* make a decisive intellectual and ethical effort to foresee the development and consequences of those phenomena, *in order to sofeguard and enhance the welfare of humanity. This is the aim that you have set yourselves. You have been studying phenomena such as* El Niño, *the monsoons and their worldwide effects, the causes of the climatic disturbances in the eastern zones of the Pacific Ocean, as well as the prolonged drought in the Sahel.*

The studies which you have carried out in the Institutes which you represent individually and which you have been

dealing with in the tranquil surroundings of the Casina of Pius IV, the seat of the Pontifical Academy of Sciences, will enable you to provide those who are threatened by these and other negative phenomena with timely weather forecasts, thus making it possible to take the necessary steps for avoiding the most serious effects of approaching natural disasters. In various parts of the world it is now possible, as a result of dedicated efforts, to set up systems for recording climatic phenomena and to gather facts on a worldwide scale which affect the entire globe.

3. *Through your work you are carrying out the Biblical command to subdue the earth, to control the catastrophes that harm the human family, and to make the earth obedient to our service. Science encourages legitimate human curiosity to know the universe and to admire and contemplate its beauty and goodness. In this way we enter into communion with God Himself, who looked upon what He had created and saw that it was very good* (cf. Gen 1:31). *But* we are also called by God to control the movements of violence and death that occur in nature, *subject as it is to inevitable adjustments of its balance. We are called to discover new sources of energy, to replace those that are non-renewable or that prove to be insufficient. Unfortunately it sometimes happens that, in order to satisfy his unlimited craving for material well-being, man corrupts and squanders the world's resources, with effects that are especially harmful to those least able to defend themselves, who possess the fewest technical skills, and who inhabit the least hospitable territories.*

You, on the other hand, are engaged in the genuine task of the scientist: you are studying in order to contemplate

and understand, to control and make fruitful. In the course of your studies, you cannot fail to admire the powerful forces of nature. *But at the same time you see that these forces can pose dangers and threats to humanity, and* you teach how to dominate them, so that they may be placed at the service of all.

4. *Ladies and Gentlemen, I am particularly grateful to the Pontifical Academy of Sciences and to its President for bringing you together. I invoke upon you the blessings of God, the Provident Creator, for the studies that you are engaged in for securing a harmonious environmental balance, which will favour human security and dignity, and which will especially benefit those who are unprepared and defenceless in the face of natural catastrophes.*

SCIENTIFIC PAPERS

The opinions expressed with absolute freedom during the presentation of the papers and in the subsequent discussions by the participants of the Study Week — although published by the Academy — represent only the points of view of the participants and not those of the Academy.

PERSISTENT METEO-OCEANOGRAPHIC ANOMALIES AND TELECONNECTIONS

SUMMARY and CONCLUSIONS

1. INTRODUCTION

Over the past three decades meteorology has evolved from a descriptive branch of physics to a quantitative science. This development has been based on an increased understanding of the mechanisms which drive the atmospheric motion on a variety of space and time scales from the global macro-scale to the micro- and meso-scales of the atmosphere.

The progress has been possible due to the advances in observational methods (using satellites), computer technology and improved modelling techniques.

Parallel with these advances in forecasting, we have also experienced a research effort leading to an ability to simulate the general circulation of the earth's atmosphere using a series of models going from quite elementary examples in 1955 to the much more comprehensive models which exist today. In addition to a good simulation of the wind, temperature and moisture fields in the atmosphere, we have also gained a new level of understanding of the heat and momentum transport processes and the energy generations, transformations and dissipations.

The research leading to these advances from a descriptive to a quantitative science is due in large measure to the desire to predict the state of the atmosphere at a future time.

The meteorological community has for more than a century been charged by society with the task of predicting the weather. The recent developments have not only changed the field of forecasting from an

empirical "art", based to a large extent on simple rules and experience, to an objective numerical application of the physical laws which govern the atmosphere, but the results have also led to increased accuracy in forecasting and an extension of the useful predictions to about one week.

The atmosphere is basically an unstable, nonlinear system, and the nonlinear aspects of the governing physical laws put a finite upper limit to the time for which reliable deterministic predictions can be made in the sense that two predictions made from two states which are initially very close to each other eventually will differ as much as two arbitrarily chosen weather states. This basic property of the atmosphere, combined with the initial uncertainty due to inadequate data and deficiencies in model formulation, sets the current limit of detailed predictions to a week. However, it does not in principle prevent us from making predictions in some averaged sense for periods much longer than 7 days.

The climate system is normally defined as consisting of the atmosphere, the oceans, the continents, the cryosphere and the biosphere. The components interact with each other in a variety of ways, but it is characteristic for some of these interactions that they take place on very long time-scales such as the interaction between the atmosphere and the cryosphere. Other interactions are much faster, but the influence on the atmosphere is often modeled as a one-way process avoiding the need for a formulation of a truly coupled system. There is no doubt, however, that a very large task facing the climate scientists is the design of models which are truly interactive, and which couple the various components to each other. Such an effort has begun only recently and mostly as a coupled ocean-atmosphere model.

The purpose of this Study Week has been to review a number of atmospheric phenomena such as the monsoon, the El Niño-Southern Oscillation, the tropical droughts and global linkages (teleconnections). The impact on society of these long-lasting phenomena is tremendous. We concentrated on the progress in understanding and predicting these episodes that are very complex in structure and show considerable interannual variability. We concluded that there is a considerable hope for predictions of some of these episodes with a useful level of accuracy in the not too distant future. We encourage society to support further research in these areas and to make better use of the recently obtained advances which are not yet fully exploited.

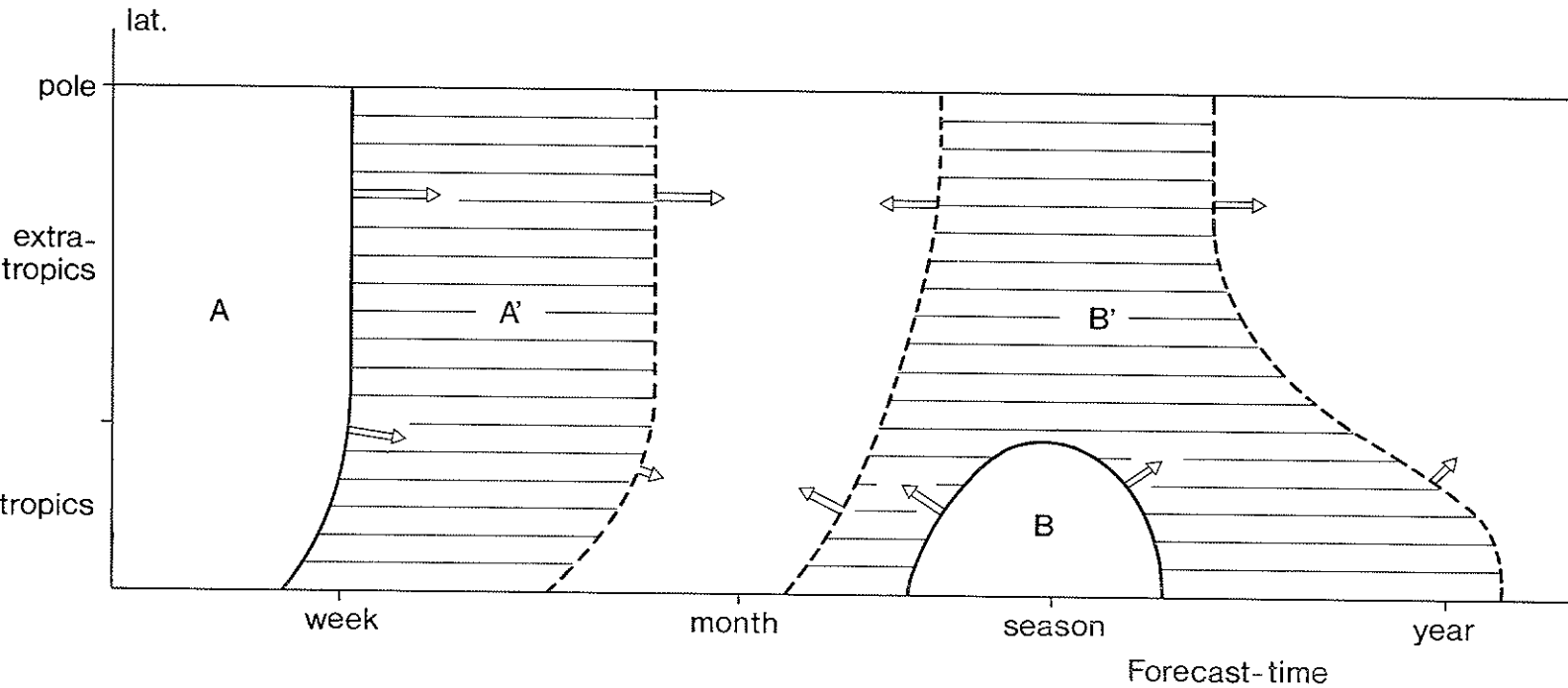

A schematic diagram with forecast time on a logarithmic scale along the horizontal axis and latitude along the vertical axis. The solid lines show present limitations for forecasts in an approximate way, while the deshed lines show the same at some future time. Arrows indicate the directions of improvements. The various areas signify the models which may be characterized as follows:

A : Forecasts performed using the most sophisticated available computer models of the atmosphere.

A¹: The possible future expansion of A.

B : Forecasts with a high statistical content, performed using a combination of statistical techniques and a variety of models representing the atmosphere and the coupled atmosphere-ocean system.

B¹: The possible future expansion of B.

2. ENSO-RELATED SECTION

I) *Introduction.* One of the great advances in our understanding of year-to-year climate variability has been the discovery, during the past few years, that a significant share — and in the tropics, probably a major share — of atmospheric variability on time-scales of months to a few years is associated with variations in tropical sea surface. The ability to model the atmospheric response to these temperature variations developed in parallel, and in the same period there emerged an understanding of how to model variations in the tropical oceans in response to changes in the tropical atmosphere. This progress has given rise to increased optimism regarding the possibilities of skillful seasonal predictions over many areas of the world.

The El Niño/Southern Oscillation (ENSO) phenomenon is the most energetic and best defined example of global climate variability on the interannual time-scale. It leads to pronounced global patterns of climate anomalies which recur every few years, and evolve over a period of about two years. These episodes are associated with massive dislocations of the rainfall régimes of the tropics, bringing drought to vast regions and torrential rains to otherwise desert areas. The related atmospheric circulation anomalies may extend deep into the extratropics, and lead to unusual winter-time conditions in both hemispheres. ENSO also causes severe disruptions of the marine ecosystem along the west coast of North and South America, affecting the fishing industry of a number of nations.

ENSO owes its existence to ocean-atmosphere interactions in the tropical Pacific, i.e., it is a fluctuation of the *coupled* ocean-atmosphere climate system, in which both components play an active role. Because of its large amplitude and two-year duration, its relatively consistent pattern of evolution, and its pronounced effect on the socio-economic well-being of a large segment of the world's population, ENSO has important implications of seasonal averaged conditions one to several seasons in advance.

There has been substantial progress in describing the climate system interactions and processes which control the evolution of the ENSO cycle. This has, in turn, stimulated major advances in our theoretical understanding of the phenomenon. This new knowledge is being exploited to develop empirical-statistical prediction schemes for many tropical and near-tropical regions. However, major advances in predictions will likely require the development and use of coupled ocean-atmosphere dynamical models.

Recent work with simple models of this kind suggests that El-Niño events are possibly predictable several seasons ahead. While this effort is in its early stages, results encourage a continuation and expansion of this promising line of research. Successes to date have employed relatively simple models, but the thorough exploitation of our knowledge of the physics of the coupled ocean-atmosphere system will require the use of general circulation models of both ocean and atmosphere.

The potential for predictability of climatic variations related to ENSO varies with region and season. Indian Monsoon rainfall, Australian-Indonesian drought, drought in southern Africa, and flooding in Peru and Ecuador are examples of important climatic events which are strongly correlated with ENSO. While there is little prospect for predicting short-time variations at single points, there is reason for optimism regarding the predictability of seasonal area-averaged rainfall. The most socially valuable forecasts are those concerning extreme events, and ENSO tends to be strongly related to such extremes.

While much of the interannual variability in the tropics is directly related to ENSO, variability at higher latitudes has many causes. Though there are areas in the extra-tropics which are strongly and consistently related to ENSO events, in most cases mid-latitude effects are complex, differing from event to event. Prospects for useful application of ENSO forecasts to these areas remain uncertain.

II) *Recommendations.* In order to deepen our understanding of the whole ENSO process, and to advance the predictive capability further, the models and routine observations must be improved considerably. The most crucial data gaps are the surface winds and the subsurface ocean temperature over the Pacific. Improved atmospheric data in the entire tropical belt is also essential. The best hope for improved observations of the surface winds over the oceans lies with scatterometer measurements by satellites, and hope for the upper air winds is in the wind profile measurements at islands and winds derived from satellite tracking of cloud elements.

In order to establish the benefits of predictions based on ocean-atmosphere coupled models, it is necessary to investigate the limits of predictability in some detail. How well can the different features of the ENSO cycle be predicted? Which are most important for predicting socially important climate variations? In the near term more detailed verification of the existing forecast system is called for. Concurrently, the development of more realistic coupled models should be accelerated. Ocean modeling

is less mature than its atmospheric counterpart, and the need for improved procedures for the assimilation of oceanic data is particularly pressing. It is to be expected that data requirements will expand as the models become more sophisticated. Along with the forecasts themselves, it is essential to provide a measure of reliability of the forecasting systems.

III) *Conclusions.* The impressive advances in both meteorology and tropical oceanography during the past two decades have resulted in a nascent ability to forecast ENSO events. Prospects now seem promising that a concerted effort would result in an operational forecasting capability within a few years. The strong role operational weather forecasting has played in the science of meteorology is indicative of the potential value of such a capability for advancing our overall understanding of short-term climate variations, and subsequently exploiting this knowledge for the benefit of mankind.

3. MONSOONS

I) *Introduction.* Monsoon rains are one of the most important sustaining factors for the vast agrarian population of Asia and Africa. Fluctuations of monsoon rains directly influence agricultural food production, energy supply and availability of drinking water. Any extreme fluctuation, whether major drought or flood, causes devastation and human misery to large populations of these areas.

On an annual time-scale, the onset and the withdrawal of monsoons and the duration of the rainy season display a remarkable degree of regularity; however, the interannual changes in the dates of onset and withdrawal, total amount of rainfall, and space-time variability of rainfall are large enough to affect the entire socio-economic fabric of these agrarian societies. Even small skill in making advance predictions of the onset and space-time fluctuations of rainfall can be of great economic value for agricultural and energy management policies; the advantages will be particularly large if extreme events could be predicted in advance.

II) *Physical nature of the monsoon.* The Asian summer monsoon is a major component of the northern summer (and southern hemisphere winter) phase of the atmosphere's seasonal cycle. It is unique for such large-scale phenomenon in the suddenness of its onset. This is felt most

dramatically over India, where the monsoon rains commence during late May or early June, although the areas affected by its circulation are in fact much larger, extending to Africa in the west and well into the southern hemisphere.

Another component of the northern summer is the west African monsoon. It is similar to the Asian monsoon in that it marks the commencement of seasonal rains, but its onset is not as dramatic, and there is no large increase in the moisture cycle.

III) *Present status of long range forecasting.* Some of the monsoon-affected countries prepare seasonal forecasts on an operational basis. These forecasts are based on statistical relationships derived from the past climatic data of atmospheric variables within the monsoon regions and outside.

The basic technique consists of developing linear regression equations or auto-regressive moving average methods using antecedent circulation features as predictor parameters. Although a comprehensive verification of such forecasts has been published, it is generally believed that these forecasts have some skill.

Development of new regression equations is an ongoing process as the significance of the predictor parameters is continuously evaluated using new data, and if the predictors are found to have reduced correlation with rainfall, they are dropped from the empirical equation used to predict rainfall.

In addition to the operational long-range forecasting, research is being conducted to investigate the possibility of using various global parameters to predict monsoon rainfall.

The examples of such studies include El Niño/Southern Oscillation (ENSO), snow cover over the Eurasian land mass, Antarctica temperature anomalies and sea surface temperature anomalies, and sea surface temperature over the Indian Ocean.

IV) *Future prospects for long-range forecasting of monsoon.* There is a considerable evidence in past observations that suggests that large-scale persistent anomalies of monsoon rainfall are associated with changes in the global scale circulation, ocean temperature and snow cover. For example, changes in sea level pressure at Darwin from winter to the spring season have been found to be a good indicator of the seasonal mean rainfall over India during the subsequent summer season. Similarly,

the establishment and northward movement of the mid-tropospheric circulation over India during winter and spring season have also been found to be good indicators of monsoon rainfall during the subsequent summer (monsoon) season. The changes in Darwin pressure are strongly related to the changes in ocean temperature over the eastern Pacific, otherwise referred to as El Niño phenomena. Thus it is clear that interactions among ocean, atmosphere and land processes can produce very large-scale slowly changing circulation systems on the globe, and depending upon the matching of monsoon season with the life cycle of these systems, they can produce either drought or flood conditions over the Asiatic monsoon region. By continuous monitoring of these global-scale circulation changes, it could be possible to estimate seasonal mean rainfall averaged over large spatial areas. In fact, currently several such techniques are being utilized to produce operational long-range forecasts of monsoon rainfall.

Our knowledge of mechanisms that determine regional scale variability of rainfall within a monsoon season is quite incomplete. There is some evidence, however, that these short period fluctuations could be related at least in part to tropical 30-60 day oscillations and mid-latitude blocking events. The present day global dynamical models show useful skill for short and medium range (up to 5 days) forecasts of circulation; however, the skill for rainfall forecasts is considerably less. With improvements in dynamical models and better treatment of forcing functions at the earth surface, it may be possible to simulate the atmospheric fluctuations more realistically. However, the degree to which dynamical models can successfully predict the short time fluctuations of rainfall at regional scales is not yet known.

A concerted effort of data analysis and modeling studies is required to make quantitative evaluation of the limits of monsoon predictability.

V) *Recommendations* (*general*). a) Noting the tremendous progress made in meteorology in recent years, all countries should be encouraged to strongly support international programs of the World Meteorological Organization (WMO) and the Food and Agriculture Organization (FAO) to exploit the full advantage of meteorological research for the benefit of all countries.

b) Governments should be urged to encourage stronger interactions between meteorologists, agriculturists and pastoral experts for proper use of forecasts and expand as necessary operational and research capabilities of weather services and research institutions.

c) Particular attention should be given to improve observational network and communication.

VI) *Technical.* a) Analysis of data should be carried out to delineate the space-time scales of droughts in the entire tropical belt.

b) Diagnostic and modeling studies should be carried out to understand the mechanisms of observed correlations and teleconnections, in particular the possible effects of land-surface processes and air-sea interactions.

c) Multi-year integrations of GCMS should be conducted to simulate the seasonal cycle; such integrations will provide an invaluable data source from which the mechanisms involved in the interannual variability of many atmospheric phenomena, particularly the monsoons, may be studied in full detail.

4. DROUGHT

In recent years there has been considerable progress in understanding meteorological conditions associated with periods of drought in different parts of the tropics and subtropics. This has come about both through improved diagnosis of available data and through the use of complex numerical models of the worldwide atmospheric circulation, which can be used to identify factors governing drought. Out of the recent advances there has emerged not only a better understanding of the causes of drought, but also the possibility that in some regions at least, especially in the tropics, its occurrence may be forecasted one season or more in advance. However, it should be emphasized that work on drought prediction is at an early stage, and, as will be discussed below, is being hampered by inadequate data in key areas of the world.

Because of the tragic human consequences, attention has focused on the drought in the African Sahel. Rainfall data has shown a fairly steady decline in annual precipitation over the Sahelian zone from the late 1950s to the present time and this has been associated with systematic changes in the strength of the prevailing winds, both near the ground and aloft. Such changes are not confined to the Sahelian region itself, but appear to extend over a broad area of the tropics. It appears that the changing pattern of these large-scale wind systems, rather than the number

or intensity of disturbances associated with individual rain events, is important for understanding the meteorological causes for Sahelian drought.

A fundamental question is whether the principal cause of the long Sahelian drought is man's influence on climate, for example through overgrazing or deforestation, or whether it is associated with decadal time-scale variability in the ocean/land atmosphere climate system. If overgrazing is the main cause of the drought, it might be possible to prevent future drought by extensive replanting over affected areas. If the latter is true, then whilst replanting may mitigate the worst effects of drought, it cannot prevent its eventual recurrence.

Complex numerical models of the atmosphere are particularly useful in simulating the possible effects of overgrazing and deforestation on climate.

The effect of reducing vegetation is to increase reflectivity of the land surface to incident solar radiation, and decrease evapotranspiration and surface roughness. Model sensitivity studies suggest that these changes can significantly reduce Sahelian rainfall.

On the other hand, there is as yet no observational evidence to support the contention that this is the fundamental cause of the drought. For example, satellite data over the last decade has not revealed a detectable increase in ground reflectivity. Furthermore, historical records reveal that Sahelian drought is a cyclical phenomenon albeit with irregular periodicity.

A second hypothesis is that on the decadal time-scale the drought may be controlled by natural variability in the coupled atmosphere/land/ocean system. In the last three decades, for example, the surface temperatures of the South Atlantic and Indian Oceans have been steadily warming relative to the North Atlantic Ocean, and this trend is correlated with the Sahel rainfall series. Model experiments also show a sensitivity of Sahel rainfall to small changes in sea surface temperature in these oceans.

If the hypothesis that sea surface temperature variations exert a controlling influence is correct, it provides an explanation of the apparent persistence of Sahel rainfall from one year to the next. However, it should be stressed that the magnitude of the trend in the ocean temperatures is small, and observational errors may be significant. Furthermore, since there are many uncertainties in the formulation of relevant physical processes in numerical models, quantitative estimates in the relationship between ocean temperatures and land rainfall are not reliable. Fully coupled atmosphere/land/ocean models are required to test the validity of these hypotheses.

Despite the above reservations, the evidence of a relationship between sea surface temperatures and Sahelian rainfall has been considered sufficiently strong to encourage preliminary attempts at forecasting Sahelian precipitation one season in advance, using statistical techniques.

Even if the natural variability mechanism is ultimately proved to be dominant, it may still be possible that the worst effects of drought can be mitigated by prudent management of the land. However, even in this case this should be seen at best as a means of alleviating the problem, rather than removing it.

Clearly, further work is required before definite conclusions can be drawn. Such work will continue to use both observational data and modeling studies. Unfortunately, there is a severe shortage of information on rainfall, temperature, wind and surface conditions over many areas within the Sahel. Furthermore, over large portions of central and eastern Africa the data network is particularly deficient. Progress in our attempts to understand the causes of Sahelian drought and find reliable means for prediction is being hampered by this paucity of data.

On the modeling side, further work needs to be done to understand better the possible feedback between land-surface processes, the ocean and the atmosphere. Furthermore, integrations of numerical models stimulating several decades using both climatological ocean temperatures and observed ocean temperature may provide a useful tool to lend more confidence to the role the oceans play in Sahelian drought. Eventually, fully coupled atmosphere/land/ocean models will be required.

In conclusion, we recommend the following as areas requiring urgent attention:

— The conventional observational network of surface and upper air needs to be drastically improved over central and eastern Africa.

— Observations of land surface properties such as vegetation cover, surface reflectivity, and soil moisture should be obtained from ground and satellite observations.

— Routine accurate global sea surface temperature measurements are also required, particularly in areas of high sea surface temperature.

— The development of interactive ocean/atmosphere/biosphere models and their application to the understanding of drought should be encouraged.

— Efforts should be made to improve methods of land use management in order to limit the possible adverse effects of drought on human

activity. Such management should take into account the large long-term variability of rainfall in future plans.

— Efforts should continue to develop statistical methods for forecasting seasonal rainfall over drought-affected areas. As interactive models become reliable, we expect them to play a larger role in such forecast studies.

5. PERSISTENT EXTRATROPICAL ANOMALIES

Numerical weather forecasts currently provide useful guidance on the evolution of the atmosphere for a period of up to a week ahead, the substantial social benefit of which is well established. Forecasts are produced using numerical models which in turn are based upon our theoretical understanding of the atmosphere general circulation and its predictability. Hence a theoretical framework is an essential ingredient to enhance our ability to design forecasting systems.

Studies to understand and forecast long-lived anomalies which occur in the extratropical region can be divided into three main topics:

a) tropical heating and its effect on a global scale circulation;

b) multiple weather régimes in middle latitude circulation;

c) predictability studies.

I) *Tropical heating and its effect in middle latitudes.* Simple models appear to give reasonable description of the near surface local response to tropical heating. Extensions of these models have been linked with ocean models to produce ideas and even forecasts of the coupled behavior of the tropical atmosphere and ocean on seasonal time-scales. Mechanisms have been exhibited by which local heating in the tropics can significantly affect the middle latitude flow, and which show that this effect may be particularly strong in certain preferred regions and patterns. The tropical heating may be fixed and associated with anomalous sea surface temperatures or may be moving in a rather systematic periodic manner on the time-scale of one or two months.

The weather in middle latitudes shows variability on a wide range of time-scales. Increased understanding of the interaction of these local weather processes with the signal forced from the tropical regions is essential.

II) *Multiple weather régimes in the midlatitude circulations.* Two phenomena of great importance in middle latitudes are the forcing by the earth's mountains and the existence of mobile weather systems. The latter tend to occur in storm track regions whose origin is due to the weavy flow associated with asymmetries in the earth's surface but which feed back strongly on the weavy flow itself.

In the last few years, it has been shown that the variability in middle latitude circulation possesses some preferred configurations. There is indeed evidence that two or more régimes do exist and in some extreme cases these régimes can persist for a season.

The severity of winters in middle latitudes (as in 1985 and 1986) strongly depends on the occurrences of some of these régimes. Possible mechanisms for their onset and decay are under active investigation. The understanding of the nature and the stability of such régimes is crucial for long-term forecasting in middle latitudes. The probability of the occurrences of mid-latitude weather régimes might be predicted, provided boundary conditions (such as sea surface temperature, ice extent and so on) are given.

Systematic studies of the physics of weather régimes must be an essential element of strategy towards long-range forecast.

III) *Predictability studies.* Theoretical studies of predictability indicate a potential for useful extension of the techniques currently used for weather forecasting to the prediction of long-lived anomalies of the extratropical atmospheric circulation on weekly to seasonal time-scales. Such techniques are now being applied experimentally to monthly prediction, and the results obtained to date show a mixture of quality ranging from remarkable successes to major failures. The central question concerns the extent to which these failures are due (1) to imperfections in our knowledge of the instantaneous state of the atmosphere at the start of the forecast, (2) to inadequacies in the representation of the atmosphere in computer models and (3) to not using these models in an optimum manner, or to some inherent turbulent characteristics of the atmosphere which limit the extent to which it can ever be predicted.

The following are needed, both to answer this fundamental question, and to exploit to the full any potential for prediction of the persistent anomalies:

— A range of theoretical and diagnostic studies of atmospheric behavior, in particular to provide a better indication of what can or cannot be predicted.

— Improved exchange of routine data between countries, and better techniques for the analysis of this data, in order to provide both a better definition of the initial atmospheric states from which forecasts are made, and more accurate and complete meteorological archives for diagnostic studies.

— Improved numerical models of the atmosphere, and their coupling with ocean models.

— Fostering of programmes of experimental predictions, including the development both of methods for extracting maximal practical information from the computational output and of the techniques for assessing *a priori* the likely reliability of the forecasts. The international collaboration that has been established in setting up such programmes is necessary particularly to compare different methodologies, and should be strengthened.

6. CONCLUDING REMARKS

The atmosphere is a part of the natural environment. It is also an essential part of the life support system for every human being. As with other parts of the natural environment, the atmosphere is mainly a resource for humanity, but also on occasion a threat to human beings.

We have considered some of these dangers appearing on long timescales.

The global meteorological community is in our opinion equipped with the necessary tools to attack these problems and to turn the knowledge and understanding, gained through research, into guidance and recommendations to decrease any negative impact on society. It is thought that the physical laws governing most aspects of the atmosphere are known, that modern technology has provided us with new tools to observe the various parts of the climate system, especially the atmosphere, and to process the vast amount of data into predictive systems, and that we are in an era where the ability to predict will increase the forecast time and the accuracy of the predictions.

If such a promising evolution will continue, or perhaps even be

accelerated in view of the severity of the problems which we have described, it is necessary that meteorology receive sufficient support to gather all kinds of data, to distribute them in a reliable way to the various parts of the globe, to be equipped with the systems necessary for data processing and predictions, and to communicate the warnings to all users. Last, but by no means least, it is necessary to attract new generations of meteorologists to the field and to permit the better ones to work on these long-term complex problems.

True understanding will come from further systematic studies of the events under consideration.

INTERANNUAL VARIABILITY IN THE EQUATORIAL BELT: EVOLUTION AND RELATIONSHIP TO EL NIÑO/SOUTHERN OSCILLATION

E. M. RASMUSSON
Department of Meteorology, University of Maryland
College Park, MD. 20742

V. E. KOUSKY and M. S. HALPERT
Climate Analysis Center, NMC, NWS, NOAA
Washington, DC. 20233

ABSTRACT

The relationship between interannual variability in the global equatorial belt, and the Southern Oscillation (SO) is examined, with emphasis on the El Niño/Southern Oscillation (ENSO) phenomenon. Data from the period 1955-86 are examined. Emphasis is on the period 1979-86, when relatively complete and homogeneous sea surface temperature (SST), outgoing long-wave radiation data (OLR) from satellites (for estimating large-scale precipitation variations), and wind data from 850 mb and 200 mb are available.

While the results are preliminary, pending a more complete analysis for the period 1955-79, they support the following conclusions applicable to anomalies in the equatorial belt.

1. The interrelationships between the large scale SST, OLR and zonal circulation anomalies are generally consistent with the premise that the circulation anomalies reflect a direct response to anomalous thermal forcing, as implied by changes in SST and SST gradients.

2. There are three important time-scales associated with the SO. The first is the dominant SO period, usually ranging between two and

seven years. The second is the biennial ENSO time-scale, most clearly evident in zonal wind anomalies over the eastern Indian Ocean-central Pacific sector, and in the migration of the SST isotherms in the western and central Pacific. Thirdly, regional ENSO anomalies may evolve as an aberration of the annual cycle. A prime example is the El Niño event of the eastern Pacific, which develops roughly in-phase and progresses westward with the annual warming cycle. The westward progression is opposite to the migration of the ENSO biennial time-scale wind anomalies

3. Zonal (east-west) wind anomalies of alternating sign, with approximately a two year period, migrated eastward across the eastern Indian Ocean-Pacific sector during the 1982-83 ENSO episode. The last pair of these anomalies slowed in its eastward progression during 1983, to become a quasi-stationary circulation couplet in the equatorial plane during the high index period which followed. These Indian Ocean-Pacific sector circulation anomalies were part of a global pattern of equatorial anomalies, previously described by Yasunari (1985), which changes phase during an ENSO episode.

4. The Indian Ocean-Pacific zonal circulation anomalies can be viewed as teleconnections in the equatorial belt, which are locally phase-locked with the annual cycle as they migrate eastward during ENSO episodes. Multi-year high index regimes are characterized by a quasi-stationary teleconnection couplet over the region, phased to provide anomalous low-level zonal inflow to the Indonesian-west Pacific convective region. These zonal teleconnections reflect the equatorial branches of large, horizontal circulation anomalies, e.g., cyclonic and anticyclonic couplets, which extend into the extratropics, and are in turn related to other extratropical patterns of teleconnections.

5. So variability in the equatorial belt has usually been viewed as primarily a standing oscillation. A different picture now emerges, in which Pacific regime "turnabouts" are not so much associated with a stationary "swaying seesaw", as with a series of eastward migrating anomalies.

6. The data suggest a relationship between the development of positive SST anomalies over the Indian Ocean and the decay phase of an ENSO episode. Thus ocean-atmosphere interaction outside the tropical Pacific may be a significant factor in the evolution of the SO.

7. More generally, SST and circulation anomalies are linked around

the entire equatorial belt. Just as a coupled ocean-atmosphere approach is ultimately required to answer fundamental questions concerning the SO, so ocean-atmosphere interaction over a single sector of tropical ocean may be influenced by remote forcing, a factor which should be considered in the design of the individual ocean basin studies.

> « There is thus ample reason for a never-ending succession of alternating trends by air-sea interaction in the equatorial belt, but just how the turnabout between trends takes place is not yet quite clear. The study of a sequence of global meteorological maps during typical turnabouts may clarify part of the problem » (Jacob A. Bjerknes, 1969).

1. Introduction

The atmosphere exhibits preferred regional or even global modes of climate variability. These fluctuations in temperature and precipitation are associated with patterns of circulation anomalies which appear over and over again in roughly the same form, often persisting or recurring throughout an entire season. These "teleconnections", which sometimes have the appearance of a wave train, with anomaly centers of opposite sign separated by thousands of kilometers, often reflect patterns of response to remote causal mechanisms (Simmons *et al.*, 1983). Such responses are a fundamental feature of atmosphere dynamics which dictate a global view of climate variability and prediction.

The year-to-year sequence of these anomaly patterns may appear, at first glance, to be essentially random in nature. However, a careful examination of the historical data reveals one dominant global mode of interannual climate variability which evolves on a time-scale of years. This phenomenon, now known as the Southern Oscillation (SO), was first clearly identified, named and extensively described by Sir Gilbert Walker (Walker, 1924; Walker and Bliss, 1932).

The SO is associated with a large-scale seesaw in surface pressure between the Indonesia-North Australian region and the southeast Pacific (Walker and Bliss, 1932; Berlage, 1957), which sways with an irregular period, generally ranging between two and seven years. It has become common to define the phase and amplitude of this pressure oscillation by the surface pressure difference between Darwin and Tahiti (Ropelewski and Jones, 1986). However, the SO has both standing and migrating

components (Trenberth, 1976), and a simple two-station index cannot properly resolve these two components. Nevertheless, the Tahiti minus Darwin SO index (SOI) has proven to be a very useful diagnostic parameter, and in subsequent discussions we will refer to "negative" and "positive" swings in the SO in the context of this index.

Major negative swings in the SO occur in conjunction with the El Niño phenomenon. The name El Niño was originally applied to a local upper ocean warming along the Peru coast, but in current scientific usage it refers to an anomalous warming over the entire central and eastern equatorial Pacific that evolves in a remarkably coherent manner over a period of about two years (Rasmusson and Carpenter, 1982). The oceanic El Niño and the atmospheric SO were discovered and for decades studied as separate entities. However, Bjerknes (1969), in a landmark paper, showed that the two phenomena are simply coupled parts of an elegant and pervasive global system of climate fluctuations, now referred to as the El Niño-Southern Oscillation (ENSO) phenomenon.

ENSO episodes are associated with massive dislocations of the rainfall regimes of the tropics, bringing regional drought to some areas and torrential rains to otherwise arid regions. The related atmospheric circulation anomalies extend deep into the extratropics, where they often result in unusual wintertime conditions over regions as far apart as the United States and New Zealand (Rasmusson, 1985). ENSO also causes severe disruptions in the marine ecosystem and fishing industry along the west coast of South and North America. Because of its large amplitude and interannual time-scale, and its consistent pattern of evolution, which is phased with the annual cycle so that specific regional anomalies occur in specific seasons, ENSO has important implications for prediction on the seasonal-interannual time-scale, especially in the lower latitudes.

During the past decade, the emphasis in SO research has been on the low index, warm episode phase of the oscillation. These periods are associated with the more disruptive climate anomalies, and seem to evolve in a more consistent, "episodic" manner than do the high index periods. However, many of the ENSO anomalies reverse sign during high index regimes (e.g., see Shukla and Paolino, 1983), indicating that there is prediction potential associated with both extremes of the SO.

There has been substantial progress in describing the climate system interactions and processes which control the evolution of low index/warm episode regimes, current diagnostic descriptions are still incomplete, particularly in accounting for the initiation and decay stages of the ENSO

phenomenon. Thus, the problem which Bjerknes posed 17 years ago, essentially how and why does the SO go from high to low index and back again, is still extremely relevant.

Current theories on the initiation of warm episodes focus on the trigger mechanism (Lau, 1985; Inoue and O'Brien, 1984), the conditioning of the tropical Pacific Ocean (White *et al.*, 1986), or both (Wyrtki, 1975, 1985). Philander *et al.* (1984) have also examined the role of instabilities of the coupled ocean-atmosphere system in the development of ENSO. The decay phase of ENSO has received less attention. One of the intriguing ingredients seems to be the appearance during some, but not all, episodes of strong easterly anomalies in the western equatorial Pacific late in what will be referred to as year (0), the year of warming in the central equatorial Pacific (Rasmusson and Carpenter, 1982). Philander (1985) comments that "the appearance of easterly winds over the western Pacific is not attributable to changes in SST but must be related to the other factors that affect the movements of the atmospheric convergence zones". Earlier in his paper, however, he suggests that an external factor for reducing the intensity of the westerly anomalies could be "a new heat source in the far western Pacific". A westward extension of the domain of investigation into the Indian Ocean seems to be a requirement for describing and ultimately understanding this stage of the episode.

There has sometimes been a tendency to view the pattern of interannual variability over the equatorial Pacific as either "normal" conditions or warm episodes during which conditions are highly anomalous, or, alternatively, to consider high and low index periods as a sequence of separate, more or less independent "events". In contrast, the SO might be viewed as a continuous process, similar to the evolution of weather on the synoptic time-scale, or 30-60 day oscillations on the intraseasonal time-scale. This is a better framework for examining the low-frequency prediction problem, assuming that an existing SO regime at least partly determines the character of the next.

The equatorial Pacific is the key region of anomalous ocean-atmosphere interaction during ENSO episodes. The role of the monsoon region (Indian Ocean-west Pacific sector) is still unclear. Except for the western Indian Ocean, equatorial sea surface temperature (SST) anomalies in this region rarely approach 1°C. However, SST's themselves are very high, usually exceeding 28°C. Thus, the atmospheric response to even small anomalies can be significant. Anomalies in the Indonesian sector tend to be opposite in sign to those over the central and eastern Pacific (Nicholls, 1984). SST

anomalies over the central and eastern equatorial Indian Ocean typically tend toward small positive values during the southwest monsoon season (June-September) of year 0 Pacific warming (Cadet, 1985). These anomalies then persist for several months, reversing sign or disappearing during the next southwest monsoon season. The degree to which these anomalies are atmospherically forced, or are themselves a source of thermal forcing, is an important question to be resolved.

The pattern of surface pressure change during swings in the SO implies significant variations in the low-level circulation over both the low-latitude Pacific and the Indian Ocean-Indonesian region (Berlage, 1957; Troup, 1966). Complex empirical orthogonal function analysis of wind data (Barnett, 1983; Gutzler and Harrison, 1986) reveals zonal wind anomalies which migrate eastward on an interannual time-scale over the equatorial eastern Indian Ocean-western Pacific. Gutzler and Harrison (1986) found these fluctuations to be phase-locked with the annual cycle, with a nominal period of two years. However, the feature appears to be an intermittent phenomenon, clearly associated with ENSO episodes. The results of Barnett (1983) are more difficult to interpret, but seem to imply a longer period associated with major swings of the SO.

These and other unresolved issues served as the motivation for an observational study in which interannual variability in the entire tropical belt is being examined. Key parameters associated with large-scale coupling of the tropical ocean and atmosphere are examined: SST, satellite measurements of outgoing longwave radiation (OLR), (which serve as an index of precipitation variability), low level (850 mb or surface) and high level (200 mb) winds. Some smoothing of the monthly data is necessary, but heavy band-pass smoothing is avoided in order to better define developments and lag relationships on the sub-annual as well as interannual time-scales. The relatively limited number of major SO swings within the period of interest (1955-86) allows an examination of the continuous time series on a case-by-case basis, with concentration on the similarities and differences in the evolution of high and low index regimes. The period 1979-86 has been analyzed in greatest detail. Time-longitude (Hovmoeller) plots along the equator are used to illustrate the variability, with additional analyses prepared as needed to describe off-equatorial features, e.g., equatorial asymmetries and global teleconnections. The results from 1979-86 are then related to more limited information available from the period 1955-1979.

2. Data and Analysis

The period 1979-86 is one of reasonably reliable and homogeneous equatorial belt data for the four parameters of interest. These data were obtained from the Climate Diagnostics Data Base (CDDB) and supporting climatological summaries of the NOAA Climate Analysis Center (CAC). The CDDB summaries were, in turn, derived from operational data and analyses acquired or prepared by the CAC, the U.S. National Meteorological Center (NMC) and the U.S. National Environmental Satellite Data and Information Service (NESDIS).

SST data consist of monthly and seasonal global analyses prepared on a 2° latitude-longitude grid. Prior to 1982, they were derived from ship and buoy observations only (Reynolds and Gemmill, 1984a). Beginning in January, 1982, AVHRR SST retrievals from U.S. polar orbiter satellites were also used as input to an analysis scheme which blends the most reliable information from both in-situ and satellite data (Reynolds and Gemmill, 1984b). The base period monthly means, from which the SST anomalies are derived, were obtained by averaging individual monthly means obtained from two data sets: (1) the Comprehensive Ocean-Atmosphere Data Set (COADS) (Slutz *et al.*, 1985) for the period 1970-79, and (2) operational data for the period 1980-85. For the earlier period (1955-79), anomalies are departures from the 1950-79 COADS means.

There is little difference in the means for these two post World War II base periods. However, they differ from the SST climatology prepared by Reynolds (1982), which included surface marine data from earlier years. The earlier observations tend toward slightly lower mean values (Rasmusson and Carpenter, 1982), and, as illustrated by Figure 1, their inclusion would result in a small but significant positive bias in the anomalies over most of the equatorial belt during the period of interest. Our primary interest is year-to-year variability, and it is easier to interpret such fluctuations about an unbiased mean than to deal with anomalies which exhibit a small but persistent bias, regardless of whether they reflect a long-term climate trend or simply inhomogeneities in the observations. That is why the shorter base period means are being used.

We are attempting to draw conclusions based on anomalies as small as a few tenths of a degree. This certainly exceeds the accuracy of individual observations, as well as the analyzed, monthly-averaged grid point values. However, our primary interest is in large spatial scale, multi-month time-scale features. While the details of these patterns may not be properly

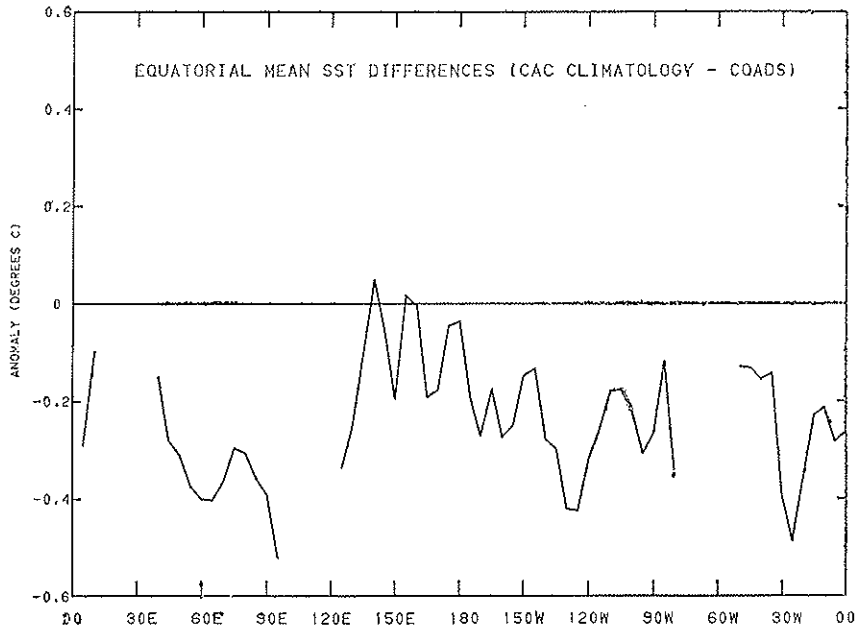

FIG. 1. Difference in SST base period means (°C). Reynolds (1982) climatology minus 1970-85 base period means.

resolved, the analyses do appear to provide useful information about the general nature of the large-scale variations.

Mean monthly values, averaged for a 10° wide strip centered on the equator, were obtained from the wind and OLR map analyses. For these parameters, monthly anomalies are computed as departures from the seven-year base period (8/79-7/86) monthly means. These values were subjected to a three-point temporal smoothing (.25, .50, .25) to remove the effects of 30-60 day oscillations. This significantly attenuates seasonal time-scale variations, but has only minor effects on the lower frequencies.

The OLR data are derived from a variety of window channel measurements from U.S. polar orbiter satellites, using a non-linear regression scheme based on model calculations (Krueger and Gruber, 1984). The data have been subjected to a retrospective correction to remove discontinuities introduced by changes in instrumentation. The day and night values have been averaged to remove the influence of the diurnal cycle insofar as possible. These data are used to infer changes in the

distribution and intensity of tropical convective rainfall. This approach is based on the hypothesis that, in the tropics, decreased OLR corresponds to increased coverage of cold (high) cloud tops, which indicates increased convective rainfall. The results of Arkin (1979), Heddinghaus and Krueger (1981), Liebmann and Hartmann (1982) and others support these assumptions.

The CAC wind fields at 850 mb and 200 mb were derived from the NMC operational global optimum interpolation (OI) analysis, which was implemented in October 1978. Using the previous 12-hour forecast as a first guess, analyses are performed twice daily, about eleven hours after the 0000GMT and 1200GMT observation times, on a 2.5° latitude-longitude grid. Since May 1980, the OI analyses have been modified by an initialization procedure to obtain the "final analysis", which is used as initial conditions for the NMC forecast cycle. Although OI remained the basic analysis routine throughnout this period, it was modified several times. In addition, the forecast model which provides the first guess for the OI has changed, as has the initialization scheme. The divergent component of the analyzed wind field may be particularly sensitive to these changes (Arkin *et al.*, 1986).

The relationships revealed by the 1979-86 data are compared with the patterns of variability during 1955-78, using more limited SST and surface wind data sets. These consist of mean monthly SST analyses from COADS data, and equatorial Pacific surface wind anomalies computed but not published as part of the study of Rasmusson and Carpenter (1982). Relevant published results of other investigators are also cited.

3. ENSO Evolution

Pacific SST and surface wind anomaly composites for six ENSO episodes between 1951-73 were presented and discussed by Rasmusson and Carpenter (1982). They described the westward migration into the central Pacific of anomalies which develop near the South American coast. Their six-event composites are dominated by the larger anomalies during the three strongest episodes (1957, 1965, 1972). Composite time-longitude plots for these three episodes (SST and SST anomalies, zonal (u) and meridional (v) wind anomaly components) are shown in Figures 2 and 3, respectively. Unlike other equatorial sections in this paper, the SST and SST anomaly composites (Figure 2) extend eastward along the equator only to 95°W, at which point they turn southeastward then angle southeast-

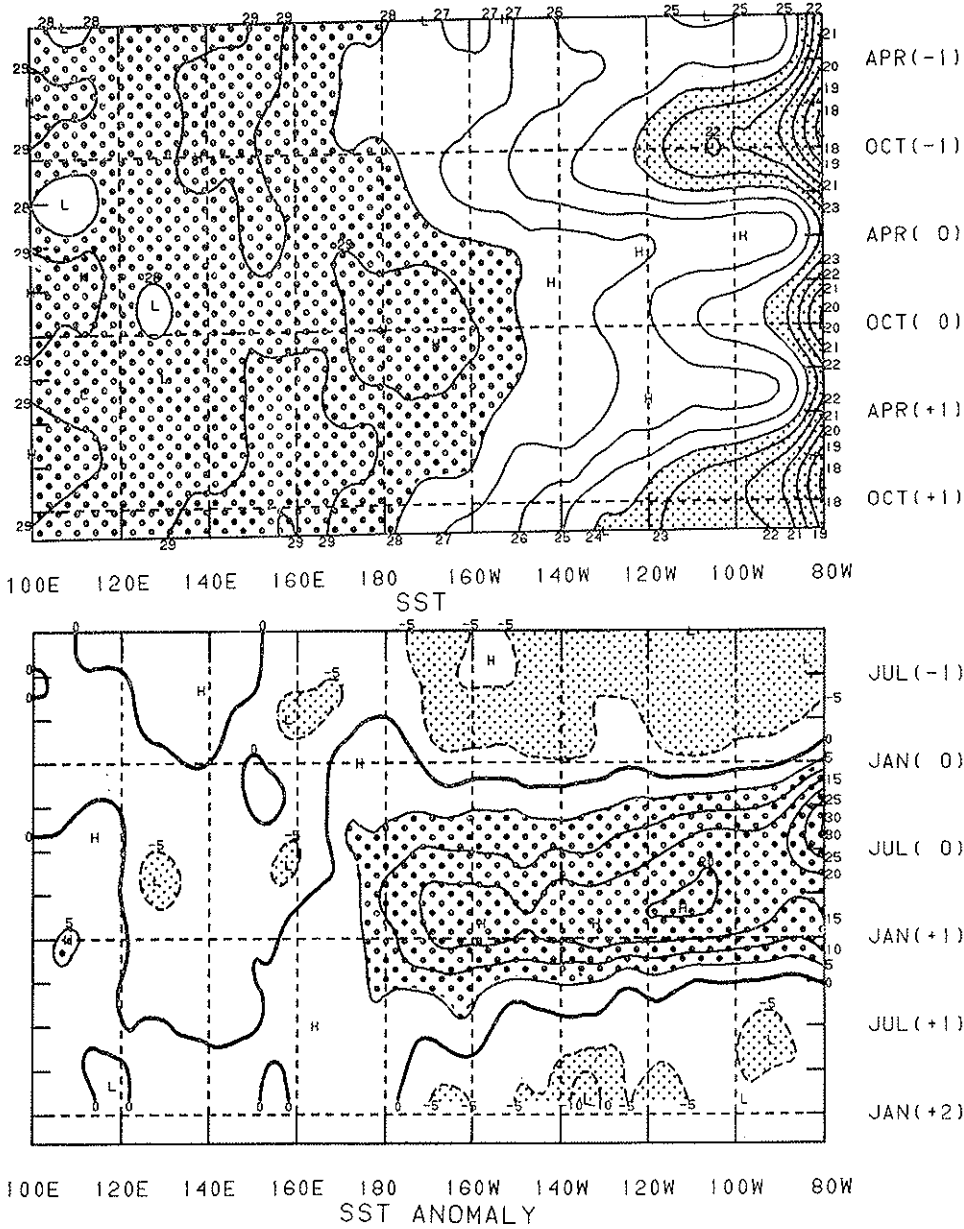

FIG. 2. SST and SST anomaly time-longitude composites for three ENSO episodes (1957, 1965, 1972). Coarse stippling indicates SST greater than 28°C, or SST anomalies greater than 0.5°C. Fine stippling indicates SST less than 24°C, or SST anomalies less than −0.5°C. −1, 0, and +1 indicate the year before, of and following the strong warming. Composites follow the equator to 95°W, then angle southeastward to intersect the Peru coast at 8°S.

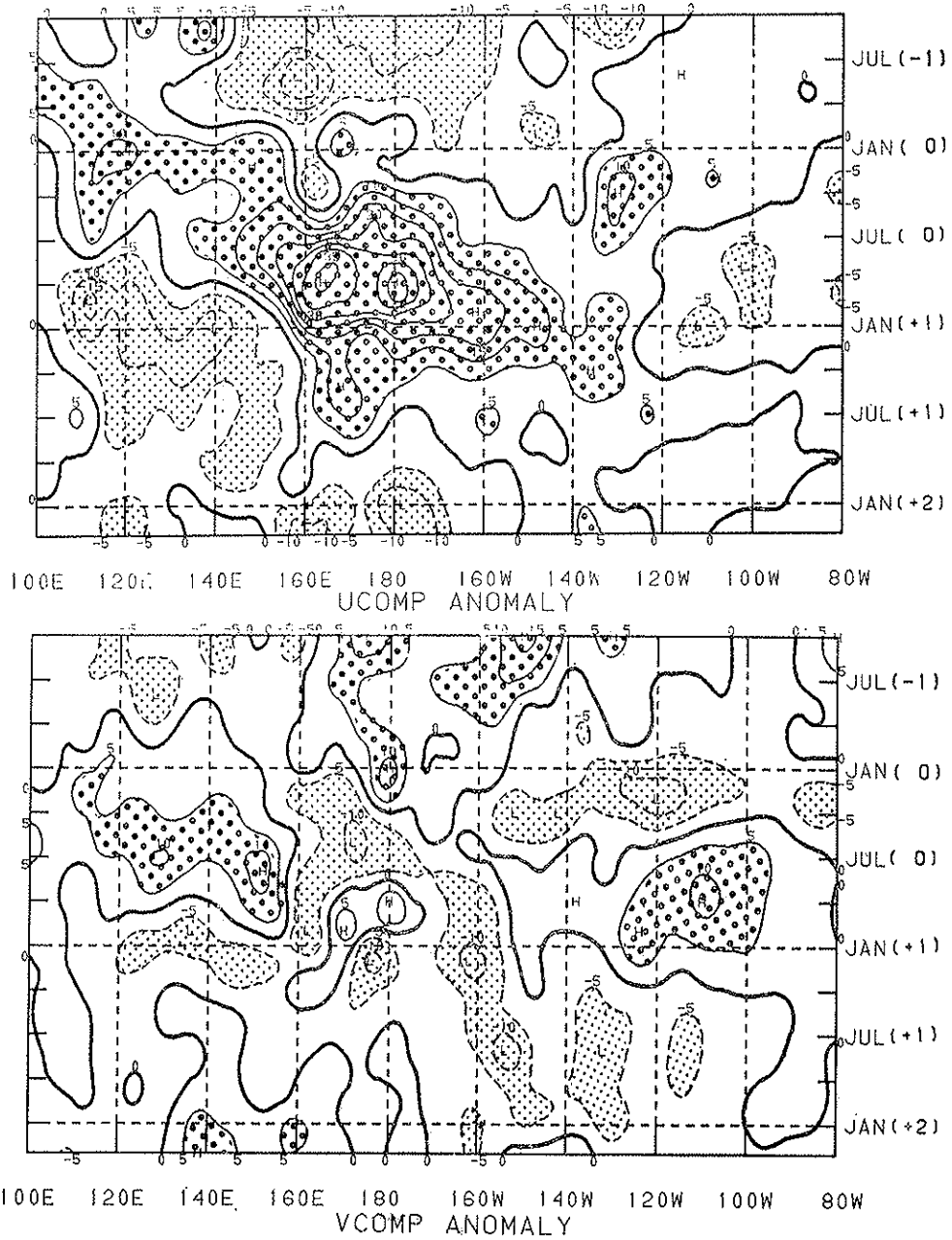

FIG. 3. Time-longitude ENSO anomaly composites along the equator for the zonal (upper) and meridional (lower) wind components. The composites are for the same ENSO episodes as Figure 2. Positive values indicate an anomalous component from the south or west. Coarse stippling indicates values greater than 0.5 m sec^{-1}. Fine stippling indicates values less than -0.5 m/sec.

ward along the climatological axis of minimum SST and maximum SST anomalies, intersecting the Peru coast at 8°S.

Significant warmings in the equatorial Pacific are generally preceded by a high index period (stronger than normal SST and surface pressure gradients between eastern and western equatorial Pacific; stronger than normal equatorial easterlies). Typically, positive SST anomalies first appear along the equator, between 160°E-180, and in the eastern Pacific, near the Ecuador-Peru coast.

The South American coastal warming is the classical El Niño phenomenon that develops early in the year, during the Southern Hemisphere warm season. This warming is one of the "events" during an ENSO "episode" that is intimately tied to the annual cycle. The annual SST warming in the eastern equatorial Pacific follows the Southern Hemisphere seasons. However, there are important east-west phase and amplitude differences; the warming progresses westward along the equator with diminished amplitude, being hardly evident west of 170°W. The low-level equatorial circulation exhibits a monsoon-like annual cycle in the meridional component of flow, associated with the seasonal waxing and waning of the tradewind regimes and the north-south migration of the Intertropical Convergence Zone (ITCZ) and South Pacific Convergence Zone (SPCZ) (Horel, 1982).

The east Pacific El Niño warming has the appearance of an enhanced and slightly delayed annual cycle. SST anomalies are largest near the coast and spread westward with diminished amplitude. The circulation anomalies have a pronounced meridional component, reflecting the anomalous equatorward displacement of the ITCZ that is associated with an enhanced rainy season along the north Peru coast. The coastal anomalies usually peak by April-June; thus, the warming has the appearance of a distinct, rapidly evolving, regional response superimposed on the more slowly evolving basin-wide ENSO anomaly pattern. The event is confined primarily to the area east of 170°W, i.e., the longitudes where there is a significant annual cycle in SST. Anomalies near the South American coast normally diminish during the subsequent cold season. However, during strong ENSO episodes there is often a brief period of re-intensification during the following Southern Hemisphere summer. This marks the mature stage of the ENSO episode (Rasmusson and Carpenter, 1982), when the low-level westerly anomalies, which appeared in the western Pacific a year earlier, have migrated eastward into the central or eastern Pacific (Figure 3). Thus, the first and second coastal warmings of a strong ENSO episode are associated

with different large-scale circulation anomaly patterns. Following the mature stage of the episode, SST and circulation anomalies enter a period of decay, which may last for several seasons.

Although the largest SST anomalies develop in the eastern Pacific, it is the more slowly evolving anomaly patterns of the western and central Pacific that establish the fundamental biennial time-scale of the ENSO phenomenon, and result in a global response. The heavy rainfall and associated heating of the atmosphere over the western Pacific-Indonesian region of high SST represent a major source of atmospheric heating that drives the large-scale circulation. As an ENSO episode develops, this west Pacific warm pool, where SST exceeds 28°C, extends eastward along the equator (Figure 2). This accounts for the initial SST increases near the date line, and is associated with an eastward extension of the heavy rainfall regime and the appearance of westerly low-level wind anomalies in the western equatorial Pacific. The enhanced eastward frictional drag of the low-level winds on the ocean results in a stronger eastward component of the upper ocean currents. This, in turn, brings warmer water farther east, resulting in a further eastward extension of the convective heat source and low-level westerly anomalies, thus closing a positive feedback loop between ocean and atmosphere (Gill and Rasmusson, 1983). The eastward migration of these features continues throughout year 0, as illustrated by Figures 2 and 3.

Rasmusson and Carpenter (1982) presented an SST anomaly composite similar to Figure 2, but did not show composites for SST or the surface zonal wind anomalies. Like Figures 2 and 3, their composites extended westward only to 100°E, and are of uncertain quality west of about 120°E. Consequently, they failed to fully describe the important eastward migrating ENSO features of the western and central equatorial Pacific. Providing such a description is a major goal of this paper.

4. Equatorial Time Series: 1979-86

The period 1979-86 encompassed a variety of climatic fluctuations: an initial period of low-amplitude fluctuations, the unusually intense ENSO episode of 1982-83, the pronounced high index period during 1983-85, and the initial stages of what appears to be a developing ENSO episode during 1986. This is a useful time series for establishing well documented benchmarks against which to compare earlier swings of the SO.

4.1 *SST Anomalies* (Figure 4)

For purposes of discussion, the Pacific-Indian Ocean sector is divided into three longitude belts: the Pacific (PA; 80°W-150°E), Indonesia (IN; 100°E-150°E), and the Indian Ocean (IA; 40°E-100°E). Since the equator passes over large land areas between 100-120E, no SST analysis is shown in that belt.

During 1979-80, SST anomalies along the equator were relatively weak and exhibited poor time-longitude continuity. The main feature was a diffuse pattern of positive anomalies in the Pacific during 1979 and early 1980. Some evidence of ENSO-like oceanic conditions was observed in the western Pacific Ocean in 1979 (White *et al.*, 1986), and a weak warming occurred along the Peru coast during late 1979-early 1980.

In retrospect, a coherent pattern of SST anomalies leading to the 1982-83 warm episode can be traced back to early 1981. More specifically, what developed into the pattern of eastward migrating positive anomalies first organized over the Indonesian-west Pacific sector during mid-1981, and there is a weak suggestion of continuity to the Indian Ocean in 1980. The simultaneous development of small but extensive negative anomalies over the eastern Pacific resulted in a steepening of the east-west SST gradient along the equator.

The anomalous SST gradient began to diminish in late 1981, as positive anomalies spread eastward across the climatological warm axis (150°E-160°E). Negative pressure anomalies developed at Tahiti, and there were indications of an incipient warming in the eastern equatorial Pacific. However, the developing El Niño pattern abruptly aborted (Rasmusson and Wallace, 1983), resulting in an atypical beginning of this ENSO episode in the east Pacific. In the west Pacific, the episode evolved in a manner similar to the SST and zonal wind composites discussed in the previous section.

The characteristics of the 1982-83 Pacific warming have been extensively documented, e.g., Rasmusson and Wallace (1983), Cane (1983), Rasmusson and Arkin (1985). However, the pattern of anomalies over Indonesia and the Indian Ocean has not been adequately described in the context of Pacific developments. Positive SST anomalies developed over the Indonesian sector during 1981, diminished in early 1982 as the Pacific warming developed, and were replaced by negative anomalies in mid-1982. By this time, small positive anomalies had developed over the Indian Ocean. The negative anomalies over the Indonesian sector, like the positive anomalies which appeared earlier, spread eastward and expanded

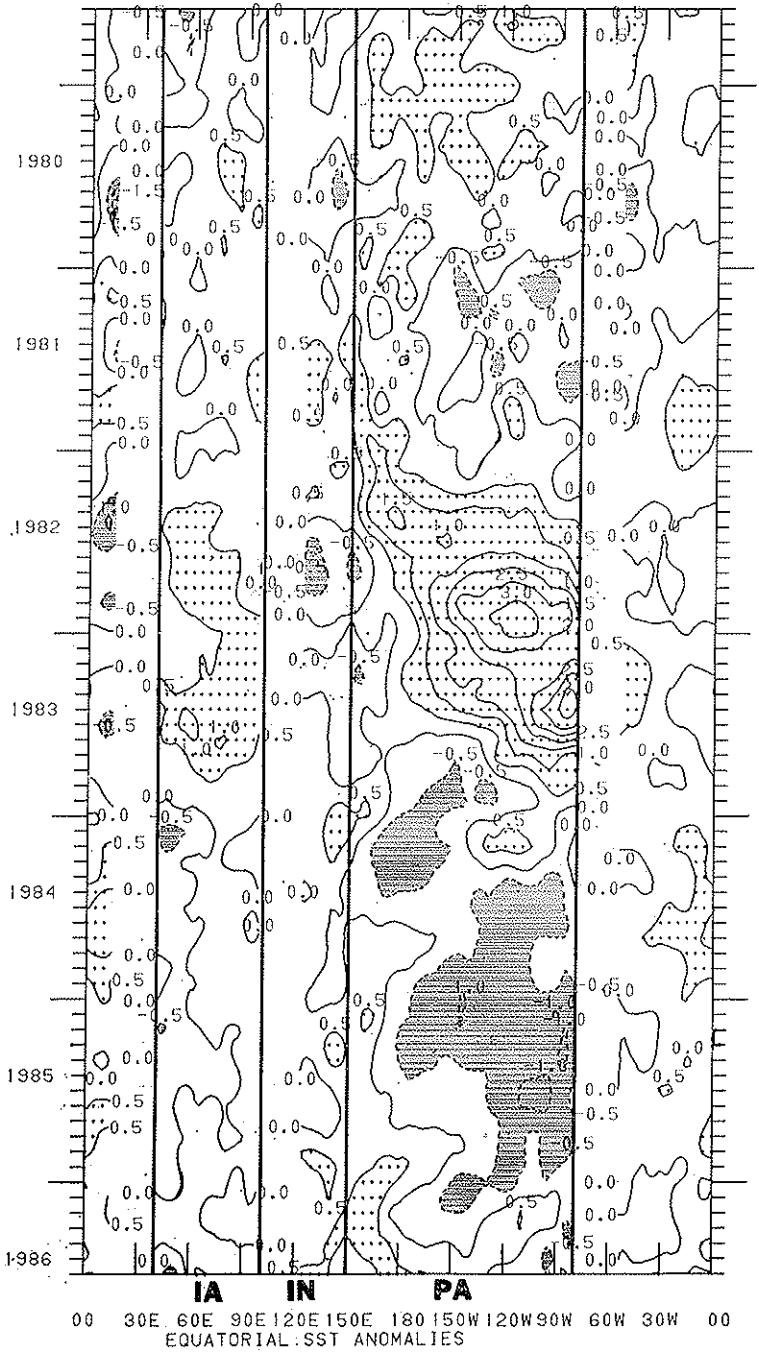

FIG. 4. Hovmoeller diagram (time-longitude section) of sea surface temperature (SST) anomalies averaged over the latitude belt 5°N-5°S. Contour interval: 0.5°C. Stippling indicated anomalies greater than 0.5°C. Shading indicates values less than −0.5°C.

in longitudinal extent. SST anomalies over the Indonesian sector changed sign again in late 1982, reflecting the eastward spread of positive anomalies from the Indian Ocean.

In summary, a coherent pattern of SST anomalies developed over the Indian Ocean-Indonesian-Pacific sectors during 1981, reaching maximum amplitude during 1982-early 1983. Moderate negative anomalies, which developed over the equatorial Pacific in 1983 with the establishment of high index conditions, continued through most of 1985. The large-scale anomaly features showed a pattern of eastward migration, most rapid during the 1982-83 warm episode, and less apparent after 1984.

The anomaly pattern in the Atlantic is also noteworthy. The west Atlantic warming of early 1983 appears to be associated with the mature stage of the warm episode in the Pacific. A second warming in the east Atlantic during 1984 also appears to have roots in the earlier ENSO episode (see 4.3). Developments in the Atlantic during 1983-84 have been discussed by Horel *et al.* (1986).

4.2 *OLR Anomalies* (Figure 5)

OLR and SST anomalies exhibited the same general pattern: weak and disorganized before 1981, large scale, large amplitude, eastward migrating features after that. The relationship between the large OLR and SST anomalies is mostly suggestive of a direct thermal response, i.e., enhanced/diminished convection over regions of positive/negative SST anomalies. However, such an interpretation must take into account anomaly gradients, and SST itself, as well as SST anomalies. For example, observations over the Indian Ocean suggest that widespread, frequent convection occurs primarily over regions where the SST equals or exceeds 28°C (Gadgil *et al.*, 1984). On Figures 4 and 5, the largest OLR anomalies are associated with the eastward migration of the 28°C isotherm across the Pacific to the South American coast during the 1982-83 ENSO episode.

SST and OLR anomalies also show a general negative correlation over the Indian Ocean. In the Atlantic, the positive SST anomalies during late 1981 and during the pronounced 1984 warming were associated with enhanced convection. This did not seem to be the case during 1983.

4.3 *850 MB Zonal Wind Anomalies* (Figure 6)

The change in character after 1980 is again apparent. The zonal anomalies are broadly consistent with the response to equatorial thermal

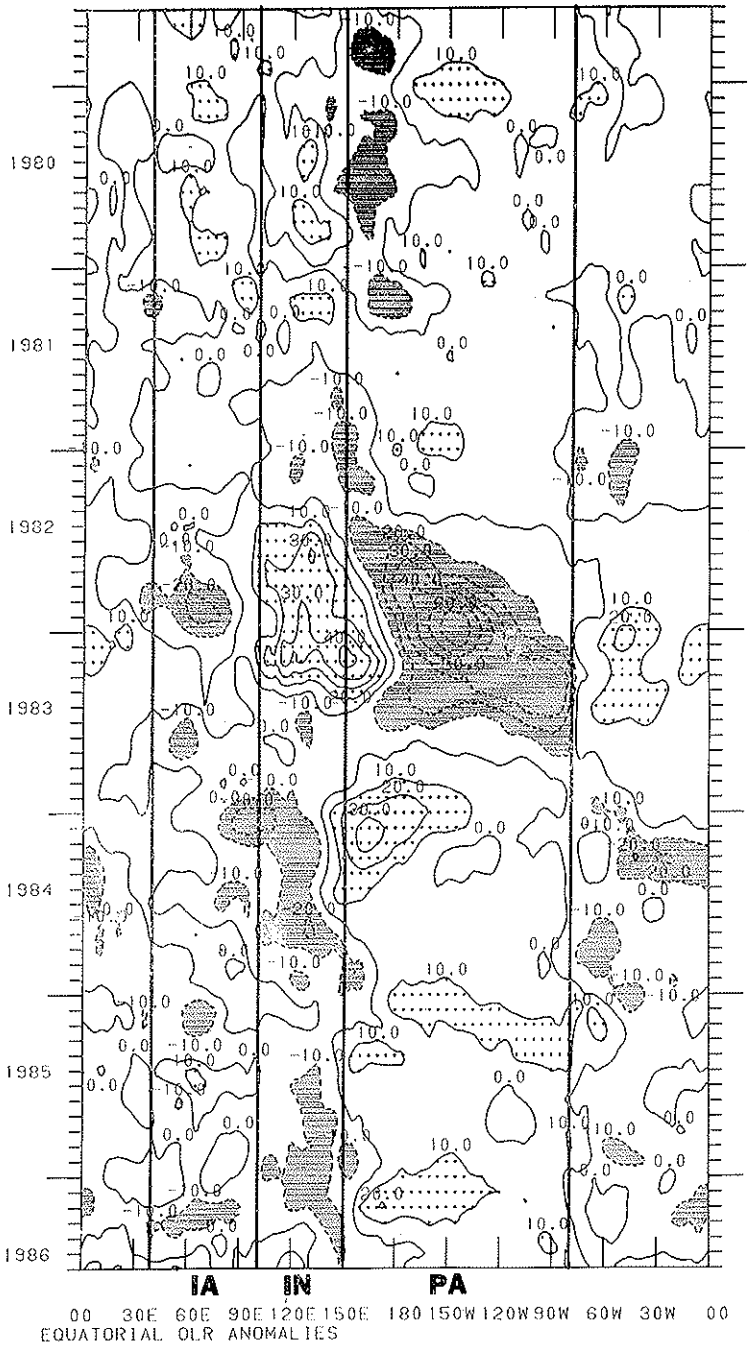

FIG. 5. Same as figure 4 except outgoing longwave radiation (OLR) anomalies. Stippled areas indicate anomalies greater than 10 watts m^{-2}. Shaded areas indicated anomalies less than -10 watts m^{-2}.

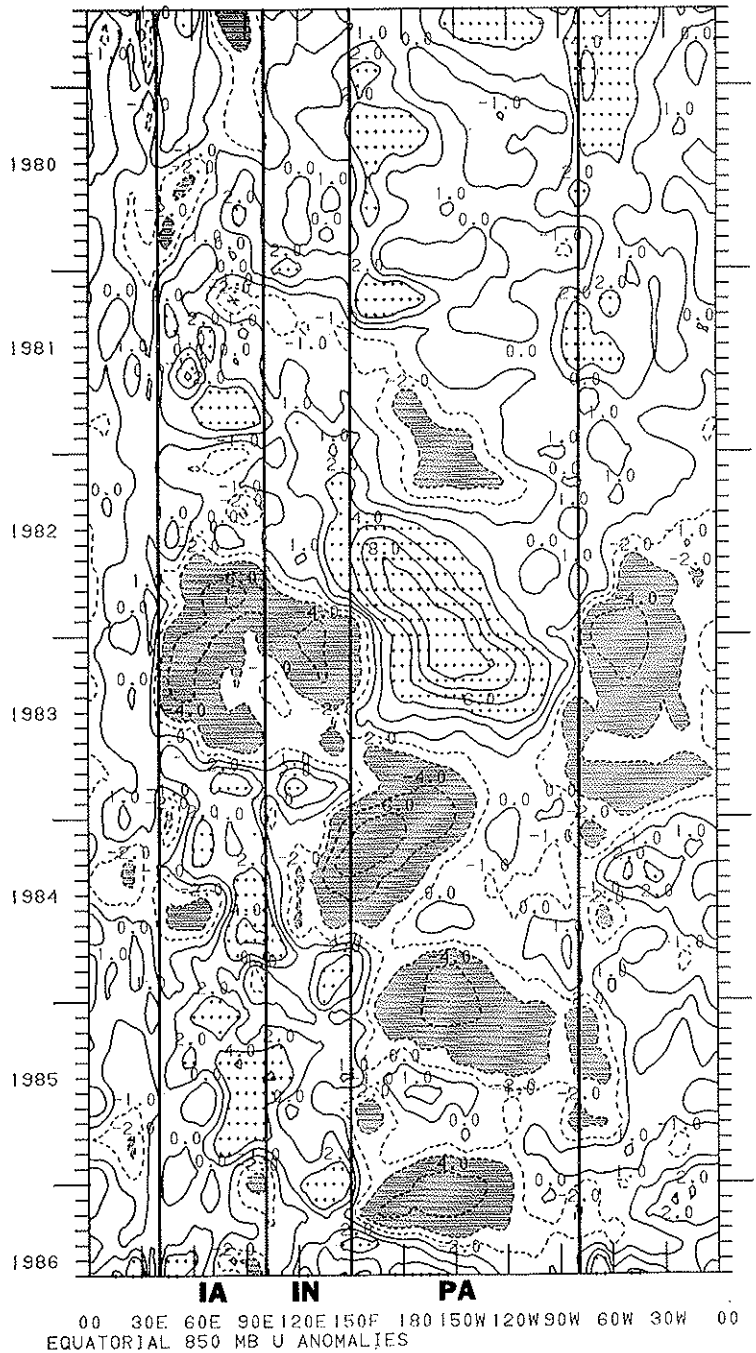

FIG. 6. Same as Figure 4 except 850 mb zonal wind anomalies. Stippled areas indicate anomalies greater than 2 m sec^{-1} (from the west); shaded areas anomalies less than -2 m sec^{-1}.

forcing indicated by simple linear models, e.g., Gill (1980), provided the SST anomalies can be considered an index of anomalous forcing.

Figure 6 shows a striking series of three eastward-migrating zonal wind anomaly maxima associated with the 1982-3 warm episode. The anomalous equatorial SST gradients resulting from the near simultaneous appearance of below normal SST over the Pacific and positive SST anomalies in the Indonesian-west Pacific sector during 1981 were associated with the development of easterly anomalies over the Pacific and westerly anomalies over the Indian Ocean. Thus, the initial appearance of positive SST anomalies over Indonesia and the west Pacific coincided with the development of a low-level inflow anomaly couplet: anomalous westward flow to the east, and anomalous eastward flow to the west of the warm anomaly. This zonal anomaly couplet migrated eastward, but the enhanced easterlies weakened as positive SST anomalies spread eastward across the Pacific during early 1982.

Typical of most episodes, easterly anomalies developed over Indonesia and the west Pacific during the last half of 1982. Comparison with the SST and OLR anomaly patterns again suggests a direct thermal response, this time to the anomalous equatorial SST gradient resulting from the development of small negative and positive anomalies over the Indonesian and central and eastern Indian Ocean sectors, respectively. If this is indeed the case, then Indian Ocean SST may play a role in the evolution of the mature and decay phases of an ENSO episode.

By late 1983, the 850 mb zonal anomalies had evolved into a high index pattern: westerly anomalies over the Indian Ocean and enhanced easterlies over the Pacific. This is consistent with the above normal SST and convection that had developed over Indonesia and the eastern Indian Ocean. Note that the high index period from late 1983 through 1985 was not reflected in the SOI (Figure 15). Both Tahiti and Darwin pressure anomalies exhibited large, interannual time-scale swings, but the low-frequency variations at the two stations were essentially in-phase, and the SOI remained near zero.

Finally, we again call attention to the interesting pattern in the Atlantic during 1983-84. The ENSO-related easterly anomalies, which prevailed during 1983, collapsed and changed to westerly anomalies in early 1984. This is the well known buildup and relaxation pattern associated with El Niño development in the eastern Pacific, and it apparently led to the 1984 warming in the Atlantic. This warming first developed

along the Angola coast, then spread equatorward and westward in a manner strikingly similar to El Niño warmings in the eastern equatorial Pacific.

4.4 *200 MB Zonal Wind Anomalies* (Figures 7, 8 and 9)

A number of investigators, e.g., Rasmusson and Arkin (1985), Yasunari (1985), Gutzler and Harrison (1986), have noted the baroclinic nature of low-latitude circulation anomalies. This is clearly illustrated by a comparison of Figures 6 and 7, which show the general tendency for large-scale anomalies of opposite sign in the upper (200 mb) and lower (850 mb) troposphere. On the global scale, both 850 mb and 200 mb zonal wind anomalies showed a dominant wave number one pattern during 1982-86. This pattern gradually shifted phase by 180° during 1982, then shifted back again in 1983. One node is tied to a migration or change in strength of the Indonesian-west Pacific equatorial easterlies; the other to similar variations in the east Pacific-Atlantic equatorial westerlies, which are primarily a Northern Hemisphere cold season phenomenon.

Yasunari (1985) analyzed the NMC 200 mb wind data from the period 1968-84, using band pass filters to display 40-60 and 20-30 month modes of variability. He found a predominant wave one pattern in the 40-60 month mode, with eastward propagating anomalies over the Indian Ocean-Pacific sector. Anomalies in the 20-30 month quasi-biennial (QBO) band showed a more rapid eastward propagation. He interpreted these results as showing a coupling/decoupling between SO and the QBO modes with strong/weak ENSO episodes. However, based on the work of Gutzler and Harrison (1986), it appears that significant QBO variations only exist in association with warm episodes.

Figure 8 shows seasonally averaged 200 mb stream function anomaly maps for December-February 1981-82, 1982-83, and 1983-84. These charts vividly illustrate the global scope of the SO. Comparison with Figure 7 shows that the equatorial zonal anomalies often reflect the common branch of large cyclonic or anticyclonic circulation anomaly couplets which straddle the equator ([1]). For example, the equatorial easterly anomalies over the Indonesian-west Pacific sector, and the westerly anomalies over the eastern

([1]) It should be noted that the use of different base periods in computing the anomalies on the two charts (16 years for Figure 8) leads to the small differences in the equatorial zonal anomalies.

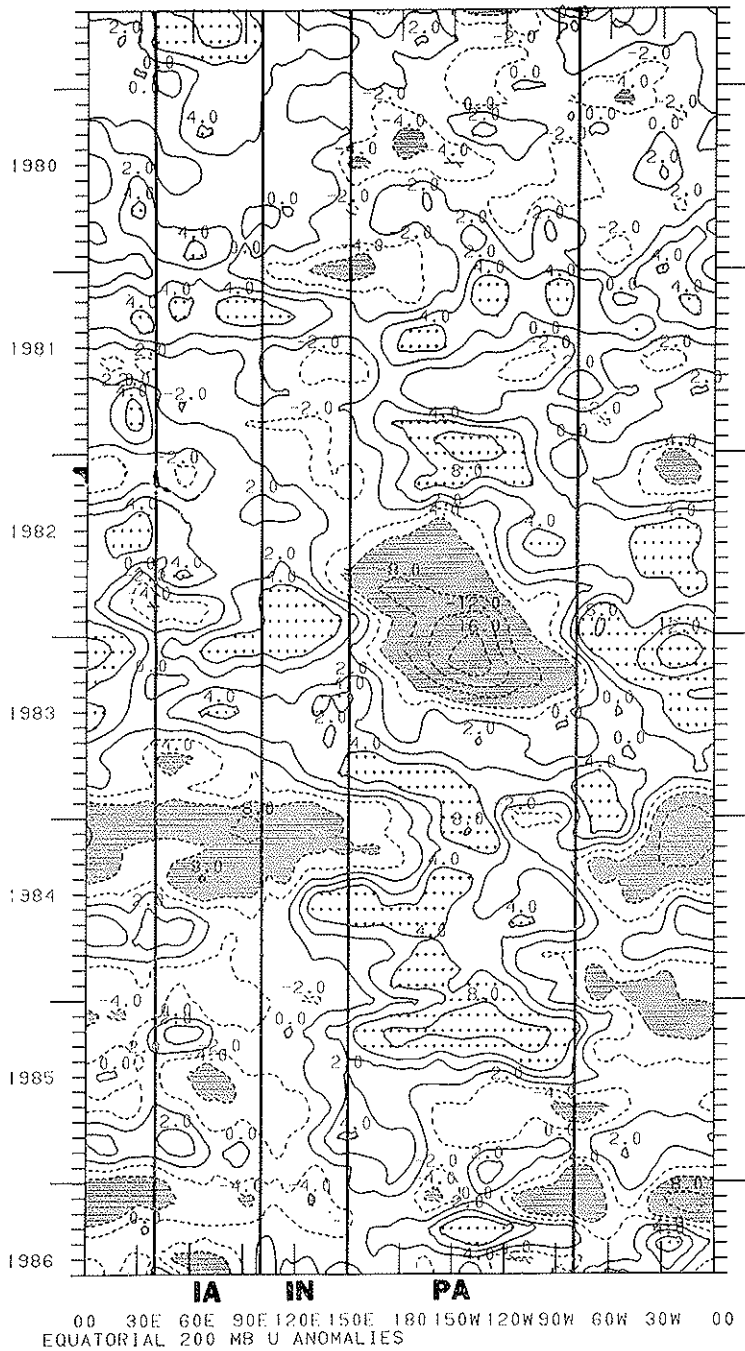

FIG. 7. Same as Figure 4 except 200 mb zonal wind anomalies. Stippled areas indicate anomalies greater than -4 m sec^{-1}; shaded areas anomalies less than -4 m sec^{-1}.

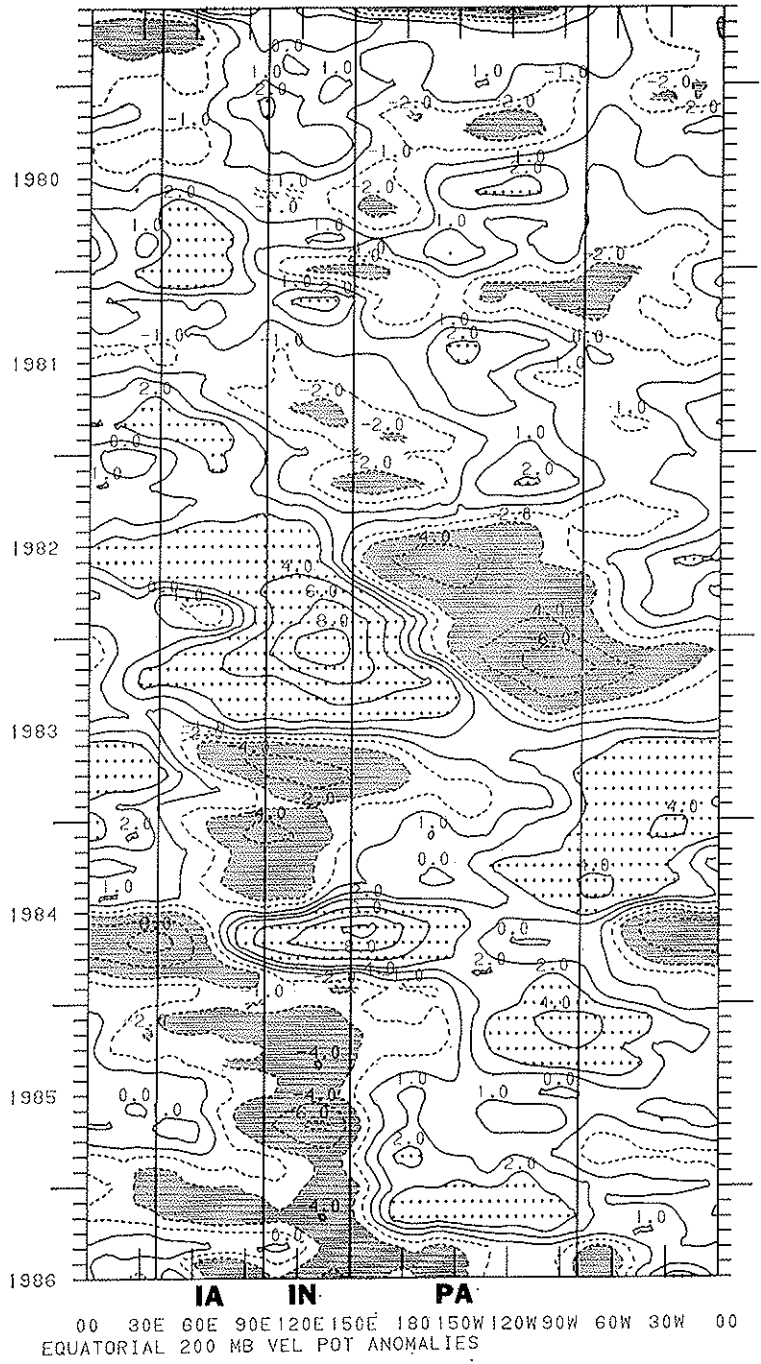

FIG. 8. 200 mb stream function anomalies 1981-2; 1982-3; 1983-4. Arrows indicate direction of anomalous flow. Contour interval: 5×10^6 m^2.

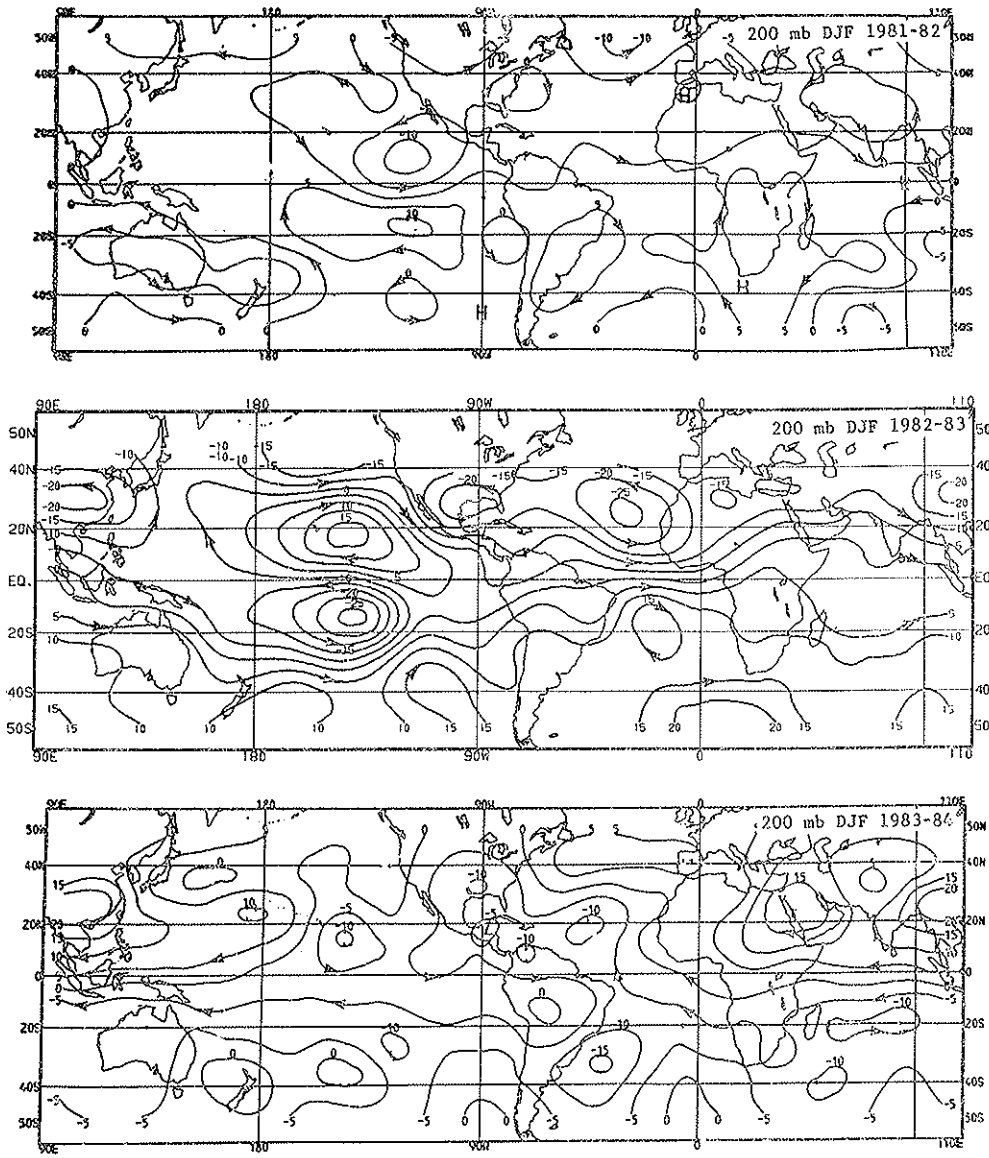

FIG. 9. Same as Figure 4 except 200 mb velocity potential anomaly. Contour interval is 1×10^6 m^{2}s^{-1}. The zonal component of the divergent wind is directed from low to high values.

Pacific during December 1981-February 1982 (Figure 7) are the common branches of Northern and Southern Hemisphere anticyclonic and cyclonic anomaly circulations, respectively (Figure 8). The poleward branches of the anomalous circulations extend into the extratropics.

The evolution from December 1981-February 1982 (Figure 8, upper) to the anomaly pattern one year later (Figure 8, center) is remarkable. The pattern over the equatorial Pacific completely reversed, and the cyclonic couplet located over the eastern Pacific in 1981-82 shifted eastward to the Atlantic. Furthermore, the amplitude of the anomaly features increased markedly. The equatorial changes are clearly associated with major circulation changes in the middle latitudes of both hemispheres. By the Northern winter of 1983-84 (Figure 8, lower), the equatorial anomaly pattern had again changed phase. The circulation anomalies were weaker over most of the world, but remained very strong over the Indian Ocean-west Pacific sector.

Anomalies of the total zonal wind component, as displayed in Figure 7, primarily reflect variation in the rotational component of flow. The 200 mb zonal divergent component along the equator, obtained from the NMC analyses, con be derived from the velocity potential anomaly (VPA) time-longitude section, illustrated on Figure 9. Since the divergent component is a linear function of the velocity potential gradient, Figure 9 illustrates the strictly defined anomalous "Walker circulation" at 200 mb. The concept of a two-dimensional Walker circulation in the plane of the equator is, however, an abstraction, since the meridional divergent flow is often quite significant. Thus, there is no assured relationship between the zonal divergent component and the local divergence or vertical motion field. In fact, comparison of the OLR anomaly section and Figure 8 indicates little relationship between the OLR anomalies and the VPA gradient. There is, however, a clear tendency for strong positive/negative OLR anomalies near VPA maxima/minima.

As with the other parameters, the anomaly pattern prior to 1981 is weak and disorganized, but a number of noteworthy features, listed below, appear after mid-1981.

1. A coherent wave two pattern developed in the VPA anomaly pattern around July, 1981. This apparently reflected an intensified zonal outflow component from the west Pacific-Indonesian region of enhanced convection, and anomalous zonal divergent flow into the east Pacific region of negative SST anomalies and enhanced low-level easterlies.

2. As was the case for the other parameters, these VPA features migrated eastward, but one year later, around July, 1982, as strong intensification began in the Pacific, a dominant wave one pattern abruptly emerged, i.e., a single "anomaly Walker Cell" around the entire equatorial belt, with the Pacific inflow-outflow couplet the dominant feature.

3. The eastward migration continued (see Rasmusson and Arkin [1985] for charts illustrating the VPA fields during June-August 1982 and December 1982-February 1983). The VPA pattern reached peak intensity around February 1983, with the dominant Pacific features 180° out of phase with those a year earlier.

4. A rapid transition occurred around July 1983, when the Pacific returned to the pattern of two years earlier. This change was consistent with the establishment of enhanced convection over the Indonesian sector. Note that while the initial 180° phase shift took place gradually, over a period of one year, the shift back, which coincided with the rapid demise of the warm episode in the Pacific, took place rapidly.

5. The pattern established in mid-1983 continued through early 1986, except for August-September, 1984. This was a period of changes in the NMC analysis-forecast cycle, which included the implementation of a diabatic initialization procedure. The unusual VPA pattern does not appear to be related to the rotational component or the OLR anomalies. We suspect it is due to analysis problems. Because of the application of the three-point smoother to the monthly data, values for the two neighboring months were also affected.

5. ENSO Episodes: 1950-1979

The evolution of atmospheric anomalies over the eastern Indian Ocean-Pacific sector during year (−1) through year (+1) of the 1982-83 ENSO episode is characterized by eastward migrating zonal wind anomalies, with a period of a little over two years. These anomalies appear to be a response to the large-scale pattern of SST anomalies. Many aspects of the evolution are quite similar to those of the typical ENSO pattern as described by a number of investigators. The most notable departure, the lack of an early warming in the eastern Pacific, has already been pointed out. Otherwise, the SST and low-level wind anomalies over the Pacific, while

unusually intense, evolved much like the patterns of the three-episode composites described in Section 4. The evolution of SST anomalies over the Indonesian sector and the appearance of positive anomalies over the Indian Ocean during year (0) is also consistent with the patterns described by Nicholls (1984) and Cadet (1985), respectively. The migration and evolution of the zonal wind anomalies over the equatorial Indian Ocean-Pacific sector were not very different from the average pattern found by Gutzler and Harrison (1986). The global wave one pattern was typical of previous swings in the SO (Yasunari, 1985). It now seems useful to establish, to the extent possible, the degree to which other warm episodes satisfied these relationships.

The SST anomalies presently being examined are illustrated in Figures 10 through 13. These diagrams reveal a rich variety of anomaly patterns associated with the SO swings (Figure 14). The poorer continuity of the SST anomalies over the west Pacific-Indian Ocean sector may be due, at least in part, to the marginal ability of the data to resolve the small anomalies. These SST analyses, together with the other sources of information, particularly the unpublished equatorial Pacific surface wind analyses prepared by Rasmusson and Carpenter (1982), the analysis of Gutzler and Harrison (1986) and Indian Ocean analyses of Cadet (1985) and Blazejewski *et al.* (1986), allow a tentative characterization of the warm episodes during this period.

The warm episodes during this three-decade period were first divided into two general classes (Table 1): episodes whose evolution exhibited the typical pattern of phase locking with the annual cycle, and the mavericks, which to some extent defy classification. We have included, for completeness, two very weak, relatively low index occurrences, that have rarely been viewed as warm episodes. The first is the "episode" of 1974. It is associated with a major negative swing but not negative values in the SOI. Therefore it represents only a relative minimum between two pronounced high index swings. This SO minimum was accompanied by a sequence of eastward migrating features in the equatorial Pacific zonal wind anomalies (not shown): a transition from strong easterly anomalies to near zero anomalies and then back to pronounced easterly anomalies. The SST section is also characterized by a period of near normal anomalies between pronounced negative anomalies. Viewed in this context, the much discussed "aborted" El Niño of 1975 corresponds to the second east Pacific warming of a typical episode. The other case not normally included as a

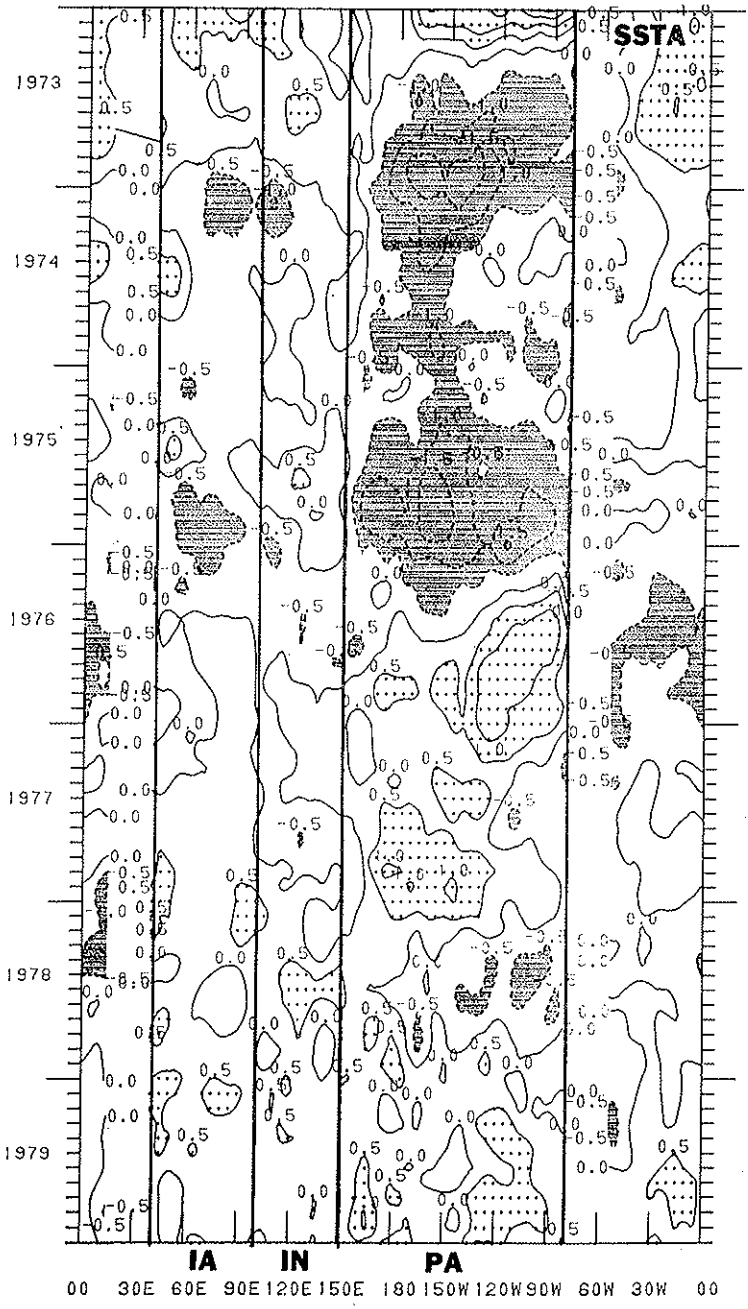

FIG. 10. SST anomalies. Stippling indicates values greater than 0.5°C. Shading indicates values less than −0.5°C.

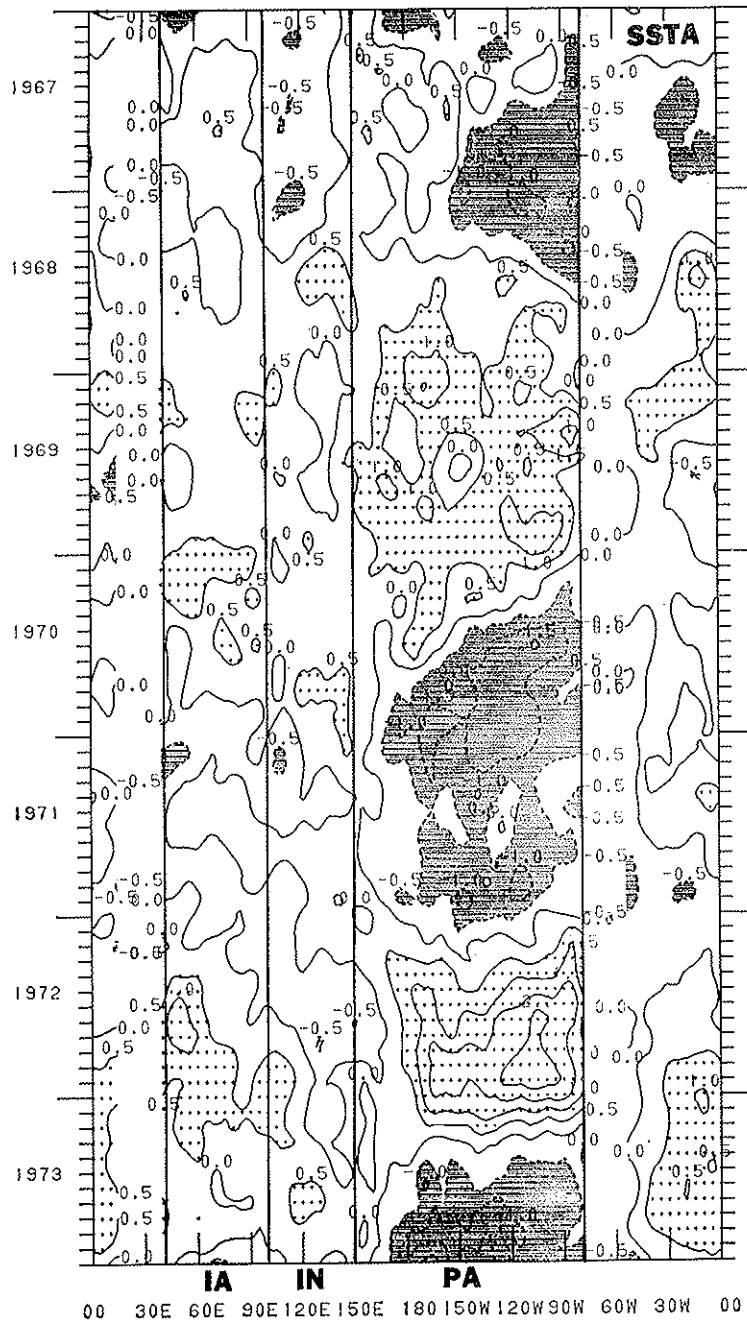

FIG. 11. Same as Figure 10.

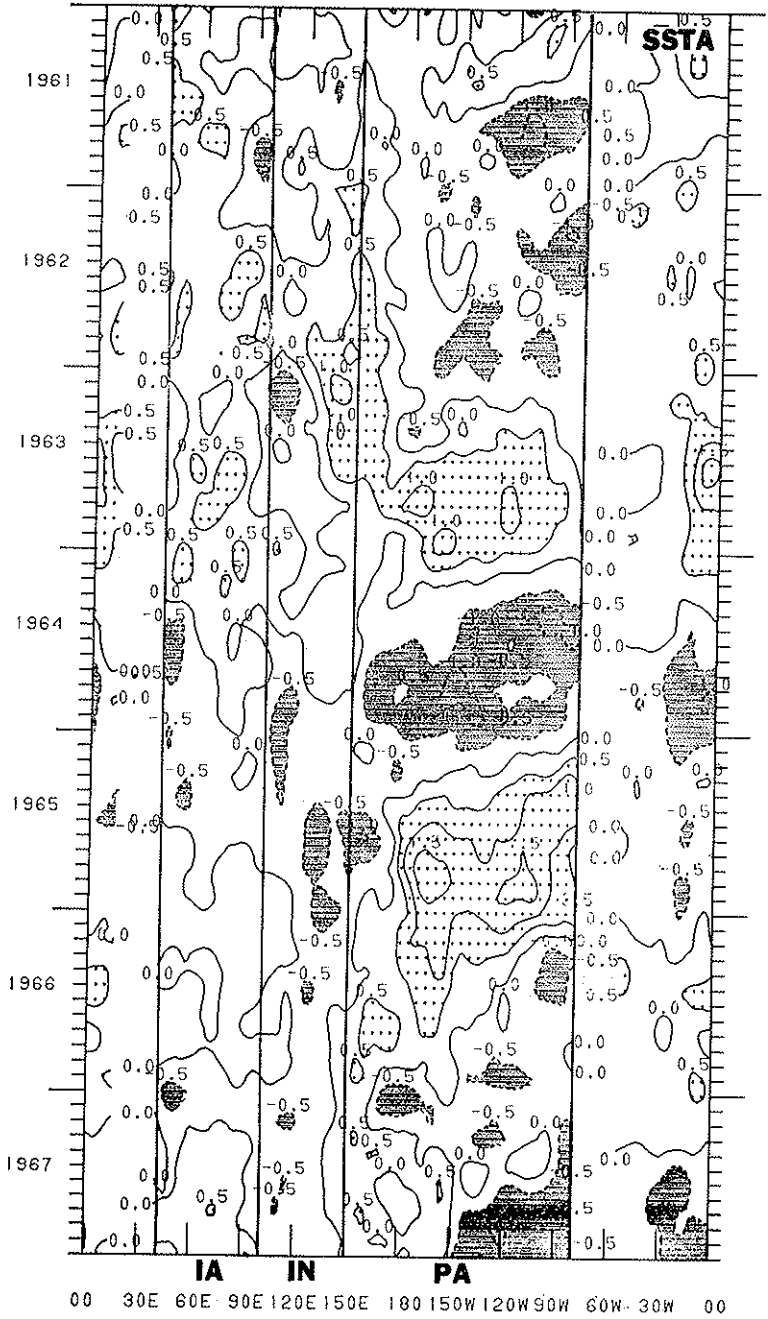

FIG. 12. Same as Figure 10.

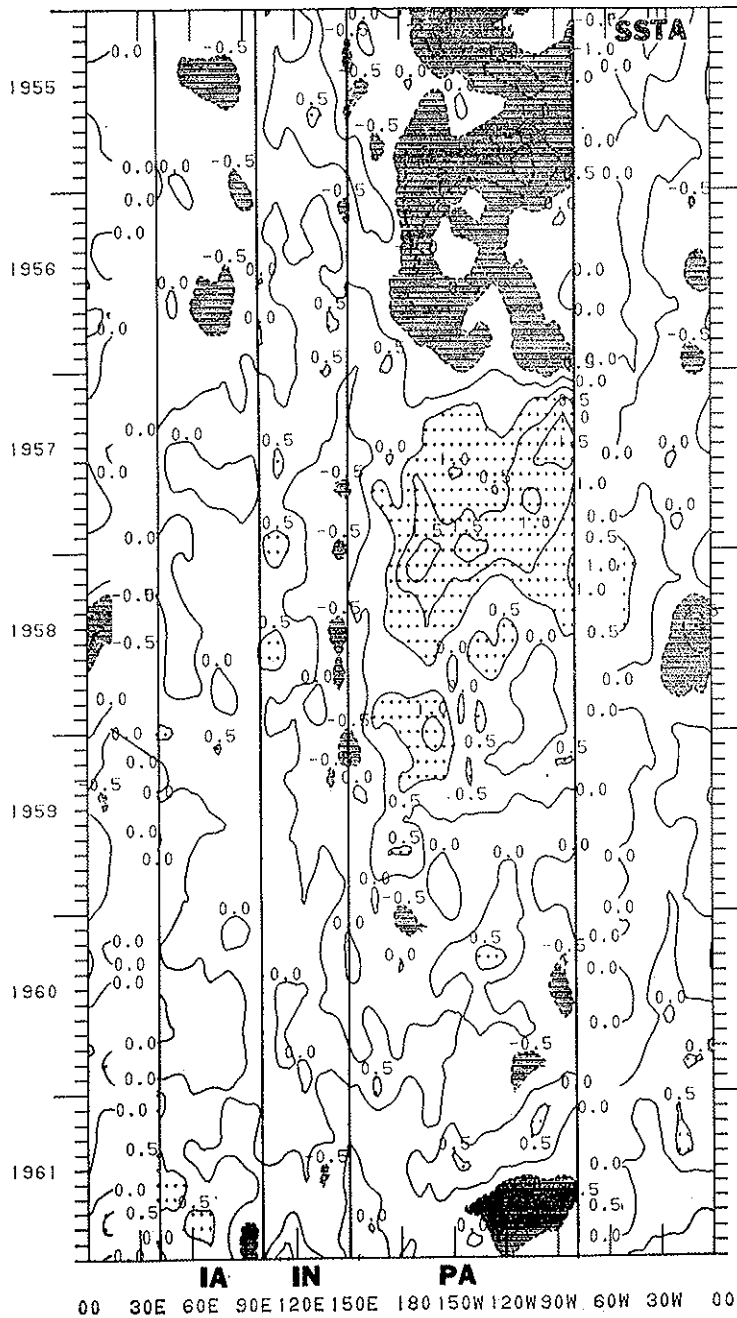

FIG. 13. Same as Figure 10.

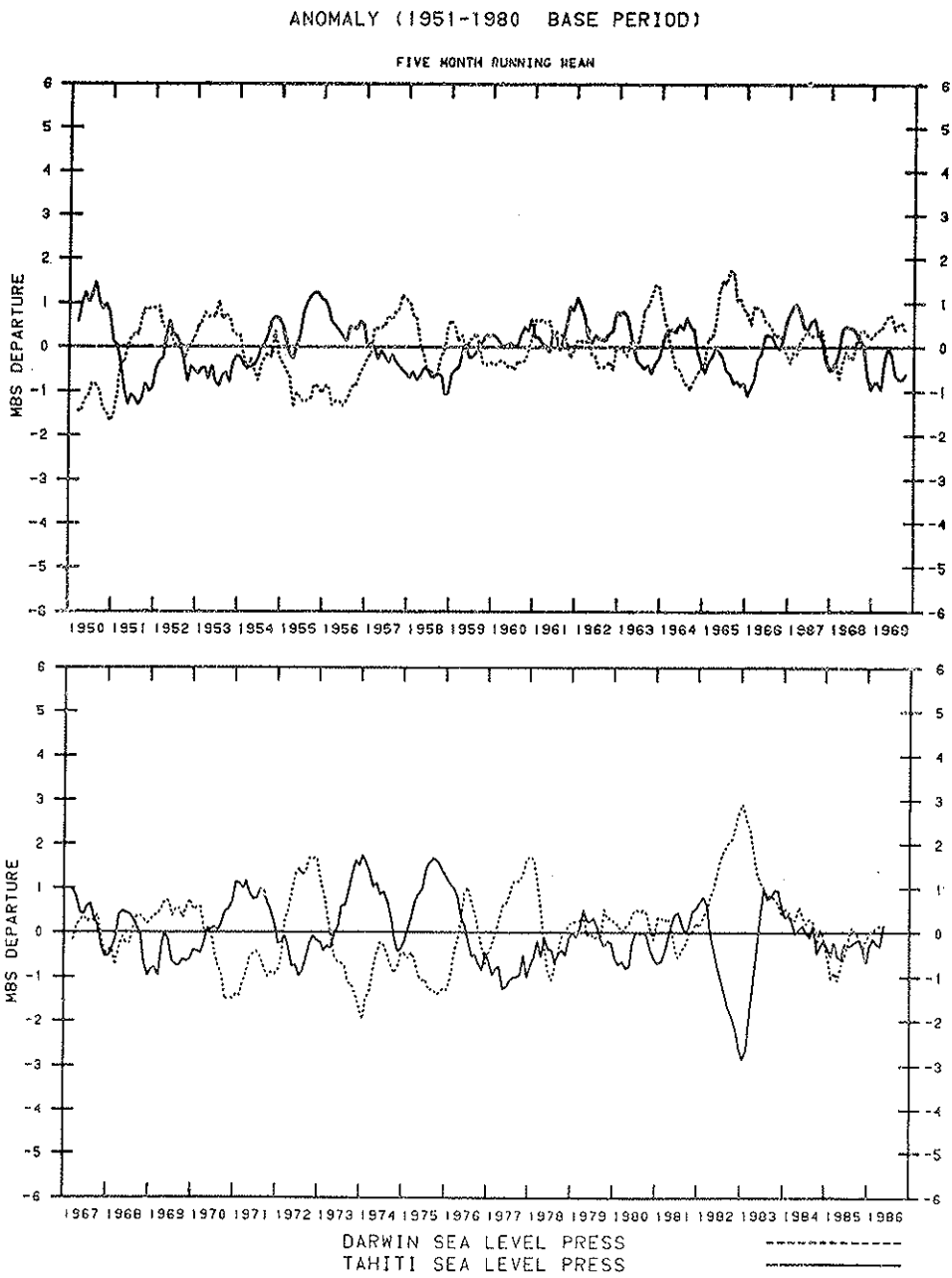

FIG. 14. Five-month running mean of the sea level pressure anomalies at Darwin (dashed) and Tahiti (solid).

TABLE 1

EPISODE[2]		YEAR[3]	ENSO CLASSIFICATION[1] PACIFIC SST EAST[4]	CENTRAL[5]	INDONESIA[7] WIND[6]	INDIAN O. SST[8]	WIND[9]
CONVENTIONAL EVOLUTION							
1982-83	(++)	(−1)	X		9/81	X		X
		(0)	O		9/82	X	X	X
		(+1)	X	X	1/84	X		X
1972	(++)	(−1)	X		6/71	X		X
		(0)	X		6/72	X	X	X
		(+1)	X	X	6/73	X		X
1957	(+)	(−1)	X		4/56	X		X
		(0)	X		1/58	O	*O*	*X*[10]
		(+1)	X	*O*	*O*	*O*		X
1965	(+)	(−1)	X		6/64	O[11]		X
		(0)	X		10/65	X	*O*	*X*[12]
		(+1)	X	*O*	*1/67*[13]	*O*		X[12]
1963	(−)	(−1)	X		6/62	X		X
		(0)	O		10/63	X	X	X
		(+1)	X	X	6/64	X		X
1974	(−−)	(−1)	X		4/73	X		M
		(0)	X		1/75	O	O	M
		(+1)	X	O	11/75[13]	O		M
MAVERICKS							
1976-77	(−)	(−1)	X		( )[14]	X		X
		(0)	X		O	X	O	O
		(+1)	O	O	O	O		M
1968-69	(−)	(−1)	X		( )[15]	O[16]		X
		(0)	O		( )[15]	O[16]	O	O
		(+1)	X	O	( )[15]	O[16]		O
1979-80	(−−)	(−1)	O		M	X		M
		(0)	O		M	O	O	M
		(+1)	X	O	M	O		M

NOTES ON TABLE 1

[1] Warmings during the period 1955-85 are compared with various aspects of a « canonical » episode, as described by a number of authors. A particular feature that evolved in a generally canonical manner is indicated in the table by an « X ». If the feature does not evolve in the canonical manner, or is weak or hard to define, it is indicated by an « O ». « M » indicated no information.

[2] Episodes are listed in order of intensity, as defined by the SST anomalies shown in Figure 4 and Figures 10-13. The following classification is adopted:

MAXIMUM SST ANOMALY (°C)	INDICATOR	DESIGNATION
$< +1.0$	— —	very weak
$\geq +1.0 < +1.5$	—	weak
$\geq +1.5 < +2.0$	+	moderate
$\geq +2.0$	+ +	strong

[3] The general timing of the anomaly feature. — 1, 0 and + 1 indicate a feature occurring the year before, of or following the major central Pacific warming, as defined by the composites of Rasmusson and Carpenter (1982).

[4] The nature of the SST anomalies in the eastern equatorial Pacific.

— 1: below normal SST
0: early year El Niño warming
+ 1: late year (0), early year (+ 1) warming

[5] The general timing of the anomaly feature. — 1, 0 and + 1 indicate a feature the early months of year (+ 1).

[6] The time of maximum low-level zonal wind anomalies at the dateline.

— 1: easterly anomaly maximum
0: westerly anomaly maximum
+ 1: easterly anomaly maximum

The dates should be considered as rough estimates.

[7] SST anomalies in the Indonesian sector based on Nicholls (1984) and an examination of Figures 4 and 10-13.

— 1: above normal
0: development of below normal
+ 1: development of above normal

[8] « X » indicates the appearance of positive SST anomalies in the central and eastern equatorial Indian Ocean during year (0).

[9] Equatorial low-level zonal wind anomalies in the eastern equatorial Indian Ocean as estimated from Figure 5 and Blazejewski *et al.* (1986).

— 1: westerly anomalies
0: easterly anomalies
+ 1: westerly anomalies

[10] Developed late.

[11] No discernible positive anomalies in the Indonesian sector, but negative anomalies in the eastern equatorial Pacific, which still resulted in a steepening of the SST gradient along the equator.

[12] Very weak anomalies.

[13] Timing very uncertain.

[14] Determined from Gutzler and Harrison (1986). The normal sequence of anomalies terminated during mid-1976, but the sequence was resumed and completed during late 1977-early 1978.

[15] No identifiable pattern.

[16] Anomalies would be « X » if 1969 were designated year (0).

warm episode is the weak, complex warming of 1979-80, which was noted in Section 4.

The warmings were further classified according to intensity, and various aspects of their evolution were compared with what we considered to be the "canonical" pattern. The results are tabulated in Table 1. For a given feature, an evolution generally similar to the "canonical" pattern is indicated by an "X". If the feature is opposite to the canonical pattern, or weak or hard to define during a particular episode, it is indicated by an "O". The marginal quality and quantity of the available information results, at times, in considerable subjectivity in the classification, e.g., the timing of the zonal anomaly maxima at the date line. Therefore, the classifications should be considered provisional at this time.

The lack of typical phase locking with the annual cycle makes it difficult to assign a year (0) to the maverick episodes. We arbitrarily labelled the initial year of warming as year (0), but this uncertainty, together with the generally weaker anomaly patterns, makes it difficult to establish convincing relationships for this class of low index regimes. Similar uncertainties exist for the extremely weak, relative low index regime of 1974. Thus, five relatively similar ENSO episodes, 1957, 1963, 1965, 1972, and 1982 remain for comparison.

In terms of the features examined, the 1972 episode emerges as canonical in every respect. The 1982-83 episode is canonical in most respects, the major departures being the failure of the early warming in the east Pacific, and a slightly delayed decay phase.

The most notable pattern of departures from canonical, indicated by the underlined items in Table 1, occurred during the 1957 and 1965 episodes. Specifically, (1) positive SST anomalies failed to develop over the Indian Ocean during year (0), and over the Indonesian sector during year (+1), (2) the easterly zonal wind anomalies were weak or late in developing over the Indian Ocean during year (0), were late in arriving at the date line during the 1965 episode, never reached the date line during the 1957 episode, (3) the central Pacific decay phase of the 1965 episode extended through much of 1966, and for the 1957 episode, high index conditions never really returned for five years. While it is certainly hazardous to generalize from two cases, the data suggest the possibility that the development of positive SST anomalies over the Indian Ocean during year (0) may be related to the development of easterly anomalies over the Indonesian-western Pacific sector, which in turn affects the

development and rhythm of the eastward moving zonal wind anomalies and the character of the decay phase of the episode.

6. Summary and Conclusions

This paper represents an interim report on an ongoing research project. The conclusions are preliminary, pending a complete analysis of the equatorial belt surface marine wind data for the period 1955-86. Nevertheless, the results to date appear to support a number of conclusions applicable to anomalies in the equatorial belt.

1. *Interrelationship of SST, OLR and circulation anomalies*

Considering the quality of the observational material, the interrelationships between the large scale SST, OLR and zonal circulation anomalies are generally consistent with the premise that the large-scale circulation anomalies during the period 1979-86 reflect a direct response to anomalous thermal forcing, as implied by changes in SST and SST gradients.

2. *Role of the Indonesian-Indian Ocean sectors*

These results provide evidence that tropical ocean-atmosphere interaction outside the equatorial Pacific may influence the course of the SO. The nature of the decay phase of ENSO is highly variable, i.e., a return of high index conditions may take place sharply and rapidly as in 1973, or not at all, as in 1958. The data suggest a relationship between the development of positive SST anomalies over the Indian Ocean during the last half of year (0) and the decay phase of the ENSO episode. While Indian Ocean SST anomalies may initially be forced from the Pacific, through atmospheric teleconnections, these results suggest that the anomalies may subsequently become an active ENSO element in their own right, influencing the later stages of the episode.

One must nevertheless remain cautious in drawing cause and effect conclusions from observational data alone, without additional support from model experiments.

3. *Origin of the SO*

Lead-lag relationships associated with ENSO do not necessarily imply causal relationships, but may simply reflect the complex time-space evolu-

tion of the phenomenon. Thus, interpretation of lead-lag relationships, without an understanding of the physical processes involved, can be extremely hazardous and misleading. This has sometimes led to poorly posed questions concerning the "origin of the SO". The geographical "origin" of circulation and pressure anomalies may be quite remote from the region of prime forcing. For example, the appearance of low-level westerly anomalies over the Indian Ocean in 1981 may be a response to SST anomalies over Indonesia. Are these anomalies to be considered the "origin" of this SO swing? This seems debatable, since the SO is a continually evolving phenomenon, and sooner or later returns to a configuration at least similar to a previous high or low index state. Thus, the question of origin may be somewhat akin to asking one to define an origin on the circumference of a circle.

4. *SO global circulation*

Zonal wind anomalies of alternating sign, with approximately a two year period, migrated eastward across the eastern Indian Ocean-Pacific sector during the 1982-83 ENSO episode. The last two of these anomaly pairs slowed in their eastward progression during 1983, and became a quasi-stationary circulation couplet in the equatorial plane during the high index period which followed (Figure 5). This remained the dominant circulation anomaly feature over the eastern Indian Ocean-Pacific sector until the breakdown of high index conditions during 1986. Globally, these Indian Ocean-Pacific sector circulation anomalies were part of a baroclinic, wave number one pattern, previously described by Yasunari (1985), which changes phase during an ENSO episode.

The Indian Ocean-Pacific circulation anomalies can be viewed as teleconnections in the equatorial belt, which are locally phase-locked with the annual cycle as they migrate eastward during ENSO episodes, and are either weak or quasi-stationary during high index regimes. These zonal teleconnections reflect the equatorial branches of large, horizontal circulation anomalies, e.g., cyclonic and anticyclonic couplets, which extend into the extratropics (Figure 9) and are in turn related to other extra-tropical patterns of teleconnections.

5. *SO time scales*

There are at least three important time-scales associated with the SO. The first is the dominant SO period, which usually ranges between two and seven years. Although irregular, it is nevertheless constrained to the

biennial-decadal time frame, which suggests some underlying control. Since this is the interval between ENSO episodes, the period may be related to an ocean circulation and/or heat content parameter (Wyrtki, 1985; White *et al.*, 1986).

An ENSO episode unfolds on a biennial sub-scale. The two-year sequence of anomalies which is nominally phase-locked with the annual cycle, and is most clearly evident in zonal wind anomalies over the eastern Indian Ocean-central Pacific sector (Figure 6) and in the migration of the SST isotherms in the western and central Pacific. The demise of a warm episode typically marks a transition from eastward migrating, biennial time-scale zonal wind anomalies, to a quasi-stationary high index anomaly pattern. On occasion, however, the biennial fluctuations may continue for more than one period. This happened between 1962-66, and 1971-76, provided we recognize the 1974 negative swing as a legitimate "event". When this happens, there is a continuous transition, during the same year, from the decay phase of one episode to the buildup phase of the next, i.e., year (+1) of the decaying episode and year (−1) of the developing episode are the same, as was the case, for example, in 1964.

Many regional ENSO anomalies may evolve as an aberration of the annual cycle. A prime example is the El Niño event of the eastern Pacific, which develops roughly in-phase and progresses westward with the annual warming cycle. The westward progression is opposite in direction to the migration of the larger-scale ENSO zonal wind anomalies. Evolving on the more rapid annual time-scale, the regional El Niño event is in decline by mid-year, while the basin-scale ENSO warming continues to develop. The relative strength of the western and eastern Pacific developments varies from episode to episode (see Figures 10-13). These differences prompted Rasmusson and Wallace (1983) to propose a two-phase framework for viewing the ENSO phenomenon.

The data from 1979-86 indicate other effects of the SO on the annual cycle in the equatorial Pacific. After 1983, the 850 mb zonal wind anomalies in the central and western Pacific (Figure 6) exhibited features with a period of one year, which migrated westward. Preliminary analyses indicate that these features in the anomaly pattern were at least partly due to the fact that the phase and amplitude of the annual cycle of the zonal wind in the central Pacific during the years immediately preceding the 1982-83 ENSO episode differed significantly from what was observed during 1984-85. This poses the question whether the annual

cycle over the central and western equatorial Pacific can be defined independent of the existing SO regime.

6. *SO regimes*

It seems that Bjerknes (1969) viewed the SO variability in the equatorial belt as essentially a pattern of standing oscillations. A different picture now emerges, involving a sequence in which the regime "turnabouts" are associated with a series of eastward migrating anomalies. Even with this improved description, the observational data give few clues as to why the turnabouts occur as they do, and the crucial question of what factors determine the amplitude of the next swing remains a mystery. These questions involve the coupled ocean-atmosphere system, and cannot be adequately addressed by analyzing atmospheric variability alone, or by observational studies alone, without the added insight obtained from carefully designed model experiments.

7. *Inter-ocean linkages*

It should be apparent that SST and circulation anomalies are linked around the entire equatorial belt. Just as a coupled ocean-atmosphere approach is ultimately required to answer fundamental questions concerning the SO, so ocean-atmosphere interaction over a single sector of tropical ocean may reflect remote influences, a factor which must be carefully considered in the design of the individual ocean basin programs of the Tropical Ocean Global Atmosphere (TOGA) Program of the World Climate Research Program.

Acknowledgements

E. Rasmusson was supported by a grant from the Climate Analysis Center. P. Arkin made constructive comments on the manuscript. We gratefully acknowledge the contributions of J. Kopman, who prepared many of the graphical products, and G. Lucas and K. Stevenson, who prepared the manuscript.

REFERENCES

ARKIN P.A., *The relationship between interannual variability in the 200 mb tropical wind field and the Southern Oscillation.* « Mon. Wea. Dev. », *110*, 1393-1404 (1982).

ARKIN P.A., *The relationship between fractional coverage of high cloud and rainfall accumulations during GATE over the B-scale array.* « Mon. Wea. Rev. », *107*, 1382-1387 (1979).

ARKIN P.A., KOUSKY V.E., JANOWIAK J.E. and O'LENIC E.A., *Atlas of the tropical and subtropical circulation derived from the National Meteorological Center operational analysis.* « NOAA Atlas », *7*, U. S. Dept. of Commerce, Washington, D. C. 95 pp. (1986).

BARNETT T.P., *Interaction of the monsoon and Pacific trade wind system at interannual time scales.* Part I: *The equatorial zone.* « Mon. Wea. Rev. », *111*, 756-773 (1983).

BERLAGE H.P., *Fluctuations in the general atmospheric circulation of more than one year, their nature and prognostic value.* « K. Ned. Meteor. Inst. Meded. Verh. », *69*, 152 pp. (1957).

BJERKNES J., *Atmospheric teleconnections from the equatorial Pacific.* « Mon. Wea. Rev. », *97*, 163-172 (1969).

BLAZEJEWSKI H., CADET D.L. and MARSAL O., *Low-frequency sea surface temperature and wind variations over the Indian and Pacific Oceans.* « J. Geophys. Res. », *91* (c4), 5129-5132 (1986).

CADET D.L., *The Southern Oscillation over the Indian Ocean.* « J. Climatol. », *5*, 189-212 (1985).

CANE M.A., *Oceanographic events during El Niño.* « Science », *222*, 1189-1194 (1983).

GADGIL S., JOSEPH P.V. and JOSHI N.V., *Ocean-atmosphere coupling over monsoon regions.* « Nature », *312*, 141-143 (1984).

GILL A.E., *Some simple solutions for heat induced tropical circulation.* « Quart. J. R. Met. Soc. », *106*, 447-462 (1980).

GILL A.E. and RASMUSSON E.M., *The 1982-83 climate anomaly in the equatorial Pacific.* « Nature », *306*, 229-234 (1983).

GUTZLER D.S. and HARRISON D.E., *The structure and evolution of seasonal wind anomalies over the near-equatorial eastern Indian and western Pacific Oceans.* « Mon. Wea. Rev. », accepted (1986).

HEDDINGHAUS T.R. and KRUEGER A.F., *Annual and interannual variations in outgoing longwave radiation over the tropics.* « Mon. Wea. Rev. », *109*, 1208-1218 (1981).

HOREL J.D., *On the annual cycle of the tropical Pacific atmosphere and ocean.* « Mon. Wea. Rev. », *110*, 1863-1878 (1982).

HOREL J.D., KOUSKY V.E. and KAGANO M.T., *Atmospheric conditions in the Atlantic sector during 1983-84.* « Nature », *322*, 248-251 (1986).

HOREL J.D. and WALLACE J.M., *Planetary scale atmospheric phenomena associated with the Southern Oscillation.* « Mon. Wea. Rev. », *109*, 813-829 (1981).

INOUE M. and O'BRIEN J.J., *A forecasting model for the onset of a major El Niño.* « Mon. Wea. Rev. », *112*, 2326-2337 (1984).

KRUEGER A.F. and GRUBER A., *The status of the NOAA outgoing longwave radiation data set.* « Bull. Amer. Meteor. Soc. », *65*, 958-962 (1984).

LAU K.M., *Elements of a stochastic dynamical theory of the long-term variability of the El Niño/Southern Oscillation.* « J. Atmos. Sci. », *42*, 1552-1558 (1985a).

LAU K.M., *Bimodal climatic state, subseasonal oscillation and the El Niño/Southern Oscillation.* Coupled Ocean-Atmosphere Models, J.C.J. Nihoul, Ed., Elsevier Oceanographic Series, *40*, 29-40 (1985b).

LIEBMANN B. and HARTMANN D.L., *Interannual variations of outgoing IR associated with tropical circulation changes during 1974-78.* « J. Atmos. Sci. », *39*, 1153-1162 (1982).

NICHOLLS N., *The Southern Oscillation and Indonesian sea surface temperature.* « Mon. Wea. Rev. », *112*, 424-432 (1984).

PHILANDER S.G.F., *El Niño and La Niña.* « J. Atmos. Sci. », *42*, 2652-2662 (1985).

PHILANDER S.G.F., *El Niño Southern Oscillation phenomena.* « Nature », *302*, 295-301 (1983).

PHILANDER S.G.F., YAMAGATA T. and PACANOWSKI R.C., *Unstable air-sea interactions in the tropics.* « J. Atmos. Sci. », *41*, 604-613 (1984).

RASMUSSON E.M., *El Niño and variations in climate.* « Am. Sci. », *73*, 168-177 (1985).

RASMUSSON E.M. and ARKIN P.A., *Interannual climate variability associated with the El Niño/Southern Oscillation.* Coupled Ocean-Atmosphere Models, J.C.J. Nihoul, Ed., Elsevier Oceanographic Series, *40*, 697-725 (1985).

RASMUSSON E.M. and CARPENTER T.H., *Variations in tropical sea surface temperature and surface wind fields associated with the Southern Oscillation/El Niño.* « Mon. Wea. Rev. », *110*, 354-384 (1982).

RASMUSSON E.M. and WALLACE J.M., *Meteorological aspects of the El Niño/Southern Oscillation.* « Science », *222*, 1195-1202 (1983).

REYNOLDS R.W., *A monthly averaged climatology of sea surface temperature.* « NOAA Tech. Rpt. NWS », *31*, U.S. Dept. of Commerce, Washington, D.C., 35 pp. (1982).

REYNOLDS R.W. and GEMMILL W.H., *A sea surface temperature analysis based on* in-situ *and satellite data.* « Proc. Ninth Annual Climate Diagnostics Workshop », Oct. 22-28. U.S. Dept. of Commerce, Washington, D.C., pp. 408-416 (1984a).

REYNOLDS R.W. and GEMMILL W.H., *An objective global monthly mean sea surface temperature analysis.* « Tropical Ocean-Atmosphere Newsletter », *23*, pp. 4-5. Available from CIMAS, Rosenstiel School of Marine and Atmospheric Science, U. of Miami, Miami, FL. (1984b).

ROPELEWSKI C.F. and JONES P.D., *An extension of the Tahiti-Darwin Southern Oscillation Index.* « Mon. Wea. Rev. », Submitted (1986).

SHUKLA J. and PAOLINO D.A., *The Southern Oscillation and long-range forecasting of the summer monsoon rainfall over India.* « Mon. Wea. Rev. », *111*, 1830-1837 (1983).

SIMMONS A.J., WALLACE J.M. and BRANSTATOR G.W., *Barotropic wave propagation and instability, and atmospheric teleconnection patterns.* « J. Atmos. Sci. », *40*, 1363-1392 (1983).

SLUTZ R.J., LUBKER S.J., HISCOX J.D., WOODRUFF S.D., JENNE R.L., JOSEPH D.J., STRUER P.M. and ELMS J.D., *Comprehensive Ocean-Atmosphere Data Set Release 1.* Document available from Climate Research Program, ERL, Boulder, CO. (1985).

TRENBERTH K.E., *Spatial and temporal variations in the Southern Oscillation.* « Quart. J. Roy. Met. Soc. », *102*, 639-653 (1976).

TROUP A.J., *The Southern Oscillation.* « Quart. J. Roy. Meteor. Soc. », *91*, 490-506 (1966).

WALKER G.T., *Correlation in seasonal variations of weather IX: A further study of world weather.* « Mem. India Meteor. Dept. », *24* (9), 275-332 (1924).

WALKER G.T. and BLISS E.W., *World Weather V.* « Mem. Roy. Meteor. Soc. », *4*, 53-84 (1932).

WHITE W.B., PAZAN S.E. and INOUE M., *Hindcast/forecast of ENSO events based upon the redistribution of observed and model heat content in the western tropical Pacific, 1964-1986.* « J. Phys. Oceanogr. », accepted (1986).

WYRTKI K., *Water displacements in the Pacific and the genesis of El Niño cycles.* « J. Geophys. Res. », *90* (c4), 7129-7132 (1985).

WYRTKI K., *El Niño - the dynamic response of the equatorial Pacific Ocean to atmospheric forcing.* « J. Phys. Oceanogr. », *5*, 572-584 (1975).

YASUNARI T., *Zonally propagating modes of the global east-west circulation associated with the Southern Oscillation.* « J. Meteor. Soc. Japan », *63*, 1013-1029 (1985).

ON THE MECHANISM OF THE EL NIÑO-SOUTHERN OSCILLATION CYCLE

MARK A. CANE and STEPHEN E. ZEBIAK
Lamont-Doherty Geological Observatory
Palisades, NY 10964

ABSTRACT

A theory for the genesis of El Niño events is developed. ENSO is seen as an oscillation of the coupled ocean-atmosphere system, but only interactions taking place in the tropical Pacific are vital to its existence. As envisioned by Bjerknes (1969), positive feedbacks between atmosphere and ocean along the equator maintain both the warm El Niño phase and the cold, non-El-Niño phase of the ENSO cycle. It is hypothesized that changes in the zonal mean heat content of the equatorial ocean are essential for the transition from one phase to another. These ideas are illustrated with a simple, numerical model of the Pacific ocean-atmosphere system. Implications for prediction are discussed.

1. INTRODUCTION

El Niño has long been considered to be an oceanographic event of great regional interest because of its effect on fisheries and the local climate of western South America. From a more global perspective it was little more than a curiosity. The Southern Oscillation, the discovery of Sir Gilbert Walker, was typically regarded as another curiosity, albeit one of global extent. Some dismissed it as a mere artifact of Walker's zealous data analysis.

El Niño and the Southern Oscillation are now recognized as the

oceanic and atmospheric manifestations of ENSO, the best defined, most prominent signal in year-to-year climate variability. The 1982-83 ENSO event had such profound global ecological, social and economic consequences that it brought "El Niño" to the public consciousness.

Scientific interest in ENSO had been building for almost 2 decades prior to the 82-83 event. In the 1960's, J. Bjerknes (and others) had pointed out observational evidence of a connection between the oceanic El Niño and the atmospheric Southern Oscillation. Bjerknes went beyond the purely descriptive to propose a hypothesis for ENSO which depends on a two-way coupling between the equatorial ocean and atmosphere.

The initial premise of our work was that Bjerknes' hypothesis is essentially correct but, as he acknowledged, incomplete. It could explain both the warm stage of the ENSO cycle (El Niño) and the cold "normal" stage, but not the perpetual alternation from one to the other. We built a relatively simple numerical model of the coupled ocean-atmosphere system to investigate his hypothesis. As discussed at length elsewhere (Cane, 1986), this construction makes use of the impressive progress of the past decades in deciphering the physics of the tropical oceans and atmosphere. This modeling work suggested an explanation for the *oscillation*. The explanation hinges on special features of equatorial ocean dynamics, features revealed by a theory developed after Bjerknes' time.

The plan of the remainder of the paper is as follows. In the next section we briefly describe the coupled ocean atmosphere model and present a few results to illustrate its general behavior. We then present our ideas on the mechanism of the ENSO cycle. Our hypotheses have some clear implications for the prediction of El Niño. After discussing these we present the results of retrospective forecasts of the years since 1970. The outcome of these experimental forecasts bears on the validity of our account of the ENSO cycle, and we conclude with a reconsideration of our hypotheses in this light.

2. Model Description

The components of our coupled model were developed and tested independently. The atmospheric component, described by Zebiak (1986) was shown to reproduce the major features of the equatorial wind anomaly field when forced by observed ENSO SST anomalies (also see Weare, 1986). The oceanic component, described in Zebiak and Cane (1986a;

also see Zebiak, 1984; Cane, 1986) was shown to simulate the overall evolution of SST anomalies during ENSO, when forced by observed tropical wind anomalies. The coupled model differs from others (see the review by McCreary, 1985) primarily in its treatment of the thermodynamics in the atmosphere and ocean, especially through the inclusion of a moisture feedback process in the atmosphere and a simple, but thermodynamically active, surface layer in the ocean.

Only a summary account of the model components will be given here. Both describe perturbations about the mean climatological state, with the climatology specified from observations. The Climate Analysis Center data set (see Rasmusson and Carpenter, 1982) was used for this purpose. For completeness the full governing equations are given in the Appendix.

a. *Atmosphere*

If SST anomalies characteristic of El Niño are given, then the principal changes in the tropical circulation may be calculated. This has been amply demonstrated by simulations with atmospheric GCM's (e.g., Shukla and Wallace, 1983; Lau, 1985). Observations show that the tropical anomalies have a simple vertical structure with a universal form, namely, a reversal of polarity between the lower and upper troposphere (e.g., regions of low level convergence lie below regions of upper level divergence). Linear dynamical models with a single degree of freedom in the vertical have proven remarkably adept at reproducing the horizontal structure of the atmosphere (Matsuno, 1966; Gill, 1980) though the physical interpretation of these models is uncertain (Geisler and Stevens, 1982; Zebiak, 1982). Our model dynamics is of this type: i.e., steady-state, linear shallow-water equations on an equatorial beta plane. Linear dissipation in the form of Rayleigh friction and Newtonian cooling are used.

The circulation is forced by a heating anomaly distribution which depends partly on local evaporation anomalies (parameterized in terms of local SST anomalies), and partly in the low-level moisture convergence (parameterized in terms of the surface wind convergence). Several observational studies (e.g., Cornejo-Garrido and Stone, 1977; Ramage, 1977) as well as GCM calculations have demonstrated the important contribution of moisture convergence to the overall tropical heat balance.

The convergence feedback is incorporated into the model, using an iterative procedure in which the heating at each iteration depends on the convergence field from the previous iteration. The scheme is analyzed in detail in Zebiak (1986). The feedback is nonlinear because the moisture

related heating is operative only when the total wind field is convergent, and this depends not only on the calculated anomalous convergence, but also the specificed *mean* convergence (see Appendix). The feedback focuses the atmospheric response to SST anomalies into or near the regions of mean convergence; in particular, the Intertropical Convergence Zone (ITCZ) and the South Pacific Convergence Zone (SPCZ). Such a focusing is conspicuous in the observed wind anomalies during ENSO (see Rasmusson and Carpenter, 1982).

b. *Ocean*

The model ocean basin is rectangular, and extends from 124E to 80W, and 29N to 29S. The dynamics of the model begin with the linear reduced-gravity model that is so successful in simulating thermocline depth anomalies and sea level changes during El Niño events (Cane, 1986, reviews this work). Such models produce only depth averaged baroclinic currents, but the ocean surface current is usually dominated by the frictional (Ekman) component. Therefore, a shallow frictional layer of constant depth is added to simulate the surface intensification of wind-driven currents. The dynamics of this layer are also kept linear, but only by using Rayleigh friction to stand in for nonlinear influences at the equator (see Zebiak and Cane, 1986b for a discussion). Upwelling velocity is computed as the divergence of the surface layer transport. Inclusion of a surface layer allows a strong response to local winds; models which omit it will understate upwelling effects. Mean currents are generated by spinning up the model with monthly mean climatological winds. These "climatological" currents are then used in the anomaly calculation.

The thermodynamics describe the evolution of temperature *anomalies* in the model surface layer. The governing equation is complete, including three-dimensional temperature advection by both the specified mean currents and the calculated anomalous currents. Although there may be local exceptions, the preponderant evidence is that surface heating does not contribute to the El Niño warming (Bjerknes, 1969, 1972; Ramage and Hori, 1981; Weare, 1983). Instead the data indicate an inverse relation between SST and heat flux into the ocean because of increased evaporation. In the model, surface heat flux anomaly is taken to be proportional to the local SST anomaly, acting always to adjust the temperature field toward the climatological mean state. This (monthly) mean temperature structure is specified from observations. The thermodynamic equation thus has

the following form (where barred quantities represent mean fields and unbarred quantities represent anomalies):

$$\frac{\partial T}{\partial t} = -\bar{u}_1 \cdot \nabla T - u_1 \cdot \nabla(\bar{T}+T) - \{M(\bar{w}_s + w_s) - M(\bar{w}_s)\} \bar{T}_z - M(\bar{w}_s + w_s) T_z - \alpha_s T, \quad (1)$$

where u_1 and w_s represent horizontal surface currents and upwelling, respectively, and the function $M(x)$ is defined by

$$M(x) = \begin{cases} 0, & x \leq 0 \\ x, & x > 0. \end{cases}$$

This function accounts for the fact that surface temperature is affected by vertical advection only in the presence of upwelling. The anomalous temperature gradient, T_z, is defined by

$$T_z = (T - T_e)/H_1, \quad (2)$$

where H_1 is the surface layer depth, and the T_e measures temperature anomalies entrained into the surface layer. T_e is parameterized in terms of T and $Td(b, \bar{h})$, a function expressing the subsurface temperature anomaly as a function of the mean and anomalous thermocline depths. The variable h is obtained from the model dynamics. Details are provided in Zebiak and Cane (1986b), where it is also shown that the full complexity of (1) is required to give realistic results.

c. *Coupling*

In the component models, the ocean affects the atmosphere exclusively through the SST field, and the atmosphere affects the ocean through the surface wind stress alone. Though it was reasonable to consider a steady-state atmosphere when prescribing seasonal mean SST forcing (as in Zebiak, 1986), this must be reconsidered when coupling to a time-dependent ocean in which the SST field can change on the timescale of a few days. For boundary forcing variations on this timescale, the atmospheric response due to moisture convergence feedback cannot reasonably be assumed to be in continuous equilibrium, since the transport time between regions of moisture input and corresponding latent heat release during ENSO can easily

aproach one month. This is an important consideration for the coupled model. If the atmospheric response is assumed to be in continuous equilibrium, then the *change* in the wind field between successive SST time steps will be overestimated. As a result, more rapid changes in SST will occur because of local wind effects. This induces yet larger changes in the atmosphere, and the combined interaction favors an artificially rapid development of anomalies, particularly at small scales where the atmospheric convergence feedback is most efficient.

To circumvent this, a procedure was adopted which effectively gives the steady-state response as before for timescales of one month or more, but restricts the feedback for shorter timescales. This is accomplished by altering the criterion governing the number of convergence feedback iterations that are performed (see Zebiak, 1984). Other methods could be used to produce a similar result. For example, a spatial smoother could be applied after each iteration, or time dependence could be added explicitly to the atmosphere model. The present method was chosen because it requires less computation.

3. Coupled Model Results

A numerical experiment with the coupled model was initiated with an imposed 2 m/s westerly wind anomaly of four months' duration beginning in December of the year designated -1. There was no external forcing thereafter: aside from the model physics, evolution of anomalies in SST, winds, etc., depends only on this initial condition and on the monthly mean climatological fields specified in the component ocean and atmosphere models. Furthermore, because of the damping in the model, the initial conditions are largely forgotten within a decade.

A 90-year time series of model SST anomaly averaged over the eastern equatorial Pacific is shown in Fig. 1. There are peaks of varying amplitude occurring at irregular intervals but typically 3 to 4 years apart. They tend to be phase-locked to the annual cycle, with major events reaching maximum amplitude at the end of the calendar year and decaying rapidly thereafter. All of these features are characteristic of observed El Niño events, as described earlier. The amplitude of model events is similar to observed ones, though the model did not produce anything as extraordinary as the 1982/83 event. The model is somewhat more regular than nature; the high frequency fluctuations present only in the real atmosphere and ocean may account for the broader natural spectrum.

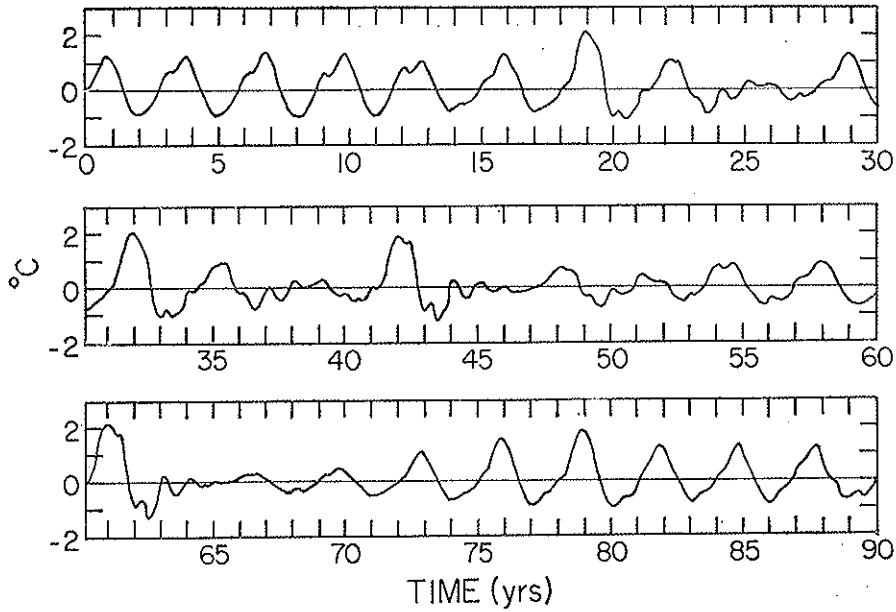

FIG. 1. SST anomalies averaged over the eastern equatorial Pacific region NINO3 (5N-5S, 90W-150W) for 90 years of coupled model integration. (From Cane & Zebiak, 1985).

Fig. 2 depicts the evolution of SST during the El Niño event of model year 31. In December of the preceding year there was no discernible anomaly; by March of year 31 there is a small but systematic warming in the eastern Pacific; by December the anomaly extends to the dateline, with a maximum at about 135°W. The model patterns and amplitudes are fairly realistic except near the South American coast, where the model's coarse resolution precludes an accurate simulation of coastal upwelling processes.

Fig. 3 shows the evolution of zonal wind along the equator. The prominent feature is the band of westerly anomalies in the central Pacific. It resembles the typical ENSO anomaly (Cane, 1983) but lacks the observed eastward progression in its early stages. What is missing is the initial anomaly west of the dateline. The ocean model exhibits too little variability in that region, so the model atmosphere has no SST anomaly to respond to. Thereafter, the spatial and temporal patterns are generally realistic until the year following the event, year 32. The model westerly anomalies persist several months longer than is typical of El Niño events.

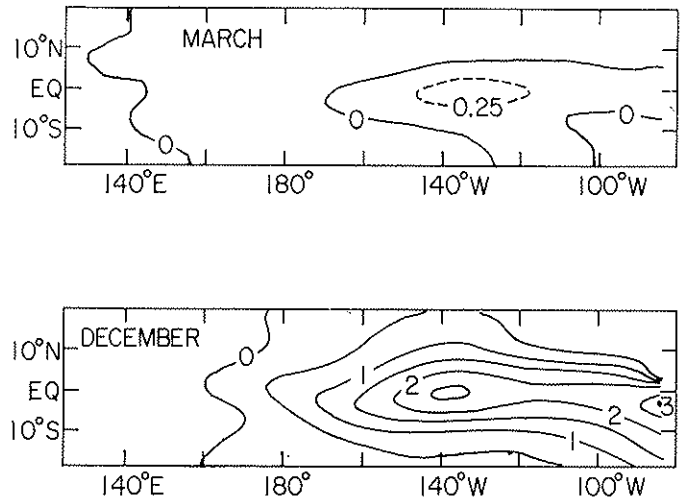

FIG. 2. Coupled model SST anomalies for March and December during the model El Niño event in year 31 (note that the contour interval for March is 0.25 C and that for December is 0.5). (From Cane & Zebiak, 1985).

The same is true for SST and other fields, and is characteristic of model events. A possible cause is the model's inability to produce the easterly anomalies in the far western Pacific which appear during the termination phase of observed events. As is the case even when observed SST anomalies are specified, the model winds are poorest in the Asian Monsoon region and in the far eastern Pacific. As with observed events, El Niño anomalies disappear quite rapidly, to be replaced by cold SST in the eastern Pacific and stronger than normal easterlies along the equator.

In summary, the coupled ocean-atmosphere model, which greatly simplifies the physics of the real ocean-atmosphere system and is certainly unrealistic in many details, nonetheless reproduces the most prominent spatial and temporal features of the evolution of El Niño events. Mechanisms internal to the model allow it to terminate events and initiate new ones in a never-ending ENSO cycle.

4. On the mechanism of the ENSO cycle

It seems fair to say that most of the work on El Niño in the past two decades has drawn inspiration from the hypothesis for El Niño

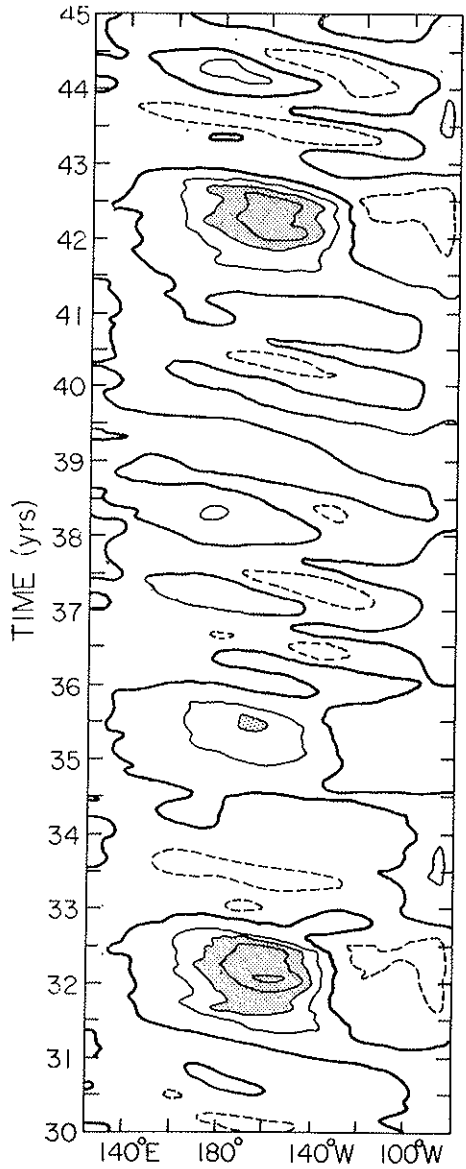

FIG. 3. Time-longitude sections for years 30-45 of the coupled model integration showing the forcing for the gravest mode oceanic Kelvin wave, a measure of zonal wind anomalies along the equator. Positive (westerly) anomalies are indicated with solid lines, and negative (easterly) anomalies are indicated with dashed lines. Large westerly anomalies (.15 dynes/cm^2) are stippled.

proposed by Bjerknes (1966, 1969, 1972). In these past decades our understanding of the tropical oceans and atmosphere has advanced substantially, (cf. the reviews by Cane, 1983, 1986; a summary is given in Cane, Zebiak and Dolan, henceforth CZD). The model described above was conceived as an embodiment of the Bjerknes hypothesis, but the advances subsequent to Bjerknes were essential in translating his ideas into appropriate physical equations.

To begin with, our ideas on the nature of the mechanism sustaining the ENSO cycle (Cane and Zebiak, 1985; CZD; Cane, 1986; Zebiak and Cane, 1986a) follow Bjerknes very closely (see especially his 1969 paper, from which we quote freely). Bjerknes points our that the eastern equatorial Pacific is unusually cold among low-latitude oceans. He attributes this to equatorial upwelling and horizontal advection of cold waters driven by the easterly trade winds prevailing along the equator. Since the western Pacific is very warm, there is a large SST gradient along the equator in the Pacific. As a result there is a direct thermal circulation in the atmosphere along the equator: the relatively cold, dry air above the cold waters of the eastern equatorial Pacific flows westward along the surface toward the warm west Pacific. "There, after having been heated and supplied with moisture from the warm waters, the equatorial air can take part in large-scale, moist-adiabatic ascent". Some of the ascending air joins the poleward flow at upper levels associated with the Hadley circulation, and some returns to the east to sink over the eastern Pacific. There is a zonal surface pressure gradient associated with this equatorial circulation cell, high in the east and low in the west.

Bjerknes named this the "Walker Circulation", because he felt that fluctuations in this circulation initiated pulses in Walker's Southern Oscillation. It can have such global consequences because "it operates a large tapping of potential energy by combining the large-scale rise of moist air and descent of colder dry air".

The Walker Circulation is the link between eastern Pacific SST anomalies and the Southern Oscillation: "A change toward a steeper pressure slope at the base of the Walker Circulation is associated with an increase in the equatorial easterly winds and hence also with an increase in the upwelling and a sharpening of the contrast of surface temperature between the eastern and western equatorial Pacific. This chain reaction shows that an intensifying Walker Circulation also provides for an increase of the east-west temperature contrast that is the cause of the Walker Circulation in the first place. Trends of increase in the Walker Circulation

and corresponding trends in the Southern Oscillation probably operate in that way. On the other hand, a case can also be made for a trend of decreasing speed of the Walker Circulation, as follows. A decrease of the equatorial easterlies weakens the equatorial upwelling, thereby the eastern equatorial Pacific becomes warmer and supplies heat also to the atmosphere above it. This lessens the east-west temperature contrast within the Walker Circulation and makes that circulation slow down".

"There is thus ample reason for a never-ending succession of alternating trends by air-sea interaction in the equatorial belt, but just how the turnabout between trends takes place is not yet quite clear".

The elements of Bjerknes' chain reactions all take place in the x-z equatorial plane. Our explanation for the turnabout turns on the refilling of the "heat reservoir" in the upper layers of the equatorial ocean. It requires consideration of the exchange of water between the equator and the higher latitudes of the tropical Pacific. The idea of coming out of the equatorial plane to account for the oscillation is not new (e.g., Julian and Chervin, 1978; McWilliams and Gent, 1978; McCreary, 1983), but our version differs from earlier ones in relying neither on the atmospheric Hadley circulation nor on freely propagating oceanic waves.

Numerical experiments with our coupled model show that the time between events changes when parameters which govern the strength of the coupling between atmosphere and ocean are varied (Zebiak and Cane, 1986a; Zebiak, 1984). The implication is that this time is an intrinsic period of the *coupled* system, not simply a function of oceanic wave speeds. However, the time is so long that the ocean clearly has a crucial role. The radiative relaxation time of the tropical atmosphere is on the order of one month, and the thermal damping time of the ocean surface layer is at most a few months (4 in the model). We therefore anticipate an active role for the subsurface ocean, with its substantially greater thermal inertia.

In the model the subsurface thermal structure reduces to a single variable, the anomaly in the heat content, or, equivalently, the thermocline depth anomaly. It is a simplification to treat the subsurface variations as having only one degree of freedom in the vertical, but observations show it to be a reasonable first approximation. The point which is essential for our argument is that wind-driven ocean dynamics are responsible for the subsurface changes. The subsurface ocean affects the atmosphere, and hence the feedback process, through the temperature of the water which is upwelled into the surface layer. Upwelling is an

important influence on SST at the South American coast and along the equator, especially in the eastern Pacific. As Bjerknes noted, this is the region where the SST variations are large. The model suggests that the warming of upwelled waters associated with the depression of the thermocline is the dominant cause of the warm anomalies there during the onset stage of an El Niño event, a result which is consistent with what data there is. It is certainly the fastest mechanism for converting a remote influence into an SST anomaly.

Our thesis is that an El Niño event cannot start until the heat content in the equatorial band is high enough to sustain the Bjerknes "chain reaction". The prevalence of 30-60 day oscillations in the western Pacific (e.g., Lau and Chan, 1985) ensures that episodes of westerly wind anomalies are frequent. They always generate oceanic Kelvin waves which tend to push down the thermocline in the east. However, if the thermocline is initially too shallow, then the resulting warming of SST will not alter the east-west temperature contrast enough to influence the atmosphere. Hence the initial wind anomaly is not reinforced and no event takes place.

Now consider the variations of the equatorial thermocline through an ENSO cycle. As the peak of an El Niño event is approached, water moves not only west to east, but also poleward, emptying the reservoir of warm water at the equator. As a result, the thermocline has already begun to shallow at the time when the wind and SST anomalies are reaching their peak. This phase relation is evident for the model by comparing Fig. 4 with Fig. 3; Fig. 5, which is based on tide gauge observations in the equatorial Pacific, shows that the heat content begins to fall before the surface anomaly maximum in December 1982-January 1983 (cf. the 76-77 event).

The decline in heat content is truly the beginning of the end of the El Niño event. The absence of the subsurface warm anomaly means that the SST anomaly can no longer be maintained. As the temperature drops in the eastern Pacific, the westerly wind anomaly loses its raison d'être. In the rapid collapse of the El Niño the ocean overshoots its mean state, leaving the eastern ocean very cold, the equatorial easterlies stronger than normal, and the heat content below its mean value. The transition back to an El Niño state cannot take place until enough warm water flows back from higher latitudes to refill the equatorial heat reservoir.

Additional support for the importance of the mean zonal heat content may be drawn from the numerical experiments illustrated in Fig. 6 and 7. For the experiments in Fig. 6 the model was simplified by eliminating

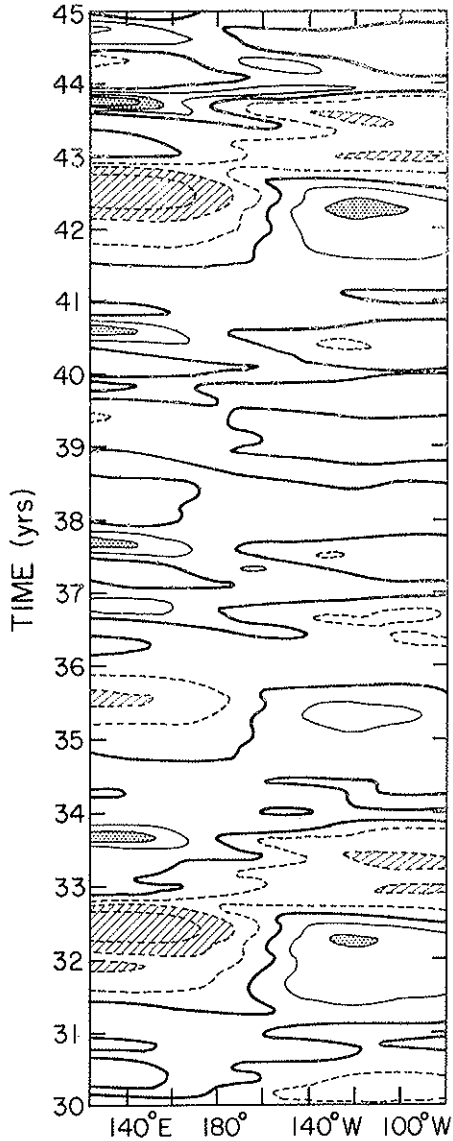

FIG. 4. Model thermocline depth anomaly at the equator, for years 30-45 of the 90-year integration. Positive anomalies are indicated with solid lines, and negative anomalies are indicated with dashed lines. The contour interval is 10 meters. Anomalies greater than +20 m are stippled; anomalies greater than −20 m are hatched.

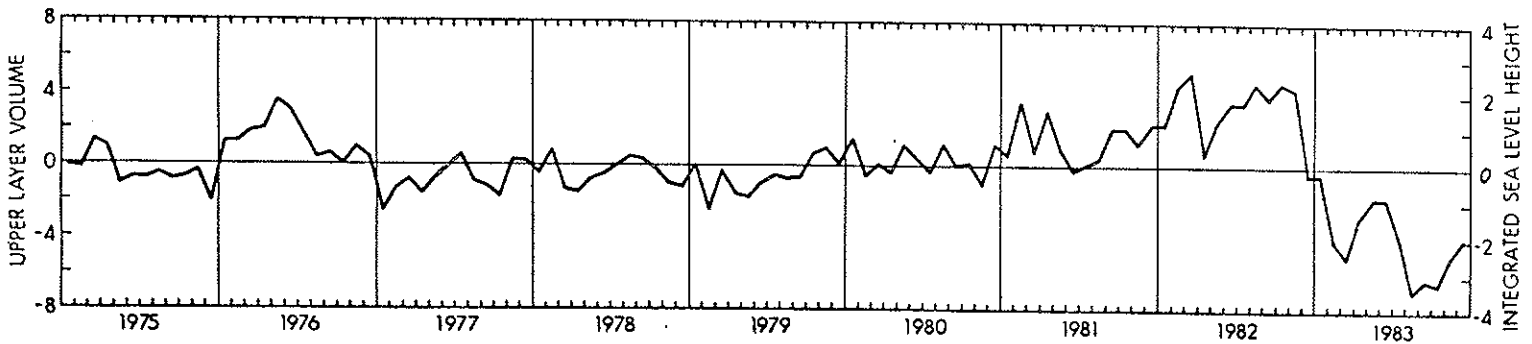

FIG. 5. Upper layer volume of the tropical Pacific (10^{14} m^3) from 1975 to 1983 relative to its mean value ($70*10^{14}$ m^3). The volume is estimated on the basis of tide gauge data for the region from 15N to 15S. (From Wyrtki, 1985).

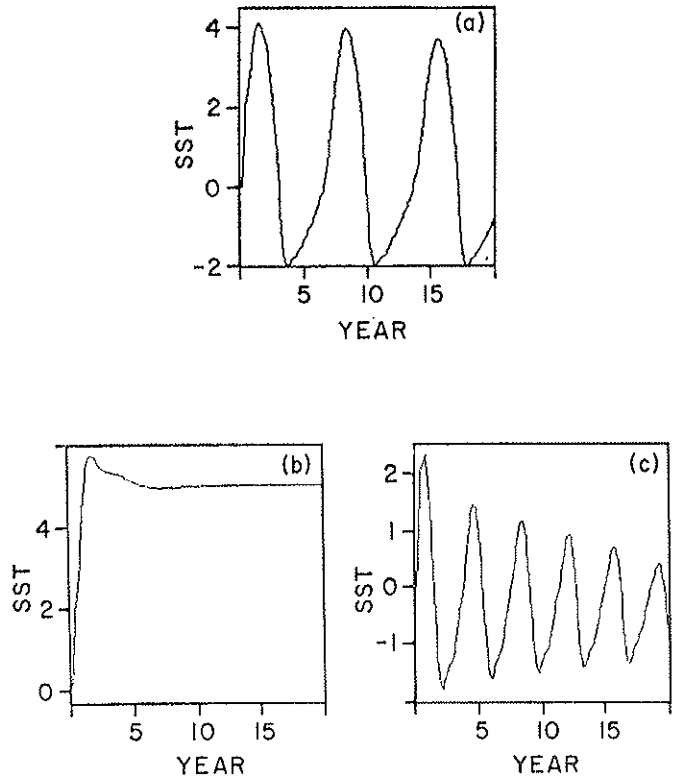

FIG. 6. NINO3 SST from model runs with the surface layer removed and perpetual July conditions. (a) Standard case. (b) Equatorial heat content held constant. (c) Changes in equatorial heat content accelerated by a factor of 2. See text.

the surface layer and holding the mean conditions fixed at their July values. The model now oscillates regularly. In these experiments the relation between the deep temperature T_d and the thermocline depth h was altered by, for example (Fig. 6c), replacing $T_d(h)$ by $T_d(h \pm 2h^*)$, where h^* is the mean thermocline depth averaged along the equator. This is tantamount to tripling the rate at which the equatorial heat reservoir is refilled. In general such changes (cf. Fig. 6) have a roughly linear effect on the period, with the experiment in which the heat content is held fixed showing no oscillation at all.

Fig. 7 shows experiments with the full model. The oscillations are now irregular. In the standard case (Fig. 7a) the preferred period is 3

years; when the rate at which the equatorial heat content refills is halved (Fig. 7b); $T_d(h)$ replaced by $T_d(h-1/2\,h^*)$ the preferred period roughly doubles to 5 or 6 years; when the rate is tripled (Fig. 7c) it decreases to 2 years. In these cases with the full annual cycle the periods are quantized in integral numbers of years, but the changes have the same sense as in Fig. 6.

The outcome of a different set of experiments exploring the role of heat content changes is summarized in Fig. 8. A coupled run, in which an El Niño was about to occur (heavy curve), was restarted 4 times with $T_d(h)$ replaced by $T_d(h-d)$ with $d=1$m, 2m, 3m and 4m (light curves, top to bottom). The effect is equivalent to reducing the heat content

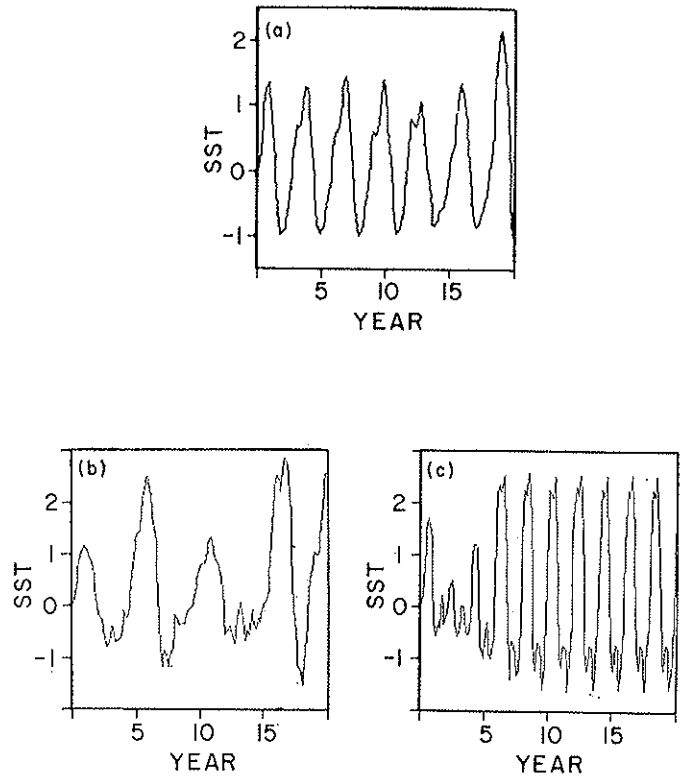

FIG. 7. Similar to Fig. 6, but with the complete model. (a) Standard case. (b) Changes in equatorial heat slowed by a factor of 2. (c) Changes in equatorial heat content increased by a factor of 2. (See text).

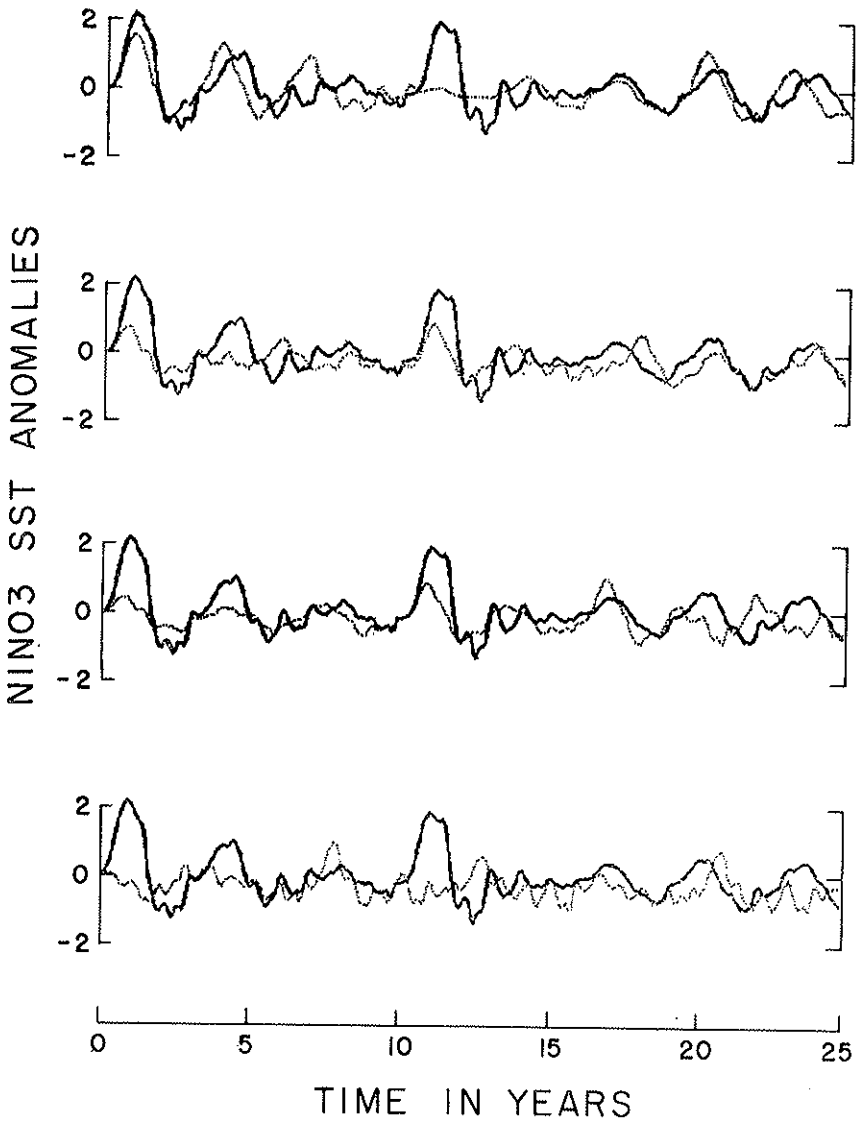

FIG. 8. NIÑO3 SST when the equatorial heat content altered as described in one text. The dark curve is the standard case. For the light curves, the thermocline was artificially lowered by 1, 2, 3, and 4 m from top to bottom.

uniformly by d meters of warm water. The El Niño occurs more or less as before in the $d=1$m case, but lowering the thermocline by another meter makes the difference between an El Niño and a mild warming. Lowering it still further eliminates the warming altogether.

That the wind and thermocline anomalies are not precisely in phase appears to be necessary for the oscillation to occur. If they were in phase, the positive feedback would simply increase the amplitude of the anomaly forever. The linear model of Philander, Yamagata and Pacanowski (1984) exhibits such growing, non-oscillatory behavior. A more realistic model would warm until the coupled system's equilibration mechanisms took over and locked the system in its maximum warm state.

If one considers how the wind anomaly is generated, it is plausible that the wind would lag the thermocline. A change in thermocline depth changes the temperature rapidly at the equator, but it takes some time for advection to spread the anomaly north and south to a scale which will fully influence the atmosphere.

It is a consequence of linear equatorial ocean dynamics that the changes in the equatorial thermocline will lead those in the wind. The slope along the equator is closely in phase with the wind; Cane and Sarachik, 1981, have shown this to be characteristic of the equatorial ocean's response to low frequency periodic wind forcing and thus to all low frequency forcing. (Here "low frequency" means time scales comparable to or greater than the time for a Kelvin wave to cross the ocean; this is about 70 days for the Pacific). The reason for the lead may be better understood by considering the response of the ocean to a wind (a westerly wind, for example) suddenly switched on over a resting ocean at $t=0$ (Cane and Sarachik, 1977).

Initially, the westerly winds induce an equatorward Ekman flux, resulting in an increase in the equatorial heat content. This begins to change as the influence of the boundaries makes itself felt. Kelvin waves leaving the western side and Rossby waves from the eastern side set up a pressure gradient across the ocean, and the accompanying poleward geostrophic flow counteracts the equatorward mass flux. The thermocline rises in the west and sinks in the east. The "hole" at the west is dug by Kelvin waves and so is equatorially confined, while at the east the Rossby waves spread the extra mass over a wide latitude band. The net result is to decrease the heat content near the equator and export mass to higher latitudes.

Thus we attribute the *oscillation* in ENSO to the special east-west

asymmetry of equatorial ocean dynamics. This is in disagreement with the contention that the oscillation is a consequence of the seasonal cycle (Philander, 1985), but we do agree that the seasonal variations modulate the ENSO cycle. An ENSO-like oscillation could take place even if the seasonal variations were suppressed, but it would have a different character. As the wind, convergence, SST and thermocline fields change during the course of the year, the strength of the coupling between the atmosphere and ocean is altered. Though the specific cause is different and more varied, the end result works either for or against the interannual changes in equatorial heat content to reinforce or weaken the feedback. From this framework one would expect ENSO to be locked to the seasonal cycle, but not rigidly: the unusual event could proceed even without optimal help from the seasons.

5. Implications for Forecasting; Forecasting Procedure

We have implied that a necessary condition for the occurrence of El Niño is that the equatorial heat content exceed a critical value. The time it takes to restore the equatorial heat content depends on a number of factors, the most important of which are dissipation times, the time for equatorial waves to cross the Pacific, and the strength of the coupling between atmosphere and ocean (Zebiak and Cane, 1986a). The phenomenological "coupling strength" is comprised of a number of factors, such as the sharpness of the thermocline, advective speeds, oceanic temperature gradients, and the sensitivity of the surface wind to SST contrasts. All of these vary seasonally and spatially, as well as changing with the state of the ocean-atmosphere system. In addition, the flow of warm water back to the equator may be influenced by higher frequency events, such as the 30 to 60 day waves in the western Pacific.

The irregularity of the interval between El Niño events reflects the variability of this refill time. This variability is what makes the prediction of El Niño nontrivial. It is an open question whether it is more a result of high frequency noise (Lau, 1985) or of the nonlinearities associated with processes intrinsic to the ENSO cycle (Vallis, 1986). While either implies the ENSO cycle cannot be predicted arbitrarily far ahead, neither precludes prediction at useful lead times.

Even in its most random variant our scenario has far different implications for prediction from those which view ENSO as quintessential-

ly random, the chance consequence of higher frequency random events (Philander, 1986; Ramage, 1986). The latter offer no hope of forecasting ENSO until its high frequency causes can be predicted, an unlikely prospect. In the former, El Niño is the outcome of a deterministic sequence, albeit one which can be distorted by chance occurrences. The prognosis for prediction is far more optimistic.

In our account of ENSO all of the essential interactions take place in the tropical Pacific region. Consequently, while information from other parts of the globe might improve the results, it is possible that predictions based solely on data from this region could be successful. There are practical advantages in limiting the region which must be covered, though it is unfortunate that the critical region is one which is so poorly observed. It is also unfortunate that data from the most important variable, the field of thermocline depth anomalies, is so sparse. For the other two most important variables, SST is known to no better than 0.5 C (Reynolds, private communication), and the surface winds to no better than 2 m/s (Halpern and Harrison, 1982). For both variables, the errors are generally higher than the quoted numbers. *In situ* wind measurements are few and are concentrated in a handful of shipping lanes. Our ENSO scenario does have the fortunate consequence that some even more inaccessible quantities, such as surface heat flux, are of secondary importance. Since available observations are insufficient to specify a complete field of thermocline depth anomalies, the following procedure was adopted. A field of monthly mean surface wind stress anomalies derived from ship observations over the tropical Pacific was obtained (Goldenberg and O'Brien, 1981). A 1-2-1 filter in time, longitude, and latitude was then applied to the analyzed winds. The anomalies used are the deviations from the average of the same calendar month over the previous 4 years; e.g., the May 1985 anomaly is the deviation from the mean of May 1982, 1983, 1984, 1985.

The period up to the forecast initial time was simulated by forcing the ocean component of the coupled model with wind stress anomaly fields specified for each month starting with January 1964. The computed SST anomalies were then used to run the atmospheric component of the model. The *calculated* anomalies in thermocline depth, currents, SST, and surface winds were then used as initial conditions for a forecast with the coupled model. Note that the *only* data used (other than climatological data) are surface wind observations. The initial SST and wind fields are calculated to be compatible with the initial thermocline displacements within the model framework; they need not agree with observed SST or

wind fields. Therefore, the procedure does not take full advantage of the available observational information. It also turned out that its expected virtue, to make the initial conditions compatible with the model, was not realized. It does have the didactic virtue of allowing the model's forecasting performance to be attributed to the wind data alone.

The coupled model runs evolve from the initial conditions as in a true forecast model: no new data is introduced after the initial time.

6. Forecast Results

Fig. 9 compares a map of observed SST anomalies during the peak period, Jan. 1983, with that from the forecast initiated in Jan. 1981. The result is typical of the more successful forecasts. As in earlier work (Zebiak and Cane, 1986a), including cases with the same ocean model driven by observed winds (Zebiak and Cane, 1986b), the gross character of the eastern Pacific El Niño SST anomaly is reproduced though its meridional and westward extent is understated.

Forecasts were initiated in the periods preceding each of the El Niño events which have occurred since 1970; i.e., 1972, 1976, and 1982. An additional set was made for the "non-event" of 1979. None were attempted

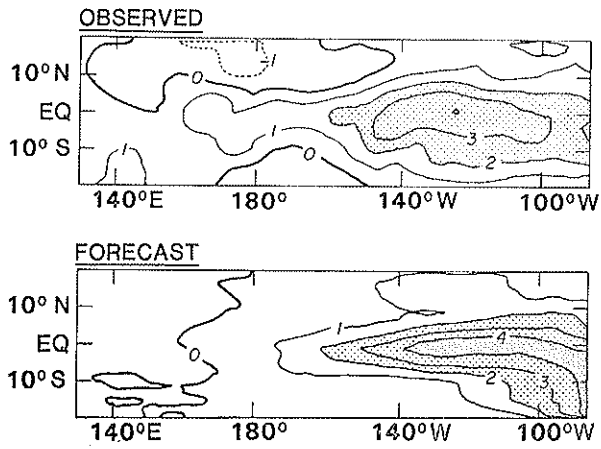

Fig. 9. SST anomalies (C) in January 1983. Top: observed, based on the analysis of the Climate Analysis Center (CAC) of NOAA. Bottom: predicted by the model forecast initiated in January 1981, 2 years earlier. (From CZD).

in the years before 1970 because the wind analyses available for these earlier years are of distinctly lower quality. In each period there are 6 forecasts spaced 3 months apart with the sequence ending in January of the nominal year. For example, for 1972 forecasts were initiated from October 1970; January, April, July, October, 1971; and January 1972.

The forecast results will be summarized in terms of the SST anomaly averaged over the eastern equatorial Pacific area NIÑO3 (Fig. 10). The NIÑO3 index was devised by the Climate Analysis Center of NOAA (National Oceanic and Atmospheric Administration) because a warming in this region strongly influences the global atmosphere (Rasmusson and Wallace, 1983). It is probably the best single indicator of an ENSO episode likely to impact global climate.

Fig. 10 shows that the model generally succeeds in predicting warmings in those years when they were observed to occur and in predicting their absence when they did not occur. As with the observed events, the peaks in the NIÑO3 index are always forecast to take place at the end of the calendar year. The individual forecasts tend to give too strong an event, especially for the 1976 El Niño. The rise in temperature during 1976 is well predicted, but 5 of the 6 forecasts begin the year at least 2°C too warm. They entirely missed the 1975 cooling trend, which culminated in the coldest NIÑO3 SST in the entire data record. This failure is present even when the model was forced by observed winds, as in the run creating initial conditions (viz., the initial SST for the January 1976 forecast in Fig. 10). On the other hand, the model never predicts an El Niño for 1975, though at the time observers saw enough precursors of an event early in the year to call an El Niño Watch.

We wish to establish that the model's ability to predict an El Niño event is significantly better than chance. Because the distribution of states in the tropical Pacific is strongly bimodal (e.g., Cane, 1983), it is straightforward to distinguish El Niño events from non-events. In terms of NIÑO3 SST we will say there is an El Niño if there is a rise of at least 2°C within 12 months leading to an anomaly of at least +1.0°C for at least 3 months. These criteria are derived from the observed events but are somewhat arbitrary; the set of forecasts would have similar scores for any other criteria able to separate observed events from non-events.

According to these criteria, 19 of the 24 forecasts are correct. (The forecasts would be judged to be less successful if more detailed agreement with observation were demanded). January 1971, April 1971, October 1975 and April 1981 fail to predict the upcoming event, while April 1978

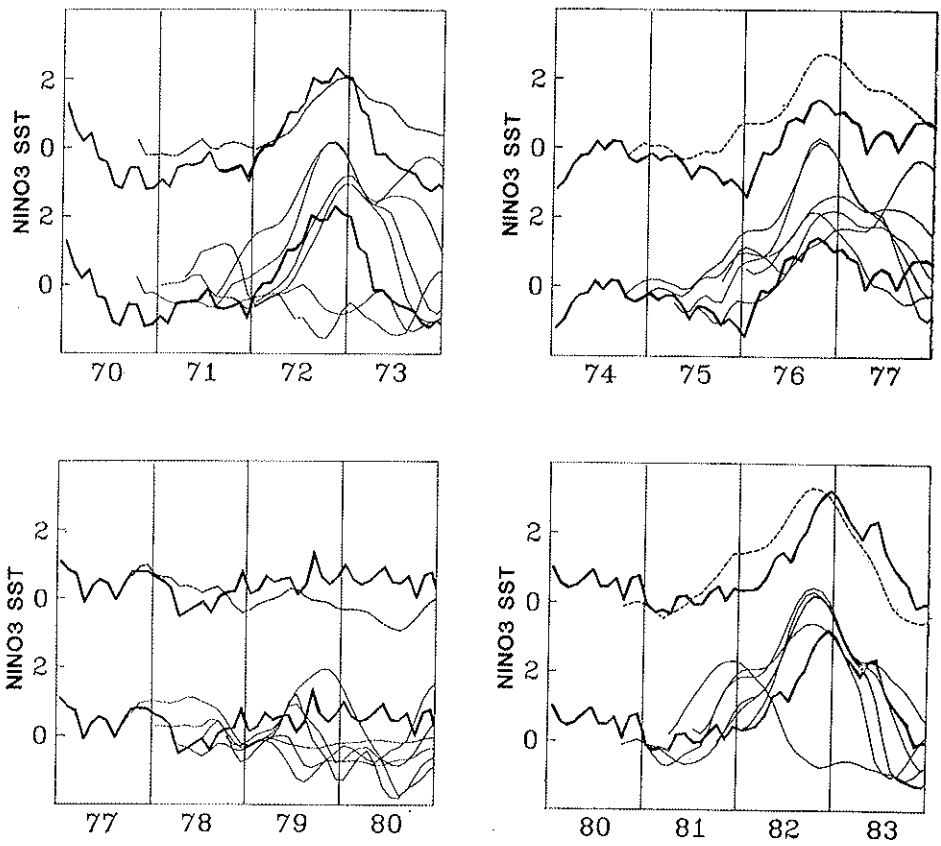

FIG. 10. Sea surface temperature anomalies (C) averaged over the eastern equatorial Pacific NIÑO3 region (90W to 150W, 5S to 5N) for four periods centered on 1972, 1976, 1979, 1982. The heavy curves are the observed values as reported by CAC/NOAA. The light curves in each panel are from 6 forecasts initiated at 3-month intervals from the October two years ahead to the January of the nominal year. The dashed curve is the average of the 6 forecasts (the consensus forecast). (From CZD).

falsely calls for an El Niño in 1979. Of the 5 failures, 3 are from April starts. In the spring the Intertropical Convergence Zone is closest to the equator and the SST in the east is warmest. As a result, the *local* coupling between model atmosphere and ocean is strong and noise in the initial state often amplifies, leading to poor results. Nature is also least predictable in the spring: it is the time when the Southern Oscillation Index shows the smallest correlation with its future value (Wright, 1985).

Meteorological forecasts are typically evaluated relative to climatology or persistence, but either inflates the skill for infrequent events like El Niño. Table 1 offers another standard. It may seem artificially favorable to compare to a guessing strategy which makes no apparent use of the known 3 to 4 year quasi-periodicity of the ENSO cycle. However, we have forecast only for periods 3 or 4 years apart when events are seemingly due. Hence the occurrence or non-occurrence of an event in any of the years in our sample is roughly equally likely, so that flipping a coin is a reasonable guessing strategy.

In order to establish a rigorous confidence level, the number of *independent* forecasts must be known. A precise determination of independence would require many more model runs, but estimates adequate for present purposes can be made readily. Treating forecasts 3 months apart as independent derives from the observation that qualitative behavior (such as incorrect forecasts or maintaining high SST in the year after an event) rarely persists longer. Doing so probably overstates the confidence level. At the other extreme, a very conservative estimate is obtained by assuming the forecasts within each set are highly correlated. Then there are only 4 independent forecasts, each given by the majority of the 6 within

TABLE 1 - Summary of Forecast Results for Past Years. Results correspond to the 24 forecasts of Fig. 9. For January "one-year forecasts" refers to the same calendar year; for all other start months, to the next calendar year. The last column shows the probability of correctly predicting at least as many cases as the model did by flipping a coin.

	Start Month	Number Right	Number of Cases	Chance by Coin Flips
ONE-YEAR	OCT	7	8	.04
FORECASTS	JAN	8	8	.004
	APR	1	4	.94
	JUL	4	4	.06
	TOTAL	20	24	.0008
TWO-YEAR	OCT	3	4	.31
FORECASTS	JAN	3	4	.31
	TOTAL	6	8	.14

each set. Since all 4 are correct there is 1 chance in 16 of doing as well by coin flipping. Our most plausible estimate is based on the fact that while indices of the Southern Oscillation can be highly correlated for many months, months preceding April of a given year correlate poorly with months following it (Wright, 1985). This motivates treating the (majority of) the first October, January and April of a set as one forecast, independent of a second forecast derived from the subsequent July, October, and January. There are now 8 independent forecasts, the last 7 of which are correct. The probability of guessing so successfully is about 0.04.

Another measure of model performance is obtained by considering events and non-events separately. Altogether, 14 of 18 occurrences of El Niño and 5 of 6 non-occurrences are forecast correctly. The joint probability of getting at least that many of each type right by an optimal random strategy is 0.004. (The optimal random strategy assumes *a priori* knowledge of the number of events and non-events in the sample, as well as the score to beat). The corresponding joint probabilities for the "conservative" and "most plausible" cases are 0.06 and 0.04, respectively.

Forecasts started from the same calendar month in different years differ only in their initial conditions. Their success attests to the thesis that the future evolution of ENSO is implicit in the initial conditions. Consider, for example, the 8 one-year forecasts initiated in January. Even if one knew in advance that there were 3 El Niño events and 5 non-events, the change of matching the model performance by guessing all 8 correctly is only 1 in 56.

Rather than considering forecasts at 3-month intervals, we now examine a more useful forecasting strategy. A forecast is initiated in each of the 6 successive months from August to January to obtain the prediction of the ensemble 1 and 2 years ahead. Table 2 summarizes the results of doing this from every year for which we have data (1970-1984) with the exception of the 3 El Niño years in the sample. A few examples are shown in Fig. 11. There are 12 sets of one-year forecasts. In 9 of these, all 6 months agree, so the interpretation of the model prediction is unambiguous. In all 9 the prediction is correct. By the rather stringent standard which scores the other 3 as wrong, the probability of doing as well or better by chance is 0.07.

It would be more accurate to judge that the 3 provide unclear guidance. In two of the cases, where there was no event in the following year, half of the months forecast correctly and the other half did not. The remaining case is the set from August 1975 through January 1976.

TABLE 2 - Summary of the sets of forecasts initiated in the 6 successive months from August through January of each year from 1970 to 1984 (excluding El Niño years). Years of El Niño events are starred. For example, in the first line of the table, the forecasts are from August 1970 through January 1971; the one-year forecasts are for 1971 and the two-year forecasts are for 1972.

Forecast from	Number Correct (out of 6) one-year	two-year	
1970	6	5*	
1971	6*	1	
1973	6	3	
1974	6	6*	
1975	2*	5	
1977	6	6	
1978	6	6	
1979	6	2	
1980	6	6*	*
1981	6*	6	
1983	3	5	
1984	3	?	

As can be seen from Fig. 11, the model actually does a good job of predicting the odd event to come. However, 4 times out of 6 our temperature rise criterion is not met because the model starts out too warm at the beginning of 1976. One might quibble with our scoring system, but it undoubtedly would have been difficult to interpret such a forecast at the time.

As might be expected, the two-year forecasts are not as successful: in 5 cases all 6 individual forecasts are correct; in 3 cases 5 of 6 are correct; in the remaining cases 1, 2, or 3 are correct. Counting 8 of the 11 as successes gives an 89% confidence level. The most consistent failure is the 1971 set, where all predicted the 1972 El Niño, but 5 of the 6 had the warming persist through 1973. Four of the 1979 forecasts predicted an event in 1981, a year early. The 1983 set is the most

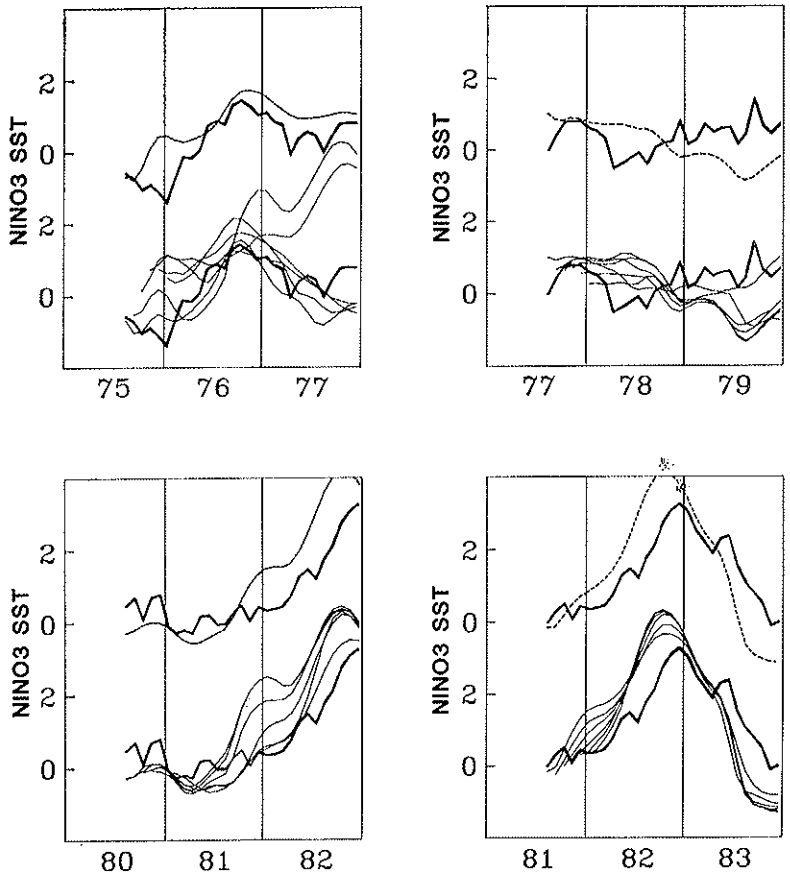

FIG. 11. Sea surface temperature anomalies (C) for selected periods averaged over the NIÑO3 region. The light curves in each panel are from forecasts initiated in the 6 successive months from August through the following January. The dashed curve is the average of the 6 (the consensus forecast) and the heavy curves are the observed values. (From CZD).

ambiguous; note that for the years since the outsized 1982 event, both the one-year and two-year forecasts have been inconsistent.

We offer one final example: the prediction for 1986. At the time of writing, September, 1986, this forecast cannot yet be evaluated. Data for August (Kousky, private communication) indicate the trades have weakened and the eastern equatorial Pacific is anomalously warm, but the amplitudes are small. Perhaps an El Niño will follow, but perhaps it will never develop beyond a mild warming. It is surprising to be so

late in the year without a definite reading as to whether or not an El Niño will occur.

Fig. 12 shows the forecasts initiated in August 1985 through January 1986. All 6 predict an El Niño. The amplitude of the consensus forecast suggests it will be a moderate event, not as strong as the events of 1982, 1972 or 1957. However, the only other moderate event in our study was the peculiar 1976 El Niño; experience with the moderate event of 1965 and the even weaker 1969 one might help in interpreting the present case. For the 3 events in our sample (1972, 1976, and 1982), the consensus overstated the maximum NIÑO3 SST anomaly amplitude by 30% (more precisely, 28%, 36% and 28%, respectively). Rescaling the 1986 forecast accordingly indicates an amplitude of 1.9°C, well below the 3.2°C of 1982 or the 2.5°C of 1972, but above the 1.4°C of 1976.

How much confidence should be placed in the prediction of a 1986 El Niño? Though all of the 1985 forecasts predict an event for 1986, none of the two-year forecasts from 1984 predict it. This is unprecedented among the limited set of cases we have studied. Also, both the 1983 and 1984 one-year forecasts lack the consistency which is typical of earlier years. On the other hand, and in our view more importantly, no previous case where all 6 one-year forecasts agreed was incorrect. More-

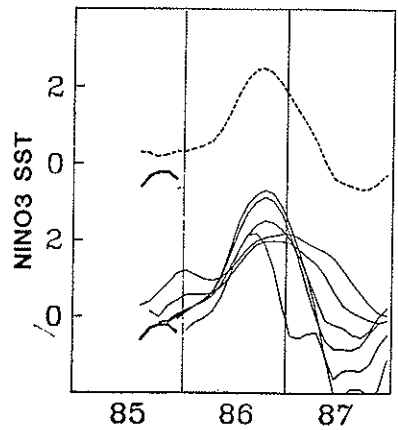

FIG. 12. Forecast for 1986: sea surface temperature anomalies (C) in the NIÑO3 region. The light curves are from the forecasts initiated in the 6 successive months from August 1985 through January 1986. The dashed curve is the average of the 6 and the heavy curves are the observed values. (From CZD).

over, except for June 1986, all forecasts from March 1985 to July 1986 give indications of a warm event at the end of 1986.

7. Implications of the Forecasts for the Nature of ENSO

The forecasts may be regarded as a set of numerical experiments bearing on the nature of ENSO. The model appears to be able to simulate the major features of observed El Niño events, and to largely avoid predicting events when it is inappropriate. Though hardly irrefutable evidence, the model's ability to generate observed El Niño events from apparently innocuous, "normal" initial conditions adds some empirical support for the contention that the cycles of ocean-atmosphere variations occurring in the model work in the same way as nature's ENSO cycle.

The degree of forecasting skill obtained despite the crudeness of the model is telling. It suggests that the mechanism responsible for the generation of El Niño events and, by extension, the entire ENSO cycle, is large scale, robust and simple: if it were complex, delicate or dependent on small scale details this model could not succeed. Neither the ocean nor the atmosphere is the prime mover in the ENSO cycle. It is essential for ENSO that the two-way coupling between ocean and atmosphere is active in both the El Niño and the non-El Niño phase of the cycle. The only region where the model does a creditable job of simulating the requisite interactions is near the equator. Its success with ENSO is a confirmation of Bjerknes' emphasis on the interactions which take place in the equatorial plane.

Our addition to the basic Bjerknes hypothesis required the model to include the dynamics of the upper layers of the tropical ocean. The tropical Pacific region remains the locus for all of the physics responsible for the existence of the ENSO cycle. This is not to deny that events in the Indian Ocean sector, in midlatitudes, etc., may influence the evolution of an El Niño event. Moreover, the evidence is compelling that the impact of ENSO is global. However, we do mean to assert that the essence of the oscillation takes place in the tropical Pacific.

Though able to generate the ENSO cycle and to forecast particular El Niño events, the model is unable to generate the 30-60 day waves. The clear implication is that these waves have no more than a minor role in ENSO. Observations seem to carry the same implication: these waves are virtually ubiquitous, and there appears to be nothing distinctive about their behavior prior to an El Niño. We believe they are properly

viewed as a rather powerful source of noise on the larger scale, lower frequency ENSO cycle. As such they have important consequences for prediction; this is discussed further below.

We have characterized El Niño as a phase of a recurring cycle, ENSO. The deterministic evolution of the cycle returns the ocean-atmosphere system to a state where small perturbations can grow into an El Niño. Our view is that a necessary condition for such an instability is that the equatorial heat content exceed a threshold value. Once El Niño is ready to happen, it can be initiated by any appropriate perturbation. The 30-60 day waves are the most likely candidate, but were they absent, something else would play this role. This description is in the spirit of the classical paradigm for hydrodynamic instability: it is assumed that a suitable perturbation will be available to grow; the crucial question is whether the necessary and sufficient conditions for instability are met.

In this scenario, the interval between events is the time for the equatorial heat reservoir to refill. In our view, the refilling does not result from the action of free equatorial waves alone. As with the events themselves, it is an interactive process, and the time it takes depends on the strength of the coupling between atmosphere and ocean. *A priori*, it seemed conceivable to us that this refill time might be determined by random events, so a scenario assigning them a dominant role could not be ruled out. The demonstrated ability of our model to forecast at long lead times suggests that the process is largely deterministic, though, as discussed below, occurrences external to the basic ENSO cycle may well exert an important influence.

A concise statement is that ENSO is a relaxation oscillation of the coupled system: the slow buildup to the necessary condition for instability during the cold phase presages the rapid warming during the event itself; an even more rapid return to cold conditions follows. In the model the mean climatic state is unstable, so a relaxation to mean conditions will lead into the next El Niño event. In both the model and nature the interval between events is irregular; as noted above, while this could be the result of random fluctuations, it could also be a consequence of the deterministic physics intrinsic to ENSO.

If ENSO is a chaotic deterministic system, then the predictability is inherently limited. There is a bifurcation surface dividing states of the ocean-atmosphere system which will soon culminate in an El Niño from those which will remain near normal. On one side, far from this surface an El Niño is sure to occur; far away on the other side its absence is

equally certain. Near the surface, where a small change in present position can result in a large difference in the future path of the system, the outcome is uncertain.

It is plausible that most of the time the system is far from this surface and its future course can be predicted for some time to come. Our forecast results suggest that this is indeed the case and that the prediction time is typically several years or more.

Accurate prediction at those times when the system is close to a bifurcation point demands that its state be known with great precision. In practice the data may be too poor to allow this, and, since the prediction model is an imperfect representation of the physical system, it may mislocate the bifurcation surface in the phase space. Fig. 13 suggests that the initial states shown in Figs. 14 and 15 are examples of states near a bifurcation point. By any obvious measure, the model initial conditions

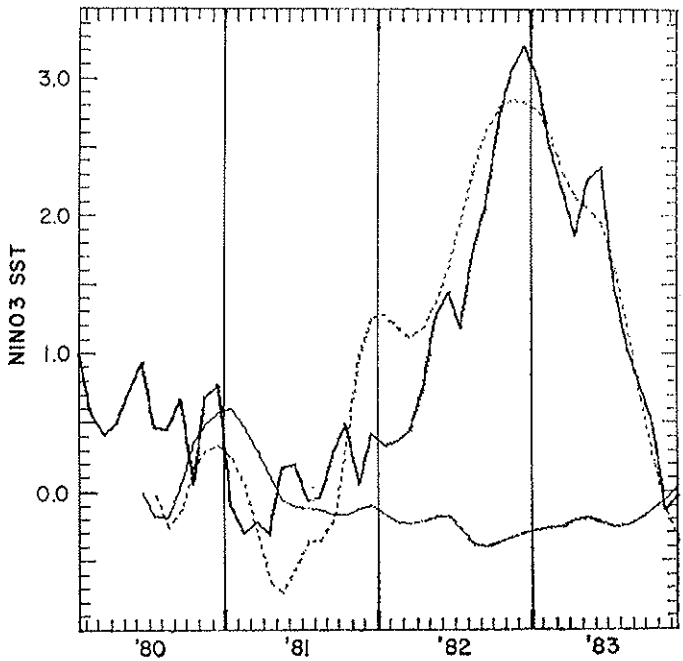

FIG. 13. Sea surface temperature anomalies averaged over the NIÑO3 region. The light curve is the forecast initiated in July 1980; the dashed curve is the forecast from the next month, August, 1980. The heavy curve shows the observed values.

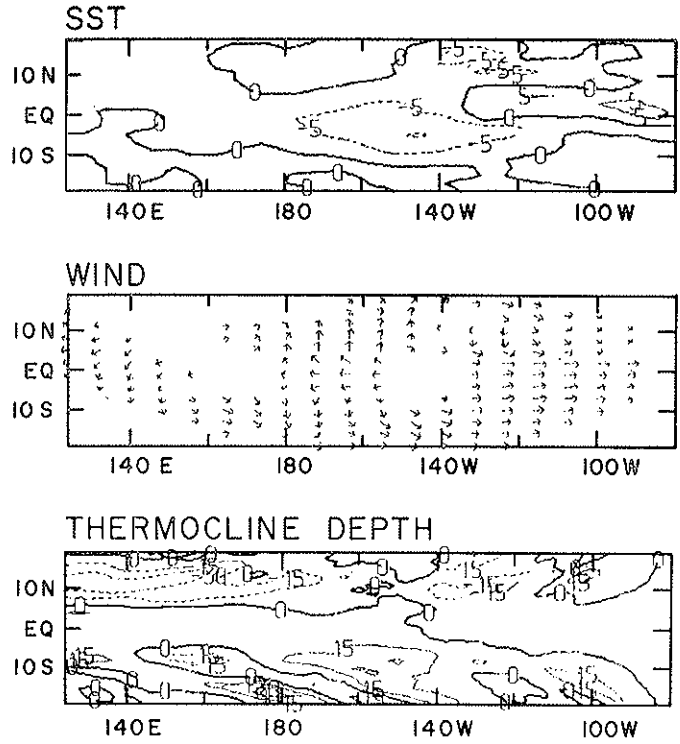

FIG. 14. Initial conditions for the forecast from July, 1980. Top: SST anomalies (units of .1 C). Middle: Surface wind anomalies (the maximum is about 1 m/s). Bottom: Thermocline depth anomalies; contour interval is 15 m.

for July 1980 are quite close to those a month later, yet the model evolution from the August start leads to the 1982 El Niño, while that from July fails to produce an event.

It may be that, at those times when the system is balanced on a knife edge, events extraneous to the ENSO cycle — noise — make the difference for the future state of the coupled system. Perhaps an additional westerly burst along the equator associated with a 30-60 day wave is all that is needed to touch off an El Niño when otherwise none would have occurred. However, the success of our forecasts suggests that if there are such times they are rare.

We have suggested a hypothesis on the nature of the ENSO cycle which draws support from numerical experiments and is not in conflict

with observations. Further tests are needed to establish its validity. It appears to be internally consistent, physically reasonable, and, on a general level, complete. While the overall picture may be clear enough, many of the specifics are hazy. Such important questions as what sets the interval between events and what is responsible for the irregularity of the cycle remain topics of ongoing research. The nature of the parameter dependences are not yet known; the nature of the "coupling strength" has not been detailed. The behavior of far simpler chaotic dynamical systems can change in complicated ways as parameters are varied, so it is not likely to prove a simple task to delineate the parameter dependencies important for ENSO. In summary, while we believe that the work reported here is a significant step toward unraveling the mysteries of the ENSO phenomenon, a great deal remains to be done before ENSO will be truly understood.

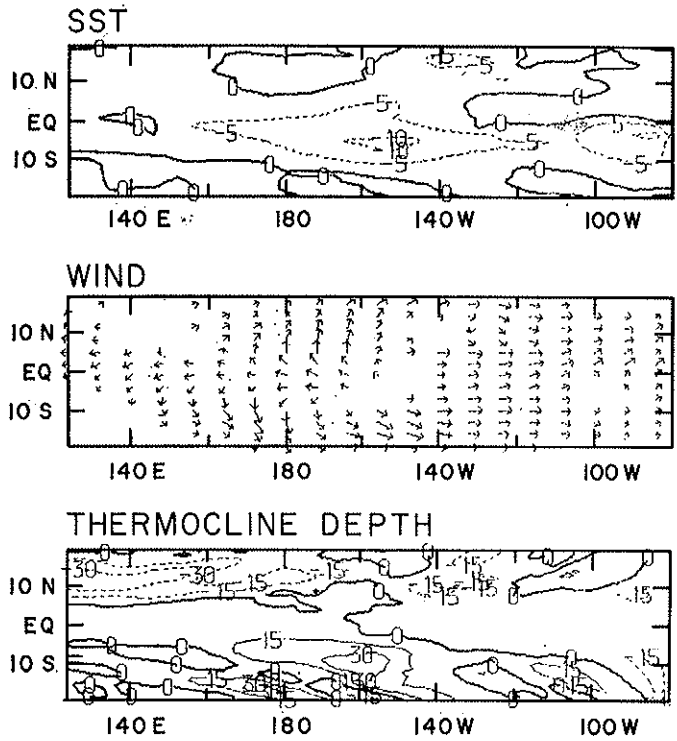

FIG. 15. Initial conditions for the forecast from August, 1980. As in Fig. 14 for July.

ACKNOWLEDGEMENTS

Our thanks to Jim O'Brien and David Legler of Florida State University for providing the surface wind analysis, and to Sean Dolan, Karen Streech and Lori Suckling for their help in preparing the manuscript and figures. This work was supported by grants NA-84-AA-D-0031 from the U.S. TOGA Office of NOAA, NA-84-RAD-05082 from EPOCS/ NOAA, and NAGW-916 from NASA. Lamont-Doherty Geological Observatory Contribution.

APPENDIX

The governing equations for the atmosphere (at iteration n) are (see Zebiak, 1986):

$$+\varepsilon u^n{}_a - \beta_o\, y v^n{}_a = -(p^n/\rho_o)_x \tag{A1}$$

$$\varepsilon v^n{}_a + \beta_o\, y u^n{}_a = -(p^n/\rho_o)_y \tag{A2}$$

$$\varepsilon\,(p^n/\rho_o) + c^2{}_a\,[(u^n{}_a)_x + (v^n{}_a)_y] = -\dot{Q}_s - \dot{Q}_l{}^{n-1} \tag{A3}$$

$$\dot{Q}_s = (\alpha' T)\,\exp\,[(\bar{T} - 30^\circ\mathrm{C})/16.7^\circ\mathrm{C}] \tag{A3a}$$

$$\dot{Q}^n{}_l = \beta\,[\mathrm{M}\,(\bar{c} + c^n) - \mathrm{M}\,(\bar{c})], \tag{A3b}$$

where
$$\mathrm{M}\,(x) = \begin{cases} 0, & x \leq 0 \\ x, & x > 0. \end{cases} \tag{A3c}$$

In (A3a), $\bar{T}\,(x, y, t)$ is the prescribed monthly mean SST, and T is the anomalous SST. In (A3b), $\bar{c}\,(x, y, t)$ is the prescribed monthly mean surface wind convergence, and c^n is the anomalous convergence at iteration n, defined by

$$c^n \equiv -(u^n{}_a)_x - (v^n{}_a)_y. \tag{A3d}$$

The governing equations for the ocean (see Zebiak and Cane, 1986a) are:

$$u_t - \beta_o\, y v = -g'\, h_x + \tau^{(x)}/\rho\,\mathrm{H} - r u \tag{A4}$$

$$\beta_o\, y v = -g'\, h_y + \tau^{(y)}/\rho\,\mathrm{H} - r v \tag{A5}$$

$$h_t + \mathrm{H}\,(u_x + v_y) = -r h\,, \tag{A6}$$

where
$$\underset{\sim}{u} = \mathrm{H}^{-1}\,(\underset{1}{\mathrm{H}}\,\underset{\sim 1}{u} + \underset{2}{\mathrm{H}}\,\underset{\sim 2}{u}). \tag{A7}$$

The subscripts 1 and 2 refer to the surface layer and underlying layer, respectively.

The equations governing the shear between layer 1 and 2 are:

$$r_s\, u_s - \beta_o\, y v_s = \tau^{(x)}/\rho\,\mathrm{H}_1 \tag{A8}$$

$$r_s\, v_s + \beta_o\, y u_s = \tau^{(y)}/\rho\,\mathrm{H}_1\,, \tag{A9}$$

where $\underset{\sim s}{u} \equiv \underset{\sim 1}{u} - \underset{\sim 2}{u}$.

Equations (A4)-(A9) allow the surface current $\underset{\sim 1}{u}$ to be determined. From this, the entrainment velocity is calculated:

$$w_s = H_1 [(u_1)_x + (v_1)_y] \tag{A10}$$

The temperature equation for the surface layer is, then,

$$\frac{\partial T}{\partial t} = -\underset{\sim 1}{u} \cdot \nabla(\bar{T}+T) - \underset{\sim 1}{\bar{u}} \cdot \nabla T - \{(\bar{w}_s + w_s) - M(\bar{w})\} \bar{T}_z - M(\bar{w}_s + w_s) \frac{T - T_e}{H_1} - \alpha_s T , \tag{A11}$$

where $\underset{\sim 1}{\bar{u}}(x, y, t)$ and $\bar{w}_s(x, y, t)$ are the mean horizontal currents and upwelling, respectively, $\bar{T}(x, y, t)$ is the prescribed mean SST, and $\bar{T}_z(x)$ is the prescribed mean vertical temperature gradient. The entrainment temperature anomaly, T_e, is defined by

$$T_e = \gamma T_{sub} + (1 - \gamma) T. \tag{A12}$$

T_{sub} has the form

$$T_{sub} = \begin{cases} T_1 [\tanh(b_1 (\bar{h}+h) - \tanh(b_1 \bar{h})] , & h > 0 \\ T_2 [\tanh(b_2 (\bar{h}-h) - \tanh(b_2 \bar{h})] , & h < 0 , \end{cases} \tag{A13}$$

where $\bar{h}(x)$ is the prescribed mean upper layer depth. Parameter values used for the coupled simulation are as follows:

$\varepsilon = (2 \text{ days})^{-1}$, $c_a = 60$ m/s, $\alpha = .031$ m^2/s^3/°C, $\beta = 1.6 \times 10^4$ m^2/s^2,
$r = (2.5 \text{ years})^{-1}$, $c \equiv (g' H)^{1/2} = 2.9$ m/s, $H = 150$ m, $H_1 = 50$ m,
$r_s = (2 \text{ days})^{-1}$, $\alpha_s = (125 \text{ days})^{-1}$, $\gamma = 0.75$, $T_1 = 28$°C, $T_2 = -40$°C,
$b_1 = (80 \text{ m})^{-1}$, $b_2 = (33 \text{ m})^{-1}$.

REFERENCES

BJERKNES J., *A possible response of the atmospheric Hadley circulation to equatorial anomalies of ocean temperature.* « Tellus », *18*, 820-829 (1966).

BJERKNES J., *Atmospheric teleconnections from the equatorial Pacific.* « Mons. Wea. Rev. », *97*, 163-172 (1969).

BJERKNES J., *Large-scale atmospheric response to the 1964-65 Pacific equatorial warming.* « J. Phys. Oceanogr. », *2*, 212-217 (1972).

CANE M.A., and ZEBIAK S.E., *A theory for El Niño and the Southern Oscillation.* « Science », *228*, 1085-1087 (1985).

CANE M.A., *Oceanographic events during El Niño.* « Science », *222*, 1189-1194 (1983).

CANE M.A., *El Niño.* « Annual Review of Earth and Planetary Sciences », *14*, 43-70 (1986).

CANE M.A. and SARACHIK E.S., *Forced baroclinic ocean motion II: The equatorial unbounded case.* « J. Mar. Res. », *35*, 395-432 (1977).

CANE M.A. and SARACHIK E.S., *The response of a linear baroclinic equatorial ocean to period forcing.* « J. Mar. Res. », *39*, 651-693 (1981).

CANE M.A. and ZEBIAK S.E., *A theory for El Niño and the Southern Oscillation.* « Science », *228*, 1085-1087 (1985).

CANE M.A., ZEBIAK S.E. and DOLAN S.C., *Experimental Forecasts of El Niño.* « Nature », *322*, 827-832 (1986).

CORNEJO-GARRIDO A.G. and STONE P.H., *On the heat balance of the Walker Circulation.* « J. Atmos. Sci. », *34*, 1155-1162 (1977).

GEISLER J.E. and STEVENS D.E., *On the vertical structure of damped steady circulation in the tropics.* « Quart. J. R. Met. Soc. », *108*, 87-93 (1982).

GILL A.E., *Some simple solutions for heat-induced tropical circulation.* « Quart. J.R. Met. Soc. », *106*, 447-462 (1980).

GOLDENBERG S.B. and O'BRIEN J.J., *Time and space variability of tropical Pacific wind stress.* « Mon. Wea. Rev. », *109*, 1190-1207 (1981).

HALPERN D. and HARRISON D.E., *Intercomparison of tropical Pacific mean November 1979 surface wind fields.* Report 82-1, Department of Meteorology and Physical Oceanography, Massachusetts Institute of Technology, Cambridge, 40 pp. (1982).

JULIAN P.R. and CHERVIN R.M., *A study of the Southern Oscillation and Walker Circulation Phenomena.* « Mon. Wea. Rev. », *106*, 1433-1451 (1978).

LAU K-M.W., *Modeling the seasonal dependence of the atmospheric response to observed El Niños in 1962-1976.* « Mon. Wea. Rev. », in press. (1985).

LAU K-M.W. and CHAN P., *Aspects of the 40-50 day Oscillation during the northern winter as inferred from outgoing longware radiation.* « Mon. Wea. Rev. », *113*, 1889-1909 (1985).

MATSUNO T., *Quasi-geostrophic motions in the equatorial area.* « J. Met. Soc. Japan », *44*, 25-42 (1966).

MCCREARY J.P., *A model of tropical ocean-atmosphere interaction.* « Mon. Wea. Rev. », *111*, 370-87 (1983).

McCREARY J.P., *Modeling equatorial Ocean Circulation.* « Ann. Rev. Fluid Mech. », *17*, 359-409 (1985).

McWILLIAMS J.C. and GENT P.R., *A coupled air-sea model for the tropical Pacific.* « J. Atmos. Sci. », *35*, 962-989 (1978).

PHILANDER S.G.H., *The effects of coastal geometry on equatorial waves.* « J. Mar. Res. », *35*, 509-523 (1977).

PHILANDER S.G.H., *El Niño and La Niña.* « J. Atmos. Sci. », *42*, 2652-2662 (1985).

PHILANDER S.G.H., *Predictability of El Niño.* « Nature », *321*, 810-811 (1986).

PHILANDER S.G.H., Yamagata T. and PACANOWSKI R.C., *Unstable air-sea interactions in the tropics.* « J. Atmos. Sci. », *41*, 604-13 (1984).

RAMAGE C.S., *Sea surface temperature and local weather.* « Mon. Wea. Rev. », *105*, 540-544 (1977).

RAMAGE C.S., *El Niño.* « Scientific American », *254*, 76-83 (1986).

RAMAGE C.S. and HORI A.M., *Meteorological aspects of El Niño.* « Mon. Wea. Rev. », *109*, 1827-1935 (1981).

RASMUSSON D.M. and CARPENTER T.H., *Variations in tropical sea surface temperature and surface wind fields associated with the Southern Oscillation/El Niño.* « Mon. Wea. Rev. », *110*, 354-384 (1982).

RASMUSSON E.M. and WALLACE J.M., *Meteorological Aspects of the El Niño/Southern Oscillation.* « Mon. Wea. Rev. », 222, 1195-1202 (1983).

SHUKLA J. and WALLACE J.M., *Numerical simulation of the atmospheric response to equatorial Pacific sea surface temperature anomalies.* « J. Atmos. Sci. », *40*, 1613-1630 (1983).

VALLIS G.K., *El Niño: A chaotic dynamical system?* « Science », *232*, 243-245 (1986).

WEARE B.C., *Interannual variations in net heating at the surface of the tropical Pacific Ocean.* « J. Phys. Oceanogr. », *10*, 1887-1908 (1983).

WEARE B.C., *A comparison of shallow water model results for three estimates of a composite El Niño forcing.* « J. Atmos. Sci. », *43*, 162-170 (1986).

WRIGHT P.B., *The Southern Oscillation: An ocean-atmosphere feedback system?* « Bull. Amer. Met. Soc. », *66*, 398-412 (1985).

WYRTKI K., *Water displacements in the Pacific and the genesis of El Niño cycles.* « J. Geophys. Res. », *90*, 11719-11725 (1985).

ZEBIAK S.E., *A simple atmospheric model of relevance to El Niño.* « J. Atmos. Sci. », *39*, 2017-2027 (1982).

ZEBIAK S.E., *Tropical atmosphere-ocean interaction and the El Niño/Southern Oscillation Phenomenon.* Ph.D. Thesis. Massachusetts Institute of Technology. 261 pp. (1984).

ZEBIAK S.E. *Atmospheric convergence feedback in a simple model for El Niño.* « Mon. Wea. Rev. », *114*, 1263-1271 (1986).

ZEBIAK S.E. and CANE M.A., *A model ENSO.* « Mon. Wea. Rev. », accepted (1986a).

ZEBIAK S.E. and CANE M.A., *A simulation of sea surface temperature anomalies during El Niño.* « J. Phys. Oceanogr. », in revision (1986b).

STUDY OF ENSO WITH AN OCEAN GCM

K. MIYAKODA, A. ROSATI, R. GUDGEL
GFDL, NOAA

and

Y. CHAO
GFD Program, Princeton University
Princeton NJ 08542, USA

ABSTRACT

A time series of surface atmospheric data is applied to an ocean GCM as a surface boundary condition. The GCM has $1° \times 1°$ grid in the global domain except $1° \times 1/3°$ high resolution in the equatorial zone, and has 12 vertical levels. The turbulence closure scheme is used for the vertical mixing. The atmospheric forcings are twice daily, based on the NMC analysis. The period simulated is the four years from 1980-1983, which include the 1982/83 El Niño. The simulation of the warm event is satisfactory. A diagnostic study on the ENSO process is performed. The time evolution of SO pressure patterns and of the surface wind fields for the 1982/83 case compare fairly well with the canonical case presented by Rasmusson and Carpenter (1982) and van Loon (1986). Based on this analysis, a hypothetical view is presented on the significance of the SO pattern and wind stress to the El Niño process.

1. INTRODUCTION

In order to investigate the mechanism of El Niño, an experiment was carried out on the simulation of the 1982/83 El Niño event, using an ocean GCM and observed atmospheric forcings. There have already been

several studies which have successfully simulated the oceanic warm events in the Equatorial Pacific, such as Busalacchi and O'Brien (1980), Philander and Seigel (1985), and Latif *et al.* (1985). The differences of the present study from those mentioned above are that the atmospheric forcings are twice daily instead of monthly means; that the ocean model is global; and that an elaborate mixed layer parameterization is used.

Because of the frequency of the atmospheric forcings, the period of the application in our study is limited. In this paper, the results for the four-year period from 1980 to 1983 will be reported. This period includes a single El Niño event for 1982/83. It has been pointed out by a number of investigators (for example, Wyrtki, 1985; Cane, 1983) that this El Niño is a large event but not a typical case. Yet we thought that it is useful to study this case in detail.

2. A TROPICAL OCEAN GCM

The ocean GCM which will be used is the world ocean model with fine equatorial mesh (Rosati and Miyakoda, 1988). The horizontal resolution is $1°\times1°$ grid over the global domain except the $1°\times1/3°$ grid within the equatorial zone (see Fig. 1). Philander and Seigel (1985) and Busalacchi and O'Brien (1980) have been successful with the equatorial fine mesh in the simulation of El Niño process. The resolution of the present model is comparable with those models for the Pacific basin. The vertical resolution is 12 levels, as is shown in Fig. 2, with 8 levels located in the upper 200 m for better treatment of the upper part of ocean, and the first layer is 5 m thick. Bottom topography is included, but the deepest level is limited to 3000 m.

This model has been adapted from that of Bryan (1969) and Cox (1984), in which the primitive equations and the salinity equation are used, and the rigid-lid condition is imposed at the surface, i.e., $w = 0$ at $z = 0$ for the computational efficiency. This last condition rules out the kinetic effect of variation in surface displacement of the ocean. The major departure of the present model from the original Bryan-Cox model is the subgrid-scale diffusion and the convective adjustment.

For vertical diffusion, the turbulence closure scheme of hierarchy level 2.5 (Mellor and Yamada, 1974) is employed. One of the merits of this treatment is that the empirical constants used are exactly the same for both the ocean and the atmosphere, which gives consistency in the

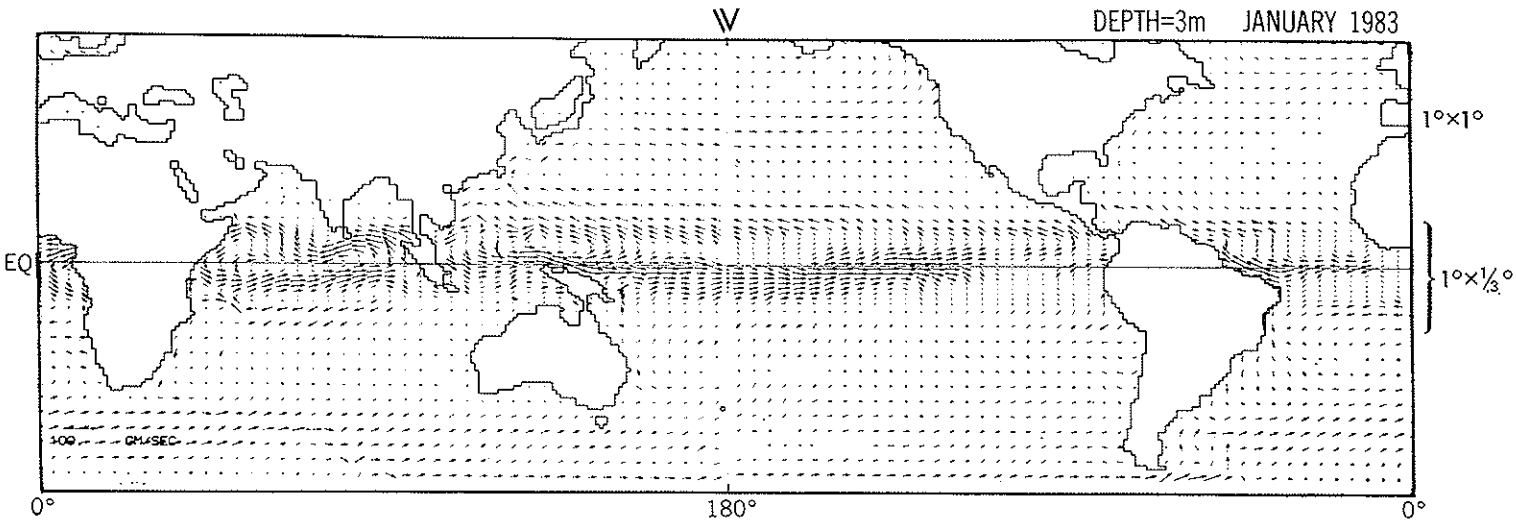

FIG. 1. Grid distribution of the ocean GCM, represented by current arrows at every 5 grid points.

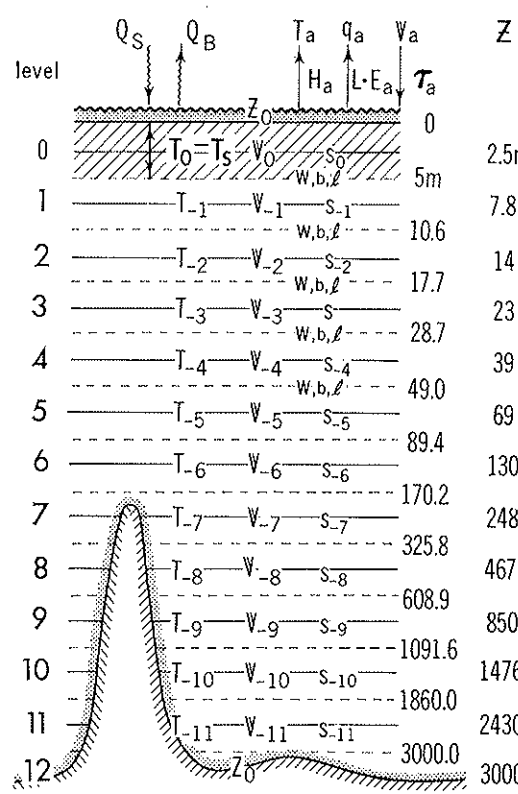

FIG. 2. A schematic diagram of the vertical resolution along with the placement of the variables.

future coupled system. Thus the stress τ, heat flux H, and salinity flux S are represented by

$$\tau_x/\rho = -\overline{u'w'} = (\nu + K_M)\frac{\partial u}{\partial z} \tag{2.1}$$

$$-H/\rho C = -\overline{T'w'} = (k + K_H)\frac{\partial T}{\partial z} \tag{2.2}$$

$$-S/\rho = -\overline{s'w'} = (k + K_S)\frac{\partial s}{\partial z} \tag{2.3}$$

where u, T, and s are the zonal current speed (τ_y is omitted here), the sea temperature and the salinity, respectively, and K_M, K_H, and K_S are the eddy coefficients, ν and k are the ambient diffusivities, ρ is the water density, and C is the heat capacity, and u', w', T', and s' are the turbulent components. The eddy viscosity coefficients are written as

$$\left.\begin{matrix} K_M \\ K_H \\ K_S \end{matrix}\right\} = \text{function of} \left(b^2,\ \ell,\ \left| \frac{\partial \mathbb{V}}{\partial z} \right|,\ g\ \beta \frac{\partial \rho}{\partial z} \right) \tag{2.4}$$

where $b^2/2$ is the turbulent kinetic energy, TKE, ℓ is the turbulent length scale, $\dfrac{\partial \mathbb{V}}{\partial z}$ is the vertical current shear, and β is the thermal expansion coefficient of water.

The TKE is governed by the equation

$$\frac{d\, b^2/2}{d\, t} = \frac{\partial}{\partial z} \left(K_b \frac{\partial\, b^2/2}{\partial z} \right) - \overline{u'w'} \frac{\partial u}{\partial z} - v'w' \frac{\partial v}{\partial z} + g\,\beta\, \overline{w'\rho'} - \frac{b^3}{\Lambda} \tag{2.5}$$

where K_b is the diffusion coefficient similar to K_M, and Λ is another turbulent length scale.

Fig. 3 is an example of the vertical distribution of the TKE, b^2. In the winter hemisphere, where convection is the prime mechanism for mixing, the TKE has penetrated down to a deep layer. With this process, the convective adjustment was not needed.

3. Performance of the GCM for the 1982/83 El Niño event

Applying the atmospheric forcings to the ocean GCM, the time integration was carried out for four years from 1980 to 1983 with $\Delta t = 3$ hours. This experiment started from initial condition of an 8-year ocean run forced by climatological atmospheric data. The atmospheric forcings

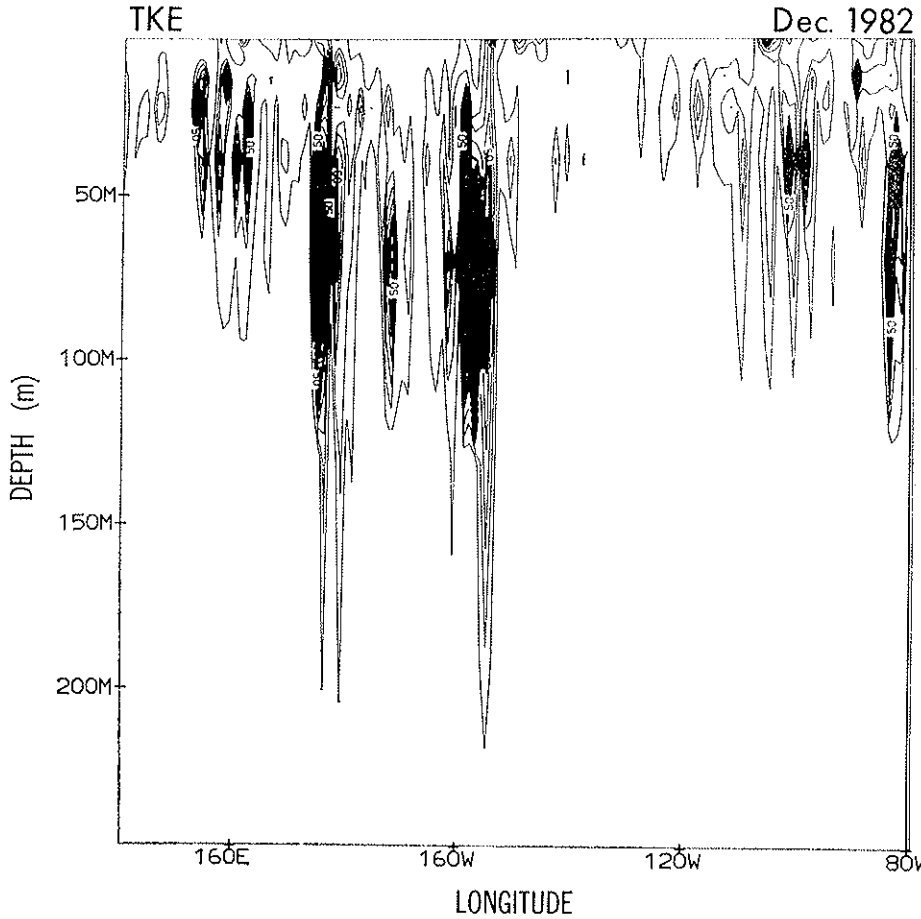

FIG. 3. Vertical distribution of turbulent kinetic energy, along the equator for the Pacific basin. Units: $cm^2\ s^{-2}$.

were taken from the NMC data for wind, air temperature and humidity at 100° mb level. The data are twice daily for the four years. The radiation was computed using climatological clouds.

Fig. 4 is the time-longitude diagrams of SST anomalies for the equatorial belt between 5° N and 5° S. The simulation is satisfactory (the observations are based on the analyses of Reynolds, 1982). Figs. 5 and 6 are the comparisons of the simulation with the observation of moored buoy (Halpern, personal communication) at the longitude 94.5°W and the

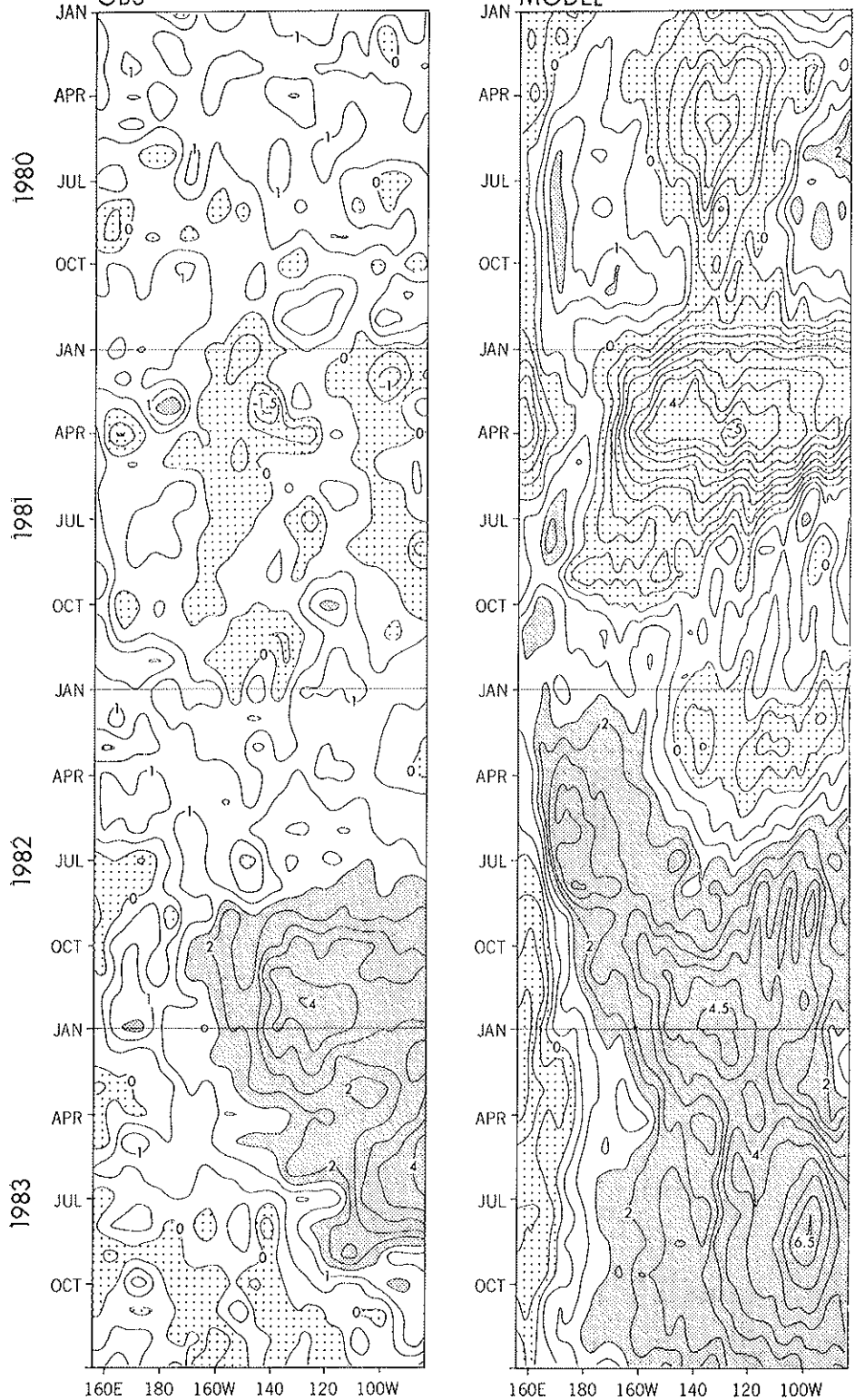

FIG. 4. The time-longitude diagram of equatorial (5°N-5°S) SST anomalies. Contour

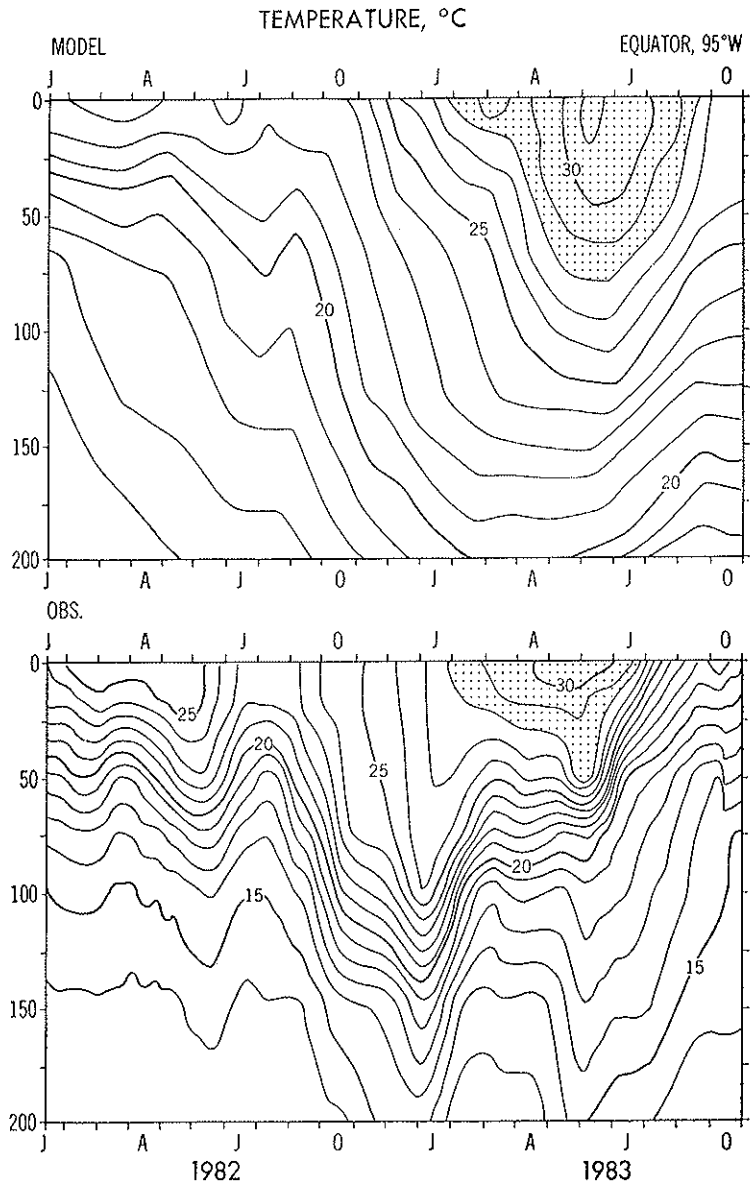

FIG. 5. Temperature (°C) at 95°W and the equator during 1982-1983. Top is the model simulation, and bottom is observation after Halpern.

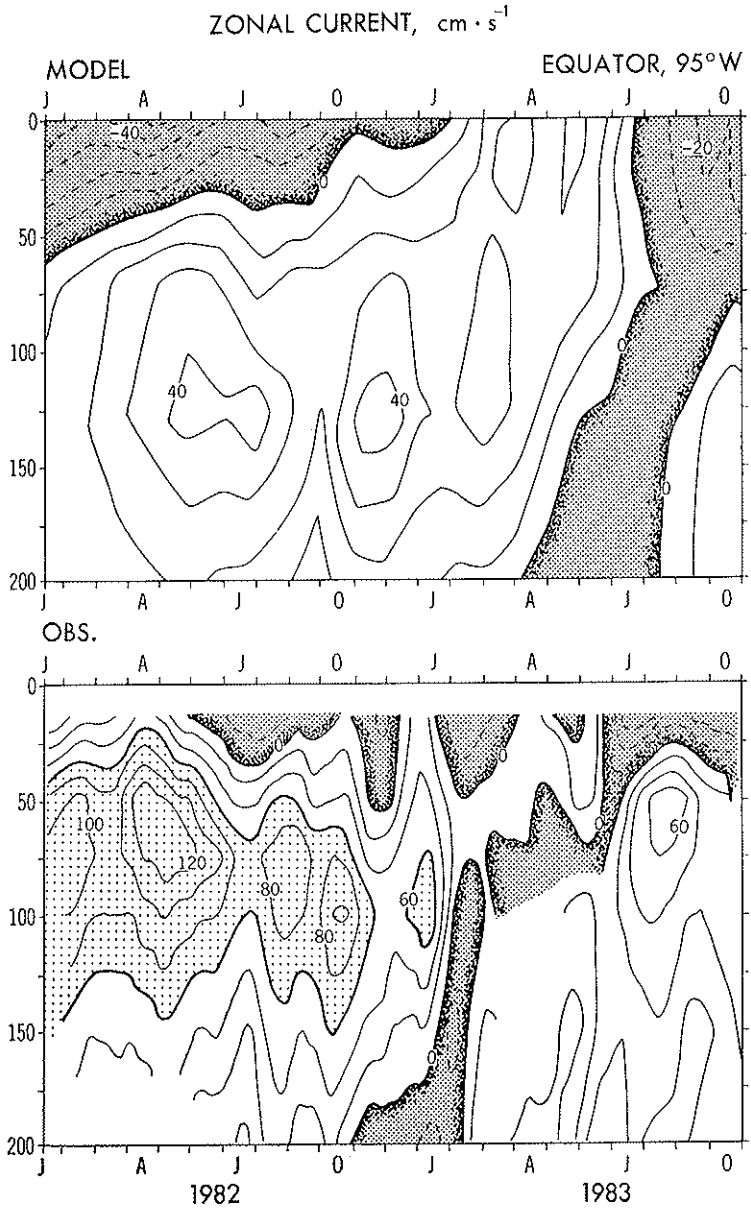

FIG. 6. As in Fig. 5 but for zonal velocity.

equator. The parameters are the water temperature and the zonal component of current as a function of time and depth. It may be safely concluded that the simulation is reasonable, the key for the success being the adequate wind data (Philander and Seigel, 1985).

Fig. 7 shows the 1980-83 evolution of the normalized ocean heat content for the equatorial belt of Pacific, derived from the GCM run. The heat content is defined by $\int_{5^\circ S}^{5^\circ N} \int_{325\ m}^{o} T\ dz\ d\phi$. The figures include the longitudinal distribution of the heat content deviation from a four-year mean. It may be clear, as was pointed out by Wyrtki (1975) and Cane (1983), that the heat content steadily increased in the western side of the Pacific from 1980 to May 1982, and then suddenly decreased, associated with the El Niño event, and that it thereafter becomes positive at the eastern side of the Pacific until September 1983. This is the "sloshing" of thermal structure in response to the changing wind stress. It is assumed that the increase of heat content at the western basin is a necessary condition for the El Niño process.

4. Consideration on 1982/83 ENSO event

In order to investigate how the 1982/83 El Niño occurred, we look into the relevant information and consider its significance. First of all, it is an established fact that a high correlation exists between the negative SO index and the positive SST anomaly (Fig. 8 — Rasmusson, 1985), and the negative SO index is likely to be a necessary condition for El Niño (van Loon, 1986).

Van Loon (1986) constructed composite maps of sea level pressure anomalies for the three consecutive years before and after El Niño. Fig. 9a shows these maps for the -1 year, the 0 year, and the $+1$ year, based on a number of the warm events (at least more than four events). For JJA (June, July and August) of the -1 year, the positive SO pattern exists (positive pressure anomaly in east and negative in west), while for JJA of the 0 year and DJF (December, January and February) of the $+1$ year, the sea level pressure anomalies are reversed, and the negative SO pattern emerges (negative pressure anomaly in east and positive in west).

Fig. 9b is the corresponding map for the case of 1982/83 El Niño, though the maps are for the geopotential height at 1000 mb instead of

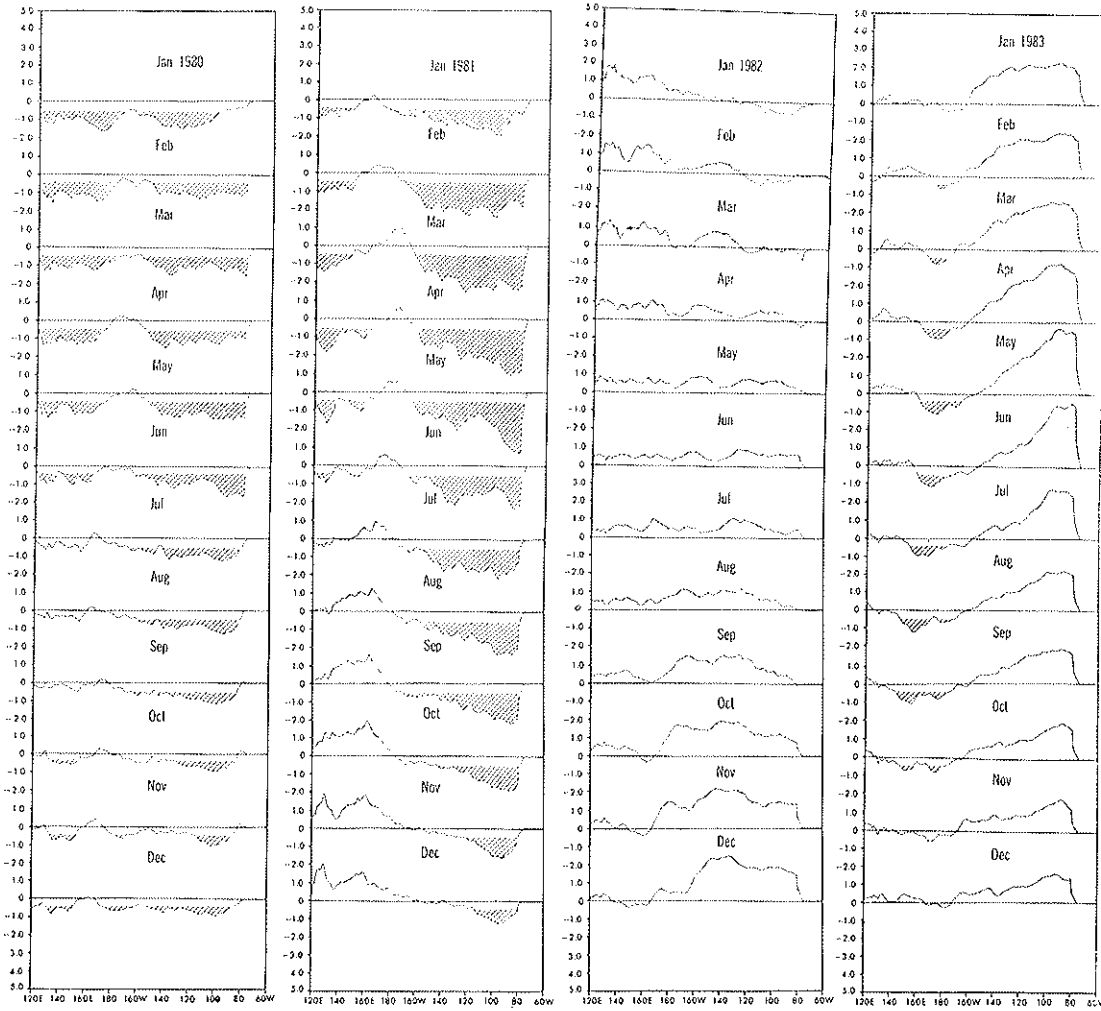

FIG. 7. Time evolution of heat content deviation along the latitude belt 5°N and 15°N. The deviation is the departure from the four year mean. Units: 10^{15} J.

sea level pressure. It appears that the correspondence of the SO patterns for this particular year to the canonical patterns in Fig. 9a is good.

Van Loon (1986) mentioned that the anomalies are small on the northern hemisphere, while they are large and significant on the southern hemisphere. He also pointed out that the SO pattern can be regarded as "a wave-train beginning in Australia and the Pacific, crossing South

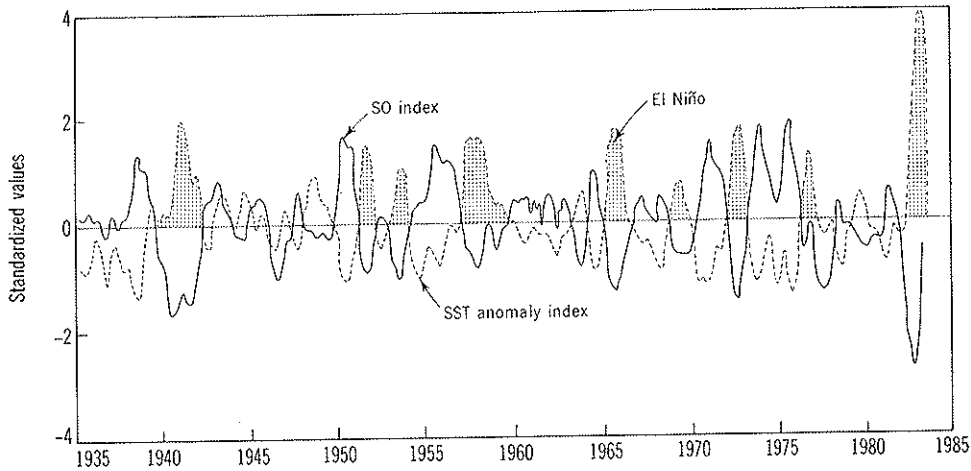

FIG. 8. Index of SST anomaly (off South American coast) and SO index. The shaded periods indicate El Niño episodes (after Rasmusson, 1985).

America, and ending in the northernmost Indian Ocean with the phase reversing from, the −1 year to the 0 year". Perhaps the most important aspects of the SO pattern for the El Niño are (i) the variation of the pressure gradient along the equator, and (ii) the intensity of southerlies in Australian monsoon and northerlies of China Sea surge. This point will be discussed later.

Rasmusson and Carpenter (1982) constructed the composite maps of surface anomaly wind field for the three consecutive years around the El Niño (see Fig. 10a). For the ASO (August, September and October) of the −1 year, the trades are strong west of the dateline and the northerlies are particularly strong off Chile. For the ASO of the 0 year, the southerlies northeast of Australia are pronounced, and the westerly anomalies are distinct over the central equatorial Pacific. For the DJF of the +1 year, the westerly anomalies are dominant, and the easterlies show up north of New Guinea. It is considered that the easterly anomaly winds in the ASO of the −1 year contribute to the piling-up of the heat content of ocean water in the western part of the Pacific. The westerly anomaly winds in the ASO of the 0 year and the DJF of the +1 year are essential for diminishing of the upwelling in the eastern Pacific, leading to the positive SST anomalies in the eastern and central basin.

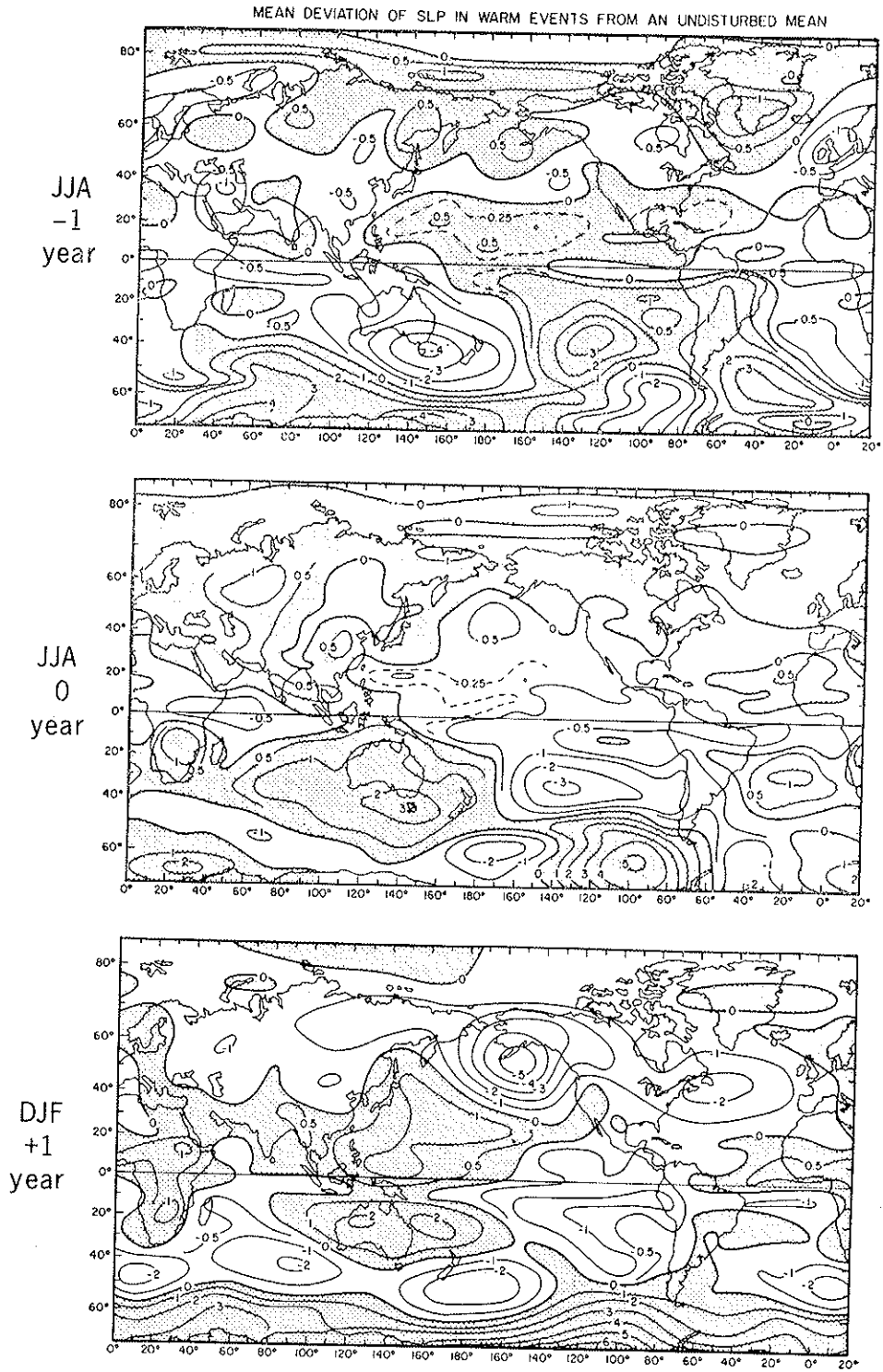

FIG. 9a. Composite maps of SLP anomalies (after van Loon, 1986).

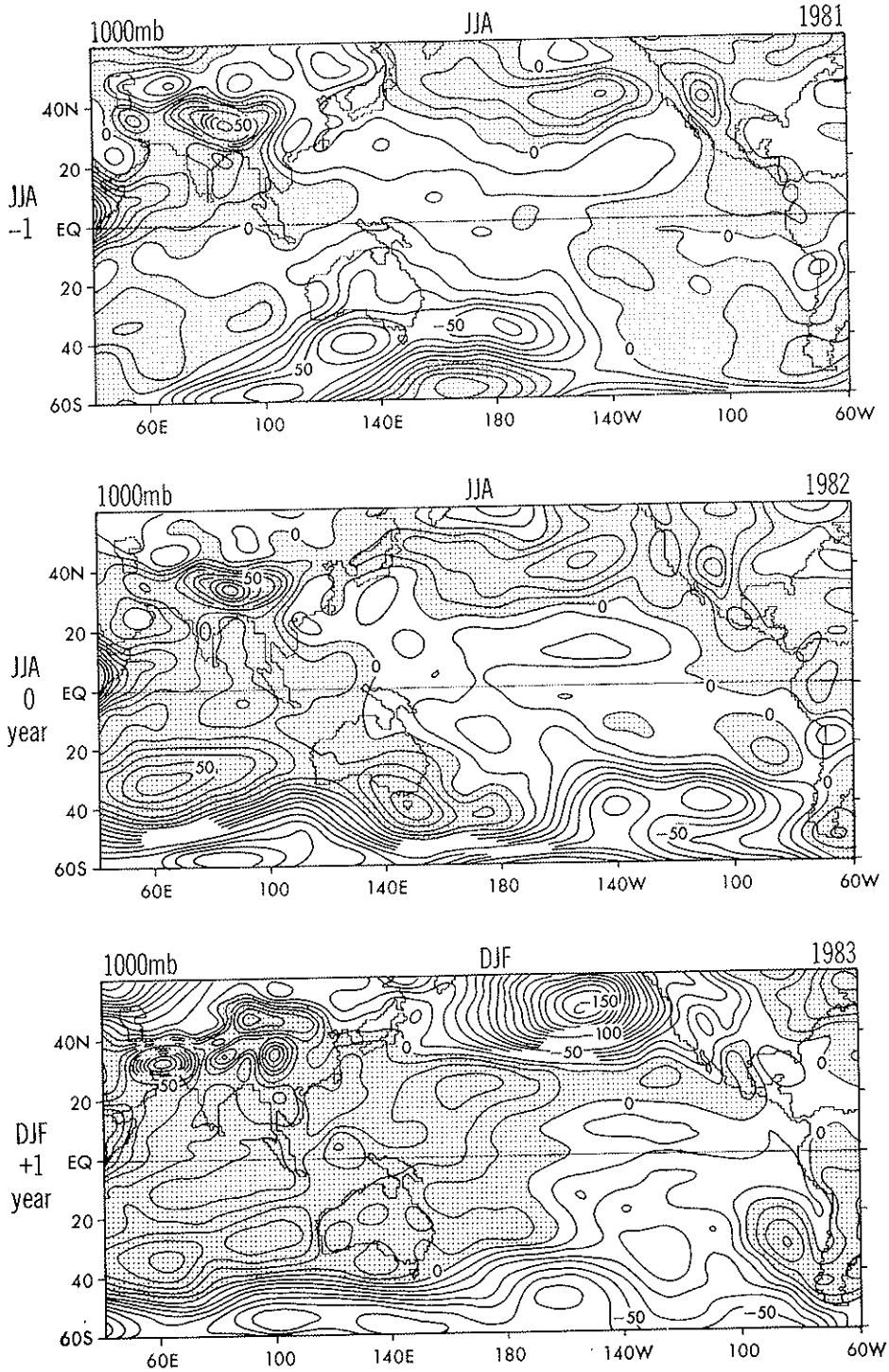

FIG. 9b. Anomaly maps of 1000 mb geopotential height for 1982/83 El Niño.

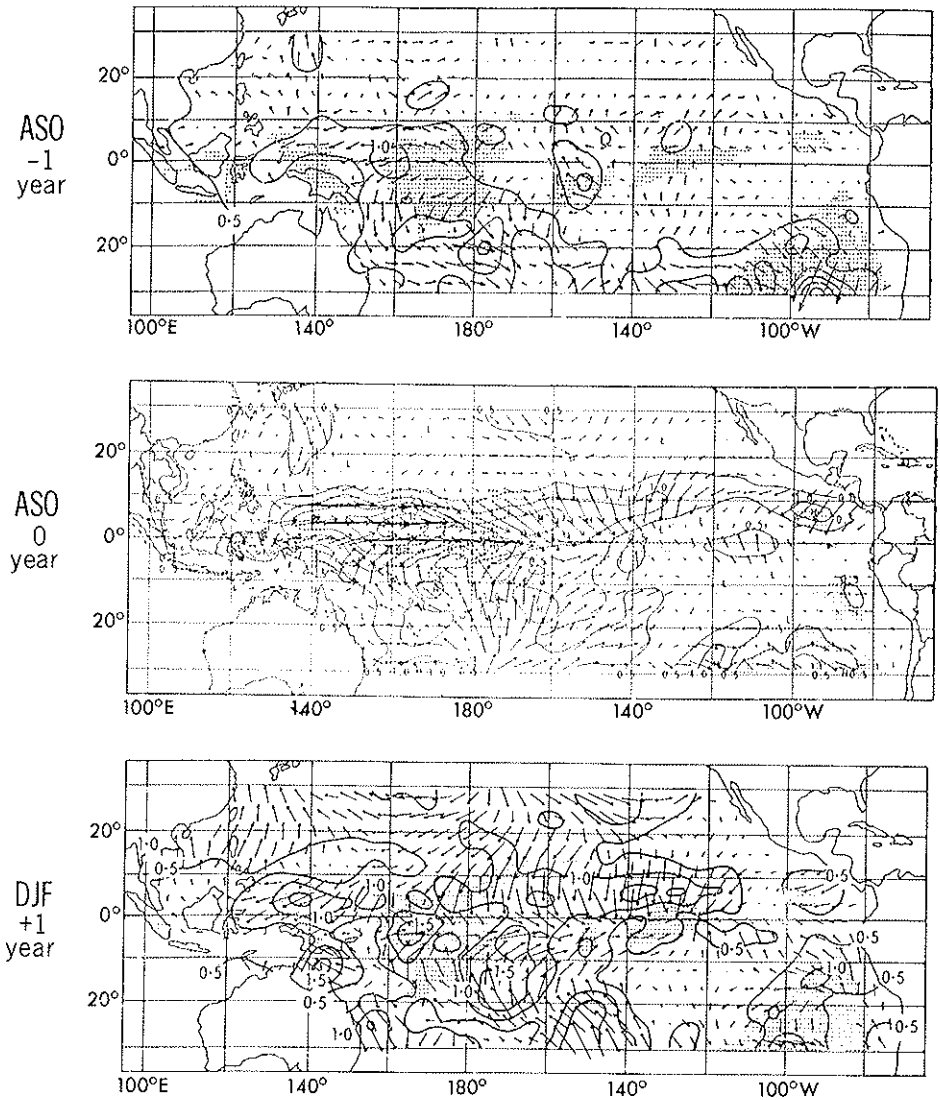

Fig. 10a. Composite maps of observed surface winds (m s^{-1}) (after Rasmusson and Carpenter, 1982).

Fig. 10b is the corresponding map for 1982/83 El Niño. It appears that the correspondence of the anomaly wind fields for this particular year to the canonical patterns in Fig. 10a is reasonably good. Even outside of 10°N-10°S belt, a number of similarities may be noticed. The exceptions are that the strong northerlies off Chile are missing in the ASO of the −1 year (though there are weak northerlies).

It is very likely that, in order to have a successful simulation of SST anomalies, as seen in Fig. 4., the role played by surface atmospheric winds is crucial. In other words, the westerlies in Fig. 10b are most essential for the case of 1982/83 El Niño. It appears that there are two important aspects for generation of the westerlies in the equatorial zone, i.e., the monsoon southerlies/northerlies in the western part of the Pacific, and the cumulus convection associated with warm SST in the middle of the Pacific.

In order to explain the westerly acceleration in the Australian monsoon region, Fig. 11 is prepared. This is the observed pattern of the zonal component of wind over the Indonesian Archipelago. The relevant dynamics is

$$\frac{\partial u}{\partial t} = f v - \frac{\partial p}{\rho \partial x} \tag{4.1}$$

Let us take the case of August, 1982. The southerlies come from south of New Guinea. If they don't cross the equator, the easterlies are generated due to the effect of fv. On the other hand, if they cross the equator, they are directed to east also due to the effect of fv. This is the mechanism of the westerlies in the equatorial zone. However, if the effect of surface pressure (the second term $\partial p/\rho\partial x$) is large, such a simple relation does not hold. Namely, if the SO pattern becomes dominant, the relation becomes complex. In reality, so far as Indonesia-Australia are concerned, the relation of the cross-equatorial wind holds well.

Fig. 12 shows the evolution of the anomalies of 1000 mb geopotential height for four years. From July 1981 to May 1982, in the Indonesia-Australia area, the height anomalies are negative, corresponding to positive SO index. Therefore, the pressure tendency along the equator tends to accelerate the trades, as has been pointed out by Wyrtki (1975) as a precursor of the warm event. Only thing is that the strengthening of trades occurred slightly late in the case of 1982/83 El Niño. After

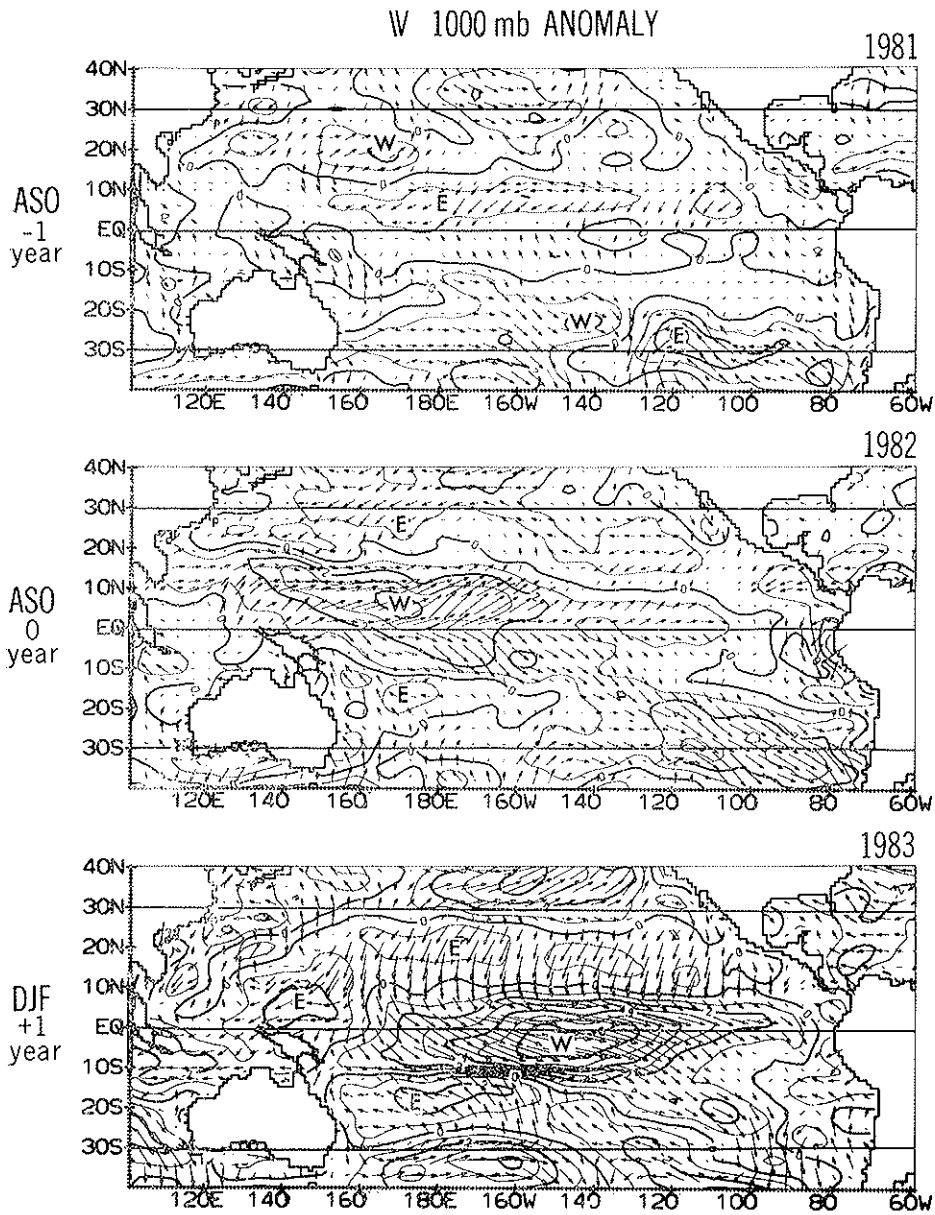

FIG. 10b. Anomaly maps of 1000 mb wind vector for 1982/23 El Niño.

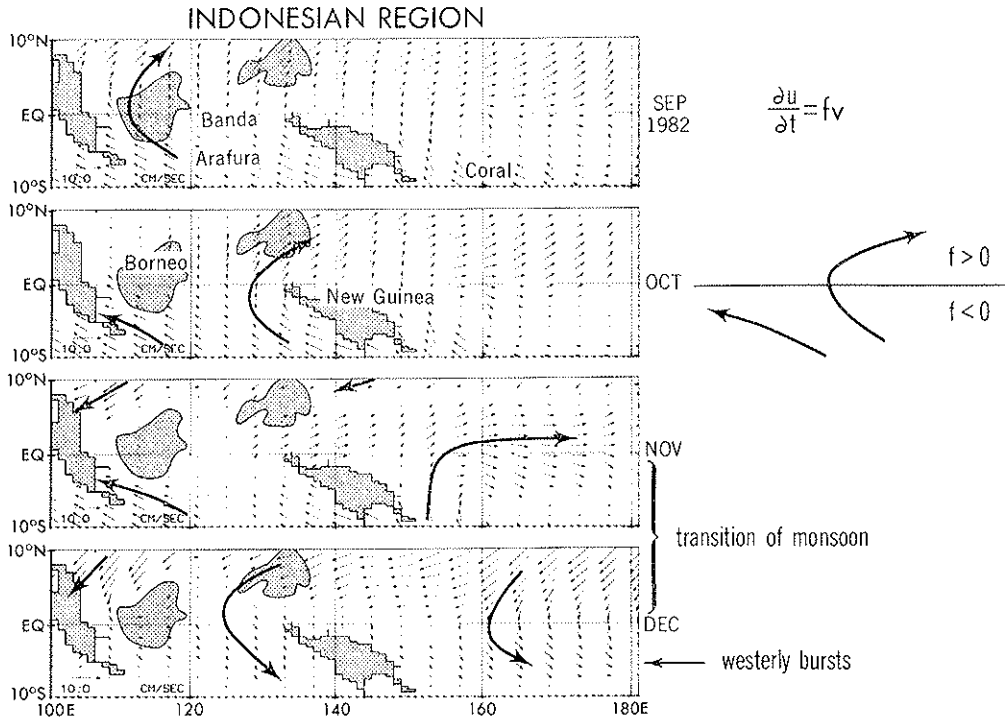

FIG. 11. Development of westerlies by the effect of cross-equatorial wind.

June 1982, the height anomaly over the Indonesia-Australia region changed to positive, corresponding to the negative SO index. The anomaly pressure gradient along the equator is now favorable for generating westerlies. As was pointed out by Gill and Rasmusson (1983), whenever cumulus convection occurs in the central Pacific, there is a tendency that the strong westerly inflow is reduced with the weaker easterly inflow, the cause of non-symmetry being the effect of the earth's rotation. Besides, in the case of negative SO pattern, such as in the present episode, the inflow westerlies are even more accelerated due to the equatorial pressure gradient.

From November 1982 through July 1983, the high pressure anomalies are located over the Indonesia-Australian region, and after that, the anomaly pressure gradient is reversed.

Fig. 13 shows the evolution of the surface wind anomalies. It reveals the following:

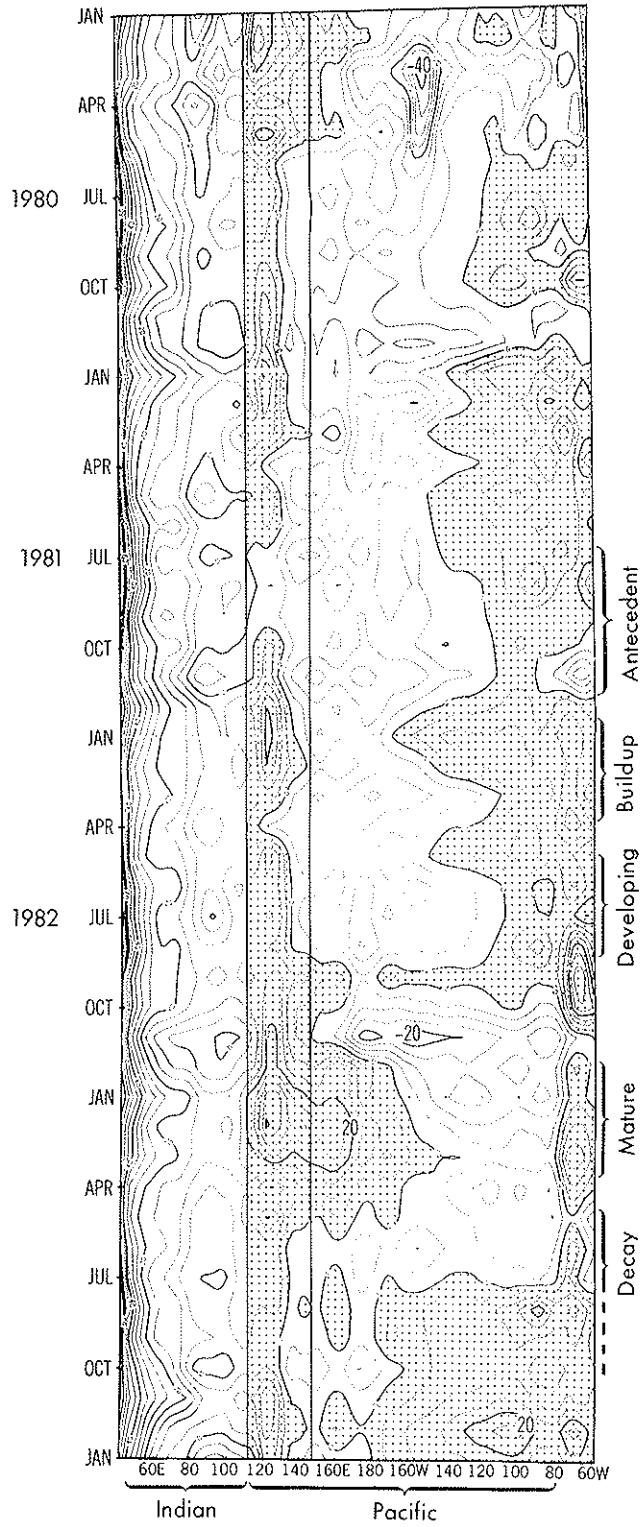

FIG. 12. Time-longitude diagram of 1000 mb geopotential height anomalies along the equator [or, the belt of 10°N-10°S. Contour interval: 5 m. The positive anomalies areas are

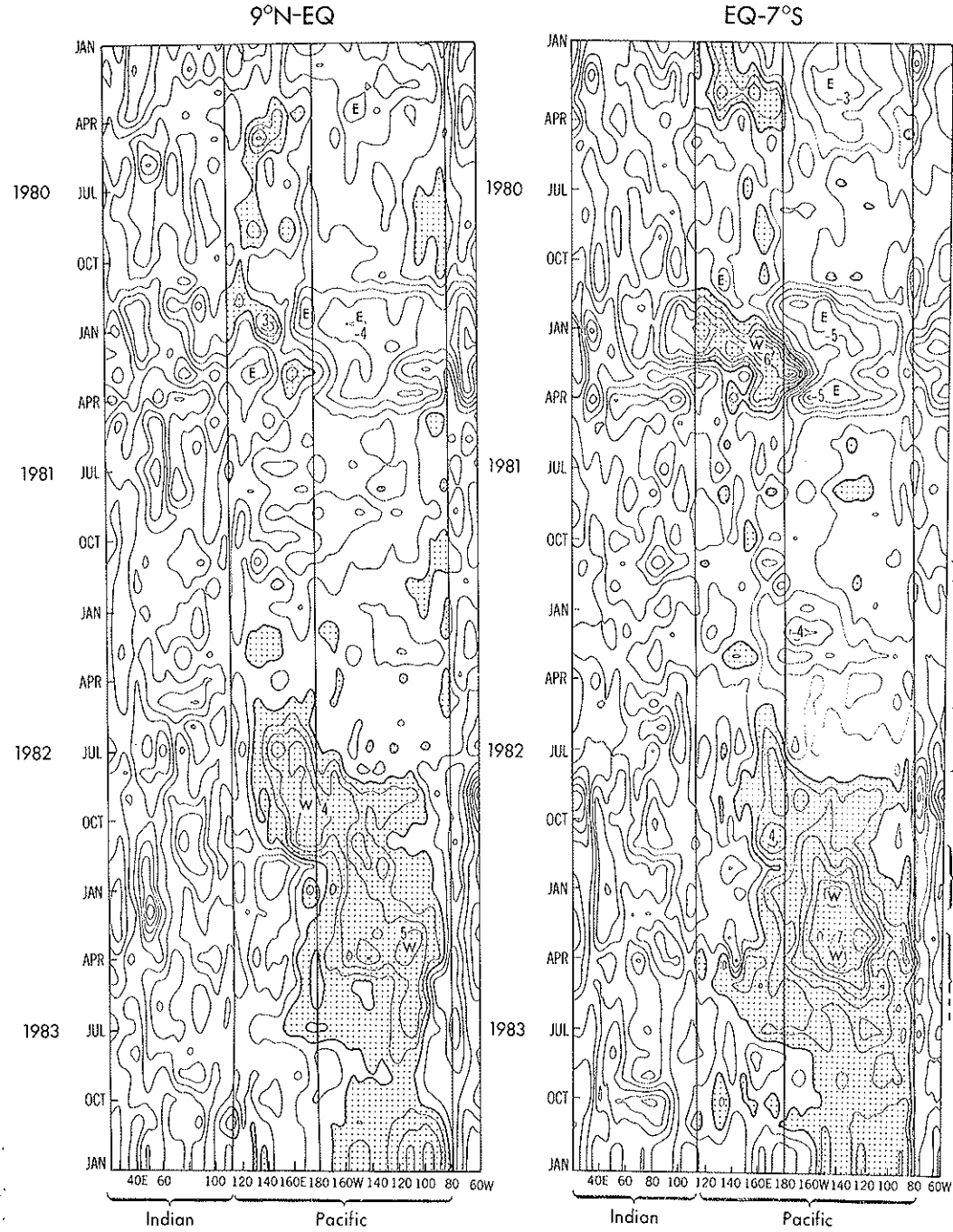

FIG. 13. Time-longitude diagram of surface zonal wind anomalies along the equator in the Pacific for the belt of Eq.-9°N (lfet) and of 7°S-Eq. (right). Contour interval: 1 m s^{-1}. The westerly regions are shaded only for the Pacific Ocean region.

(i) From May 1981 to April 1982, in the Indonesian region, there are strong trades, as was mentioned previously.

(ii) From June to November 1982, in the Indonesian region, the westerlies tend to be stronger, probably due to strong southerlies east of Australia and the higher pressure in the Indonesian region associated with the SO cycle.

(iii) From September 1982 to July 1983, in the central Pacific, the westerlies develop. The reason of the westerlies at 120° W in September 1982 is that the equatorial pressure field tends to accelerate westerlies (high pressure in Indonesian side), and that the activity of the cumulus convection in the central Pacific regions associated with the emergence of warm SST easily induces westerlies. These westerlies in turn induce the warm SST (Gill and Rasmusson, 1983).

(iv) It is likely that the main process of SST warming is due to the relaxing of upwelling associated with the westerlies *in situ*, so far as this El Niño is concerned.

(v) As seen in September 1982-March 1983, there are southerlies at 160°W-140°E and 20°S, which are associated with the SO pressure patterns in the midlatitude of the southern hemisphere. However, these southerlies are not contributing to the generation of equatorial westerlies.

Concerning the long-term behavior of the surface pressure pattern, Barnett (1985) hypothesized the eastward propagation of the large-scale pattern in the complex EOF mode 1 from India to eastward. In fact, he showed this pressure propagation for the case of 1982/83 event though the validity of his hypotheses remains to be seen.

5. Remarks and conclusions

Using an ocean GCM and the atmospheric forcings based on the NMC surface analyses, the simulation of the 1982/83 El Niño event has been, to some extent, successfully performed. Thus this system of GCM provides a useful tool which enables one to investigate some of the mechanisms of the El Niño phenomenon. Diagnostic analyses of the wind stress and the 1000 mb geopotential height fields have revealed that the evolution of wind fields and SO patterns in the case of the 1982/83 El Niño have a great deal of similarity to those of the canonical case, presented by Rasmusson and Carpenter (1982) and van Loon (1986).

The analysis of these results raises the following questions:

a) In May 1981-April 1982, there are strong trades (or less westerlies) west of the dateline. Are they indeed important for the El Niño?

b) Are these trades related to the negative pressure gradient along the equator (positive SO index) in the Indonesian region?

c) Are the strong monsoon southerlies over Indonesia-Australia or the cold surge over South China Sea important for the El Niño?

d) Nicholls (1984) has pointed out the relationship between the Indonesian SST and SO as well as the eastern Pacific SST some seasons later. Is it important?

e) Is the Australian monsoon stronger in the year of negative SO index than in the year of positive index?

In June-November 1982, the westerlies are dominant in the central equatorial Pacific. It is now known that they are related to the positive SST anomalies. Wind stresses are responsible for the emergence of the SST anomaly.

It may be reasonable to note that the real understanding of the whole ENSO process requires the simulation study with an atmospheric GCM as well. (See Zebiak and Cane, 1987). In particular, the evolution of SO pressure patterns is most difficult to unravel.

f) In October-December 1982, the westerlies become pronounced, as described above. In this process, is the atmospheric pressure gradient along the equator indeed crucial?

Although the delineation of the mechanism could be of "chicken-and-egg" nature, the critical analysis of each process may be useful for the ultimate understanding of the whole phenomenon.

g) Is Barnett's hypothesis true (the eastward propagation of the large-scale atmospheric pressure)? Is the standing oscillation of the SO pattern alone not sufficient for the generation of El Niño?

REFERENCES

BARNETT T.P., *Variations in near-global sea level pressure.* « J. Atmos. Sci. », *42*, 478-501 (1985).

BRYAN K., *A numerical method for the study of the world ocean.* « J. Comput. Phys. », *4*, 347-376 (1969).

BUSALACCHI A.J. and O'BRIEN J.J., *The seasonal variability in a model of tropical Pacific.* « J. Phys. Oceanogr. », *10*, 1929-1951 (1980).

CANE M.A., *Oceanographic events during El Niño.* « Science », *222*, 1189-1195 (1983).

COX M.D., *A primitive equation, 3-dimensional model of the ocean.* « GFDL Ocean Group Tech. Rept. », No. 1, 143 pp. (1984).

GILL A.E. and RASMUSSON E.M., *The 1982-83 climate anomaly in the equatorial Pacific.* « Nature », *306*, 229-234 (1983).

LATIF M., MAINER-REIMER E. and OLBERS D.J., *Climate variability studies with a high-resolution equatorial model of the Pacific ocean.* Elsevier Oceanogr., Ser. 40, *Coupled Atmosphere-Ocean Models*, edited J.C.J. Nihoul. Elsevier Science Publishers E.V. Amsterdam (1985).

MELLOR G.L. and YAMADA T., *A hierarchy of turbulence closure models for planetary boundary layers.* « J. Atmos. Sci. », *31*, 1791-1806 (1974).

NICHOLLS N., *The Southern Oscillation and Indonesian sea surface temperature.* « Mon. Wea. Rev. », *112*, 424-432 (1984).

PHILANDER S.G.H. and SEIGEL A.D., *Simulation of El Niño of 1982-1983.* Elsevier Oceanogr. Ser. 40, *Coupled Ocean-Atmosphere Models*, edited by J.C.J. Nihoul, 511-541. Elsevier Science Publishers B.V., Amsterdam (1985).

RASMUSSON E.M. and CARPENTER T.H., *Variations in tropical sea surface temperature and surface wind fields associated with the Southern Oscillation/El Niño.* « Mon. Wea. Rev. », *110*, 354-384 (1982).

RASMUSSON E.M., *El Niño and variations in climate.* « Amer. Scientist », *73*, 168-177 (1985).

REYNOLDS R.W., *A monthly averaged climatology of sea surface temperature.* « NOAA Tech. Rep. NWS », *31*, Washington, DC., 33 pp. (1982).

ROSATI A. and MIYAKODA K., *A GCM for upper ocean simulation* (to be submitted to J. Phys. Oceanogr.) 1987.

VAN LOON H., *The characteristic of sea level pressure and sea surface temperature during the development of warm event in the Southern Oscillation.* « Namias Symposium », Scripps Institution of Oceanography, University of California, San Diego, La Jolla, Ca., 160-173 (1986).

WYRTKI K., *El Niño - The dynamic response of the Equatorial Pacific Ocean to atmospheric forcing.* « J. Phys. Oceanogr. », *5*, 572-584 (1975).

WYRTKI K., *Water displacements during 1982-83 and the genesis of El Niño and the Southern Oscillation.* « J. Geophys. Res. », *90*, 7129-7132 (1985).

ZEBIAK S.E. and CANE M.A., *A Model El Niño Southern Oscillation.* « Mon. Wea. Rev. », *115*, 2262-2278 (1987).

THE ASIAN SUMMER MONSOON ONSET — A PLANETARY-SCALE PHENOMENON

R. P. PEARCE
Department of Meteorology
University of Reading
Reading RG6 2AU, U.K.

1. Introduction

Many analyses have been carried out of the 1979 Asian summer monsoon and recently analyses from global prediction centres have also been used to study, not only subsequent onsets, but also the entire tropical circulation including estimates of the distribution of large-scale heat sources and sinks. It is when the monsoon circulation is viewed in the global and seasonal context that its planetary scale nature is revealed. It is this perspective which is presented in the next section. The onset process is then described in Section 3, where its two main phases are described. The first is a moisture build-up over the Arabian Sea and the second a rapid intensification when the main monsoon rains over India commence. It is also at this time that a strong cross-equatorial upper return flow over the Arabian Sea is set up. Some experiments in the numerical simulation of the 1979 onset are briefly described in Section 4 in order to stress the importance of realistic modelling of the physical transfer of heat and moisture by small-scale convection and of radiation. These difficulties highlight the sensitivity of the atmosphere itself to these factors and the crucial role of cumulus convection in the large-scale monsoonal circulation. Finally, in Section 5, a simple zonally-symmetric model of a narrow E-W convective band in the tropical belt is used to suggest what are the essential geographical and atmospheric circulation features responsible for the observed characteristics of the Asian Summer Monsoon — and the less dramatic characteristics of monsoons elsewhere.

2. The Asian summer monsoon and the seasonal variation of the global atmospheric circulation

Historically the Asian monsoon has been regarded essentially as a regional phenomenon, its onset being identified with the outbreak, in late May or early June, of extensive rainfall over India. Since 1979, the year of the First Global Weather Experiment (FGGE), operational daily global analyses of wind, temperature and other variables computed by numerical weather prediction (NWP) models have become available and, although incorporating much less observational data than in 1979, nevertheless enable useful climatological analyses to be carried out. Figure 1 shows the winds for the tropical belt together with the vertically integrated heating averaged for the seasons December, January and February (DJF) and June, July and August (JJA) 1979-84. The heating rates were obtained as a residual in the thermodynamic equation expressed as

$$\left(\frac{p_0}{p}\right)^{R/c_p}\frac{\bar{Q}}{c_p} = \frac{d\bar{\theta}}{dt} = \bar{\omega}\frac{\partial\bar{\theta}}{\partial p} + \bar{\underline{v}}\cdot\nabla\bar{\theta} + \left(\overline{\omega'\frac{\partial\theta'}{\partial p}} + \overline{\underline{v}\cdot\nabla\theta}\right) \qquad (1)$$

(i) (ii) (iii) (iv)

where $\overline{}$ denotes a seasonal average and $'$ a departure; the storage term $\frac{\partial\bar{\theta}}{\partial t}$ is essentially zero for a solsticial season.

(ii), (iii) and (iv) are referred to as the steady vertical transport, steady horizontal transport and transient eddy transport terms respectively.

Note in Figure 1:

(a) The seasonal shifts of the main heating regions;

(b) The pair of anticyclones at 150 mb linked with equatorial easterlies over Indonesia in DJF, with westerlies over the E. Pacific; and over the W. Pacific, Indian Ocean and Africa in JJA;

(c) The low level trade winds over the Atlantic and Pacific Oceans;

(d) The Asian summer (JJA) and winter (DJF) monsoon circulations.

The contributions of the individual terms (i)-(iv) in Eq. (1) to the heat balance of JJA are shown in Figures 2.

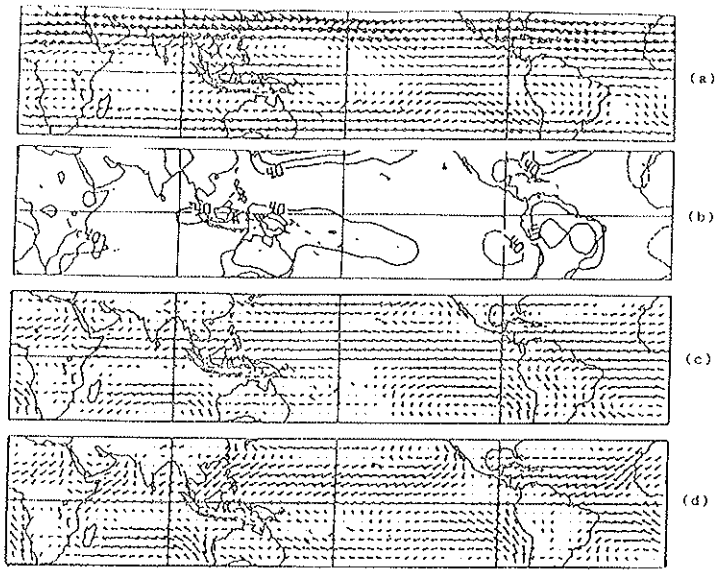

FIG. 1. Mean winds during December-February, based on data for the years 1979-84, between 35°S and 35°N at (a) 150, (c) 850 and (d) 1000 mb. A 3 mm long arrow corresponds to a wind speed of 27 m s^{-1} in (a), and 13.5 m s^{-1} in (c) and (d). The pattern of large-scale, vertically integrated diabatic heating is shown in (b). The contour interval is 40 Watts/m^2; heating is indicated by solid and cooling by dashed contours. The zero contour is not shown for clarity. The field has been smoothed prior to plotting with an isotropic filter that effectively retains length scales up to spherical wavenumber n = 24.

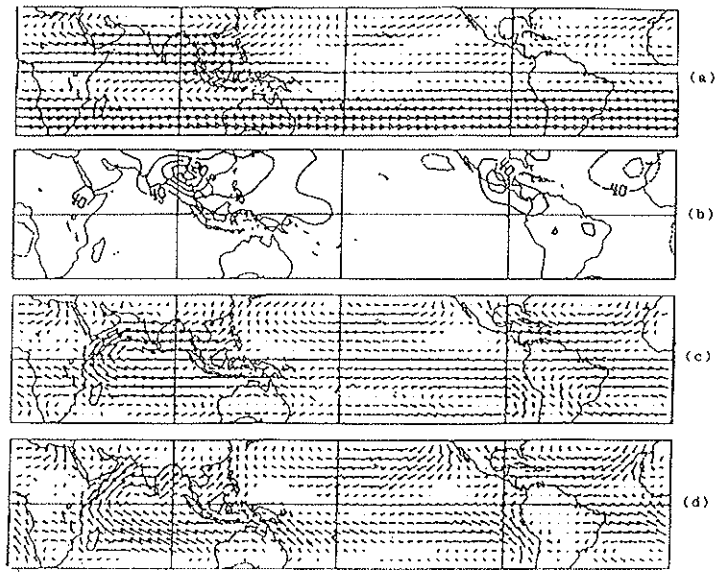

As above but for June-August.

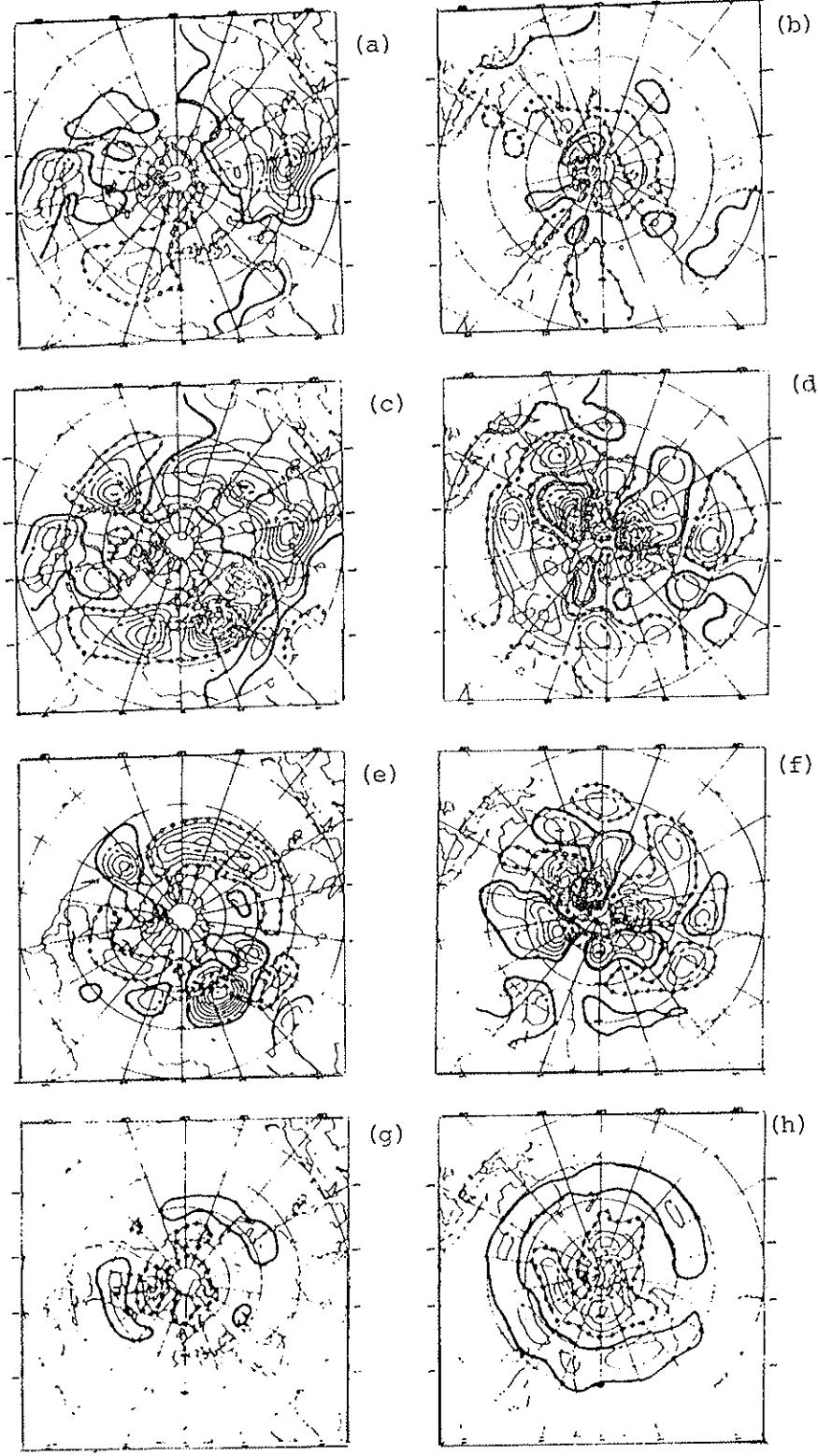

FIG. 2. HA components of the thermal energy equation (Eq. (1)), calculated from ECMWF

Note:

(a) The relatively small contribution of (iii) and (iv) equatorward of 20°, i.e., the balance is mainly between heating and vertical transport by the mean flow.

(b) The important role of steady horizontal transport in the subtropics largely offsetting vertical transport in the planetary waves.

The observed flow patterns, which are related not only to the large-scale heat sources and sinks, but also to the large mountain masses and the continent-ocean configuration, may usefully be analysed by separating them into non-divergent (rotational) and irrotational (divergent) parts.

The dynamical influence of these large-scale heat sources and sinks, particularly on the upper-tropospheric flow, is readily studied using this approach, particularly the configuration of the stationary planetary waves. [See the contribution by B.J. Hoskins in this volume.] The latter include the upper anticyclones associated with the tropical heat sources.

The Asian summer monsoon onset, when seen in its global context, is thus the final stage in the establishment of the JJA global flow regime; its retreat is linked to the first stages in the setting up of the DJF regime.

3. The onset process during May-June

The Asian summer monsoon circulation at both upper and lower levels, characterised by its heat source well-displaced from the equator, is a major zonally asymmetric general circulation feature and, for a feature of this magnitude, is established with remarkable rapidity during April-June. The onset during 1979, as inferred from FGGE level IIIb data (see Pearce and Mohanty, 1984, for details) is shown in Figures 3-7 (see captions for details).

Note in particular:

(a) the moisture build-up over the Indian Ocean between the first half of May and the first half of June (Fig. 4 (b)) and subsequently over the Arabian Sea (Fig. 4 (c)); also the accompanying latent heat release (Fig. 5).

(b) The rapid intensification of the 850 mb winds over the Arabian Sea during the first half of June (Fig. 6 (c)) and the accompanying rise of mean tropospheric temperature (Fig. 6 (b)), and surface moisture flux (Fig. 7 (b)).

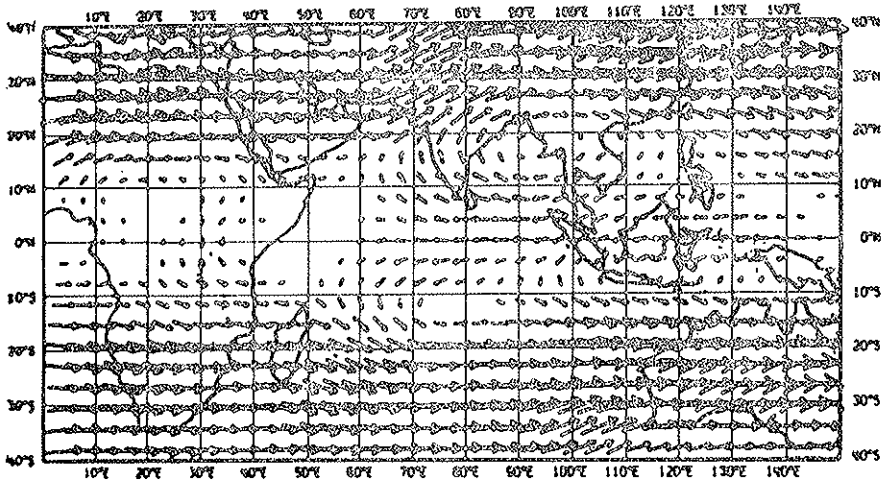

(a)

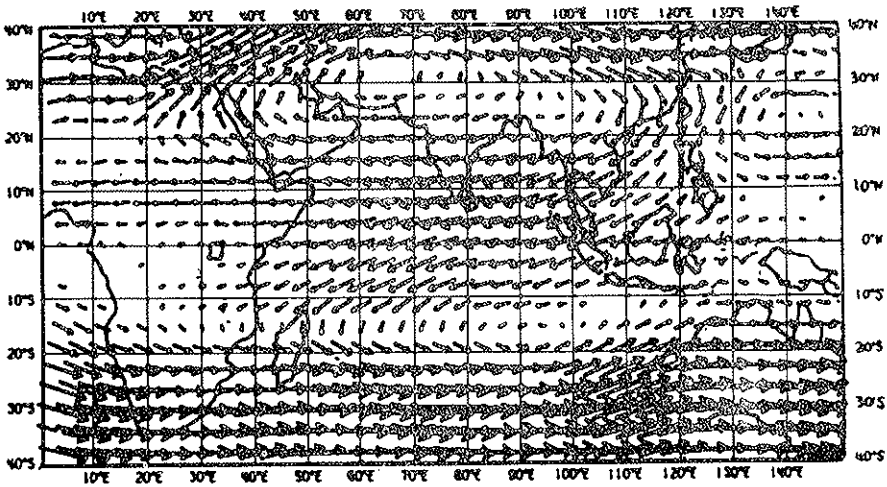

(b)

FIG. 3

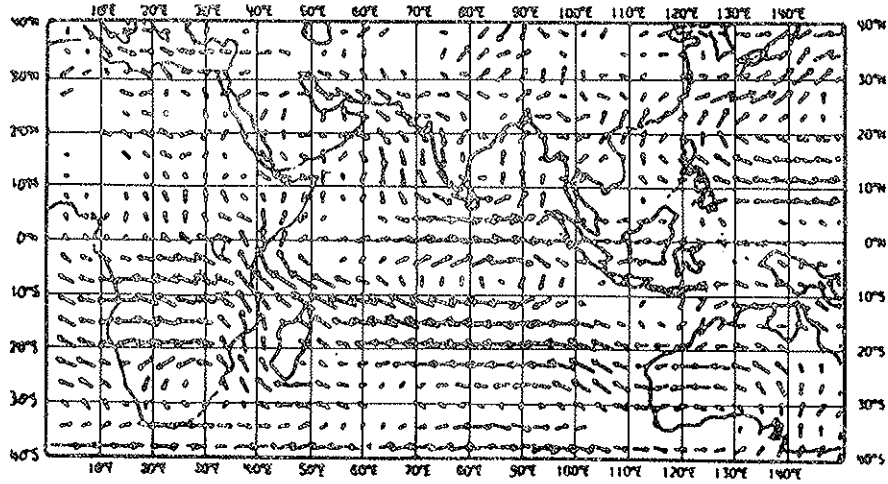

(c)

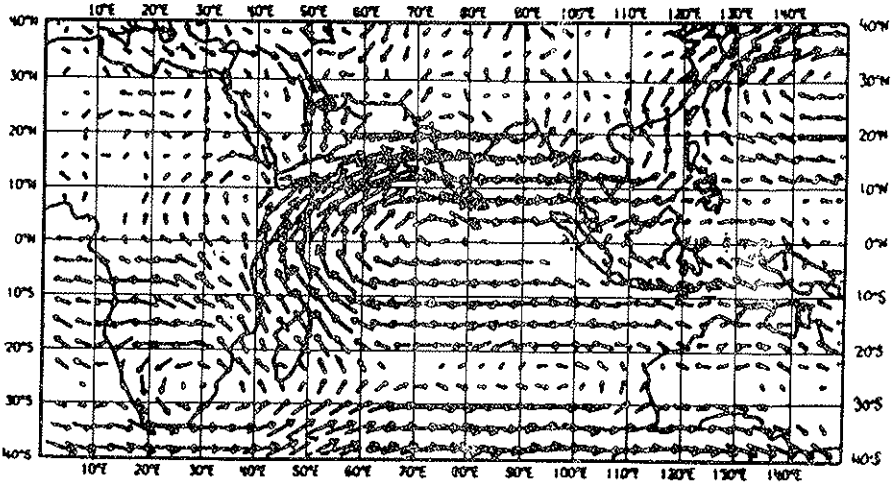

(d)

FIG. 3. Mean wind vectors (scale 1 mm = 10 m s^{-1} at 150 mb, 7 m s^{-1} at 850 mb); (a) 150 mb, Period 1 (1200 1 May 79 to 1200 15 May 79); (b) 150 mb, Period 4 (1200 16 Jun 79 to 1200 30 Jun 79); (c) 850 mb, Period 1 and (d) 850 mb, Period 4.

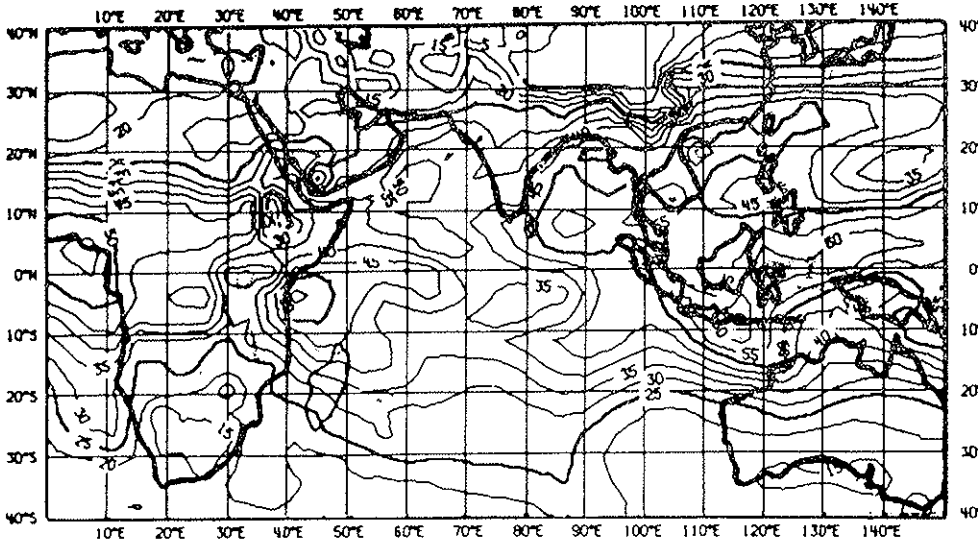
10°E 20°E 30°E 40°E 50°E 60°E 70°E 80°E 90°E 100°E 110°E 120°E 130°E 140°E
40°N 30°N 20°N 10°N 0°N 10°S 20°S 30°S 40°S

(a)

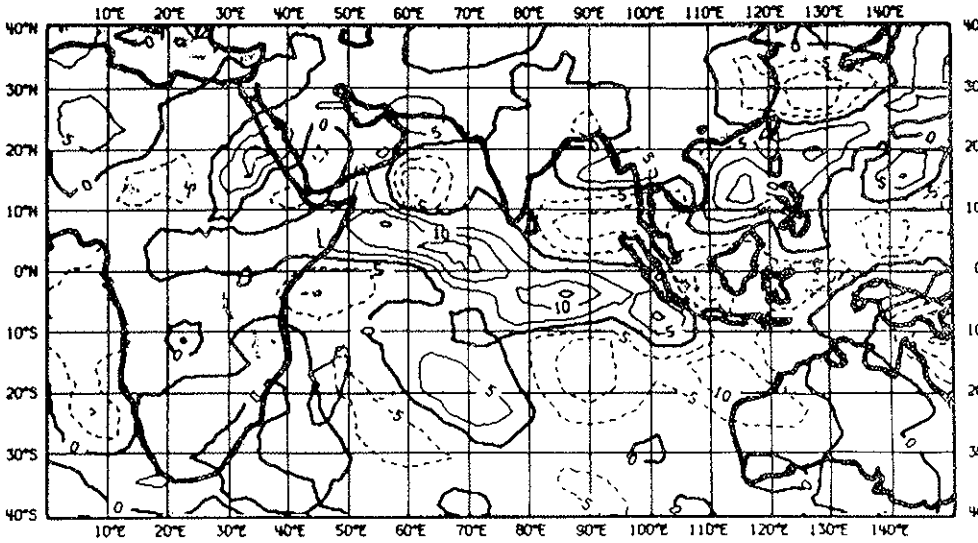
10°E 20°E 30°E 40°E 50°E 60°E 70°E 80°E 90°E 100°E 110°E 120°E 130°E 140°E
40°N 30°N 20°N 10°N 0°N 10°S 20°S 30°S 40°S

(b)

FIG. 4

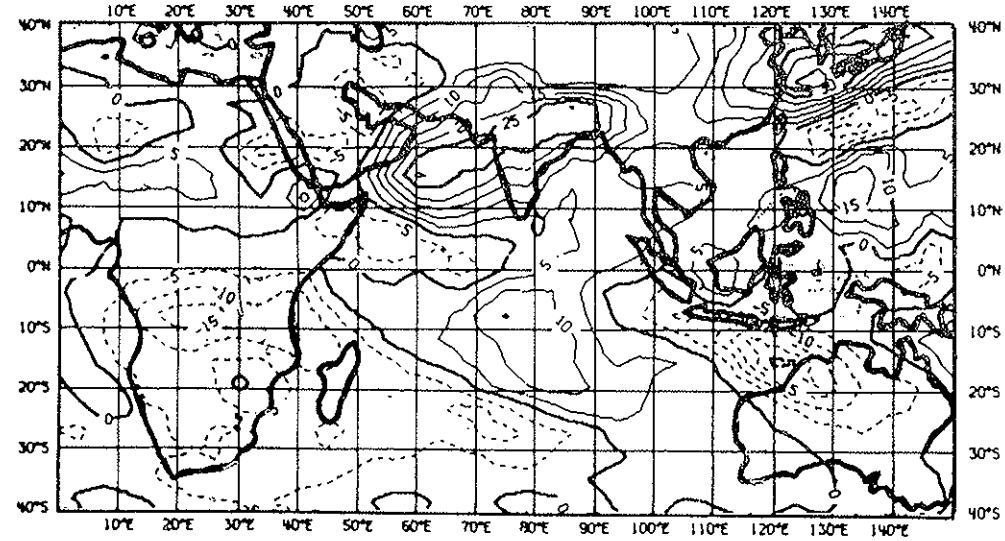

(c)

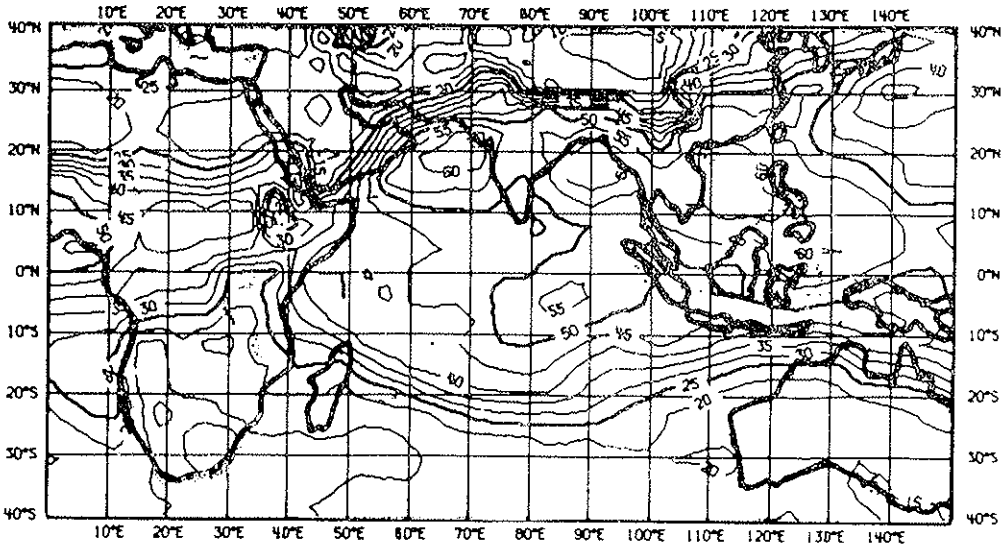

(d)

FIG. 4. Mean net tropospheric moisture $\hat{q}$ in mm: (a) period 1 and (d) Period 4. Increase in $\hat{q}$ (mm) between (b) Period 1 and Period 2, and (c) Period 2 and Period 4. Solid lines denote positive and dashed lines negative values.

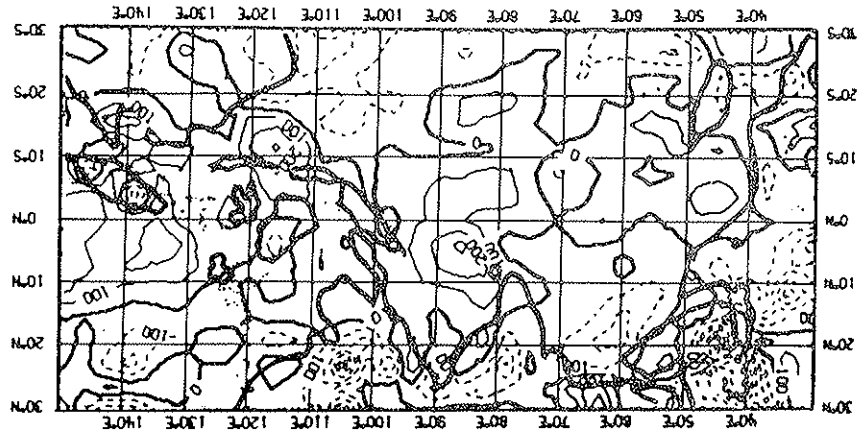

(a)

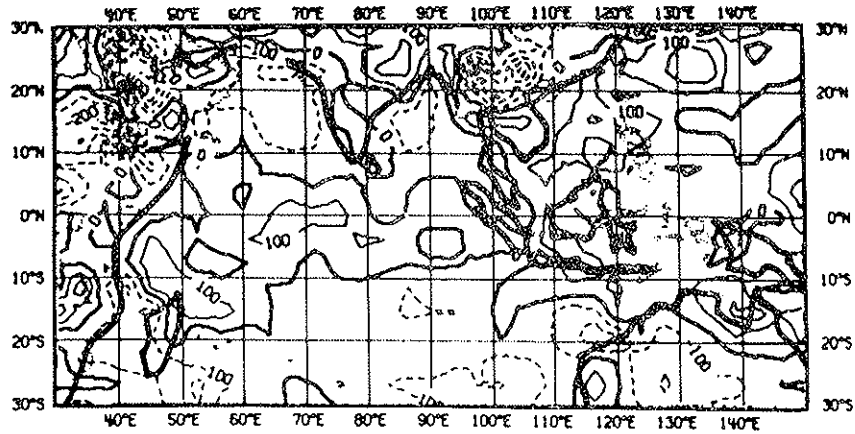

(b)

FIG. 5

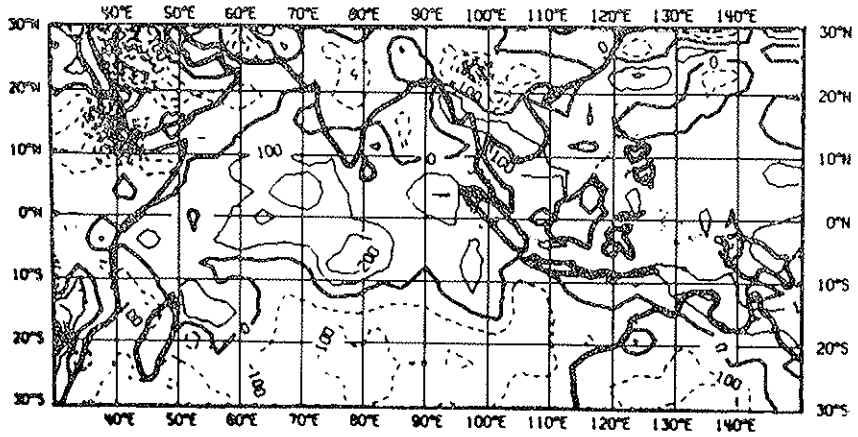

(c)

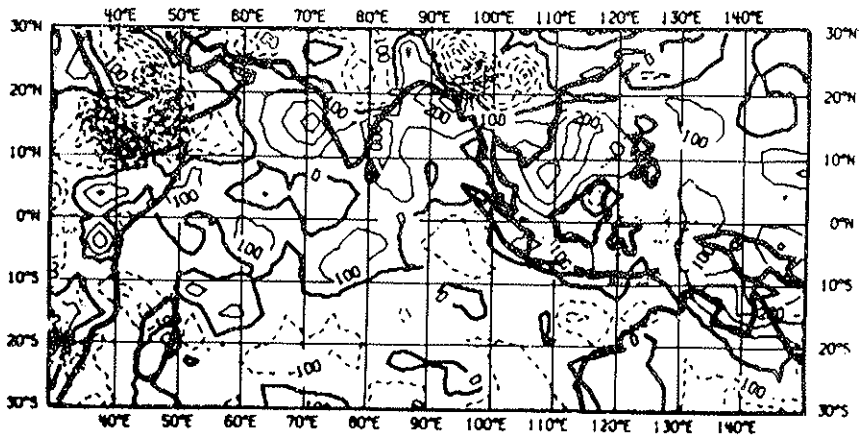

(d)

FIG. 5. Net tropospheric heating (W m^{-2}) for (a) Period 1, (b) Period 2, (c) Period 3 and (d) Period 4.

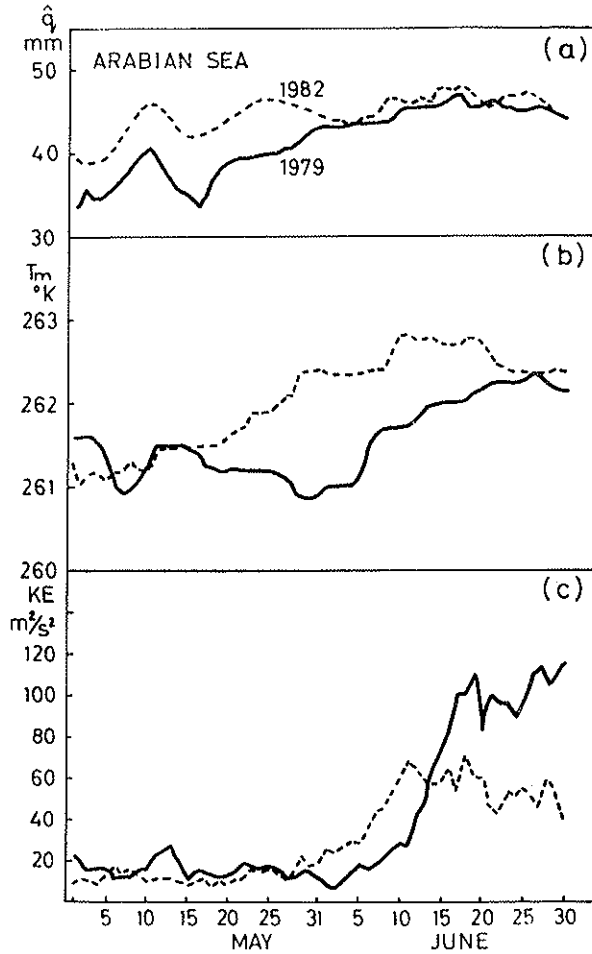

FIG. 6. Time sequences for Region C (0 - 22.5°N, 41.25 - 75°E) of daily (1200) values of (a) total moisture $\hat{q}$ in mm, (b) mean tropospheric temperature T_m; and (c) mean kinetic energy per unit mass of 850 mb flow. Solid curves 1979, dashed curves 1982.

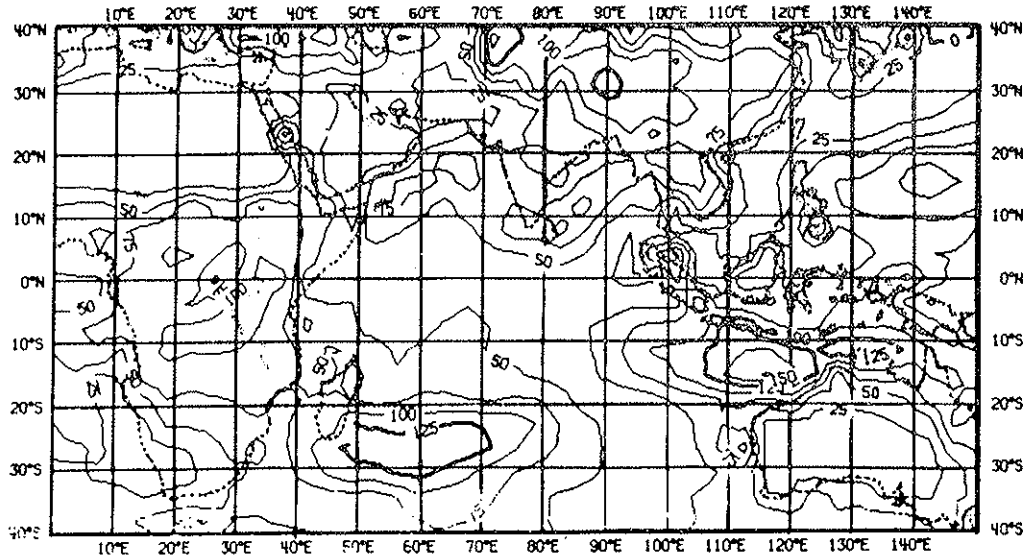

(a)

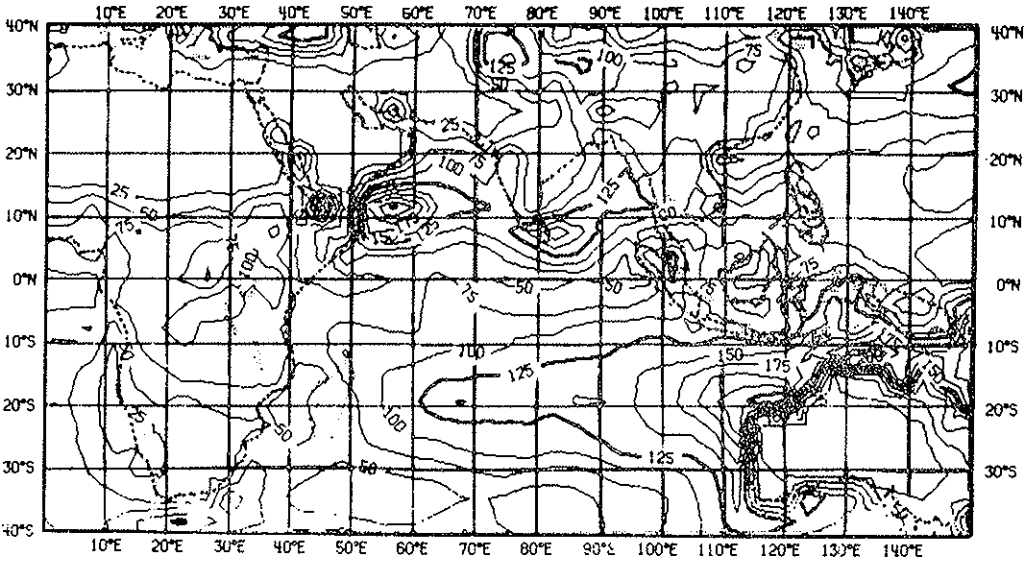

(b)

FIG. 7. Mean surface flux of latent heat (W m $^{-2}$) for 1982 for (a) Period 1 (1-15 May) and (b) Period 4 (16-30 June).

(c) The extensive cross-equatorial flow at 150 mb in the second half of June, when the monsoon is fully established (Fig. 3 (b)).

These features suggest that the monsoon onset process comprises two phases — a moisture build-up over the Arabian Sea followed by a rapid intensification involving feed-back between low-level winds (surface moisture flux) and large-scale latent heat release. Also that when fully established both hemispheres are intimately linked with strong cross-equatorial flow, northwards at low levels and southwards in the upper troposphere.

Similar analyses carried out using ECMWF archived operational initialised fields for subsequent years show that these features are typical of the onset process, although the actual date of the start of the intensification period may vary. Time sequences for 1982 of total moisture, mean tropospheric temperature and kinetic energy per unit mass at 850 mb over the Arabian Sea are shown in Fig. 6. This was a more typical year than 1979, in which the onset date over S. India (13 June) was later than the 'normal' date of 31 May, and the intensification more pronounced (in comparing these time sequences the much poorer data coverage in 1982, particularly of moisture, must be borne in mind).

4. Modelling the onset

There have been several recent attempts at modelling the intensification phase of the 1979 monsoon onset, e.g., Krishnamurti *et al.* (1984), Mohanty *et al.* (1984) and Kershaw (1985). Full details of the present status of the numerical prediction of the onset are given by other contributors to this report; only a brief outline is presented here.

Both Krishnamurti (1984) and Kershaw (1985) succeeded in simulating the 'onset vortex', a cyclonic storm in the eastern Arabian Sea the occurrence of which coincided with the 1979 onset of the monsoon rains over S.W. India but which is not observed every year. Krishnamurti emphasises the importance of correctly specifying the initial state, including convection and also the steepness of the orography if the vortex is to be properly predicted; Kershaw emphasises the importance of including correct sea-surface temperatures.

Mohanty *et al.* (1985) describe a series of numerical experiments on the 1979 monsoon onset with different convective and radiative schemes in the ECMWF operational prediction model. They emphasise that the

most realistic results, including simulation of the upper tropospheric cross-equatorial flow during the intensification phase, are obtained only when the (1985) operational Kuo convective scheme and radiation schemes are modified and a shallow convection scheme is added.

Fig. 8 shows their time sequences of the simulated KE of the 850 mb winds over the Arabian Sea together with those obtained by Krishnamurti and Kershaw over almost the same region. Fig. 9 shows meridional cross-sections of the 10-day averaged meridional wind zonally meaned over 45°E-75°E, observed and simulated by Mohanty *et al.* The upper cross-equatorial flow in the fully modified case (Fig. 9d) is particularly evident, being in close agreement with the observed distribution (Fig. 9a).

One aspect of the prediction of the monsoon onset on which all modellers agree is that it is extremely sensitive to its representation of moisture in low latitudes. The model convection and radiation are both highly sensitive to the moisture distribution and there is strong feedback, particularly in the tropics, with the low-level winds and surface moisture transfer over the oceans. Observations suggest that it is precisely these processes which are involved in the monsoon onset. The numerical experiments described above illustrate this sensitivity. However, even with the FGGE data coverage, the initial moisture fields are subject to quite large error (see, e.g., Cadet (1983)). The situation with operational data

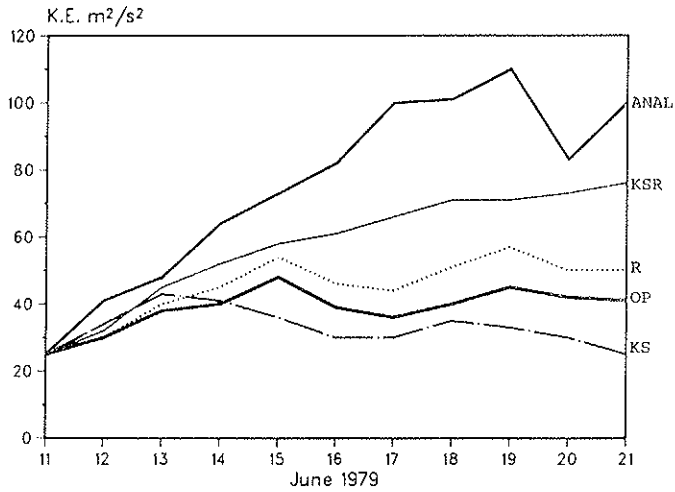

FIG. 8. Time series of the kinetic energy of the 850 mb flow over the Arabian Sea region (0-22.5°N, 41.25° - 75°E). See Fig. 9 for legends.

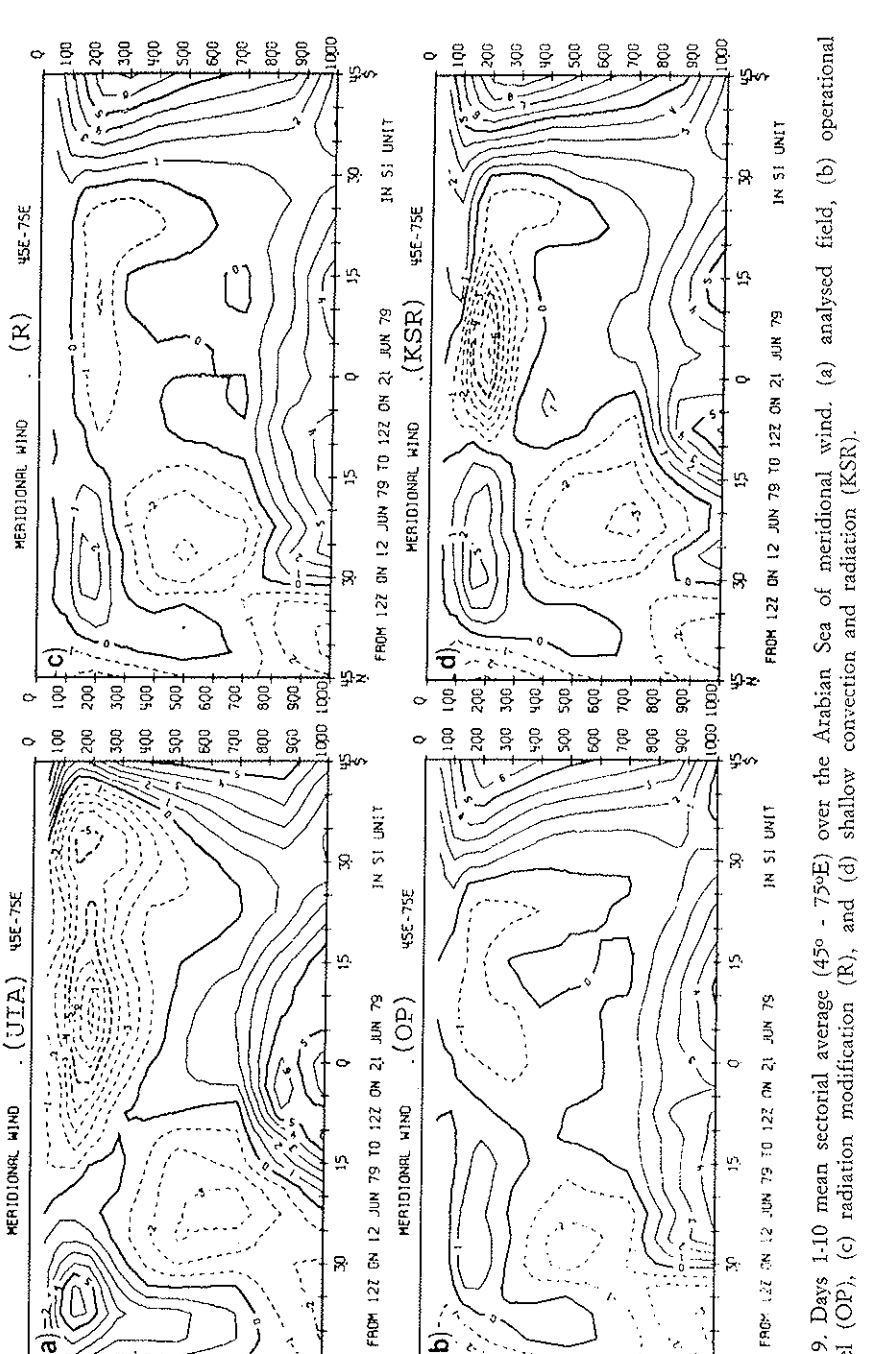

FIG. 9. Days 1-10 mean sectorial average (45° - 75°E) over the Arabian Sea of meridional wind. (a) analysed field, (b) operational model (OP), (c) radiation modification (R), and (d) shallow convection and radiation (KSR).

in subsequent years up to the present time is appreciably worse, with approximately half the FGGE year coverage over the Indian Ocean. One of the most urgent requirements for the improvement of monsoon onset predictions is an increase in data over the monsoon region, particularly the Arabian Sea and the low-latitude Indian Ocean.

5. A simple model of the ITCZ and the Asian monsoon

Interesting insight into the dynamics of the monsoonal flow is provided by a simple two-dimensional model of the tropical belt. Such models have been considered by other authors, e.g., Webster (1983) who inferred from a coupled air-sea model that the hydrological cycle could be responsible for low-frequency monsoon variability. The model considered here, however, regards the monsoon convection as concentrated into a narrow zonal strip and examines the factors controlling its location. The essential characteristics of the model are that it assumes that

(i) thermodynamically the region is almost everywhere subject only to radiative cooling; only in a relatively narrow zonal band does latent heat release occur;

(ii) the low-level wind is zero at the lateral boundaries (the latitudes of the centres of the low-level anticyclones), the positions of the boundaries being determined by the planetary-scale dynamics; and

(iii) the msl pressure at the lateral boundaries is also determined by the planetary-scale dynamics.

Consider the vorticity equation applied to the steady-state boundary layer on the equatorial β-plane, with all variables independent of longitude (x), i.e.

$$v\left(\frac{\partial \zeta}{\partial y}+\beta\right)+w\frac{\partial \zeta}{\partial z}=(f+\zeta)\frac{\partial w}{\partial z}-\alpha\zeta\ , \qquad (1)$$

α is a constant friction parameter, and each of the variables is taken as a mean over the layer $0 \leqslant z \leqslant H$. Thus $w \cong \frac{w(H)}{2}$, $\zeta \cong \zeta(H)/2$ and

$w \dfrac{\partial \zeta}{\partial z} \cong \zeta \dfrac{\partial w}{\partial z} \cong \dfrac{w(\mathrm{H})\zeta(\mathrm{H})}{2\mathrm{H}}$, and these terms approximately cancel. The vorticity equation is thus approximated as

$$0 = -v\left(\frac{\partial \zeta}{\partial y} + \beta\right) + \beta y \frac{\partial w}{\partial z} - \alpha\zeta \,. \tag{2}$$

Consider the boundary layer flow satisfying (2) in an equatorial strip $-\mathrm{Y} \leqslant y \leqslant \mathrm{Y}$ (Fig. 10). Take as boundary conditions

$$u = v = 0 \text{ at } y = \mathrm{Y}\,, y = -\mathrm{Y} \tag{3}$$

— assumed to be determined by planetary-scale processes. Suppose also that over most of the strip these processes (mainly radiative cooling) imply $w(\mathrm{H}) = w_0\,(< 0)$.

The mass continuity equation is taken as

$$\frac{\partial v}{\partial y} + \frac{\partial w}{\partial z} = 0 \tag{4}$$

so if $v(y)$ is to satisfy both (2) and (3) it must have at least one discontinuity; a form of v, with w_0 and H taken as constants, is

$$v = \begin{cases} \dfrac{w_0}{\mathrm{H}}(\mathrm{Y} - y)\,, & \mathrm{Y} \geqslant y > y_c \\ -\dfrac{w_0}{\mathrm{H}}(\mathrm{Y} + y)\,, & -\mathrm{Y} \leqslant y < y_c \end{cases} \tag{5}$$

This assumes a single discontinuity in v at $y = y_c$; its magnitude is $-\dfrac{2w_0\mathrm{Y}}{\mathrm{H}}$ (Fig. 10).

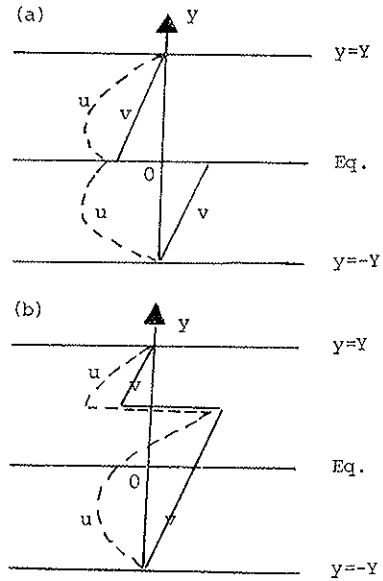

FIG. 10. Model distributions of u(y) and v(y) for (a) the symmetric case and (b) the asymmetric case with a region of westerlies.

Substituting (5) into (2), noting $\zeta = -\dfrac{\partial u}{\partial y}$ and $\dfrac{\partial w}{\partial z} = \dfrac{w_0}{H}$, and using the boundary conditions (3) gives

$$u = \begin{cases} -\dfrac{\beta}{\alpha'(1+\alpha')}(Y - y)(Y + \alpha' y), & Y \geqslant y > y_c \\ -\dfrac{\beta}{\alpha'(1+\alpha')}(Y + y)(Y - \alpha' y), & -Y \leqslant y < y_c \end{cases} \tag{6}$$

where $\alpha' = -\dfrac{\alpha H}{w_0}$ (> 0 for $w_0 < 0$ typically of order 5 to 10). Thus $u(y)$ is a pair of parabolic profiles (Fig. 10), with discontinuities at $y = y_c$. Note that at the equator u is always negative, equal to $-\beta Y^2/\alpha'(1 + \alpha')$,

and is zero at $y = \pm y_0$ where $y_0 = \dfrac{Y}{\alpha'}$, thus westerlies can occur only if $y_c > y_0$.

This idealised solution of the vorticity equation with its discontinuities in v and u can be reconciled with the physical system if the discontinuity is interpreted as a narrow strip of width Δy in which strong convergence and ascent ($w(H) = w_c > 0$) occurs with v changing sign and u and v continuous across it. Continuity of mass is assured if $w_c \Delta y + (2Y - \Delta y) w_0 = 0$, i.e., $w_c = -w_0 \left(\dfrac{2Y}{\Delta y} - 1 \right) \cong - \dfrac{2 w_0 Y}{\Delta y}$ and (2) may be satisfied approximately by suitable choice of Δy. The implication of the position of this zone on the surface moisture flux is now considered. (It may, in fact, be inferred from the zonal momentum equation that, in the absence of a zonal pressure gradient, the convective region can exist only if westerlies are present, i.e., with $y_c > y_0$). This flux is assumed to be proportional to the area-averaged value of $\hat{V}$ of the low-level wind speed $V (u^2 + v^2)^{1/2}$). Figure 11 is a graph of $\hat{V}$ as a function of the latitude of the convective region y_c. This shows the increase of $\hat{V}$ with y_c, and, by implication, the increase in the surface moisture flux with the northward progression of the convergence zone. However, this increase is not large — only a few percent as the zone moves north from the position of minimum moisture transfer (around 15°N) to 25°N.

An important constraint on the northward extent of the convergence zone is obtained if the low-level pressure (or geopotential ϕ_s) difference across the zone is considered. The meridional component of the momentum equation is

$$v \frac{\partial v}{\partial y} + \beta y u = - \frac{\partial \phi_s}{\partial y} - \alpha v \ . \qquad (7)$$

Continuity of ϕ_s at the convection zone enables (7) to be integrated across the entire model strip for any value of y_c using (5) and (6), to give $\Delta\phi_s = \phi_s(Y) - \phi_s(-Y)$. Fig. 12 shows $\phi_s(y)$ for a prescribed value of y_c and Fig. 13 is a graph of $\Delta\phi_s$ as a function of y_c.

If now it is assumed that, across the monsoon region, $\Delta\phi_s$ is determined by planetary scale effects, including heating of the Asian land mass, it is seen that this imposes a limitation on the value of y_c. Taking a typical

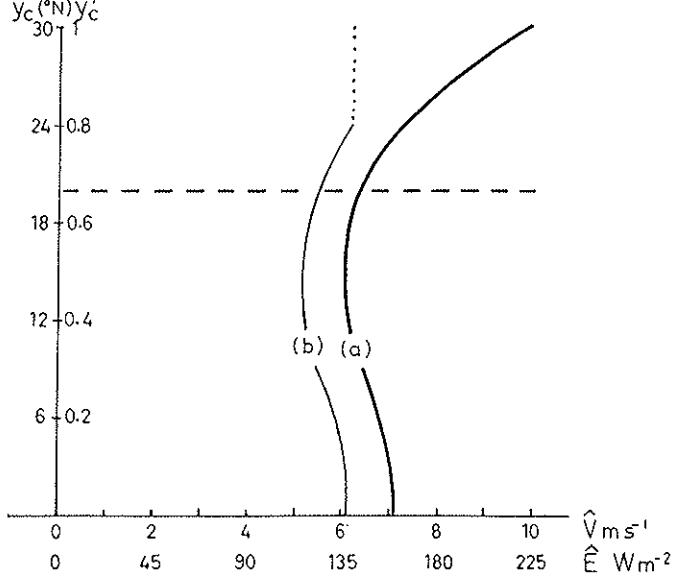

FIG. 11. Model mean wind speed over the tropical belt $\hat{V}$ in m s^{-1} (a) 30°S to 30°N and (b) 30°S to 24°N) as a function of the latitude of the convection zone y_c. Also shown are the mean evaporation rates $\hat{E}$ in W m^{-2} (weighted in (b) by 0.9, the assumed fraction of the width occupied by ocean) using the formula $\hat{E} = c_D \rho_s \hat{V} L(q_{sat}(T^*) - q(T_s))$; here $c_D = 1.5 \times 10^{-3}$, $\rho_s = 1.2$ kg m^{-3}, $L = 2.5 \times 10^6$ J kg^{-1} and $q_{sat}(T^*) - q(T_s)$, the water vapour mixing ratio difference between the sea surface and air at ship deck level, is taken as 5×10^{-3}. The values of the friction parameter α and boundary layer divergence are taken as 4×10^6 s^{-1} and 10^{-6} s^{-1} respectively. The dashed line corresponds to 20°N.

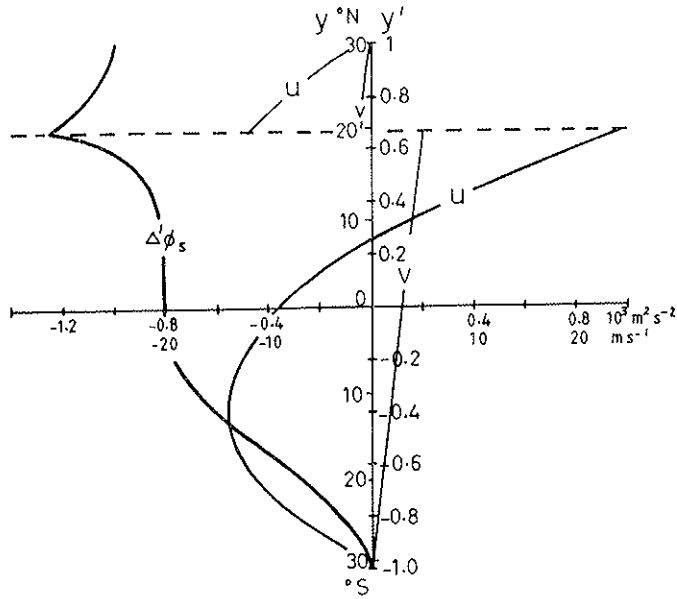

FIG. 12. The geopotential difference $\Delta'\phi_s = \phi_s(y') - \phi_s(-1)$ in 10^3 m^2 s^{-2} as a function of y' with the convection zone at 20°N (dashed). Also shown (thin lines) are the distributions of zonal wind u and meridional wind v in m s^{-1} satisfying Eqs. (5) & (6) with $\gamma' = 2/3$

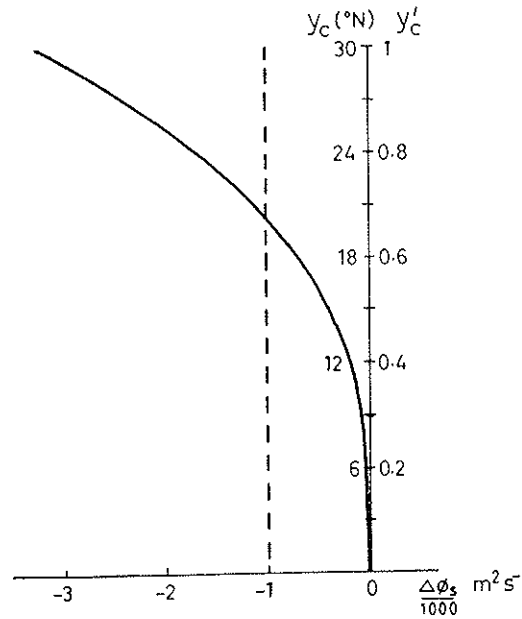

FIG. 13. Latitude of the model convection band (y_c) as a function of the sea-level geopotential difference across the tropical belt 30°S to 30°N ($\Delta\phi_s$ in 10^3 m^2 s^{-2}). The dashed line corresponds to the observed June-August climatological value of $\Delta\phi_s$ in the Indian Ocean sector.

observed value of $\Delta\phi_s$ corresponding to the established monsoon as 1000 $m^2 s^{-2}$, and identifying the convection band as the monsoon trough, gives the position of the trough as at about 20°N.

A similar model may be constructed for the upper level outflow, linked to the boundary layer model. Fig. 14 shows such a solution with $v(y)$ equal in magnitude but opposite in sign to that in the boundary layer. To satisfy (2) the absolute vorticity is zero and the source of vorticity due to stretching just offsets the frictional sink.

Clearly zonal asymmetries play a very important role in the monsoon circulation and one must not draw conclusions on the basis of a zonally symmetric model concerning features which are strongly influenced by such asymmetries. The constraint on the position of the monsoon trough does, however, seem to be a very strong one, this not being very sensitive to the magnitude of $\Delta\phi_s$ when the latter reaches values typical of the summer mean over the tropical belt in the Asian sector; the convection band does

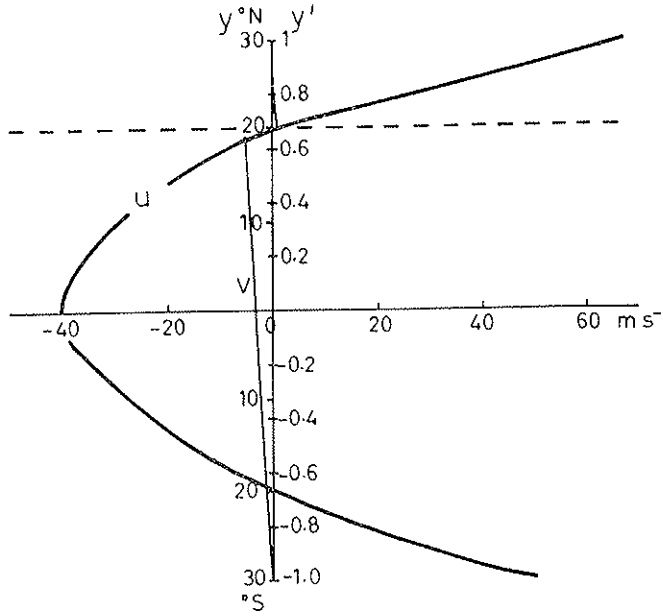

FIG. 14. Model outflow distributions of u(y′) and v(y′) for $y_c = 20°N$, taking v(y′) equal and opposite to the values in Fig. 12 and assuming $u = 0$ at $y = y_c$.

not extend much further north than 20° over the Arabian Sea. The model suggests that this is primarily because of the restriction on $\Delta\phi_s$ imposed by the planetary scale circulation and the surface heating over the Asian land mass. If the region were any further north, the westerlies would be too strong to be in near-geostrophic balance consistent with the low-level pressure gradient.

It is also reasonable to infer from the model that for feed-back involving surface moisture transfer from the ocean to occur, the convection zone must be able to exist poleward of about 15° and still be over the ocean. It is only when it reaches this latitude that further displacement polewards involves an increase in the surface evaporation, this being associated with the stronger westerlies. It is not perhaps surprising, therefore, that such an intensification is not observed in the case of the West African and Asian winter monsoons where the land-masses involved, North Africa and Australia, are not sufficiently far removed from the equator for westerlies to extend as far polewards as 15° and still be over the ocean in their respective sectors.

ACKNOWLEDGEMENTS

The author would like to express his gratitude to Dr. P. Sardeshmukh for providing the climatological analyses referred to in this paper, and to the Director of ECMWF for allowing access to the ECMWF data archives; also to Mrs. N.F. Spicer for typing the manuscript.

REFERENCES

CADET D.L., *Mean fields of precipitable water over the Indian Ocean during the 1979 summer monsoon from TIROS-N soundings and FGGE data.* « Tellus », *35B*, 329-345 (1983).

KERSHAW R., *Onset of the south-west monsoon and sea-surface temperature anomalies in the Arabian Sea.* « Nature », *315*, 561-563 (1985).

KRISHNAMURTI T.N., INGLES K., COCKE S., KITADE T. and PASCH R., *Details of low latitude medium range weather predictions using a global spectral model.* II. *Effects of orography and physical initialisation.* « J. Met. Soc. Japan », *62*, 613-649 (1984).

MOHANTY U.C., PEARCE R.P. and TIEDTKE M., *Numerical experiments on the simulation of the 1979 Asian Summer Monsoon.* Tech. Rep. No. 44, ECMWF, Reading, U.K. (1984).

MOHANTY U.C., SLINGO J.M. and TIEDTKE M., *Impact of modified physical processes on the tropical simulation in the ECMWF model.* Tech. Rep. No. 52, ECMWF, Reading, U.K. (1985).

PEARCE R.P. and MOHANTY U.C., *Onsets of the Asian Summer Monsoon 1979-83.* « J. Atmos. Sci. », *41*, 1620-1639 (1984).

WEBSTER P.J., *Mechanisms of low-frequency variability: surface hydrological effects.* « J. Atmos. Sci. », *40*, 2110-2124 (1983).

LONG RANGE FORECASTING OF SUMMER MONSOON RAINFALL OVER INDIA

J. SHUKLA, D.A. MOOLEY and D.A. PAOLINO
Center for Ocean-Land-Atmosphere Interactions
Department of Meteorology, University of Maryland
College Park, Maryland 20742

1. Introduction

The monsoon rains are perhaps the most important natural phenomena that sustain the large agrarian populations of Asia. On an annual time scale, there is a remarkable degree of regularity in the occurrence of the rainy season; however, there are large interannual variations in the amount of seasonal rain, its space-time variability and the timings of the onset and withdrawal of the rains. The agricultural production, the availability of drinking water and the generation of hydro-electric power critically depend upon these fluctuations. Because of the unique geographical location of India, the atmospheric circulation displays a spectacular annual cycle of rainfall in which more than 80% of the annual rain falls during the summer monsoon season comprised of the months June through September. Attempts to predict seasonal rainfall over India started more than 100 years ago. (The present paper is an outgrowth of a lecture given by one of the authors [J.S.] at an international conference held at New Delhi during April, 1986, to celebrate 100 years of long-range forecasting of monsoon rainfall over India). It is natural that considerable efforts have been made towards diagnosing the interannual variability and predicting the onset, withdrawal and total amount of monsoon rains. In this paper we shall confine our discussion mainly to the long-range forecasting of summer monsoon rainfall over India. However, in order to provide a suitable context to the prediction problem, we give below a summary of main conclusions drawn from

various diagnostic studies on interannual variability of monsoon rainfall (Shukla, 1986; Mooley and Shukla, 1987).

a. Long term seasonal mean (June, July, August, September) rainfall over India is about 850 mm, its standard deviation is about 84 mm and the coefficient of variability is about 10%. The standard deviation of the percentage departure from normal rainfall for seasonal and monthly averages is about 13% and 25% respectively, and it reduces only to 21% if the seasonal mean is removed before calculating the standard deviation of the monthly percentage departure.

b. During the past century monsoon rainfall over India was more than one standard deviation above normal about 15% of the time and more than one standard deviation below normal about 18% of the time. For convenience we will refer to these years as excess rainfall years and deficient rainfall years, respectively. All the remaining years with the absolute value of the rainfall anomaly being less than one standard deviation would be referred to as the normal rainfall years.

c. During the excess rainfall years and the deficient rainfall years, the rainfall anomaly over most of India is of the same sign with the exception of northeast India where it is of the opposite sign and of small magnitude. This suggests that the spatial scales of the seasonal mean anomalies are quite large.

d. During the excess rainfall years and the deficient rainfall years, the monthly mean rainfall anomaly for each of the four individual months is generally similar to the seasonal mean rainfall anomaly. This is particularly true for the drought years. This suggests that the major anomalies of monsoon rainfall are not only of large scale but also persist for the entire season. However, for a large number of normal rainfall years there is a large month to month rainfall variability.

e. It is only during the excess and deficient rainfall years that significant anomalies of the global circulation are also observed.

f. It is reasonable to conjecture that intraseasonal fluctuations of monsoon rainfall are related to differences in the characteristics of the synoptic scale disturbances, quasi-periodic oscillations and interactions with circulation in the midlatitudes.

g. There appears to be a good potential for predictability of the large space-time average circulation and rainfall because they are related to the slowly varying global boundary conditions, and low-frequency planetary scale fluctuations. The degree to which the regional intraseasonal fluc-

tuations can be predicted is uncertain because they appear to be caused by internal dynamical processes.

In the next section we present a historical review of the early efforts of Walker and his predecessors to predict monsoon rainfall. In section 3, we summarize the current efforts to search for possible relationships between monsoon rainfall and a variety of atmospheric circulation parameters. In section 4, we present an empirical method for predicting monsoon rainfall over India, and in section 5, we present concluding remarks and our opinions on the prospects for the future.

2. Historical Review

A large number of monsoon failures over India during the nineteenth century and the adverse impact of these failures on the economy ultimately led to the establishment of the India Meteorological Department in September 1875 for the improvement of meteorological observations in India and for study of weather and climate of India. Shortly thereafter, the country was struck in 1877 with severe drought over most parts of the country, resulting in intense suffering by the people. The government of India constituted the First Famine Commission to look into the Indian famines and suggest remedial measures. The Famine Commission collected valuable data for all past famines from 1770 and submitted a report to the government in 1880. After considering the report, the government took action on the recommendations of the commission. H. F. Blanford, the Meteorological Reporter was called upon by the government of India to take action for preparation of monsoon forecasts. Blanford (1884), who studied meteorological conditions in relation to the monsoon rainfall of India, concluded that Himalayan snow cover could influence climate and weather of the plains of India. He postulated that excessive winter and spring snowfall in the Himalayas and Hindukush delays the advance of summer monsoon and results in less rainfall during monsoon season. He also observed that droughts may be associated with high pressure in Mauritius, Australia and over a great part of Asia. He issued tentative forecasts of monsoon rainfall for the years 1883-85 on the basis of snowfall in the Himalayas. The success achieved by these tentative forecasts created a climate of confidence, and it was decided in 1885 that a monsoon forecast be issued routinely every year. The first regular forecast for India and Burma was prepared on

June 4, 1886, on the basis of general weather conditions over India and on snowfall in the Himalayas and Sulaiman range during January-May preceding the monsoon.

Sir John Eliot, who succeeded Blanford in 1887, included conditions over the whole of India as a predictor parameter, and in the next year he also included the conditions over the Bay of Bengal and the Arabian Sea. In 1888 and 1889, the forecast consisted of two parts — the preliminary memorandum issued in the third week of May and the final memorandum issued about the 9th of June. From 1890, the preliminary memorandum was dropped. The forecasts became more and more ambitious and the size of the forecast grew from 3 pages in 1886 to 22 pages in 1892. India experienced another great famine in 1899 which was not predicted and the newspapers made scathing comments on the forecasts. In 1902, the Government decided that forecasts should be issued only to the Provincial Governments as confidential documents. However, in 1906, the Government decided that forecasts of (i) monsoon rainfall, (ii) August-September rainfall and (iii) winter (December-February) rainfall be prepared regularly and after approval by the Government be published in the Gazette of India supplement.

Sir Gilbert T. Walker, a Senior Wrangler at Cambridge, succeeded Eliot in 1904. Walker knew that an accepted theory of general circulation was necessary for putting seasonal prediction on a scientific basis. He argued that in the absence of such a theory statistical studies can be pursued since the results of such studies are likely to give clues to a possible physical basis. He commenced studies of statistical relationships, both concurrent and antecedent, between Indian weather and world weather. His studies on world weather confirmed two pressure oscillations — North Atlantic (between the Azores high and Icelandic low) and North Pacific (between the North Pacific high and the Aleutian low). His search for global predictors for forecasting Indian monsoon rainfall brought out the important result that the oscillation suggested by Hildebrandson (1897) and confirmed by Lockyer and Lockyer (1904) as a pressure see-saw between the Indian Ocean and Argentina is a very large-scale phenomenon. For the first time Walker called this phenomenon the Southern Oscillation. He described this oscillation as a tendency for air to be removed from the Pacific areas for accumulation in and around the Indian Ocean and vice versa. As mentioned by Normand (1953), the most remarkable of Walker's results was the discovery that the June-August Southern Oscillation Index had a correlation coefficient of 0.8 with the

same index for the following winter season (December-February) and only 0.2 with that for the preceding winter.

Walker (1910) developed regression equations with the predictors: snow accumulation over the Himalayas at the end of May, South American pressure (mean of March, April and May), May Mauritius pressure, Zanzibar rain for April and May, for forecasting monsoon rainfall over India and Burma. During 1907 and 1908, this regression equation was used only as a guide to the inferences drawn from the current forecast method in use. The issue of official forecasts based on Walker's regression equation commenced from 1909. The objective approach of Walker's forecast method helped in the deletion of detailed discussions about the behavior of the factors and their anticipated influence on monsoon rainfall and thereby considerably reduced the size of the forecast memorandum.

Walker also examined the relationship between solar activity, as measured by the annual value of the mean sunspot number, and meteorological parameters at many stations. Based on his empirical studies, Walker was apparently convinced about the reality of the solar-weather relationship, but he concluded that sunspot numbers play only a minor role in influencing the seasonal weather over India.

Up to 1915, the monsoon forecasts were being issued for the whole of India and Burma. Thereafter, Walker divided the country into four fairly homogeneous divisions on the basis of correlation with the predictors, and forecasts for these divisions were being issued till 1922 when the areas were again revised. On partition of India in 1947, the areas were changed. In 1961, the areas were changed again. Fig. 1 shows the subdivisions of India.

After several revisions of the predictors and divisions of India, Walker (1924) developed in 1924 the following regression equations for forecasting the normalized anomaly of monsoon rainfall over Peninsular (ΔRP) and Northwest India (ΔRNW).

$$\Delta RP = 0.20P_1 - 0.32P_2 - 0.24P_3 - 0.22P_4 - 0.26P_5 - 0.12P_6 \quad (1)$$

$$\Delta RNW = 0.04P_1 - 0.14P_4 - 0.48P_5 - 0.30P_7 - 0.24P_8 - 0.06P_9 \quad (2)$$

where the predictor parameters are,

P_1 = normalized anomaly (i.e., anomaly divided by standard deviation) for April and May South American Pressure (mean of Santiago, Buenos Aires and Cordoba)

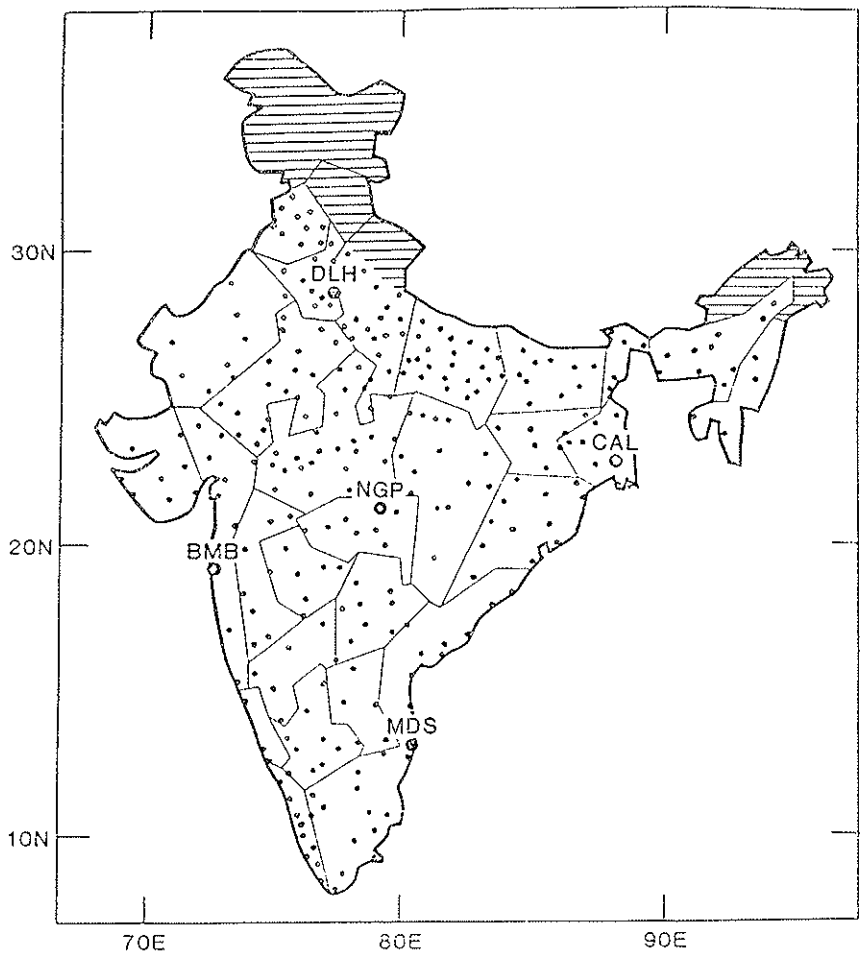

FIG. 1. Locations of the stations and the subdivisions for which rainfall is averaged. Hatching indicates the hilly regions not included in the averaging.

P_2 = normalized Zanzibar May rainfall anomaly
P_3 = normalized Java rainfall (October-February) anomaly.
P_4 = normalized Cape Town pressure (September-November) anomaly
P_5 = normalized South Rhodesian rainfall (October-April) anomaly
P_6 = normalized Dutch Harbor temperature (December-April) anomaly
P_7 = normalized anomaly of snow accumulation over the western Himalayas by the end of May

P_8 = normalized anomaly of Dutch Harbor temperature (March-May)
P_9 = normalized anomaly of equatorial pressure.

Equatorial pressure = 1/3 [1/2 Seychelles Pressure (February + March) + 1/4 Batavia Pressure (January-April) + 1/3 Port Darwin Pressure (March-May)]

Walker (1924) has mentioned that the multiple correlation coefficient between monsoon rainfall and the predictors used is 0.76 for peninsular as well as northwest India monsoon rainfall.

Until 1955, the predictors used in the regression equations for forecasting monsoon rainfall were from the surface or sea level. In 1956, Calcutta and Bangalore upper level winds were introduced as predictors in the regression equation for forecasting Peninsular monsoon rainfall, and Agra-Gwalior and Calcutta upper level winds in the regression equation for forecasting northwest India monsoon rainfall.

For the first time, Jagannathan and Khandekar (1962) examined the relationship between contour heights of different isobaric surfaces up to 400 mb at Indian radiosonde stations for the months March through May and Indian Peninsular monsoon rainfall, based on the data for 1944-58. They showed that the height and thickness between two pressure levels for some locations are useful predictors. Utilizing these predictors, they obtained three regression equations based on all data up to 1958 and verified for one independent year 1959. The three regression equations gave forecast departures of Peninsular rainfall as 7.5, 7.9 and 6.1 inches against the actual departure of 11.2 inches.

At present, the India Meteorological Department gives its long-range forecast in seven categories, large defect ($\leq$ 50% of normal), moderate defect (50% to 74% of normal), slight defect (75% to 89% of normal), normal (90% to 110% of normal), slight excess (111% to 125% of normal), moderate excess (126% to 150% of normal) and large excess ($>$ 50% of normal) (Thapliyal, 1981). Normand (1953), Jagannathan (1960) and Rao (1964) have reviewed the seasonal forecasting of monsoon rainfall in India.

Ramdas *et al.* (1954) evolved a regression equation for forecasting the date of establishment of the summer monsoon over Travancore-Cochin (the present Kerala state), south Kanara, Ratnagiri district and Colaba district. They used April Seychelles rain, mean westerly wind component over Agra (or average of Delhi and Gwalior) from 1 to 3 km during the first half of May, April Darwin pressure, Cochin pressure minus Jaipur pres-

sure in April, October-April south Rhodesian rainfall and April Rhodesian rainfall as predictors. The regression equations were developed on the basis of all available data up to 1950. They have not given any verification on independent years 1951-54. However, on the basis of the general indication of the behavior of the predictors, they have inferred for these independent years whether the onset over the west coast (which covers all the four areas) would be about the normal date, not far from the normal date, later than a particular date or earlier than a particular date, and have tried to verify such general forecasts for the west coast.

Montgomery (1940a,b) who reviewed the work of Walker examined the stability of the predictors used by Walker (1910, 1922, 1924) in the preparation of forecasting formulae for monsoon rainfall, by computing the correlation coefficients between monsoon rainfall and these predictors for later periods and comparing these correlation coefficients with those obtained by Walker. Among the predictors used by Walker in his 1924 formula for forecasting of monsoon rainfall for Peninsular India, Montgomery (1940b) found that South American pressure, Dutch Harbor temperature and south Rhodesian rainfall have maintained their original correlation, and have thus exhibited stability. In this connection, it may be mentioned that the lengths of periods over which the correlation coefficients for the predictors for forecasting Peninsula monsoon rainfall have been compared are very dissimilar, the periods used by Montgomery (1940b) being much smaller.

Jagannathan (1960) studied the stability of the different predictors used by the India Meteorological Department in the regression equations for forecasting the monsoon rainfall over Peninsular and northwest India over different decades of the period 1881-1960. According to him none of the predictors showed stable correlations over all the decades of the period. It may, however, be mentioned that a decade is perhaps too small for studying the stability of a relationship. The mean, standard deviation and covariance and consequently the correlation coefficients for 10-year periods are subjected to high random sampling fluctuations. In view of this, fading of the relationship, or change of the relationship from direct to inverse and vice versa could be due to random sampling fluctuations. On the basis of study by Jagannathan (1960), American pressure, Dutch Harbor temperature and Bangalore 6 km wind have shown good stability.

Montgomery (1940b) carried out verification of Walker's (1922, 1924) formulae for forecasting monsoon rainfall for the Peninsula. Using Walker's formulae, he computed the forecasts for the later periods 1920-

36 and 1924-36 and as a measure of verification of these forecasts he computed the correlation coefficients between the forecast and actual rainfall. For the 1919 and 1924 formula the correlation coefficients were 0.21 and 0.12. These small and nonsignificant correlation coefficients showed that the earlier good relationship was not sustained for later periods. Walker (1922, 1924, 1933) himself verified his forecasting formulae. He computed a forecast of All-India rainfall for the later periods 1909-21 and 1909-27 by using the "1908 forecast formula", and then computed correlation coefficients between forecast and actual rainfall. The correlation coefficients for these periods are 0.55 and 0.56, suggesting fairly good stability in the later periods. He also verified the two "1924 forecast formulae" for northwest India and Peninsula for the later period 1924-36. In all, there were 18 forecasts — 9 for northwest India and 9 for the Peninsula. According to Walker, forecasts should be issued only when there is a 4 to 1 chance of success. In 8 of these forecasts, this condition is satisfied but in 2 cases only the sign of the forecast departure is correct. On a careful scrutiny by Walker (1933) of the forecasts issued before the monsoon seasons of 1905-32, two-third were correct. However, the verification of such general forecasts is subject to uncertainty.

Normand (1953) verified the monsoon forecasts issued during the period 1931-48, 16 each for the Peninsula and northwest India for the whole season, and 14 for the Peninsula and 15 for northwest India for August-September rainfall. Of these 61 forecasts, 10 were wrong. On pure chance, the numbers of forecasts estimated wrong on the basis of a normal distribution, and on the basis of actual distribution for 1931-48 are 23 and 17, respectively. The number of the wrong forecasts allowable on the 4 to 1 standard was 12. Thus the regression forecasts have done much better than chance forecasts, but only slightly better on the 4 to 1 standard. However, the period 1931-48 is not quite typical in that it has experienced relatively less droughts. It was also found that the proportion of wrong forecasts for the worst monsoon years was 66 percent, which is large. Considering all these points, Normand posed the question, "Are the relationships, though real, now so small that they are of insufficient value for the issue of useful forecasts?" Finally, Normand (1953) expressed the hope that persistent patterns of flow in the middle or upper troposphere may prove to be of prognostic value, but lacking a background of theory we will still have to depend on statistical methods. As mentioned in Section 3, the development during the last decade, as hoped by Normand, has brought out the April ridge at 500 mb as a middle tropospheric

flow parameter characterized by some persistence and well-related to the Indian monsoon rainfall. However, we have yet to understand the physical mechanisms that produce statistically significant empirical relationships between monsoon rainfall and other circulation features.

3. Current Research

In this section we have summarized the results of several investigations that have appeared during the last 10 years. The current approach is not different from the one used by Walker more than 75 years ago in that empirical relationships are sought between monsoon rainfall and global circulation features; however, the choices of predictor parameters are different. We have divided this section into the following subsections to present separate descriptions of various predictor parameters.

3.1 Mid-tropospheric circulation over India

3.2 Boundary conditions at the Earth's Surface
- 3.2.1 Snow Cover
- 3.2.2 Sea Surface Temperature

3.3 Southern Oscillation

3.4 Surface Temperature over India

3.5 Surface Pressure over the Northern Hemisphere

3.6 Upper Air Flow over India

3.1 *Mid-Tropospheric Circulation over India*

The tropospheric circulation over India is characterized by the subtropical ridge, which can be identified at and above the 500 mb level along 75°E in the monthly mean wind charts. As observed from the normal charts (India Meteorological Dept., 1972), based on the data for 1951-65, the 500 mb ridge along 75°E is located at 11.5°N in January, 15°N in April, 28.5°N in July and 20°N in October (Fig. 2). The seasonal shift is largest from April to July, the period covering the transition from summer to the monsoon season. However, the mean seasonal shift from January to May is only 4-5° of latitude. Thus, during the onset and establishment of the monsoon during June and July, the normal 500 mb ridge location undergoes a rather large and rapid shift. At 200 mb level, the mean ridge shifts from 4°N in January to about 10°N in April and shifts

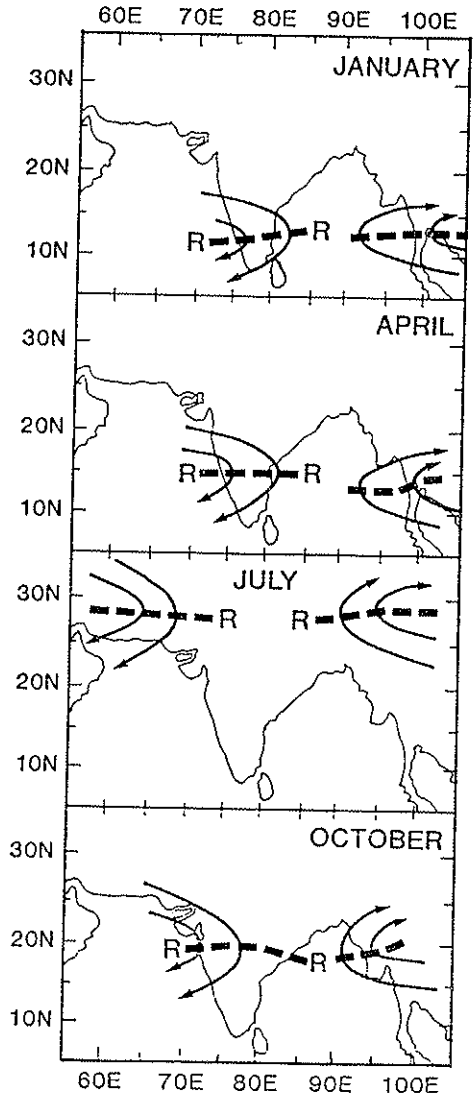

FIG. 2. Schematic representation of the climatological monthly mean circulation and location of the ridge (R) at 500 mb during January, April, July and October. Based on actual streamline maps published by the India Meteorological Department (1972).

further northward to 15°N in May and to 25°N in June. The shift in the 200 mb ridge is thus not regular. Moreover, due to paucity of wind observations at 200 mb in the earlier portion of the period, these normal charts do not adequately represent the ridge at this level. Since the observational coverage is much better at 500 mb level, it has become customary to use the ridge at 500 mb as a possible predictor parameter.

Interannual variability of the ridge during April through July

The Monthly Weather Report in the India Weather Review, published by the India Meteorological Department, includes a monthly 500 mb wind flow chart for India and neighborhood for the years 1948-67. The mean monthly locations of the 500 mb ridge along 75°E for the months April through July for each of the years 1948-67 were estimated from these flow charts by Shukla and Mooley (1986). From these mean locations of the ridge, the mean, standard deviation (S.D.) and the extreme locations of the ridge for the period 1948-67 have been obtained for the months April, May, June and July. These are given below. It should be noted that the ridge could not be located in June in 8 years, and in July in 2 years.

	April	May	June	July
Mean	15.7°N	18.6°N	23.1°N	28.3°N
S. D.	2.3°	2.4°	2.5°	2.4°
Northernmost location	19.5°N	24.5°N	26.5°N	31.6°N
Southernmost location	11.0°N	14.8°N	18.0°N	23.7°N

It can be seen that the range of variation of the ridge is about 8°-9° of latitude. The extremes are generally observed to lie within two standard deviations from the mean.

Relationship of the 500 mb ridge with rainfall

Banerjee *et al.* (1978) showed for the first time that the cube-root of the percentage of Indian meteorological subdivisions with normal or above normal monsoon rainfall (i.e., $\geq$ 81% of the normal) is significantly correlated with the latitudinal position of the subtropical ridge along 75°E on the 500-mb mean circulation chart of April. They obtained the regression equation between these two parameters for the period 1950-

70 and verified the same on the independent years 1939-49 and 1971-75 and found that the mean error for the number of subdivisions with normal or above normal rainfall was 6 percent. They also showed that at 500 mb level, the normal northward seasonal movement of the ridge axis from January to May was regular and organized. Mooley *et al.* (1986) have pointed out that the Indian Meteorological subdivisions vary largely in size, by more than one order of magnitude, the ratio of the largest to the smallest being about 13. Therefore, in a particular year, when all except five subdivisions have normal to above normal monsoon rainfall, it may appear to be a normal rainfall year; however, if the five subdivisions with deficient rainfall happen to be large, they could cover 30% of the country. In view of this, the number of subdivisions with normal to above normal monsoon rainfall cannot be considered to be a satisfactory measure of the monsoon rainfall over the country. The percentage area of the country with normal to above normal monsoon rainfall might have been a relatively better measure of monsoon rainfall over India than the percentage of the number of subdivisions with normal to above normal monsoon rainfall. Mooley *et al.* (1986) have shown that the relationship of the Indian monsoon rainfall with the location of April 500 mb ridge is positive (correlation coefficient = + 0.71) and highly significant and that even over periods as small as 20 years, the relationship is stable and consistent. They have also shown that ridge location south of the normal by more than one standard deviation is a much better indicator of deficient monsoon rainfall (i.e., normalized rainfall anomaly ≤ -1.0 S.D.) than ridge location north of normal by more than one standard deviation, of excess monsoon rainfall (i.e., normalized rainfall anomaly of ≥ 1.0 S.D.). They developed a regression equation on the basis of data for the period 1939-80 and verified it for the independent years 1981-84. Estimates for 1982 (a drought year) and 1984 (a near-normal monsoon rainfall year) were very close to actual rainfall, and those for 1981 (a near-normal activity year) and 1983 (an excess rainfall year) deviated from the actual rainfall by + 7.6% and − 15%. However, the verification sample was rather too small to judge the efficacy of the regression relationship. Mooley *et al.* (1986) also examined the relationship between monsoon rainfall of each of the subdivisions and the location of the ridge on the basis of data for the period 1939-80, and found that the rainfall for the subdivisions mostly north of 12°N and west of 84°E is positively and significantly related. It may be mentioned that the monsoon rainfall series used by Mooley *et al.* (1986) is based on monthly rainfall from a fixed network of 306 evenly distributed rain gauge

stations for the period 1939-80 and about 250 rain gauge stations for the period 1981-84.

Thapliyal (1981, 1982) showed on the basis of data for 1944-73 that the relationship between monsoon rainfall in Peninsular India and the April 500 mb ridge is highly significant. He developed an Auto-Regressive Integrated Moving Average (ARIMA) model for forecasting monsoon rainfall for the Indian Peninsula, with April 500 mb ridge as the leading indicator. For forecasting Peninsular monsoon rainfall, using data for 1939-76, he obtained an expression which involves rainfall of the preceding thirteen years and changes in the ridge location from the current year to the preceding year for the preceding five years. He obtained forecasts of Peninsular monsoon rainfall for the years 1977-80 by ARIMA as well as a regression model and found that error by the ARIMA model was smaller than that by the regression model in each of these four years. It may, however, be mentioned that the sample size for verification was rather too small.

Intra-seasonal relationships among 500 mb ridge locations

Over the period 1948-67, correlation coefficients have been obtained between the April ridge location and the May through July ridge locations and between May and July ridge locations. These are, cc (April, May)=0.63, cc (April, July) = 0.55, cc (May, July) = 0.47. The first two correlation coefficients are significant at 5% level and the third is very close to significance at 5% level. The correlation coefficient of 0.55 between April and July ridge locations suggests the persistence in the ridge location from April through July.

The years with normalized monsoon rainfall anomaly with absolute value larger than 1.0 have been classified as years of deficient (negative) or excess (positive) monsoon rainfall and 500 mb ridge locations have been

Years of deficient monsoon rainfall	Ridge location anomaly (°lat.)			Years of excess monsoon rainfall	Ridge location anomaly (°lat.)		
	April	May	July		April	May	July
1951	−3.0	−3.8	−0.8	1956	3.8	5.9	2.7
1965	−0.7	−2.5	−4.4	1961	1.8	0.3	1.7
1966	−1.7	0.4	−3.7				
Mean	−1.8	−2.0	−3.0	Mean	2.8	3.1	2.2

examined for such years for the months April, May and July. The anomaly of the ridge locations during these years and in these months is given below.

Thus, the mean anomaly of the ridge location in each of the months April, May and July is negative/positive for years of deficient/excess monsoon rainfall and the difference between the two means is 4-5° of latitude which is about twice the S.D. of the monthly ridge location. In addition, in each deficient rainfall year the ridge anomaly is generally negative and relatively large, and in each excess rainfall year the anomaly is positive and relatively large. Thus in these years, the anomaly in April ridge location is found to persist through July.

Indian monsoon rainfall in years of low/high latitude April ridge location

As an illustration, Fig. 3 shows the April 500 mb ridge location for 1951 and 1956, which were respectively years of deficient and excess monsoon rainfall.

We have classified the years in which the April ridge was located south/north of the mean position by more than one standard deviation as years of low/high latitude ridge location. The years of low latitude ridge location are 1941, 1951, 1952, 1963, 1966, 1968, 1972, 1974, 1979 and 1982 and those of high latitude ridge location are 1942, 1946, 1947, 1956, 1964, 1967, 1969 and 1975. Indian rainfall for the two bimonths (June-July, August-September) and the same for the low/high latitude ridge location years falling within the period 1939-78 are given below:

Years of low latitude ridge	Indian rainfall mm		Years of high latitude ridge	Indian rainfall mm	
	June-July	Aug-Sept		June-July	Aug-Sept
1941	389	358	1942	502	471
1951	411	331	1946	501	415
1952	453	352	1947	414	531
1963	401	472	1956	556	437
1966	416	343	1964	467	475
1968	436	334	1967	442	436
1972	311	356	1969	430	416
1974	389	374	1975	480	503
Mean	401	365	Mean	474	461

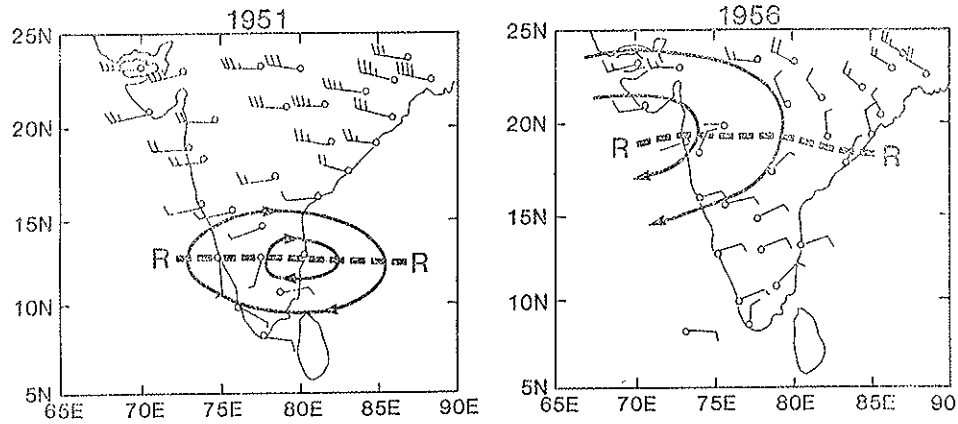

FIG. 3. Monthly mean (April) winds at the Indian upper air stations at 500 mb for the years 1951 and 1956.

Mean rainfall amounts for the two halves, June-July and August-September, for the period 1939-78 are 443 and 432 mm respectively.

These rainfall values show clearly that (i) the mean for each half of the monsoon season is much higher for the years of high latitude ridge location than that for low latitude ridge location; (ii) in most of the years of low/high latitude of the ridge location, the rainfall anomaly is negative/positive for both halves of the monsoon season. This suggests that low/high latitude location of April ridge is an indicator of low/high rainfall in each half of the monsoon season, apparently through persistence of the anomaly of April ridge location through July.

Possible physical basis for influence of the ridge location on rainfall

As mentioned before, the mean 500 mb ridge undergoes an annual oscillation of about 17° of latitude. The ridge demarcates the westerly circulation regime to the north from the easterly tropical regime to the south. During January, the westerly circulation regime at 500 mb reaches its southernmost position. As the season advances, the westerly circulation regime shifts north. The anomaly in the magnitude of this northward shift of the westerly circulation could therefore result either from the anomaly in the characteristics of the mid-latitude westerly flow, or from anomalous tropical heat sources. Anomalous snow accumulation over Eurasia and anomalies in incoming/outgoing radiation could also affect

the ridge position. A rather large negative anomaly of the ridge location in April or May could be associated with colder tropospheric conditions whose persistence through July could adversely affect the establishment and activity of the monsoon. This apparent relationship between the anomaly of the April 500 mb ridge and the anomaly of the Indian monsoon rainfall appears to be quite complicated, and in the present stage of our inadequate knowledge of these factors and their interactions it is not possible to offer any explanation for the observed relationship.

3.2 *Boundary Conditions at the Earth's Surface*

3.2.1 *Snow Cover*

Blanford (1884) utilized the winter and spring snowfall in the Himalayas to predict the subsequent summer monsoon rainfall over India. The inverse relationship between snow cover and rainfall which was suggested by Blanford and later used by Walker gave consistent results during the period 1880-1920; however, for the following 30-year period the relationship was either weak or opposite, and after 1950 the India Meteorological Department dropped this parameter as a predictor.

Hahn and Shukla (1976) utilized a short series of satellite-derived snow cover over Eurasia for 9 years (1967-1975) and showed that the original suggestion by Blanford for inverse relationship between winter-spring snow cover and monsoon rainfall was strongly supported by satellite-derived snow cover data.

Dickson (1984) further extended this study by including data up to 1980 and found that the correlation coefficient for the period 1967-1980 was only -0.59 compared to -0.74 for the period 1967-1975.

The physical mechanism responsible for this relationship is not clearly understood. It has been conjectured that excessive snow cover could contribute towards a weaker summer monsoon intensity in two ways: colder tropospheric temperatures over Eurasia could delay the establishment of meridional temperature gradients, or wetter soil could dissipate most of the solar heating for evaporation rather than heating of the continental land masses. There is some evidence that during the years of excessive snow cover, the mid-tropospheric ridge over India is to the south of its normal position during the spring season.

3.2.2 *Sea Surface Temperature*

Angell (1981) used seasonal Sea Surface Temperature (SST) anomaly time series for the eastern equatorial Pacific (0-10°S and 90°W-180°W) for the period 1868-1977 to examine the relationship between SST and Indian monsoon rainfall. He found a highly significant inverse relationship (correlation coefficient = − 0.62) between Indian monsoon rainfall and the SST anomaly two seasons later. He also observed that in 20 years during the period, SST anomaly during an El Niño season, was at least 0.8°C.

Mooley and Parthasarathy (1984) examined the sea surface temperature (SST) over the eastern equatorial Pacific Ocean (0-10°S and 90°W-180°W) in relation to the Indian monsoon rainfall for the period 1871-1978. They utilized the seasonal anomaly series which they obtained from Angell (1981). In addition to computing the lag/lead correlation coefficients for the whole period, they computed these for the two halves of the period to find out whether the relationships exhibited any stability. The correlation coefficients obtained by them are given below.

SST Season	CC for Period 1871-1978	1971-1924	1925-1978
DJF (−2)	0.08	+0.02	+0.13
MAM (−1)	−0.22*	−0.29*	−0.17
JJA (0)	−0.47**	−0.46**	−0.52**
SON (+1)	−0.60**	−0.66**	−0.55**
DJF (+2)	−0.58**	−0.65**	−0.52**

* Significant at 5% level.
** Significant at 0.1% level.

The figure after the season indicates the number of seasons before (if negative) or after (if positive) the monsoon season. It can be seen that the relationship between SST for the concurrent and the succeeding two seasons and Indian monsoon rainfall is highly significant and stable, but for the preceding MAM season, the relationship is much weaker and is not stable. SST in the DJF season preceding the monsoon season has no relationship with Indian monsoon rainfall.

Association between Indian monsoon rainfall and El Niño events

El Niño is an anomalous oceanic and meteorological event involving the sudden appearance of abnormally warm surface water off the Peru-Ecuador coast (equator - 12°S). The warm water spreads westward to the central Pacific Ocean. The event generally starts around March or April, and may last for one year or more and attains maximum sea surface temperature in late December. The Southern Oscillation is closely linked to this event and the two are referred to as ENSO event.

Using the Line Islands Precipitation Index (LIPI) as indicator of El Niño events during the period 1922-74, Sikka (1980) brought out a general association between El Niño events and deficient rainfall. But as mentioned by Rasmusson and Carpenter (1983), since LIPI has a tendency to peak near the end of the El Niño year, they listed all El Niño events as occurring during pairs of consecutive years. As a result of this ambiguity in identification of the years of El Niño events, the degree of correspondence and lead/lag relationship could not be fixed.

Rasmusson and Carpenter (1983) examined Indian monsoon rainfall with reference to warm episodes (El Niño events) during the period 1875-1979. They took years of El Niño as those listed by Quinn *et al.* (1978) during the periods 1875-1920 and 1939-1947, and for the remaining periods, i.e., 1921-38 and 1948-79, when they had adequate surface marine data, they determined the years of El Niño events from these data. Their study showed that during 21 out of 25 El Niño years, Indian monsoon rainfall was below the median rainfall, and in 19 years it was below the mean rainfall.

Mooley and Parthasarathy (1983) examined the association between Indian summer monsoon rainfall and El Niño during the period 1871-1978. They considered 22 El Niño events — severe and moderate — as categorized by Quinn *et al.* (1978). They used two categories of rainfall, the first with rainfall in standard units (i.e., normalized anomaly) ≤ -0.84, calling this category as "Drought", and the second with rainfall > -0.84, calling this category as "No Drought". By considering "Drought" and "No Drought" as two categories of rainfall and "El Niño" (severe and moderate) and "No El Niño" as two categories of El Niño events, they prepared 2×2 contingency tables for India and for the different Indian meteorological subdivisions. They tested these contingency tables for significant association by applying Chi-square test. The association between drought and El Niño is found to be significant (at 5% or above) for India and 19 subdivisions mostly located west of 80°E. They also found that the worst

drought years in the history of Indian drought, viz., 1877, 1899, 1918 and 1972, were severe El Niño years. Out of 22 El Niño (moderate and severe) years, in 17 El Niño years Indian monsoon rainfall was below normal, in 4 El Niño years the normalized anomaly of Indian monsoon rainfall was between +0.52 and 0.92, and in one El Niño year the rainfall was very close to normal.

Parthasarathy and Mooley (1985) examined the average monsoon rainfall of India for severe, moderate, weak and very weak El Niño events as classified by Quinn *et al.* (1978) during the period 1871-1980 and found that mean rainfall increased with the decrease of intensity of El Niño. They also showed through a student's t-test that the difference between the means for the 22 El Niño years (moderate and severe) and the remaining 88 years was significant at 0.1% level and brought out the influence of El Niño events on Indian monsoon rainfall.

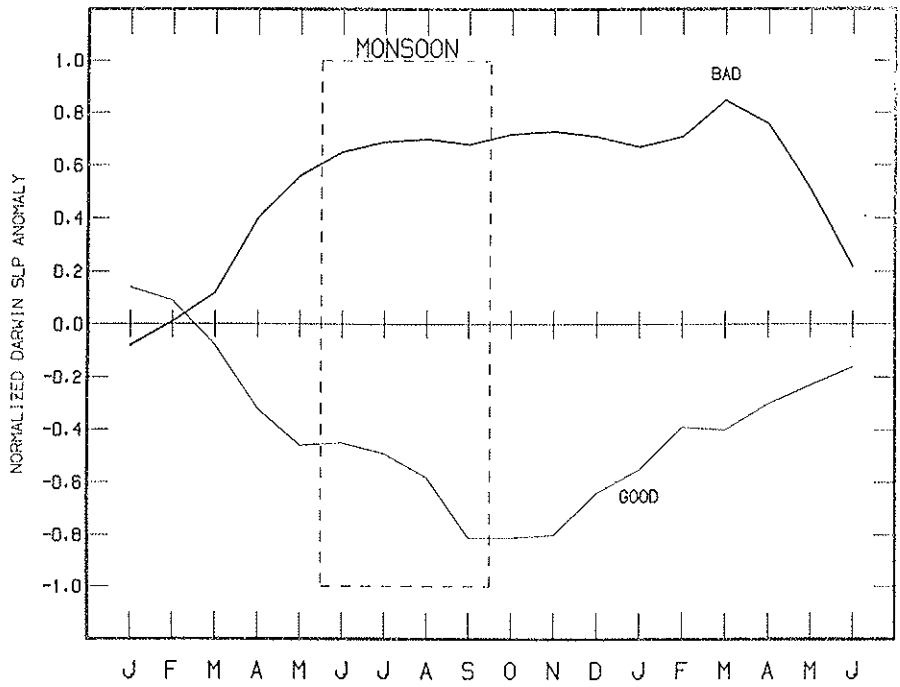

FIG. 4. Composite of normalized Darwin pressure anomaly (three-month running mean) for good monsoon rainfall years and bad monsoon rainfall years.

3.3 *Southern Oscillation (SO)*

As described in the section entitled Historical Review, the basic relationship between the Southern Oscillation and Indian monsoon rainfall was utilized by Walker as two of the predictor parameters (P_1 and P_9) in equation (1) which represent the two nodes of SO. However, in a recent study Shukla and Paolino (1983) found that the mean Darwin pressure anomaly during the spring season preceding the monsoon season composited separately for all the drought years and flood years were not very different from each other (see Fig. 4). The winter to spring tendency of the Darwin pressure appeared to be a more useful predictor for summer monsoon rainfall over India. Figure 4 gives composite Darwin sea level pressure anomalies for deficient rain years (1899, 1901, 1904, 1905, 1911, 1918, 1920, 1928, 1941, 1951, 1965, 1966, 1968, 1972, 1974, 1979, 1982) and excessive rain years (1892, 1893, 1894, 1916, 1917, 1933, 1942, 1947, 1956, 1959, 1961, 1970, 1975, 1983).

We have also examined the stability of correlation between Darwin pressure tendency and Indian rainfall, and it is found that this relationship is statistically significant for the entire record length; however, during the past 50 years the correlation coefficient is considerably higher than that for the previous years.

3.4 *Surface Temperature over India*

Mooley and Paolino (1986) have examined the surface maximum and minimum temperature over India during the pre-monsoon months March, April and May in relation to Indian monsoon rainfall. They found three areas for which temperature is significantly related to the Indian monsoon rainfall. These three areas are: south Gujarat and adjoining parts of Maharashtra and of Madhya Pradesh (area A), north Tamilnadu coast and adjoining parts, (area B), and south Gujarat State and adjoining parts of southwest Madhya Pradesh (area C). The mean monthly April minimum temperature for areas (A) and (B) and mean monthly May minimum temperature for area (C) are significantly (5% or over) related with Indian monsoon rainfall. The best relationship (cc = 0.60) is between Indian monsoon rainfall and mean monthly minimum temperature during May over south Gujarat and adjoining parts of southwest Madhya Pradesh (area C). This area is apparently located east of the Intertropical Convergence Zone (ITCZ) over the Arabian Sea and the anomalous thermal

conditions over this area possibly represent the anomalous thermal conditions over the Arabian Sea ITCZ.

Bhalme and Mooley (1980) found that the mean heights of the 200 mb surface were much below (above) normal over the belt 15°-30°N along 70°E during drought (good monsoon) years, suggesting colder (warmer) upper troposphere. Verma (1980, 1982) showed a good association between cooler (warmer) upper troposphere over north and northwest India and poor (good) summer monsoon rainfall. He also found that a cooler (warmer) upper troposphere in May generally persists during the monsoon season. However, for later years, i.e., after 1977, we did not find good association between upper tropospheric temperature and Indian monsoon rainfall.

3.5 *Surface Pressure over the Northern Hemisphere*

Hemispheric analyses of seasonal mean sea level pressure (SLP) were used to investigate relationships with monsoon rainfall. These fields were available for a long period of record and are of good quality. The period of record used for the SLP is from Dec. 1924 through Nov. 1977.

Correlation coefficients were computed between seasonal SLP and Indian monsoon rainfall for seasons preceding, during, and following the monsoon. Maps of correlation coefficients showed a continuity of pattern from one season to the next, but did not show any statistically significant persistent patterns. The correlation map for summer SLP anomalies one year before the monsoon showed a large negative pattern significant above the 5% level off the east coast of North America. We do not know if this relationship has any physical significance. The correlation map for spring SLP anomalies immediately preceding the monsoon showed an area of statistically significant positive correlation in the North Pacific, south of 30°N.

An empirical orthogonal function (EOF) analysis was performed on the seasonal SLP data, in the hope that certain dominant patterns of SLP variability, as isolated by the analysis, might be related to the Indian monsoon. The coefficient time series for the dominant EOFs in each season were correlated with the all-India monsoon rainfall time series, but no significant correlations were found.

We have also examined SLP at selected stations in India, Pakistan, Bangladesh and Sri Lanka, with periods of record from 20 to 85 years, and their relationships with monsoon rainfall. Correlation coefficients were computed between monthly and seasonal station SLP time series and

India monsoon rainfall. Our motivation was to see if relationship between monsoon rainfall and SLP at the Indian stations is as strong, or even stronger than Darwin SLP. It was found that for none of the Indian stations were the correlation efficients as high as that for Darwin.

3.6 *Upper Air Flow over India*

Joseph (1978) examined the meridional flow in the upper troposphere over India during May, June, July and August and found that during years of large-scale monsoon failure the meridional flow in the upper troposphere during June through August was southerly, and that during May in such years, southerly meridional flow over India at the 150 mb level was stronger than that in other years. Utilizing this persistence of upper tropospheric flow associated with monsoon failure, Joseph *et al.* (1981) developed relationship between a meridional wind index (Vm) and Indian monsoon rainfall. This index is the mean of the meridional winds at Madras, Bombay, Nagpur, Delhi and Srinagar for May at the 200 mb level. This index had a highly significant correlation coefficient of -0.89 with Indian monsoon rainfall for the period 1964-78. They used the Indian monsoon rainfall series constructed by Parthasarathy and Mooley (1985). They developed a regression equation between Indian monsoon rainfall (R) and (Vm) which is given by $R = 92.55 - 3.15\ Vm$, where R is in cm, Vm in m. sec^{-1}, southerly meridional wind is taken as positive. Joseph (1983) verified the regression equation for the independent years 1979-82. The percentage errors of the forecast rainfall for these years were, -6.0, -9.7, $+3.3$ and 5.3 respectively. Mooley and Shukla (1987) examined the relationship between mean April 500 mb ridge along 75°E and the meridional index for May, Vm, of Joseph *et al.* (1981) and found the correlation coefficient between the two parameters to be -0.73 for the period 1964-78. The relationship is inverse and is highly significant. Thus, the meridional wind index, Vm, and April 500 mb ridge are not independent. With the April 500 mb ridge as predictor, the forecast of monsoon rainfall can be prepared earlier and hence it is more useful than the mean May meridional wind index, Vm.

Thapliyal (1979) has shown that the circulation features at the 50 mb level in January during westerly and easterly Quasi Biennial Oscillation (QBO) years are very different and that they can provide useful guidance for forecasting Indian monsoon rainfall. But in view of the fact that drought is also seen to follow both easterly and westerly phases of QBO

in January, it is difficult to use these circulation features as predictors for monsoon seasonal rainfall in any individual year.

Kung and Sharif (1980) developed a regression equation for prediction of the date of onset of the summer monsoon over the Kerala coast from 700 and 100 mb circulation parameters. They considered geopotential heights, temperature, kinetic energy, zonal and meridional wind components at the 700 and 100 mb levels (in all, 10 predictors) over the point, 12.4°N, 76.5°E on the Kerala coast, for April. They used data for the period 1958-78. They obtained the dates of monsoon onset over Kerala from the India Meteorological Dept., and data for geopotential heights and temperatures at 700 and 100 mb from the National Meteorological Center's octagonal grid data archived at the National Center for Atmospheric Research (NCAR). The wind components were approximated by the computed geostrophic components. On experimentation, they found that the addition of the zonal wind component at 100 mb and the meridional wind component at 700 mb did not improve the fit of the regression equation. In view of this, they deleted these two parameters. The standard deviation of the observed date of onset is about a week. The error in the forecast of date of onset exceeded one S.D. in 4 years out of 19 years. The largest error of 17 days occurred in 1972, actual onset being much later than the forecast date of onset.

In another study, Kung and Sharif (1981, 1982) considered the additional predictors, 700 mb January zonal wind and 700 mb March temperature over Australia, April Indian Ocean temperature over the area 10°-20°N and 60°-70°E and developed regression equations for forecasting the monsoon onset date over Kerala and for forecasting monsoon rainfall over Central India, using data for 1958-77. According to them, forecasts of the onset date had an average accuracy of 5% and forecasts of rainfall over Central India had an average accuracy of 6%.

4. An Empirical Prediction Scheme

In this section we have summarized the results of Shukla and Mooley (1986), who have presented a multiple regression equation to predict seasonal rainfall over India. They have suggested that since the two most important circulation anomalies that influence the Indian monsoon rainfall appear to be the Southern Oscillation and the latitudinal location of the 500 mb ridge, and since there is no significant correlation between these, they should be used as predictors in a linear regression equation.

Based on data for the period 1939-1984, they have developed a regression equation:

$$Y = aX_1 + bX_2$$

where Y = Normalized rainfall anomaly for India for the summer monsoon

X_1 = Normalized anomaly of the location of the 500 mb ridge during April along 75°E

X_2 = Normalized anomaly of January to April change in Darwin sea level pressure.

Table 1 gives the values of seasonal rainfall, latitudinal location of ridge and Darwin pressure change for the 46 year period used in that study. Table 2 gives the regression coefficients (a) and (b) for the successive 30 year periods. Table 2 also gives correlation coefficients between monsoon rainfall and the two predictors. Regression equations are developed for each 30 year period and utilized to predict rainfall for two independent years, one immediately preceding and one immediately succeeding the 30 year period. The results of independent verification for 32 years are shown in Figure 5. Actual rainfall is along the abscissa and the predicted rainfall is along the ordinate. The two dotted lines represent ± 5% of the actual rainfall. It can be seen from this Figure that prediction of droughts is especially better. The root mean square error is 35.8 mm, which is only 4.2% of the mean rainfall. The root mean square error for the climatic mean to be the forecast each year would have been 82 mm, which is 9.6% of the mean rainfall.

The multiple correlation coefficient is 0.82, which means that only 67% of the variance is explained by these two predictors. While a regression equation on this level of explained variance might provide some useful guidance in operational forecasting of monsoon rainfall, it is clear that a substantial percentage (33%) of variance remains unexplained, and therefore it will be necessary to investigate other factors which might be related to the summer monsoon rainfall over India.

5. Prospects for the Future and Concluding Remarks

From a practical standpoint, there are two aspects to the problem of monsoon prediction:

— Prediction of seasonal mean rainfall
— Prediction of space-time variability of rainfall

There appear to be statistically significant relationships between monsoon rainfall and anomalies of planetary scale circulation and boundary

Table 1 - Indian Monsoon rainfall, April 500 mb ridge location along 75°E ar Darwin Mean Sea Level pressure (SLP) change from January to Apr (1939-84).

Year	Rainfall (mm)	Ridge (°N)	Darwin SLP Change (mb)	Year	Rainfall (mm)	Ridge (°N)	Darwin Sl Change (m
1939	788.9	14.0	4.4	1963	855.2	13.5	2.6
1940	850.2	15.3	5.0	1964	919.9	18.3	1.8
1941	729.0	11.2	2.8	1965	706.8	14.0	4.9
1942	958.3	17.5	1.8	1966	735.2	13.5	2.4
1943	866.1	16.0	2.5	1967	858.6	17.5	5.7
1944	921.3	14.5	3.0	1968	753.7	12.5	5.6
1945	907.3	16.7	3.8	1969	829.3	17.3	5.1
1946	901.3	17.3	4.1	1970	939.4	15.8	1.8
1947	942.3	18.0	2.1	1971	885.8	16.7	2.2
1948	872.4	14.5	1.7	1972	653.2	11.0	4.8
1949	901.8	17.0	2.8	1973	911.6	16.7	1.7
1950	874.9	17.0	3.0	1974	746.9	13.5	4.8
1951	736.9	12.0	4.1	1975	960.1	17.5	1.3
1952	791.7	13.5	3.6	1976	854.7	17.0	4.8
1953	919.7	17.0	2.0	1977	880.5	14.0	3.4
1954	885.3	16.5	2.8	1978	908.0	14.0	1.9
1955	929.9	15.5	0.6	1979	746.0	12.5	3.7
1956	979.5	17.5	3.5	1980	881.0	15.0	3.8
1957	784.3	16.0	3.0	1981	842.0	17.0	4.8
1958	886.3	17.0	0.4	1982	736.0	11.3	3.8
1959	938.1	16.0	2.8	1983	959.0	14.5	0.3
1960	839.4	16.7	2.0	1984	835.0	14.8	3,0
1961	1017.0	15.0	1.9				
1962	806.9	14.8	4.7	Mean	857.1	15.3	3.0
				S.D.	82.2	2.0	1.3

TABLE 2 - Values of regression coefficients a(1) and b(2); multiple correlation coefficients mcc (3); cc for rainfall and ridge location only (4); and cc for rainfall and Darwin pressure tendency only (5) for the successive 30 year periods and the whole 46 year period.

Period	(1)	(2)	(3)	(4)	(5)
1939-68	0.624	−0.294	0.77	0.71	−0.49
1940-69	0.607	−0.333	0.75	0.68	−0.47
1941-70	0.594	−0.361	0.76	0.67	−0.50
1942-71	0.522	−0.389	0.72	0.62	−0.52
1943-72	0.577	−0.368	0.77	0.69	−0.55
1944-73	0.576	−0.370	0.78	0.69	−0.56
1945-74	0.603	−0.369	0.81	0.73	−0.59
1946-75	0.588	−0.387	0.83	0.74	−0.63
1947-76	0.577	−0.406	0.83	0.73	−0.64
1948-77	0.551	−0.412	0.81	0.70	−0.63
1949-78	0.524	−0.434	0.80	0.68	−0.64
1950-79	0.540	−0.425	0.81	0.69	−0.65
1951-80	0.542	−0.413	0.80	0.69	−0.64
1952-81	0.524	−0.439	0.79	0.66	−0.63
1953-82	0.544	−0.429	0.80	0.68	−0.62
1954-83	0.513	−0.487	0.79	0.63	−0.64
1955-84	0.513	−0.487	0.79	0.63	−0.64
1939-84			0.82	0.71	−0.58

conditions. The most significant association is found with the El Niño-Southern Oscillation phenomena and the mid-tropospheric circulation over India. This is indeed encouraging because if the fluctuations of seasonal mean were merely the consequences of interannual variability of the intra-seasonal variability, the problem of monsoon prediction would have been reduced to predicting the intraseasonal fluctuations themselves.

In order to make further progress it would be essential to understand the relationship among the synoptic scale, intraseasonal variability and planetary scale circulations which appear to influence the seasonal mean rainfall. There have been several suggestions that eastward propagating 30-60 day oscillations might play an important role in determining the intraseasonal fluctuations of monsoon rainfall over India. This deserves further investigation. It is quite likely that a suitable phase relationship between the Southern Oscillation (2-4 years) and 30-60 day oscillations

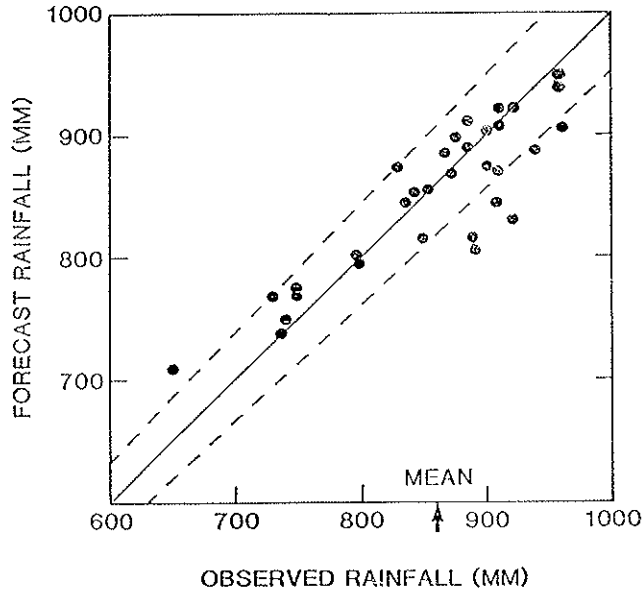

FIG. 5. Observed and forecast rainfall (mm) for 32 years of verification. The arrow indicates the long term mean rainfall (753 mm). The dashed lines represent the ± 5% of the solid line.

might provide important insight into the mechanisms of intraseasonal and interannual variability of monsoon rainfall over India.

On a day-to-day basis, the rainfall fluctuations are associated with synoptic scale disturbances (lows, depressions) and fluctuations of the monsoon trough; however, it needs to be investigated if planetary scale circulation anomalies (which are apparently related to seasonal mean monsoon rainfall) influence the statistics of these synoptic scale disturbances. If this were found to be the case, prospects for long range forecasting of monsoon would be quite good.

Another important question from a practical standpoint is the predictability of monthly and seasonal rainfall anomalies over smaller spatial regions. We have examined the multiple correlation coefficients between seasonal rainfall over each of the 30 subdivisions of India, Southern Oscillation tendency, and 500 mb ridge location. We find that the multiple correlation coefficient is considerably less for subdivisions than for all India rainfall. This suggests that the relationships between planetary scale

circulation anomalies and seasonal mean rainfall over India do not necessarily hold for anomalies over smaller regions and that it would be necessary to gain a better understanding of the mechanisms of intraseasonal variability at regional scale before we could attempt to predict rainfall anomalies over smaller regions of India. At this time we do not have any clear evidence that it would be possible to predict rainfall anomalies over smaller regions empirically.

REFERENCES

ANGELL J.K., *Comparison of variations in Atmospheric Quantities with Sea Surface Temperature variations in equatorial eastern Pacific.* « Mon. Wea. Rev. », *109*, 230-243 (1981).

BANERJEE A.K., SEN P.N. and RAMAN C.R.V.R., *On foreshadowing southwest monsoon rainfall over India with mid-tropo-spheric circulation anomaly of April.* « Indian J. Met. Hydrol. Geophy. », *29*, 425-431 (1978).

BHALME H.N. and MOOLEY D.A., *Large-scale droughts/floods and monsoon circulation.* « Mon. Wea. Rev. », *108*, 1197-1211 (1980).

BLANFORD M.F., *On the connection of Himalayan snowfall with dry winds and seasons of drought in India.* « Proc. Roy. Soc. London. », *37*, 3 (1884).

BOX G.E.P. and JENKINS G.M., *Some recent advances in forecasting and control.* « Appl. Stat. », *17*, 91-109 (1968).

BOX G.E.P. and JENKINS G.M., *Time Series Analysis, forecasting and control.* San Francisco, Holden-Day (1970).

HILDEBRANDSSON H.H., *Quelques recherches sur les entres d'action de l'atmosphère.* « Kon. Svenska Vetens.-Akad. Handl. », *29*, 1-36 (1897).

India Meteorological Department, *Upper Air Atlas of India and neighbourhood.* India Met. Dept., New Delhi, 60 maps (1972).

JAGANNATHAN P., *Seasonal forecasting in India, a review.* India Meteorological Department, Special Publication, DG. 82/650. Available from Director General, Lodi Road, New Delhi-3, India (1960).

JAGANNATHAN P. and KHANDEKAR M.L., *Predisposition of upper air structure in March to May over India to the subsequent monsoon rainfall of Peninsula.* « Indian J. Met. Geophys. », *13*, 305-316 (1962).

JOSEPH P.V., MUKHOPADHUAYA R.K., DIXIT W.V. and VAIDYA D.V., *Meridional wind index for long range forecasting of Indian summer monsoon rainfall.* « Mausam », *32*, 31-34 (1981).

JOSEPH P.V., *Sub-tropical westerlies in relation to large-scale failure of Indian monsoon.* « Ind. J. Met. Hydrolo. Geophys. », *29*, 412-418 (1978).

JOSEPH P.V., *Inter-annual variability of summer monsoon rainfall.* Ph. D. thesis, University of Poona, 106 pp. (1983).

KUNG C.E. and SHARIF T.A., *Regression forecasting of the onset of the Indian summer monsoon with antecedent upper conditions.* « J. Appl. Meteor. », *19*, 370-379 (1980).

KUNG C.E. and SHARIF T.A., *Long-range multi-regression forecasting of the Indian summer monsoon onset and rainfall with antecedent upper air pattern and sea surface temperature.* International Conference on « Early results of FGGE and large-scale aspects of monsoon », 12-17 January 1981, Tallahassee, Florida, pre-print vol., 5-57 to 5-60 (1981).

KUNG C.E. and SHARIF T.A., *Long-range forecasting of the Indian summer monsoon onset and rainfall with upper air parameters and sea-surface temperature.* « J. Meteor. Soc. of Japan », *60*, 672-681 (1982).

LOCKYER N. and LOCKYER W.J.S., *The behavior of the short-period atmospheric variation over the earth's surface.* « Proc. Roy. Soc. », *73*, 457-470 (1904).

MONTGOMERY R.B., *Report on the work of G.T. Walker.* « Mon. Wea. Rev. », Supplement, *39*, 1-22 (1940a).

MONTGOMERY R.B., *Verification of three of Walker's seasonal forecasting formula for India monsoon rain.* « Mon. Wea. Rev. », Supplement, *39*, 23-24 (1940b).

MOOLEY D.A. and PARTHASARATHY B., *Indian summer monsoon and El Niño,* « PAGEOPH », *121*, 339-352 (1983).

MOOLEY D.A. and PARTHASARATHY B., *Indian summer monsoon and east equatorial Pacific Sea Surface temperature.* « Atmosphere-Ocean », *22* (1), 23-35 (1984).

MOOLEY D.A. and PAOLINO D.A., *Indian monsoon signal in surface level thermal field.* Personal communication (1986).

MOOLEY D.C., PARTHASARATHY B. and PANT G.B., *Relationship between Indian Summer Monsoon Rainfall and the location of the ridge at 500 mb level along 75°E.* « J. Clim. and Appl. Met. », *25*, 633-640 (1986).

MOOLEY D.A. and SHUKLA J., *Variability and Forecasting of the Summer Monsoon Rainfall over India,* in: « Reviews in Monsoon Meteorology », Editors, C.-P. Chang and T.N. Krishnamurti, Oxford University Press 1987.

NORMAND C.W.B., *Monsoon seasonal forecasting* (presidential address to Royal Meteorological Society). « Quart. J. Roy. Met. Soc. », *79*, 463-473 (1953).

PARTHASARATHY B. and MOOLEY D.A., *Relationship between AU-India summer monsoon rainfall and ENSO during last one century.* Proc. First WMO workshop on « The Diagnosis and Prediction of Monthly and seasonal atmospheric variations over the Globe », held at University of Maryland, College Park, Maryland, U.S.A., 29 July - 2 August 1985, published by World Meteorological Organization in publication series, Long Range Forecasting Research, Re-print No. 6, Vol. I, 265-273 (1985).

QUINN W.H., ZOPF D.O., SHORT K.S. and KUO YANG R.T.W., *Historical trends and statistics of Southern Oscillation, El Niño and Indonesian droughts.* « Fish. Bull. », *76*, 663-678 (1978).

RAMDAS L.A., *Prediction of the date of establishment of southwest monsoon along the west coast of India.* « Ind. Jour. of Meteor. and Geop. », *5*, 305-314 (1954).

RAO K.N., *Seasonal forecasting - India.* WMO/IUGG Symp. on « Long Range Forecasting », Boulder, Colorado, published in WMO Tech. Note No. 66, 1965, 17-30 (1964).

RASMUSSON E.M. and CARPENTER T.H., *The relationship between eastern equatorial Pacific Sea Surface temperature and rainfall over India and Sri Lanka.* « Mon. Wea. Rev. », *111*, 517-528 (1983).

SHUKLA J., *Interannual variability of monsoons. Monsoons,* Eds: Jay S. Fein and Pamela L. Stephens, John Wiley & Sons, Inc. (1986).

SHUKLA J. and MOOLEY D.A., *Empirical prediction of summer monsoon rainfall over India.* « Mon. Wea. Rev. », *114* (1986).

SIKKA D.R., *Some aspects of the large-scale fluctuation of summer monsoon rainfall over India in relation to fluctuations in the planetary and regional scale circulation parameters.* « Proc. Ind. Acad. Sci. (Earth Planet. Sci.) », *89*, 639-653 (1980).

THAPLIYAL V., *ARIMA model for long-range prediction of monsoon rainfall in peninsular India.* India Met. Dept. Mono. Climatology, No. 12/81, 12 pp. (1981).

THAPLIYAL V., *Stratospheric circulation in relation to summer monsoon over India.* Symp. on « Hydrological aspects of Droughts, I. » Indian National Science Academy, pre-print. volume, New Delhi, pp. 341-363 (1979).

THAPLIYAL V., *Stochastic dynamic model for long-range prediction in peninsular India.* « Mausam », *33*, 399-404 (1982).

VERMA R.K., *Importance of upper tropospheric thermal anomalies for long-range forecasting of Indian summer monsoon activity.* « Mon. Wea. Rev. », *108*, 1072-1075 (1980).

VERMA R.K., *Long-range prediction of monsoon activity: a synoptic diagnostic study.* « Mausam », *33*, 35-44 (1982).

WALKER G.T., *Correlations in seasonal variation of weather*, II. « Mem. India Meteor. Dept. », *21*, 22-45 (1910).

WALKER G.T., *Correlations in seasonal variation of weather*, VII. *The local distribution of monsoon rainfall.* « Mem. India Meteor. Dept. », *23*, 23-29 (1922).

WALKER G.T., *Correlations in seasonal variations of weather*, X. « Mem. India. Met. Dept. », *24*, 335-345 (1924).

WALKER G.T., *Seasonal weather and its prediction.* British Association for Advancement of Science. Report 103, 25-44, reprinted, Annual Report Smithsonian Institute, for 1935, 117-138 (1933).

ON UNDERSTANDING THE METEOROLOGICAL CAUSES OF SAHELIAN DROUGHT

RICHARD J. REED
Department of Atmospheric Sciences
University of Washington, Seattle, Washington 98195

1. Introduction

The great human suffering engendered by the recent prolonged shortage of rainfall in sub-Saharan Africa has focussed world-wide attention on the problem of Sahelian drought and has inspired much research into the meteorological and related causes and manifestations of this phenomenon. The unusual severity and persistence of the latest drought episode is illustrated in Fig. 1 which depicts standardized annual rainfall anomalies for the Sahel for the years from 1901 to 1985. Significant drought has persisted now for 18 consecutive years, and in five of these years the negative rainfall anomaly exceeded any recorded previously in the century. Not since 1958 has there been a positive anomaly comparable in size to the negative anomalies of the 1970's.

This paper addresses the problem of understanding the causes of sub-Saharan or Sahelian drought. It does not pretend to review all aspects of the subject nor does it try to draw final conclusions regarding causes. Rather its main object is to elucidate the meteorological and related features that control rainfall production and distribution over Africa north of the equator in summer and to document how these features change regionally, and to a lesser extent globally, between dry years and wet years. In addition we will touch briefly on the problem of obtaining improved data sets for future studies of Sahelian drought.

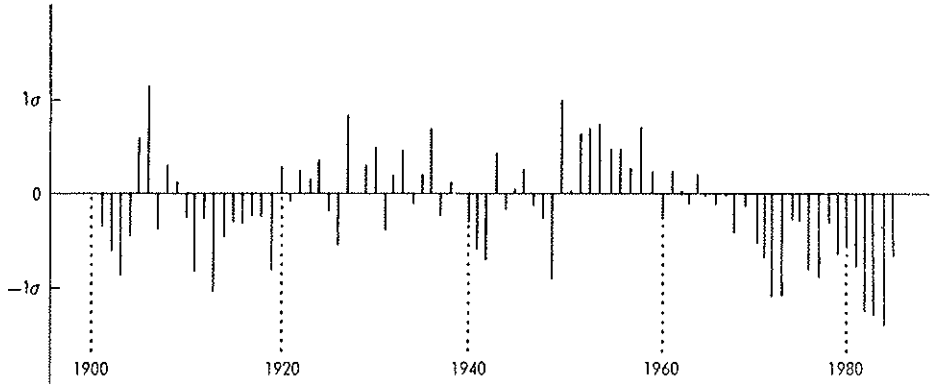

FIG. 1. Standardized annual rainfall anomalies for the Sahel, 1901-1985. (Folland *et al.*, 1986).

2. METEOROLOGICAL FACTORS AFFECTING RAINFALL PRODUCTION IN THE SAHEL

Before examining these factors, it is appropriate to look at the rainfall itself. Figure 2, taken from Tanaka *et al.* (1975) shows the average August precipitation for the decade 1941-1950 (top) and 1951-1960 (bottom). The former was a slightly drier than normal period in the Sahel and the latter a much wetter than normal period. Main features evident on both maps are (1) the rainfall maximum running approximately east-west near 10°N, (2) the strong gradient of rainfall between 15°-20°N and (3) the minimum near the Gulf of Guinea associated with the so-called "little dry season". In view of the strong precipitation gradient in the Sahel, it might appear at first sight that rainfall deficiency in that region arises from an abnormal southward displacement of the axis of maximum precipitation (or failure of the axis to move sufficiently far northward during its seasonal migration), but the explanation is not quite so simple as shown by Fig. 3, also taken from Tanaka *et al.* In 1968, a drought year, the axis was abnormally far south. However, in 1972, when there was an even stronger rainfall deficiency, the axis was situated not far from its position in the wet decade of the 1950's. The deficiency in 1972 was connected with reduced amounts virtually everywhere. Nicholson (1980) has stressed the fact that Sahelian drought is associated with more than one type of anomaly pattern over West Africa.

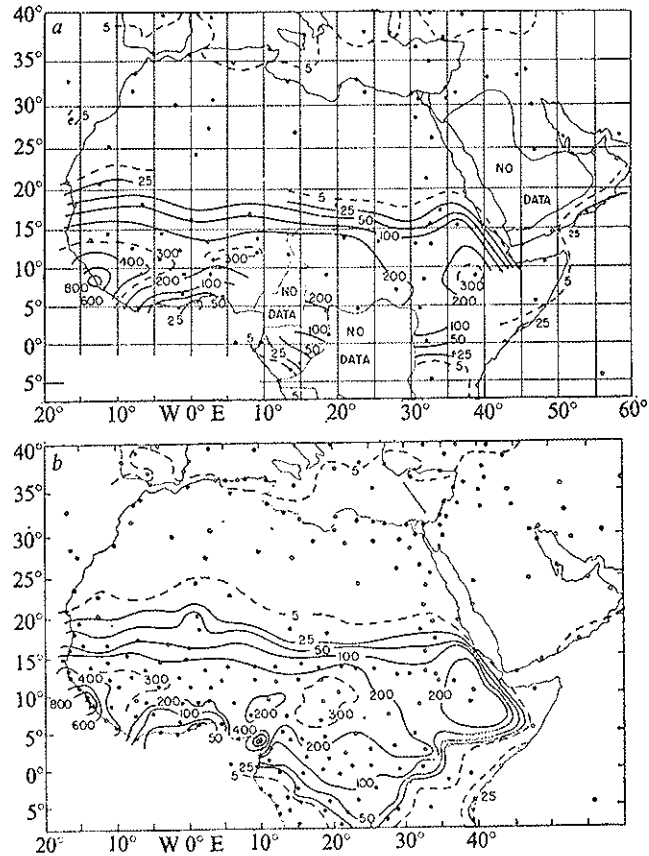

FIG. 2. Analyses of average August precipitation data (mm) for 1941-50(a) and 1951-60(b) for the African region (Tanaka *et al.*, 1975). Dots indicate positions of reporting stations.

We turn now to an examination of the large-scale circulation features associated with Sahelian rainfall. For economy of presentation we have chosen to base the discussion largely on a few schematic diagrams rather than on illustrations taken from original sources. Major features of the surface circulation are shown in Fig. 4 where it is seen that two contrasting flows exist over Africa during the rainy season: a warm moist flow that originates in the Southern Hemisphere and a hot, dry flow that originates over the North Atlantic and Mediterranean. These meet at what is usually termed the Intertropical Convergence Zone (ITCZ). At the surface this kinematic ITCZ lies close to 20°N across much of the

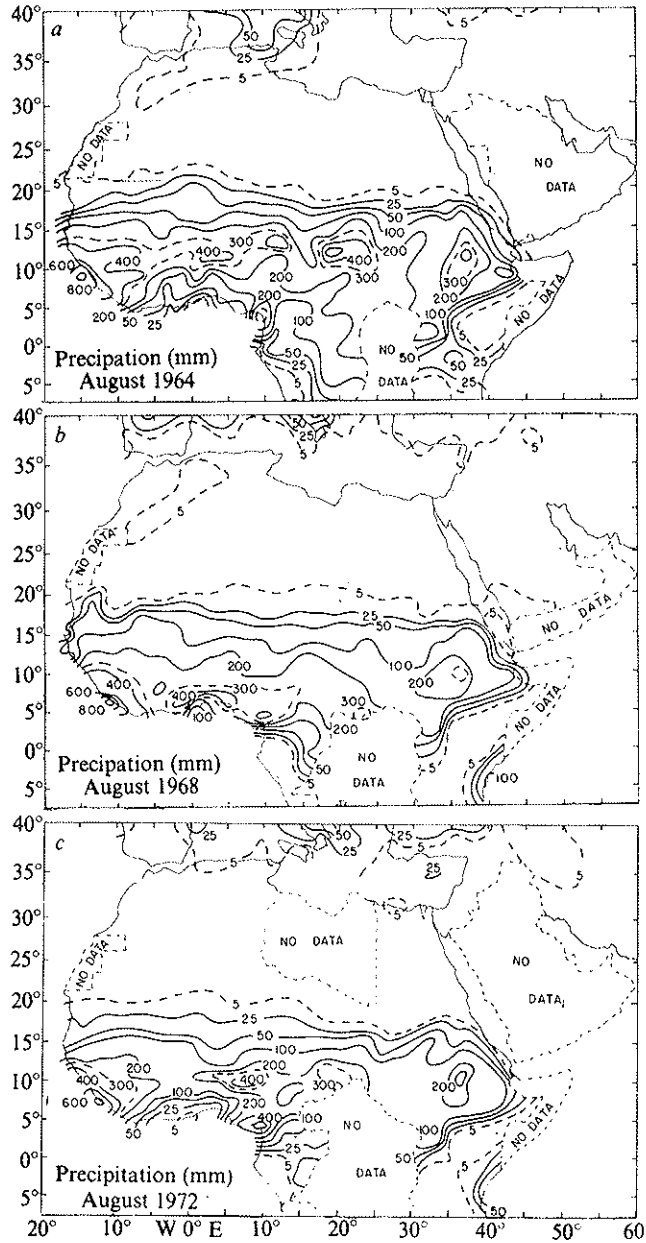

FIG. 3. Analyses of August precipitation data for 1964(a), 1968(b) and 1972(c) for the African region. (Tanaka *et al.*, 1975).

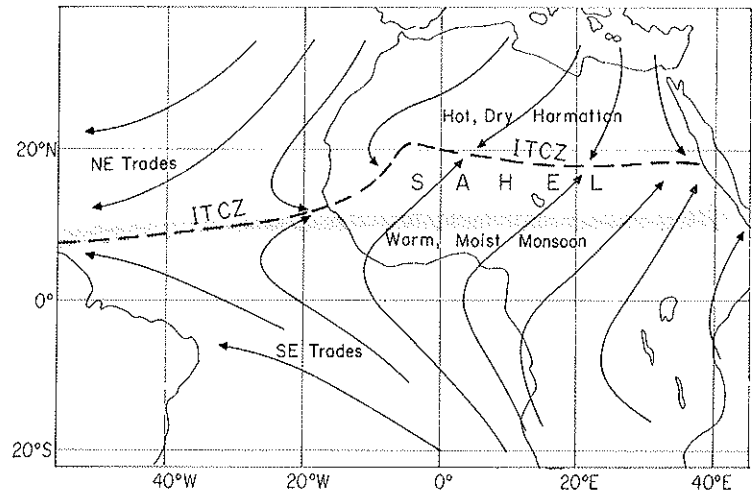

FIG. 4. Schematic diagram of surface flow over tropical and subtropical Africa during summer. Heavy dashed line represents Intertropical Convergence Zone or monsoon trough. Stippling indicates blet of maximum rainfall.

continent. The position is well to the north of the belt of maximum rainfall (shown by stippling). The picture is quite different from that over the ocean, where the kinematic ITCZ and the convergence associated with the rainfall maximum tend to be nearly coincident. The moist southwesterly flow south of the ITCZ is generally referred to as the African monsoon and the trough of low pressure associated with the ITCZ is often called the monsoon trough.

Over the Atlantic the ITCZ is located farther south, near 10°N, and in the west represents the line of confluence between the northeast and southeast trades. Warmest sea-surface temperatures and the band of heaviest precipitation are situated close to the ITCZ.

Important features of the middle and upper tropospheric flow are depicted in Fig. 5. Extending across much of Africa near 15°N is a mid-tropospheric jet stream, centered usually between 700 and 600 mb, which we will refer to as the African easterly jet (AEJ). It is produced by the strong thermal contrast between the hot desert air to the north and the cooler air in the continental rain belt and ocean area to the south. A separate easterly jet stream exists at higher levels (near 200 mb) to the south of the AEJ. This is commonly termed the Tropical Easterly

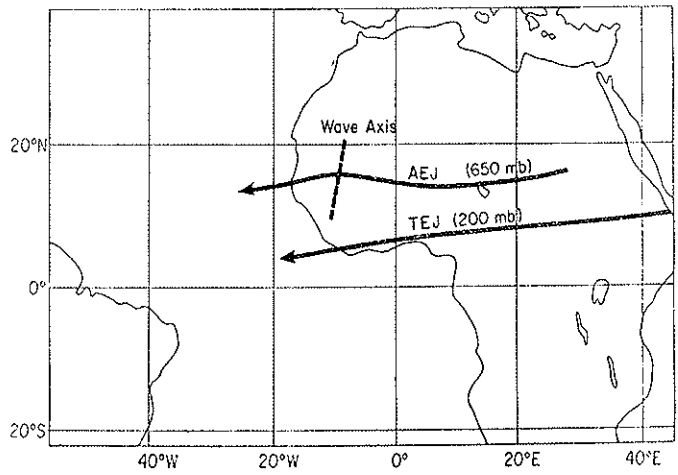

FIG. 5. Schematic diagram showing locations of the African Easterly Jet (AEJ) and Tropical Equatorial Jet (TEJ). Dashed line represents axis of easterly wave disturbance.

Jet (TEJ). It originates over and to the east of the Indian Ocean and is a component of the Asiatic monsoon circulation.

The AEJ is particularly relevant to Sahelian rainfall. It is known to be baroclinically-barotropically unstable, the instability being manifested in the form of synoptic-scale easterly wave disturbances that form at 3-4 day intervals over West and Central Africa and that travel westward at speeds of 6-7° long d^{-1}. (Burpee, 1972; Norquist *et al.*, 1977). The depicted undulation in the AEJ is meant to suggest the associated waves. It has been shown (Reed *et al.*, 1977) that the waves exert a substantial modulating effect on convective activity and precipitation, at least over West Africa and the Atlantic. Presumably, too, they distribute moisture and precipitation over a broader latitudinal range than would happen in their absence.

Meridional cross sections through the aforementioned features appear in Figs. 6a and b. A series of mean charts for August-September 1985 prepared from ECMWF initialized analyses for 0000 and 1200 GMT have been particularly helpful in constructing these diagrams. The charts, taken from Reed *et al.* (1986a), are reproduced in the appendix (Figs. A1-3).

The schematic diagram for 20°W (Fig. 6a) shows previously mentioned features — the AEJ, the TEJ, the low-level monsoon flow, the locations of the surface ITCZ and rainfall or cloud maximum — and additionally

portrays the Hadley or mass circulation. The oceanic extension of the Saharan Air Layer (SAL) is also shown. Since only the divergent component of the wind enters into the mass flow, greater weight has been put on the divergence fields (Figs. A2b and d) than on the total meridional winds (Figs. A1b and d) in depicting the horizontal branches of the meridional circulation. The upward branch of the mass circulation at 20°W is situated near 10°N, somewhat south of the surface position of the ITCZ, but not as far removed as over the interior. The sinking branch occurs near 30°N,

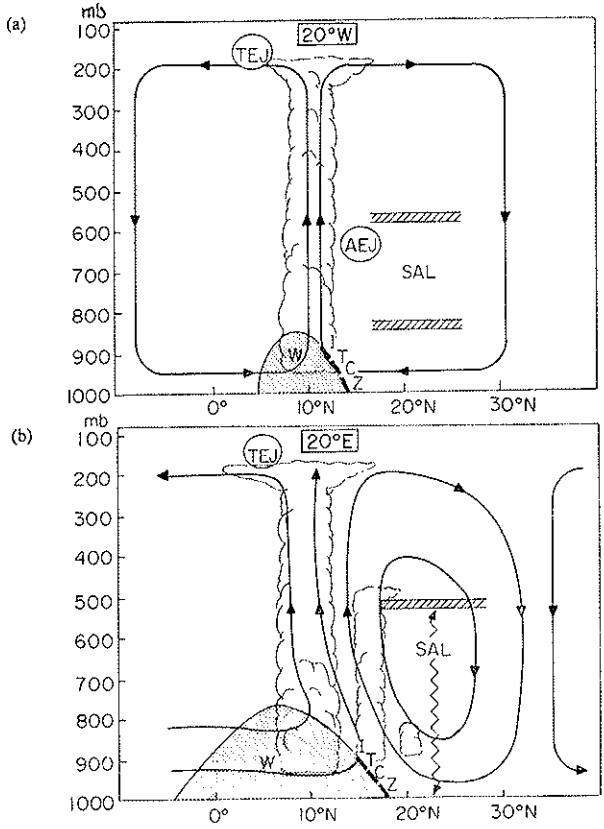

FIG. 6. Schematic meridional sections for (a) 20°W and (b) 20°E. Solid lines depict mass circulation. Stippling represents westerly monsoon flow; heavy broken line the ITCZ. Width and depth of clouds indicate relative rain amounts. Also shown are African Easterly Jet (AEJ), Tropical Easterly Jet (TEJ) and Saharan Air Layer (SAL). Boundaries of SAL are indicated by cross hatching. Zigzag line depicts dry convective mixing of the SAL.

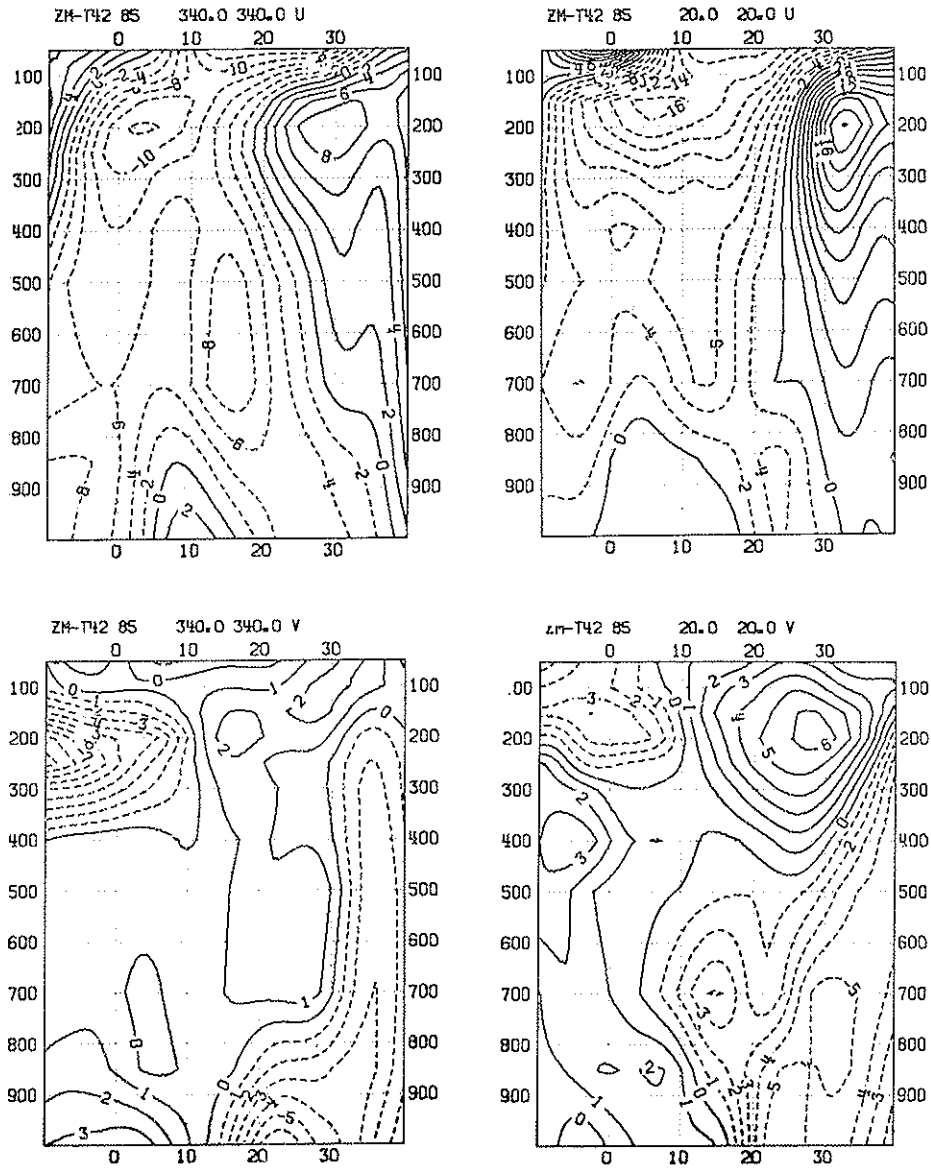

FIG. A1. Meridional sections of mean zonal u and meridional winds v for August-September, 1985, at 20°W (a, b) and 20°E (c, d). Unit m s^{-1}.

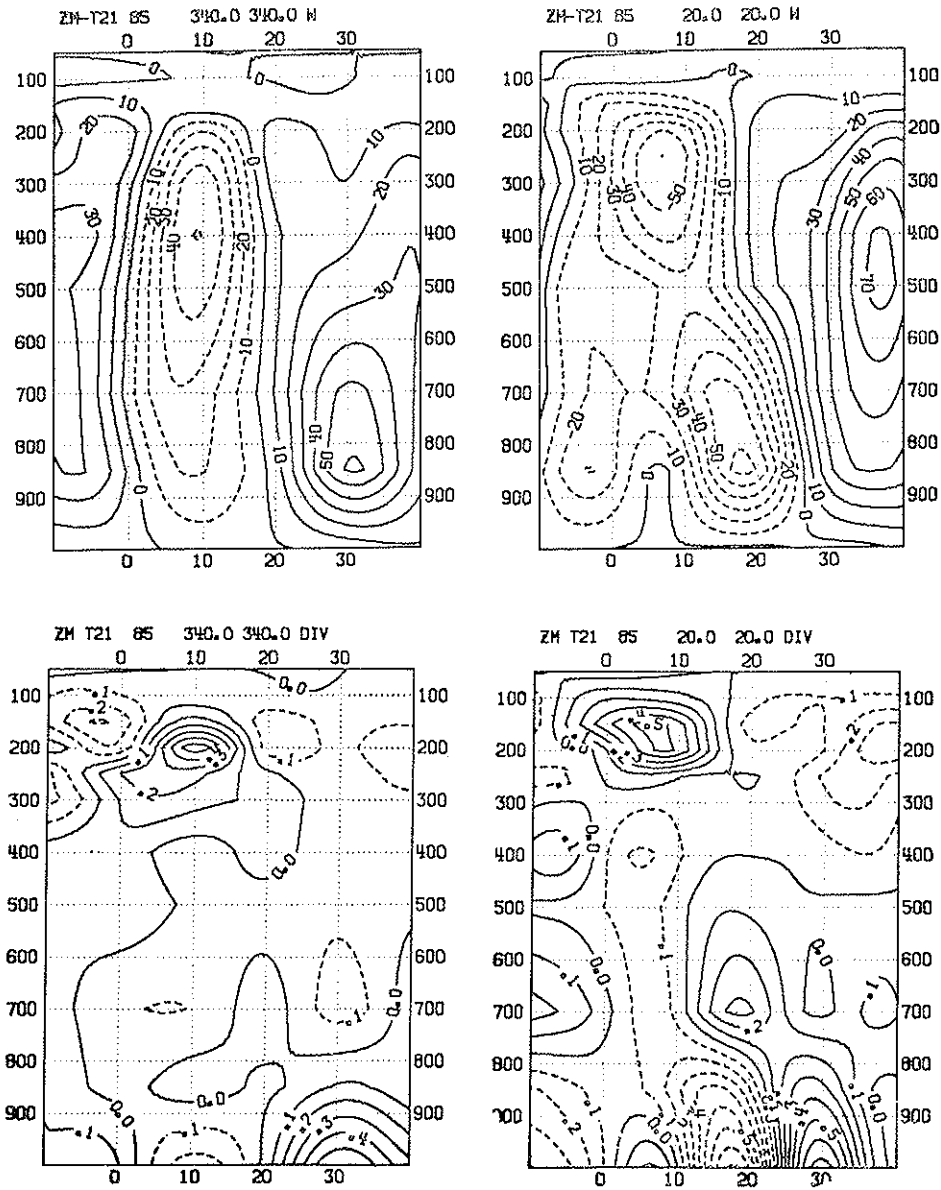

FIG. A2. As in Fig. A1 for mean ω (10^{-5} mb s^{-1}) and divergence (10^{-5} s^{-1}).

slightly to the south of the axis of the Atlantic subtropical high. The model generated vertical motions and divergences that form the basis of the picture are, of course, subject to considerable uncertainty, but the essential correctness of the model analyses at 20°W is attested to by moisture budgets (not shown) constructed from the mean motion and moisture fields shown in Figs. A1b, A2a and A3b of the appendix. Divergences of moisture flux along the 20°W meridian are reasonable in terms of precipitation and evaporation estimates appearing in the literature.

The cross section along 20°E (Fig. 6b) presents a somewhat different picture, though the mass flow may be characterized as a Hadley circulation that is highly skewed at lower levels. The moist monsoon flow is deeper than over the eastern Atlantic and penetrates northward in the form of a thin wedge to almost 20°N. Hot, dry and often dusty desert air rises over the wedge, mixing with the monsoon air that pulses upward in convective plumes. Presumably the low-level ascent over the southern desert is caused by the intense sensible heat flux from the surface and is much deeper than the shallow frictionally-driven circulation postulated by Charney (1975). The top of the desert mixed layer or SAL lies near 500 mb (Carlson and Prospero, 1972). The strongly subsiding flow over the northern desert should not be regarded as representing only the downward branch of the Hadley circulation, since the subsidence seems more closely linked to cold air advection over the Mediterranean (Figs. A1d and A3c) than to radiative cooling aloft.

Because of the dryness of the desert air, little cloudiness or precipitation is observed near the nose of the wedge (or surface ITCZ position). Further south the monsoon layer deepens and increasing amounts of moisture penetrate into the overlying dry easterlies, gradually moistening them. Thus shower activity becomes more frequent and intense towards the south, reaching a peak near 10°N. Unlike over the ocean, the belt of maximum rainfall, as remarked previously, is well removed from the region of strongest low-level convergence. The precipitation maximum evidently results from a northward increase in convection as the monsoon air from the ocean is increasingly destabilized over the heated land and from a subsequent northward decrease in convection as the moist monsoon flow becomes increasingly diluted by mixture with the overlying dry air. From the foregoing description it is clear that the strength and depth of the monsoon flow should be a major factor in determining the overall amount of precipitation in sub-Saharan Africa, a point that has been made by numerous authors (e.g., Landsberg, 1975).

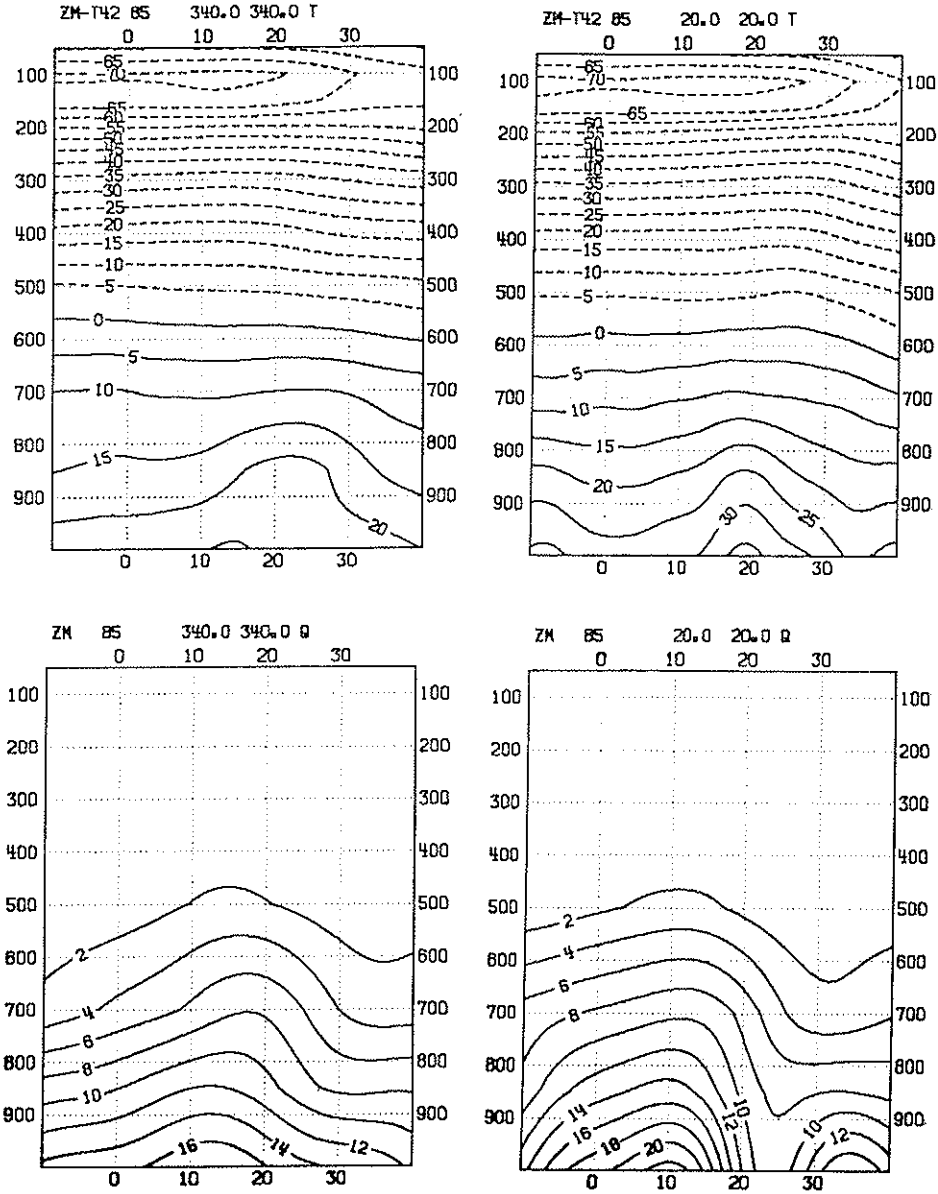

FIG. A3. As in Fig. A1 for mean temperature T(°C) and specific humidity q (10^{-3}).

It should be mentioned that moisture budgets along 20°E computed from the mean fields shown in Figs. A1-3, are not nearly as satisfactory as those obtained for 20°W. They show larger moisture convergence and hence rainfall over the Sahel than in the region of the observed rainfall maximum near 10°N. This result suggests that the strong rising motion over the desert at 18°N (Fig. 6b and Fig. A2c) may be wrong or exaggerated. However, basic principle requires that the strongly heated desert air should rise. The problem may lie with the moisture analysis (Fig. A3d) which shows much larger mixing ratios over the Sahara than the 4 g kg^{-1} value found by Carlson and Prospero (1972) to characterize the Saharan air layer (SAL).

3. Differences between Dry and Wet Years

3.1. *Circulation changes over Africa*

Mean wind changes over Africa between wet and dry periods in the Sahel have been documented by Newell and Kidson (1974). Wet periods chosen by them were August 1958-62; dry periods were August 1970-73. According to Fig. 1, the wet years were, with the exception of 1958, years of near normal rainfall. The dry years were all marked by much below normal rainfall. Meridional cross sections along 10°E of the mean zonal winds for the wet and dry periods and for the wind difference appear in Figs. 7a-c. Corresponding sections for the mean meridional wind appear in Figs. 8a-c. Prominent features of the sections are:

(1) A stronger and deeper southwesterly monsoon in the wet years than in the dry years (positive differences in both zonal and meridional winds below 800-700 mb between the equator and about 20°N).

(2) A stronger and more southward extending AEJ in dry years than in wet years (positive maximum at 700 mb near 10°N in Fig. 7c).

(3) A stronger TEJ in wet years than in dry years (negative maximum near 5°N, 200 mb in the same figure).

(4) Stronger southerlies at upper-levels in the northern hemisphere subtropics in wet years (positive maximum near 30°N in Fig. 7a).

(5) A stronger upper-level jet stream in the southern hemisphere subtropics in the dry years (negative maximum at 20°S in Fig. 7b).

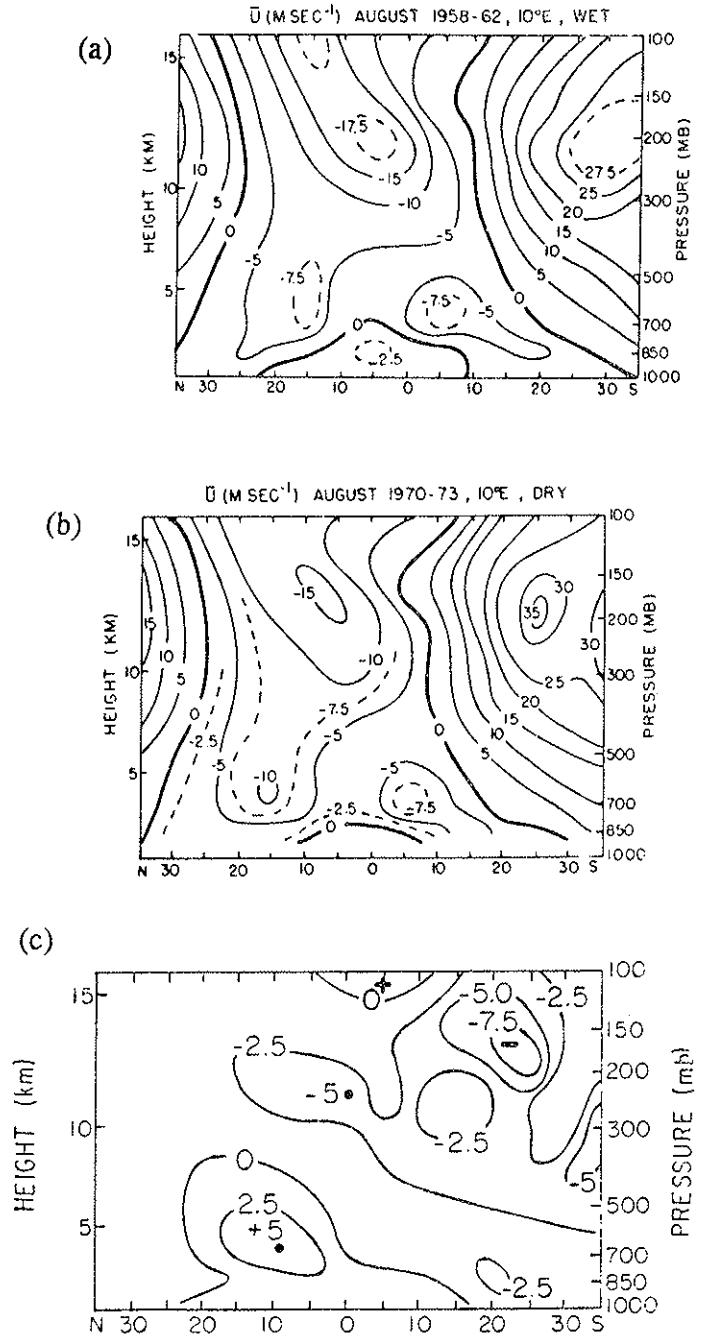

FIG. 7. Meridional cross-sections along 10°E of mean zonal wind for (a) August 1958-62 and (b) August 1970-73 and (c) differences. (Newell and Kidson, 1974). Units: m s^{-1}.

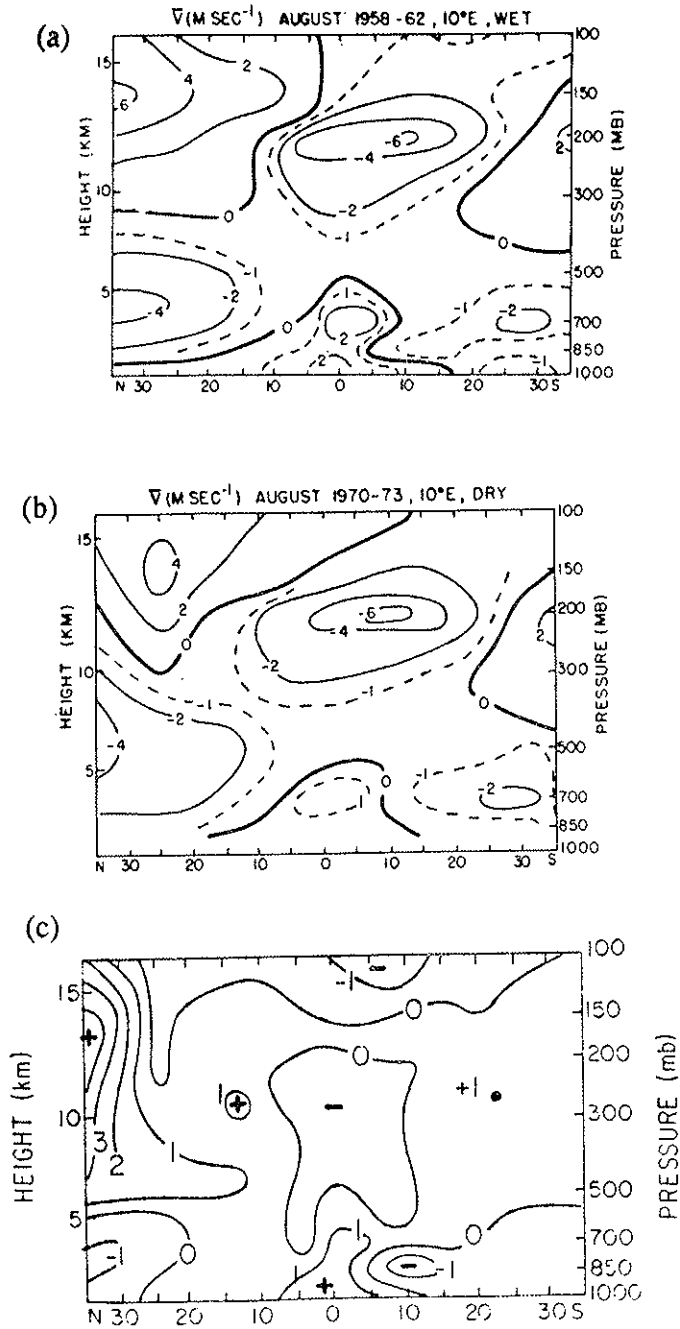

FIG. 8. As in Fig. 7 for mean meridional wind.

The finding of a deeper and stronger monsoon flow in wet years (item 1 above) confirms the expectations of Landsberg (1975) and others. However, such a sharp distinction was not observed in a study by Lamb (1983) that compared three drought years (1968, 1971 and 1972) and three non-drought years (1967, 1969 and 1975).

Newell and Kidson (1974) discussed possible causes of the strengthening of the AEJ in dry years (item 2), pointing out that the enhancement was associated with increased easterly wind shear between 850 and 700 mb and hence from thermal wind arguments with an increased temperature rise between the equator and the Sahel. They cited evidence from Tanaka *et al.* (1975) and Schupelius (1976) to support the idea that Sahelian temperatures are indeed warmer in dry years. In explanation of the warmer temperatures, they postulated the existence of enhanced subsidence connected with global-scale circulation changes. As an alternative explanation they pointed out that reduced rainfall leads to decreased evapotranspiration and therefore to an increased input of sensible heat from the earth's surface.

In an earlier paper Kidson (1977) proposed that the strengthening of the TEJ on wet years was associated with a strengthening of the meridional or Hadley circulation, the mechanism of the easterly acceleration being the added Coriolis torque exerted on the equatorward flowing upper branch of the circulation. The difference chart for the meridional wind (Fig. 8c) only weakly supports this hypothesis. However, it may be that the explanation is correct but that the main effect lies upstream of the 10°E meridian of the cross section. Figure 9, taken from Newell and Kidson (1974), reveals that the enhancement of the TEJ on wet years is considerably stronger in the Gulf of Aden, at the eastern edge of their figure than at 10°E, suggesting a possible linkage to the Indian Ocean region. The previously mentioned large wind differences at sub-tropical latitudes of both hemispheres also suggest the importance of considering distant events in seeking to understand Sahelian drought. This is a theme that will be returned to later.

3.2. *Circulation and related changes over the Atlantic*

These are of particular interest with respect to the drought problem. They have been investigated by Lamb (1978) with use of seasonal (July-September) composites for dry years (1942, 1949, 1970, 1971 and 1972) and for wet years (1943, 1950, 1952, 1954 and 1957) and by Hastenrath

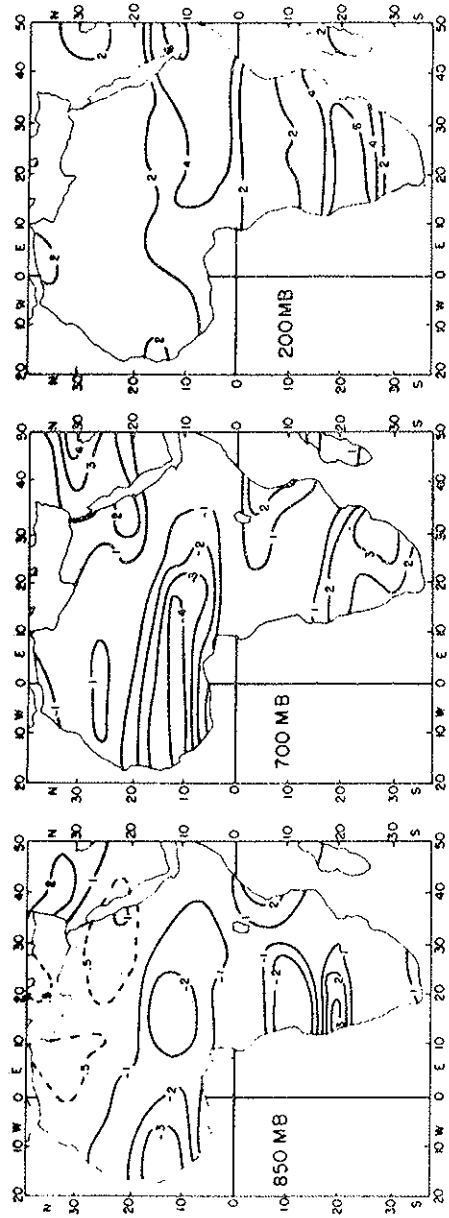

FIG. 9. Maps of zonal wind difference between dry (1970-73 and wet (1958-60) Augusts at 850, 700 and 200 mb. (Newell and Kidson, 1974). Units m s^{-1}.

(1984) with use of July-August composites for the same wet years and for slightly different dry years (1941, 1942, 1944, 1968, 1970, 1971 and 1972). Differences between the wet and dry years (wet minus dry), taken from Hastenrath appear in Fig. 10. The dot pattern represents positive differences; the thin and heavy broken lines enclose areas significantly different at the 5 and 10% levels, respectively.

Significant positive zonal wind differences exist in a broad region extending from West Africa to the northern coast of South America and the Caribbean. Where the positive anomalies coincide with the trade winds, they indicate stronger than normal trade easterlies during dry years. Where they coincide with the southerly monsoon flow near and south of Senegal, they signify a weaker than normal onshore flow during dry years. The meridional wind component exhibits several significant positive differences and one significant negative difference. The positive differences again signify stronger than normal northeasterly trades and weaker than normal southwesterly monsoon flow in dry years. These results accord with those of Newell and Kidson for the adjoining land area. The negative difference on the equator to the west of the Gulf of Guinea indicates that the southeasterly trades have a stronger than normal southerly component on dry years. This feature, coupled with the tendency for the zonal component in the Gulf of Guinea to be stronger than normal on dry years suggests southward displacement at times of drought of the ridge of high pressure that extends west-northwestward through the Gulf.

The sea-level pressure differences between the wet and dry years show higher than normal pressures to the south of the equator and lower than normal pressures off Africa to the north of 10°N and over the Caribbean. This pattern of differences is consistent with the above described zonal wind changes. The southward displacement of the near equatorial pressure trough on dry years associated with these pressure changes has been illustrated by Lamb (1978). The latter also noted that the North Atlantic subtropical high is situated abnormally far north on dry years despite the southward displacement of the near equatorial trough and the stronger pressure gradient (or easterlies) in the trade wind belt.

A distinctive pattern of sea-surface temperature differences accompanies the foregoing features. Wet years are marked by warmer than normal SST's in a belt stretching from the Mauritanean coast to the Caribbean. Colder than normal SST's extend across the Atlantic from the Gulf of Guinea to northeast Brazil. A similar relationship between SST's and Sahelian drought was found by Lough (1986) based on principal component

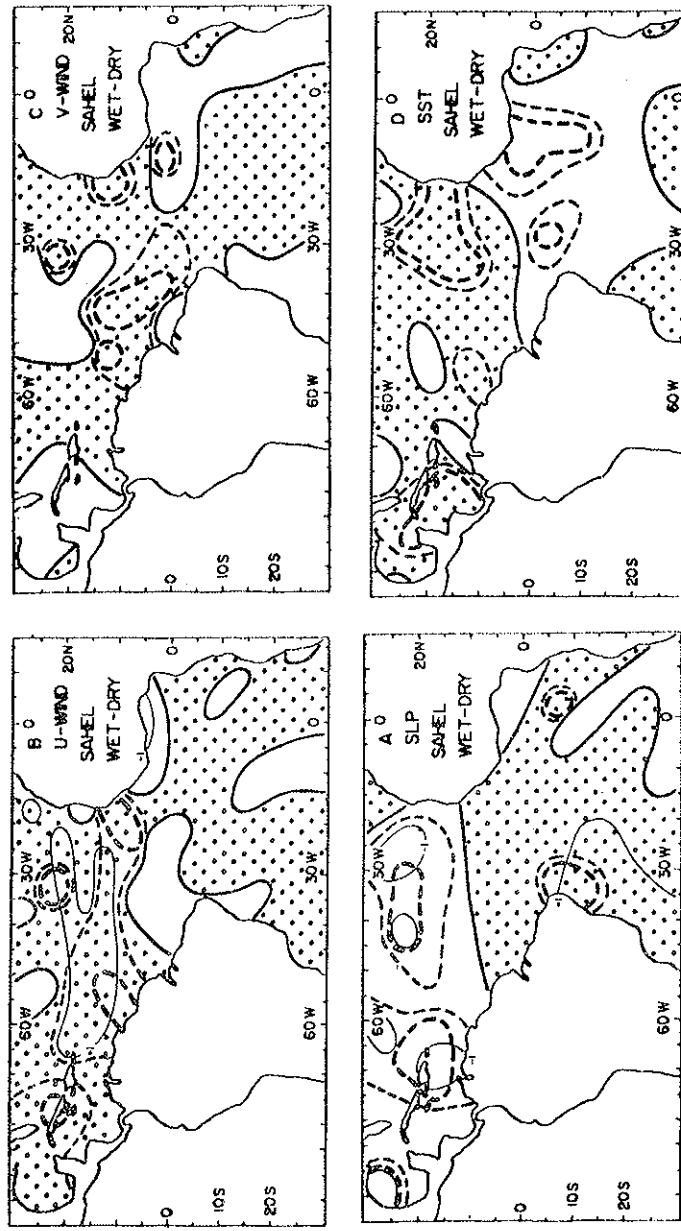

FIG. 10. Maps of July-August circulation departures associated with rainfall anomalies in sub-Saharan Africa (Hastenrath, 1984). Dots denote areas of positive departures. Areas significant at the 5 and 10% levels are enclosed by heavy and thin broken lines.

analysis. She obtained a -0.64 correlation between the second eigenvector of the monthly normalized SST departures for the period 1948 to 1972, shown in Fig. 11, and the Sahel rainfall index (SRI) of Nicholson (1979). However, although the second eigenvector for the period 1911-39 was similar to that for the later period, little correlation of it with the rainfall index for the 1911-39 period was found.

Folland *et al.* (1986) have also observed a similar pattern of temperature differences between wet and dry periods using data from years that partly overlap those employed in the previously mentioned studies (wet: 1950, 1952-4, 1958; dry: 1972-3, 1982-4). An important result of their work is the finding that Sahelian drought appears to be as closely related to SST anomalies in the Pacific and Indian Oceans as to those in the Atlantic. Particularly impressive is their graph showing for the period 1901-1985 the difference between July-September SST anomalies in the Southern Hemisphere and northern Indian Ocean minus those in the Northern Hemisphere excluding the northern Indian Ocean. The association of major features of the positive and negative anomaly differences with dry and wet periods in the Sahel is obvious. Evidently a more stable relationship between SST's and Sahelian drought emerges when the oceans are considered on a global basis rather than when only the Atlantic is considered. Recent modelling results (Palmer, 1986) provide support for the idea that rainfall in the Sahel is sensitive to SST anomalies in all three major oceans.

Lamb (1978) and Lough (1986) have looked at lag relationship in SST and other anomaly patterns. Some encouraging results for drought

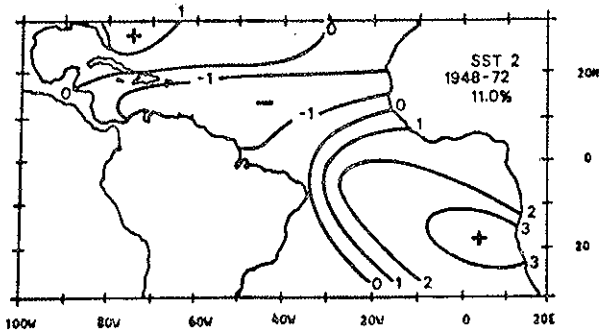

FIG. 11. Second eigenvector of monthly normalized SST departures, 1948 to 1972 (Lough, 1986). Loadings are multiplied by 10.

prediction 3 to 6 months in advance were obtained by Lamb, but this subject and the subject of modelling results are beyond the scope of the present paper.

3.3. *Sahelian drought in relation to African wave disturbances and Atlantic hurricanes and depressions*

In the previous subsections it was shown how a number of the quasi-stationary features of the summertime large-scale circulation over Africa and the Atlantic differ between drought and non-drought or wet years. It is natural to inquire whether related changes occur with respect to the transient, synoptic-scale systems that frequent the tropical belt north of the equator from central Africa to the Caribbean during the May-November period. Information on this subject is scattered. For continental Africa some pertinent statistical data on wave behavior can be found in studies by Albignat and Reed (1980) and Mouzna (1984) and by recent results obtained at ECMWF by Reed *et al.* (1986b). For coastal Africa, the annual summaries of tropical Atlantic systems prepared by the National Hurricane Center in Miami for the years 1967-1979 inclusive and appearing in *Monthly Weather Review*, contain information of value. Unfortunately, most of the years examined in these studies and summaries were drought years. Four can be characterized as years of minor drought (1969, 1974, 1975 and 1978) and only one (1967) as a non-drought (but not wet) year. The continuing annual summaries of the Atlantic hurricane season, also prepared by the Miami center and appearing in *Monthly Weather Review*, are rich sources of information on tropical cyclones (storms with winds ≥ 18 m s^{-1}) and hurricanes (storms with winds ≥ 33 m s^{-1}) in the Atlantic and Caribbean.

Considering first the African region, we present in Figs. 12-14 band-pass filtered amplitudes or variances of the 850 mb meridional wind for oscillations of roughly 3-4 day period for seven different years. (Amplitudes can be converted to variances by squaring and dividing by two). The variance patterns define the regions of maximum wave intensity or activity and, in view of the westward travel of the waves, the upstream and downstream regions of development and decay. An exact comparison of the intensities is not possible because of the slightly different bandwidths and shorter sampling periods employed in Figs. 12 and 13 than in Fig. 14. Moreover, there is some possibility that the variances in Fig. 14 were

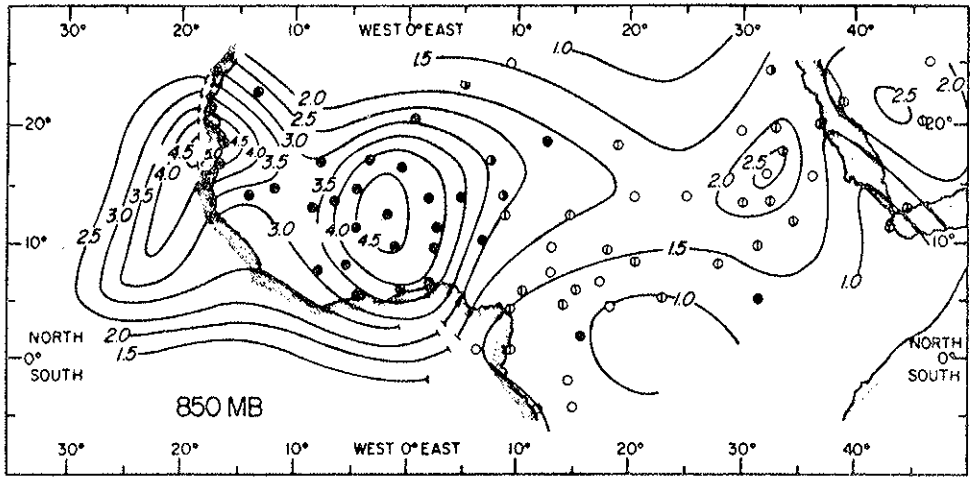

FIG. 12. Amplitude of meridional wind oscillation (m s^{-1}) in the frequency band 0.2-0.4 cpd at 850 mb during Phase III of GATE (Albignat and Reed, 1980).

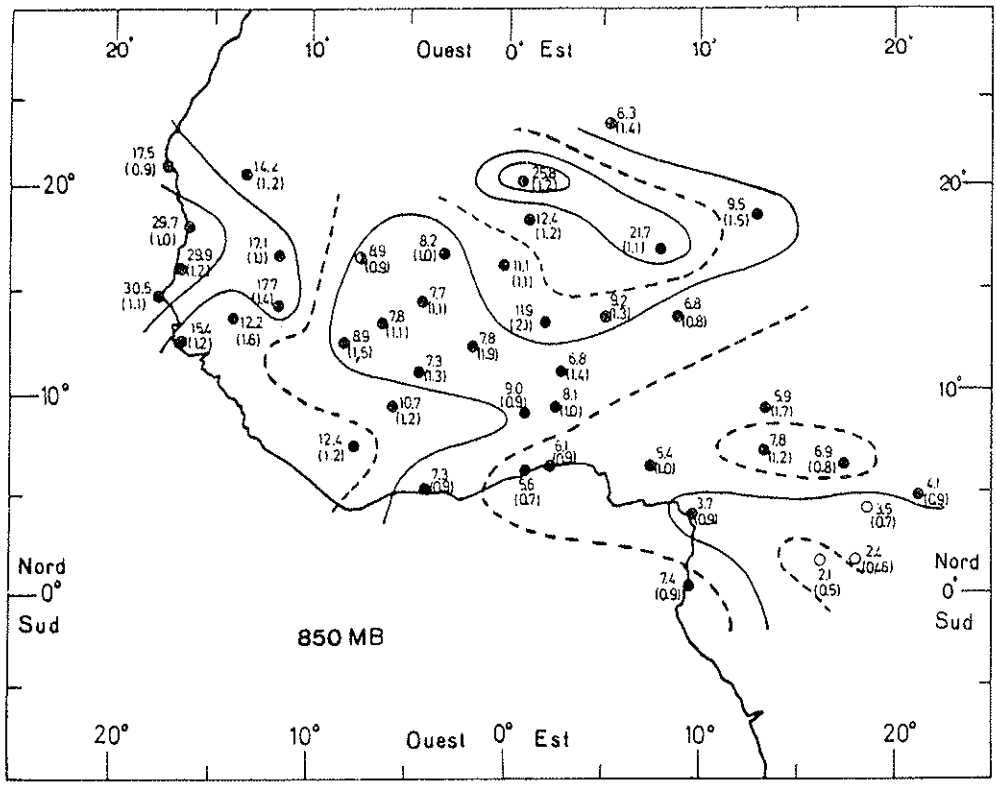

FIG. 13. Variance of the 850 mb meridional wind component in the frequency band 0.2-0.4 cpd for the period 15 July-15 August 1978 (Mouzna, 1984).

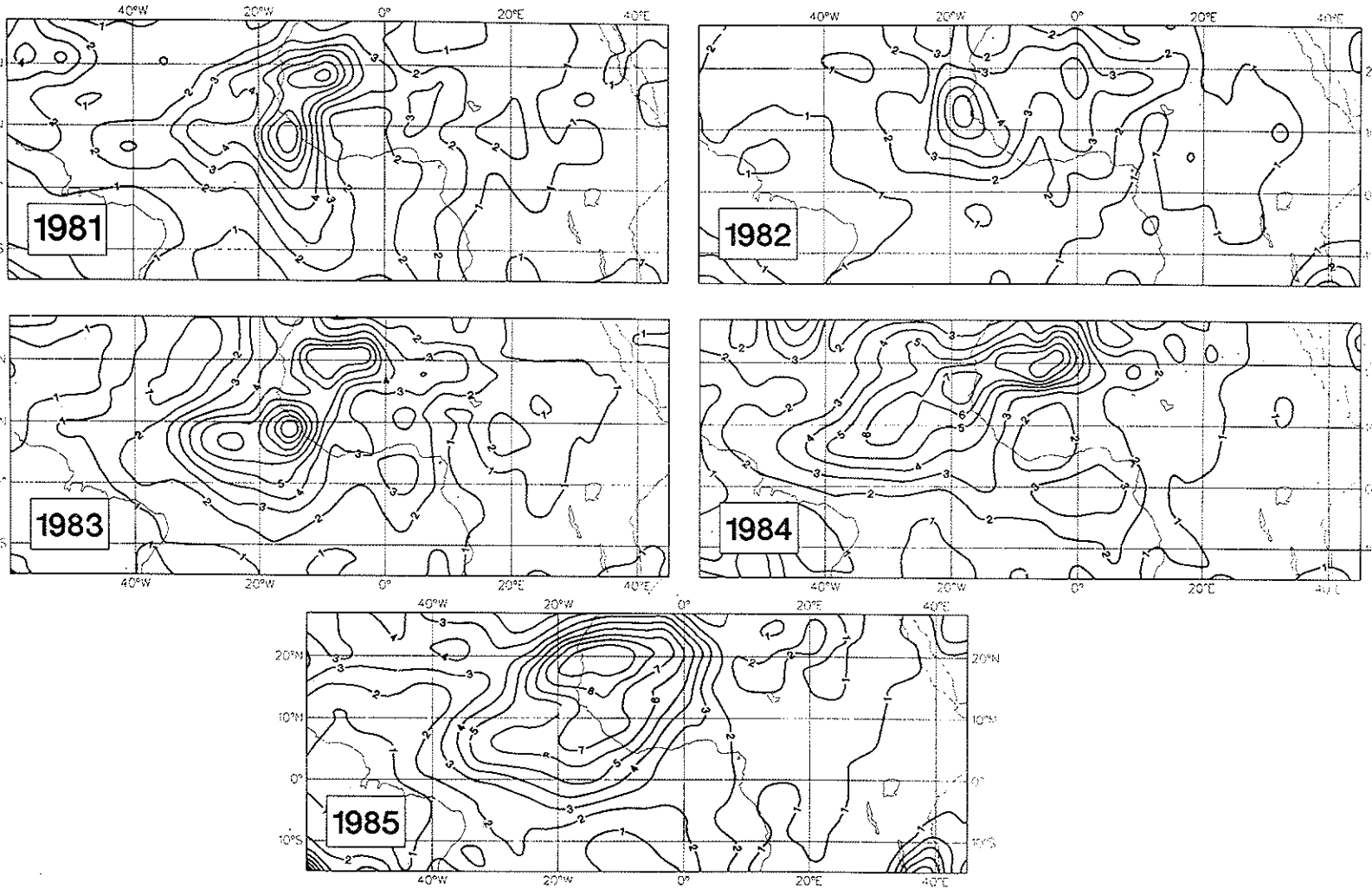
40°W
20°W
0°
20°E
40°E
1981
1982
1983
1984
1985
20°N
10°N
0°
10°S

affected by changes in model resolution and physics that occurred during the 5 years covered by the figure.

Of the years depicted, 1974 was least deficient in rainfall. Figure 12, taken from Albignat and Reed (1980), shows two areas of maximum amplitude (variance) in the four week period from 23 August to 19 September of that year, one situated on the coast between 15°N and 20°N and a second inland at 10°N centered just to the west of the Greenwich meridian. All other years display dual maxima but in none of these years was the inland maximum displaced so far to the south. As noted first by Carlson (1969) and later by Burpee (1975) and Reed *et al.* (1977), African waves often possess two circulation centers at low levels, a nearly cloud-free center in the monsoon trough over the sub-Sahara and a second one marked by greater cloud, and presumably precipitation, amounts in the rain belt to the south. The northernmost center is thought to be an outgrowth of dry baroclinic instability. It has hypothesized (Norquist *et al.*, 1977) that the southern center is energized by convective heat release or wave-CISK (Lindzen, 1974). Thus it is perhaps of significance that the inland maximum was located farthest south on the wettest year.

Somewhat countering this suggestion, however, is the picture for 1978, the third wettest of the years considered. According to Fig. 13, taken from Mouzna (1984), the coastal maximum was similarly located in the period 15 July-15 August 1978. However, the interior maximum was located 10 deg north of its 1974 position. (Peak variances in this figure are at least double those of other years, raising a question of whether the variances are in error by a factor of two).

Variances for waves with periods of 2.9 to 5.1 days, obtained from the initialized ECMWF analyses (Reed *et al.*, 1986b) for August-September 1981 to 1985 inclusive, appear in Fig. 14. These were years of moderate (1981 and 1985) to severe (1982-84) drought (see Fig. 1). Patterns for 1981, 1983 and 1985 were most similar, possessing maxima near 9°N, 18°W and 20°N, 10°W. In 1984 the coastal maximum was displaced well to the north in a position similar to that in 1974 and 1979, and in 1982 the inland maximum, though much weaker, was located in nearly the same position as in 1979. Taken as a whole the results indicate considerable year-to-year fluctuation in the variance patterns but not a sequence of changes that can be related to the drought intensity.

A longer and perhaps more revealing picture of changes in wave behavior appears in Fig. 15. This figure, based on data in the annual summaries of Atlantic tropical systems (e.g., Simpson *et al.*, 1968) shows

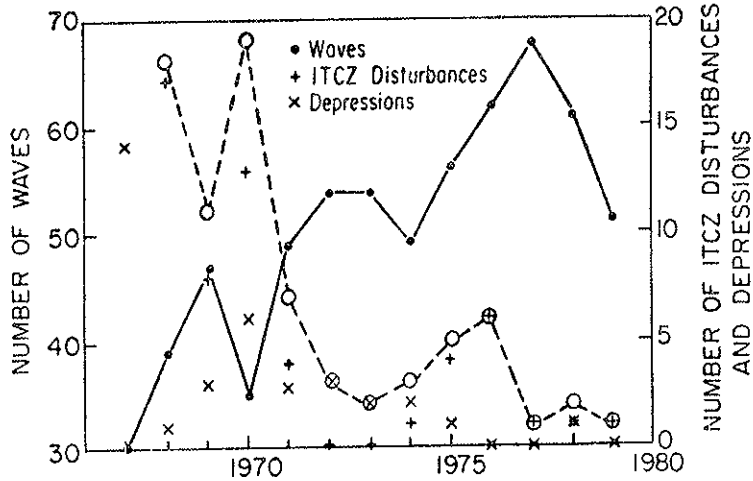

FIG. 15. Number of waves (solid line) and sum of numbers of ITCZ disturbances and depressions (dashed line) in vicinity of West African coast during the years 1967 to 1979. (ITCZ disturbances not counted in 1967).

the number of waves, depressions (defined as systems with closed circulations but maximum winds < 18 m s^{-1}) and ITCZ disturbances that crossed the African coast during the years 1967 to 1979 inclusive. (The latter are defined by the above authors as "a discrete system of apparently organized convection, generally 100 to 300 mi in diameter, originating in the tropics or subtropics, having a non-frontal, migrating character, and having maintained its identity for 24 hr or more."). The striking feature of the diagram is the dramatic increase in the number of waves (solid line) beginning in 1970 and the equally dramatic decrease in the combined number of depressions and ITCZ disturbances (dashed line). If uniform counting procedures were maintained during the interval, a pronounced change in the character of the disturbances crossing the coast is indicated during the persistent drought of the 1970's. Again the correlation of year-to-year changes with drought intensity (see Fig. 1) is not large, but the trend for the period as a whole is remarkable. If real, it suggests that more of the wet type of system existed prior to or early in the drought period than later on, since ITCZ disturbances are by definition convective in character and depressions invariably have large masses of convection associated with them. It should also be noted from Fig. 14 that the total number of systems has changed little, if at all, during the period. A

tentative conclusion is that the ever present sub-Saharan baroclinic zone and near equatorial rain belt jointly spawn about the same total number of disturbances over Africa each year, whatever the rainfall amount, but that fewer strong and/or highly convective disturbances occur near the coast during periods of extended drought. If this conclusion is correct, a passive role for the disturbances in drought formation is suggested. When wetter conditions prevail, they exhibit a more convective character than during dry periods, but they are not more plentiful.

More provocative than the relationship of African waves to drought is the relationship of Atlantic (including the Caribbean Sea and Gulf of Mexico) tropical cyclones and hurricanes. Particularly impressive is the association shown in Fig. 16 between the annual number of hurricane hours and the SDI. It is apparent from the figure that the yearly number of hurricane hours fell below the long term average in nearly every year between 1971 and 1984. This was also true, though not to such an extreme degree, for the actual number of hurricanes. Also remarkable in Fig. 16 is the correspondence between extreme drought and minimal hurricane activity. The years 1972, 1973, 1977, 1982 and 1983, all years

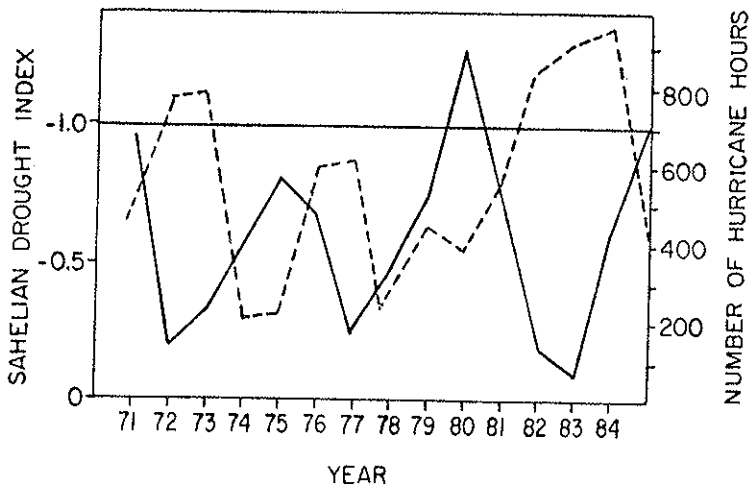

FIG. 16. Number of hurricane hours from Lawrence and Clark (1985), solid line and right axis, and Sahelian drought index (SRI), dashed line and left axis, for years 1970-85. Horizontal line indicates average number of hurricane hours for years 1954-68. Note that the SDI has been plotted with scale reversed.

of extremely deficient hurricane activity, ranked 5th, 4th, 6th, 3rd and 2nd in drought severity according to the SDI. The years 1972, 1982 and 1983 were in succession the least active years since 1930. It is perhaps worth noting that 1972-73, 1976-77 and 1982-83 were also El Niño years or years of negative SOI (Southern Oscillation Index).

The conditions associated with the decline in hurricane activity during the drought period of the 1970's have been remarked on repeatedly in the annual summaries of the Atlantic hurricane season. These are (1) abnormally strong upper westerlies or tropospheric westerly wind shear in the customary cyclogenetical areas and (2) below normal SST's in the Atlantic between West Africa and the Antilles. The latter condition has already been mentioned in previous discussion of the works of Lamb (1978), Hastenrath (1984), Lough (1986) and Folland *et al.* (1986). The former condition, the presence of abnormal westerlies or westerly shear, is linked to abnormal behavior of the mid-ocean upper-tropospheric trough.

Another interesting and related facet of the behavior of synoptic systems in the tropical and subtropical Atlantic during the decade of the 1970's pertains to the ratio of the number of depressions of tropical origin to the total number of depressions. Concomitant with the increased strength of the upper westerlies and with the negative SST anomaly in the Atlantic a change occurred in the proportion of systems that were of purely tropical origin and those ascribed to a "baroclinic" origin (Fig. 17). The latter term is used by the Miami group to denote systems that form either in low-level frontal zones that push far southward or beneath the cold lows that frequent the upper tropospheric, mid-Atlantic trough. From Fig. 17 it is evident that the 1970's were marked by a far greater proportion of the "baroclinic" type systems than were the late 1960's.

Taken collectively, the foregoing results show that during the recent (or present?) prolonged drought episode substantial shorter period changes occurred in the behavior of both the quasi-stationary and transient components of the flow in the tropical and subtropical Atlantic. These changes appeared to be connected with pronounced fluctuations in the severity of drought. The subject requires more attention than can be given it here, but certainly the evidence gathered thus far reinforces the view that teleconnections may play an important role in the drought problem.

Finally, in order to avoid planting the idea that a simple, universal relationship exists between hurricane activity and Sahelian drought, we present a much longer record of the number of hurricane hours (days) in the Atlantic taken from a recent paper by Gray (1984). This longer record

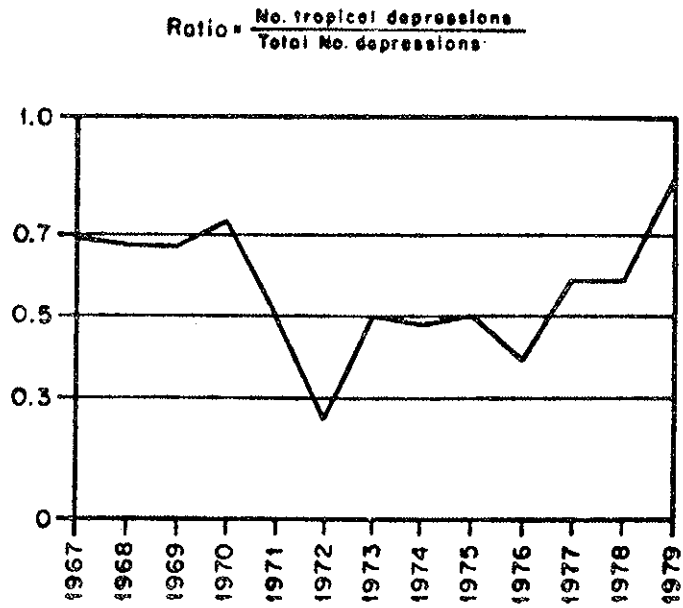

FIG. 17. Ratio of the number of depressions of tropical origin to the total number of depressions, 1967-79 (Frank and Clark, 1980).

(Fig. 18) indicates that the relationship of hurricane activity to the El Niño holds up reasonably well for the century as a whole. Comparison of this figure with Fig. 1 reveals a much less impressive relationship between hurricane days and Sahelian drought.

4. FUTURE NEEDS

A prime requisite for improved understanding of Sahelian drought is the availability of high quality data sets for the Sahel and adjacent regions. Two types of data are commonly used to advantage in modern diagnostic studies: original observations and model-generated grid point data. Our purpose here is to point out briefly the severe deficiencies that exist with respect to both types of data in the regions of interest.

The availability of data over Africa and nearby areas for a typical recent month (August 1985) is shown in Figs. 19a-f, taken from Reed

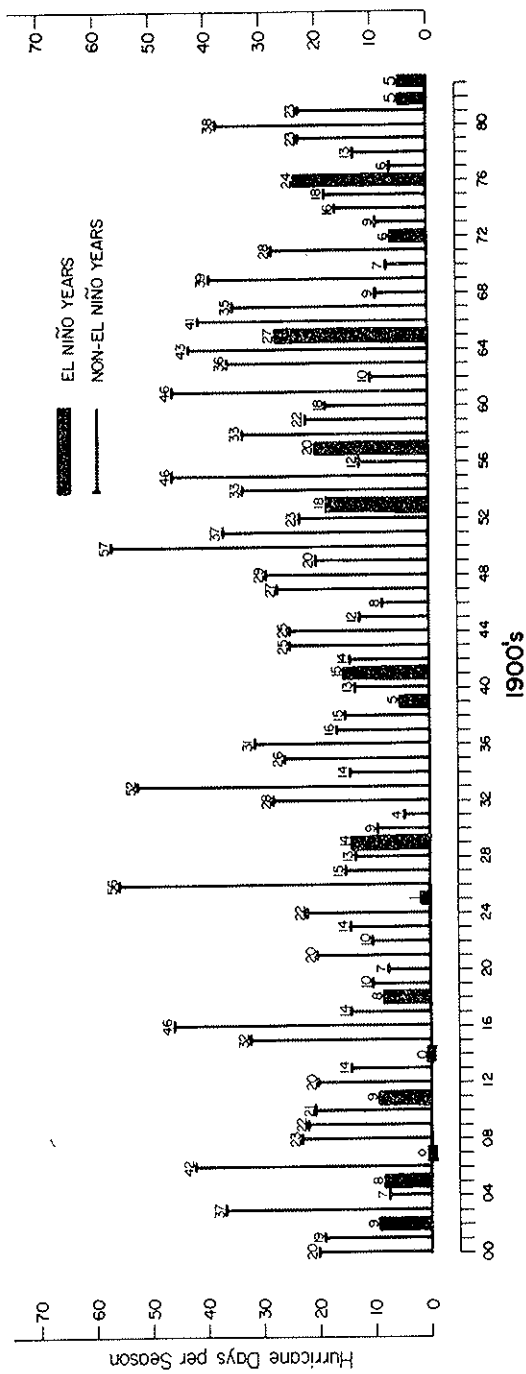

FIG. 18. Number of hurricane days (given at top of lines) in El Niño and non-El Niño years from 1900 to 1982 (Gray, 1984).

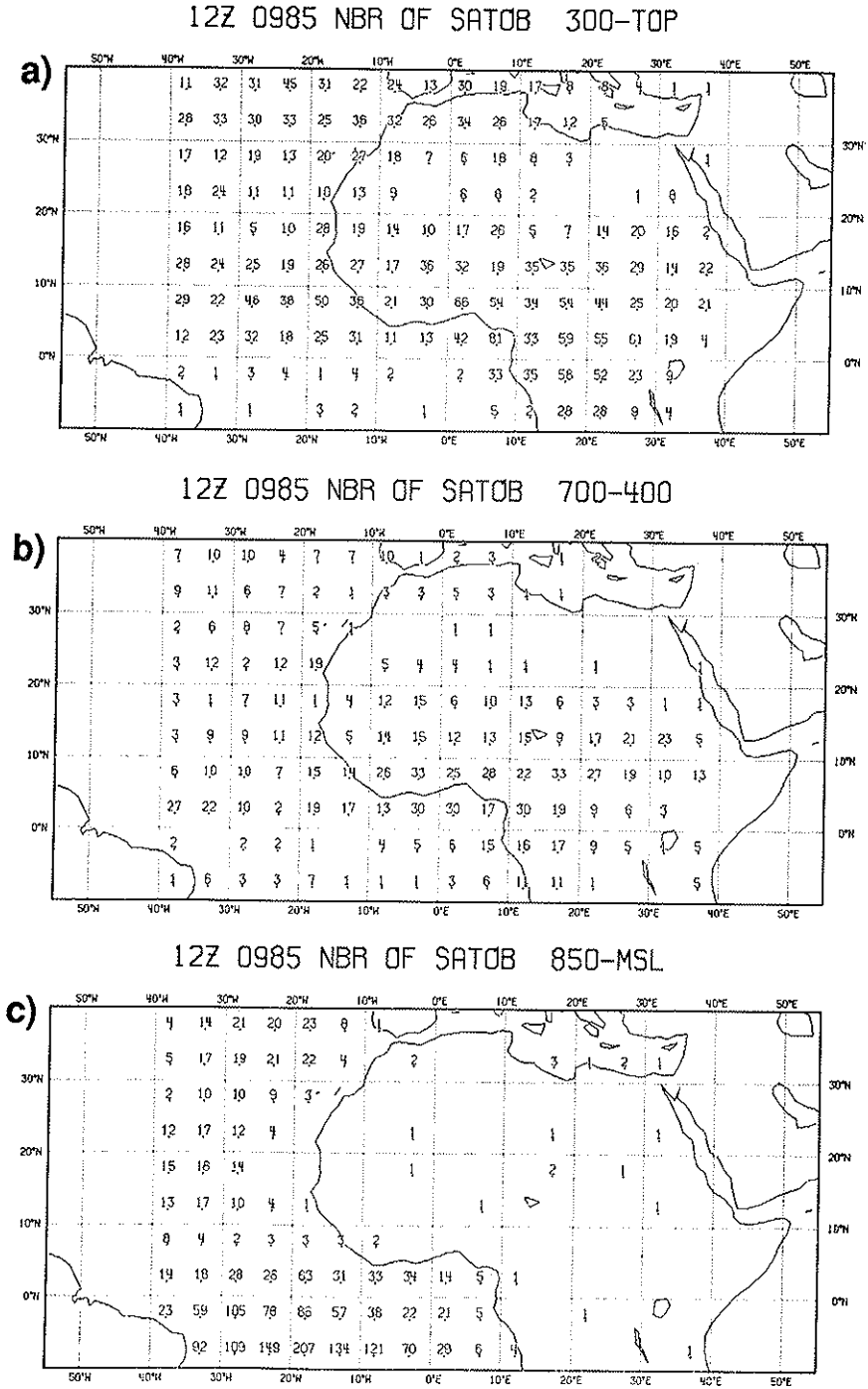

FIG. 19. Number of observations received at 1200 GMT in August 1985 for (a) aireps, (b) balloons at 250 mb, (c) balloons at 850 mb and satellite winds (d) above 300 mb (e), between 700 and 400 mb and (f) 850 mb and the surface (Reed *et al.*, 1986a).

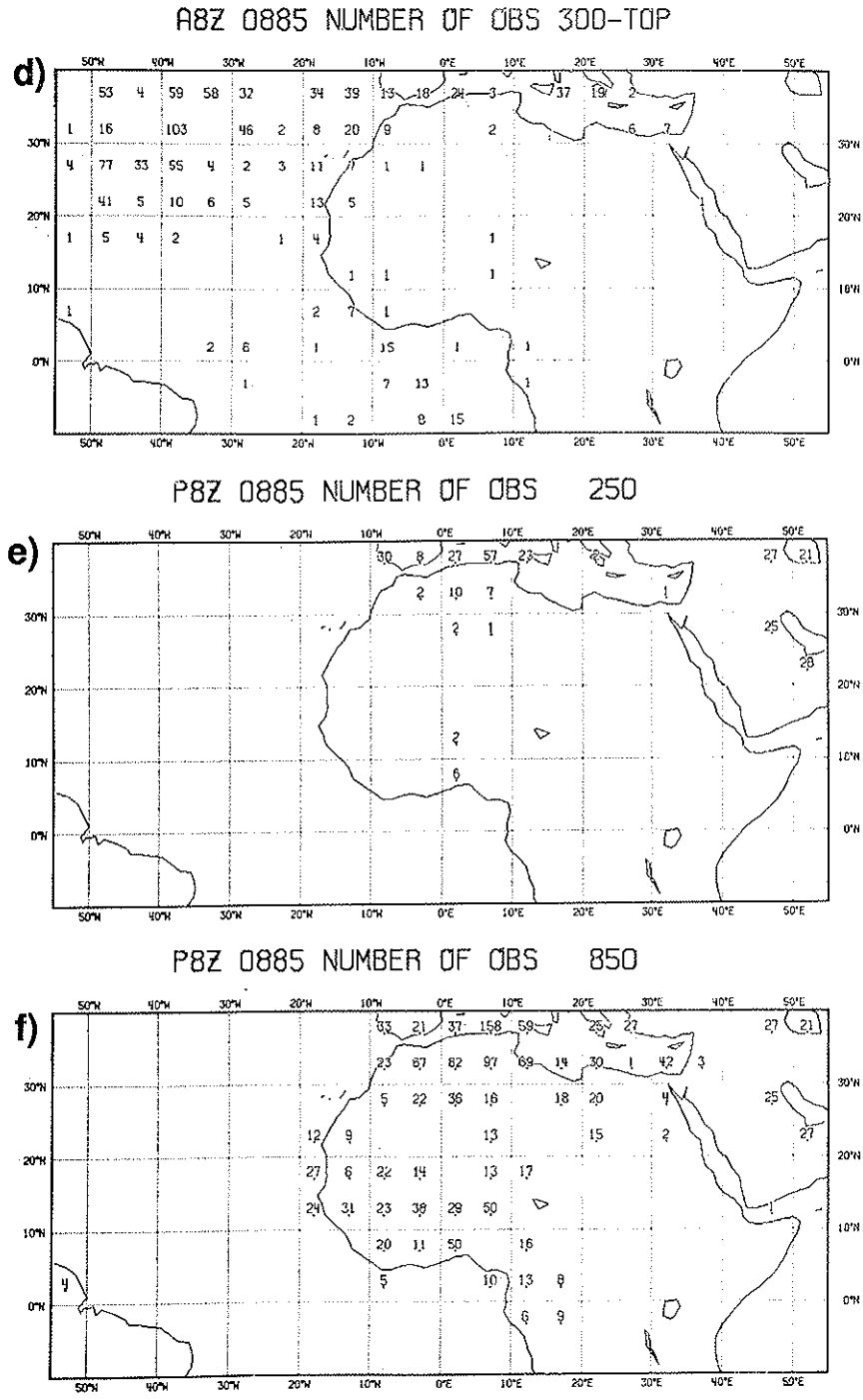

FIG. 19 continued.

et al. (1986a). The numbers of various types of observations taken within ± 3h of 1200 GMT and received at ECMWF via the Gobal Transmission System by 2000 GMT are plotted at the center points of 5° lat./long. squares. It is apparent from Figs. 19a-c that large data gaps exist over the Sahara and also over parts of Central and East Africa. The data deficiency over the Sahara is not surprising, though it might be hoped that with modern technology some way could be found to alleviate it. The situation with respect to Central and East Africa is especially regrettable, since in previous years, and even previous decades, observations have been forthcoming from areas that are now blank. Satellite cloud-track wind observations (Figs. 19d-f) help to overcome the problem at middle and upper levels but are rarely obtainable at lower levels, where data are especially needed. The writer does not know whether the deficiency is as severe for archived data as for operational data. However, the efficient preparation of gridded data sets requires that the observations be available in nearly real time.

A possible problem connected with the use of gridded data concerns the accuracy of certain of the analyzed or initialized data fields in Saharan and sub-Saharan Africa, in particular the fields of divergence, vertical motion, moisture and precipitation. Mention was made earlier of the difficulty that arose when we attempted to obtain moisture budgets along 20°E from ECMWF mean fields. The computations yielded very heavy precipitation over the Sahel. The same problem seems to afflict the British Meteorological Office general circulation model, as evidenced by the excessive rainfall amount in the region to the northeast of Lake Chad shown in Fig. 20 (reproduced from Folland *et al.*, 1986). Karyampudi (1986) has described the difficulties encountered in adapting the PSU/NCAR mesoscale model to prediction over Africa. The amount of tuning of this already much used model that was needed in order to achieve reasonable simulations for the Saharan and nearby regions was an eyeopener for this non-modeller. These pieces of evidence suggest a need for closer attention to the problem of modeling the atmospheric structure in these regions. In middle latitudes much confidence can be placed in gridded data sets generated by existing forecast models. It is not certain, however, that current models perform well enough in all parts of the tropics for the data sets to be used with the same degree of confidence. The Sahel, in particular, is a region where model behavior needs more careful scrutiny.

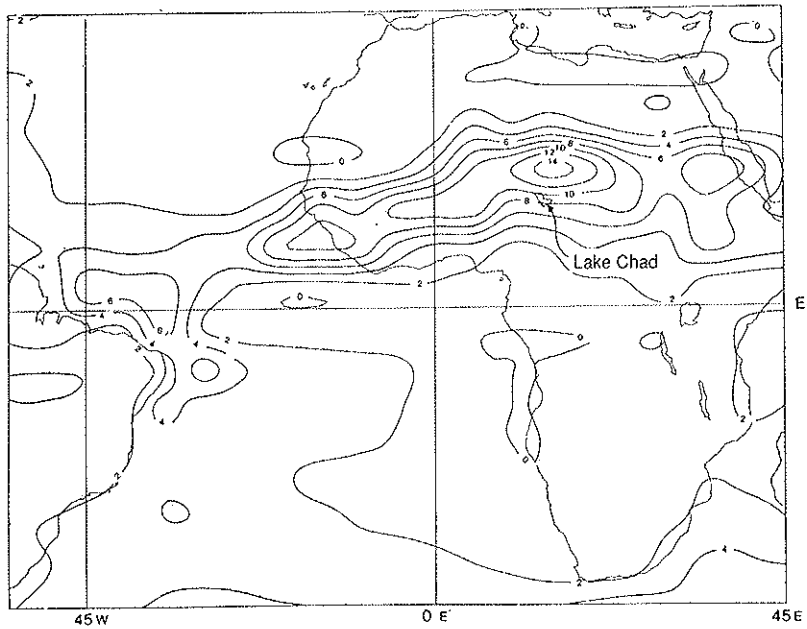

FIG. 20. Mean rainfall (mm d^{-1}) in 180 day control run (Folland *et al.*, 1986).

5. SUMMARY AND DISCUSSION

From the foregoing account it is seen that the Sahel in summer is a transition zone between the rain belt that stretches across Africa to its south and the dry Sahara that lies to its north. Within this zone, hot dry desert air rises over a thin wedge of warm moist monsoon air, intermixing with the convective plumes that emanate from the boundary layer. Indeed, the Sahelian zone can be viewed as a weak frontal zone wherein the warm air mass is exceedingly dry and essentially cloudless and the (relatively) cool air mass is moist and populated by cumulus clouds of varying amounts and depths. The preference of a mid-tropospheric jet stream is a further manifestation of the frontal character of the zone, as are the wave disturbances that form within the zone and exert a modulating influence on the precipitation.

On the basis of the above picture it can be argued that rain production in the Sahel must depend on the strength and depth of the monsoon current and on the dryness of the subsided desert air that intermixes with

it. From the limited evidence presented here the production does not appear to depend on the number or geographical position of the wave disturbances, since they seem to be as plentiful in dry years as in wet and their tracks during the recent drought episode were little related to drought severity. No reliable information exists on the variations in strength of the desert subsidence, though enhanced subsidence has been proposed as a possible explanation for the warmer lower tropospheric temperatures observed over the Sahel during drought periods. Rain production also depends on evapotranspiration, or recycling of moisture, and hence on soil moisture. These factors were not discussed in this presentation, but it might be assumed that reduced evapotranspiration and soil moisture are more likely to be consequences of drought than causes.

The wider factors affecting Sahelian rainfall are not fully understood, though there is considerable evidence that distant events may be of importance. Since the 1940's a distinctive pattern of SST anomalies, characterized by below normal temperatures in the tropical North Atlantic and above normal temperatures in the Gulf of Guinea, has prevailed during periods of drought. There is also evidence, based on records for the entire century and on numerical modeling results, that rainfall in the Sahel is linked to SST anomalies in the Pacific and Indian Oceans, as well as in the Atlantic.

Circulation features, too, suggest the importance of large or planetary-scale influences. The subtropical jet streams of both hemispheres exhibit changes between wet and dry years that are as large as those occurring within the sub-Saharan region. Since 1970 the severity of drought appears related to hurricane activity in the Atlantic as measured by the number of hurricane days. Years of severe drought have tended to coincide with years of much reduced hurricane activity. The reduced hurricane activity of the 1970's has been shown by investigators to be related to two factors: below normal SST's between Africa and the Antilles and enhanced westerly shear, or upper tropospheric westerlies, in the formative regions. Thus a tie-in is implied between Sahelian drought and circulation features of the Western Atlantic.

Much remains to be done before Sahelian drought can be fully understood. Clearly the problem must be examined on a global scale in view of the aforementioned evidence of significant teleconnections. The problem must also be better understood regionally. In this regard we have pointed out the need for vast improvement of the African data network and also for improved numerical modeling of the sub-Saharan atmosphere.

REFERENCES

ALBIGNAT J.P. and REED R.J., *The origin of African wave disturbances during Phase III of GATE.* « Mon. Wea. Rev., *108*, 1827-1839 (1980).

BURPEE R.W., *The origin and structure of easterly waves in the lower troposphere of North Africa.* « J. Atmos. Sci. », *29*, 77-90 (1972).

BURPEE R.W., *Some features of synoptic-scale waves based on compositing analysis of GATE data.* « Mon. Wea. Rev. », *103*, 921-925 (1975).

CARLSON T.N., *Some remarks on African disturbances and their progress over the tropical Atlantic.* « Mon. Wea. Rev. », *97*, 716-726 (1969).

CARLSON T.N. and PROSPERO J.M., *The large-scale movement of Saharan air outbreaks over the Northern Equatorial Atlantic.* « J. Appl. Meteor. », *11*, 283-297 (1972).

CHARNEY J.G., *Dynamics of desert and drought in the Sahel.* « Quart. J. Roy. Meteor. Soc. », *101*, 193-202 (1975).

FOLLAND C.K., PALMER T.N. and PARKER D.E., *Sahel rainfall and worldwide sea temperatures 1901-85: Observational, modelling and simulation studies.* To appear in « Nature » (1986).

FRANK N.L and CLARK G., *Atlantic tropical systems of 1979.* « Mon. Wea. Rev. », *108*, 966-972 (1980).

GRAY W.M., *Atlantic seasonal hurricane frequency.* Part I: *El Niño and 30 mb quasi-biennial oscillation influences.* « Mon. Wea. Rev. », *112*, 1649-1668 (1984).

HASTENRATH S., *Intrannual variability and annual cycle: Mechanisms of circulation and climate in the tropical Atlanitc sector.* « Mon. Wea. Rev. », *112*, 1097-1107 (1984).

KARYAMPUDI V.M., *A numerical study of the evolution, structure and energetics of the Saharan Air Layer.* Ph. D. Thesis. The Pennsylvania State University, University Park, Pennsylvania, 287 pp. (1986).

KIDSON J.W., *African rainfall and its relation to upper air circulation.* « Quart. J. Roy. Meteor. Soc. », *103*, 441-456 (1977).

LAMB P.J., *Large-scale tropical Atlantic surface circulation patterns associated with Subsaharan weather anomalies.* « Tellus », *30*, 240-351 (1978).

LAMB P.J., *West African water vapor variations between recent contrasting Subsaharan rainy seasons.* « Tellus », *35A*, 198-212 (1983).

LANDSBERG H.E., *Sahel drought: change of climate or part of climate?* « Arch. Meteorol. Geophys. Bioklin. », *B23*, 193-200 (1975).

LAWRENCE M.B. and CLARK G.B., *Atlantic hurricane season of 1984.* « Mon. Wea. Rev. », *113*, 1228-1237 (1985).

LINDZEN R.S., *Wave-CISK in the tropics.* « J. Atmos. Sci. », *31*, 156-179 (1974).

LOUGH J.M., *Tropical Atlantic sea surface temperatures and rainfall variations in Subsaharan Africa.* « Mon. Wea. Rev. », *114*, 561-570 (1986).

MOUZNA N., *Les caractéristiques de propagation des ondes tropicales en Afrique de L'ouest observées pendant l'expérience WAMEX.* Thesis, University of Clermont, 52 pp. (1984).

NEWELL R.E. and KIDSON J.W., *African Mean Wind Changes between Sahelian Wet and Dry Periods.* « J. Climatol. », *4*, 27-33 (1974).

NICHOLSON S.E., *Revised rainfall series for West African subtropics.* « Mon. Wea Rev. », *107*, 620-623 (1979).

NICHOLSON S.E., *The nature of rainfall fluctuations in subtropical West Africa.* « Mon. Wea. Rev. », *108*, 473-487 (1980).

NORQUIST D.C., RECKER E.E. and REED R.J., *The energetics of African wave disturbances as observed during Phase III of GATE.* « Mon. Wea. Rev. », *105*, 334-342 (1977).

PALMER T.N., *The influence of the Atlantic, Pacific and Indian Oceans on Sahel rainfall.* Sumbitted to « Nature » (1986).

REED R.J., NORQUIST D.C. and RECKER E.E., *The structure and properties of African wave disturbances as observed during Phase III of GATE.* « Mon. Wea Rev. », *103*, 317-333 (1977).

REED R.J., HOLLINGSWORTH A., HECKLEY W.E. and DELSOL F., *An evaluation of the performance of the ECMWF operational forecasting system in analysing and forecasting tropical easterly wave disturbances.* Part I. *Synoptic investigations.* To be published as an ECMWF Technical Memorandum (1986a).

REED R.J., KLINKER E. and HOLLINGSWORTH A., *An evaluation of the performance of the ECMWF operational forecasting system in analysing and forecasting tropical easterly wave disturbances.* Part II. *Spectral investigations.* To be published as an ECMWF Technical Memorandum (1986b).

SCHUPELIUS G.D., *Monsoon rains over West Africa.* « Tellus », *28*, 533-536 (1976).

SIMPSON R.H., FRANK N., SHIDELER D. and JOHNSON H.M., *Atlantic tropical disturbances, 1967.* « Mon. Wea. Rev. », *96*, 251-259 (1968).

TANAKA T., WEARE B.C., NAVATO A.R. and NEWELL R.E., *Recent African rainfall patterns.* « Nature », *225*, 201-203 (1975).

STUDIES OF THE ROLES OF LAND-SURFACE PROCESSES AND SEA TEMPERATURE ANOMALIES ON AFRICAN DROUGHTS OF RECENT YEARS

Y. C. SUD, F. SEMAZZI,* A. MOLOD** and E. KALNAY
Laboratory for Atmospheres, NASA/Goddard Space Flight Center
Greenbelt, MD 20770

ABSTRACT

In this paper we review the physical mechanisms that result in a positive feedback between reduced vegetation and decreasing rainfall over the sub-Saharan region. These include soil moisture and evapotranspiration, albedo, and surface roughness. Several general circulation model (GCM) experiments that validate the role of land-surface processes in desertification are discussed.

A series of model parameterization experiments were performed in order to explain and eliminate spurious precipitation in and adjacent to the Sahara desert in previous simulations with various versions of the Goddard Laboratory for Atmospheres (GLA) model. These experiments contribute to clarify the important role of dry convective instability over dry and hot deserts in suppressing precipitation.

The land-surface processes described above may help to explain the long term tendency towards reduced precipitation observed in the Sub-Sahara over the last 25 years 1960 through 1985.

An investigation of the relationship between observed annual rainfall

* Department of Meteorology, University of Maryland, College Park, MD 20742.
** M/A Com Sigma Data.

in the Sahel and Sudan regions of Sub-Sahara and sea surface temperature anomalies during the 15-year period 1970-1984, suggest that shorter time scale interannual fluctuations in the rainfall may be associated with changes in the global ocean atmosphere interactions and resultant changes in the circulation from patterns such as those observed in El Niño episodes.

1. Introduction

Droughts are a recurring phenomenon in many parts of the world, particularly the semi-arid regions; but the recent droughts over Africa, which started around 1968 and have persisted thereafter across Sub-Saharan North Africa, i.e., from Senegal to Ethiopia, have had a truly devastating effect on the entire region. In all the analyses of rainfall records (Nicholson, 1983, 1985; Nicholson and Entekhabi, 1986; Lamb, 1983; Lamb, 1985; Lough, 1986) the frequent presence of African droughts is evident. In this paper we examine the nature of African droughts and review various studies, including some recent results obtained at the Goddard Laboratory for Atmospheres (GLA, formerly known as GLAS), that suggest an important role of various physical processes in maintaining these droughts.

In Fig. 1, we show the time evolution of the normalized rainfall index for the Sudan and Sahel regions of Africa after Nicholson and Entekhabi (1985) and the corresponding network of rainfall stations used to compute these indices. Two main features of rainfall anomaly index time-series are clear. First, there is a steady increase of departure rainfall anomaly index from the mean for both regions with a steady trend of increasing drought severity up to 1984. Second, there is a vacillatory component of rainfall anomaly superimposed on the steady rainfall decrease. The latter might be reflecting the inter-annual variability of rainfall which may, in turn, be due to changes in the large scale forcings such as sea surface temperatures (Lamb, 1978; Covey and Hastenrath, 1978; Folland *et al.*, 1986).

It must be emphasized that the real causes of African droughts are not at all well understood. Speculative hypotheses that have some proven validity, at least in the context of General Circulation Model (GCM) simulation studies, have implicated some aspects of the earth's surface processes. We shall describe them and discuss some modelling and data analysis evidences of the validity of such hypotheses.

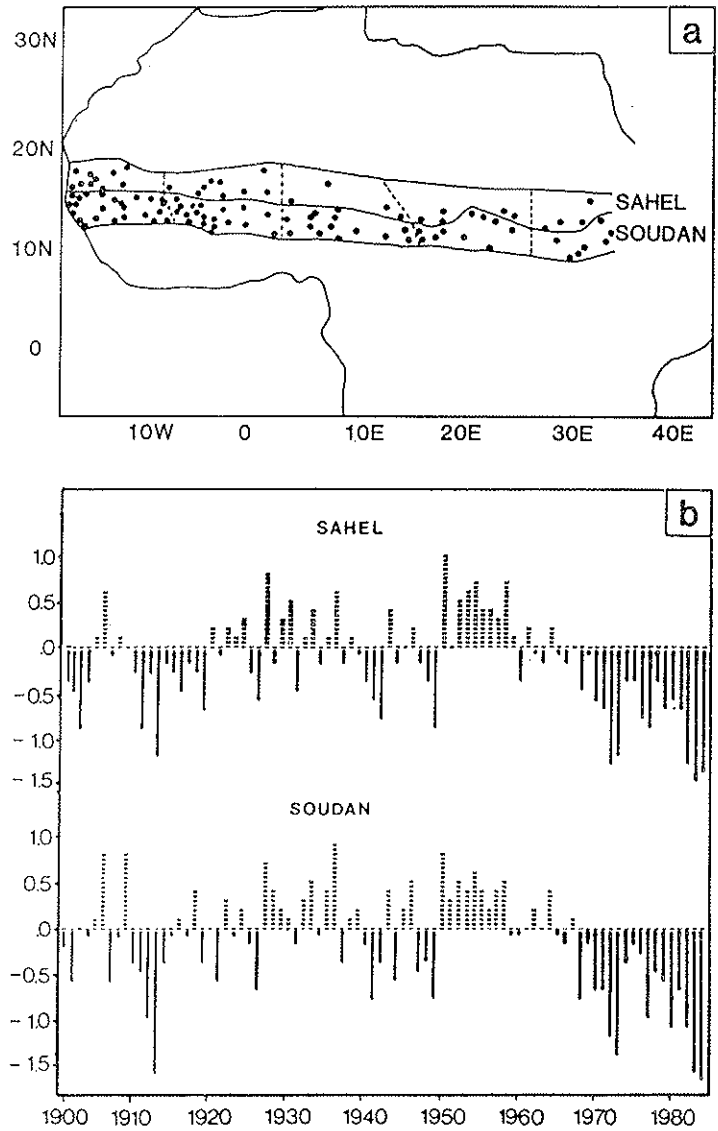

FIG. 1. (a) Station network and location of rainfall zones. (b) Standardized annual rainfall index for the Sahel and Soudan zones of West-African (Nicholson and Entekhabi, 1985).

2. Land Surface Processes

Charney (1975) proposed a surface albedo feedback hypothesis for explaining Sahelian droughts of the early seventies; he argued that high surface albedo of deserts or desert border regions reduces the net solar energy absorption at the surface which, in turn, causes BPL cooling, sinking and drying aloft with reduced convection and moisture convergence, all of which contribute to reduction in rainfall. Charney (1975) also postulated that such an increase in surface albedo, could be brought about by destruction of vegetation, excessive land use, or the antecedent vagaries of weather.

Subsequently, Charney *et al.* (1977) used GCM simulations to demonstrate the role of surface albedo of some chosen desert border regions. That study was followed by several surface albedo sensitivity studies (Idso, 1978; Chervin, 1979; Carson and Sangster, 1981; Sud and Fennessy, 1982; Laval, 1983; Henderson-Sellers and Wilson (1983) and Henderson-Sellers and Gornitz, 1984) employing GCM's of varying degree of complexity. All these surface albedo anomaly studies have shown that increases in surface albedo reduce the rainfall.

Other researchers pointed out the need for investigating the role of evapotranspiration which, in turn, depends on soil moisture. Consequently, other GCM simulation sensitivity studies were performed on the influence of soil moisture (see, for example, Manabe, 1975; Kurbatkin *et al.*, 1979; Walker and Rowntree, 1979; Shukla and Mintz, 1982; Carson and Sangster, 1981; Sud and Fennessy, 1984; Rowntree and Bolton, 1983; Yeh *et al.*, 1985; and Cunnington and Rowntree, 1985). Most of these studies started the simulations from all dry or all moist land at the initial time; in the course of the integration, the soil moisture was either allowed to evolve or held constant. Except for the study by Sud and Fennessy, all these studies have shown a positive feedback between evapotranspiration and rainfall. The Sud and Fennessy study was rather unique because it was carried out for chosen desert border regions with an earlier version of the GLAS GCM (Somerville *et al.*, 1974) which had somewhat unrealistic dry convective parameterization. This will be further discussed in Section 3.

Recent simulation studies by Sud and Smith (1984, 1985) and Sud *et al.* (1986) have identified the important role of yet a third component of land surface characteristics, i.e., the surface roughness. On the scale of the Planetary Boundary Layer (PBL) turbulence, surface roughness

depends upon the vegetation. Indeed, surface albedo, evapotranspiration and surface roughness all depend on vegetation. Hence, feedback between rainfall and vegetation is to be naturally expected; however, this problem can only be realistically studied with a coupled biosphere-atmosphere GCM model. Our current understanding of the three land-surface dependent processes, which is essentially based on the GCM simulation studies reviewed above, can be explained schematically as follows (Fig. 2):

The upper panel of Fig. 2a shows how an increase of surface albedo reduces the net solar radiation absorbed at the ground. If the region were a desert border region the evapotranspiration would be negligibly small. Therefore, the outgoing energy fluxes essentially will be those of sensible heat and longwave radiation. Moreover, if the PBL were deep, which happens during the day, most of the longwave flux from the surface would be absorbed by the moisture in the PBL. In other words, both longwave and sensible heat fluxes result in the heating or cooling of the PBL. High surface albedo causes radiational cooling, reduced sensible heating of the PBL, both of which produce sinking in the atmosphere aloft; the overall effect is that of drying the PBL by moisture divergence, and, in that way, the net result is the suppression of the cumulus convection and rainfall.

The middle panel, Fig. 2b, shows the effect of changing the soil moisture and/or evapotranspiration. In this case the net radiation balance at the surface of land is essentially the same. However, increased evapotranspiration, i.e., more $\Delta(\lambda q)$ into the PBL, implies a correspondingly lower sensible heat flux, i.e., $\Delta(C_pT + gz)$. Here, q is the water vapor mixing ratio, λ the coefficient of latent heat, C_p the air heat capacity at constant pressure, T the absolute temperature, g gravity acceleration, and z the height. Since the moist static energy, $h \equiv C_pT + gz + \lambda q$, is unaffected by equivalent exchanges between sensible and latent heat, one cannot expect any changes in moist static energy and the corresponding moist convective instability condition for cumulus convection. Nevertheless, high relative humidity ($\sim$ 90% or so) at the base of the cloud, which is also the top of the PBL, is required for the onset of moist convection because condensation occurs only after the lifting condensation level is reached by the air parcels (Helfand, 1979). Thus, evapotranspiration helps to promote moist convection. Without adequate relative humidity, latent energy λq will not be released. In that case, the relevant energy is dry static energy: $C_pT + gz$; and, under unstable conditions dry convective mixing will take place which has the effect of further drying

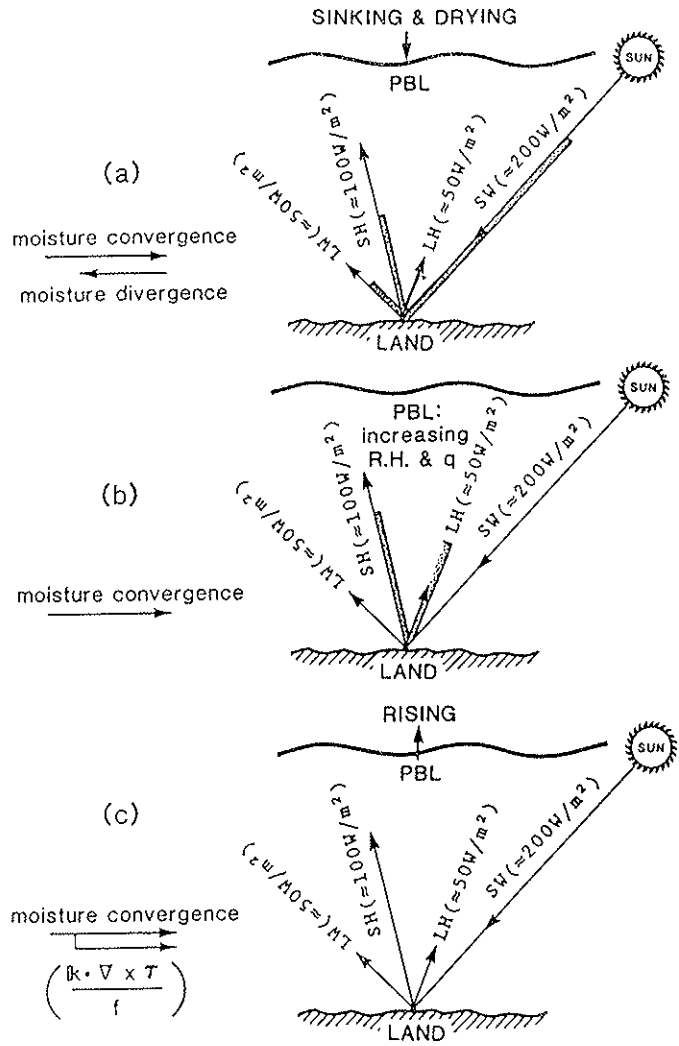

FIG. 2. Schematic balance of energy at the surface showing the effects of changes in (a) surface albedo. (b) Evapotranspiration, and (c) surface roughness. The arrows and values in parentheses show typical subtropical energy components (SW: net shortwave influx; LW, SH and LH: long-wave, sensible heating and latent heating respectively). The shaded bars denote the values modified by a land surface properly.

the PBL because moisture is mixed aloft into the dry diverging air. These arguments suggest that reduced evapotranspiration also reduces rainfall.

The bottom panel of Fig. 2c, shows the role of surface roughness. Surface roughness influences the bulk aerodynamic surface drag $C_D = C_D(Ri_B, h/z_0)$ where Ri_B is the bulk Richardson number and h/z_0 is the PBL height divided by surface roughness length. Since surface stress is given by $|\tau| = C_D U_s^2$ where U_s is the surface wind speed, its dependence on surface roughness is evident. However, since C_D affects heat and moisture surface fluxes equally, its influence on these fluxes is negligible because the surface stratification must adjust to maintain a quasi-equilibrium between net radiation balance at the surface and the PBL fluxes of heat and moisture plus a heat flux into the ground. Thus, the primary influence of surface roughness takes place through its effect on surface stress and cross-isobaric moisture convergence which depends on the curl of surface stress.

It must be pointed out that each of the above mechanisms has a positive feedback effect on rainfall. Although the physical roles of surface albedo, soil moisture and surface roughness can now be identified independently, they are also intimately coupled through the vegetation which reduces surface albedo, while increasing evapotranspiration and surface roughness, all of which have a positive feedback on rainfall.

In the future we propose to examine the dependence of rainfall on vegetation in more detail by implementing a simple but realistic model of the biosphere developed by Sellers *et al.* (1986). Nevertheless, we do not expect to obtain results too different from our current understanding of the basic influences of surface albedo, evapotranspiration and surface roughness, all of which have been confirmed through various GCM simulation studies at GLA and elsewhere. In this context, semi-arid tropical region studies are particularly valid because, being driven by heat and controlled by friction, the tropical circulation is strongly influenced by land-atmosphere interactions (Charney *et al.*, 1977).

3. Role of Convection

We have recently performed several studies modifying the parameterization of moist convection in the GLA GCM in order to improve the climatology of the model simulated rainfall. In the process, these experiments have contributed to a better understanding of the role of dry

and moist convection in the suppression of rain over subtropical deserts such as Sahara.

In the past, GLA GCM simulations always produced spurious rainfall in summer simulations over the Sahara desert. This, has been a major weakness of the current GLA GCM (Kalnay *et al.*, 1977, 1983) and its predecessor models that employed the three-level Arakawa (1972) cumulus parameterization. This deficiency has been pointed out or is evident in many simulation studies with GLA(S) GCM (Charney *et al.*, 1977; Halem *et al.*, 1979; Shukla *et al.*, 1981; Randall, 1982; and Kalnay *et al.*, 1983; and Sud and Smith, 1984). Mintz (1984) attributed the simulated rain in Sahara that is apparent in Charney *et al.* (1977) to excessive evapotranspiration associated with too much soil moisture. Accordingly, it was believed that the spurious rain over Sahara was due to deficiencies in surface fluxes over land and that their improvement would largely eliminate it. In fact, Sud and Smith focused on the problem of the influence of desert surface roughness in an attempt to address the question of spurious rain over Sahara and discovered that reducing the surface roughness over the Saharan region (Fig. 3a), reduces rainfall in the northern Sahara, (Fig. 3b). Analysis of that simulation revealed that the decreased rainfall was produced by reduced cross-isobaric moisture convergence caused by reduced surface stress, (Fig. 3c).

Recently, it became clear that the spurious Sahara desert rainfall in all the July simulations could not be entirely due to deficiencies in surface flux parameterizations. Sud and Molod (1986) examined the possibility of deficiencies in the parameterization of convection. They implemented the Arakawa-Schubert (1974) cloud parameterization in the GLA GCM but that parameterization still produced rain over Sahara in a July simulation.

Two further changes that were then included in the parameterization resulted in the suppression of Saharan rain. The first one was the requirement of at least 90% relative humidity in the PBL for the onset of moist convection (as discussed before). The second was the mixing of moisture and momentum in the dry convective adjustment, which previously only mixed heat (Manabe, 1965). Of the two changes, the most important was the latter, particularly allowing the PBL moisture to be mixed aloft.

Since the Sahara is essentially dry and arid, the intense solar heating during the day in summer causes vigorous dry convective mixing and provides an escape for the converging moisture in the PBL. Without this

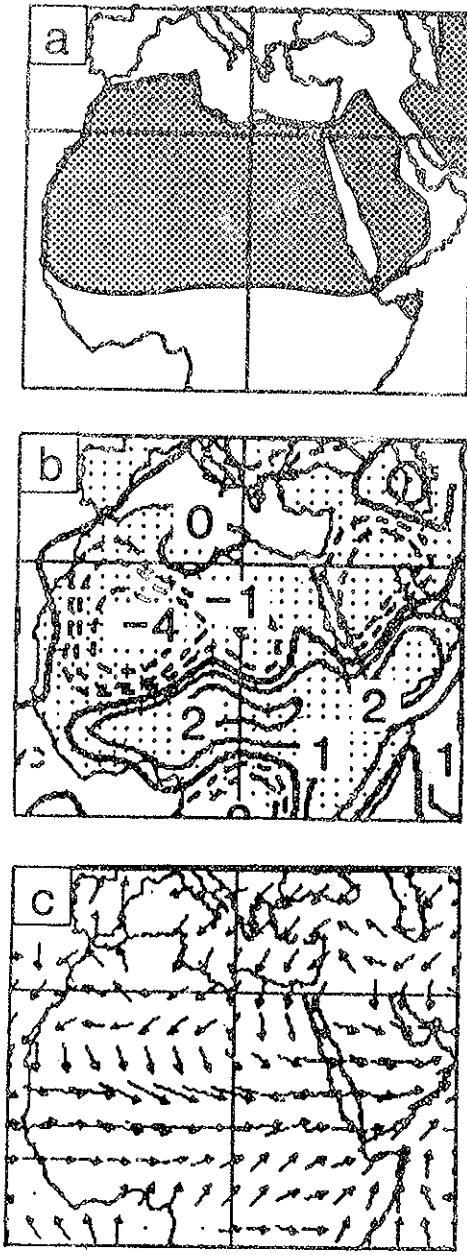

FIG. 3. (a) Region where the desert surface roughness was decreased; and its influence on (b) rainfall (mm/day); and (c) moisture flux vq (10^6 mm/day · m).

dry convective mixing, the PBL moisture would build up until moist convection takes place in order to neutralize the moist convective instability and would result in rain. These studies clarify the role of dry convection in maintaining the desert that is caused by increased sensible heat fluxes from dry. The results suggest that if the Sahara desert had soil moisture consistent with desert grasses, even a small amount of evapotranspiration ($\sim$ 2-4 mm/day) would keep the PBL cool, suppress dry convection, and enhance rainfall. Further experiments with simulated increased soil moisture over the Sahara, (Fig. 4a), and correspondingly reduced sensible heat flux (Fig. 4b) resulted in somewhat more evapotranspiration than was actually intended ($\sim$ 4-6 mm/day); but, as expected, this was accompanied by even larger increase in precipitation (Fig. 4c). This investigation indicates that an amelioration of North African droughts could be brought about by vegetation cover producing evapotranspiration and PBL moistening. This would replace sensible heating on the dry desert with evapotranspiration and moistening of the PBL as well as promote enhanced moisture convergence through its contribution to the surface roughness.

Even though the mechanisms responsible for the increased rainfall through the enhancement of vegetation are becoming clear only recently, the role of vegetation in promoting rainfall has been suspected by scientists and keen observers alike for a long time (see, e.g., Brooks, 1928; Hora, 1952; Charney, 1975; Charney *et al.*, 1977; Schickedanz, 1976; Henderson-Sellers, 1980; Dickinson, 1980; Hare, 1983; Mintz, 1984; Anthes, 1984; and Rowntree *et al.*, 1983.

4. Role of Sea-Surface Temperature

In the previous section we discussed several land-surface processes that produce a positive feedback between vegetation and rainfall. They could, perhaps, be responsible for the steady trend of diminishing rainfall observed between the 1960's through 1985, (Fig. 1). The shorter time scale oscillations cannot be so explained and may be associated with interannual changes in circulation, possibly in association with sea surface temperature (SST) anomalies.

The role of sea surface temperature anomalies in producing and maintaining global scale circulation and rainfall anomalies has been a subject of intensive investigation in recent years. As a result, it is now well recognized that El Niño and the Southern Oscillation (ENSO)

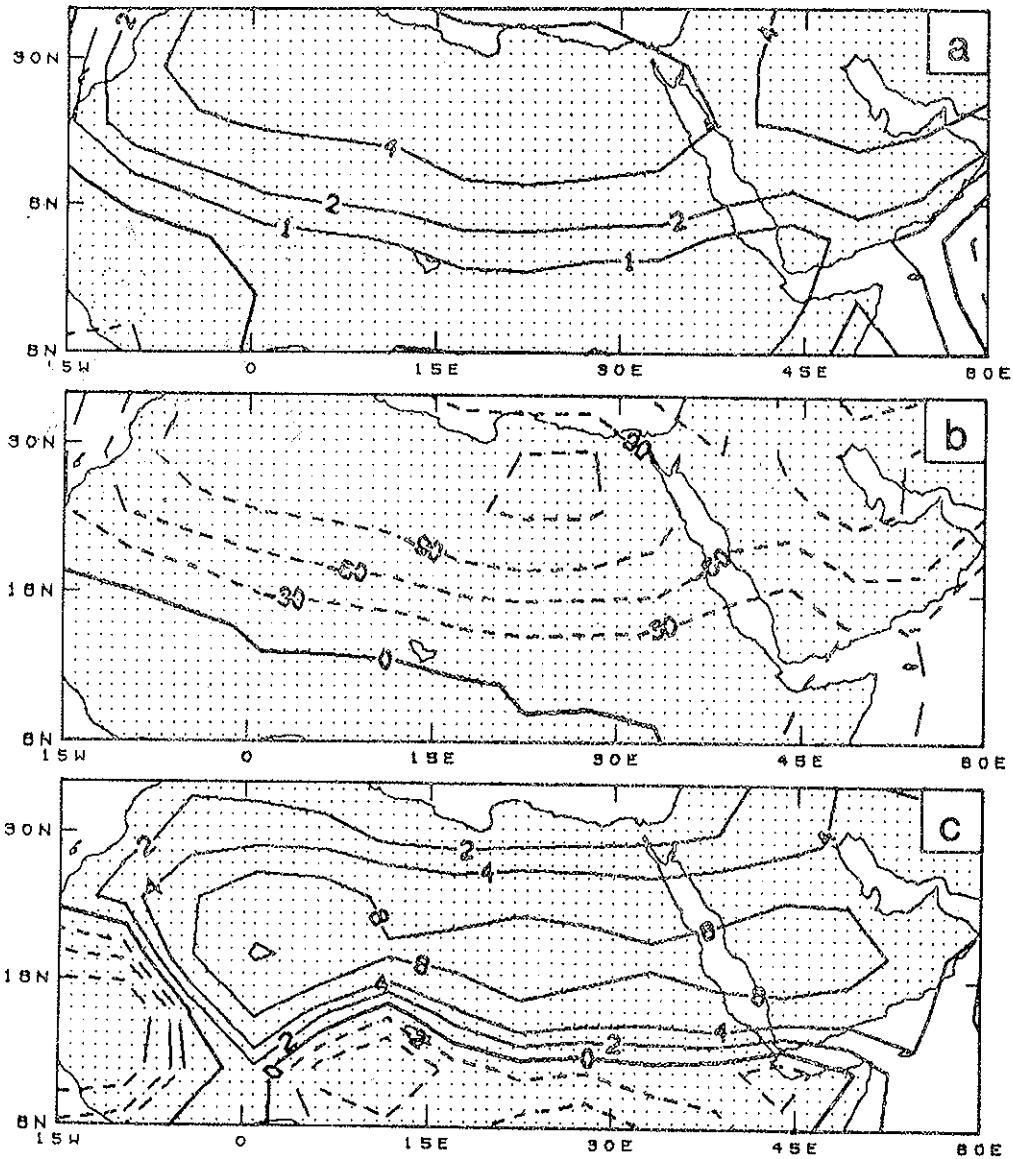

FIG. 4. Changes in (a) evapotranspiration (mm/day); (b) sensible heat flux (w/m^2); and (c) rainfall (mm/day), produced by a simulated increase in the Saharan soil moisture.

phenomena produce large scale anomalies in monsoon circulation and rainfall which also affect the north African region. However, the role of SST anomalies on African droughts has not been researched adequately. Kraus (1977) was the first to point out the relationship between Sahelian rainfall and north-south SST gradients over the Atlantic Ocean. Hastenrath and Lamb (1977) and Covey and Hastenrath (1978) also point out different aspects of SST anomaly and north African rainfall. More recently, Lough (1986) used an EOF (Empirical Orthogonal Function) analysis to explore some relationships between Atlantic SSTs and Sahelian rainfall for the periods of 1911-1939 and 1948-1972.

Semazzi *et al.* (1986) have recently investigated the relationship between SSTs and north African rainfall for a fifteen year period 1970-1984. They use a global SST dataset described by Reynolds and Gemmil (1984), for the fifteen year period which includes the recent African droughts. The SST data used in this study is a 4° latitude × 5° longitude monthly averaged from the Reynolds 2° × 2° monthly data. The rainfall data used is the annual mean standardized rainfall anomaly index, produced by Nicholson (1983, 1985) and Nicholson and Entekhabi (1985) for the Sahel and Soudan region. Our rainfall index and SST anomalies are taken as departures from the fifteen year mean.

a. *Correlation between SST and Rainfall*

First we show the straight rainfall-SST correlation between the annual Soudan and Sahel rainfall and the point SST anomalies for the months of February and August, (Fig. 5a and 5b). The patterns have a striking resemblance with El Niño modes of SST, which is not surprising since El Niño events represent a large part of the SST variance; nevertheless, the magnitude of the correlations (up to 0.85) is remarkable.

b. *EOF analysis of SST Data*

We analysed the SST data using Empirical Orthogonal Function (EOF) analysis following Von Storch and Hannoschock (1984), and Legler (1984). Three separate EOF analyses were performed for the global, Atlantic and Indian Oceans. Table 1 gives the percentage variance explained by the first three most dominant modes, namely, EOF1, EOF2 and EOF3. There is a close correspondence between the global and regional first modes (EOF1) both in the time evolution, and in the spatial pattern, (Fig. 6a, 7a and 8a).

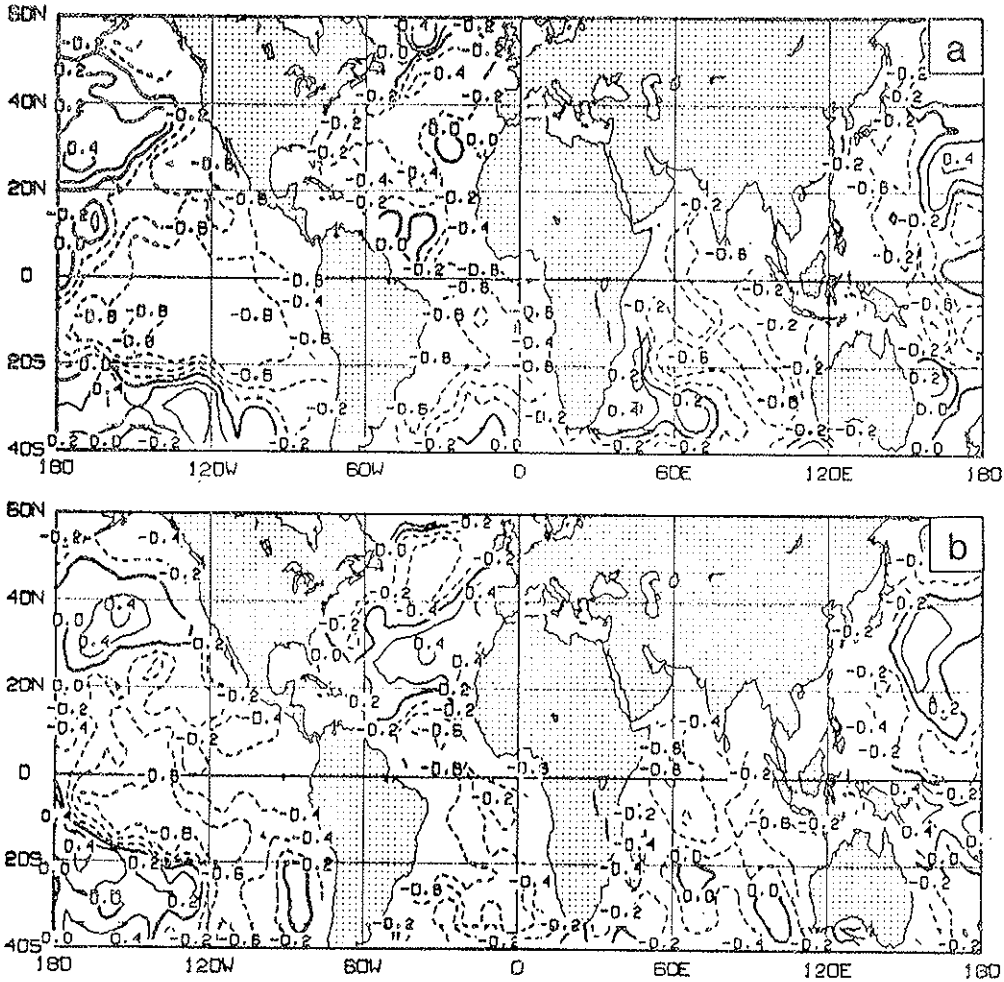

FIG. 5. Soudan region rainfall index and global SST correlation coefficient for (a) February and (b) August. Correlations with greater than 0.6 are shaded.

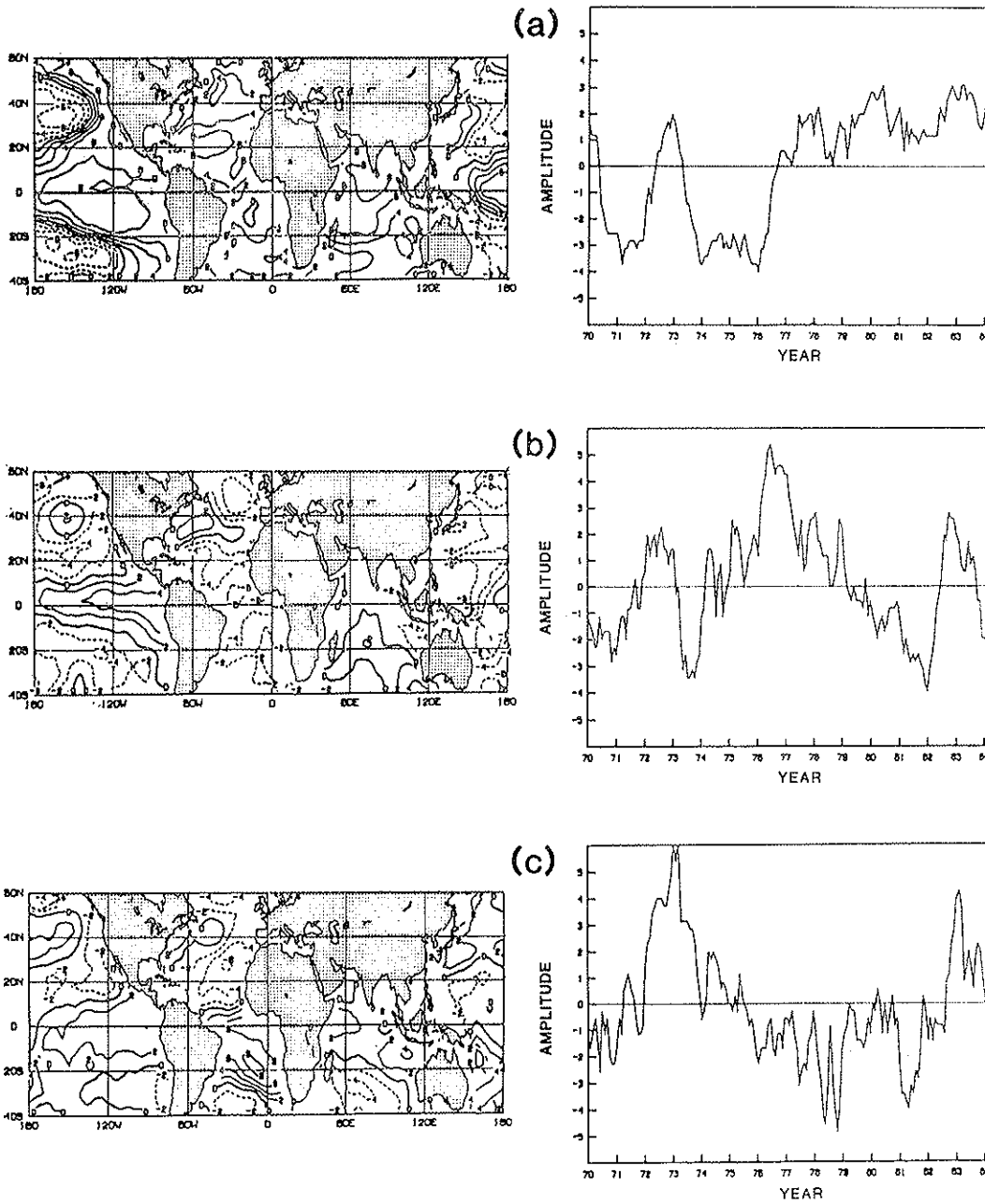

FIG. 6. (a) EOF1, (b) EOF2 and (c) EOF3, eigenvector patterns (left) and time series (right) for the global analysis; 1970-1984. (Loadings of the SST EOF patterns are multiplied by 10).

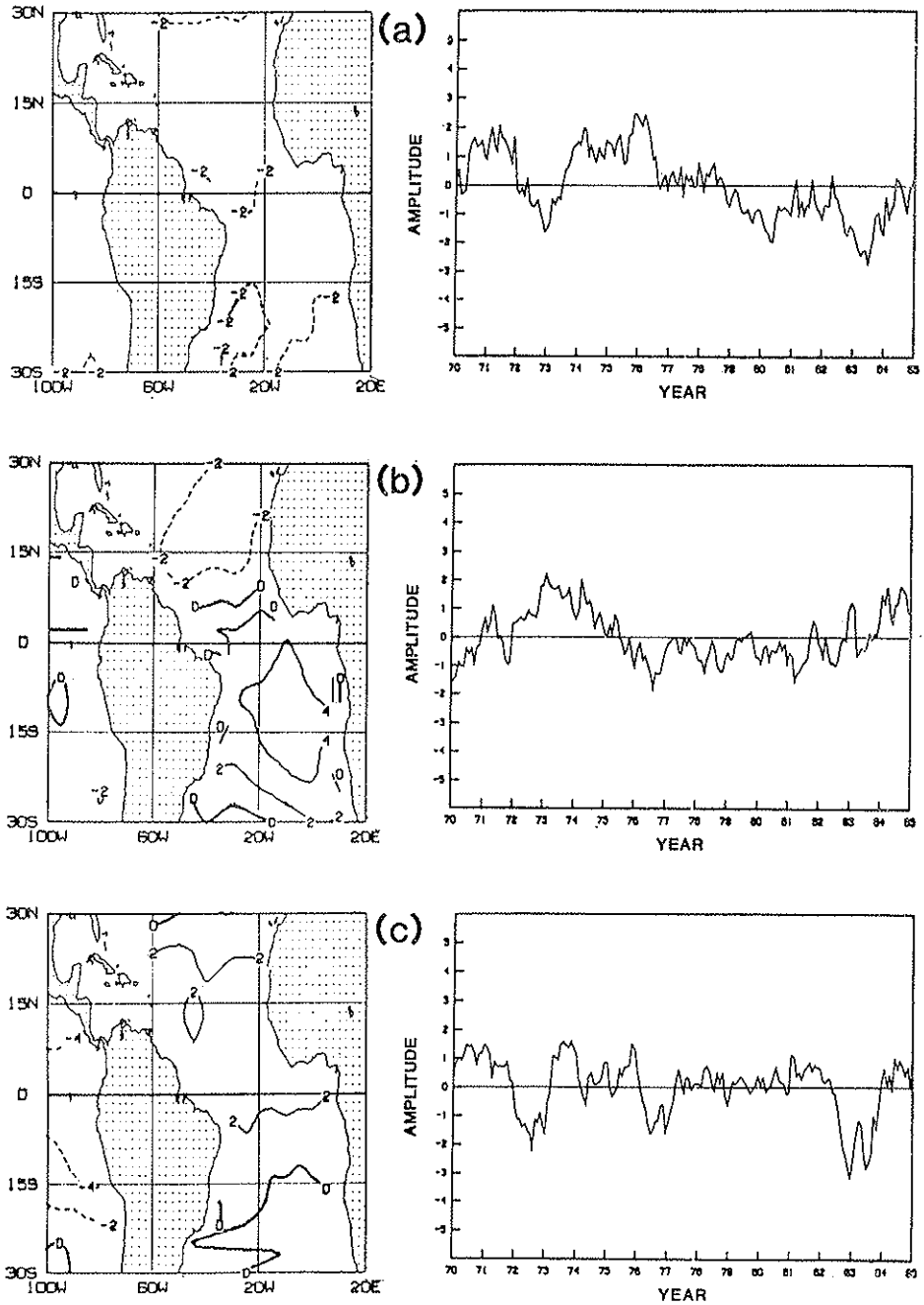

FIG. 7. (a) EOF1, (b) EOF2 and (c) EOF3, eigenvector patterns and time series for the Atlantic Ocean analysis; 1970-1984. (Loadings of the SST EOF patterns are multiplied by 10).

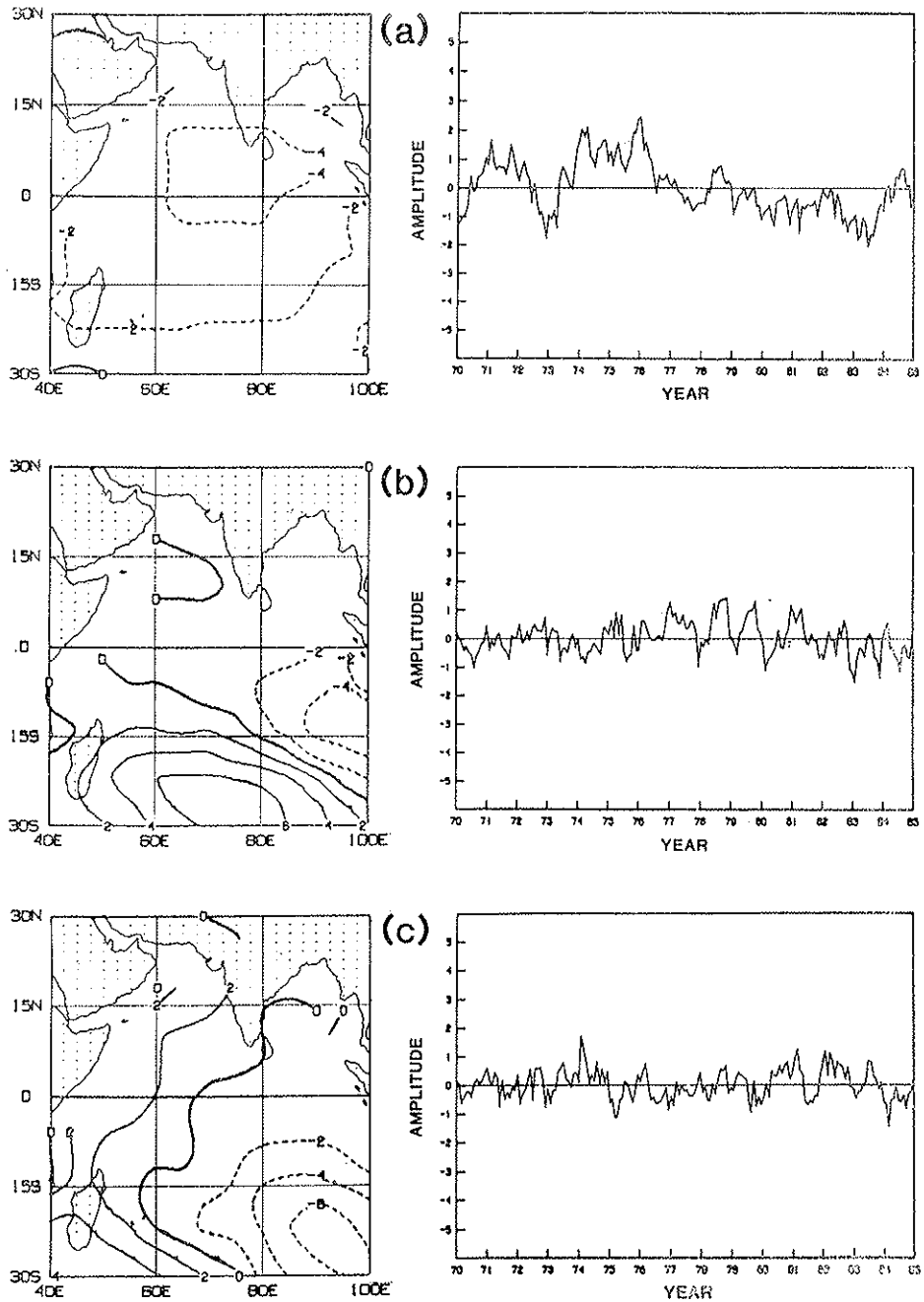

FIG. 8. (a) EOF1, (b) EOF2 and (c) EOF3, eigenvector patterns and time series for Indian Ocean analysis; 1970-1984. (Loadings of the SST EOF patterns are multiplied by 10).

TABLE 1 - *Variance represented by EOF modes in the SST time series: 1970-84.*

EOF mode	Global	Atlantic 100W - 20E 40S - 60N	Indian 30S - 22N 40E - 100E
EOF1	17%	23%	35%
EOF2	6%	19%	11%
EOF3	5%	11%	9%

The global EOF1 pattern over the Pacific ocean is typical of the El Niño SST anomaly, with warm water over eastern equatorial Pacific and cold water over surrounding region; simultaneous warming also takes place for the Atlantic and Indian Oceans. Estimation of the frequency spectra and autocorrelation of EOF1 time series (results not displayed) indicate a peak between 4 and 7 years, which is typical of the El Niño recurrence time scale. Notice that two of the three most recent El Niño events (1972-1973, 1976-77 and 1982-1983) coincide with large positive EOF1 amplitudes. The global EOF2, (Figs. 6b) corresponds to the Atlantic EOF3 (Fig. 7c), with a cross-correlation of 0.6 between the two time series. The loading for the Global EOF3, (Fig. 6c) is dominated by the Atlantic north-south anomaly dipole; it corresponds to the Atlantic EOF2 pattern, (Fig. 7b) and the corresponding time series have a cross-correlation coefficient of 0.7. The EOF2 and EOF3 for the Indian Ocean, Figs. 8b and 8c, do not have a coherent relationship with the modes for the global and Atlantic analyses; the corresponding cross-correlations are low and in this sense EOF2 and EOF3 appear to be of regional character, an observation which is partly substantiated by their resemblance to the atmospheric component of the monsoon flow over this region.

c. *Relationship between SST EOF modes of African Droughts*

We now focus on the relationship between the first two EOFs of SST for the Atlantic Ocean and Sub-Saharan rainfall. The first mode EOF1 explains the largest variance of the data, and is a global mode therefore similar for the global, Atlantic and Indian Ocean analyses. The

Atlantic EOF2, on the other hand, which is important because of its correspondence with the third global mode, has significant variance and is characterised by a dipole pattern previously suspected to be associated with the Sub-Saharan droughts, (Lough, 1986).

The annual rainfall over Sahel and Soudan regions represents essentially the monsoon rainfall because over 95% of the rainfall in both regions falls between April and October whereas the monsoon season is June to September.

Fig. 9 shows the correlation between the amplitude of the monthly Atlantic EOF1 and EOF2 time series, and the annual Sahel and Sudan rainfall index. The largest corresponding correlations are observed with

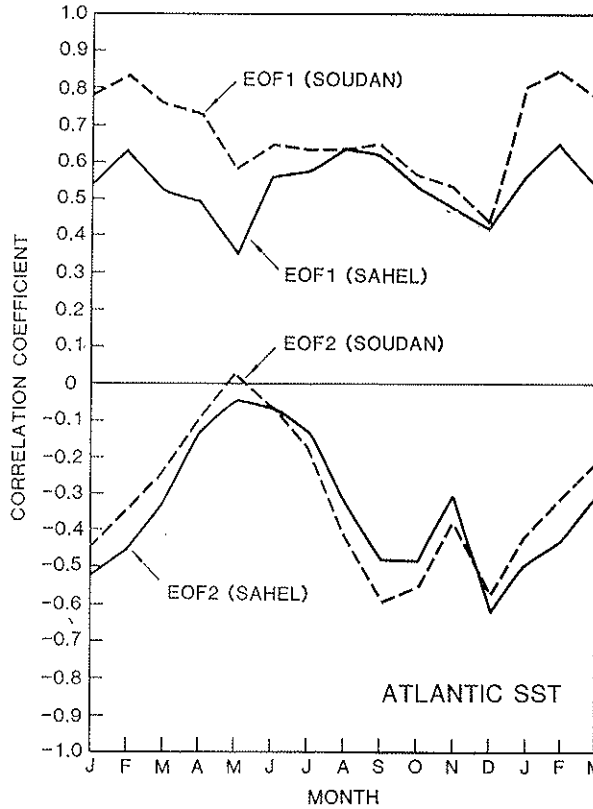

FIG. 9. Monthly stratified correlations of Atlantic EOF1 and EOF2, time series with the Sahel and Soudan Standardized rainfall index: 1970 to 1984.

EOF1, which is characterized by the warming or cooling of the entire Atlantic Ocean basin. As stated before, this mode is also a part of the global EOF1. The highest correlations between the monthly SST and the annual rainfall are observed in February. The values are 0.84 for the Soudan and 0.65 for the Sahel. The correlation between the Soudan rainfall and the monthly amplitude of the Atlantic EOF1 remains above 0.5 throughout the year except in December. The correlation with the Sahel region is only slightly smaller. This result is so striking that it deserves to be confirmed by means of GCM simulations.

The second Atlantic mode, EOF 2, is negatively correlated with the rainfall, the negative (positive) anomaly in north (south) Atlantic is associated with negative rainfall anomaly. The correlation increases during the monsoon season and remains above 0.4 between August and January. This phase relationship suggests that EOF2 reflects the dependence of future SST on the antecedent monsoon rainfall. We hypothesize that it is related to evaporation from the ocean surface that may be caused by global scale ocean-atmosphere interaction anomalies. Because there is high evaporation from the tropical Atlantic Ocean during the monsoon period, a good (or bad) monsoon may imply ~ 1-2 mm/day higher (or lower) evaporation from the oceans, which translates to 1-2°C warming (or cooling) of the 100 m deep mixed layer of the ocean over a period of about 90 days. This hypothesis needs to be verified using diagnostics from a GCM simulation, or from 4-dimensional analysis of the atmosphere.

5. Conclusions

There are three main inferences that can be drawn from studies that were reviewed or reported in this paper.

The first two refer to the physical mechanisms that result in a positive feedback between reduced vegetation and desertification. They may explain the trend towards reduced rainfall observed since the 1950's. The third one, showing the relationship between rainfall and SST anomalies associated with changes in the global circulation, may be responsible for the interannual changes in the precipitation.

First, land-surface processes which are dependent on land surface albedo, evapotranspiration and surface roughness can have a strong influence on monsoonal circulation and rainfall over north Africa. Since vegetation is the key element that affects all of these land-surface processes, the

dependence of African rainfall (droughts) on vegetation (or lack of vegetation) can be easily inferred.

Second, the dry convective mixing of PBL moisture into diverging air aloft has an important role in suppressing the rainfall over North Africa. If the moisture mixing is not allowed or the dry convection is arrested through increased evapotranspiration over the Sahara in GCM simulations, the rainfall reappears over the Sahara and increases over the Sub-Sahara (Sud and Molod, 1986). This suggests that desiccating the Sahara region would lead to reduced rainfall even if the normal moisture convergence were to take place. If the converging moisture mixed upwards to a large depth, only fair weather cumuli may form.

The third study deals with possible causes for oscillations in rainfall during the recent African droughts. Fluctuations in rainfall have led some scientists to interpret that the drought was over. However, in every case the drought returned with even more severity. Our investigations suggest that sea surface temperature anomalies which are dominated by the El Niño/Southern Oscillation events have a strong correlation with rainfall anomalies, which could explain the fluctuating component of African droughts.

It is important to determine whether the trend towards reduced African rainfall has a component which may be related to the land surface processes that have been altering slowly but steadily. In this context the influence of deforestation of African rainforest, which is continuing at the rate of about 4% or so, cannot be ruled out. To examine the influences of these changes this requires many more GCM simulation studies. We plan to examine some of these hypotheses in the future using our newly developed Simple Biosphere (SiB) model and parameterization of ocean surface fluxes.

ACKNOWLEDGEMENTS

This paper reviews some of the ongoing studies at GLA and elsewhere of earth's surface influences on African rainfall including droughts and desertification. Useful input has been provided by W. E. Smith, V. Mehta on the analysis of results. African rainfall data was provided by Drs. Sharon Nicholson and P.J. Lamb. Discussions with Prof. Y. Mintz and Dr. Max Suarez were very helpful in including the Arakawa-Schubert scheme in the GLA GCM as well as in the planning of the series of experiments summarized in this paper. The paper was typed by M. A. Wells and B. Richardson, and the figures prepared by L. Rumburg.

REFERENCES

ANTHES R.A., *Enhancement of Convective Precipitation by Mesoscale Variations in Vegetative Covering in Semi-arid Regions.* « J. Climate and Appl. Meteorol. », *23*, 541-554 (1984).

ARAKAWA A., *Design of the UCLA General Circulation Model, Numerical Simulation of Weather and Climate.* Tech. Rep. No. 7, Dept. Meteorol., UCLA (1972).

ARAKAWA A. and SHUBERT W.H., *Interaction of a Cumulus Cloud Ensemble with the Large-Scale Environment,* Part I. « J. Atmos. Sci. », *31*, 674-701 (1974).

BROOKS C.E.D., *The Influence of Forests on Rainfal and Runoff.* « Quart. J. Roy. Meteor. Soc. », *54*, 1-7 (1928).

CARSON D.J. and SANGSTER A.B., *The Influence of Land-surface Albedo and Soil moisture on General Circulation Model Simulations.* In: I.D. Rutherford (ed.), GARP/CRP: *Research Activities in Atmospheric and Oceanic Modelling, Numerical Experimentation Programme,* Report No. 12, pp. 5.14-5.21 (1981).

CHARNEY J.G., *Dynamics of Deserts and Drought in the Sahel.* « Quart. J. Roy. Meteorol. Soc. », *101*, 193-202 (1975).

CHARNEY J.G., QUIRK W.J., CHOW S.H. and KORNFIELD J., *A Comparative Study of the Effects of Albedo Change on Drought in Semi-arid Regions.* « J. Atmos. Sci. », *34*, 1366-1385 (1977).

CHERVIN R.M., *Response of the NCAR General Circulation Model to Changed Land Surface Albedo.* Report of the JOC Study Conference on Climate Models: Performance, Intercomparison and Sensitivity Studies, Washington, DC, 3-7 April, 1978. « GARP Publ. Series », No. 22, Bol. 1, pp. 563-81 (1979).

COVEY D.L. and HASTENRATH S.L., *The Pacific El Niño phenomenon and the Atlantic circulation.* « Mon. Wea. Rev. », *106*, 1280-1286 (1978).

CUNNINGTON W.M. and ROWNTREE P.R., *The Sensitivity of the Saharan Region in a General Circulation Model.* « Meteorological Office » Bracknell, UK (1985).

DEARDORFF J.W., *Parameterization of the Planetary Boundary Layer for use in General Circulation Models.* « Mon. Wea. Rev. », *100*, 93-106 (1972).

DICKINSON R.E., *Effects of tropical deforestation on climate. From Blowing in the wind: deforestation and long-range implications.* No. 14, Studies in Third World Societies, « Dept. Anthropology, College of William and Mary, Williamsburg, Va », pp. 411-441 (1980).

FOLLAND C.K., PARKER D.E. and PALMER T.N., *Sahel rainfall and worldwide sea surface temperature: 1901-1985.* « Nature », *320*, 602-607 (1986).

HALEM M., SHUKLA J., MINTZ Y., WU M.L., GODBOLE R., HERMAN G. and SUD Y., *Comparisons of Observed Seasonal Climate Features with a Winter and Summer Numerical Simulation produced with the GLAS General Circulation Model.* « GARP », Publ. Series No. 22, 207-253, WMO, Geneva, Switzerland (1979).

HARE F.K., *Climate and Desertification.* WMO/UNEP, WCP-44 (1983).

HASTENRATH S. and LAMB P.J., *Climate atlas of tropical Atlantic and eastern Pacific oceans.* The University of Wisconsin Press, 112 pp. (1977).

HENDERSON-SELLERS A., *The Effects of Land Clearance and Agricultural Practices Upon Climate.* « Blowing in the Wind: Deforestation and Long-Range Implications ». Studies in Third World societies, Pub. No. 14, Dept. Anthropology, College of William and Mary, Williamsburg, Va., pp. 443-485 (1980).

HENDERSON-SELLERS A. and GORNITZ V., *Possible climatic impacts of land cover transformations, with particular emphasis on tropical deforestation.* « Climatic Change », 6, 231-257 (1984).

HENDERSON-SELLERS A. and WILSON M.F., *Surface albedo Data for Climate Modelling.* « Rev. Geo. and Space Phys. », *21*, 1743-1778 (1983).

HELFAND H.M., *The Effect of Cumulus Friction on the Simulation of a January Hadley Circulation by the GLAS Model of the General Circulation.* « J. Atmos. Sci. », *36*, 1827-1843 (1979).

HORA S.L., *Hora's Satpura Hypothesis: An Aspect of Indian Biogeography.* « Current Science, Bangalore », *19*, 364-370 (1952).

IDSO S.B. and DEARDORFF J.W., *Comments on the Effect of Variable Surface Albedo on the Atmospheric Circulation in Desert Regions.* « J. Appli. Meteorol. », *17*, 560 (1978).

JAEGER L., *Monatskarten des Niederschlags fur die ganze Erde.* Berichte des Deutschen Wetterdienstes, 18, No. 139. Im Selbstverlag des Deutschen Wetterdienstes, Offenbach, W. Germany (1976).

KALNAY-RIVAS E., BAYLISS A. and STORCH J., *The 4th order GISS model of the global atmosphere.* « Beitr. Phys. Atmos. », *50*, 299-311 (1977).

KALNAY *et al.*, *Documentation of the GLAS Fourth-Order General Circulation Model* « NASA Tech. Memo 86064 », Vol. 1 NTIS, Washington, DC (1983).

KRAUS E.B., *Subtropical droughts and cross-equatorial energy transports.* « Mon. Wea. Rev. », *105*, 1009-1018 (1977).

KURBATKIN G.P., MANABE S. and HAHN D.G., *The moisture content of the continents and the intensity of summer monsoon circulation.* « Soviet Meteorology and Hydrology », *11*, 1-6 (1979). English translation.

LAMB P.J., *Large-scale tropical Atlantic surface circulation patterns associated with sub-Saharan weather anomalies.* « Tellus », *30*, 240-251 (1978).

LAMB P.J., *Sub-Saharan rainfall update for 1982: continued drought.* « J. Clim. », *3*, 419 (1983).

LAMB P.J., *Rainfall in sub-Saharan West Africa during 1941-1983.* « Arch. Met. Geoph. Biokl. », *196*, 131-139 (1985).

LAVAL K., *GCM experiments with surface albedo changes.* Paper presented at Third International School of Climatology. Erice, Italy, October 1983.

LEGLER D.M., *Papers from 1982-83 El Niño/Southern Oscillation Workshop.* NOAA/AOML, Miami, Florida, 229 pp. (1984).

LOUGH J.M., *Tropical Atlantic sea surface temperatures and rainfall variations in sub-Saharan Africa.* « Mon. Wea. Rev. », *114*, 561-570 (1986).

MINTZ Y., *The Sensitivity of Numerically Simulate Climate to Land surface Boundary Conditions.* In: J.T. Houghton (ed.), *The Global Climate.* Cambridge University Press, London, pp. 70-105 (1984).

NICHOLSON S.E., *Sub-Saharan rainfall in years 1976-1980: evidence of continued drought.* « Mon. Wea. Rev. », *111*, 1646-1654 (1983).

NICHOLSON S.E., *Sub-Saharan Rainfall 1981-1984.* « J. Climatol. », *23*, 1388-1391 (1985).

NICHOLSON S.E. and ENTEKHABI, *The quasi-periodic behavior of rainfall variability in Africa and its relationship to the Southern Oscillation.* « Arch. Met. Geoph. Biocl. », Ser. A., *34*, 311-348 (1985).

RANDALL D.A., *Monthly and seasonal simulations with GLAS climate model.* Proceedings of the Workshop on Intercomparison of Large-Scale Models used for Extended Range Forecasts of the European Centre for Medium Range Weather Forecasts, Reading, England, pp. 102-166 (1982).

REYNOLDS R.W. and GEMMIL W.H., *An objective global monthly mean sea surface temperature analysis.* « Tropical Ocean-Atmosphere Newsletter », *18*, 14-15 (1984).

RIND D., *The Influence of Ground Moisture Conditions in North America on summer Climate as Modelled in the GISS GCM.* « Mon. Wea. Rev. », *110*, 1487-1494 (1982).

ROWNTREE P.R., *The influence of tropical east Pacific Ocean temperatures on the atmosphere.* « Quart J. R. Met. Soc. », *98*, 290-321 (1972).

ROWNTREE P.R., *Sensitivity of general circulation models to land surface processes.* In Proceedings of Workshop on Intercomparison of Large-Scale Models for Extending Range Forecasts. ECMWF, 1982, pp. 225-261 (1983).

ROWNTREE P.R., *Review of general circulation models as a basis for predicting the effects of vegetation change on climate.* Proceedings of the United Nations University Worksnop on « Forests, climate and hydrology regional impacts » at Oxford, March 1984 (to be published). Also Met. 0 20 Tech Note II/225 (1984).

ROWNTREE P.R. and BOLTON J.A., *Simulation of the atmospheric response to soil moisture anomalies over Europe.* « Quart J. R. Met. Soc. », *109*, 501-526 (1983).

SCHICKENDANZ P.T., *The Effect of Irrigation on Precipitation in the Great Plains.* Final Report, Illinois State Water Survey, University of Illinois (1976).

SELLERS P.J., MINTZ Y., SUD Y.C. and DALCHER A., *A simple biosphere model (SiB) for use within general circulation models.* « J. Atmos. Sci. », *43*, 505-531 (1986).

SEMAZZI F.H.M., METHA V. and SUD Y., *The relationship between sub-Saharan rainfall and global sea surface temperature: 1970-1984.* In preparation (1986).

SHUKLA J., STRAUS D., RANDALL D.A., SUD Y. and MARX L., *Winter and Summer Simulations with the GLAS Climate Model.* NASA Tech. Memo. 83866, p. 282 (1981).

SHUKLA J. and MINTZ Y., *The Influence of Land Surface Evapotranspiration on Earth's Climate.* « Science », *215*, 1498-1501 (1982).

SOMERVILLE R.C.J., STONE P.H., HALEM M., HANSEN J.E., HOGAN J.S., DRUYAN L.M., RUSSELL G., LACIS A.A., QUIRK W.J. and TENENBAUM J., *The GISS model of the global atmosphere.* « J. Atmos. Sci. », *31*, 84-117 (1974).

SUD Y.C. and FENNESSY M.J., *A Study of the Influence of Surface Albedo on July Circulation in Semi-Arid Regions using the GLAS GCM.* « J. Climatol. », *2*, 105-125 (1982).

SUD Y.C. and FENNESSY M.J., *A Numerical Study of the Influence of Evaporation in Semi-arid Regions on the July Circulation.* « J. Climatol. », *4*, 383-98 (1984).

SUD Y.C. and MOLOD A., *Influence of land surface processes on convection on circulation and rainfall in North Africa.* NASA Tech. Memo. (1986).

SUD Y.C. and SMITH W.E., *Ensemble Formulation of Surface Fluxes and Improvement in Evapotranspiration and Cloud Parameterization in a GCM.* « Boundary-Layer Meteorol. », *29*, 185-210 (1984).

SUD Y.C. and SMITH W.E., *The influence of surface roughness of deserts on the July circulation: A numerical study.* « Bound. Layer Meteor. », *4*, 383-398 (1985).

SUD Y.C., SHUKLA J. and MINTZ Y., *Sensitivity of circulation and rainfall to land surface roughness: A numerical study with the GLAS GCM.* Accepted for publication in « Journal of Climatology and Applied Meteorology » (1986).

VON STORCH H. and HANNOSCHOCK G., *Comments on empirical orthogonal function analysis of wind vectors over the tropical Pacific region.* « Bull. Am. Meteor. Soc. », *65*, 162 (1984).

WALKER J. and ROWNTREE P.R., *Effect of Soil Moisture and Rainfall in a Tropical Model.* « Quart. J. Roy. Meteor. Soc. », *103*, 29-46 (1979).

YEH T.C., WETHERALD R.T. and MANABE S., *The Effect of Soil Moisture on the Short-Term Climate and Hydrology Change - A Numerical Experiment.* « Mon. Wea. Rev. », *112*, 475-490 (1984).

DROUGHT, SEA-SURFACE TEMPERATURE, AND ATMOSPHERIC TELECONNECTIONS

T. N. PALMER
European Centre for Medium Range Weather Forecasts
Shinfied Park, Reading

ABSTRACT

GCM integrations using worldwide SST anomalies observed during anomalously wet or dry periods in the African Sahel, suggest that there are dynamical links between ocean variability, in all three major oceans, and rainfall over the African Sahel. Variability occurs on a variety of timescales from inter-annual to inter-decadel.

Inter-annual variability in the tropical Atlantic appears also to be related to drought in the Brazilian Nordeste. However, in this case, modelling and observational evidence is put forward suggesting that this variability arises from atmospheric forcing in the extratropical Northern Hemisphere.

1. INTRODUCTION

In this paper I will consider the relationship between worldwide sea surface temperature (SST) and drought in two regions of the world, the African Sahel, and the Brazilian Nordeste. In both cases, positive relationships appear to exist, and these involve teleconnections with other parts of the world.

In Section 2 I shall discuss some general circulation modelling experiments which test, dynamically, the observed relationships between Sahel drought, and worldwide SST discussed by Folland, elsewhere in this volume.

In Section 3 I shall outline some modelling and observational evidence which suggests that anomalous Atlantic SST may be an intermediary in a teleconnection between the North Atlantic Oscillation and Brazilian drought. In this case, the observations suggest that drought may be forced by anomalous circulations in the extratropics.

2. Influence of the Atlantic, Pacific and Indian Oceans on Sahel Rainfall

Folland *et al.* (1986) and Folland (this volume) have reported that persistently dry and wet periods of several years in the Sahel have been accompanied by global scale patterns of SST.

Fig. 1 shows the worldwide SST difference field between the five driest and five wettest years in the Sahel after 1949 and is discussed in more detail in Folland *et al.* (1986). Note that whilst this field does represent differences between extreme years, values in the South Atlantic are not as large as anomalies (> 2 K) observed during the exceptional warm event of 1984. Similarly, values in the East Pacific are not as large as observed anomalies following the 1982-83 El Niño event.

Results were obtained from several 180-day fixed July integrations of the Meteorological office 11-layer GCM (Slingo, 1985) using the full difference field in Fig. 1, and its components in the three principal oceans. The integrations are identified as follows. The control integration has fixed climatological average July SSTs, and the anomaly integration (TOT) has the full field in Fig. 1 added to these values. Integration ATL, PAC and IND have only those SSTs in Fig. 1 from the Atlantic, Pacific and Indian Oceans respectively, added to climatological values.

Fig. 2a shows the model's Sahel rainfall with climatological SSTs; the response of an AGCM to a particular SST anomaly is strongly dependent on its climatology without the anomaly. Over the western and central Sahel, between about 15°W and 10°E, the model's rainfall climatology is in good agreement with Jaeger's (1986) observed climatology. East of this region, the model's climatological rainfall extends north and south of the observed limits; the maximum northeast of Lake Chad is excessive. Over the western Sahel, model rainfall exceeds evaporation (not shown) by about 4 mm per day and moisture is supplied to this region by the horizontal moisture flux. The 'steady' component of this flux is shown in Fig. 2b for the 950 mbar level.

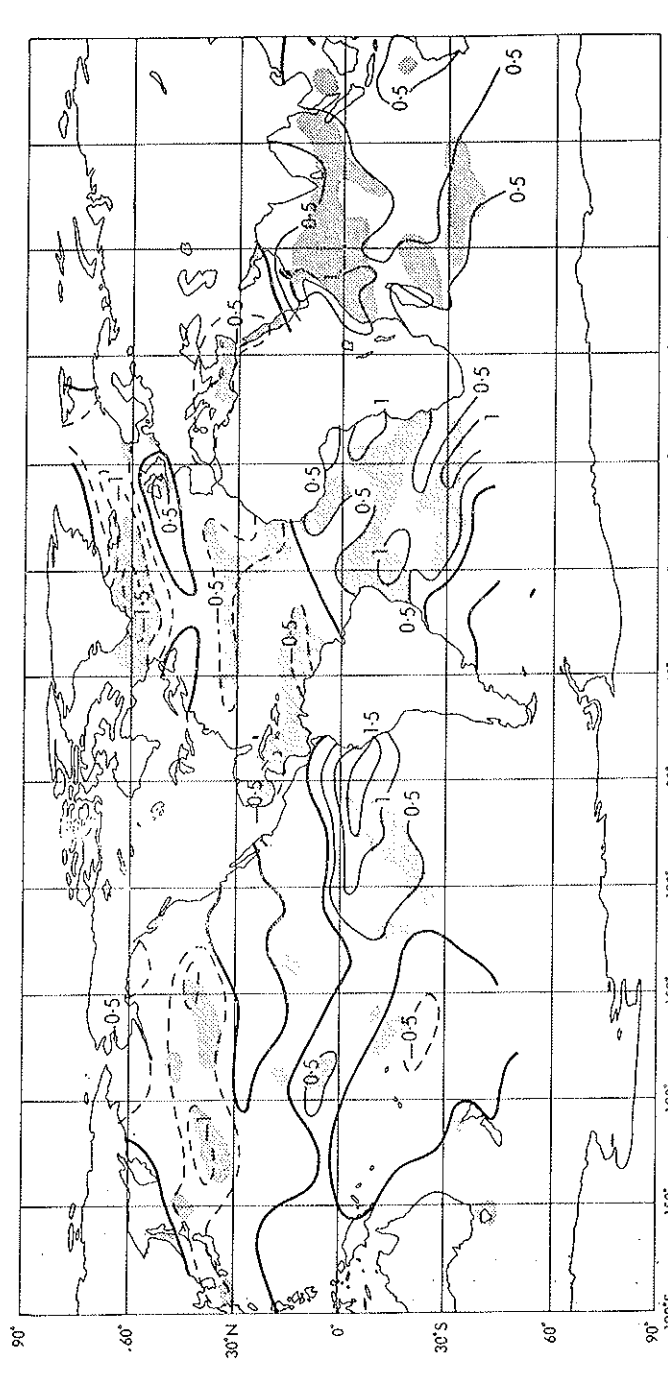

FIG. 1. SST, July to September: average of (1972-73, 1982-84) (Sahel dry) minus average of (1950, 1952-54, 1958) (Sahel wet). Contours every 0.5°C. Shaded areas are different from zero at the 90% level of significance according to a t-test.

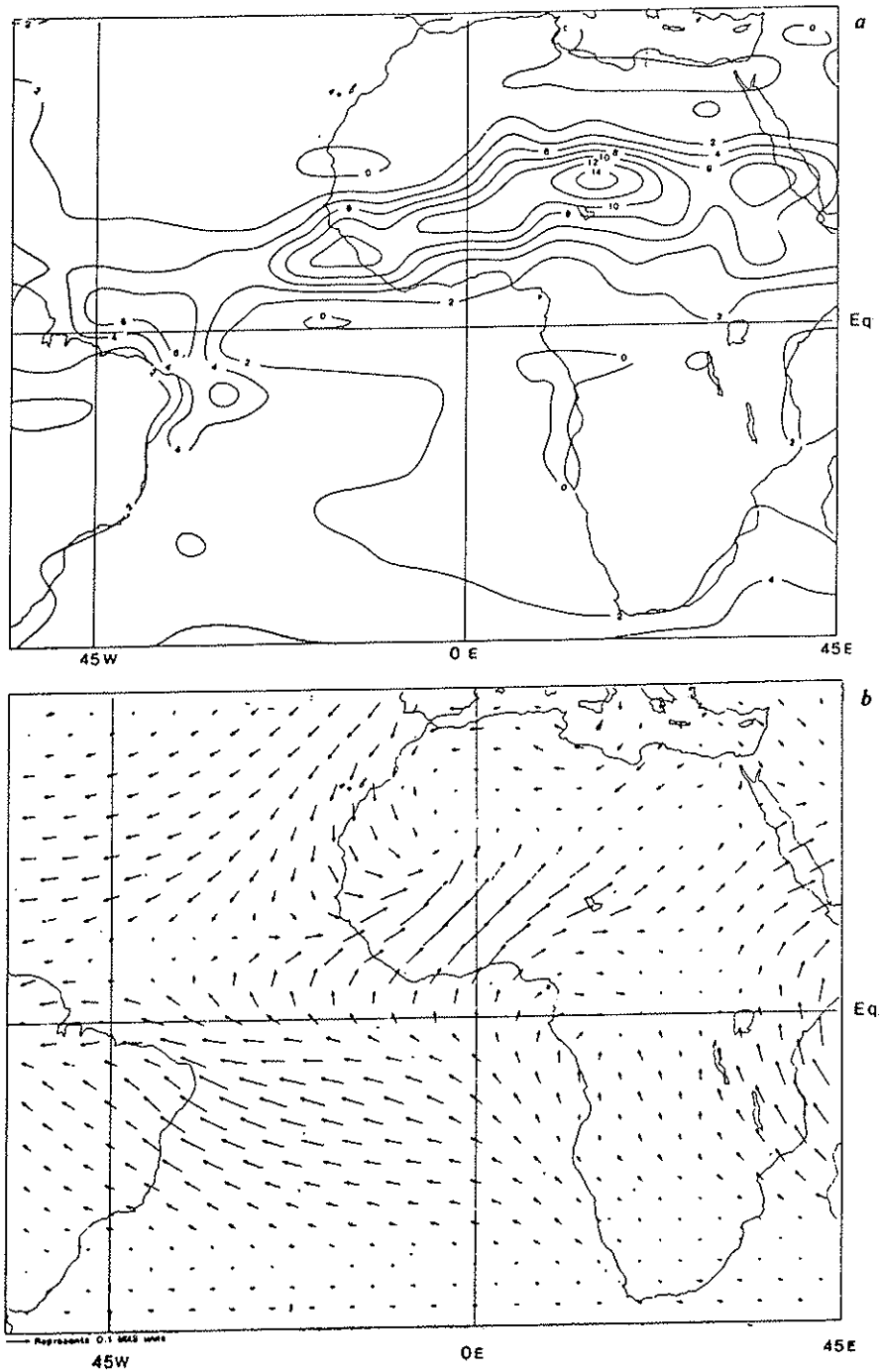

FIG. 2. (a) Mean rainfall (millimetres per day) in a 180-day control run. (b) Average 950-mbar steady moisture flux in a 180-day control run.

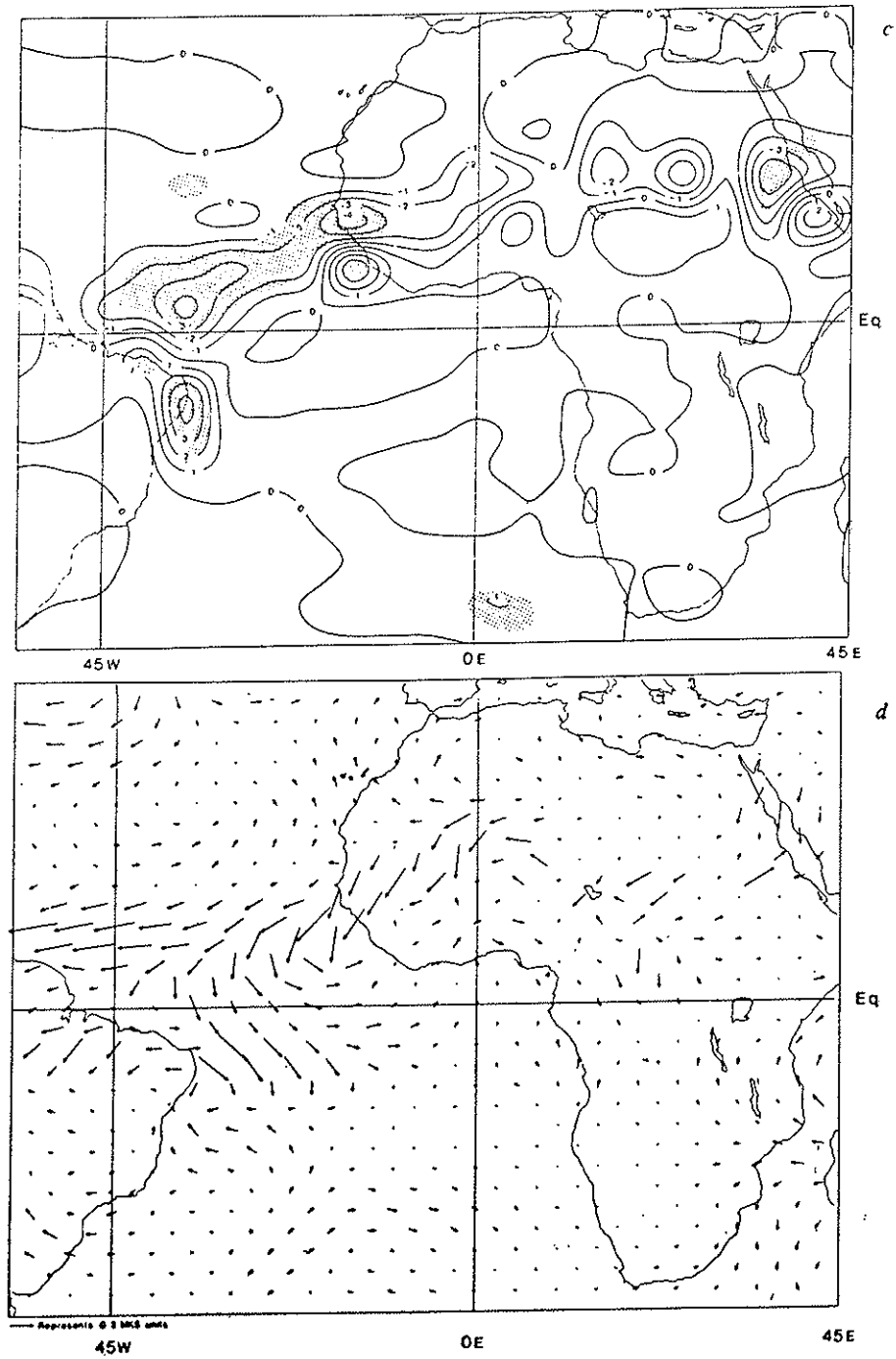

FIG. 2. (c) 180-day mean rainfall (millimetres per day); anomaly integration minus control. (d) 180-day mean 950 mbar steady moisture flux; anomaly integration minus control. The scale of the arrows shown in panel (d) is 5 times that in (b).

Fig. 2c shows the rainfall in the integration with the full observed composite SST anomaly, minus the control rainfall. Over the western Sahel, rainfall is decreased on average by about 30% of the model's climatological values. Over the eastern Sahel there is a smaller but coherent reduction of about 1-2 mm per day, with reductions of up to 50% over the mountains of south-east Sudan and north-east Ethiopia. Fig. 2d shows that the model's steady 950 mbar flux of moisture from the South Atlantic into the western Sahel is decreased by about 20-50%. This experiment therefore shows that the observed SST difference pattern of Fig. 1 can provide a coherent change in Sahel rainfall mainly through a reduction in moisture flux convergence, with perhaps a small southward displacement of the ITCZ in the western Sahel. The effect of warmer SSTs in the Southern Hemisphere in increasing low-level saturation mixing ratios may therefore be much less important than the impact of the SST anomalies on the dynamics of the tropical atmosphere. This conclusion is consistent with the reduced divergence at 250 mbar in the model (not shown) over almost the whole Sahel belt, from south of 10°N up to 20°N and from the Atlantic to the Red Sea.

Fig. 3 shows 180-day mean-rainfall difference fields between the four anomaly integrations and the control. For integration ATL, the pattern of rainfall reduction over the Atlantic and the Western Sahel is similar to, but ~ 30% weaker than, that for integration TOT. Over the eastern Sahel, the reduction in rainfall is much less substantial in ATL.

For integration PAC, surprisingly at first sight, there is a similar pattern of rainfall reduction to that in TOT and ATL. Over the Atlantic, values are smaller than in ATL, and the rainfall enhancement to the south is absent. However, inland, over the Sahel, rainfall reduction seems to be larger than that in ATL.

Results from IND are different. Inland, over the western and central Sahel, an enhancement in rainfall of over 1 mm per day is apparent. Further east, over Sudan and northern Ethiopia, there is a decrease in rainfall by up to 50% of climatological values. Finally, over the western Indian Ocean itself, values are strongly enhanced. (Although not shown, rainfall over the eastern Indian Ocean is also increased).

An assessment of whether these rainfall anomalies are significant was made by calculation a t-variate from the six pairs of non-overlapping 30-day mean values of the control and anomaly integrations. If the conditions of the t-test were satisfied, then anomalies with $|t|>2$ would be accepted at about the 7% significance level, using a two-sided test. T-values with

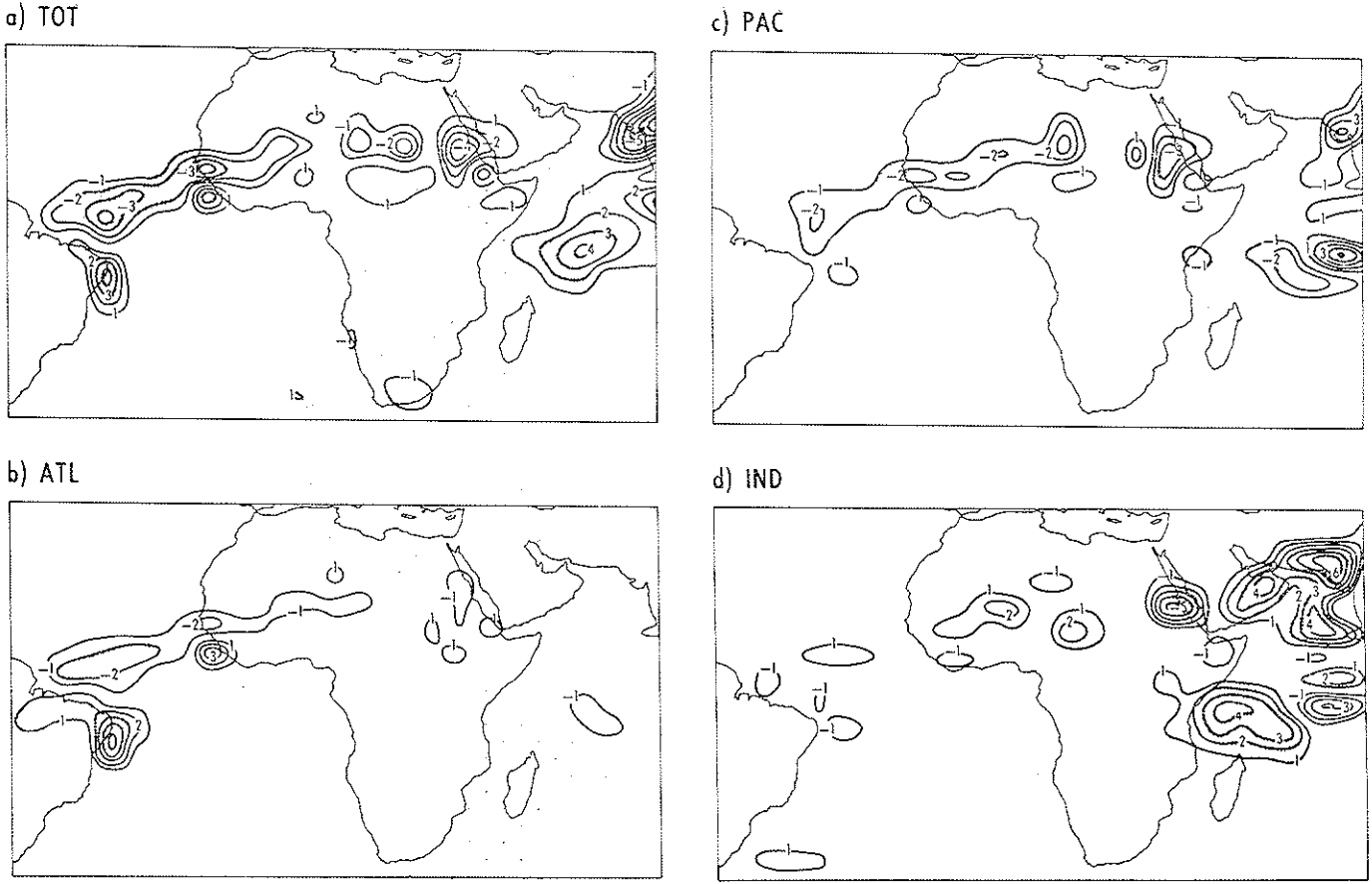

FIG. 3. Rainfall anomaly (relative to control integration) for experiment with: (a) Full SST anomaly in Fig. 1 (TOT); (b) Atlantic portion of Fig. 1 only (ATL); (c) Pacific portion of Fig. 1 only (PAC); (d) Indian Ocean portion of Fig. 1 only (IND). Contour interval, 1 mm per day. Stippling indicates areas where the magnitude of the t-variate exceeds 2.

magnitude >2 are shown stippled in Fig. 3. The reduction in rainfall across the Atlantic and into the extreme western Sahel is extremely reproducible in experiment TOT whilst values of t are smaller in this region for ATL and, except for a small neighbourhood of the West African coast, $t<2$ in PAC. In experiment IND, the increase in rainfall over the Indian Ocean is significant, as is the principal area of decrease over Sudan. In TOT, and more so in ATL, the increase in rainfall over north-east Brazil appears to be highly reproducible (although the northern summer is not the main rainy season in this area).

The addition of the SST anomaly in ATL reduces the meridional gradient of Atlantic SST just south of the inter-tropical convergence zone (ITCZ). As a result, the Atlantic Hadley cell south of the ITCZ is weakened and, as Fig. 4a shows, the low-level south-east trade winds are weakened. The flux of moisture into the ITCZ is reduced, producing less latent heating there, consistent with the weaker Hadley cell. Whilst the main change in precipitation occurs over the Atlantic, Fig. 4a shows that reduction in low-level flow into the ITCZ also reduces the south-west monsoon flow into the western Sahel.

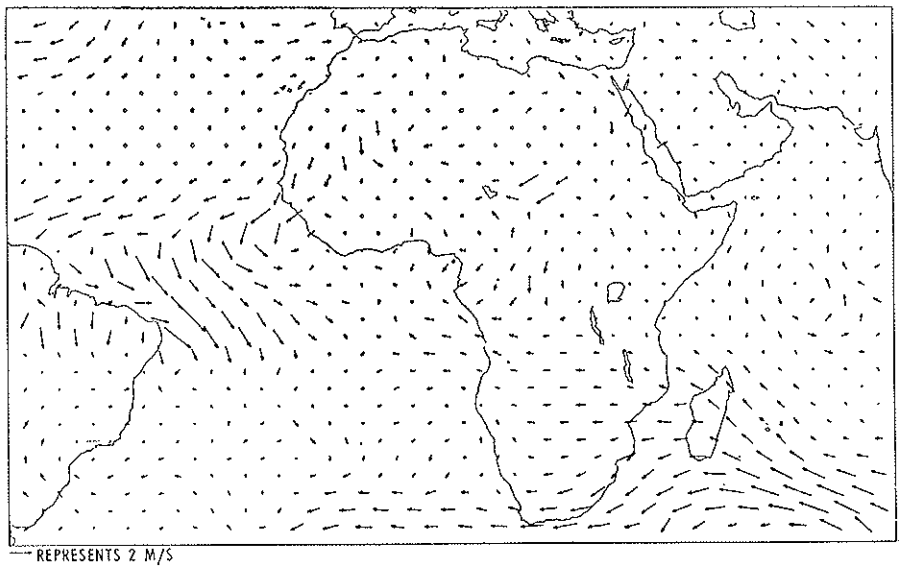

FIG. 4. (a) 950-mbar wind anomaly for experiment ATL.

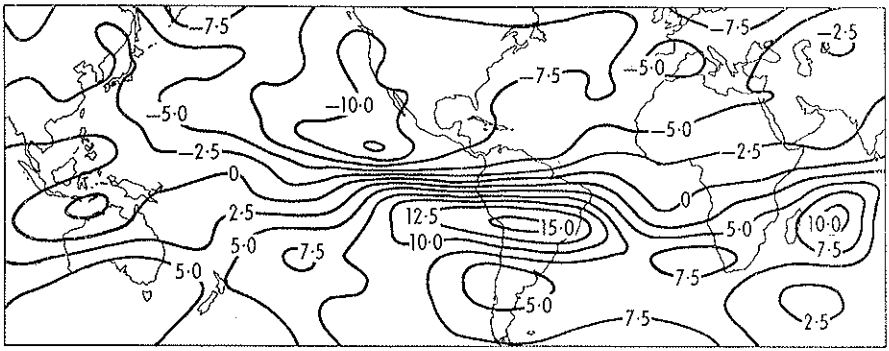

FIG. 4. (b) 250-mbar streamfunction anomaly ($x10^6 m^2 s^{-1}$) for PAC.

As mentioned above, the composite SST anomaly in Fig. 1 is considerably weaker, particularly in the Gulf of Guinea, than SST anomalies observed during the exceptional warming of 1984. Hence, it is very likely that a more marked weakening of the south-west monsoon flow into the western Sahel would have resulted if the 1984 SST anomalies had been used in place of those in Fig. 1. We hope to test this speculation in a future integration.

Whilst the SST anomaly field in Fig. 1 has negative values over 1 K in the north Pacific, the principal influence of SST anomalies in PAC on rainfall is over the tropical Pacific. With water at 28°C or warmer extending across most of the tropical Pacific north of the Equator in the climatological normal, the anomaly near the dateline in Fig. 1 produces a substantial increase up to 10 mm per day over the central and west Pacific, whilst anomalies west of Central America (which weaken the meridional SST gradient there) are associated with a reduction of the maximum of rainfall west of Mexico by up to 10 mm per day. Previous GCM studies with El Niño SST anomalies have shown that enhanced latent heat release in the central equatorial Pacific excites an atmospheric Kelvin wave which can propagate across the Atlantic and Africa without complete dissipation. As a result the equatorial upper troposphere is warmed, geopotential height is raised and anomalous equatorial westerlies are produced, in agreement with results from thermally forced linear equatorial ß-plane models (Gill, 1980). Figure 4b shows the 250-mbar streamfunction anomaly from PAC. The north-to-south gradient indicates that the anomalous non-divergent wind in the tropics at 250 mbar indeed

has a westerly component, strongest over the east Pacific, but extending over the Atlantic and Africa. The wind anomalies have a baroclinic vertical structure near the ITCZ over the Pacific, Atlantic and Sahel, with an easterly component at low levels.

This again reduces the south-west monsoon flow into the western Sahel, and thereby the supply of moisture for precipitation. The fact that there is no significant increase in rainfall over the Atlantic south of the ITCZ in PAC is consistent with the divergent circulation anomalies being mainly east/west oriented ('Walker cell') rather than north/south ('Hadley cell') as in ATL.

Results from IND are more easily understood. In Fig. 3d, there was substantial enhancement of rainfall over the Indian Ocean; Fig. 4c shows anomalous divergence at 250 mbar associated with this enhancement. The correspondence between divergence and rainfall arises from the local thermodynamic balance in the tropics between adiabatic cooling by vertical motion and latent heat release. The main area of descent required by mass continuity appears to be located over Ethiopia and Somalia, consistent with the rainfall decrease there. The anomalous low-level wind in this region (not shown) flows from land to ocean, similar to Fig. 4a for ATL.

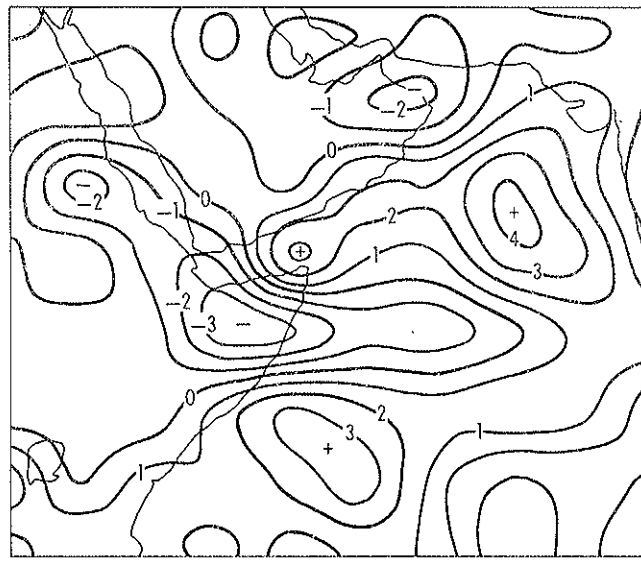

FIG. 4. (c) 250-mbar divergence anomaly ($x10^6 s^{-1}$) for IND.

These results certainly lend support to the hypothesis that changes in worldwide SST are responsible for Sahel drought, though it could be argued that a rather large SST anomaly (the difference between extreme wet and dry years) has been used, and that a weaker and less significant response might result if the anomaly was halved, making it representative of deviations from climatology. I would like to argue, however, that uncertainties in how to parameterize possible feedbacks between land-surface processes and the atmosphere, on these long timescales, make it impossible to be confident about the reality of the magnitude of the model's response over the Sahel, and that it could indeed be somewhat larger than shown above.

The impact of possible land-surface feedback processes has been studied by Rowntree *et al.* (1985), through integrations of the Meteorological Office climate model in annual cycle mode. Firstly, they considered the impact of reducing the capacity of the soil to hold water, accessible to the atmosphere for evaporation, from a value of 15 cm, appropriate for deep rooting vegetation such as trees and permanent grasses, to 1 cm, more appropriate for bare soil. This was done between 10-32.5N, 20W-60E. Secondly, they studied the impact of increasing the albedo in the region 10-17.5N over Africa. In Fig. 5 are shown results from an experiment combining both of these effects. It should be noted that the rainfall differences are shown relative to a control integration which was integrated with an annual cycle. In this control run, the excessive rainfall rates over the central and eastern Sahel, noted above, are largely absent. The reduction in rainfall in Fig. 5, expressed as a percentage change, is very comparable to that for experiment TOT.

In the Meteorological Office climate model, there is no direct coupling between albedo and rainfall rate, or between soil moisture capacity and rainfall rate. It is not difficult to imagine that some relationship might exist, on a timescale of a few years, if reduced rainfall were to lead to a reduction in deep-rooting, low albedo vegetation. However, data on such effects are sparse, and uncertainties great. Nevertheless, if some such relationship were to be incorporated into the model's parametrization of land/surface processes, then the results from Rowntree *et al.*'s experiments indicate that the impact of the observed SST anomalies in Fig. 1 might indeed be quite larger than suggested by the results given in Fig. 3. At present, we can only conclude that further research is needed to reduce the uncertainties in modelling atmospheric variability on these timescales.

Of course, none of this discussion has addressed the question of the origin of decadel variability in the ocean temperatures. One might speculate

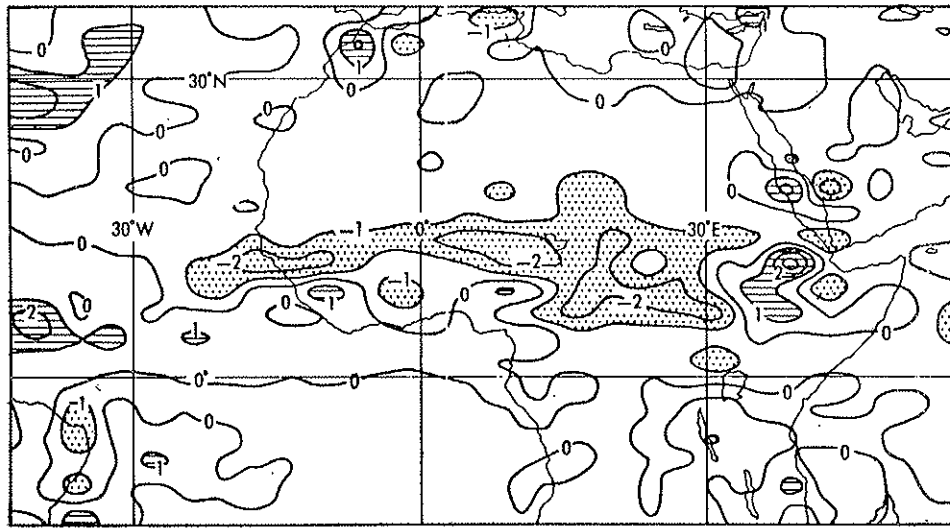

FIG. 5. Differences in rainfall (mm/day) relative to a control average for June to August of an annual cycle experiment with reduced soil water capacity and increased albedos (from Rowntree *et al.*, 1985).

with some confidence that the development of coupled ocean/atmosphere GCMs, will, within the next decade, shed considerable light on the matter.

3. TELECONNECTION BETWEEN BRAZILIAN DROUGHT, SST, AND THE NORTH ATLANTIC OSCILLATION

Moura and Shukla (1981) have found dynamical relationships between sea surface temperature (SST) anomalies in the tropical Atlantic and rainfall in the drought-prone region of Northeast Brazil. In Fig. 6, composite March SST anomalies are shown for five drought years since 1950, using the Meteorological Office Historical SST dataset (Minhinick and Folland, 1982). In particular, during these years, the tropical North Atlantic is warmer by up to one degree (whilst the tropical South Atlantic is cooler than normal). Fig. 7 shows the composite March PMSL anomaly for the same drought years. Largest positive values ($\sim$ 8 mb) occur in high latitudes near Greenland. In the subtropical North Atlantic there are negative pressure anomalies in excess of 2 mb. Essentially opposite results

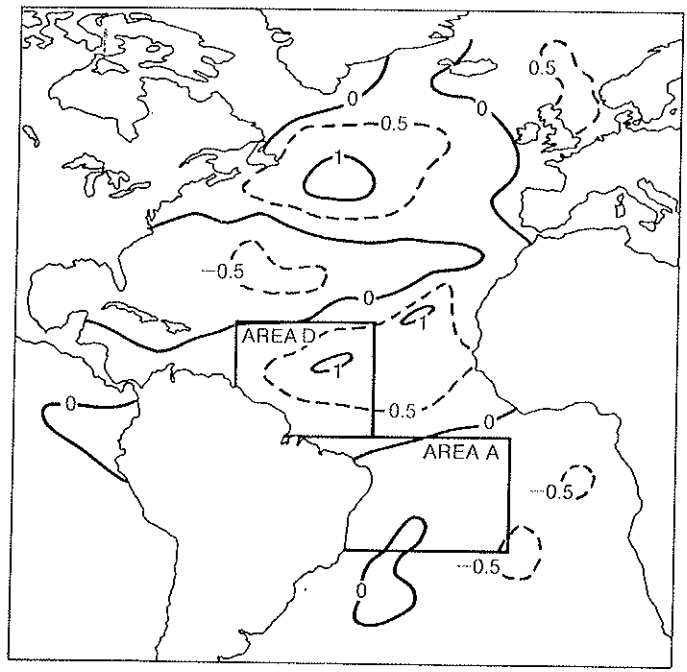

FIG. 6. Composite SST anomalies (relative to 1951-80) during March of 5 years of severe drought (1951, 1953, 1958, 1970, 1979) in Brazil (contour interval. .5K). Definition of areas 'A' and 'D' used to define correlation between SST and Northern Hemisphere PMSL are shown.

(not shown) obtain for SST and PMSL composites of 'wet' years in Northeast Brazil. This pattern of PMSL anomaly is associated with variability in the so-called North Atlantic Oscillation (NAO) (Wallace and Gutzler, 1981) associated with fluctuations in the strength of the climatological-mean jet stream over the extratropical NW Atlantic. These results are consistent with those of Namias (1972), Hastenrath and Heller (1977) and Nobre *et al.* (1985).

In order to understand better the relationship between SST in the region of the tropical Atlantic adjoining the Nordeste, synchronous and lagged correlation between SST and Northern Hemisphere PMSL over the period 1891-1980 have been studied. In order to remove effects due to climate fluctuations on time scales of a decade or more (Folland *et al.*, 1984), the data has been divided into three epochs (1891-1920,

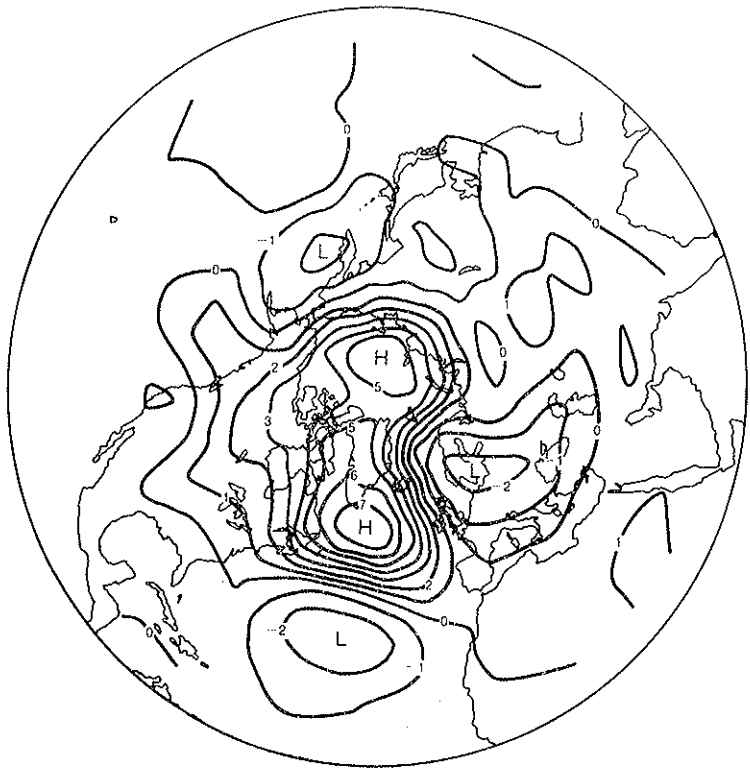

FIG. 7. Composite PMSL anomaly (relative to 1951-80) during March of years used to form Fig. 1 (contour interval 1 mb).

1921-1950, 1951-1980) and correlations calculated independently for each of the three epochs. A single field representative of the entire 90 year period was then formed using a Fisher z-transform technique. The statistical significance of the correlation was assessed using a t-test.

Following Xavier *et al.* (1985) we define two areas north and south of the equator (Fig. 6), and for each March of the 90 year period mean SST in these areas were calculated. Fig. 8a shows the synchronous correlation coefficients between March SST in area 'D' (0-20N, 35-60W) and March Northern Hemisphere PMSL. The NAO pattern shown in Fig. 7 is clear, with a correlation of — 0.8 over the subtropical North Atlantic, and a value of 0.5 over Greenland. The stippled areas indicate significance at 5% or better. It is clear that the entire NAO pattern is significant.

(By contrast, over Asia and much of the Pacific, the pattern was weak and regions of significance small. A possible exception to this may be the tropical East Pacific).

Fig. 8b,c shows lagged correlations between March SST in area 'D' and PMSL in February and January, respectively. With a lag of one month correlation between SST and PMSL over the North Atlantic is almost as strong as the synchronous correlation. Negative correlations over the East Pacific extending northward into mid-latitudes are also apparent. In Fig. 8c, with two months lag, the NAO pattern is weaker than in the earlier diagrams, though both positive and negative centres are significant at the 5% level. With a lag of three months (not shown) there was a (significant) negative correlation of -0.4 in the subtropical NW Atlantic but only weak (~ 0.2) and insignificant correlations over Greenland.

In Fig. 8d we show the correlation between March SST and PMSL in April. A significant area of negative correlation, up to -0.5 exists over the Caribbean area, but over the North Atlantic values are weak. Generally correlations with SST in area D leading PMSL gave weak and insignificant results over the North Atlantic. For this reason we believe it much more likely that the NAO is responsible for forcing SST anomalies in area D, than vice versa.

Simultaneous and lagged correlations between Northern Hemisphere PMSL and SST in area A have also been studied. Unlike results using area D, however, we have been unable to find, with confidence, any significant regions of correlation.

The results of this article, together with the modelling study of Moura and Shukla (1981) suggest that SST in the tropical North West Atlantic may provide an intermediate link between occurrence of drought in Northeast Brazil, and the North Atlantic Oscillation in the Northern Hemisphere PMSL field.

It should be noted that the NAO is a dominant mode of variability, on a monthly time scale, in general circulation models with only climatological SSTs (Lau, 1983). Hence, observations of anomalous values of the NAO need not imply forcing by enhanced tropical SST anomalies. Indeed, it appears likely from the lagged observations above that the persistence of an anomalous NAO index during the Northern Hemisphere winter provides the principal forcing for anomalous SST in area D.

On the other hand the persistence of an anomalous NAO index over the three months, from January to March, appears to require some explanation, and it is possible that some co-operative ocean/atmosphere feed-

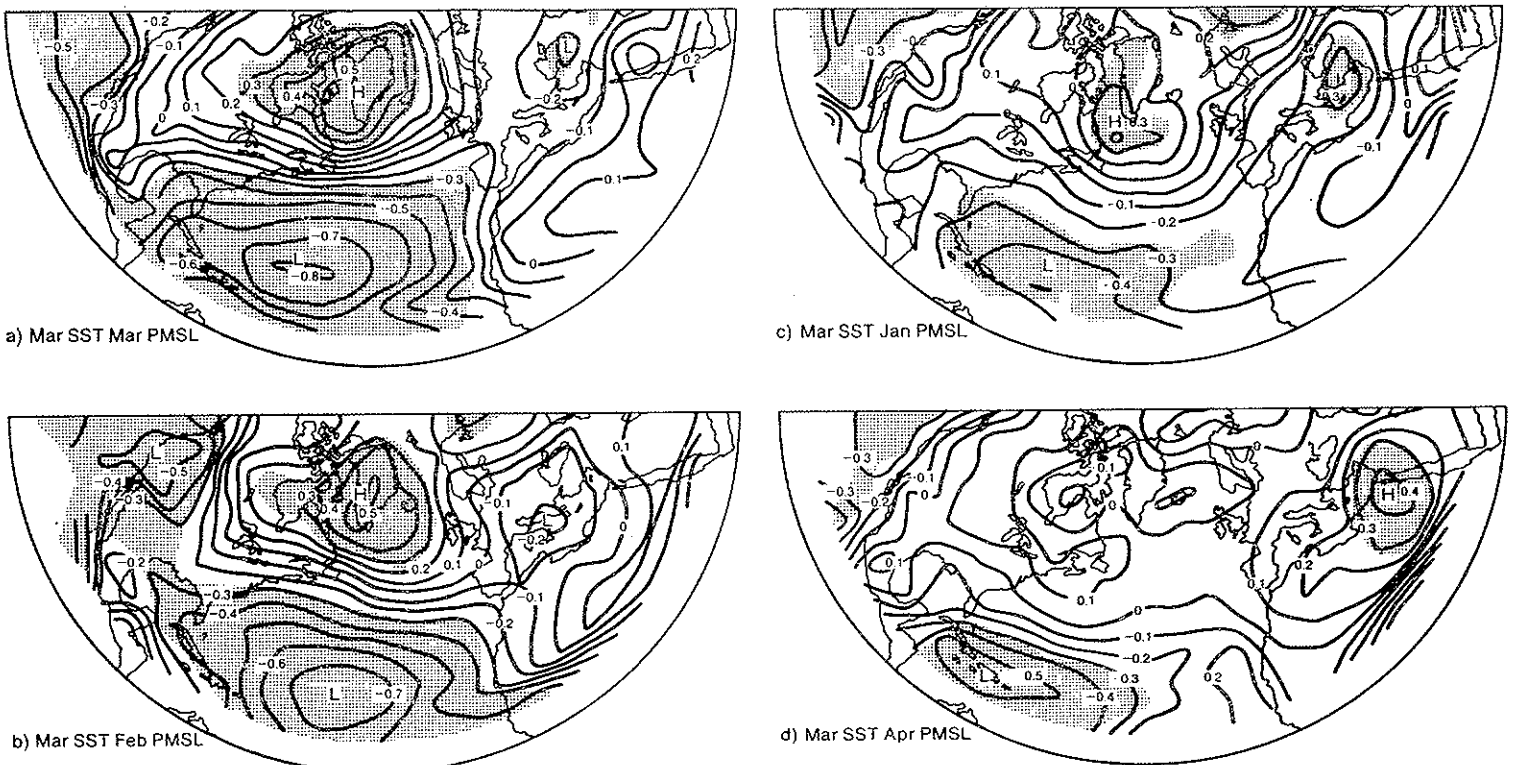

FIG. 8. Correlation coefficient between SST in area D and Northern Hemisphere PMSL. Data from 1891-1980 with climatic trends removed (see text). Stippled areas indicate significance at the 5% level.

back, not necessarily in the tropics, is playing a role. For example, in Fig. 6, the largest SST anomalies in the Atlantic, during periods of Brazil drought, occur to the east of Newfoundland. Palmer and Sun (1985) have found that this may indeed be an area where the atmospheric general circulation is responsive to extratropical SST anomalies, though their study was for late autumn/early winter conditions.

Xavier *et al.* (1985) have found strong correlations between SST in area A and Northeast Brazil rainfall. In our study, SST in area A was only weakly correlated with PMSL over the North Atlantic. Hence, there is no reason to expect the occurrence of drought to be invariably related to the strength of the NAO index.

REFERENCES

FOLLAND C.K., PALMER T.N. and PARKER D.E., *Sahel rainfall and worldwide sea temperatures, 1901-85.* « Nature », *320*, 602-607 (1986).

GILL A.E., *Some simple solutions for heat-induced tropical circulation.* « Quart. J. R. Met. Soc. », *106*, 447-462 (1980).

HASTENRATH S. and HELLER L., *Dynamics of climatic hazards in northeast Brazil.* « Quart. J. R. Met. Soc. », *103*, 77-92 (1977).

JAEGER L., *Monthly and areal patterns of mean global precipitation and variations in the global water budget.* Street-Perrott (Ed.), D. Reidel Publ. Co. Dordrecht. pp. 129-140 (1986).

LAU N-C., *Mid-latitude wintertime circulation anomalies appearing in a 15 year GCM experiment.* Large-scale dynamical processes in the atmosphere edited by Brian Hoskins and Robert Ptarce. Academic Press, 397 pp. (1983).

MINHINICK J.M. and FOLLAND C.K., *The Meteorological Office historical sea surface temperature data set.* Met 0 13 Branch Memorandum No. 137, Meteorological Office, Bracknell, England (1982).

MOURA A.D. and SHUKLA J., *On the dynamics of droughts in Northeast Brazil: Observations, Theory and Numerical Experiments with a General Circulation Model.* « J. Atmos. Sci. », *38*, 2653-2675 (1981).

NAMIAS J., *Influence of Northern Hemisphere general circulation on drought in Northeast Brazil.* « Tellus », *24*, 336-343 (1972).

NOBRE P., MOURA A.D. and NOBRE C.A., *Planetary-scale circulation anomalies associated with droughts over Northeast Brazil.* « Tropical ocean-atmosphere Newsletter », *30*, 11-13 (1985).

PALMER T.N. and SUN ZHAOBO, *A modelling and observational study of the relationship between sea surface temperature in the Northwest Atlantic and the atmospheric general circulation.* « Quart. J.R. Met. Soc. », *111*, No. 470 (1985).

ROWNTREE P.R., WILSON M.F. and SANGSTER A.B., *Impact of land surface variations on African rainfall in general circulation models.* Met O 20 DCTN 30. Meteorological Office, Bracknell, Berkshire (1985).

WALLACE J.M. and GUTZLER D.S., *Teleconnections in the geopotential height field during the Northern Hemisphere winter.* « Mon. Wea. Rev. », *109*, 784-812 (1981).

XAVIER T., DE MA B.S., XAVIER A.F.S. and PIMENTEL T., *Sea Surface temperatures of the tropical Atlantic Ocean and Solar Activity: Relationships with rainfall at Ceara-Northeast Brazil.* Internal report. Instituto de Estatistica e Informatica do Estado do Ceara. Ceara, Brazil (1985).

MONSOON DYNAMICS, RAINFALL AND TELECONNECTIONS

R.K. DATTA
Director (NWP) Mausam Bhavan
India Meteorological Department
Lodi Road, New Delhi, India

ABSTRACT

Summer monsoon circulation is a planetary scale phenomenon and accounts for a large fraction of the variance of the global motion field. This planetary scale circulation is constantly perturbed by synoptic and meso scale circulation features which to a large extent control the intra-seasonal monsoon fluctuations. The first part of the paper describes in some details various dynamical aspects of these features with special emphasis on onset and break monsoon processes. The second part is a discussion on the possible regional and global linkages and teleconnections with a special reference to temperature anomaly over Antarctica and its relationship with monsoon rainfall anomalies.

1. INTRODUCTION

The word 'MONSOON' is derived from the Arabic word 'MAUSAM' which means season. The name seems to have been coined long ago by seamen navigating the Indian seas, to describe a system of alternating winds over the Arabian Sea. A reference to festivals associated with various phases of monsoon exists in the classical literature of India. Kalidas, a famous Indian poet and writer, in a classical Sanskrit book 'Meghdoot' (means cloud as messenger) around the Sixth century A.D. referred to these wind systems and the onset of monsoon.

The monsoon as experienced over the Indian sub-continent is rather a remarkable phenomenon. Seasonally varying circulation systems associated with the annual heating and cooling of the earth are experienced over certain other parts of the globe, especially over the parts of Asia and Africa. In order to include the monsoonal characteristics of global circulation systems, meteorologists have now adopted a broader meaning of monsoon. Monsoon is now generally referred to as seasonal migration of the planetary pressure and wind belts in continental areas of the globe. Ramage (1971), reviewing the definitions provided by earlier workers, stated that a region is considered as a monsoon region if it satisfies the following surface circulation criteria:

i) the prevailing wind direction shifts at least 120° between January and July,

ii) the average frequency of prevailing wind direction in January and July exceeds 40%,

iii) the mean resultant winds in at least one of the months exceeds 3 m/sec, and

iv) fewer than one cyclone-anticyclone alteration occurs every two years in either month in a 5° latitude-longitude rectangle.

The region satisfying all the above criteria lies between 25°S to 35°N and 30°W to 170°E and may be classified as monsoon area.

This delineation of the monsoon area was based on surface level circulation features only. But the monsoon is now understood to be controlled by circulation features within the whole depth of the atmosphere, especially tropospheric and lower stratopheric circulations seem to play a significant role. In order to study this we present in Fig. 1.1 (a,b), the mean monthly upper wind cross-section for the years 1977 and 1979 for a number of stations in the region of the tropical belt throughout the world. The selection of the years 1977 and 1979 is important because these were the years of contrasting monsoon activity, the former being a year of good summer monsoon activity over the Indian subcontinent and later being a drought year. Moreover, both these years were years of International Monsoon Experiments.

These plots bring out the following significant features related to the upper air wind system in the equatorial belt:

i) At stations north of 10N and between 20W to 100E, there is a significant reversal of tropospheric wind regime between summer and

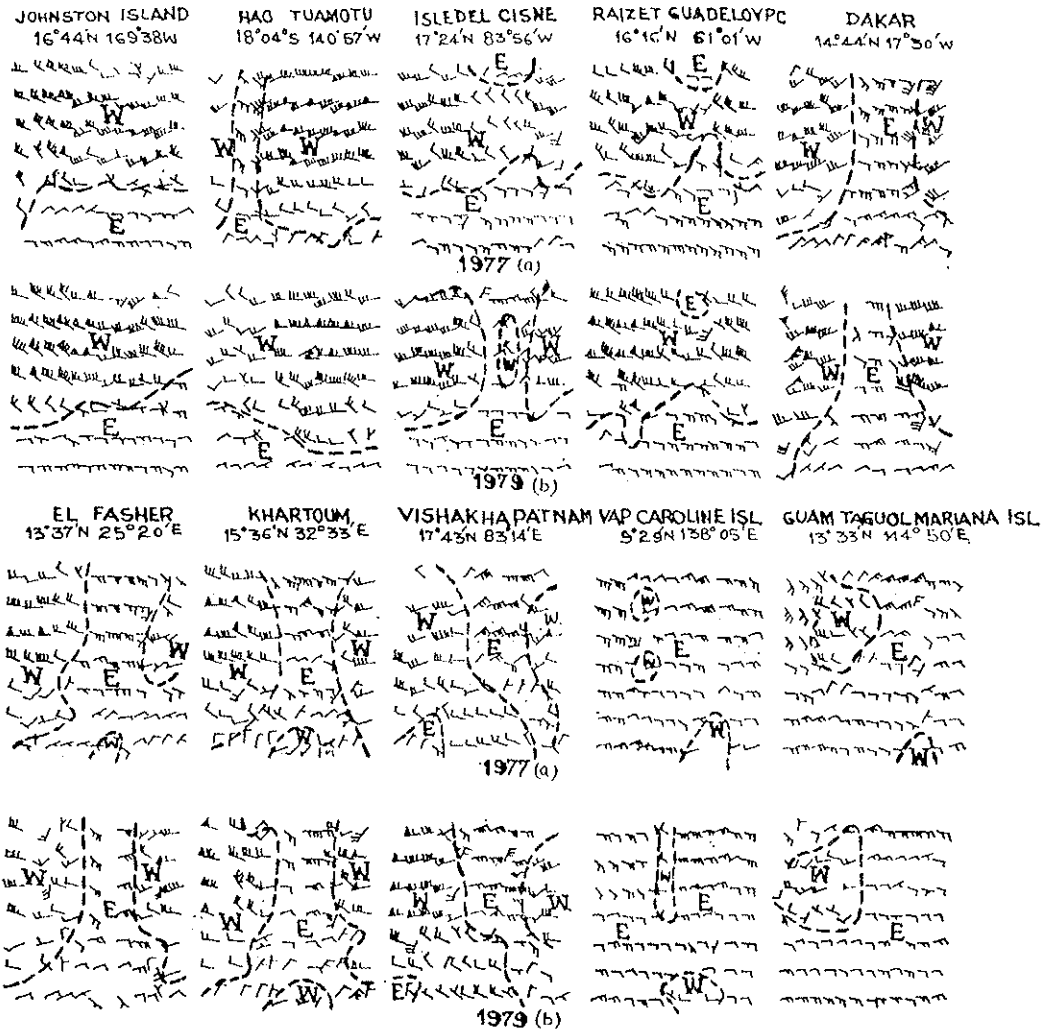

FIG. 1.1. Mean Monthly vertical cross section of winds for stations in the tropical belt.

winter months. Reversal is similar during both the years 1977 and 1979, except that the intensity was higher during 1977 compared to 1979.

ii) For stations east of 100E, there are no significant changes in circulation pattern between summer and winter months except at or near sea level.

iii) At stations west of 60W also there are no significant changes in wind flow from season to season, although there seem to be some apparent variations between 1977 and 1979.

It may be clear from the above description that out of the region which has been marked as monsoon area, the region 20W to 100E has reversal in flow patterns over the whole of the troposphere. We will further show that the Indian summer monsoon has other spectacular features connected to its onset and day to day variations in its intensity. Thus, monsoon circulation over and adjoining the Indian sub-continent has a special importance and its study has thus been of considerable interest to the meteorologists all over the world. We would, however, confine our attention mainly to monsoons of the Indian sub-continent.

1.1 Monsoons of the Indian Sub-Continent

From general consideration, the Indian sub-continent encounters two types of monsoons. These are:

i) The summer monsoon, also well known as the Southwest monsoon, which influences this sub-continent from the beginning of June to the middle of September.

ii) The winter monsoon, also well known as the Northeast monsoon, running from October to December.

The southwest monsoon is more important from both economic and scientific considerations. During this short spell of over 100 days (June to September), India gets over 70% of the total annual rainfall.

The monsoon circulation also accounts for a large fraction of the variance of the global motion field. The numerical models therefore fail to successfully simulate the global circulation, if the processes which drive the monsoon circulation are not explicitly incorporated. The proper understanding of physical processes which drive the monsoon circulation is therefore very important both for proper prediction on regional as well as on global scales. For convenience, in future discussions 'monsoon' will refer to SW monsoon until and unless specified otherwise.

1.2 Monsoon Circulation Pattern

In 1921, Sir George Simpson hypothesized that the monsoon is a continuation of southeasterly trade winds of the Indian ocean, which after crossing the equator attain southwesterly direction due to the turning effect of coriolis force. Although doubts prevailed, Simpson's hypothesis held the ground until the fifties. Observations made over the Arabian Sea during the International Indian Ocean Expedition (IIOE) 1963-65, however, divided the scientists into two schools of thought. One school believed that the Simpson's hypothesis is not valid and monsoon air need not bring moisture from the Indian Ocean but evaporation from the Arabian Sea itself can provide a potent source of moisture required for the monsoon rainfall, thus implying that the monsoon need not originate from the southern hemisphere. The other school, however, strongly supports cross-equatorial flow and moisture source of crucial importance to the origin of the monsoon. The detailed observations showing strong cross-equatorial flow particularly off the east coast of Africa (well known as Low Level Jet or Somali Jet) provide enough evidence for this hypothesis.

MONEX-79 data set has further confirmed the significance of cross equatorial flow as an important feature for the onset of monsoon. This data set has also provided a lot of information on teleconnections between systems of southern hemisphere and fluctuations in monsoon circulation.

Since early periods, differential heating has been considered the main mechanism for driving the monsoon circulation. This still seems to be valid, but weather systems associated with monsoon circulation cannot be described simply by a 'Chimney effect', which means that the air heated over the continent rises and is replaced near the ground by moist maritime air masses (Wagner, 1931).

There seems to be a general agreement that besides other physical processes which are not fully understood, the following factors play a significant role to drive the monsoon circulation and associated rainfall:

i) Differential heating of land and sea;

ii) The Tibetan plateau located at about 5-6 km height which acts as a raised platform for a heat source, and

iii) The inffluence of western and eastern Ghats running parallel to the west and east coast of peninsular India, the Arakan Yoma and the Garo-Khasi Jaintia hill ranges to the east, Kirther and Suleman ranges to the west and Vindhya and Satpura over Central India.

1.2.1 *Sea Level Flow Pattern*

With the advent of summer, development of heat low starts even by March with slightly higher pressure over the oceanic regions. By April, the sub-tropical anticyclone of the southern hemisphere shifts northward carrying with it SE trades to the north. The large-scale heat low from Africa in the west to Burma and further east over SE Asia gets established.

By May, the continental heat low dominates the low level circulation pattern, with a dominant heat low pressure zone extending from northwest parts of India and adjoining Pakistan to the northern angle of the Bay of Bengal and thence through Burma and China into the Pacific ocean. The heat low further intensifies as the season advances and the low pressure zone acquires the popular name, monsoon trough. The chief features of monsoon circulation at the sea level over the Indian sub-continent may be summarized as follows:

i) Heat low over Pakistan and adjoining area, with the zone of low pressure extending from heat low to the northern portion of the Bay of Bengal. The surface wind flow is thus westerlies south of the trough and easterly to the north of the trough zone.

ii) Strong pressure gradient with minimum pressure in the north and higher pressure to the south. In good monsoon situations, pressure gradient between Bhuj (23.3N, 69.6E) and Trivandrum (85N, 76.9E) may be of the order of 10-12 mb. This pressure gradient pattern is entirely the reverse of the winter pattern, during which period the pressure is higher in the north and lower in the south.

1.2.2 *Upper Air Flow Pattern*

As the sea level circulation evolves into a typical monsoon circulation, there are certain changes which take place in the upper air flow pattern. These may be summarized briefly as follows:

i) Building up of cross equatorial southerly flow near Somali coast of east Africa with wind speed reaching 60 kt, well known as low level jet (Findlater, 1969a). Features of low level westerly jet are also observed over the peninsula with a core of maximum wind near 850 mb (Koteswaram, 1960; Joseph and Raman, 1966).

ii) Establishment of an east-west trough over the southern peninsula, with quite often embedded vortices in Bay and/or Arabian sea. This east-

west trough at the initial stage is generally most prominent at 700 mb (Yin, 1949; Datta *et al.*, 1981, 1982). With the advance of season, this trough builds up to 500 mb level. At this stage, there seems to be a dynamic link between the lower tropospheric flow pattern and the trough sloping southwards with height. This brings in gradual increase of depth of westerlies to the south and easterlies to the north of the trough. 500 mb being transitional level, the flow pattern above this level is predominantly governed by the sub-tropical ridge and its gradual northward shift.

iii) Sub-tropical ridge which, as mentioned earlier, is one of the significant circulation features, especially of mid and upper tropospherical flow patterns, is also a prominent feature of monsoon circulation. It is also known as Tibetan High. As it shifts northwards with the advance of the season, the sub-tropical westerly jet (STJ) shifts north of the Himalayas. A tropical easterly jet (TEJ) appears on the southern periphery of the ridge with its core speed between 150 and 100 mb and around 10-13N (Koteswaram, 1960). Koteswaram also pointed out that the STJ sometimes persists over NW India even after the onset of the monsoon over Kerala.

iv) With the advance of season, another significant change is the shift of the upper tropospheric (200 mb) trough from its mean winter position of 90E to 75E. This change-over has been associated with the onset of the monsoon over India (Riehl, 1954).

1.2.3 *Zonal Circulation*

In fig. 1.2 (a,b,c,d,e,f), we present the zonal wind charts based on the mean data computed by Boogard (1977) for the month of July. The typical features are:

i) General westerlies over the Arabian sea, Bay of Bengal and adjoining Indian Ocean up to the equator, and easterlies south of it. This pattern is more or less similar up to 500 mb level, with intensity of westerlies being maximum at 850 mb level over the SE Arabian Sea and level to level it is higher over the Arabian Sea than over the Bay of Bengal. Although not reflected in mean pattern, we observe on occasions, especially associated with the formation of monsoon depression, westerly winds of jet speed and jet characteristics at low level around 850 mb. It is still not fully known whether low level jet is a consequence of the formation of a mon-

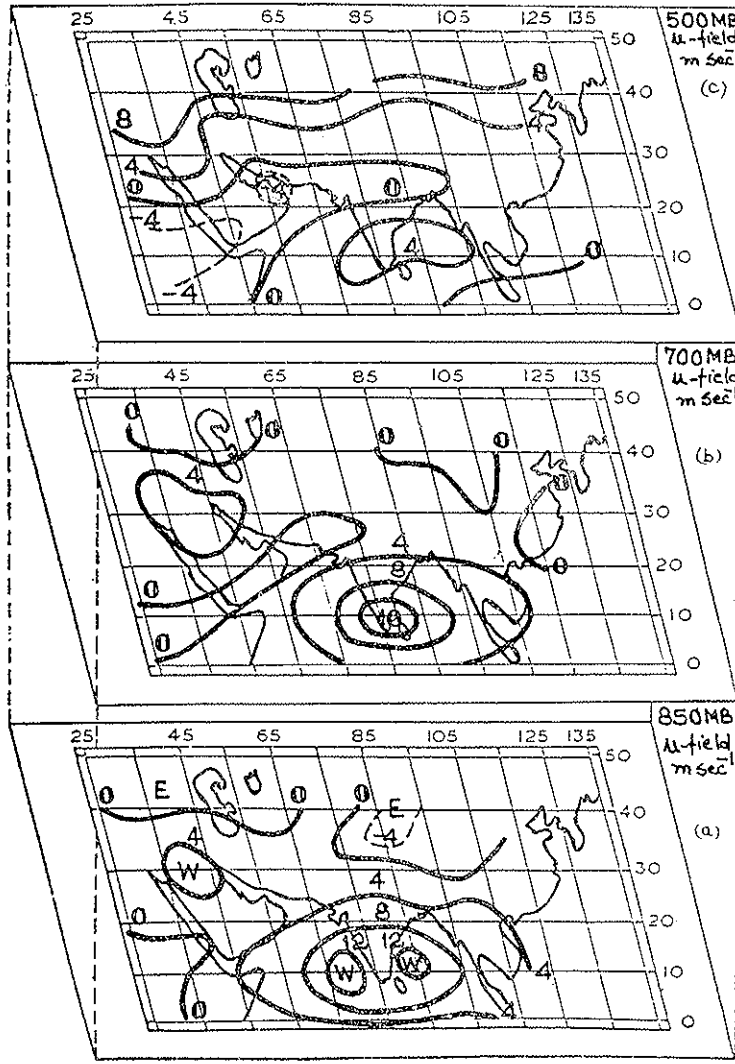

FIG. 1,2. Mean July zonal flow pattern for various levels.

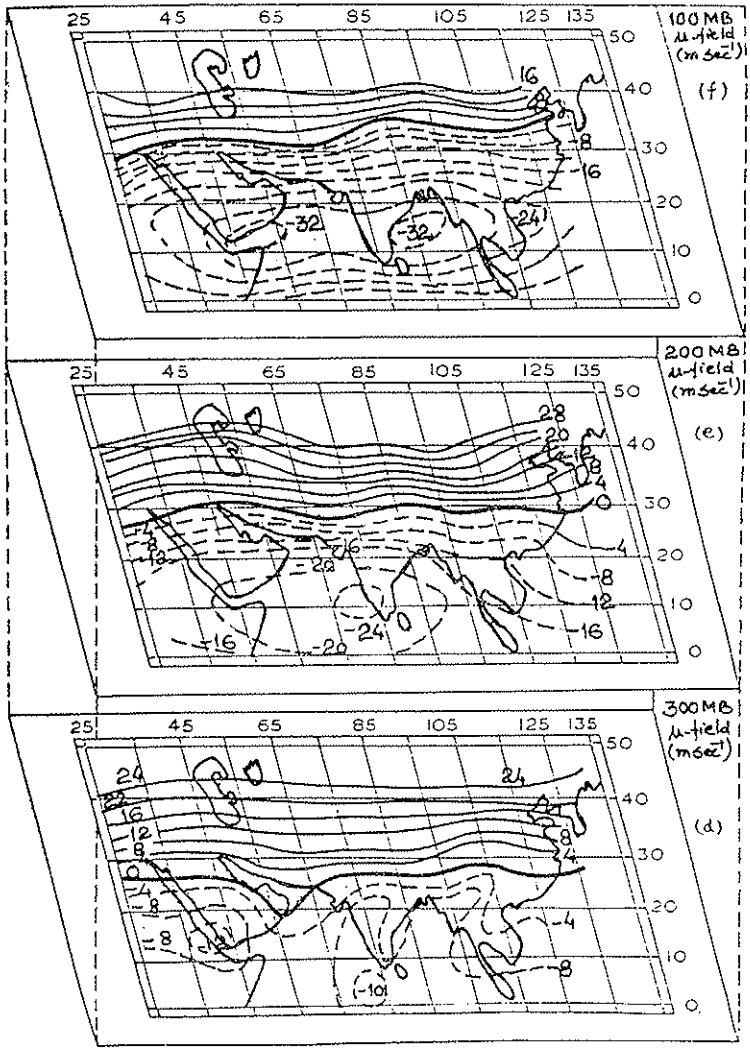

FIG. 1.2. Same as on previous page.

soon depression or establishment of low level jet is a signal for the intensification of the existing disturbance.

ii) The upper tropospheric flow pattern is predominantly easterly with westerlies confined to north of 25N and south of the equator. The intensity of easterlies increases with height, being maximum at 150 mb. A comparison of this flow, with the winter (January) flow, shows a complete reversal of easterly and westerly fields. Transition starts by April and by July the monsoon flow gets completely established. Significantly, the monsoon current over the Indian sub-continent is predominantly westerly (south of the trough axis) in the lower troposphere with easterlies overlying it.

As already mentioned, TEJ can be seen quite prominent in the upper troposphere. TEJ was studied in detail by Koteswaram (1958), who explained their dynamics and their links with the onset and day to day activities of monsoon. The Sub-tropical Westerly Jet (STJ) is prominent at about 200 mb level but its axis is shifted to north of 40N.

1.2.4 *Flow Across the Equator and Meridional Circulation*

Cross equatorial flow from the southern to the northern hemisphere has been considered a significant component of the monsoon circulation (Simpson, 1921). In spite of certain contrary views, it has stood tests of recent observations.

Rao (1964) showed that there is an interhemispherical circulation across the equator from the winter to the summer hemisphere. Findlater's (1969 a and b) work has also clearly established cross equatorial flow. In the lower troposphere, the south to southwesterly winds of jet structure have been observed by Findlater over and near the Somalian coast of East Africa during the monsoon, which is well known as Somali Jet. Krishnamurti (1976) explained the dynamics of this LLJ through the influence of beta effect (i.e., the effect of variation of coriolis' parameter with latitude) and the orography of East Africa.

Monex 1979 data, especially the Balsamine experiment data, also provides excellent information on the low level flow from the southern hemisphere to the northern hemisphere as a precursor to the onset of the monsoon.

In figure 1.3, we present the mean meridional circulation pattern for the month of July. The data for the preparation of these charts was also taken from Boogard (1977).

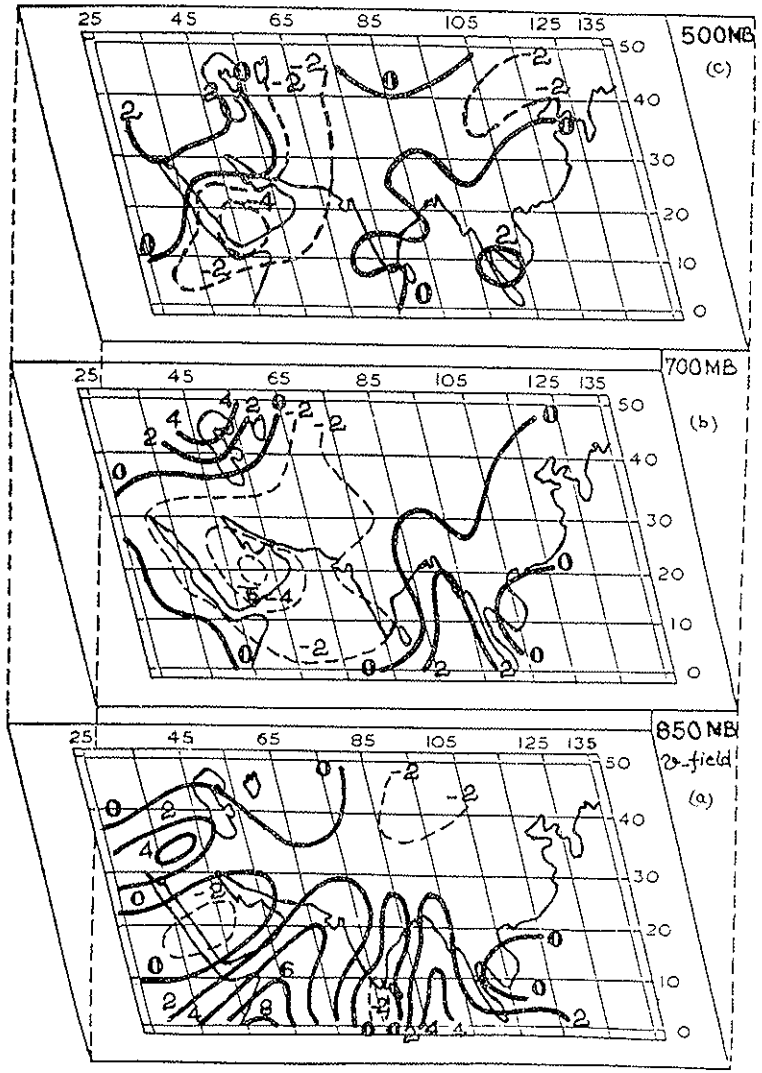

FIG. 1.3. Mean July meridional flow pattern.

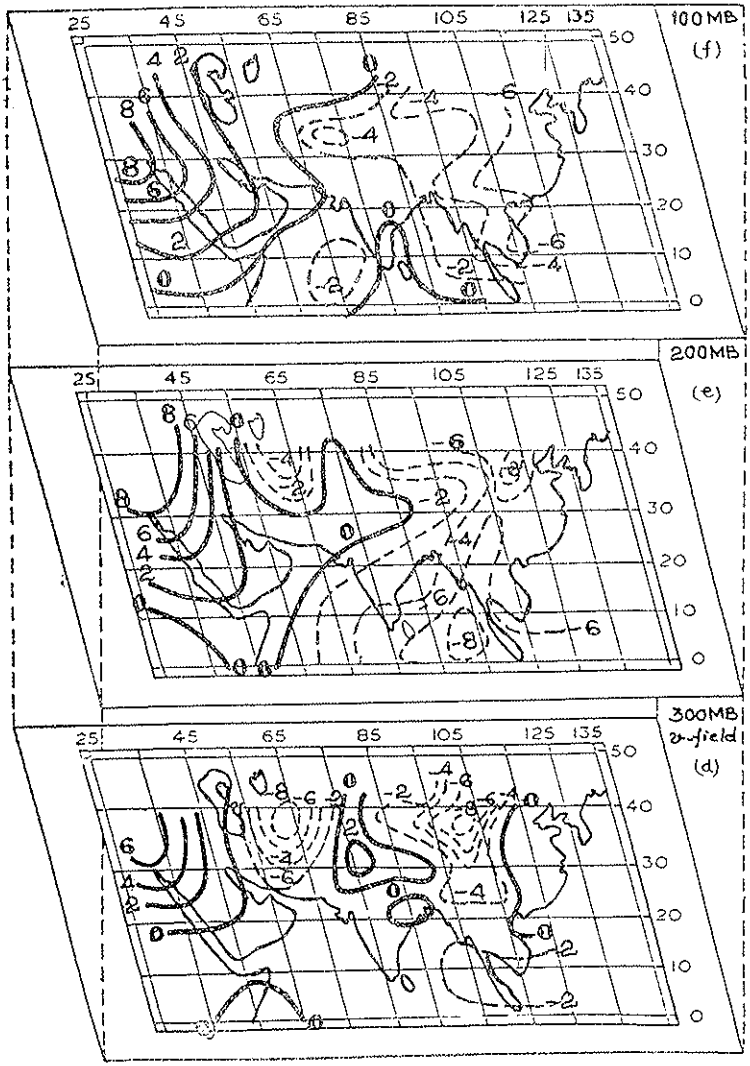

FIG. 1.3. Same as on previous page.

Though the meridional wind components are considerably weaker than the zonal components in the monsoon region, their study is important to understand the exchange of heat and momentum between hemispheres and the tropics and middle latitudes. The significant feature at the surface and 850 mb level is the general southerly flow over coastal regions of East Africa and adjoining the Arabian Sea. There is another region of southerly flow located over the Bay of Bengal together with a small region of northerly flow bounded by 70 to 80 degrees. The strongest southerlies are located over the East African region at 850 mb.

At higher levels (700/500 mb), southerlies change over to northerlies over the Arabian Sea and continue so in the upper troposphere. In the Bay of Bengal, southerly flow, though weak, is maintained up to 500 mb level but it becomes predominantly northerly aloft.

1.2.5 *Vertical Circulation*

Koteswaram (1960) postulated a meridional circulation model (fig. 1.4) which is a reverse 'Hadley Cell'. He explained the mechanism of this circulation by taking into account the upper level anti-cyclogenesis caused by the heating of the elevated Tibetan Plateau and latent heat released by convective hot towers in the monsoon trough. The upper tropospheric easterly jet stream has been explained as an effect of south-

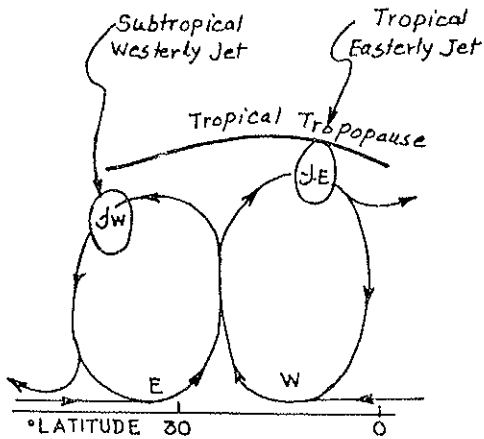

FIG. 1.4. Idealized monsoon circulation model (after Koteshwaram, 1960).

ward displacement of air from Tibetan anticyclone under conservation of absolute angular momentum. Thus, the heat source provided by the elevated Tibetan Plateau and the monsoon trough region and the sink over the equator helps the establishment of the reverse 'Hadley Cell', and the monsoon current is driven as a return current in the lower troposphere.

Das (1962), using a 10-layer quasi-geostrophic model, computed vertical motion for a typical monsoon month (July) and showed the region of ascent over northeast India and the region of descent over northwest India, thereby depicting a heat source over the northeast and heat sink over northwest India. This type of zonal vertical circulation was later postulated by Bjerknes (1969) along the equatorial region. In order to explain the observed belt of low level westerlies and reversed easterlies aloft, Frost and Stephensen (1965) proposed a zonal circulation cell with an ascending branch over the heated land mass of Indonesia and a descending branch over the equatorial Indian ocean along about 60E.

Flohn (1964) schematically presented the vertical motion field in the low latitude in two longitudinal belts 10W to 75E and 90E-130E (fig. 1.5).

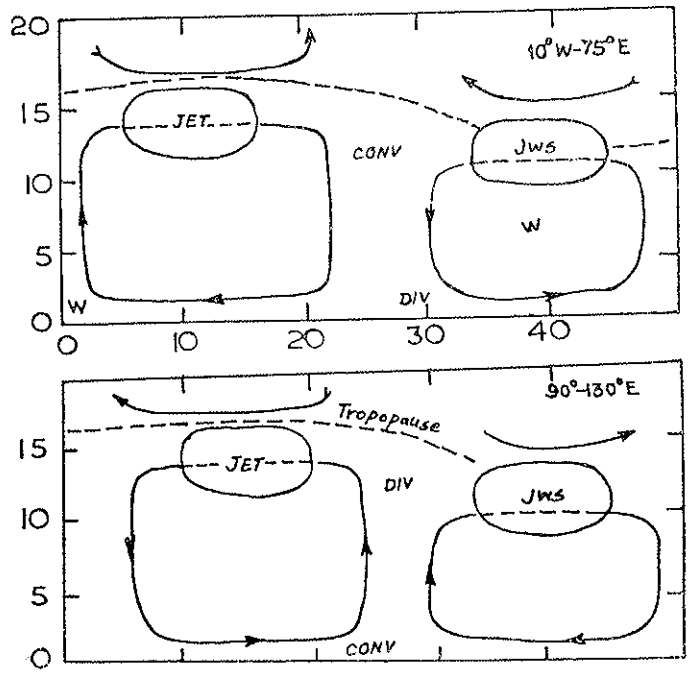

FIG. 1.5. Schematic vertical motion field (after Flohn, 1964).

From our consideration the second circulation pattern is more restricted and would be more valid for the region 75E to 110E.

A quasi-Geostrophic model (QGM) was used by Datta and Mukherji (1975) for computation of the 'w' field, during two typical situations of active and weak monsoon conditions. Based on that, we schematically derived a vertical motion pattern (fig. 1.6 a to e). It may be seen from the figures that the active monsoon condition is characterised by reversal of ascent to descent at about 600 mb level, south of 20N. Thus the monsoon circulation is largely controlled by large scale-meridional (Hadley) and zonal (Walker) overturning.

1.2.6 *Temperature Distribution*

In fig. 1.7 (a to f), we present the temperature distribution over the Indian sub-continent and adjoining region during July. The results are based on climatological data derived by Boogard (1977). The significant features are a marked region of high temperature running east-west approximately in the latitude belt 25-30N with centres of high temperature located over Sahara and Saudi Arabia in the lower troposphere. At sea level a minor centre of high temperature is also located in China, north-west of Tibet. At lower levels, (below 850 mb), there is a north-south thermal ridge as a result of greater heating of peninsular India in comparison to the adjoining oceanic surfaces. The oceanic region near the equator is colder.

At 500 mb (mid-troposphere), the thermal ridge runs along approximately 25N, but the centre of the warmest temperature is located over the Tibetan Plateau. The temperature gradient to the north is sharper in comparison to the south. The region of the cold centre lies over the Indian Ocean near the equator.

In the upper troposphere, up to 200 mb, the thermal ridge axis runs more or less along the same parallels but there is a gradual build-up of southward gradient, so that at 200 mb level, the southward temperature gradient southwards is larger than the gradient northwards.

150 and 100 mb are characterised by warmer temperatures in the north with no thermal ridge but with a significant thermal trough running along the equator.

This temperature distribution during July, which is obviously caused by the land-sea distribution in the area, and the existence of an elevated heat source over the Tibetan Plateau are important features for understanding the monsoon dynamics.

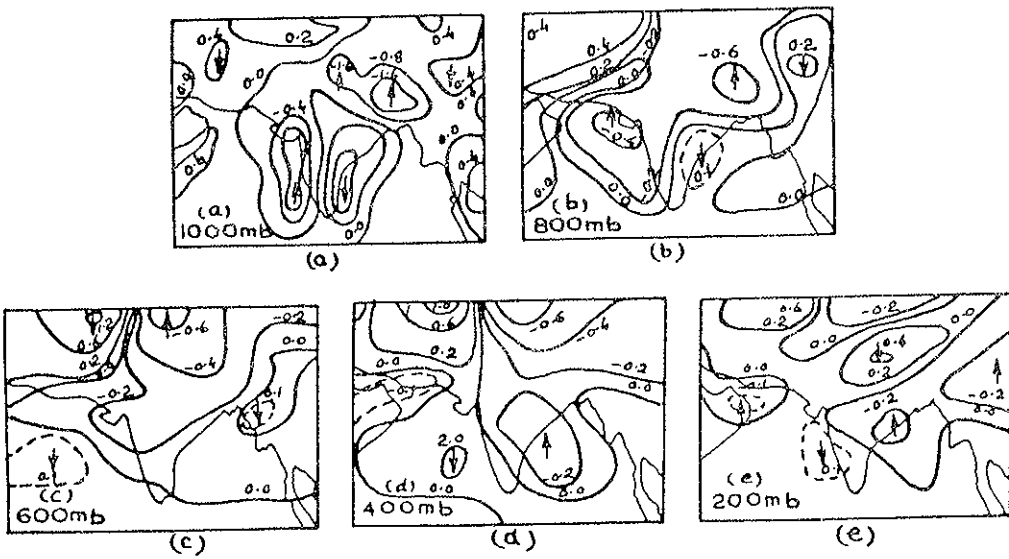

FIG. 1.6. Vertical motion ω field during active monsoon situation 23 and 27 August 1967.

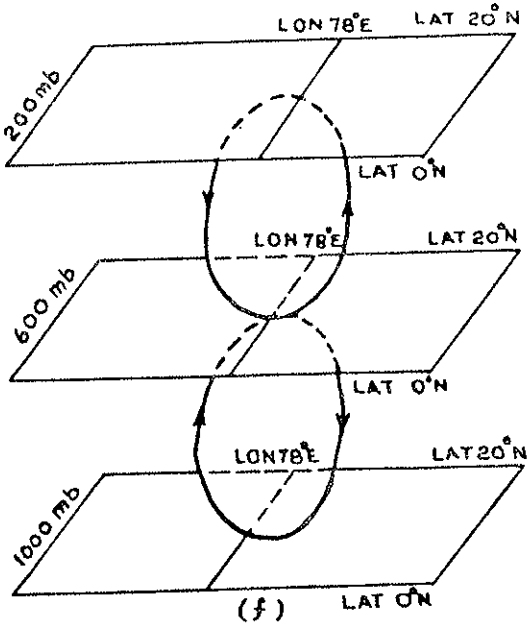

FIG. 1.6. Schematic representation of vertical motion field during active monsoon.

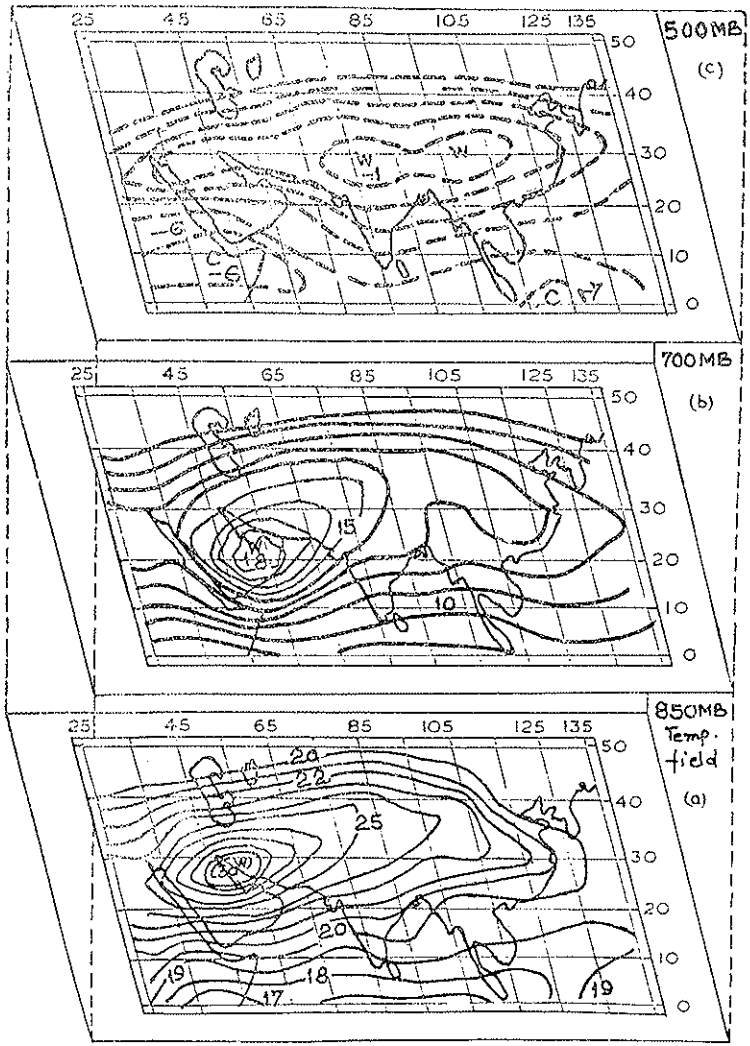

FIG. 1.7. Mean July temperature distribution.

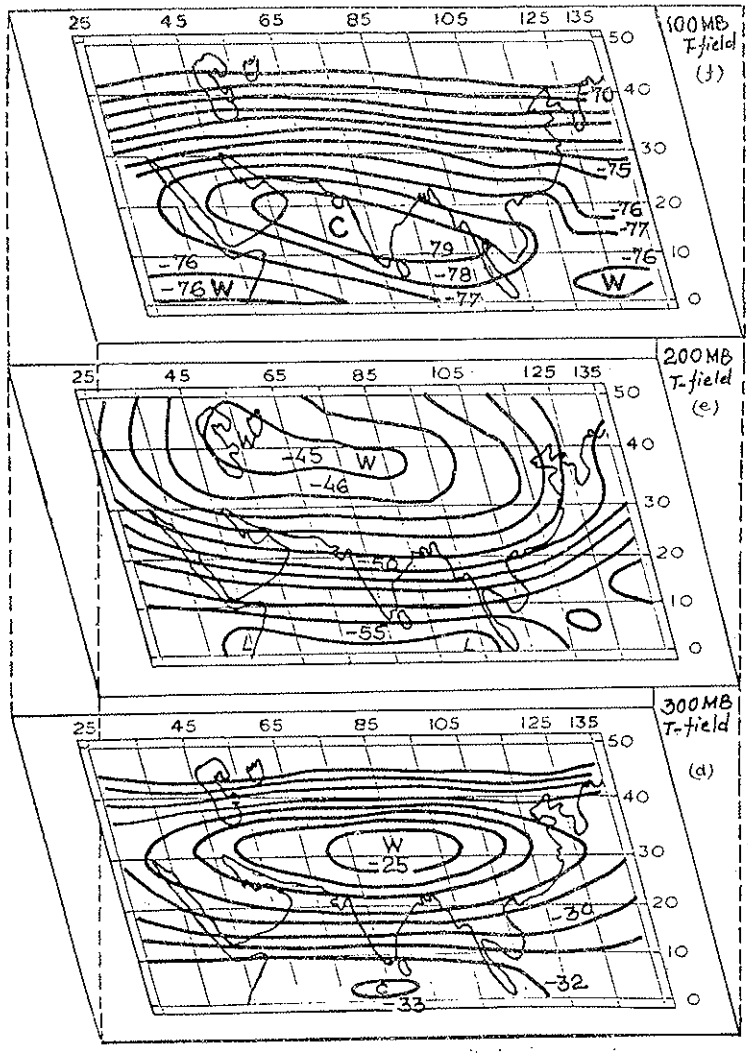

FIG. 1.7. Same as on previous page.

1.2.7 *Rainfall Distribution*

In fig. 1.8, we present normal rainfall distribution over the country during the monsoon season, June to September. The rainfall distribution clearly shows a marked influence of orography of the Western Ghats, the Khasi-Jaintia, the Vindhyas and the Himalayas. There are regions of heavy rainfall over the west coast of India and the Khasi-Jaintia hilly areas. Cherra-

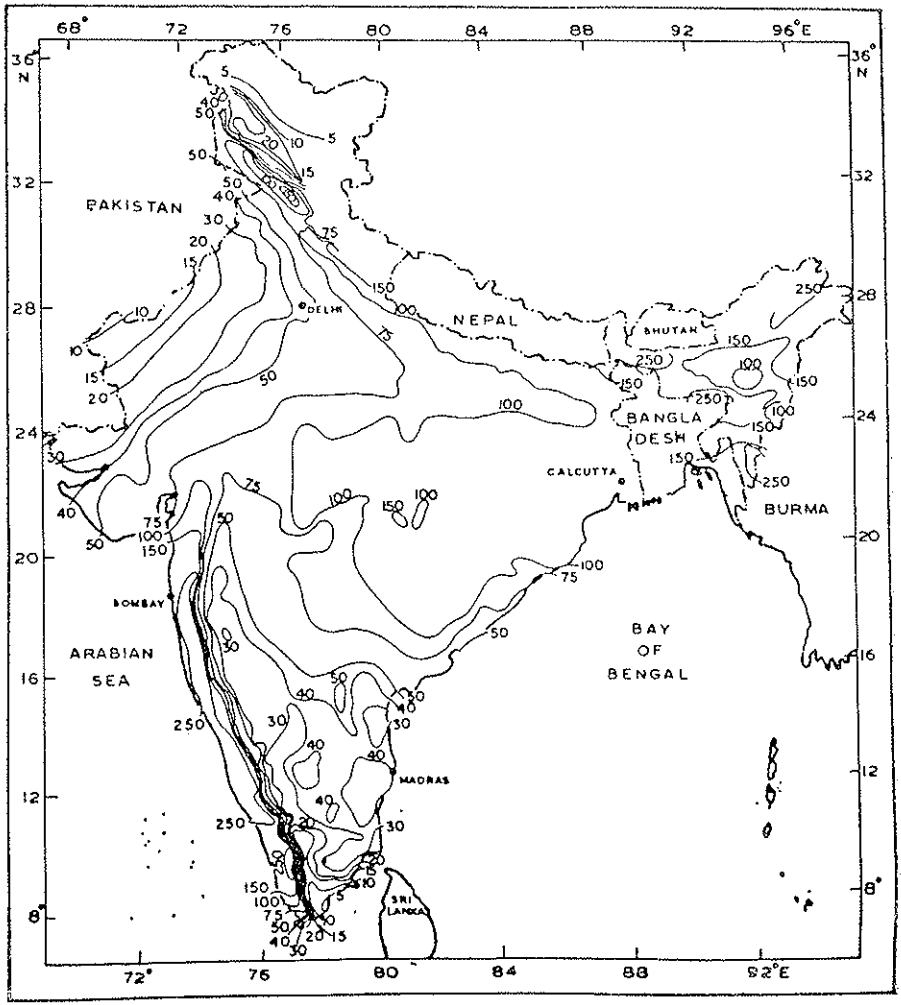

FIG. 1.8. Normal monsoon rainfall distribution.

punji (25-15N, 91-44E) in the latter region gets the world's highest annual rainfall of 1145 cm. The latest records however place MAWSYNRAM 25.30N and 91.58E as the wettest station with annual rainfall of 1188 cm. There is a rapid decrease of rainfall from the west coast as we proceed inland to the lee of Ghats. Immediately south of Vindhyas again is a region of heavy rainfall decreasing southwards. Along the west coast itself, also, there is vast variation in the rainfall, the maximum being over 250 cm between 12-18N and decreasing on either side: such that the southeastern parts of the peninsula as well as the northern parts of Sri Lanka, are very dry. There is a gradual decrease of rainfall over the Gangetic plain from east to west, decreasing from about 100 cm over West Bengal to less than 10 cm over West Rajasthan. Another region of heavy rainfall is located over the foothills of the Himalayas, which is in excess of 150 cm over Himachal Pradesh and reduces sharply as we proceed west to west-northwest, getting almost negligible rainfall in Ladakh valley being on the leeside for the monsoon wind.

The above is a picture of normal distribution of rainfall over India during the monsoon. But in any particular year, there may be marked variations in the rainfall from its normal value. This feature is reflected in fig. 1.9, which depicts the coefficient of variability of rainfall. Coefficient of variability (CV) is defined as the ratio of the standard deviation of the season's rainfall to the mean amount. CV as a whole for India is only 10 percent, but it has large variations for certain regions in the country. The regions which get larger normal rainfall are the regions with lower CV, whereas the regions of lesser normal rainfall have higher CV values

Generally the NW part of India and peninsular India are the regions of higher CV (CV $>$ 30 percent) and are therefore more susceptible to year-to-year variations of rainfall.

In fig. 1.10, we show the mean rainy days (daily rain $\geqslant$ 0.1 mm) during the period June-September. It is interesting to note that except over the west coast and parts of Assam where the number of rainy days during the period June 1 to September 30 exceeds 75 days over the rest of the country, the number of rainy days is less than 50. If, however, spells of heavy rainfall be considered, as shown by Ananthakrishnan (1976) for 4 representative stations (Bombay, Calcutta, Delhi and Madras), 50 percent of the rainy days in the low intensity end of the spectrum account for less than 10 percent of the total rainfall, while 10 to 15 percent of the rainy days on the high intensity end of the spectrum account

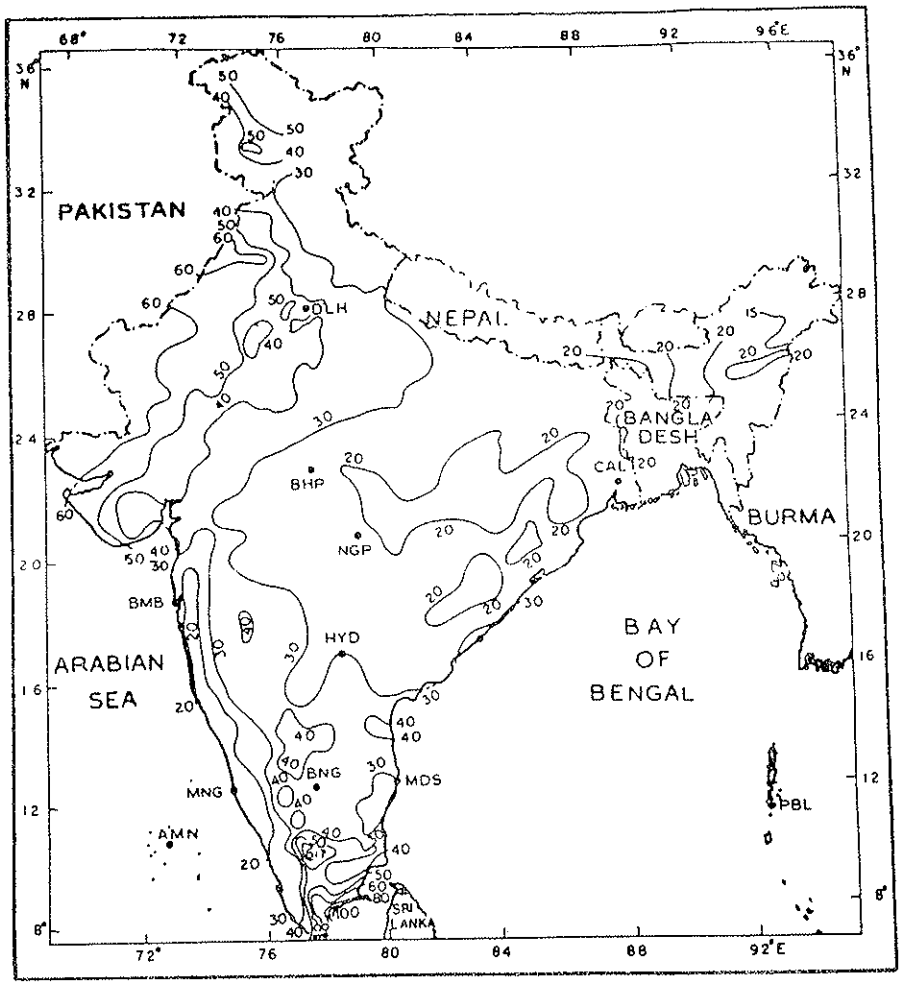

FIG. 1.9. Coefficient of variability of rainfall during monsoon.

for over 50 percent of the total rainfall. 55 to 60 percent of the rainy days have intensity less than 10 mm/day and for 85 to 90 percent of the rainy days the intensity is less than 50 mm/day. Thus the monsoon period may not be considered as a period of continuous rainfall but a period where a few spells of rainy days, e.g., 10 to 15 percent of rainy days, may account for most of the rainfall during the season.

It is also noticed that several stations show double rainfall maxima

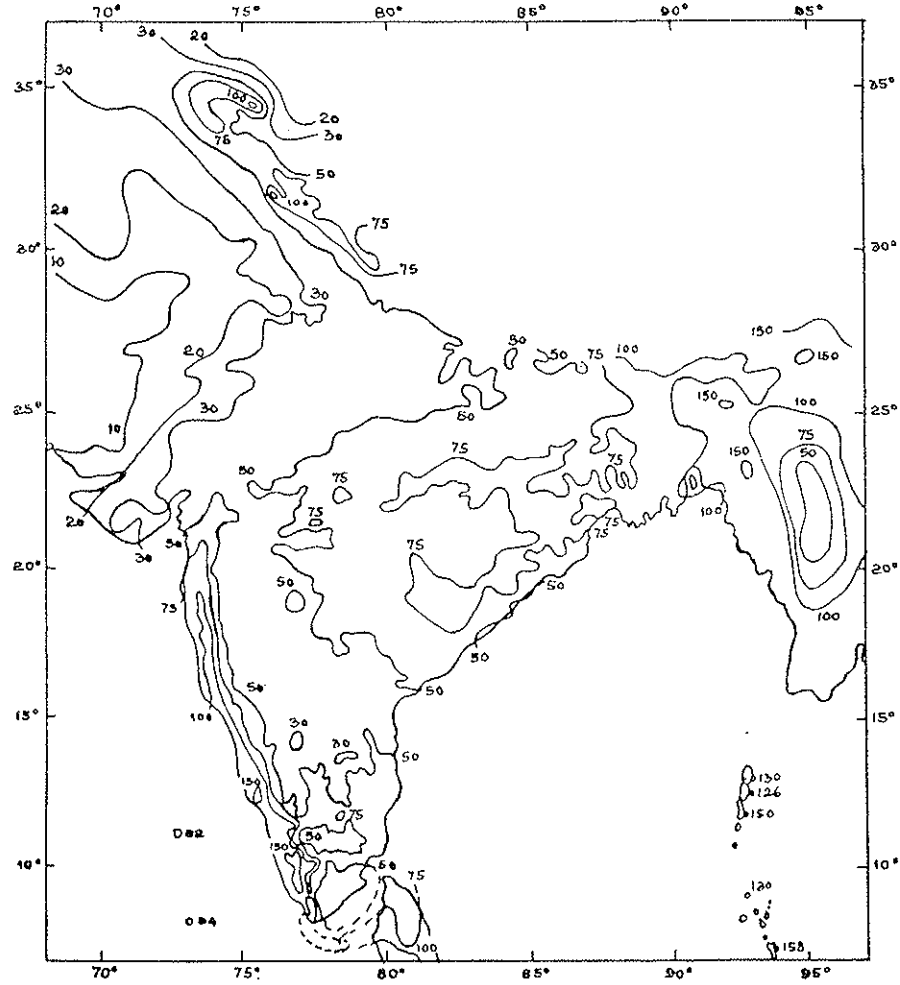

FIG. 1.10. Mean annual number of rainy days.

during the monsoon season. Similar double maxima were observed over the region of Lake Victoria (Datta, 1980).

1.2.7.1 *Diurnal Variation of Rainfall*

It is interesting to examine the diurnal variation of rainfall to understand significant precipitation formation processes.

While examining the diurnal variation of rainfall for stations located

around Lake Victoria in east Africa, Datta (1980), found very interesting features pertaining to the interaction of land and lake breezes and their influence on precipitation dynamics in the region.

In a similar study in India (Datta, 1986) mean clock hour precipitation data over 7 representative stations for the period 1948-1965 was subjected to fourier analysis. The list of the stations is given in the Table.

LIST OF STATIONS

Name	*Coordinates*
Bombay	19.1N 72.7E
Mahabaleshwar	17.9N 73.7E
Sagar Island	21.6N 88.1E
Cherrapunji	25.3N 91.7E
Madras	13.0N 80.2E
New Delhi	28.6N 72.2E
Hyderabad	17.5N 78.5E

Bombay and Mahabaleshwar represent the west coast, Madras the east coast, also the lee-ward side of monsoon winds, Saugar Island, an island on the east coast. Cherrapunji lies in the northeast part of the country and records the world's highest precipitation in the world (though the recent world record is of Mawsynram, a station near Cherrapunji). New Delhi and Hyderabad represent continental stations in the northern and southern parts of the country. The fourier analysis depicts the following interesting features.

i) Bombay, Cherrapunji, Saugar Island show single peak near early morning (0300 to 0500 hr). First harmonic explains over 85 percent of the variance. Radiation cooling seems to play a significant role in precipitation forming processes besides orographic and other dynamic features.

ii) Madras and Hyderabad show peak around late evening/early night (20-22 hr). First harmonic here also accounts for about 90 percent of variance. This may suggest afternoon insolation as an important triggering mechanism.

iii) Whereas the 5 stations discussed earlier had significantly unimodal hourly rainfall distribution, Mahabaleshwar (a hill station on Western Ghats) and New Delhi have bimodal rainfall distribution with peaks

during the afternoon and early morning. The first harmonic corresponding to afternoon accounts for 41 percent variance over Mahabaleshwar and about 65 percent variance over New Delhi. The second harmonic corresponding to early morning peak explains 47 percent variance over Mahabaleshwar and 19 percent over Delhi.

1.2.7.2 *Periodicity in Monsoon Rainfall*

During recent years, a number of studies have reported low frequency modes with time scales less than the seasonal time scale. These low frequency modes are related to the Intra-seasonal monsoon fluctuations.

Krishnamurti and Bhalme (1976) found that during the monsoon of 1967, the various meteorological elements including rainfall exhibited fluctuations around the time scale of 2 weeks. Shorter time scale fluctuations around 2-3 days were also observed.

Madden and Julian (1971) were probably the first to show the existence of oscillations with a period around 40 days. Their results were based on ten years' data of one tropical station (CANTON ISLAND, 3S, 172W). In their subsequent study (Madden and Julian, 1972) they confirmed the existence of these low frequency oscillations in tropical regions in general.

Yasunari (1980), using satellite cloud observed data for the years 1966 to 1972 as well as 1 June-30 September 1973, came to the conclusion that the daily cloudiness has a periodicity of 30 to 40 days as a predominant mode. Modes of 30-50 days have also been shown in the meridional propagation of the east-west oriented trough/ridge system over the Indian area during the monsoon of 1979 (Krishnamurti and Subrahmanyam, 1982). Sikka and Gadgil (1980) studied the northward propagation of maximum cloud zones (MCZ) and suggested the low frequency mode of propagation of MCZs (they really observed two MCZs which can be compared with ITCZ and ET defined by Sud and Datta (1980) and Datta *et al.* (1981).

Goswami and Shukla (1984) carried out several long time Integrations with a symmetric version of the GLAS Climate Model. They observed strong and weak episodes of the Hadley circulation. The oscillation of the Hadley circulation seems to occur in two dominant ranges of periodicity, one with a period of 10-15 days and the other 20-40 days.

All the above mentioned and earlier studies (not quoted here) suggest that the intra-seasonal fluctuations are dominated by significant

modes, namely 2-3 days, about 2 weeks and 20-40 days. It is generally believed that the similar modes are present in monsoon rainfall.

Daily rainfall data for long time periods is being examined critically at the India Meteorological Department to confirm the existence of these modes and their possible application in long-range forecasting.

1.3 Onset of the Monsoon

The monsoon advances into India towards the end of May or early June with a good degree of regularity in a statistical sense (i.e., with a standard deviation of about a week). It marches northwards starting from the west coast of India (Kerala Coast) to the other parts of the country. By July, it covers the whole of India. It starts withdrawing from the extreme northwest parts of India by the 1st of September and withdraws from most parts of the country by the middle of October, except south peninsular India, where it is difficult to distinguish between the withdrawal of the SW monsoon and the onset of the NE monsoon.

Fig. 1.11 (a and b) represents normal dates of onset and withdrawal of the monsoon respectively.

The apparent regularity of the onset of the monsoon may lead one to think that the prediction of the onset of the monsoon is a trivial matter, but this spectacular phenomenon is full of vagaries. While onset, some years, is abrupt, associated with formation of a depression/cyclone and its northwards movement (e.g., onset of 1979), in other years, it may be a quite slow process associated with a formation of a zone of low pressure extending east-west and its gradual northward progress.

After the first burst/onset of the monsoon over the Kerala coast, further northward progress may be smooth till it covers the whole country, or erratic after initial good progress. As an illustration, during the 1982 monsoon, onset over the Kerala coast was on 30th May, i.e., 2 days before the normal date, and it progressed rapidly up to 15N during the next 3-4 days. Afterwards, there was no significant progress for over 10 days and Bombay got its first monsoon spell only on 17th June, 7 days after the normal date. In 1978, however, the progress of the monsoon was very smooth.

For showing the year-to-year variations in the date of onset, we

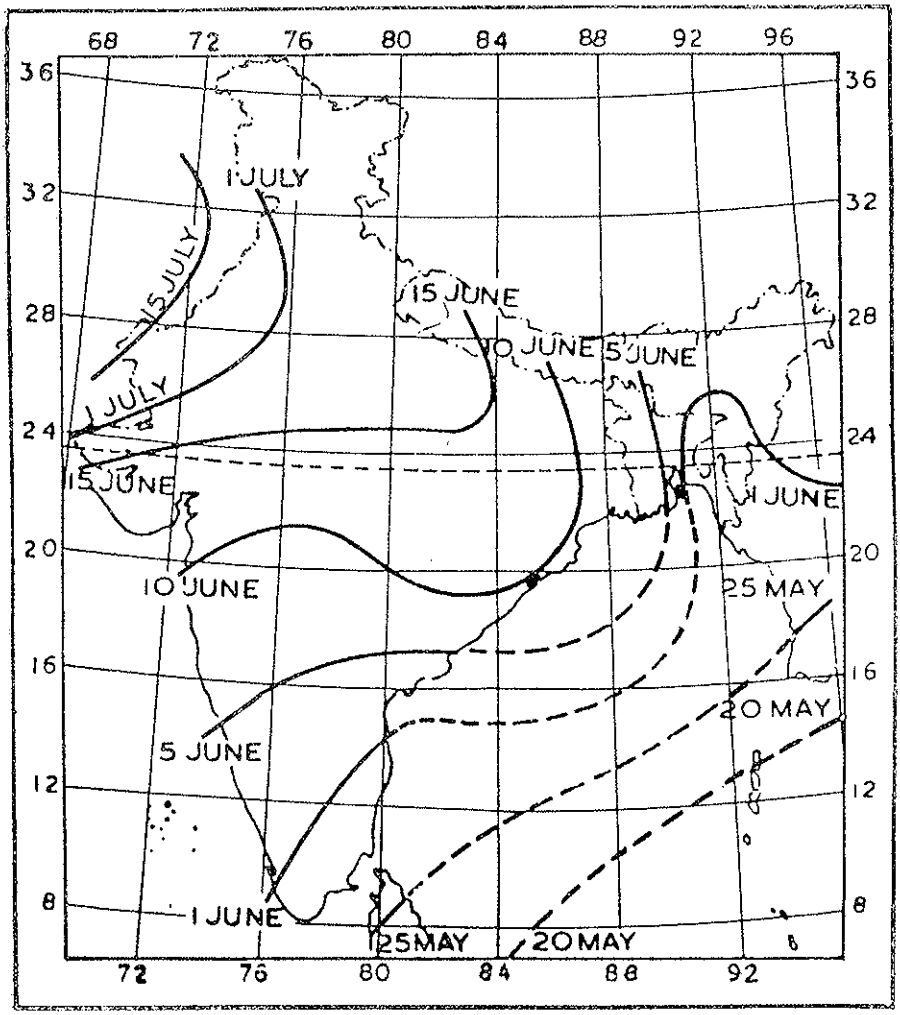

FIG. 1.11a. Normal dates of onset of s.w. monsoon.

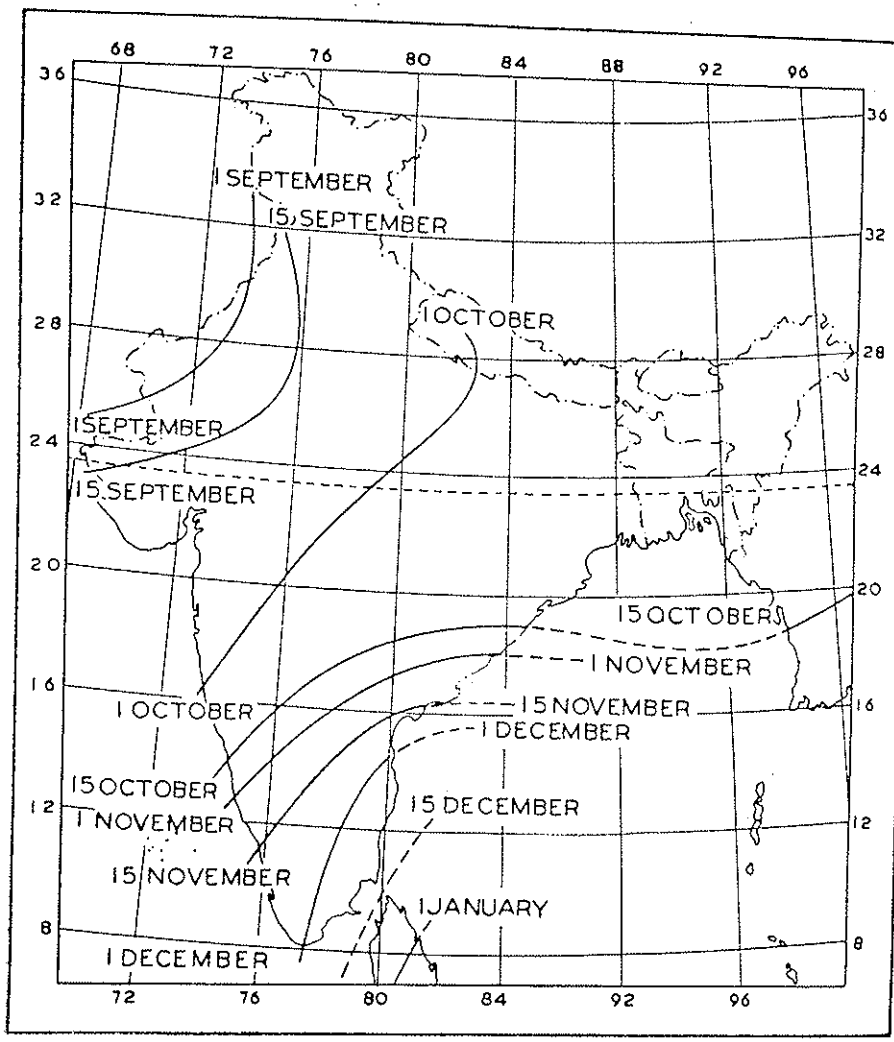

FIG. 1.11b. Normal dates of withdrawal of s.w. monsoon.

present in fig. 1.12 (a, b, c and d) actual dates of onset of monsoon at four representative stations, viz., Cochin, Bombay, Calcutta and New Delhi. This clearly brings out the marked year-to-year variation in the progress of the monsoon in the country.

The onset process being a very important component of the monsoon is discussed in detail in Section 2.

1.4 Significant Synoptic Features During Monsoon

Some of the synoptic systems which play a significant role in maintaining the monsoon circulation are:

i) Monsoon trough
ii) Monsoon depressions
iii) Mid-tropospheric Cyclones (MTC)
iv) Off-shore vortex
v) Waves in easterlies
vi) Break in monsoon

1.4.1 *Monsoon Trough (MT)*

The monsoon trough is an elongated zone of low pressure, which on a sea level synoptic chart, during the normal monsoon conditions, runs from the centre of heat low over north-west India and adjoining Pakistan to the northern angle of the Bay of Bengal along the Gangetic Plain. Normally, by monsoon trough, we refer to its position at sea level, although it has been observed to extend up to about 500 mb, tilting southwards with height.

The Monsoon trough is a quasi-permanent feature of monsoon circulation but in the absence of the other monsoon disturbances, the intensity of the monsoon activity largely depends upon the location and intensity of the monsoon trough. Because of its importance, we have discussed this system in detail and some of its features related to onset are discussed in Section 2 and those related to break monsoon in Section 3. The monsoon trough has been re-defined in these sections.

1.4.2 *Monsoon Depression*

There are low-pressure systems which normally form over the Bay

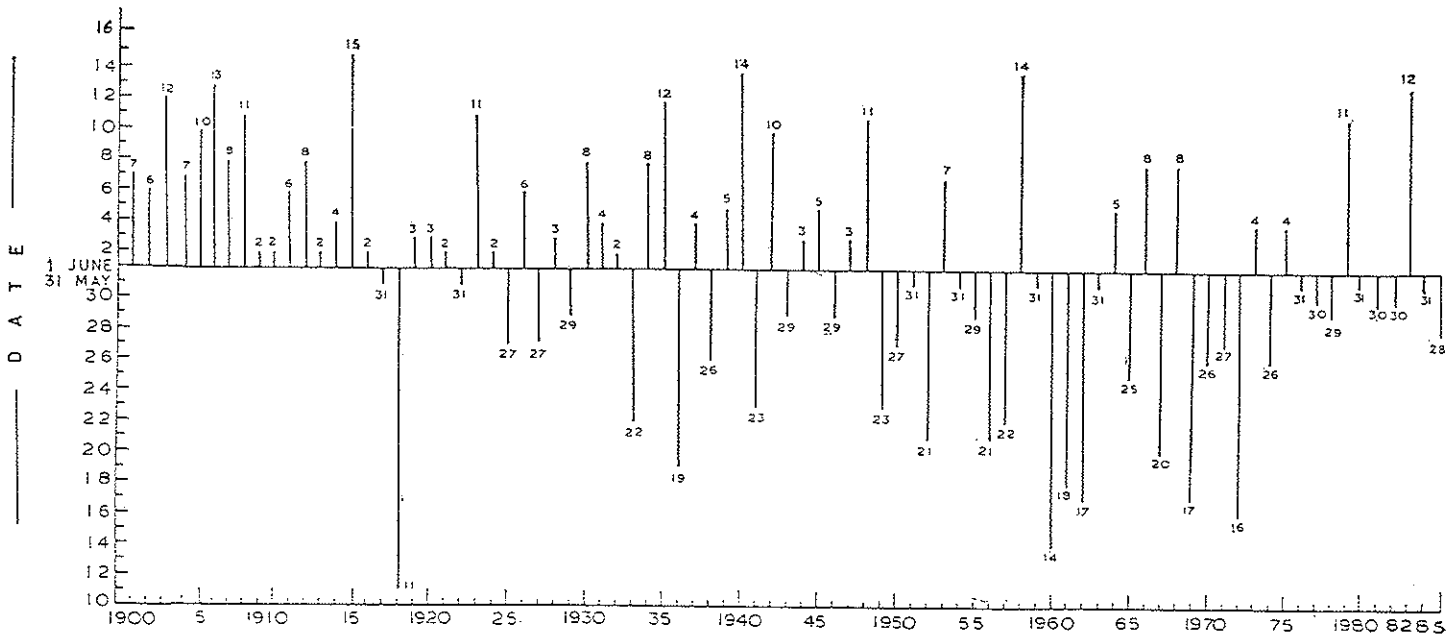

FIG. 1.12a. Actual dates of onset of southwest monsoon, « Kerala », normal date 1 June.

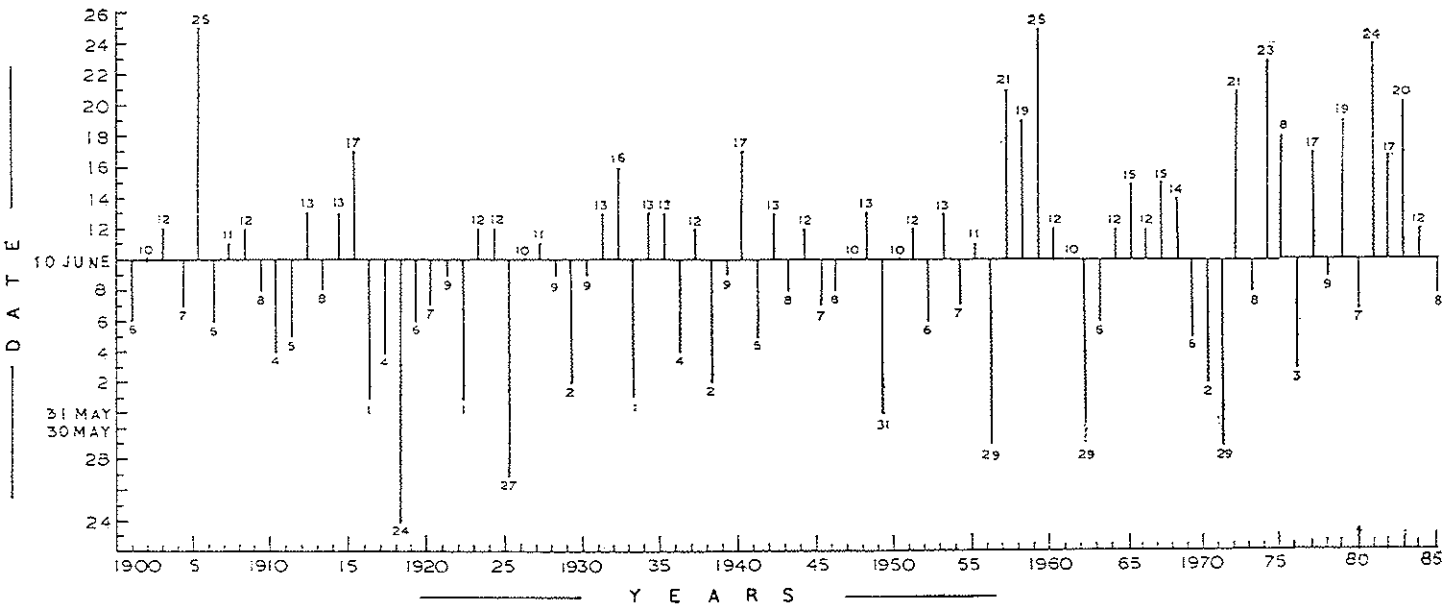

FIG. 1.12b. Actual dates of onsete of southwest monsoon, « Bombay », normal date 10 June.

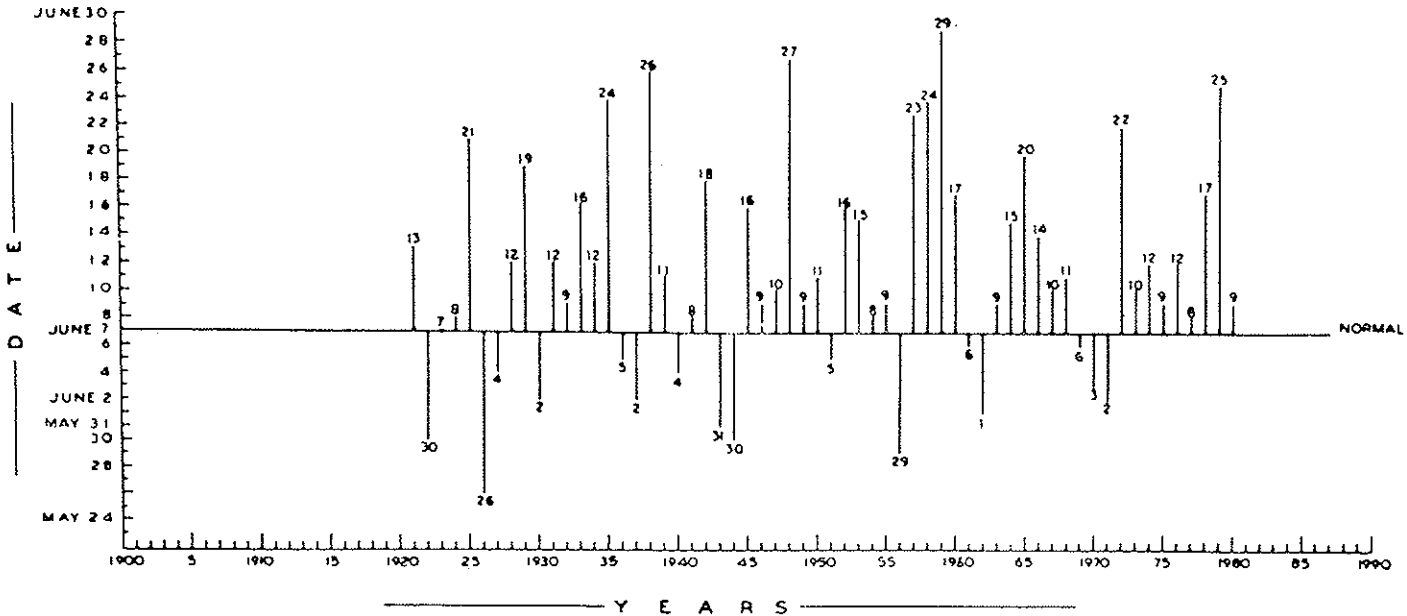

FIG. 1.12c. Actual dates of onset of southwest monsoon, « Calcutta », normal date 7 June.

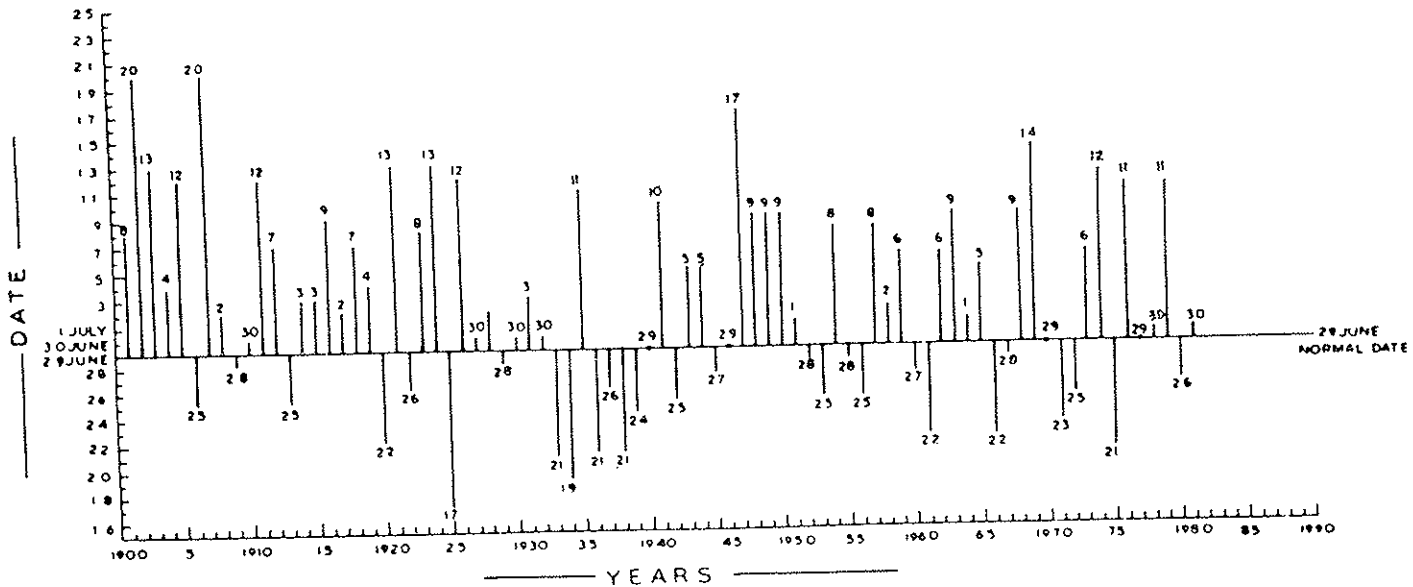

FIG. 1.12d. Actual dates of onset of southwest monsoon of « Delhi », normal date 29 June.

of Bengal (less frequently over the Arabian Sea) and move west-northwestwards along the Gangetic plain and give copious rainfall in their wake. Normally over 6-7 disturbances form during the whole season and their intensity rarely exceeds the limit of deep depression (wind speed less than 37 km per hour or less than 4 closed isobars at the interval of 2 mb). Some of the monsoon disturbances also originate over land rather than over oceanic surfaces and are well known as land depressions.

It is observed that these disturbances first appear at the upper level and then descend to the sea level under a) weak or after break monsoon conditions; b) during transition period, i.e., late May or early June and late September. During normal and active monsoon conditions (also during July and August), however, they generally first appear as sea level circulations or trough of low.

Recently Koteswaram *et al.* (1986) have coined a name MRD (Monsoon Revival Depressions) for the disturbances which develop to finish the break spell. These disturbances according to him also first appear as cyclonic circulation at 700/500 mb.

These disturbances play a very significant role in the maintenance of the monsoon circulation. Till the Sixties, the frequency of formation of the monsoon depression was given so much importance that the activity of the monsoon and thus the economy of India was directly related to this frequency. Structure and physical processes which lead to the formation of monsoon depressions are discussed in Section 4.

1.4.3 *Mid-Tropospheric Cyclones (MTC)*

Although mid-tropospheric lows have been observed and studied quite early over the Bay of Bengal (Koteswaram, 1950), the nomenclature MTC was coined during the International Indian Ocean Expedition (IIOE) period by Miller and Keshavamurty (1968) to represent a vortex between 700 to 500 mb (not reflected at sea level) over the north-eastern parts of the Arabian Sea. Ramage (1971) called these vortices subtropical cyclones, a term used to describe winter-time upper-level cut-off lows which develop over the eastern Pacific north of Hawaii. Some of these are also associated with surface cyclones. But this term could be confused with tropical cyclones, so the MTC term has better acceptability to describe such systems. MTC seems to form *in situ*, and remains quasi-stationary for a period of one week or so before dissipation. Disturbances similar to MTC have also been observed in other parts of the tropical oceans.

Carr (1978) has discussed in detail the MTC of the summer monsoon. He has also presented experiments to simulate numerically an MTC. All these studies show that MTCs generally have the following significant structure and dynamic characteristics.

i) These disturbances appear as close circulation only in and near the mid-troposphere. A unique feature of the MTC is the weak or non-existence of surface vortex and the equally significant lack of circulation above 400-300 mb. The role of critical level absorption may be important in confining the vorticity to the mid-troposphere.

ii) The horizontal scale of these disturbances is of the order of 1000 km and the vertical scale of the order of 6 km, the largest amplitude being at 600 mb.

iii) They are warm cored above the middle level and slightly cold cored below the middle level. The lapse rate is lower within the circulation than on its periphery. Recent observations during Monex-1979 show (Joseph, 1981) that the temperature gradient within an MTC at 700 mb is considerably higher than noted by Miller and Keshavamurty (1974) and is cold cored.

iv) There are many possible triggering synoptic situations for MTC formation. Pre-existence of disturbance in the Bay of Bengal may help formation of MTC (though an important but not necessary condition). If weak vorticity is already present in a region of imminent MTC formation, an increase in moisture flux or cumulus activity above could initiate the development sequence. Once the MTC is initiated, the latent heat release plays the dominant role in creating and maintaining the temperature and vorticity structure and in driving the energy cycle.

1.4.4 *Off-Shore Vortex*

These are sub-synoptic scale systems with a horizontal scale of 30-150 km and are generally observed off the west coast of India during the monsoon period. They are very shallow systems and are normally confined to the low levels below 850 mb.

The first detailed study on the formation of an off-shore vortex along the west coast of India was done by George (1956). These vortices have been associated with heavy rainfall over the west coast.

As already mentioned, from scale consideration these vortices are sub-synoptic systems and it would be normally difficult to track them from

one synoptic chart to the other, but Mukherjee and Shah (1981) claim to have tracked an off-shore vortex during the period of Monex-79. We, however, believe that these are sub-synoptic scale systems and the movement of these systems is a regeneration process at a new location like the movement of a squall line.

1.4.5 *Waves in Easterlies*

The nomenclature waves in Easterlies is popularly associated with a type of disturbance in the Caribbean Sea discussed by Riehl (1954). These are westward moving disturbances of the tropical lower tropospherical easterlies. The disturbance axis, usually oriented SSW-NNE, coincides with a pressure trough. Riehl studied the dynamics of easterly waves based on the conservation of potential vorticity and explained the existence of fair weather to the east of the axis or vice versa depending upon the phase speed of the waves vis-à-vis the prevailing wind speed.

But these criteria cannot be applied in the monsoon region, because this region is influenced by the East-West oriented lower tropospherical trough with easterlies poleward and westerlies equatorward of the trough. The characteristics of these systems are entirely different. On the trough zone, however, the disturbances do show movement east to west.

As discussed under monsoon depressions, these systems move east to west and in a large number of cases, their origin can be traced to the tropical disturbances far in the east. While simulating the characteristic features of the tropical atmosphere for the period June to August 1974, using the Goddard Laboratory of Atmospheric Science (GLAS) general circulation model, Estoque and Jing (1981) found westward moving disturbances of the type discussed by Riehl in all tropical belts except in the region between 40E to 180E, the origin of the monsoon. In this region, they see different features from those observed in the other regions. This analysis also confirms the difference in the characteristics of the disturbances in the monsoon region compared to those in the other parts on the tropics.

Disturbances similar to waves in easterlies are observed to influence southern peninsular India during pre-monsoon and post-monsoon periods. But these are not observed to conform to the usual weather sequence observed in the Caribbean Sea.

1.4.6 *Break in Monsoon*

Within the monsoon season, there are periods when the monsoon activity considerably decreases or ceases over the plains of India but increases over the foot of the Himalayas and the southern peninsula (especially the coastal regions of Tamilnadu). This situation is referred to as a 'break in monsoon'. The duration of the break, once it sets in, may last for a couple of days. The longest break so far was 21 days. If the break sets in during late August, in most cases it may bring in early withdrawal of the monsoon from NW India, as happened during 1979 and 1986.

These breaks with their associated dry spells and flooding of Himalayan rivers have great impact on the agricultural economy of India. We discuss in detail the synoptic and dynamic feature pertaining to break monsoon conditions in Section 3.

1.5 Teleconnection and Monsoon

The conventional forecaster bases his prediction on synoptic associations and linkages besides other dynamical factors. These linkages could be, on a regional scale, useful for foreshadowing the events in the next few days, or they could be on global scales which could be useful for prediction for a period of a few weeks to a season or more in advance.

For long-range forecasting, Sir Gilbert Walker carried out a very systematic study to derive distant relationship. One of the associations, discovered by Walker, well known as 'Southern Oscillation' (SO), stands out to be an important parameter which has significant association with the performance of the monsoon.

Recently Das and Datta (1985) and Datta (1986) observed interesting relationships between the surface temperature anomalies over Antarctica in the months of January to May with the subsequent performance of the monsoon. In Section 5, we discuss these important distant relationships with the performance of the monsoon.

2. DYNAMICS OF ONSET OF MONSOON

2.1 Onset of Monsoon

The onset of the monsoon during late May or early June over the Kerala coast (southwestern tip of India), which acts as a gateway for

the entry of the monsoon over the Indian sub-continent, is one of the most significant seasonal events. The onset is associated with the advance of the summer season and associated redistribution of seasonal heat sources and sinks and resultant wind régimes.

A precise definition of the term 'onset' is very difficult as it depends on many parameters, and thus it could be determined by various criteria such as changes in circulation pattern, rainfall distribution, etc. Ananthakrishnan *et al.* (1967) suggested an objective criterion for onset. Ananthakrishnan *et al.* (1968) in another study also gave an excellent review of the latest information (to 1968) on the studies by various workers on the onset of monsoons. In this section, we have attempted to answer some of the questions about the monsoon onset problem posed by MONEX planners, viz.:

(i) What is a monsoon trough? Is it another name for ITCZ, such that ITCZ merely loses its identity into the monsoon trough under the influence of the continentality? Or is it another name for equatorial trough (ET)?

(ii) What are the dynamical mechanisms that describe the replacement of oceanic ITCZ or ET by the monsoon trough and how are they related to the onset of the monsoon?

(iii) What is the structure of the monsoon trough?

Before we try to give plausible answers to the above questions, we discuss certain aspects connected with the onset problem.

2.1.1 *Criteria for onset*

From the atmospheric scientific point of view the onset of monsoon refers to the setting in of typical seasonal circulation patterns in the atmosphere. However, to the public at large, the onset of a monsoon is practically synonymous with rainfall. As the economy of India is closely linked with rainfall during the monsoon, the Meteorological Department of India (IMD) has also adopted rainfall as the criterion for declaring the onset of a monsoon. Rainfall in any case, as the end product of various physical and dynamical processes taking place in the atmosphere, could on its own merit also be taken as the primary index of monsoon activity over land. The normal date of onset at a place depicted in the climatological charts presented in Fig. 1.11a generally refers to the middle date of a pentad, the normal rainfall for which shows a characteristic rise. For the stations

which do not show a significant rise between two successive pentads, other subjective considerations (not very clearly spelt out) were used in deriving the normal date of onset.

The forecasters in their operational work are in a dilemma every year to declare the 'onset', and in this decision process they are generally led by subjective reasonings. To provide an objective aid, Ananthakrishnan *et al.* (1967) studied the problem through the analysis of rainfall series (1901 to 1967) for stations along the Kerala-Karnataka coast. They suggested the following objective criterion for declaring the date of onset over the Kerala coast.

After May 10, if at least five of the stations (listed in table 2.1) report 24 hourly rainfall of 1 mm or more for two consecutive days, the second day is declared as the onset day.

It may be seen that this criterion is based on synoptic climatological reasoning and as such is backed by sound and large statistical information. For example, selection of a date after May 10 is based on the statistics of 80 years, which show that onset over Kerala is unlikely before May 11, therefore any rainfall prior to May 11 may be associated with premonsoon thunderstorm activity.

The above empirical criterion suggested by Ananthakrishnan *et al.* has been found to be satisfactory and the dates of monsoon onset determined on its basis are not very different from the dates given by operational forecasters for period 1901-1967.

The Meteorological Department of India nowadays follows the above

TABLE 2.1 - *List of stations used for declaring onset of monsoon over Kerala.*

Station	Index	Lat N	Long E
COLOMBO	43466	7.9	19.9
MINICOY	43369	8.3	73.0
TRIVANDRUM	43371	8.5	76.5
ALLEPPEY	43352	9.5	76.4
COCHIN	43353	9.9	76.2
KOZHIKODE	43314	11.4	75.7
MANGALORE	43284	12.9	74.9

criterion and in our study also we have used the dates of onset based on this.

2.1.2 *Review of Earlier Work — Synoptic Features Associated with Onset*

The significant changes which occur in the flow pattern and the other physical parameters like SST, moisture distribution, etc., have been the subject of study by many earlier workers. Some of the prominent changes that have been identified regularly have been reviewed by Ananthakrishnan *et al.* (1968). Some of these studies have emphasized surface synoptic features and other upper level features. We give below the results of some of these significant studies.

(i) Roy (1946) associated onset with the advance of equatorial maritime air from south to north (it may be recalled, that was the period of air mass enthusiasts). The thunderstorm/showerly activity, according to him, was a consequence of development of instability with lower level moist maritime air being over-run by dry continental air. Without going into details of air mass analysis, we note that Roy envisaged flow from the southern hemisphere across the Indian Ocean as a precursor of onset.

(ii) Malurkar (1950) envisaged the pulsatory nature of the burst of monsoon from the south. According to him, low pressure areas south of the equator, carrying fresh monsoon or maritime air travelling in a westerly direction, gets deflected northward if a ridge in the west blocks its passage and also if pressure rises in the south of it. Thus according to him, the monsoon consists of pulses coming from south and the first pulse may thus cause onset.

In the present context, we can correlate ideas of Malurkar with the recent studies pertaining to the influence of Mascarenes High. The pulsatory nature can be compared with various periodicities discussed earlier (2-3 days, about 2 weeks and 30-40 days).

(iii) Yin (1949) associated the onset of the monsoon with the westward shift of the trough in the westerlies at 500 mb from 90E to 80E and development of shear line in the south and its northward progress. This northward shift, according to him, could be facilitated by the shift of the sub-tropical westerly jet, north of the Himalayas.

(iv) Riehl (1954), reviewing the work of Yin (1949), associated the onset with the forward edge of the shear line, which could be best delineated at 700 mb level.

(v) Sutcliffe and Bannon (1954) observed an interesting association between the dates of appearance of the first easterlies at 200 mb over Aden about 5-16 days before the onset of the monsoon over the Kerala coast. Ananthakrishnan and Ramakrishnan (1965) however found no regular lag between the first appearance of easterlies over the middle east (Aden and Bahrain) and the date of onset over Kerala coast. It may thus seem that this parameter has little prediction value.

(vi) Yeh, Dao and Li (1959) studied the onset of 1956 and confirmed Yin's association of the sudden disappearance of strong upper level westerlies on the southern rim of the Himalayas and the onset of the monsoon. Flohn (1965) supported this view and further suggested that this process results in the establishment of two quasi-permanent troughs on either side of the Tibetan plateau, i.e., along 65E and 100-105E.

(vii) Koteswaram (1958, 1960) and Koteswaram and Bhaskara Rao (1963), discussing the dynamics of low latitude upper tropospheric easterly jet (TEJ), concluded that the setting in of TEJ coincides with the burst of the monsoon. This idea was contested by Raman and Ramanathan (1964), but our studies support and confirm the observations and findings of Koteswaram.

(viii) Flohn (1960) postulated that the Tibetan Plateau acts as an elevated heat source in the mid troposphere and helps in reversing the normal temperature and pressure gradients over south Asia to south of 35N between the layers of 600 and 300 mb. This process, according to him, provides a switch for the lower level flow producing the burst of the monsoon over the west coast of India.

Although the influence of the Tibetan plateau as an elevated heat source to generate reverse Hadley Cell is well supported, but since the sub-tropical anticyclone in the upper air (the region of the highest pressure and the highest temperature) is well to the south of the Tibetan plateau at the time of onset over Kerala, the postulate of Flohn may not explain the onset over Kerala.

(ix) Nataraja Pillai (1965) observed that the onset and its northward advance is linked to the cyclonic and anticyclonic vortices at 700 mb level.

(x) Ramamurthi and Jambunathan (1965) associated the onset with the formation of a near equatorial trough between 700 and 400 mb levels over Kerala. They considered all other features such as appearance of TEJ, disappearance of upper level westerlies or their shift to the north of the Himalayas as secondary features.

On the basis of the above, and our own examination, we summarize the significant synoptic situations associated with the onset of the monsoon as follows:

a) Establishment of low level trough or (extending to 1.5 km or so) heat low over NW India and adjoining Pakistan.

b) Disappearance or shift to north of the Himalayas of upper level strong westerly winds.

c) Shift of trough in westerlies from its winter position of 85-90E to 75-80E. Also establishment of another quasi-stationary trough along 100-110 (east of the Tibetan plateau).

d) The appearance of TEJ over south India.

e) Significant cross equatorial flow at the lower levels.

f) Formation of a marked shear line or near equatorial trough between 700-400 mb levels.

g) Sharp increase in pentad mean rainfall and a large number of stations reporting rainfall consecutively for 2 days or more.

2.1.3 *Year to Year Variability in Onset of Monsoon*

The onset of the monsoon over Kerala coast as well as other places in the country is quite regular in a statistical sense. This can be inferred from the fact that the standard deviation of the date of onset is just about a week.

A bird's-eye view of the year-to-year variation in the dates of onset of the monsoon at four representative places, namely Kerala coast (Cochin), Bombay, Calcutta and New Delhi for the period 1901-1982 can be seen in fig. 1.12. The extreme dates of onset over the Kerala coast are 11th May and 18th June, i.e., a difference of 5 weeks.

The physical understanding and the prediction of the seasonal transition is very important. The early or late onset of the monsoon is controlled by transient disturbances on planetary and regional scales. One could also study the year-to-year variations from synoptic-dynamic consideration or by numerical simulation. In the present study we will discuss the results of the former approach.

2.2 Synoptic Dynamic Consideration of Onset

The process of onset of the monsoon is not the same every year. While it is spectacular (called burst of monsoon) and may be associated

with a formation of monsoon depression/cyclone or trough of low pressure, in some years it is gradual, while in other years it may show no significant difference between pre-monsoon and monsoon activity. Having reviewed the findings of various workers in the previous section, an attempt is made to project new concepts based on studies conducted by the author in this section. These studies may be divided into the following topics:

i) Synoptic-climatology of the onset-vortex.

ii) SST and moisture distribution during the pre-onset and onset phases.

iii) The role of the equatorial trough (ET) and ITCZ in the onset process.

iv) A new concept of the monsoon tough.

For these studies, we examined the weather reports for the period 1901 to 1980 covering a few days on either side of the date of onset. Finally, out of these years, we critically selected the monsoon onset processes during the decade 1970-79, which covered (i) years of early onset as well as delayed onset; (ii) years of slow and erratic northward progress after the onset or smooth progress, and (iii) years of droughts (1972, 1979) as well as good monsoon (1977, 1978).

The weather charts prepared at Northern Hemisphere Analysis Centre (NHAC), New Delhi, were used. The special data sets of Monsoon-77 and MONEX-79 were used for detailed computations of dynamic parameters.

2.2.1 *Onset Vortex*

During the monsoon season of 1979, the monsoon onset over the Kerala coast occurred on June 11 under the influence of an upper air circulation between 700-400 mb levels over the extreme southern peninsula. A low formed at sea level on June 12 over the southeast Arabian Sea; while moving slowly northwards, it concentrated into a depression on the 16th at about 400 km west of Mangalore (12.9N and 74.9E) and into a cyclonic storm on the 18th (near 18.5N, 63E). The cyclonic storm moved away westwards to Oman on the 21st. The system was observed with the best summer MONEX observing system and has been studied in detail by various workers who participated in the Monex-79. During the operational phase of Monex-79, a new term, 'onset vortex', was coined, and many authors now believe that such a vortex is usually associated with

the onset. To understand it more precisely we examined the weather reports during onset for the period 1901-1979. For the period 1901-1961, we were guided by the Indian daily weather reports (IDWR), whereas for the years 1962 onwards we also referred to the weather charts prepared at NHAC New Delhi. Based on our critical examination of these weather maps, we could identify that the onset in the South Kerala coast is associated with any of the following four synoptic situations: (i) formation of a cyclonic storm (wind speed greater than 33 kt) in the Arabian Sea and/or the Bay of Bengal; (ii) formation of cyclonic systems of an intensity of a depression (wind speed greater than 17 kt but less than 33 kt), or even well marked low pressure areas (wind speed less than 17 kt); (iii) existence of upper air circulation not marked at the surface level; and (iv) no significant system.

In table 2.2 we have given the years with their associated synoptic features during the onset. This table brings out the following salient features.

i) For about 50 percent of the years, the onset was associated with the formation of a well marked system at the surface.

ii) In a large number of cases, depression/cyclonic storm formed after the actual onset, or following old terminology in front of advancing monsoon current, the onset during 1979 being one of such cases.

iii) For the remaining 50 percent of the years, the onset was associated with the formation of upper air circulation systems or trough at the surface. The years under category (iv), i.e., years of no significant systems have also been included in this category (iii), as the observational networks, especially before 1940, were not adequate to properly observe upper air circulation systems.

From these statistics, we can tentatively conclude that precursor to the onset is the formation of cyclonic circulation in the Arabian Sea or in the Bay of Bengal or in both the regions. Further, the formation of a depression or a cyclonic storm is not a necessary condition, but when they exist and move in a favourable direction, i.e., a westerly direction for a system in the Bay of Bengal and in a northerly direction for a system in the Arabian Sea, the northward progress of the monsoon after the onset in the south Kerala coast is smooth and rapid. The type of sequence presented by Yin (1949) also fits very well with the above statistics.

2.2.2 *SST and Moisture Distribution Over Arabian Sea During the Pre-Onset and Onset Phases*

The sea surface temperature (SST) and its variations have an important role on the rate of evaporation from the sea surface. We examined SST for the decade 1970-1979. However, the data were quite dense only for the period of international experiments, namely Monsoon-77 and MONEX-79. During the 1979 monsoon we had special coverage through research vessels and satellite-derived observations. We used these observations to

TABLE 2.2 - *Yearwise Classification of Synoptic Features During Onset.*

Nature of system	Year of Occurrence		
	Both in Arabian Sea & Bay of Bengal	In Arabian Sea only	In Bay of Bengal only
Cyclonic storm	1901	1911**, 1916*, 1933**, 1948, 1959, 1960, 1961, 1964*, 1970, 1975, 1976, 1979*.	1914*, 1925**, 1962***, 1965, 1969.
Depression or well-marked low	1904, 1932	1919, 1920*, 1926, 1934*, 1938*, 1946*.	1917, 1922, 1927, 1929, 1936, 1941, 1943, 1949*, 1950, 1951, 1960*, 1974.
Surface level trough with low (unsettled condition) or upper air circulation	1902, 1906, 1908, 1912, 1913, 1918, 1955, 1957, 1958, 1963, 1972, 1973.	1907, 1910, 1915, 1940, 1945, 1954, 1956, 1967, 1968, 1971, 1973, 1978.	1905, 1954, 1947, 1953.
No significant system	1903, 1909, 1921, 1923, 1924, 1928, 1930, 1931, 1935, 1937, 1939, 1942.		

* Refers to years when system formed in front of advancing current of monsoon, i.e., onset, precedes the system.

** Weaker system is also present in the other region.

*** System formed in Bay and moving in a westerly direction emerged into the Arabian Sea.

determine whether variations in the depth of precipitable water could provide any clue for the onset.

We present below the salient features of SST and moisture distribution during these years:

2.2.2.1 *SST Distribution*

SST as derived from satellite measurements for the period May 25 to June 15, 1979, were plotted on charts and isotherms analysed. The satellite information provided almost one observation for every 5° square in the area between 25S to 20N and 45E to 125E, which was supplemented with the observations of the MONEX ships and other commercial ships in the region. For comparison, we also plotted SST for the period May 25 to June 15 for the year 1977, although data for this period was only confined to a limited region and made on board the special monsoon research ships and other commercial ships in the region. Assuming that there is no significant diurnal variation in the SST values, composite data for 24 hours was utilized and meridional time cross sections drawn along meridians 60E, 65E, 70E and 75E to study the day-to-day variations. These are presented in figs. 2.1 and 2.2 for the year 1977 and 1979, respectively.

The significant features depicted by the cross sections may be summarized as below:

a) The SST values near the equator were generally lower at all meridians compared to the northern latitudes. The day-to-day variations were also not marked except on days of prevailing northerly winds, as on 27 and 28 May, 1979.

b) The warmest SST are located near 15°N.

c) The onset of the monsoon is found to be associated with decrease in the SST, especially north of 5N which is more marked to the west of 65E. The plausible reasons for cooling may be (i) northeastward transport of cold water from the Somali coast; (ii) large scale evaporational cooling; and (iii) dense clouding during the onset.

d) We also noticed that cold and warm SST patterns showed some sort of alterations. Because of small data set we have not attempted any time series analysis, but a comparison of 1977 and 1979 sections clearly shows that penetration of surges of cold waters is more frequent during 1977 compared to 1979. It may be recalled that 1977 was the year of early onset and normal monsoon activity, whereas 1979 was the year of late onset and poor monsoon activity.

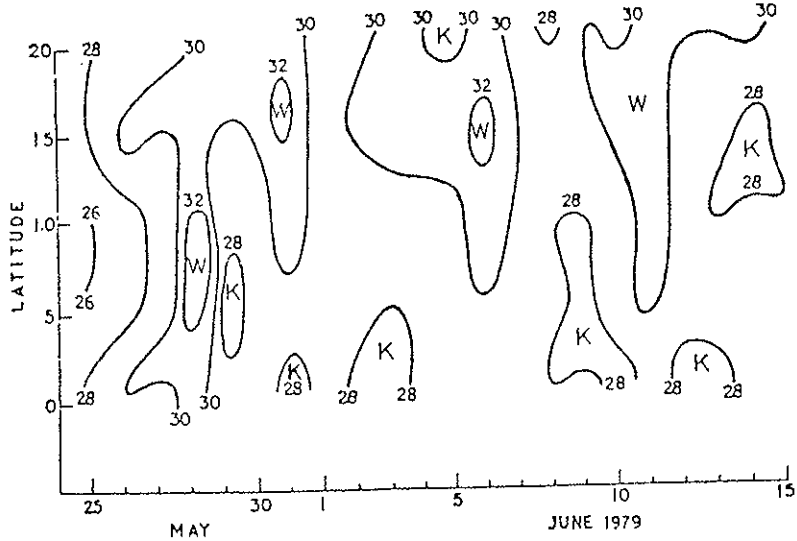

FIG. 2.1a. Time section for sea surface temperature (SST) distribution along 60° meridian.

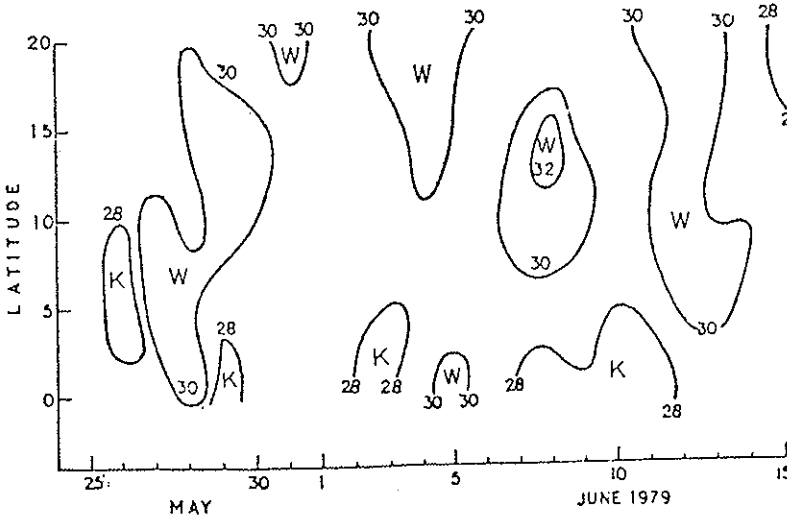

FIG. 2.1b. Time section for sea surface temperature (SST) distribution along 70° meridian.

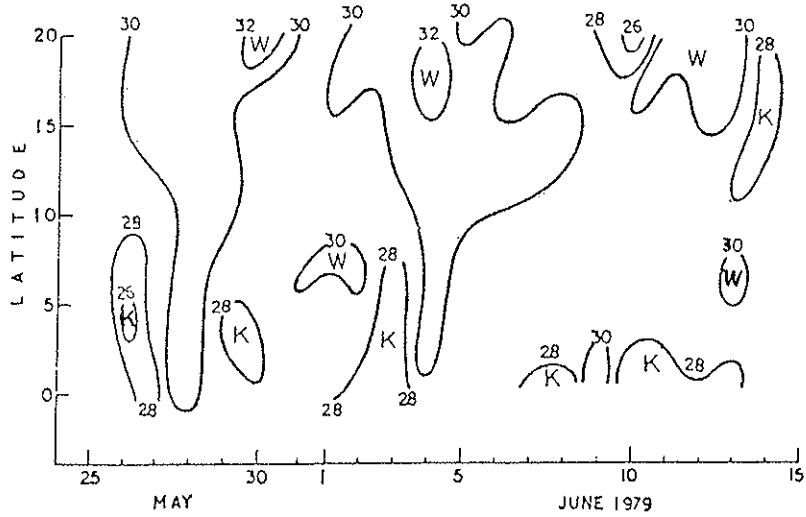

FIG. 2.2a. Time section for sea surface temperature (SST) distribution along 65_{0} meridian.

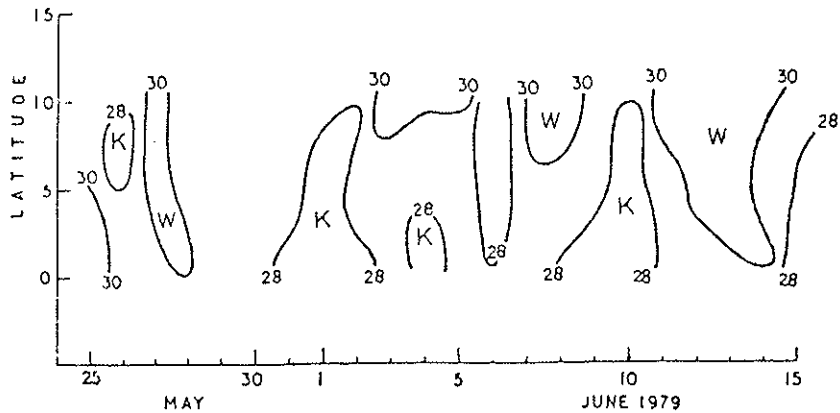

FIG. 2.2b. Time section for sea surface temperature (SST) distribution along 75° meridian.

2.2.2.2 *Moisture Distribution*

The satellite data provided us useful information about the cumulative precipitable water for levels up to 700, 500 and 300 mb. The amount of precipitable water from the data of research ship observations was also computed. The precipitable water values as derived from the satellite observations and those computed from ascents of the nearest Monex ships agreed very closely.

The time section analysis for the total precipitable water was done for the period 25 May to 15 June, 1979, in a similar manner to that for SST; the results are depicted in fig. 2.3. The interesting features revealed by the plots are given below:

a) Moist area along the 60 degree meridian with precipitable water of the order of 5.5/kg was located near the equator between May 29 and June 3, and also again during June 7-10 just before the onset. The driest area with precipitable water of the order of 2-3 gm/kg was along 20N. Similar moisture distributions were also observed along 65° and 70° meridians. However, a significant difference in moisture distribution to the east of 60E as compared to west of it is that during the onset phase (June 9-12), there was a significant increase of moisture in the northern latitudes. Such variations are very clearly observed along 65E.

b) A dry tongue extended southwards to the equator from 20N during 27-28 May. This, as discussed earlier, is associated with the marked incursion of hot and dry northerlies. This is also confirmed by observations of Debois and Cadet (1979).

c) The area of maximum moisture showed a progressive shift north-eastward with the progress of the season. Earlier studies by Mukherjee (1962) did not show any build-up of depth of precipitable water from pre-monsoon to monsoon conditions at Trivandrum. Pant and Vernekar (1963) also did not find significant changes in wet bulb potential temperature (Θw) over Trivandrum between pre-monsoon and monsoon conditions, although they did observe gradual variations of Θw in Bombay. We believe their studies could not reveal any significant variations, because moisture distributions over equatorial land stations are already modified by the pre-monsoon thunderstorm activity. This study, though based on small data samples, shows a promise that moisture distribution in the Arabian Sea might provide an advance signal for onset.

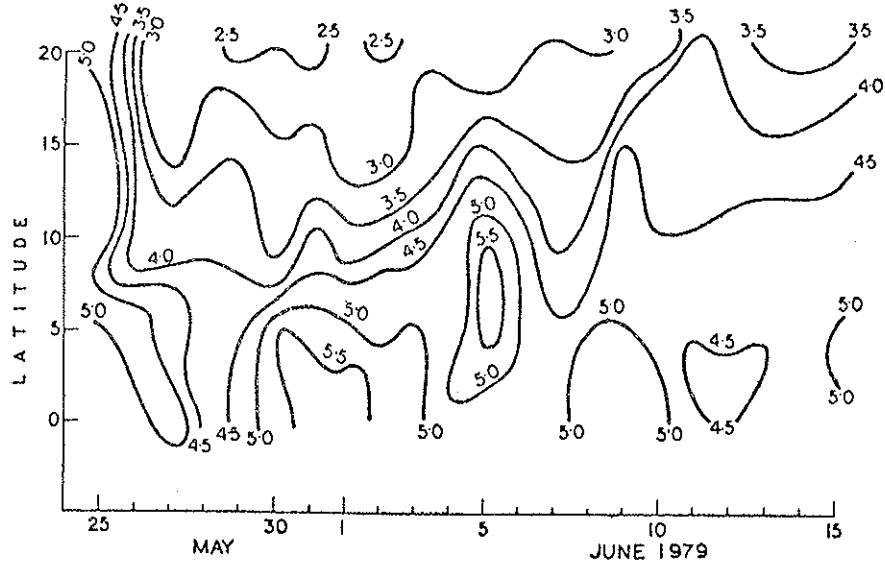

FIG. 2.3a. Time section for moisture field distribution (gm) along 60° meridian.

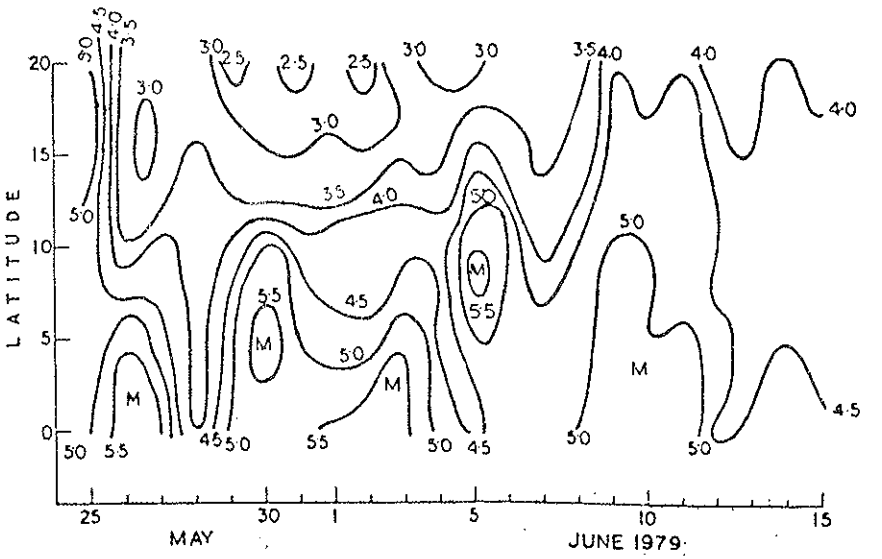

FIG. 2.3b. Time section for moisture field distribution (gm) along 65° meridian.

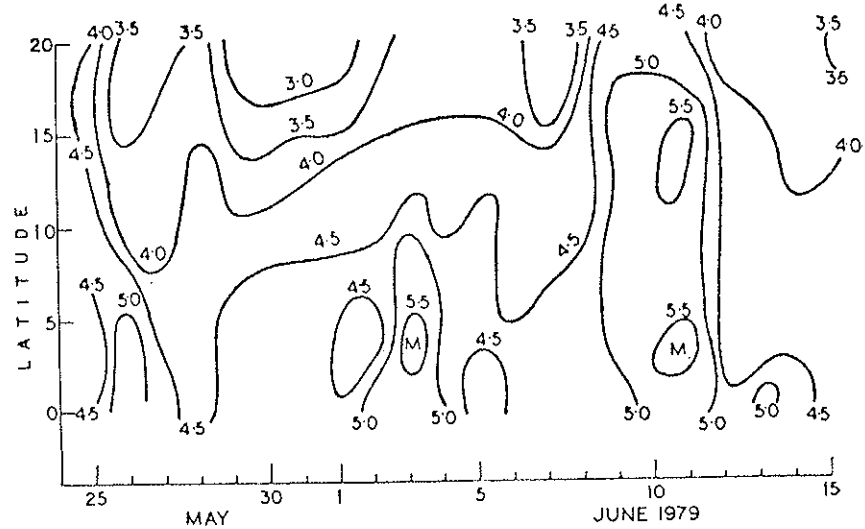

FIG. 2.3c. Time section for moisture field distribution (gm) along 70° meridian.

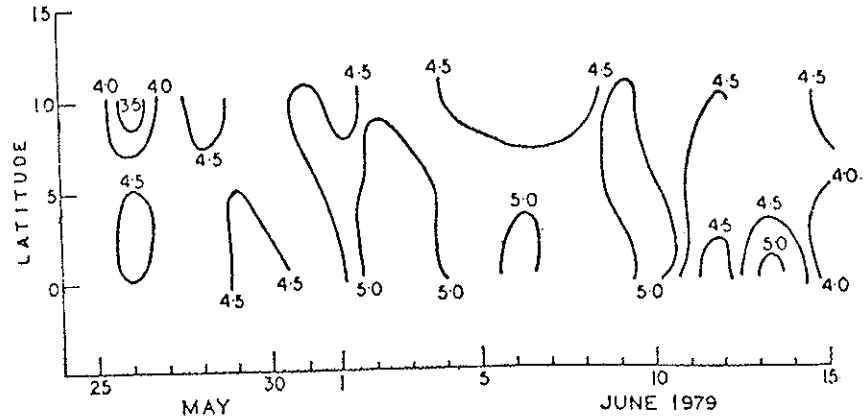

FIG. 2.3d. Time section for moisture filed distribution (gm) along 75° meridian.

2.2.3 *Onset, ITCZ and ET*

For the purpose of delineating ITCZ and ET from the daily weather charts, we (Sud and Datta, 1980) assumed the following definitions. It will be shown later, by the computations of vorticity and vertical motion, that our assumption of considering ITCZ and ET as separate features is valid. These two separate features can also explain the two zones of maximum cloudiness — one over the continents and the other over the oceans, observed by Sikka and Gadgil (1980).

i) ET is a trough in the pressure field with associated wind flow being easterlies to the north and westerlies to the south. The easterlies and westerlies may not be from two different hemispheres and thus ET may be located in the same air mass of either hemisphere.

ii) ITCZ is a zone where northerlies of the northern hemisphere and the southerlies from the southern hemisphere converge, i.e., a region of convergence of two different air masses.

Keeping the above definition in view, the streamlines/trajectories were drawn and daily positions of ITCZ and ET at 850, 700 and 500 mb levels were recorded along 75, 80 and 85E during the period May 15 to June 30 for the decade 1970-79. On some occasions, when one or both of these features are not well defined at one or the other level, we made use of time continuity. To remove the minor fluctuations in positions, a five day average position was computed, and for plotting purposes, this position was assigned to the middle date of the pentad.

In most of the cases, we noticed that both ITCZ and ET could be better identified at 700 mb level compared to the other levels. For the purpose of illustration, we show position of ITCZ and ET at 700 mb level on two typical dates in 1977 and 1979, in fig. 2.4a and 2.4b. In 1979, the ET consists of mainly dry continental air mass, whereas during 1977, ET consists of moist air mass from the southern hemisphere.

As the 75°E meridian is more representative of the Indian sub-continent, and further since these features are more marked at 700 mb level, we present in fig. 2.5 the position of ET and ITCZ at 700 mb level along 75E for the years 1972, 73, 75, 77, 78 and 1979. Our study of the position of ET and ITCZ at 700 mb for different years brings out the following salient features:

i) Both ET and ITCZ show northward progression with the advance of the season. Marked fluctuations were noticed in some years than in others.

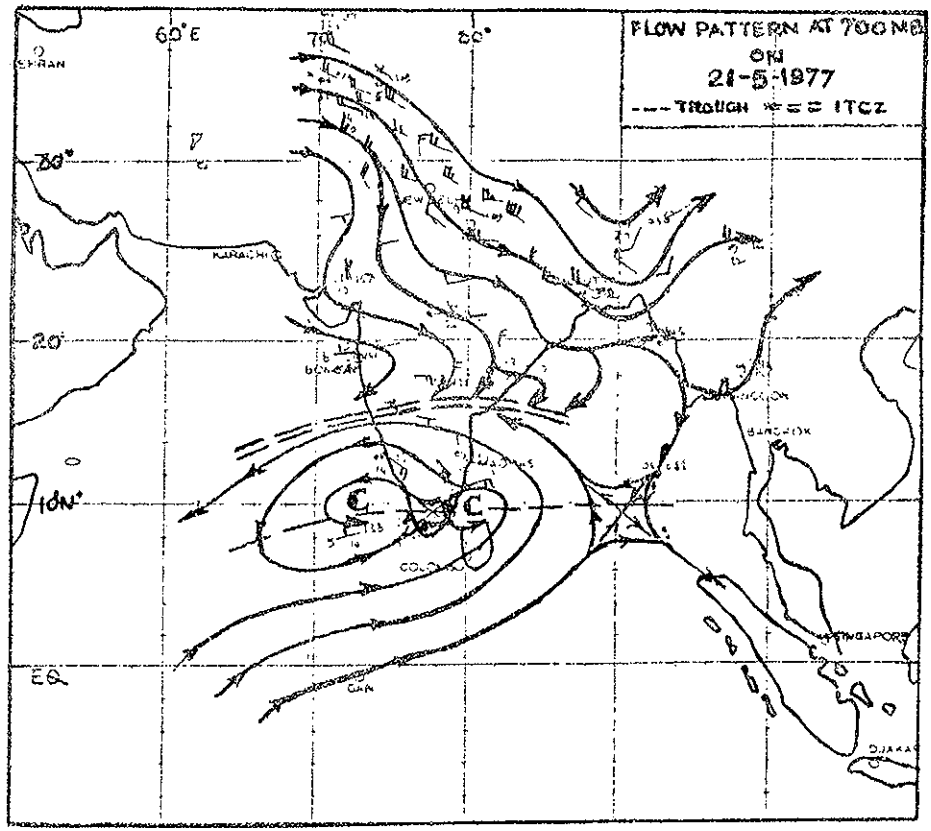

FIG. 2.4a.

ii) In the years when the ITCZ was generally located northward of ET, as in 1973, 1977 and 1978, the onset of the monsoon was timely, and its northward progress was also smooth. These cases are similar to those depicted in fig. 2.4a, where ET consists of maritime air mass.

iii) In the years 1972, 1975 and 1979, the ITCZ was south of ET for a part of the season. The onset in these years was either delayed, or after onset the northward progress was erratic and slow. These cases are similar to those depicted in fig. 2.4b, when ET consists of dry continental air mass.

This analysis indicates that for a smooth and timely onset, the ITCZ

should be always north of the ET during their northward progression. For delayed monsoon cases, the shift of ITCZ south of ET has been observed and is found to be associated with the penetration of strong northerlies from middle latitude. Such a circulation is associated with the development of a marked north-south ridge over and near the Caspian Sea.

Based on these contrasting features, we developed conceptual flow patterns to depict these variations. Fig. 2.6 (a and b) represent schematically these flow patterns pertaining to delayed onset and normal onset, respectively. From this analysis, one is tempted to conclude that the location of ET vis-a-vis ITCZ and type of air masses which are primarily responsible for the formation of ET in the contrasting years could explain to considerable degree the normal and delayed onset of monsoon.

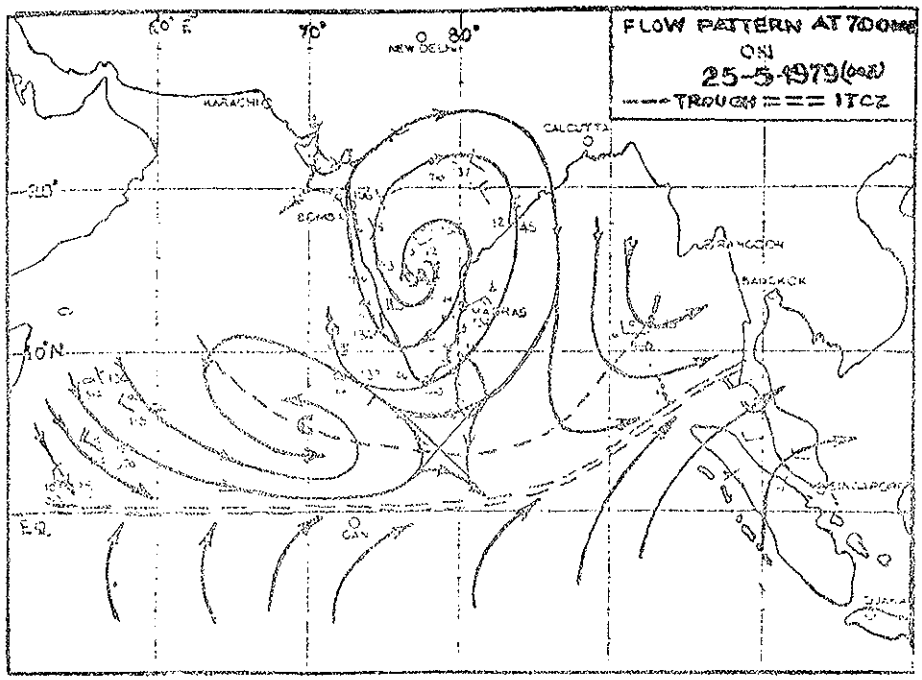

FIG. 2.4b.

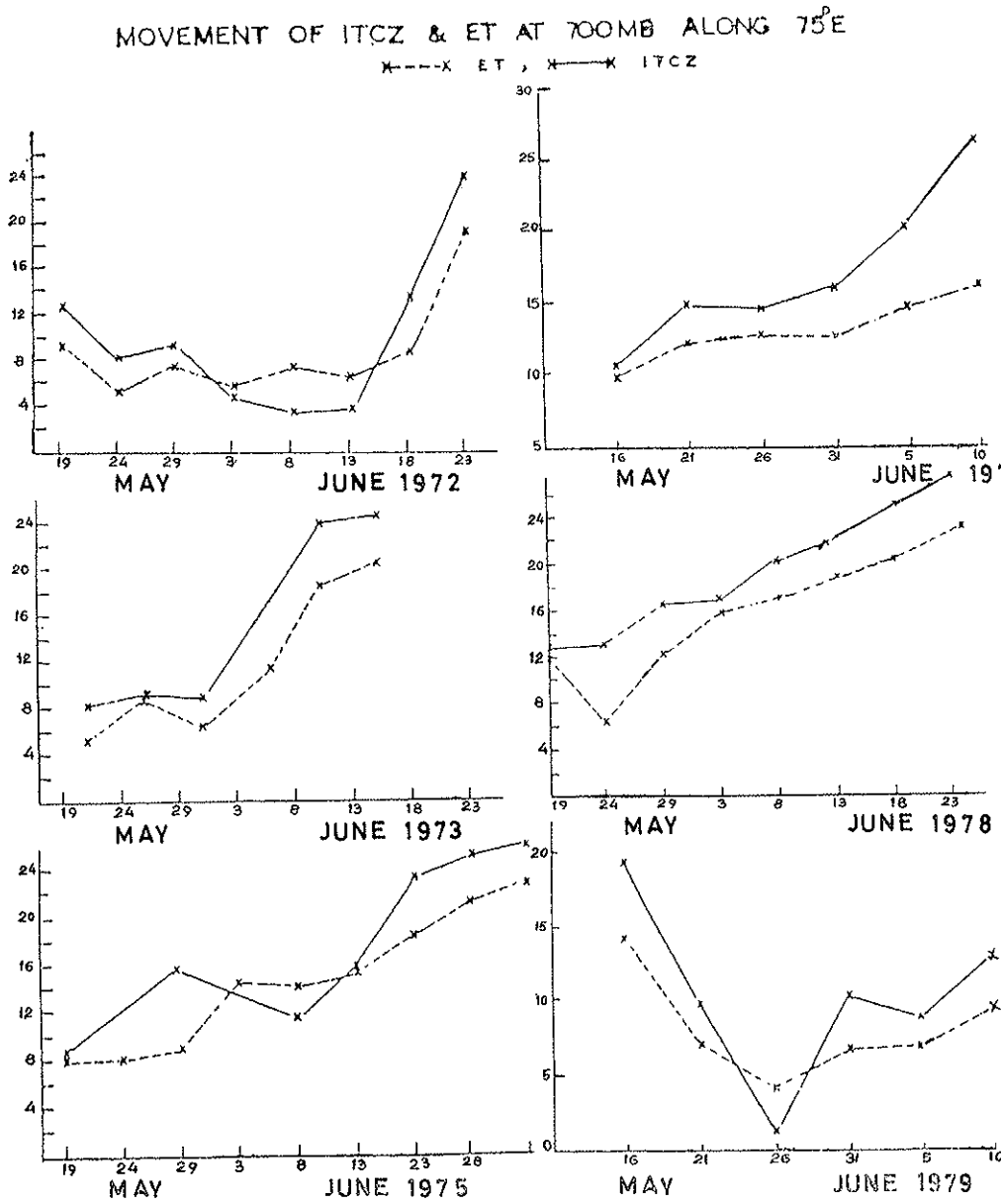
MOVEMENT OF ITCZ & ET AT 700MB ALONG 75°E
ET , ITCZ
MAY
JUNE 1972
MAY
JUNE 19
MAY
JUNE 1973
MAY
JUNE 1978
MAY
JUNE 1975
MAY
JUNE 1979

FIG. 2.5.

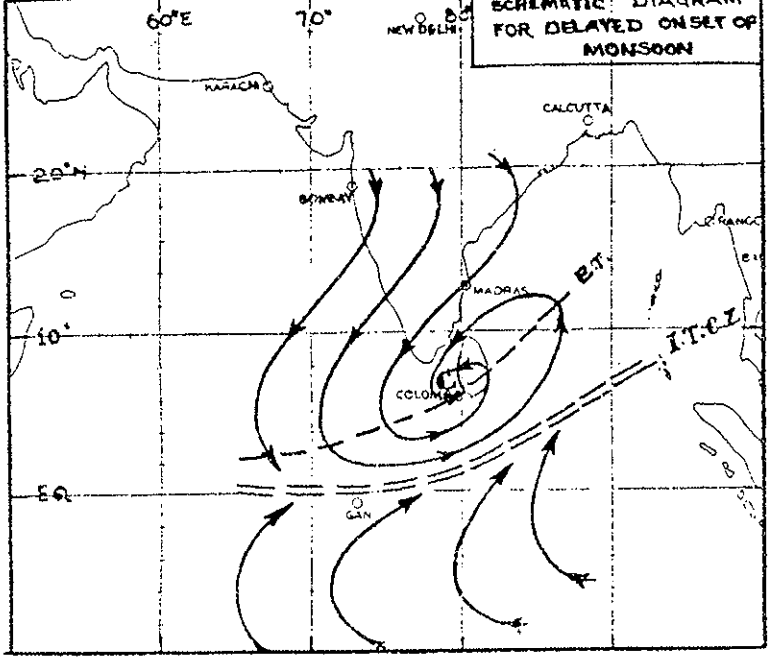

FIG. 2.6a.

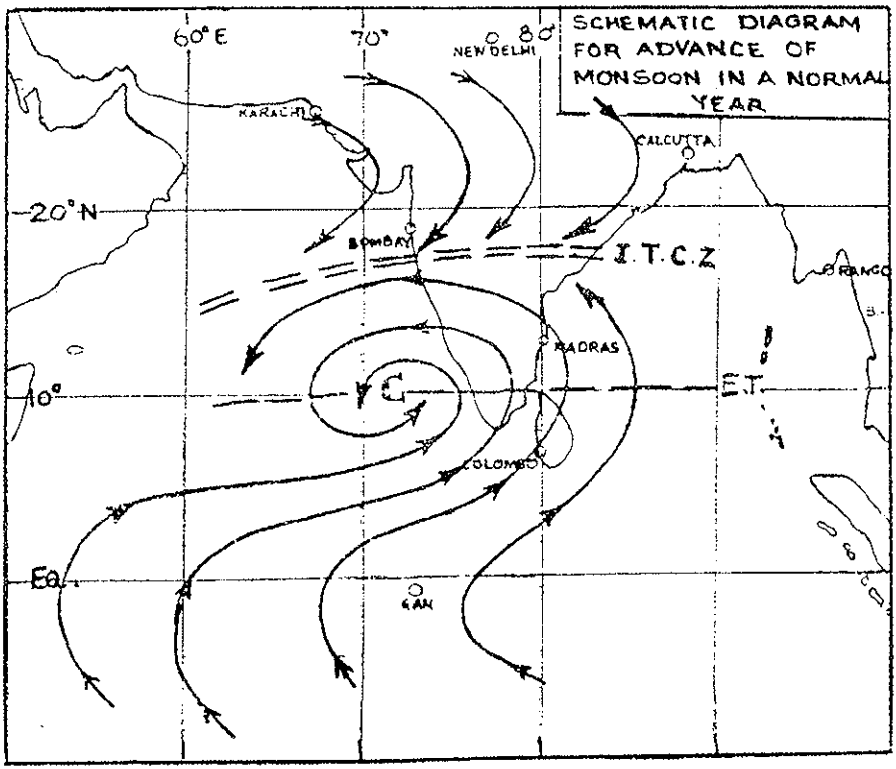

FIG. 2.6b.

2.2.3.1. *Vorticity and Vertical Velocity Fields Associated with ITCZ and ET*

ITCZ and ET have been observed as separate synoptic features. It is interesting to examine if the same could be reflected in vorticity and vertical motion fields. For this purpose, we selected two typical situations, one each during 1977 and 1979. These are 4th June 1977 and 30th May 1979. The availability of data from specialized observing research ships and research aircrafts for the period, besides typically of the synoptic situation, prompted us to select these dates.

2.2.3.1.1 Error Analysis

In order to understand the reliability of observations for the vorticity and 'ω' computations, we conducted experiments by introducing random errors in the wind observations in ITCZ region for 30th May, 1979. Errors of the order of ± 5 kt in speed and ± 20 degrees in wind direction were introduced randomly. Three trials were made. Results of the trials are presented in fig. 2.7. It was noticed that there is no appreciable shift in the location of vorticity maxima and vertical motion field though their magnitudes varied from 3 to 25%.

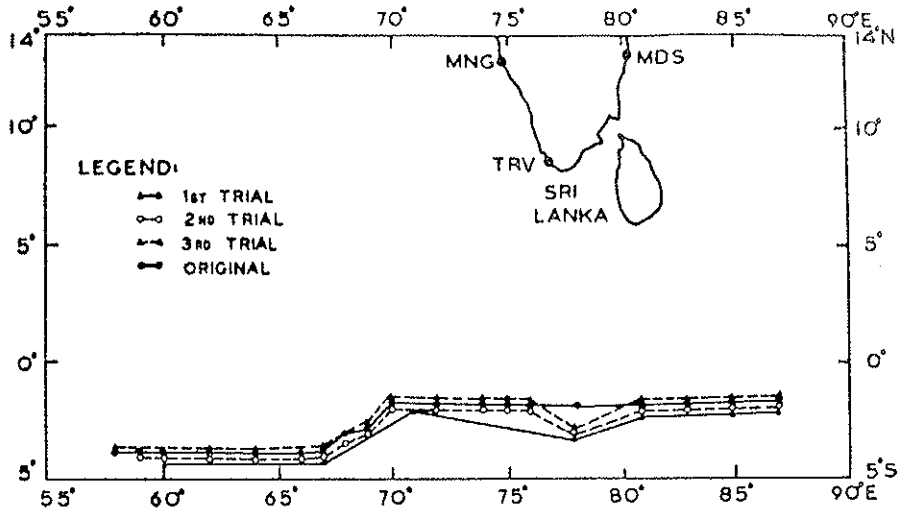

FIG. 2.7. Position of ITCZ on 30th May 1979, with random errors.

2.2.3.1.2 Vorticity Field

The vorticity field for both situations was computed for various levels. Vertical cross sections of the vorticity field along 70 and 75 meridian were prepared. In fig. 2.8a and 2.9a, we show the cross section for 4th June, 1977. We present the cross section for 30th May, 1979 in fig. 2.10a and 2.11a.

These illustrations show two distinct areas of cyclonic vorticity separated by anticyclonic vorticity. Regions of two positive vorticity maxima coincide with the synoptic location of ET and ITCZ. It is also noticed that magnitude of vorticity is higher in association with ET than with that of ITCZ. Vorticity is maximum at 700 mb where ET and ITCZ are generally better defined.

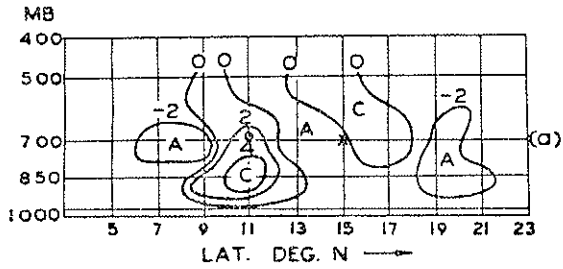

× : ITCZ ⊛ : ET

FIG. 2.8a. Vertical cross section, along 70°E, 4 June 1977. Vorticity, unit: 10^{-5}/sec.

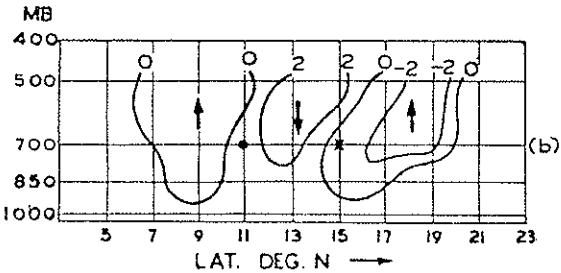

× : ITCZ ● : ET

FIG. 2.8b. Vertical cross section, along 70°E, 4 June 1977. Vertical velocity, unit: 10^{-3}mbs/sec.

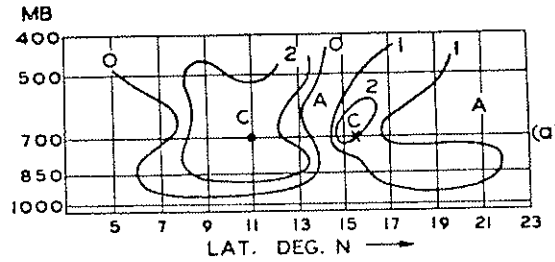

× : ITCZ ● : ET

FIG. 2.9.a Vertical cross section, along 75°E, 4 June 1977. Vorticity, unit: 10^{-5}/sec.

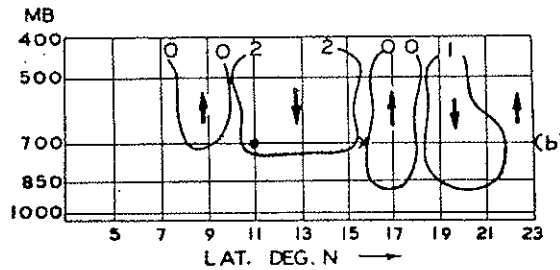

× : ITCZ ● : ET

FIG. 2.9b. Vertical cross section, along 75°E, 4 June 1977. Vertical velocity, unit: 10^{-3}mbs/sec.

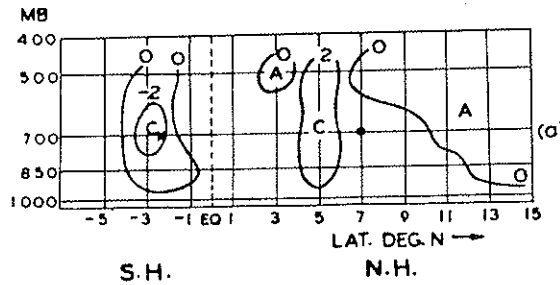

× : ITCZ ● : ET

FIG. 2.10a. Vertical cross section, along 70°E, 30 May 1979. Vorticity, unit: 10^{-5}/sec.

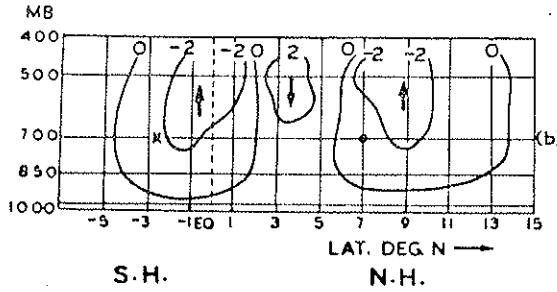

× : ITCZ ● : ET

FIG. 2.10b. Vertical cross section, along 70°E, 30 May 1979. Vertical velocity, unit: 10^{-3}mbs/sec.

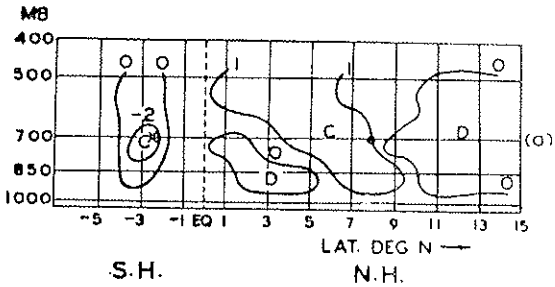

× : ITCZ ● : ET

FIG. 2.11a. Vertical cross section, along 75°E, 30 May 1979. Vorticity, unit: 10^{-5}/sec.

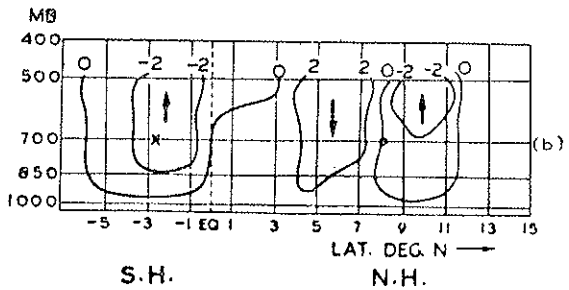

× : ITCZ ● : ET

FIG. 2.11b. Vertical cross section, along 75°E, 30 May 1979. Vertical velocity, unit: 10^{-3}mbs/sec.

2.2.3.1.3 Vertical Motion Field

The vertical motion (ω) field was computed by kinematic method. The vertical cross sections of the 'ω' field along 70 and 75° meridian are presented in fig. 2.8b and 2.9b for 4th June 1977, and for 30th May 1979 they are presented in fig. 2.10b and 2.11b. In this case again we observe two distinct regions of upward 'ω' separated by a region of downward 'ω'. Further, the regions of upward 'ω' are located approximately at the same position as ET and ITCZ.

Although in the vorticity field, the maximum was of higher magnitude for ET compared to ITCZ, the magnitude of 'ω' is higher in the region of ITCZ compared to ET.

2.2.3.1.4 Satellite Cloud Imagery

In fig. 2.12, we present cloud imagery as observed by GOES on May 30, 1979, wherein we have also super-imposed location of ITCZ and ET as on May 30, 1979. It shows more or less two distinct bands of cloudiness, one roughly along 3-5S and the other along 6-8N over the Indian Ocean between the 70 and 80° meridians.

The cloud band in the southern region, which is associated with ITCZ and larger 'ω' values, seems to be more intense.

The agreement between the locations of ET and ITCZ and distinct cloud bands is fairly good.

2.2.4 *Monsoon Trough, ITCZ and ET*

The position of a monsoon trough and its day-to-day variations has been found to affect considerably the rainfall distribution, especially over the Gangetic plains.

The first fundamental question which needs clear understanding refers to the definition of a monsoon trough. Is it the sea level feature, which is even present during late May, when the monsoon is still in early onset phases? The question has remained unanswered for several years. The planners of MONEX-79 included the proper definition of the monsoon trough as one of the important scientific objectives of the experiment. From our critical examination of weather charts during the monsoon period, we observed the following significant features.

From early May onwards, a thermal trough develops with heat low over northwest India and the adjoining Pakistan region. This is a shallow

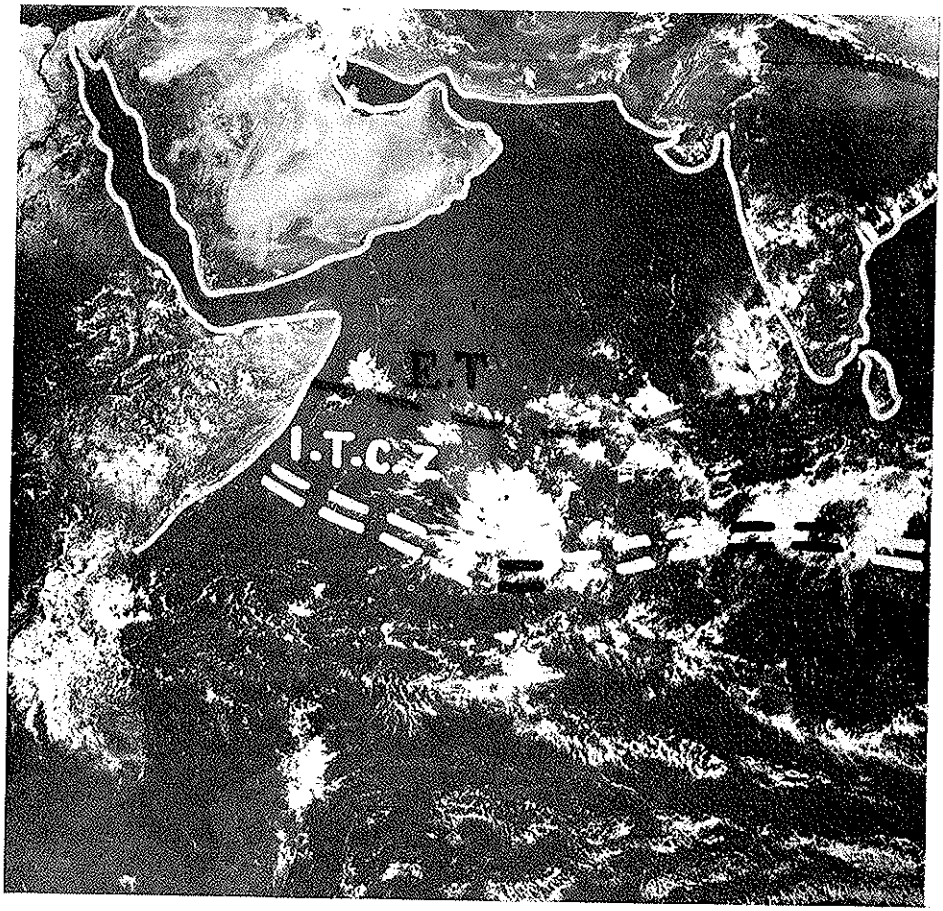

FIG. 2.12. ITCZ and E.T. Vis-a-vis cloud imagery.

system and hardly extends up to 850 mb level. This during early periods (late May) has no link with the ITCZ/ET, which are located far to the south. The ET region is associated with general cloudiness and thunderstorm activity, but the region of the thermal trough is free of cloud. With the advance of season as ET progresses northwards, a dynamic link seems to get established between sea level features and ET at 700/500 mb levels. We postulate that this dynamic coupling is developed through cumulus convection and large-scale vertical motion associated with ET. After this dynamic coupling, we observe the coherent movement of ET

at all the levels from surface to 500 mb level. We are thus convinced that ET, as it advances northward, gets linked with the thermal trough and this vertically coupled system (from surface to mid troposphere) is a real monsoon trough. It attains a well defined structure, sloping southward with height, and controls the monsoon activity.

Further aspects on the variations in the slope and its characteristics will be discussed in the next Section on 'Break monsoon'.

In the following we summarize some of the interesting concepts on onset processes:

i) Formation of ET as an upper air circulation (better defined at 700 mb level) in the Arabian Sea or in the Bay of Bengal or in both the regions is a precursor to the onset.

ii) The formation of a depression or a cyclonic storm, termed as onset-vortex by various authors (Krishnamurti *et al.*, 1980), is not a necessary event, but when it forms and moves in a favourable direction (westward in the Bay of Bengal and northward in the Arabian Sea), the northward progress of the monsoon after the onset over south Kerala coast is smooth and rapid.

iii) ITCZ and ET are two distinct synoptic features associated with fairly well defined positive vorticity maxima and upward 'ω' field. In the initial period, these are better defined at a 700 mb level than at other levels.

iv) It is not only the northward progression of ET and ITCZ which is important but also their relative positions. ITCZ, being north of ET, is associated with smooth northward progression of monsoon, whereas ITCZ, being south of ET, is an indication of erratic northward progress of monsoon.

v) Satellite cloud imagery also shows two separate cloud bands confirming the distinct existence of ITCZ and ET.

vi) With the advance of season, northward progressing low latitude ET gets dynamically coupled with sea level shallow thermal trough and this three-dimensional coupled system attains the characteristics of the monsoon trough. ET thus loses its identity into the monsoon trough.

vii) Time section of the distribution of SST over the Arabian Sea shows frequent penetration of surges of cold waters from south to north. Sample data for 2 years show that the more frequent the surges, the better is the monsoon activity.

viii) Location of ET vis-a-vis ITCZ and their impact on onset, and study of lag relationship between changes in various physical parameters like SST, depth of moisture, wind speed, etc., and onset could provide some clues for advance information on onset.

3. CIRCULATION FEATURES IN BREAK MONSOON

Within the monsoon season, there are periods when the monsoon activity in terms of rainfall considerably decreases or ceases over the plains of India but increases over regions near the foot of the Himalayas and the south peninsula (Tamilnadu). During this period, the monsoon trough also shifts to the foot-hills. This situation is referred to as 'break in monsoon'. This phase may last for a couple of days to as much as 3 weeks. Ramamurthy (1969) has prepared the statistics of breaks for the period 1888 to 1967, the results of which were summarized by Rao (1976) and are presented in Table 3.1. The statistics will show that August is more susceptible to breaks.

In a broad sense, the inter-annual variability of monsoon precipitation over India is related to four main events:

i) Date of onset and smooth or otherwise northward progress of monsoon;

TABLE 3.1 - *Statistics of breaks in monsoon.*

Month	No. of breaks	No. of break days	Average duration	Longest break days	Most frequent duration days	No. of break days in		
						First 10 days	Second 10 days	Last days
Jul	53	306	5.8	17	4	81	117	108
Aug	55	356	6.5	20	3	115	159	82
Commencing July, ending in Aug.	5	47		21				

ii) Number of cyclonic systems (depressions or low pressure areas) affecting the country;

iii) Frequency and duration of breaks; and

iv) Date of withdrawal of monsoon.

All these events are inter-related. It has been observed that the frequency and duration of breaks contribute in a large measure to the year-to-year variability of monsoon rainfall. Because of the significant impact of rainfall within the monsoon season on the Indian economy and the scientific importance of the break phase in the season, proper understanding of the circulation features associated with the break and their modelling is very necessary. A number of recent studies relate the active and break situation to the low frequency (30-50 days) modes of tropical circulation. This section is an in-depth-study of circulation features related to break monsoon conditions.

3.1 Synoptic Situations Associated with Breaks

Besides significant changes in rainfall distribution over most parts of the country, there are important changes in the flow patterns which have been studied by various workers. Koteswaram (1950), Ramaswamy (1962), Datta and George (1966) and Ramamurthy (1969) have described detailed synoptic situations preceding the establishment of break conditions. These are summarized below:

3.1.1 *Sea Level Pattern*

i) Shift of the monsoon trough northwards near the foothills of the Himalayas and absence of any low pressure or trough of low pressure in the north Bay of Bengal.

ii) General decrease in pressure gradient over the country. For illustration, the pressure gradient between Bhuj (23.3N and 69.6E) and Trivandrum (8.3N, 76.9E) may reduce to 1-3 mb during break situation, compared to 7-10 mb in good monsoon conditions.

iii) The gradual change of run of isobars from the normal west-east to north-south direction bringing ridging pattern over the country (like pre-monsoon conditions).

3.1.2 *Flow Pattern in the Lower Troposphere*

i) The monsoon trough at 850 mb and 700 mb levels also shifts northwards near the foothills or disappears. Instead, there is development of ridge over northwest India.

ii) The above changes result in the general absence of easterlies over Uttar Pradesh, Bihar and adjoining regions. There is also a general decrease of strength in westerlies over peninsular India, where flow starts developing a more northerly component.

iii) In a large number of cases, a trough of low or a cyclonic circulation, similar to the development of ET during the onset phase, develops over the South Andaman sea. Then westward movement of the system in most cases helps in the revival of the monsoon activity.

3.1.3 *Flow Pattern in Upper Troposphere*

i) General shift of upper tropospheric subtropical ridge southward by over 2-3° latitude.

ii) Occurrence of double easterly jet maxima over India, one around 10N and another fairly north near 20N. Sometimes instead of double maxima, we observe generally strong easterlies spread over a very broad area.

iii) Appearance of a westerly jet over the northern parts of the country.

iv) In some cases, the ridge-trough system at 500 mb over and east of the Caspian Sea may extend up to 300 or even 200 mb level.

3.2 Break Monsoon and Ridge-Trough System Over the Caspian Sea

As already stated the establishment of a well marked anticyclone with north-south ridge axis over and near the Caspian Sea in the lower and mid-troposphere has been observed to cause interruption in the normal monsoon activity. Strong northerlies east of the anticyclone thwart the normal northward progress of ITCZ during the onset phase and cause break monsoon conditions if this occurs later in the season. Fig. 3.1 depicts a typical flow pattern, a few days before the occurrence of a break condition. In years of prolonged break conditions, this feature is also

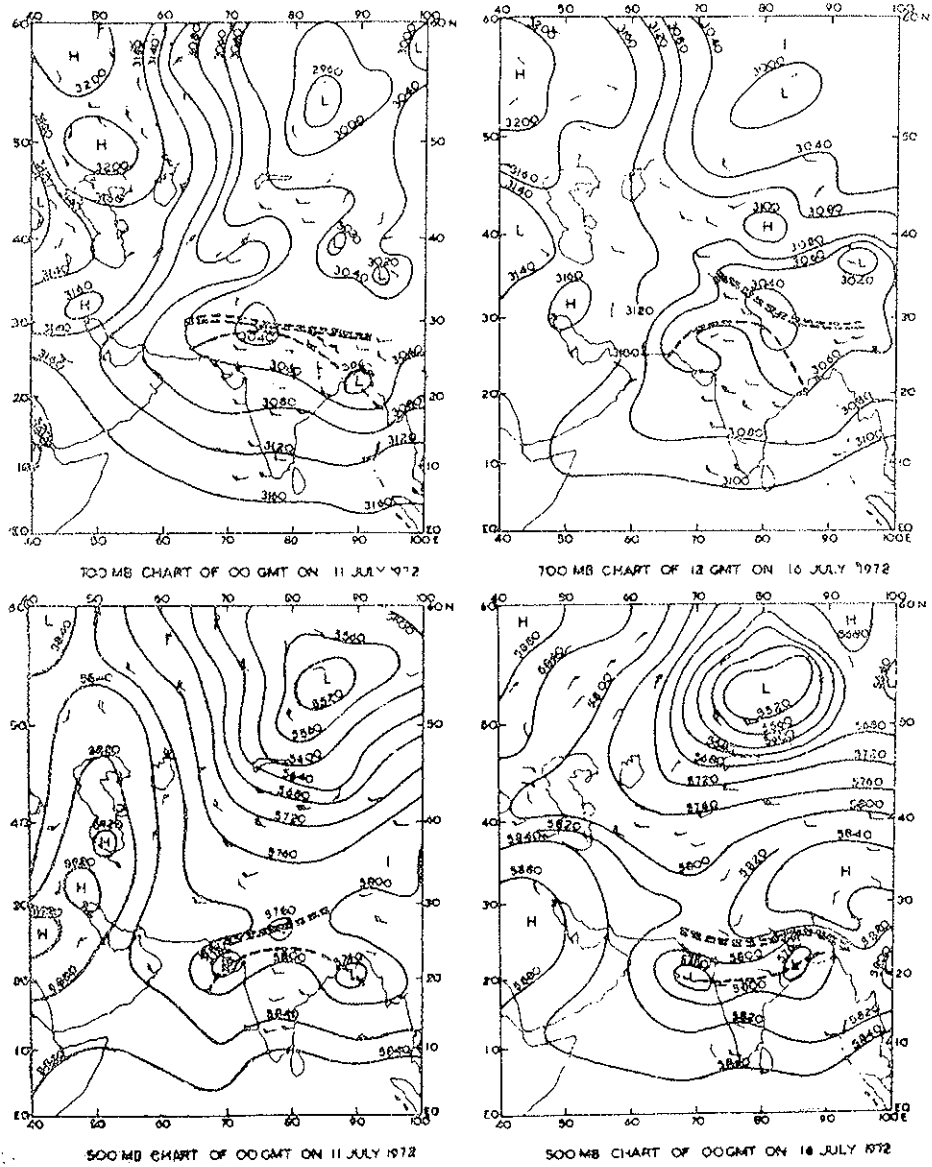
700 MB CHART OF 00 GMT ON 11 JULY 1972
700 MB CHART OF 12 GMT ON 16 JULY 1972
500 MB CHART OF 00 GMT ON 11 JULY 1972
500 MB CHART OF 00 GMT ON 16 JULY 1972

FIG. 3.1a.

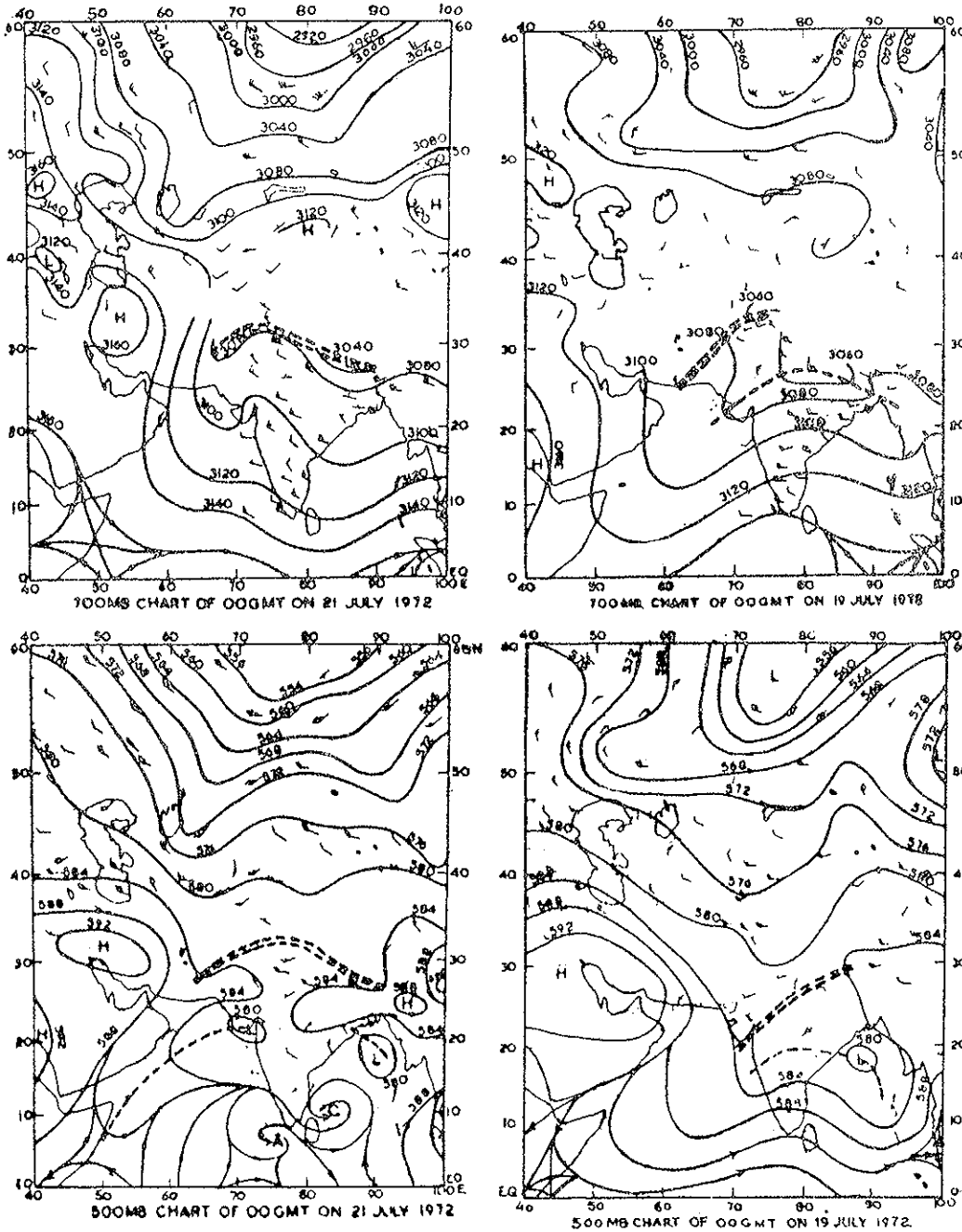
700MB CHART OF 00GMT ON 21 JULY 1972
700MB CHART OF 00GMT ON 19 JULY 1972
500MB CHART OF 00GMT ON 21 JULY 1972
500MB CHART OF 00GMT ON 19 JULY 1972

FIG. 3.1b.

reflected in the mean flow in contrast to years of normal monsoon activity. For example, fig. 3.2 (WMC MOSCOW mean charts for 700 mb for August of years 1972, 1975, 1976, 1977 and 1978) clearly illustrates the dominant role of the anticyclone in the year 1972 (which incidentally was a drought year) compared to the other years. A similar feature was observed in 1979. The prominent existence of the anticyclone is also seen in the large positive geopotential anomaly (difference of monthly mean from long-term mean monthly geopotential field) in the lower troposphere in 1972 and 1979 compared to other years (fig. 3.2). We also examined individual break conditions during the years 1971-1980. There were break situations during (i) 17 July to 4 August, 1972; (ii) 1 Sept. to 7 Sept., 1974; (iii) 25 July to 28 July, 1975; (iv) 15 to 18 August, 1976; (v) 21 July to 5 August 1979 and 17 to 20 July, 1980. All these cases were associated with significant development of the north-south ridge at 700/500 mb over and near the Caspian Sea. These observations lead to the conclusion that with the development of a marked N-S ridge over the north Caspian Sea, the northerly flow ahead of the ridge penetrates into the monsoon area and disrupts the normal monsoon flow pattern. The present observations support earlier studies pertaining to the occurrence of weak monsoon flow associated with the eastward movement of large amplitude trough in the westerlies, protruding into Indian latitudes. The effect of this blocking high over India was also observed earlier by the author (Datta, 1966). This high was then termed as 'Ural High'. Its influence on the recurvature of a monsoon depression and ushering in of early winter conditions over northwest India were examined in that study.

3.3 Monsoon Trough and Break

As discussed in the previous section, the sea level shallow thermal trough which exists right from late May takes the shape of the monsoon trough as it gets dynamically coupled with the northwards advancing ET at 700/500 mb levels.

Normally the monsoon trough slopes south-wards with height (slope being 5-6° between sea level and 500 mb level positions), the slope being more in the western sector than in the eastern sector. Preceding the establishment of break conditions, however, the slope of the trough gradually decreases and trough axis at various levels up to 500 mb shows northward progression to the foothills and finally trough axis becomes

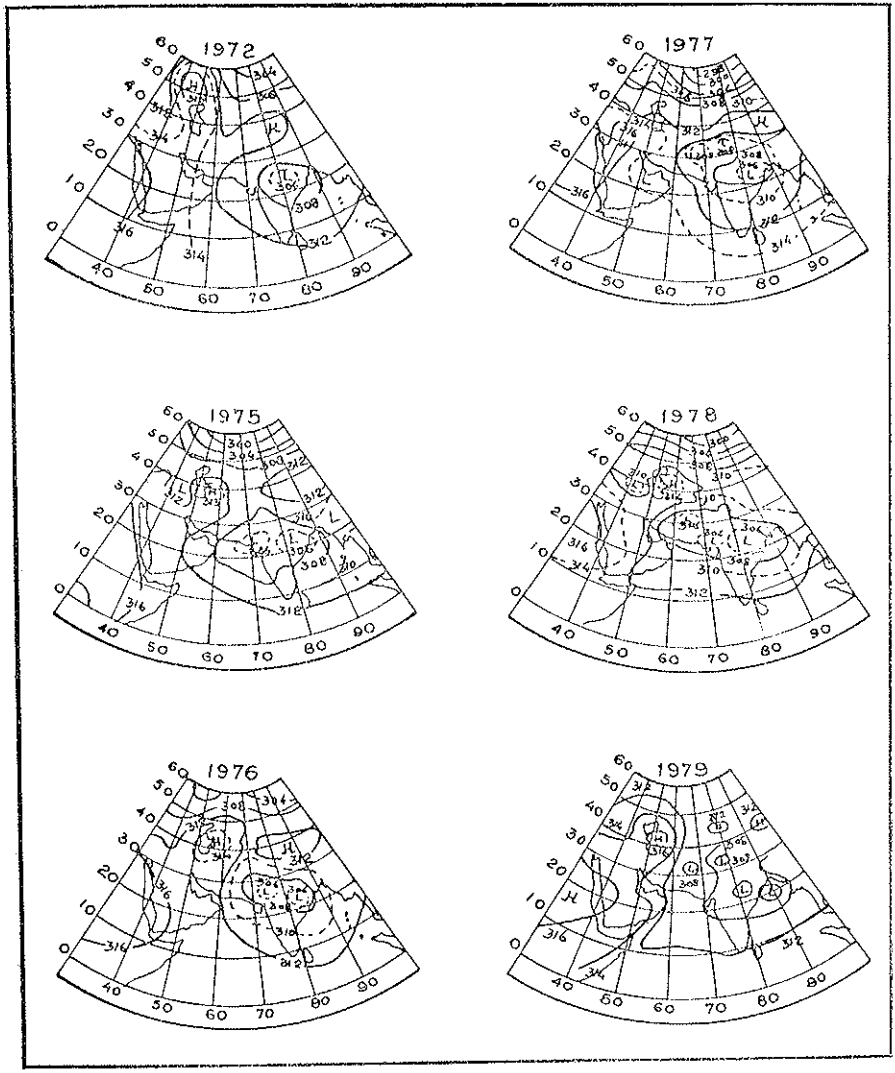

FIG. 3.2. 700 mb mean charts (August).

vertical. At this stage, it is a critical situation which generally leads to a 'break situation'.

If there is no system over the North Bay and the ridge-trough system over the Caspian Sea region is prominent, the break becomes quite persistent.

During the 2nd half of July, 1972, break conditions began to get established. The monsoon trough started progressing northward by 14th July, and the break was fully established by 20th July. The marked ridge-trough system at 700/500 mb levels which appeared even as early as on 11 July was a good indicator of the possible forthcoming break conditions.

This break was prolonged up to 4th August 1972. Revival took place under the influence of the formation of a low pressure area in Bay, which concentrated into a depression on the 5th and affected most of the northern parts of India. This resulted in a shift of the monsoon trough to its normal position. The ridge-trough system also collapsed during the same period, making the flow zonal. In fig. 3.3 for illustration, we present the flow pattern on July 11, 16, 19 and 21 at 700/500 mb levels. We note the build-up of a high amplitude ridge over the Caspian Sea area and gradual northward shift of the monsoon trough, till the break condition is established. The slope of the trough along 70, 80 and 90E for the same period is present in fig. 3.4, which clearly marks the decrease of slope till the slope almost disappeared on 21.7.1972.

The normal activity is generally restored under the following conditions, which may exist individually or together:

i) The advection of a low pressure system from the far-east into north Bay of Bengal or its in-situ development.

ii) Collapse of the ridge-trough blocking system over the Caspian Sea.

iii) Fresh formation of ET (upper air circulation) in the low latitude and its north-northwestward progress proceeding almost in the same manner as the onset process, except that this process is very rapid compared to onset (Koteswaram, 1950).

3.4 Vertical Motion Field Associated With Break

To derive the 3-dimensional structure of break monsoon circulation, it is necessary to study the vertical motion field associated with a typical break situation. The situation chosen was during August 23-27, 1966. It

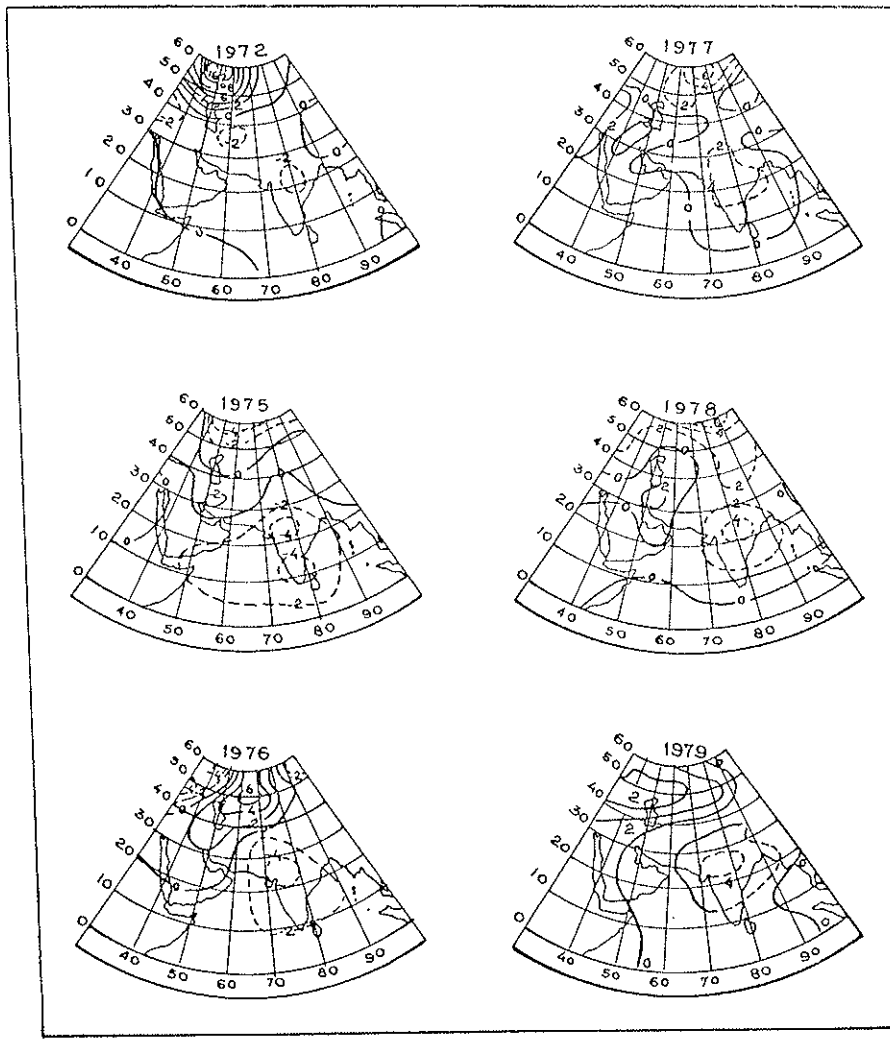

FIG. 3.3. 500 mb geopotential anomaly charts (August).

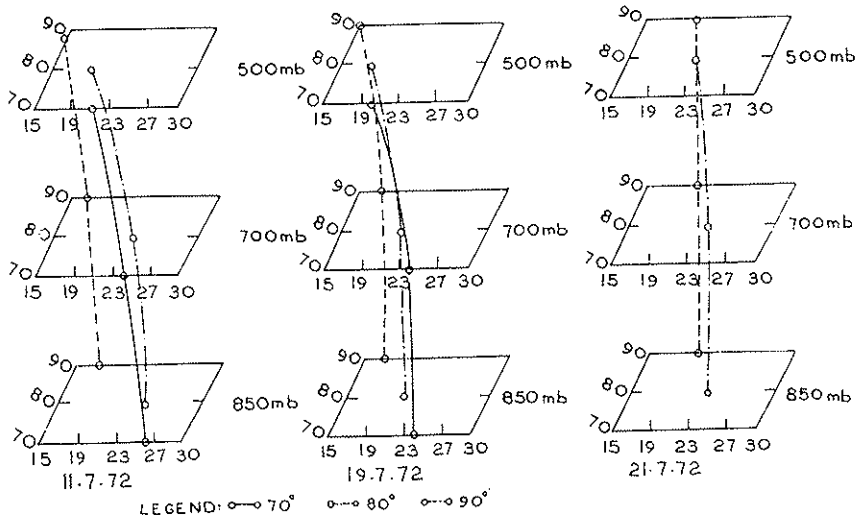

FIG. 3.4. Position of monsoon trough during typical break situation.

was a typical break situation as is reflected in the pentad rainfall (fig. 3.5). As the situation was quasi-persistent and in order to smooth out errors of the individual days, we derived the vertical motion field for average pentad flow pattern during the period. A 5-layer quasi-geostrophic model was used to derive the vertical motion field.

The vertical motion (ω) field at different levels for the above period, based on the mean flow for 5 days, is given in fig. 3.6. The salient features of the vertical motion field typical of break are given below:

i) At 1000 mb level, we have weak areas of ascent over the west coast of India and areas of descent over the east coast of India. Another area of ascent is observed over China and a feeble area of ascent is also observed in Indo-China.

ii) At 800 mb level, we have a region of ascent over the north Arabian Sea. Two other cells of ascent lie over the foothill regions of northwest India and southwest China. A centre of descent lies over West Pakistan which extends towards the east coast of India through the central parts of the country.

iii) At 600 mb level, the 'ω' pattern is similar to that at 800 mb level with the regions of descent over the central parts of India becoming

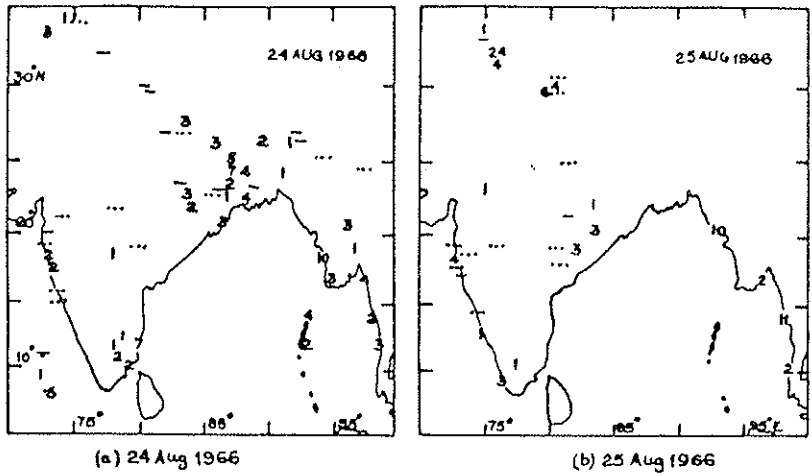

FIG. 3.5. 4hr. Rainfall in break monsoon.

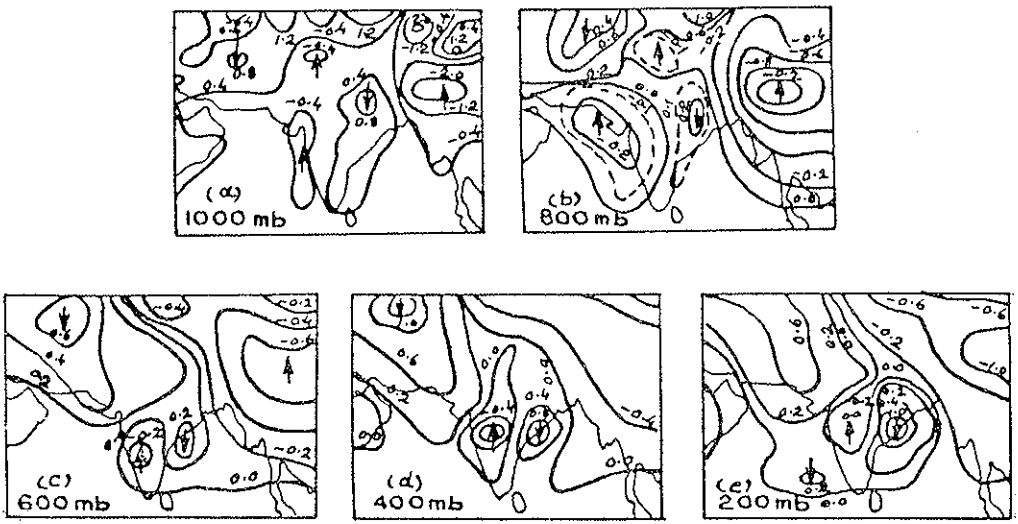

FIG. 3.6. Vertical motion (ω field) during break monsoon (23 to 27 August 1966).

more prominent. Regions of ascent lie over the west coast and extreme northern parts of India and southwest China.

At 400 mb, the 'ω' pattern is similar to that of 600 mb, except that the vertical motion field over the China region is slightly less prominent. At 200 mb level, there is no further significant change except the descent becoming more prominent over the south Arabian Sea and the east coast of India.

Thus the vertical motion field in a typical weak monsoon condition is well organised into large-scale descent extending from Pakistan to the north-west Bay of Bengal. This large-scale subsidence which takes place over the usual monsoon trough region during the weak phase, dessicates moisture and suppresses rainfall over those parts of the country.

In fig. 3.7, we present schematically the three dimensional vertical motion field for the break conditions. If we compare this circulation pattern with fig. 1.6 depicting the circulation pattern during the active monsoon condition, it is noticed that the break monsoon condition is associated with a single cell resembling large convection, where an active monsoon condition is characterized by reversal of ascent to descent at about 600 mb level. These features are specifically valid for the region south of 20N.

3.5 Vertical Circulation During 'Break' — A Proposed Model

Considering the large-scale changes which take place in the circulation patterns and related rainfall distribution over the Indian sub-continent during break, Rao and Datta (1975) proposed a circulation model, which

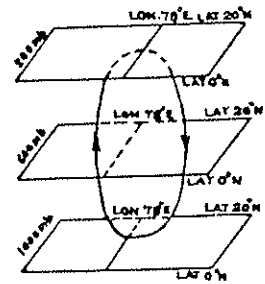

Fig. 3.7. Schematic representation of vertical motion field during break conditions.

is presented in fig. 3.8. On comparison with the circulation model proposed by Koteswaram (fig. 1.4), it can be noted that the main changes are in the reverse Hadley cell which is shifted northwards in fig. 3.10 and is broken up into two sub-cells, one extending from the equator to 10-12°N and the other between 20-30°N.

The proposed model depicts westerlies south of 10°N, weak westerlies between 20-30N and easterlies north of it.

Koteswaram *et al.* (1986) have recently postulated a circulation model for the break situation, which is generally similar to the one described above. The salient features of this section can be summarized as follows:

i) An establishment of a large amplitude trough and its slow eastward movement is a precursor to the onset of break monsoon conditions.

ii) Formation of a trough of low or a cyclonic circulation over the south Andaman Sea and adjoining areas also precedes establishment of break in a number of cases.

iii) Persistence of the break monsoon conditions is linked with the establishment of an N-S ridge over the Caspian Sea region in the layer 700-300 mb. This ridge acts like a typical blocking situation in the subtropical latitudes.

iv) Northward movement of the monsoon trough in the lower and middle troposphere and gradual decrease in its slope precede the onset of break-monsoon conditions.

v) The vertical motion field typical of the 'break' is characterised by a region of ascent over the foothills of north India at lower and middle

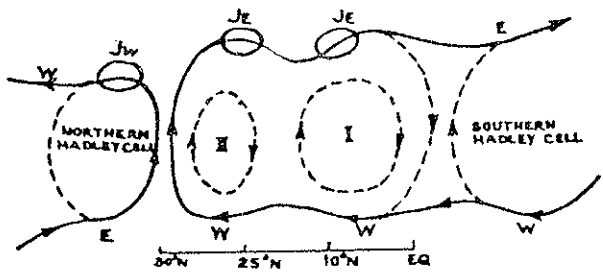

FIG. 3.8. Proposed circulation model for break monsoon.

troposphere and the region of descent extending from Pakistan toward northwest Bay of Bengal through central India.

vi) The vertical cell over the Indian region during the 'break' is similar to a large convection cell whose centre lies over central India.

We also notice that after the initial onset, the two states of monsoon circulation, i.e., one pertaining to a normal monsoon and the other pertaining to a break monsoon, are two probable modes linked with the location and vertical structure of the monsoon trough. This leads us to think that the monsoon trough has at least two states of equilibria, i.e., (i) active monsoon mode, and (ii) break monsoon mode. Charney and De Vore (1979) have introduced a theoretical concept of existence of multiple equilibria in atmospheric circulations under critical forcings. We observe that when the slope of the monsoon trough with height decreases and becomes more or less vertical, it reaches a critical stage, where under certain synoptic conditions it leads to a 'break situation' or back to normal monsoon activity. We therefore postulate that the active/break monsoon modes are two possible modes of the regional monsoon trough system, whose critical forcing mechanisms are as yet not fully understood.

4. MONSOON DEPRESSIONS

The formation of a marked low pressure system over Bay of Bengal, its intensification and movement west-northwestwards over the Gangetic plain is a very important synoptic situation. Its existence and its pre-eminent position as a rain-producing system were recognized as early as 1884 by Sir John Eliot. According to him, atmospheric whirls of all degrees of intensity and magnitude pass from the Bay of Bengal to the coastal districts and interior of India. He named a class of these whirls as the "Smaller or the Minor Storms", which are now known as monsoon depressions. According to the present definition followed in the India Meteorological Department, a monsoon disturbance is termed as depression when the surface winds in cyclonic circulation are between 17 and 33 kt, and as a cyclonic storm if wind speed increases exceed 33 kt. Normally 6-7 disturbances form during the whole monsoon season. They cause heavy rain along their track during their passage.

In earlier periods, so much importance was given to monsoon depressions that the activity of the monsoon for the year was directly related

to their frequency. Dhar and Bhatacharaya (1973) have however shown that the contribution of the rainfall caused by depression over the basins of the rivers Ganges and Godavari is only 8 to 12 percent of the total basin rainfall, respectively. This analysis and other analyses of long-term data clearly show that, whereas there is no one-to-one relationship between the total seasonal rainfall in the country and the number of monsoon depressions, the formation and movement of depressions do significantly affect the distribution of precipitation. Another important characteristic of a monsoon depression is its flood potential, especially if the track of a particular depression is properly oriented with respect to the catchment of a river system.

Table 4.1 gives the number of depressions and cyclonic storms that formed from June to September in the Bay of Bengal, the Arabian Sea and over land for the period 1891-1970 (Rao, 1976).

TABLE 4.1

Region of formation	June		July		August		September	
	D	S	D	S	D	S	D	S
Bay of Bengal	71	35	107	38	132	26	141	32
Arabian Sea	18	15	9	3	2	2	9	5
Land area	12	1	39	1	42	0	21	1

D: Depression S: Cyclonic storm

It can be seen from this table that the region of maximum cyclogenesis is the Bay of Bengal; next comes the land area and last the Arabian Sea. Month-wise distribution suggests that September is the most active and June the least. However, June is also the month where a large number of disturbances intensify into cyclonic storms.

Meteorologists in India have undertaken a large number of case studies to document the synoptic situations which favour the intensification of disturbances in the Bay to monsoon depression. The salient situations are:

i) Southward shift of the eastern end of the monsoon trough and its dipping into the Bay of Bengal.

ii) Increase in strength of the lower troposphere westerly current over peninsular and central India.

iii) Formation of a well-marked cyclonic circulation in the lower troposphere and its gradual descent to surface. In a large number of cases, however, the development of disturbances is from lower to higher levels. It is generally during the early and later parts of the monsoon season that the development proceeds from the upper levels to the surface. One such case during early July, 1979, has been extensively studied by various workers (Sanders, 1981).

iv) Existence of a well-organised or organizing bright cloud mass over the Bay of Bengal and its persistence for 24 hours or so.

v) Pressure fall in the north Bay of Bengal and increase in rainfall activity in the coastal regions, Saugor and other Bay islands and Sandhead ship position.

vi) Existence of a well marked trough in upper level easterlies (300-200 mb) providing significant upper level divergence over the region of incipient disturbance.

4.1 Mechanism for the Development

Some or all the conditions mentioned above may exist but still the low pressure systems may not intensify into a depression. Whereas, in other cases even though the conditions may be marginally satisfied, still depressions may develop. What are the crucial factors or mechanisms which help in intensifying the existing cyclonic circulation into a depression? Several workers have postulated various possible mechanisms, although a precise answer is not known, but the existing theories explain to a great extent the formation of a monsoon depression.

4.1.1 *Synoptic-Dynamical Views*

Eliot (1884) believed that the cloud builds up over the region of cyclonic vorticity and the vertical motion associated with lower level convergence of moist air over the north Bay of Bengal. Heavy precipitation

caused therefrom helps in the release of latent heat, which in turn maintains the monsoon depression.

With the success of the frontal theory for the middle latitude weather systems, the air mass concept took prominence and theories were postulated to explain the formation of a depression on the concept of the convergence of three different air masses (Roy and Roy, 1930). A large number of case studies were undertaken to prove their hypothesis. Mull and Rao (1949), however, showed that there was no significant temperature contrast between different air masses considered. Many other workers also got similar results and this led to the dropping of the air mass concept.

Koteswaram and George (1960) applied the concept of Sutcliffe's development equation modified by Petterssen (1956) for study of the development of cyclones of the mid-latitudes, which states that it is the imbalance between the vorticity advection term and Laplacian of the thermal term that causes development at sea level.

According to Koteswaram and George, this imbalance is brought about by the advance of the upper easterly wave with its associated vorticity advection and/or the favourable position of the tropical easterly jet (TEJ). This structure when it overlays the existing trough (fig. 4.1) of low pressure at the sea level brings in the development and formation of monsoon depression. This system is further maintained by thermal advection term. Cyclonic vorticity will be produced ahead of the depression and destroyed in the rear. This would therefore not only explain further intensification of the depression but also its movement towards the region of rising cyclonic vorticity. In the case study for a depression of August 1957, they observed these features and arrived at the following conclusions:

i) The depression was formed from the pre-existing sea level trough under the influence of upper vorticity advection with very little influence of low level thermal advection during the formative stage.

ii) Thermal advection, which occurred after the initial formation, helped to further intensify and maintain the system.

iii) The movement of the depression was also governed by the same mechanism, maximum contribution being the thermal advection term, and the system moved to the region of warm advection (i.e., vorticity rising area).

This concept is still largely used by conventional forecasters to predict formation of monsoon depression (George and Datta, 1965). Prasad and Krishna Rao (1974) observed that cut-off low in the mid-latitude westerly

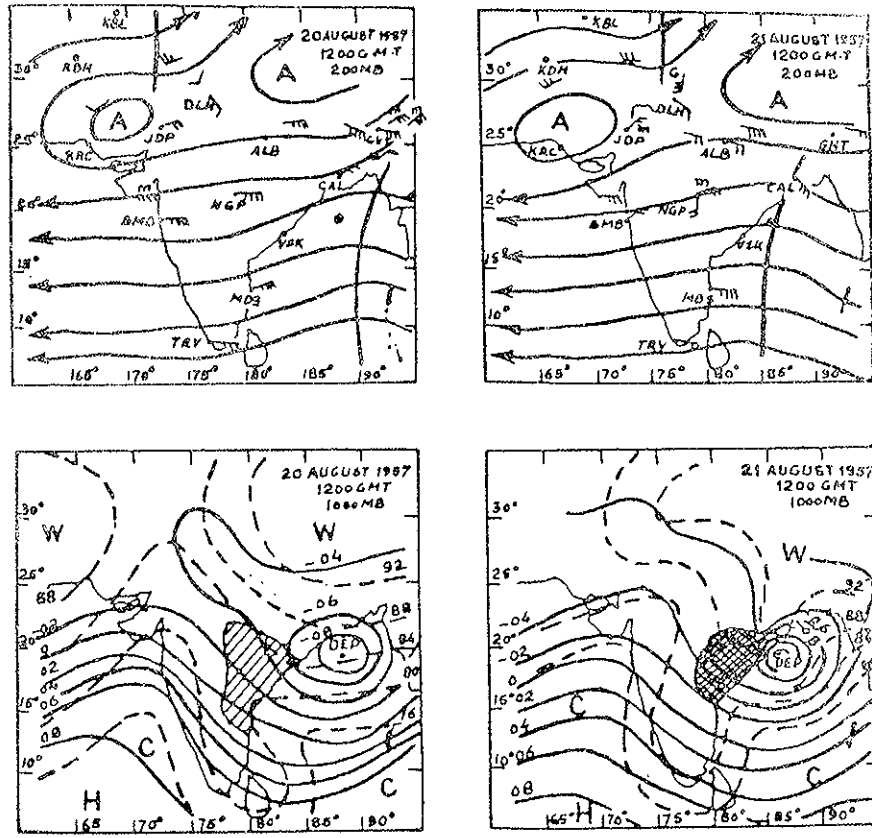

FIG. 4.1. Upper diagrams-200 mb streams lines at 1200 GMT. (winds at 12 km plotted, low level and 0000 GMT. winds indicated by l and m heavy lines-wave throughs). A-anticyclone, C-cyclone. Lower diagrams-1000mb contours and 1000 ~ 500mb relative topography at 1200 GMT. (L-low, H-high, DEP-surface centre of depression shown by a big dot, C-cold, W-warm, contours-solid lines, value in tens of metres, thickness-dashed lines, values in tens of metres, thousandth figure omitted. Areas of continuous rainfall have been given single hatching and heavy rainfall of 5cm and more double hatching), (after Koteswaram, 1960).

trough may, under favourable conditions, induce a perturbation in the easterlies.

Raman *et al.* (1979) gave special emphasis to a parameter pertaining to the decrease in vertical wind shear; this is one of the six genesis parameters (Gray, 1979).

The main problem in a proper understanding and prediction of formation of monsoon depressions in the Bay of Bengal is the lack of data, especially on the upper air in the region. The upper wind data derived from cloud imagery of INSAT-1 (Indian National Satellite) will hopefully provide very useful information.

4.1.2 *Theory of Instability*

The dynamics of monsoon depression has also been studied by instability analysis of horizontal and vertical sheering mean monsoon flow. Daggupatty (1967) applied the linear instability analysis, using quasi-geostrophic and P.E. Model, and concluded that the waves are not baroclinically unstable under the prevailing vertical wind shear and the value of 'f' over the Indian region, unless the static stability parameter is considerably reduced.

Analysis by Krishnamurti *et al.* (1976) of the data of a case of the monsoon depression of August, 1968, showed the existence of combined barotropic-baroclinic instability. But the existence of the condition could not be treated as conclusive as far as the initiation of the disturbance was concerned. Their study, however, brought very interesting conclusions on the maintenance of the depression through cumulus convection.

Detailed barotropic and combined barotropic-baroclinic instability analysis of the monsoon flow was carried out by Shukla (1977, 1978). We reproduce below the results summarized by Shukla (1981).

i) Monsoon depressions over the Bay of Bengal are caused either by amplification of westward-propagating weak disturbances or by downward propagation of the internal jet instability of the easterly jet.

ii) The barotropic instability of the low level flow over the Bay of Bengal is conducive to the growth of weak disturbances. The presence of surrounding terrain contributes to the establishment of such a large-scale flow (monsoon trough over the head Bay) which is barotropically unstable.

iii) CISK is the primary driving mechanism for the rapid growth

of a pre-existing weak perturbation. However, if the amplitude of the disturbance at the lower levels is not sufficient to draw on the low level moisture convergence, the disturbance does not grow to a deep depression.

iv) Once the disturbance has attained adequate amplitude in the lower levels (either by downward propagation of wave energy or by CISK), the low level moisture convergence and latent heat of condensation are utilized more efficiently for the development of a vertically coupled disturbance, which, along with upper-level easterlies, contributes to the westward propagation of the disturbance. Absence of strong vertical coupling leads to vertical tilt and decay of the disturbance.

Study by Shukla explains the formation processes in the Bay to a great extent, but no attempt has been made by any worker to explain the formation processes of depressions of land origin or those forming over the Arabian Sea. What are the conditions in these regions?

Mishra and Salvakar (1980) brought out the significance of baroclinic instability in the formation of monsoon depression, but their conclusions are questionable because of unrealistic meridional temperature-gradient at the ground and arbitrary vertical wind shear at the lower levels used by them.

Studies by Shukla provide concrete evidence that combined barotropic-baroclinic instability alone cannot explain the formation of the monsoon depression. Proper inclusion of moist convection heating is essential to explain the growth, the initial trigger being provided by terrain friction which helps in generating a barotropically unstable trough of low over head Bay.

Similar studies for the depressions of land origin, because of availability of better data, may lead to a better understanding of formation processes of monsoon depression.

4.1.3 *Rainfall Distribution Associated with Monsoon Depressions*

Pisharoty and Asnani (1957) studied the rainfall associated with three cases of depression by compositing them with reference to the centre and track of the depressions. Heavy rainfall of 7.5 cm and above in the preceding 24 hours was confined to a belt 400 km wide to the left of the track and extending 500 km in advance and an equal distance to the rear along the track (fig. 4.2).

Bedekar and Banerjee (1969) also observed by a similar technique that the region of heavy precipitation (5.0-7.5 cm) was concentrated to

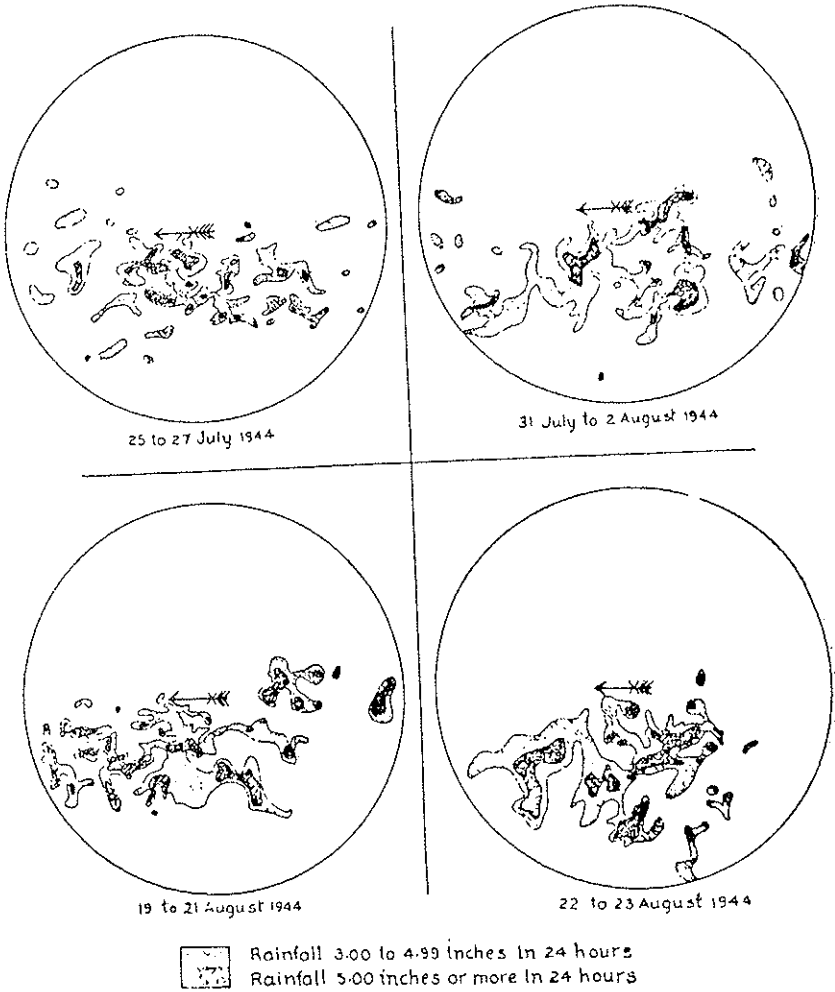

FIG. 4.2. Composite charts of rainfall for area 350 miles around depression centres (after Pishority and Asnani, 1957). (Scale 1" = 140 miles).

the left of the track within a narrow belt of 2-3° in width and 7° in length. In case of recurving systems, the increase in rainfall to the right of the track has been observed.

In case of depressions of land origin, we observe two centres of maxima (fig. 4.2): one to the left of the track (Southwest) and the other to the right (Northeast) of the track.

Das, Datta and Chabra (1971) observed that the 'ω' field at 800 mb provides excellent guidance to delineate the region of heavy precipitation.

Rao and Rajmani (1972) also found a similar relationship between the 'ω' field and rainfall distribution.

In the following, we specifically discuss further the following aspects of monsoon depressions.

i) Origin of depressions;
ii) Genesis potential of various regions in India;
iii) Movement of monsoon depressions; and
iv) Structure of monsoon depressions of land origin.

4.2 Origin of Depressions

It has generally been observed that monsoon depressions generate from the incipient cyclonic circulation. This cyclonic circulation may appear first as a diffuse low pressure system or trough of low with the monsoon trough dipping into the Bay of Bengal, or it may first appear as a circulation in the upper air anywhere up to mid-troposphere. Some of these disturbances (as shown by the above statistics) also intensify into cyclonic storms, whereas some remain as low pressure systems, where surface wind does not exceed 17 kt and no more than one closed isobar could be drawn. Some of the systems have also been observed to dissipate *in situ*.

4.2.1 Source Regions of Bay Depressions

Iyer (1938), in his classical paper, postulated that most of the depressions which form over the Bay of Bengal have their genesis associated with the disturbances in the Pacific or China sea. George and Datta (1965) studied a monsoon depression of September 1963, formed out of the remnants of a typhoon from the Pacific ocean under upper level divergence (200 mb anticyclone). Ramanna (1965) found that about 17

percent of depressions are formed out of the remnants of Pacific typhoons.

We studied 64 cases of monsoon depression which formed during the decade from 1970-1979 in the months of May to September.

To trace the origin of the systems, synoptic charts, a few days prior to the formation of the low pressure area (LPA) in the Bay of Bengal, were studied. Besides well-defined low-pressure systems moving westwards, the pressure changes and the rainfall pattern were also considered to trace a source of the systems which intensify in the Bay.

Table 4.2 gives the monthwise classification of the cases studied. The frequency of the systems was highest in August, followed by July, September, June and May.

TABLE 4.2

Month	No. of cases studied	% of system from E to SE
May	7	90
June	12	75
July	15	83
August	17	87
September	13	75

From the table it may be noted that about 82 percent of the total number of disturbances seem to have their sources either in the east or southeast. Some of the disturbances could be distinctly seen to originate from the remnants of Pacific typhoons. Very few, i.e., about 15-20 percent, of the total disturbances seem to have formed *in situ*.

4.3 GENESIS POTENTIAL OF VARIOUS REGIONS IN INDIA

From the table 4.1, it is seen that the maximum frequency of depressions is in the Bay of Bengal. It is therefore interesting to study the general condition of this zone, which makes it very favourable for cyclogenesis:

i) High sea surface temperatures of the order of 29°C or more (> 26°C).

ii) Frequent dipping of the monsoon trough in the Bay creates initial positive vorticity which acts as incipient disturbance.

iii) Weak vertical wind shear in the basic current over the region.

All these conditions, which were listed by Palmen (1956) for cyclogenesis, are found over this region (Bansal and Datta, 1972). Gray (1979) proposed six primary climatological parameters for the genesis of tropical storms; these are (i) low level vorticity; (ii) coriolis force; (iii) vertical wind shear; (iv) ocean thermal energy (SST); (v) equivalent potential temperature and (vi) middle troposphere humidity. All these parameters were used to define seasonal genesis parameters (SGP) by Gray. The first three parameters constitute dynamical parameters and the last three thermal parameters.

The values of each parameter, as well as total SGP are given in table 4.3.

TABLE 4.3 - *Computation of Seasonal Genesis Potential.*

Area	Vorticity parameter 10^{-6} sec^{-1}	Coriolis parameter 10^{-5} sec^{-1}	Vertical shear parameter (700 mb sec/m)	Ocean energy parameter 10^3 Cal/cm^2	Moist stability parameter °K/510 mb	Humidity parameter	SGP 1.37×10^{-8} Cal °K sec^{-1} cm^{-3}
NW Bay of Bengal centred 20°N 90°E	30.0	4.99	0.062	10.8	10	1	10
SW Arabian Sea centred 10°N 73°E	9.0	2.53	0.026	9.6	11	1	1
Source region of land depression centred 25°N 87°E	22.0	6.16	0.062	—	11	1	—

This table shows that the genesis potential of the NW Bay of Bengal during July is higher than the south Arabian Sea. Comparing these values

with the composited picture presented by McBride (1979), we find that the SGP value for NW Bengal as comuted for mean July conditions compares favourably with a value of SGP 12 for the pre-hurricane cloud cluster in the Atlantic Ocean. The Southwest Arabian Sea, however, gives a value of SGP which in the Atlantic ocean corresponds to cloud clusters (non-developing).

As it is difficult to compute thermal parameters over land area, we have presented only the values of various dynamical parameters for the NE Indian region centred at 25N 87E in the table 4.3. This is a prominent source region for the depression of land origin. The values of dynamical parameters compare favourably with the parameters of the NW Bay of Bengal.

These computations support the statistics on frequency of formation of cyclonic disturbances given in table 4.1. Note for the period 1891-1970, there were 155 disturbances formed in the Bay of Bengal, 12 in the Arabian Sea and 40 in the land during July. Thus during July, the Bay of Bengal is the most potential region for the formation of tropical disturbances, the next being the land area, and the last being the Arabian Sea. SGP computations also show the same results.

4.4 Movement of Monsoon Depressions

If one examines the tracks of depression and cyclones during the months of June to September, it may seem paradoxical that the track of these disturbances is against the mean zonal flow of the lower troposphere, which is westerly. But it might be noted that there is large vertical shear and the flow reverses to easterlies in the upper troposphere, reaching jet speed between 150 to 100 mb (TEJ). George and Datta (1965) and Bhagare and Datta (1971) have shown that in most cases these disturbances are steered by upper tropospheric flow.

The climatology of these depressions brings out the following noteworthy points:

i) June to August, disturbances in the Bay generally form north of 18N (mostly north of 20N) and west of 92E; in a few cases during June and August they also form at southern latitudes extending to 15N. June is also an active month for the formation of disturbances in the Arabian Sea, the number being small during the other months. In September, generally the disturbances form at the southern latitudes.

ii) During July, the depressions move mainly on a west to west-northwest track and cases of recurvature are few. Depressions of June and September show a greater spread and more tendency of recurvature. The depressions in August are characteristically similar to those of July, but have slightly more spread and more cases of curvature.

iii) A few depressions from the Bay moving westwards also emerge into the Arabian Sea.

iv) The average speed of movement of depressions in July is 5-10 km/hr east of 85E, becoming more (10-20 km/hr) in the west. In certain cases, the speed of 30 km/hr has also been observed over central India. In other months, similar conditions held good but speed is slightly lower.

v) Systems have less recurving tendencies (i.e., changing course to northerly or northeasterly) in the month of July and maximum during September. Systems generally show recurving tendency west of 85E, and maximum frequency of recurvature is west of 80E.

vi) Before recurving, systems show considerable decrease in speed, and increase in speed after recurvature.

vii) On climatological consideration, the movement of disturbances in the Bay of Bengal is largely governed by the location of upper tropospheric anticyclone (Datta, 1967).

4.4.1 *Synoptic Consideration and Movement of Depression*

We studied in detail the life history of a monsoon depression which formed out of the remnant of a typhoon in the South China Sea. It crossed over to the Bay of Bengal as low pressure system and intensified into a depression on Sept. 11, 1963. The track of the depression is given in fig. 4.3. It might be noticed that it initially moved west-northwestwards from the 11th to the 14th, when it started recurving and changed to a more northerly track after Sept. 14. George and Datta (1965) tested the well known synoptic features to explain and to provide suitable techniques (thumb rules) to forecast the track of monsoon depressions. The various features considered were:

(i) pressure changes and rainfall distribution; (ii) high-level steering and location of upper-level ridge axis; (iii) warm tongue analysis and (iv) trough in mid-latitude westerlies. The critical examination of data during the life history of this depression and the many other recent cases showed

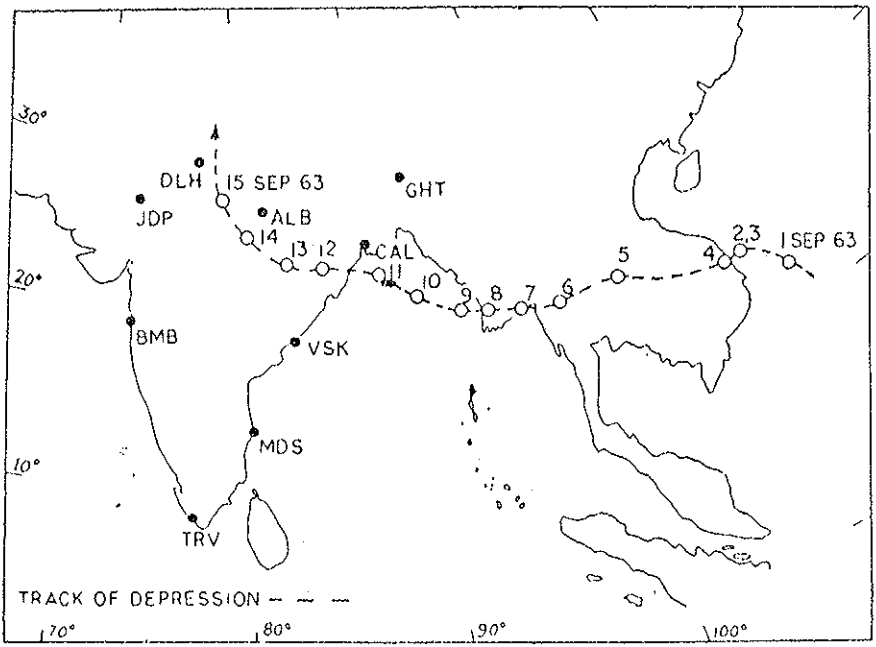

FIG. 4.3. Track of the depression — 1 to 15 September 1963.

the following significant features, which we recommend for use as guidance factors in day-to-day forecasts:

a) The changes in the orientation of the rain belt could provide good guidance. In the present case, the rain belt was extending westwards of the position of the centre up to the 13th but showed northward extension on the 14th (fig. 4.4). This shift is a good indication of recurvature after the 14th. Pressure changes (short term and 24 hours) also showed a shift from west to north.

b) Upper tropospherical winds near the centre of the depression, as well as location of the depression with respect to the upper air level anti-cyclone, provide another forecasting tool. For example, note from figs. 4.5 and 4.6, the cases of monsoon depressions of Sept. 1963 and August 1978 respectively as to how the 300 mb flow has been guiding the movement of the depressions. Initial westward movement and later recurvature has been well brought out.

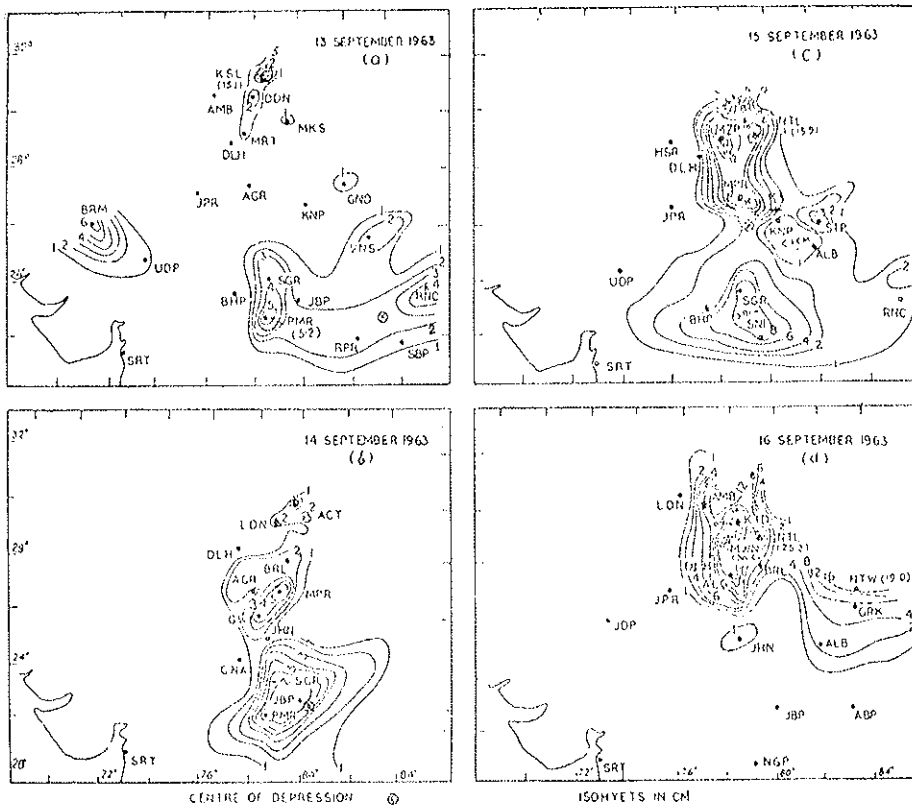

FIG. 4.4. Rainfall pattern for the period 13-16 September 1963.

c) Another synoptic technique found useful to predict the movement of tropical disturbances is the "Warm tongue analysis". The warm outflow from tropical disturbances produces a belt of warm air ahead of the disturbances. Fig. 4.7 depicts the thickness (500-700 mb) pattern on Sept. 13 and 14. It is noticed that on the 13th a thermal high is located to the west of the depression centre, whereas it is northeast of the centre on the 14th. This change-over provides an excellent clue for the change of track from its more westerly to northerly direction.

d) Ananthakrishnan (1958) emphasized the role of the trough in upper level westerlies in recurving the depressions. A high amplitude trough along 70E or east of it, modifies the upper-level anticyclone and the steering field. Figs. 4.5 and 4.6 depict these features.

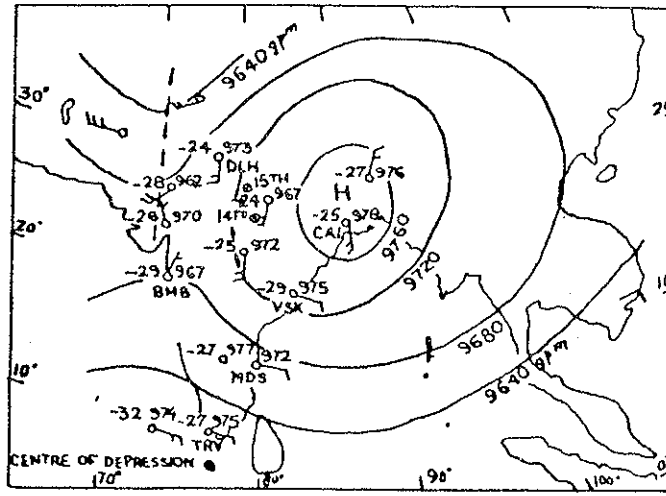

FIG. 4.5. Flow pattern at 300mb at 12 GMT of 14 September 1963. The contours have been drawn at an interval of 40 GPM.

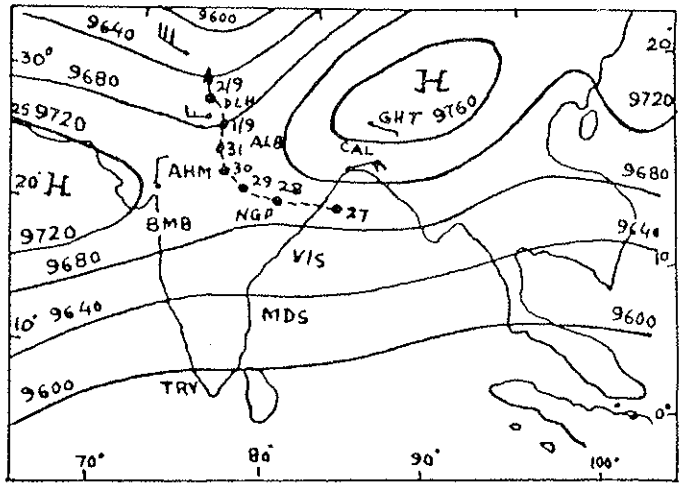

FIG. 4.6. Flow pattern at 300mb at 00 GMT of Sept. 1, 1978.

● Position of depression from Aug. 27-Sept. 2, 1978.

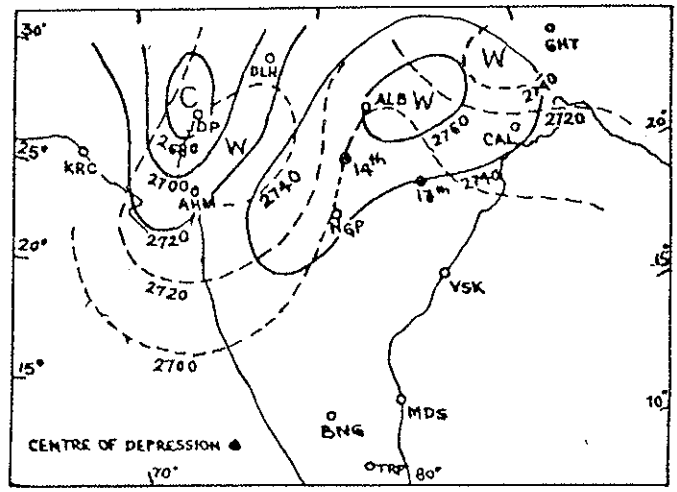

FIG. 4.7. Thermal thickness 700-500mb.

------ Thermal thickness at 00 GMT of 13 September 1963.
——— Thermal thickness at 00 GMT of 14 Septembre 1963.

The synoptic features can provide very useful guidance in predicting the movement of the depression. In cases where all the above conditions exist simultaneously, the forecasting is easy; however, in cases of contradictory conditions, guidance from other statistical and numerical techniques is very essential.

4.5 Structure of Monsoon Depressions

Various studies have been conducted to understand the three-dimensional structure of Monsoon Depressions (Mulki and Banerjee, 1960); Chaudhary and Rao, 1976; Godbole, 1977). All these studies were based on the composition of data for monsoon depressions which formed in the Bay and moved inland.

From these studies, the following conclusions may be drawn on the structure of depressions:

i) The monsoon depressions have horizontal dimensions of about 1500 km and vertical dimensions of about 8 km and horizontal wind speeds of more than 20 m/sec.

ii) The vergence, vorticity and 'ω' fields show that the strongest

activity is concentrated in a narrow vertical tube ahead of the depression and relatively weak field in the rear. The field is strongest near the 800 mb level.

iii) It is cold-cored in the lower level up to 700 mb and warm-cored aloft, amplitude being maximum near 300 mb level.

iv) The flow changes from cyclonic to anticyclonic near 200 mb. The changes from inflow to outflow take place around 300 mb.

v) Its vertical axis tilts eastward with height.

vi) Very moist air prevails to the southwest of the depression centre.

vii) From the above distribution of various fields, it can be noted that monsoon depressions are not symmetric with respect to these parameters.

The sample for compositing, as far as we are aware, was not homogeneous with reference to the track. Recurving types of disturbances have probably been also clubbed with westward moving disturbances. The selection of cases also did not consider if the disturbances were formative, mature or dissipating phases.

In order to avoid some of the above-mentioned drawbacks, we have attempted a study of the composite structure of land depressions. Details of this work are discussed in a subsequent section.

4.5.1 *Monsoon Depressions of Land Origin*

Statistics presented in table 4.1 clearly show that the land depressions are one among the major rain-producing systems in India during the monsoon months. However, their frequency is low compared to depressions of Bay origin (about 1.6 per year, 117 during 1891-1970). Copious rainfall occurs over India in association with such land depressions. In this connection, the land depressions of September 1978 (Mandal *et al.*, 1979) is an excellent example. This depression caused record rainfall in various places in Bihar and West Bengal along its track and caused deluge in the city of Calcutta. It is interesting to study these depressions of land origin because the data is generally available during all the development phases, compared to depressions of oceanic origin.

Specifically, the present study is unique as:

i) It specifically considers the monsoon depressions of land origin.

ii) The life cycle of a depression has been divided into three stages,

viz., formative, mature and dissipative. The formative stage is taken as the day before the system was declared as depression. The mature stage refers to the synoptic hour when the system is found to be the most intense with reference to central pressure and pressure gradient force around the centre. The dissipating stage is taken when the system again weakens into a low.

iii) The sample is ensured to be homogeneous with respect to intensity and track of the system.

In order to maximize the data, the well known technique of compositing has been used. For this purpose, we have utilized upper air data of 11 land depressions which originated over the Gangetic West Bengal and adjoining areas of Bihar and moved in a westerly direction.

Data for 11 cases of land depressions were picked during the period 1971-1979. To maximize the data, we used a compositing technique similar to one used by Pisharoty and Asnani (1957) and Gray, 1979).

Specifically, a circular grid extending to 1000 km with each circle of 100 km radius has been used. The circles are then divided into 12 equal sectors, each sector making an angle of 30°. Thus, the circular grid system is divided into $12 \times 10 = 120$ sections. Datta *et al.* (1978) proposed compositing of land depression by considering separately various phases. Upper air data for 11 cases of the land depressions in three stages, i.e., (i) formative, (ii) mature and (iii) dissipative, were composited separately according to their stages. The grid is so adjusted that the centre of the depression always lies at the centre of the grid and the direction of the grid has been kept to coincide with the direction of the movement of the depression. The upper air data falling in any sector for all land depressions accounted here have been taken into consideration for finding out the mean parameters. The mean value for various meteorological parameters for the levels 950, 850, 700, 500, 300, 200 and 100 mb levels were considered. Meteorological parameters considered were wind speed and direction, contour values, temperature, specific humidity and potential buoyancy. The composited data thus obtained have been analysed. The composited data has been also used to compute various dynamical parameters, such as relative vorticity, vergence field, vertical motion field, etc. The salient features on the structure as obtained from the above data are given below:

4.5.1.1 *Wind Field*

The cyclonic circulation in all the three stages of depression

(formative, mature and dissipative) is extending up to 400 mb. At 200 mb, the wind field around the depressions changes to anti-cyclonic with the centre of the anticyclone about 400 to 600 km north of the low level depression centre. Another cyclonic circulation at about 7 hundred km to the east of the depression centre is observed in the lower level in the formative stage. However, this circulation is not present in the mature and dissipative stages. The eastwest trough extends up to 500 mb with a slight tilt to the south with height, this being prominent in the mature stage.

The system is most intense at 850 mb level, where wind speed is 10-15 kt during the formative and dissipative stages and 15-20 kt during the mature stage.

From the wind circulation field, it could be concluded that the horizontal scale of the system is of the order of 1000 km.

4.5.1.2 *Contour Field*

Associated with depression (fig. 4.8 - 4.10), the low pressure extends up to 300 mb, in all the three stages of the depression and changes into high pressure aloft. Consistent with the wind field, another lower level low exists about six to seven hundred km east of the depression centre. In the formative stage, a third low also exists in the lower level about 700 km south of the system. Chaudhary and Rao (1976) in their study also observed similar low to the south within the depression field. The low associated with the depression is more intense in the mature stage than in the formative and the dissipative stages. Though no significant tilt of the low with height could be observed, a slight slope towards south with height was noticed.

4.5.1.3 *Temperature Field*

Temperature patterns associated with various phases of composited land depression were analyzed for 950, 850, 700, 500, 300, 200 and 100 mb levels; however, for economy of space we present in fig. 4.11 to 4.13, temperature patterns for 850, 500 and 200 mb for the three phases.

The temperature pattern clearly indicates that the system in all three phases has cold cored structure at the lower levels and warm cored at 200 mb. There are, however, some significant differences in three stages of depression, which are given below:

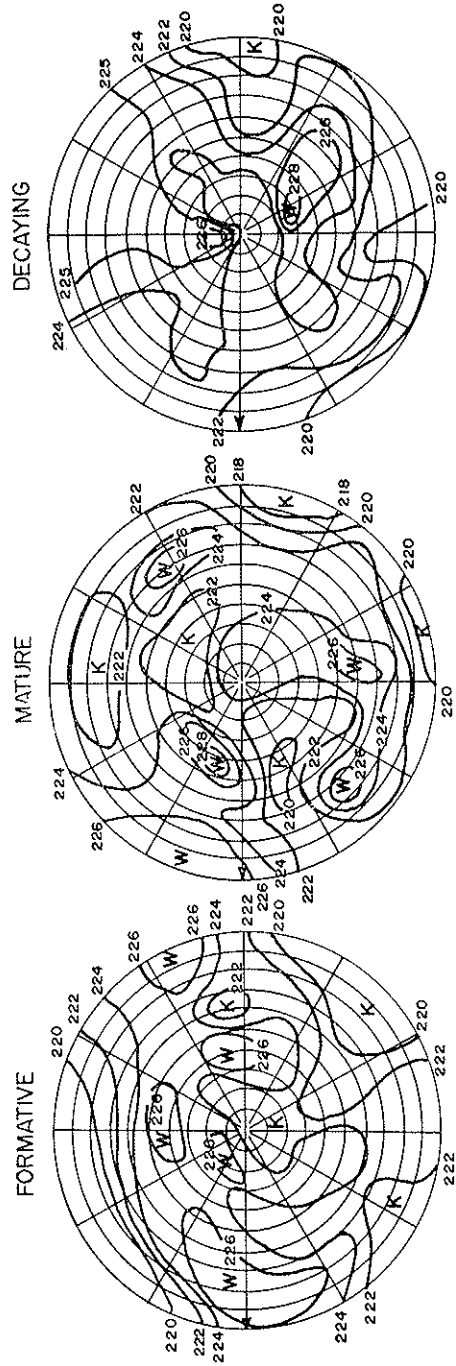

FIG. 4.8. Composite contour field for different phases at 850 mb.

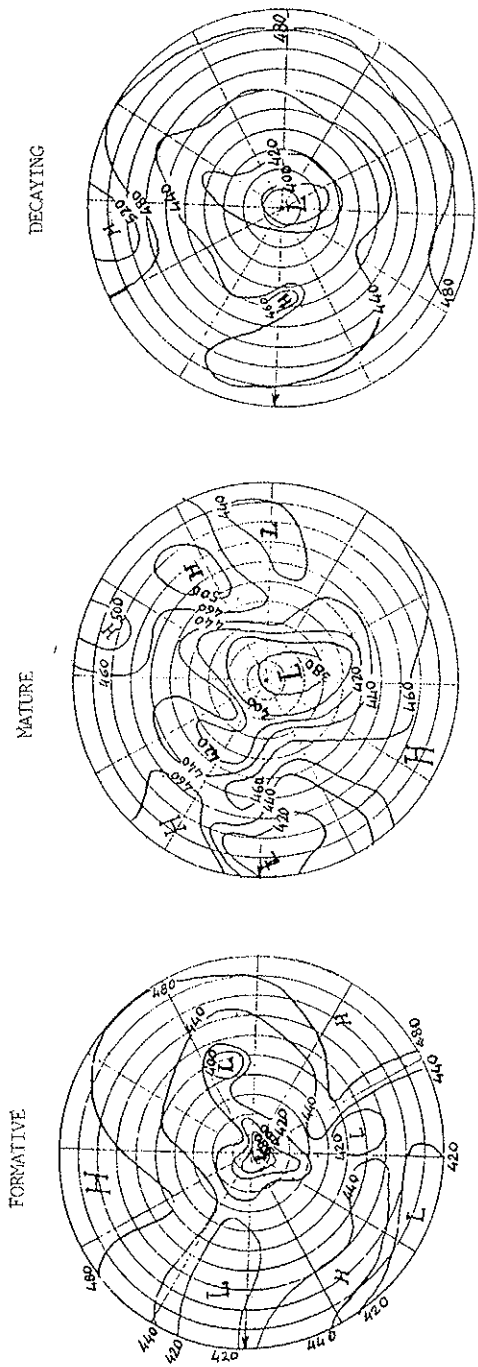

FIG. 4.9. Same as in fig. 4.8 at 500 mb.

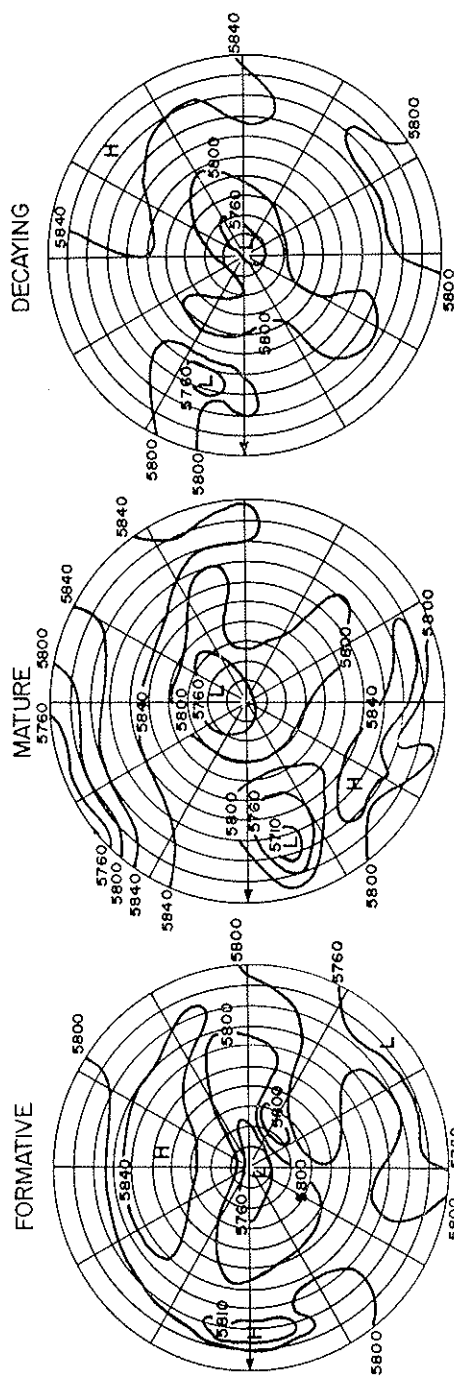

FIG. 4.10. Same as in fig. 4.8 at 200 mb.

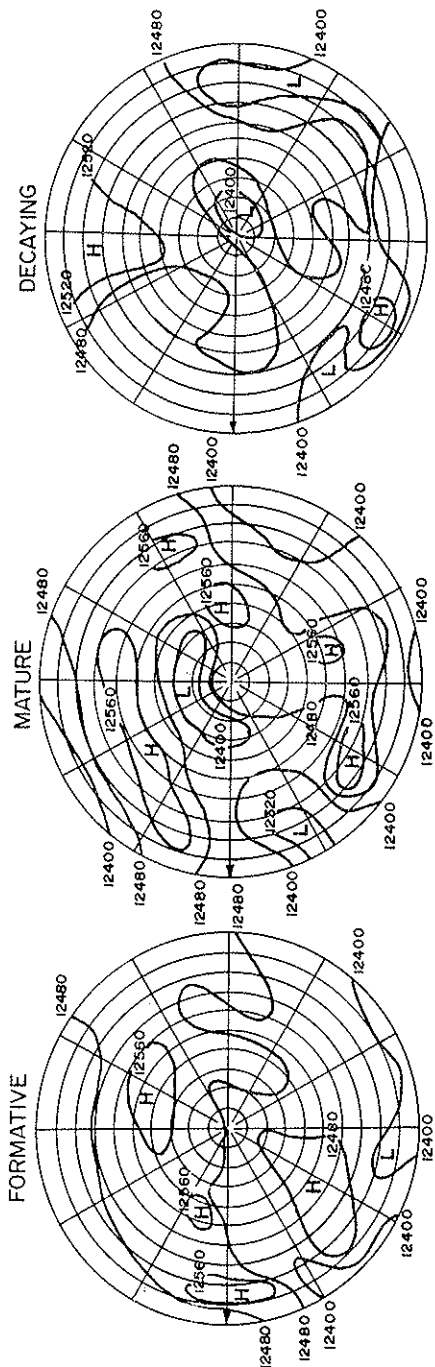

FIG. 4.11. Composite temperature field for different phase at 850 mb.

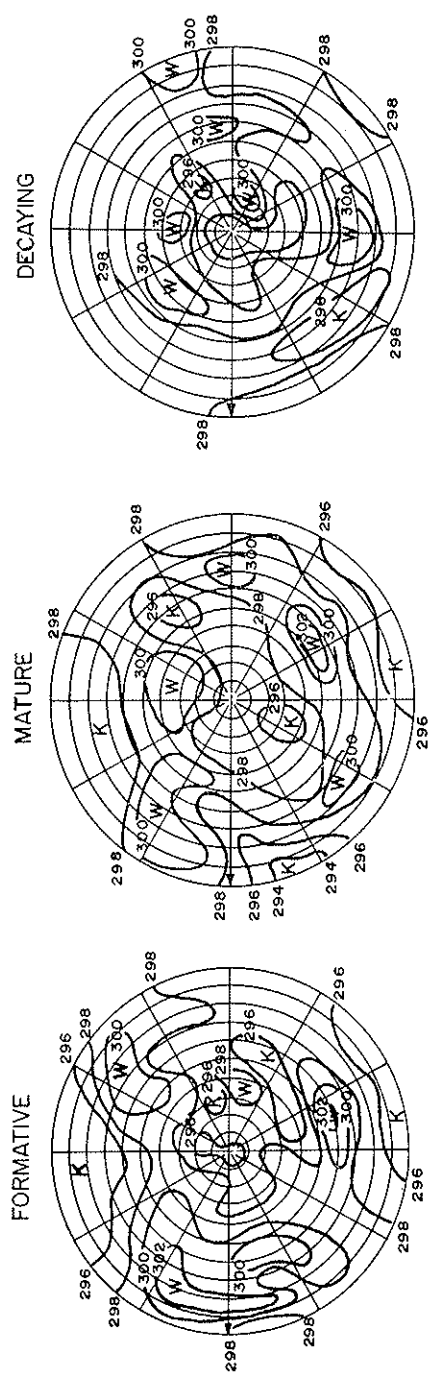

FIG. 4.12. Same as in fig. 4.11 at 500 mb.

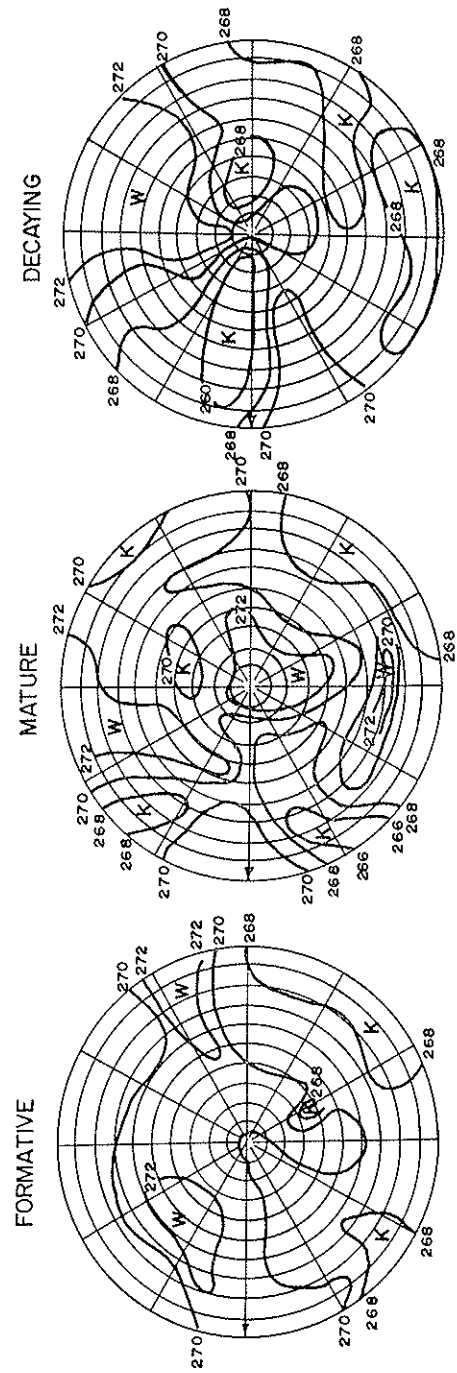

FIG. 4.13. Same as in fig. 4.11 at 200 mb.

i) The cold core extends to 700 mb during formation and dissipating stages but is confined only to 850 mb during the mature stage.

ii) Even within the region of cold core, level to level the temperature is comparatively warmer at the mature stage than at the other two stages.

iii) The warm core is observed up to 300 mb in all the three stages. At 200 mb level, the central region is warm cored in the mature stage, but is cold core during the formative and dissipative stages.

iv) A well marked warm sector is located to the west of the centre of depression at lower level during mature and dissipating stages.

It appears that there is a tendency for warm core to develop to the lower levels as the system reaches the mature stage. This is a significant observation which needs special attention. This observation might suggest that CISK plays a prominent role during development.

It is interesting to compare our results with similar work done by other authors. Murakami (1977) observed that the monsoon lows over the inland areas have a diffused temperature structure (no obvious cold core) at the lower levels and warm core in the upper levels. Chaudhary and Rao (1976) observed that monsoon depressions had cold core up to 850 mb and warm core from 700 mb to 300 mb. Above 300 mb, again the temperature field around depressions was found to be cold cored. Godbole (1977) also observed that monsoon depressions are cold cored in the lower troposphere from surface to 700 mb and become warm core at 500 mb to 300 mb.

In the present study, the temperature structure generally agrees with the one observed by Chaudhary and Rao (1976) and Godbole (1977). The levels up to which the cold core extends vary from 850 mb during the mature stage to 700 mb during the formative and decaying stages. In the middle and upper troposphere, the thermal structure shows a warm core in all the three stages except at 200 mb level and above where it is cold cored during formative and decaying stages.

As a contrast to the thermal structure observed by Murakami (1977), in the present study both during formative and decaying stages, (when the systems could be compared with land lows studied by Murakami) the cold core in the lower levels is quite prominent.

4.5.1.4 *Moisture Field*

Composited specific humidity values for various levels were also analyzed for all the levels. The isolines for only two levels, viz., 950 and

500 mb, are presented in the figs. 4.14 and 4.15. The salient features are:

i) At the lower level (950 mb), the depression field in all the phases is generally moist, being more moist in the northern sector during formative and mature stages.

ii) During the dissipating stage, there is a decrease in moisture around and along the northwest sector of the depression field compared to formative and mature stages.

iii) In the mid-troposphere (500 mb level), the central region of depression (within 500 mb) is more moist than the surrounding areas, particularly in the mature and dissipative stages.

iv) In the upper troposphere (300 mb and above), moisture is not very significant and the specific humidity is less than 1 gm/kg.

The moisture structure is found to be such that the northern sector is more moist than the southern sector. This finding agrees with the findings of Godbole (1977). However, according to Murakami (1976), monsoon lows of coastal regions have positive moisture anomaly east of the axis and inland lows (Murakami, 1977) have positive anomaly to the west of axis.

It has been observed that the middle troposphere (700 to 500 mb) is more moist around the depression field than its surroundings, which agrees well with the general findings of Gray (1979) and Sikka (1978).

4.5.1.5 *Relative Humidity*

Fig. 4.16 shows the mean two-dimensional (x - p) relative humidity profile. It shows high values of relative humidity, particularly in the middle troposphere in the mature stage. This feature is highly conducive to convection with minimal entrainment drying (Gray, 1979) and there fore favourable for development.

4.5.1.6 *Equivalent Potential Temperature* (Θ_E)

The value of Θ_E at the surface minus the saturated values at mid-troposphere (600 mb) gives a measure of the atmosphere's potential to sustain deep cumulus buoyant moist convection (Gray, 1979).. Cumulonimbus convection on the other hand acts as a primary mechanism for the vertical coupling between lower and upper troposphere necessary for development.

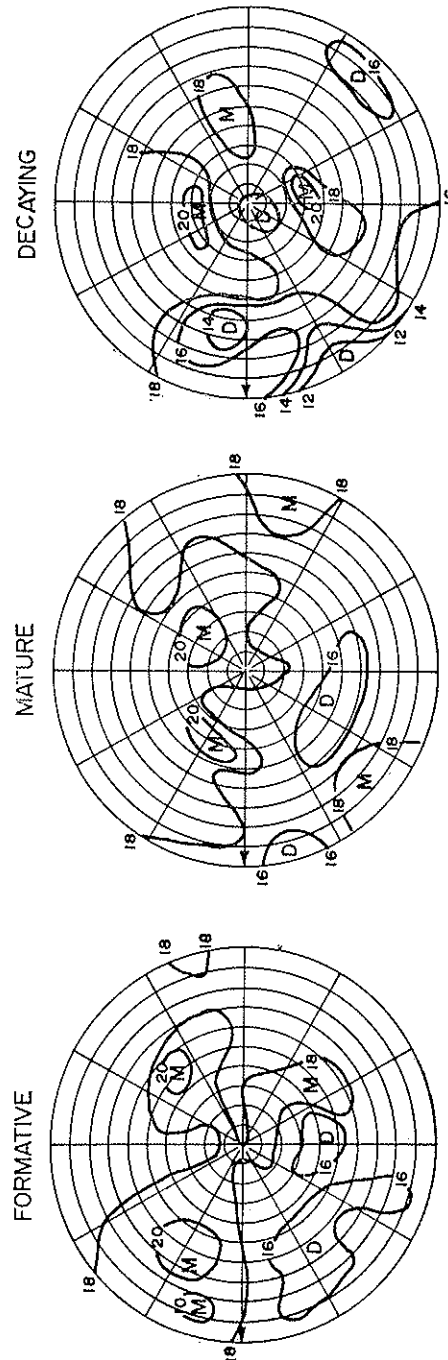

FIG. 4.14. Composite moisture field for different phase at 950 mb.

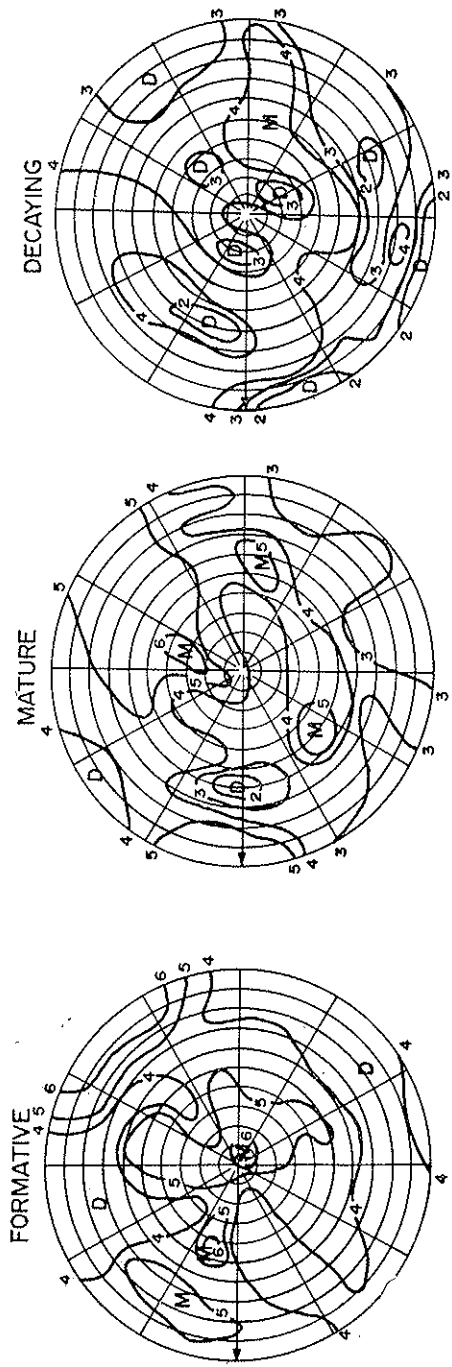

FIG. 4.15. Same as in fig. 4.14 at 500 mb.

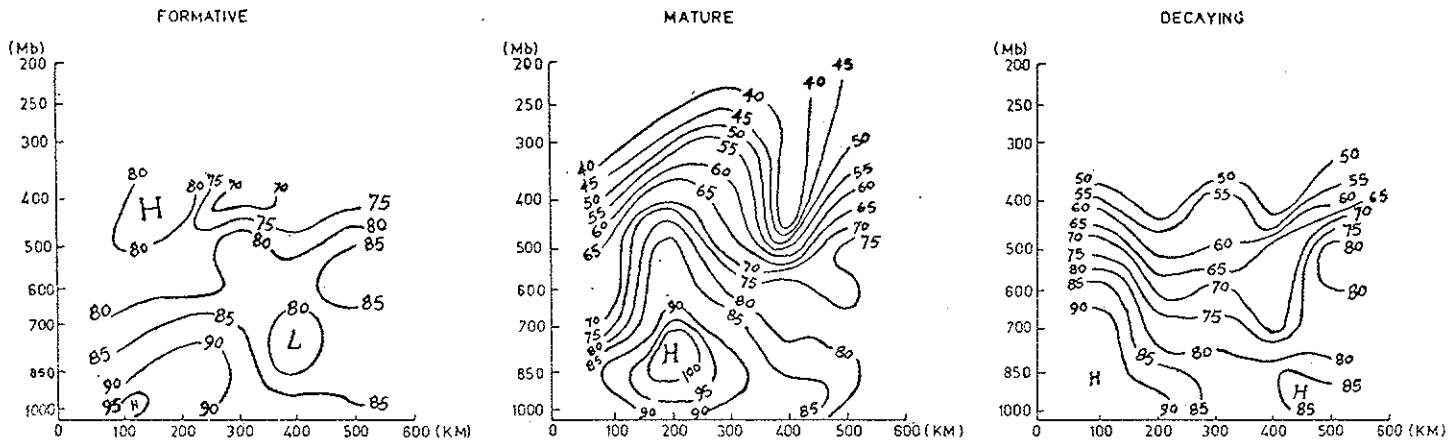

FIG. 4.16. Distribution of relative humidity for different phases.

Fig. 4.17 shows the values of surface to 600 mb gradient. It is observed that the values around the depression field increased from 10°K in the formative stage to 14°K in the mature stage and decreased to 4°K in the dissipative stage. Decreased vertical coupling due to decrease in convection may be one of the causes of dissipating of such depressions.

4.5.1.7 *Distribution of Precipitation*

In fig. 4.18 (a, b and c), we show the precipitation distribution around the centre of depression. The salient features are given below:

i) In all stages, there are two prominent maxima of rainfall, one in the northern sector and the other in the west-southwest sector, the latter being more prominent.

The WSW sector maxima is similar to the one reported by earlier workers (Pisharoty and Asnani, 1957), Bedekar and Banerjee, 1969) and could be explained from the consideration of inflow and moisture convergence.

The northern sector maxima about 300 km from the centre which was not reported earlier, could be explained with regard to orographic lifting of moist easterlies/southerlies.

ii) Another maxima in the forward sector (800 km ahead of the centre) is observed in the mature stage. Similar distance effect is noticed in the decaying stage but in the SSW sector. Such distance effect was observed in the case of tropical storm and has been discussed by Mukerjee *et al.* (1979).

iii) As expected, rainfall is maximum in the mature stage, when the centre of highest rainfall of the order of 7 cm lies in the SSW sector about 200 km from the centre.

4.5.1.8 *Vergence and Vorticity Field*

In table 4.4 and 4.5, we present vergence and vorticity values at different radii with reference to the centre. Lower level convergence and upper level divergence are prominent in all stages. The divergence at 200 mb shows a decrease with increase in radial distance except in the mature stage, where divergence increases with the decrease in radial distance.

Vorticity has the usual pattern, with positive vorticity at the lower levels changing to anticyclonic above 300 mb level.

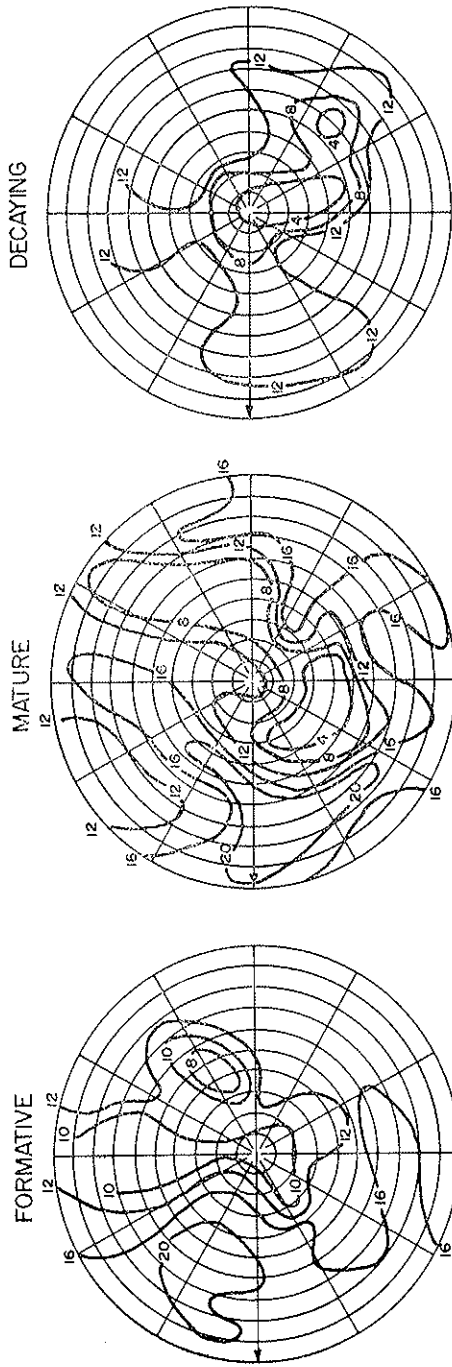

FIG. 4.17. Surface to 600 mb gradient of equivalent potential temperature.

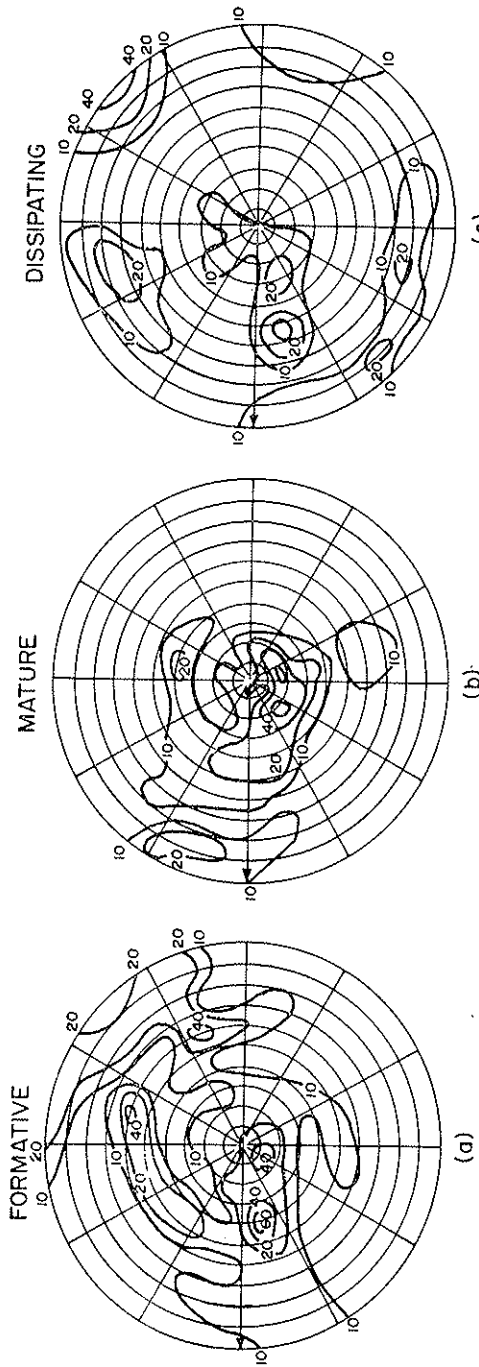

FIG. 4.18. Precipitation distribution.

4.5.1.9 *Vertical Motion*

The vertical motion field was computed by the Kinematic method. The total divergence in the column is adjusted to be zero by distributing the net divergence to the various levels. O'Brien (1970) made a comprehensive analysis of adjustment techniques. He assumes that the error in the mean divergence for each level is a linear function of the net error determined at the top of an atmospheric column.

For better understanding the structure, plots of the vertical motion field were drawn by taking east-west and north-south cross sections through the centre of the depression. These are presented in fig. 4.19 (a, b and c) and fig. 4.20 (a, b and c) separately for different phases.

The salient features observed in the vertical motion field are summarized below:

i) During the formative stage, the vertical motion is not well organized. There are alternate regions of upward and downward vertical motion fields with respect to the centre, both in the vertical and east-west direction.

The N-S cross section depicts the general region of upward motion near the centre except small pockets of subsidence between 850-700 mb levels.

ii) The picture is markedly changed during the mature stage, and the well organized vertical motion field is observed around the centre.

E-W cross section shows a marked region of upward motion just west of the centre extending up to mid-troposphere with maxima between 850-700 mb levels. Other maxima are also present about 300-500 km east of the centre and 500-700 km west of the centre.

N-S cross section however shows two regions of upward motion, one north of the centre and the other about 300 km south of the centre.

The vertical motion field therefore supports the existence of two precipitation maxima, one in the west-south-west sector and the other in the northern sector. The region of the upward motion 500-700 km west of the centre could explain the third (distance effect) precipitation maxima reported under 4.5.1.7.

iii) The dissipation stage is marked by the large scale subsidence near the centre. The rest of the region consists of alternate areas of upward and downward motions. This feature is quite consistent with the dissipation stage.

TABLE 4.4 - *Vergence Field* (Unit 10^{-5} sec^{-1}).

	Formative state					Mature stage					Decaying stage				
200	1.5	6.8	3.8	2.5	0.2	−0.4	−0.3	0.2	0.5	0.7	1.8	0.1	0.2	0.1	0.4
300	−0.02	0.1	−0.1	−0.02	−0.1	−1.9	−1.1	−0.5	−0.5	−0.4	−0.8	−0.8	−0.5	−0.4	−0.2
500	−0.4	0.1	0.1	2.0	0.1	−1.0	−1.1	−0.6	−0.1	−0.1	−0.7	−0.7	−0.3	−0.2	−0.2
700	−2.9	−0.7	−0.2	−0.2	−0.01	−2.5	−0.8	0.1	0.2	0.2	−0.4	−0.6	−0.4	−0.3	−0.2
850	−0.8	−0.4	0.1	0.03	−0.1	−2.5	−1.0	−0.1	−0.1	−0.1	−1.8	−1.2	−0.6	−0.5	−0.5
950	−1.7	−0.8	−0.6	−0.2	−0.1	−0.9	−0.7	−0.4	−0.1	−0.2	−1.33	−1.6	−0.9	−0.7	−0.5
	1	2	3	4	5	1	2	3	4	5	1	2	3	4	5

Distance from centre in deg latitudes

TABLE 4.5 - *Vorticity Field* (Unit 10^{-5} sec^{-1}).

	Formative state					Mature stage					Decaying stage				
200	−2.1	−1.5	−1.3	−0.8	−0.6	−3.2	−1.7	−1.6	−1.8	−1.6	−4.5	−2.5	−1.4	−0.5	−1.0
300	0.3	0.8	0.6	0.7	0.7	1.3	0.8	0.4	−0.2	−0.7	2.3	1.9	1.0	0.3	−0.3
500	7.9	2.9	1.4	1.04	0.9	8.8	6.4	3.4	1.8	1.1	4.9	3.1	2.3	1.6	1.0
700	8.1	4.7	2.8	1.7	1.2	12.1	6.2	3.6	1.7	1.0	2.6	3.8	2.8	1.7	1.1
850	8.2	4.3	2.3	1.6	0.9	9.5	5.5	3.4	1.9	1.4	6.0	3.9	2.6	2.0	1.5
950	8.3	4.2	2.3	1.3	0.9	8.7	4.7	2.9	1.6	0.9	7.3	4.2	2.1	1.2	1.0
	1	2	3	4	5	1	2	3	4	5	1	2	3	4	5

Distance from centre in deg latitudes

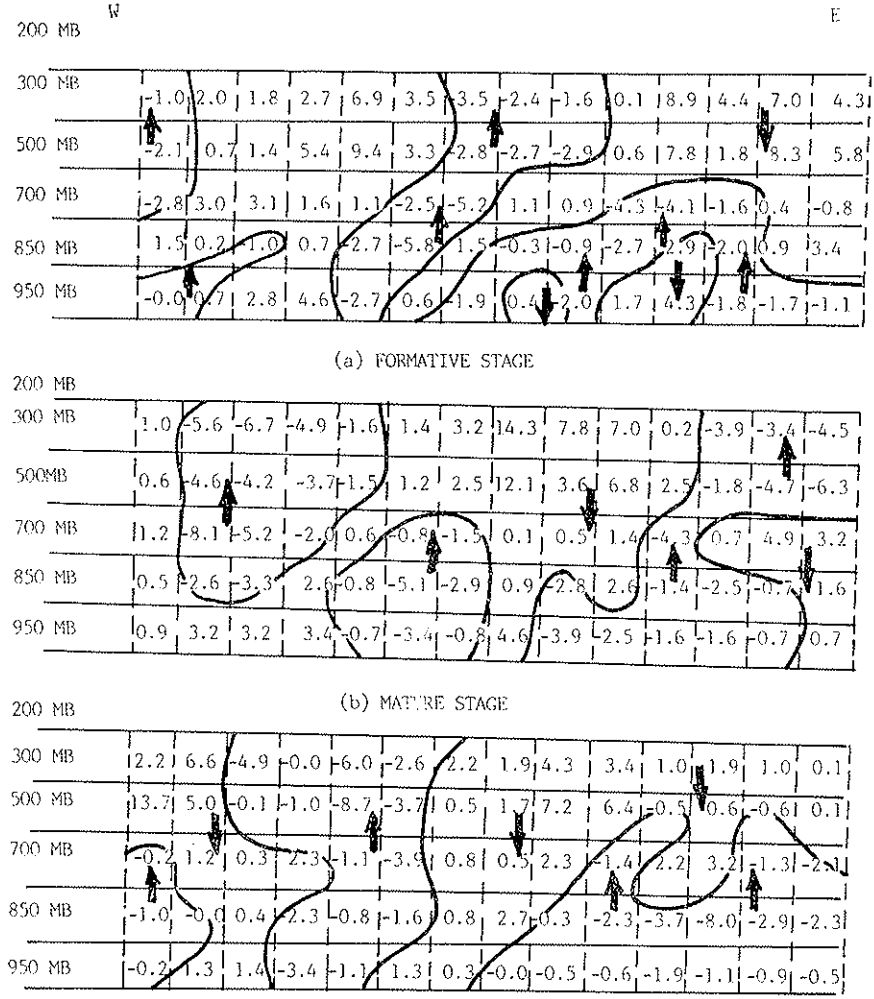

FIG. 4.19. E-W. Cross section of the vertical motion field through the centre (units = 10^{-3}mb/sec.).

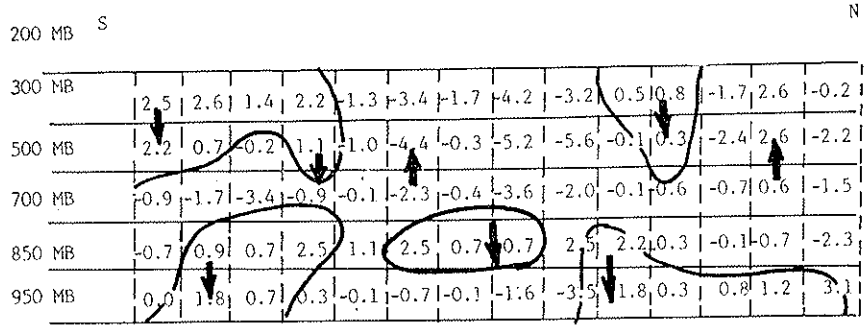

(a) FORMATIVE STAGE

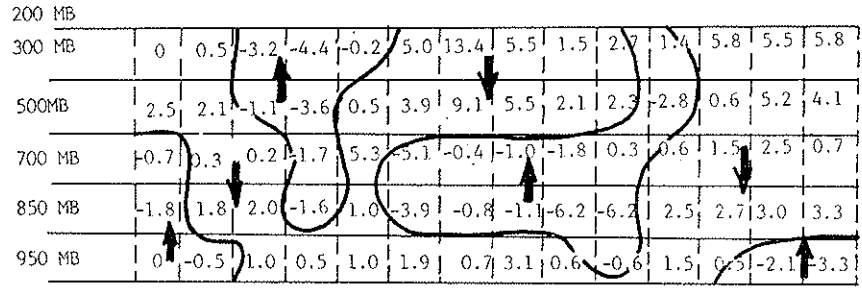

(b) MATURE STAGE

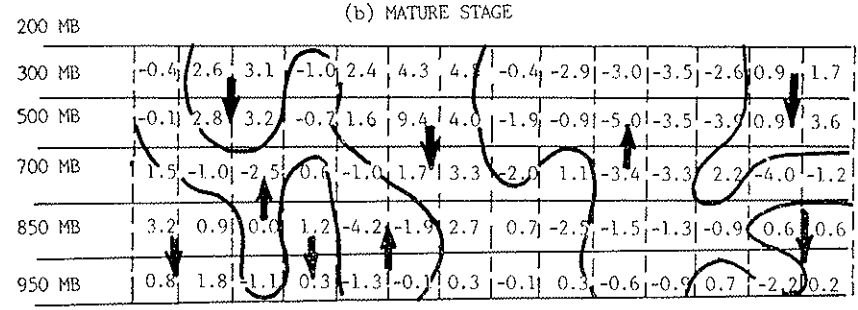

(c) DISSIPATION STAGE

FIG. 4.20. N-W. Cross section of the vertical motion field through the centre (units = 10^{-3}mb/sec.).

4.6 Summary

The salient features from the studies discussed in this section are given below:

i) Over 80 percent of monsoon depressions forming in the Bay of Bengal seem to develop out of the remnants of the tropical disturbances from the east. 15 to 20 percent depressions form *in-situ* in the Bay of Bengal.

ii) Northwest Bay of Bengal has the highest SGP for the genesis of tropical disturbances and is comparable to the developing pre-hurricane clusters in the Atlantic Ocean.

iii) The steering concept and other synoptic associations like shift of rain belt, pressure departure, thermal thickness and the existence of a high amplitude trough can provide good aid for forecasting the movement of tropical depressions.

iv) The thermal structure of the composited land depressions is cold cored in the lower level (up to 700 mb), becoming warm cored between 500 and 300 mb level and again cold cored beyond 200 mb level.

v) Compared to non-deepening lows studied by Murakami, the systems investigated in the present study even in a formative state (low stage) show cold cored structure. This is an important observation which could be useful for prediction purposes.

vi) The warm core descends to the lower levels during the mature stage, suggesting that CISK is playing an active role during development. *At the mature stage, the central region is warmer level by level compared to the formative stage.*

vii) Besides getting a rainfall maximum in the southwest sector as in the case of depressions of sea origin, there is another rainfall maximum to the north of the centre at about 300 km. The vertical motion field also supports this observation. This information could be very useful for the issuance of heavy rainfall warnings.

5. TELECONNECTIONS AND MONSOON ACTIVITY

Right from the beginning, man has been seeking linkages of weather events occurring at different places. The lag in their occurrence becomes a useful predicter. The linkages could be on a smaller or regional scale

with lag relationship of a few hours to a few days. This knowledge is used by conventional weather forecasters. In the other cases the linkages could be on a planetary or global scale with lag relationships varying from a few weeks to months, season or more. These long period links are generally associated with low frequency motions, which in the case of monsoon are associated with 10-20 day, 30-50 day time-scales to several longer time-scales such as semiannual, the annual, the quasi and southern oscillation (SO)/El Niño.

Since the last century, meteorologists have been searching for relationships of monsoon rainfall with weather events of distant regions. Above normal snowfall over the Himalayas in the pre-monsoon period was found to be negatively correlated with subsequent monsoon rainfall over India. Indian droughts were also associated with high pressure over Mauritius and Australia. Although there were other studies on the distant relationship (Hildebrandsson, 1897; Lockyer and Lockyer, 1902; the real detailed study was conducted by Sir Gilbert Walker, 1923, 1924). He observed that there are three dominant circulation features which he called North Atlantic, North Pacific and Southern Oscillations. The two northern oscillations can be represented mainly by opposition between the sub-tropical anticyclones and the low pressure areas on their poleward sides. One measure of this opposition is a measure of the strength of the westerlies of mid-latitudes. The southern oscillation (SO) is however regarded as a large seasaw of atmospheric mass between the Pacific and the Indian Ocean in the tropics and subtropics. The main opposing centres of action of the SO are located near Indonesia and the South Pacific anticyclone covering the sub-tropical eastern Pacific. Walker did not stipulate any satisfactory physical basis for these oscillations except the possibility of SO being related to some emanation from the sun. The chart of lines of equal relationship of pressure with SO showed considerable resemblance with that of equal relationship of pressure with sunspots. Nevertheless the distant relationships determined by Walker were found to be very useful for foreshadowing Indian Monsoon rainfall.

SO out of the above three oscillations gained prominence in the mid-sixties, when the observational, theoretical and modelling studies showed a strong relationship of sea surface temperature anomalies (SSTA) over the tropical eastern Pacific with SO and associated atmospheric response characteristics. Thus phenomena relating to abnormal SSTA, well known as El Niño, a Spanish name, which was originally applied to a weak warm coastal current which annually runs southwards along the coast of

Ecuador around the Christmas season. In the present scientific usage El Niño is associated with extreme warming of SST which occurs every few years with its preferred period lying in the range of 2-7 years. Various workers (Berlage, 1966 and Doberitz, 1968) provided support of a strong relationship between SSTA and atmospheric characteristics. The studies by Bjerknes (1966, 1969, 1972) and information from satellite clearly showed physical linkage of the interannual fluctuations of SST over the broad expanse of the eastern equatorial Pacific (El Niño), with SO related changes in the atmospheric fields such as changes in the zonal wind components near the equator and the large scale equatorial Pacific precipitation regimes. Notably, thus, El Niño (also called warm event) is considered an important index of SO and more broadly these phenomena are synthesized into one and also sometimes referred to as ENSO.

Sikka (1980) showed that during the period 1879-1975, 15 cases of monsoon failure were associated with El Niño events but there were 3 cases of monsoon failure which were not associated with El Niño and there were 7 El Niño events which corresponded to normal monsoon rainfall. Shukla and Paolino (1983) also found very close relationship between El Niño/SO and performance of summer monsoon. Ramage (1973) and Chiu and Lo (1979) from case studies showed significant relationship between El Niño and monsoon circulation.

In two other companion papers by Shukla and Rasmusson, there is a detailed description on ENSO and their impact on various tropical circulation features. Raman and Maliekal (1985) observed that a steep poleward directed pressure gradient anomaly gradient during January to April has a significant correlation with the monsoon activity over India. According to the authors, preceding above normal monsoon performance, there exists a negative anomaly with a steep gradient of about 15 mb directed polewards from nearly 45N. Reverse is the case preceding below normal performance of the monsoon. The authors believe the trend once set during January to April, tends to continue during June to September when the flow becomes dominating meridional which is related to below normal performance of monsoon. There are a number of questions, namely (i) are the surface pressure features so stable as to retain the same trend for such a long period of time? (ii) the significant variations are between 45N to pole with practically no significant changes equatorward of 45N. (iii) how strong is this signal and if we consider only this factor how much variance can it explain? etc.

In this section, we present re-examination of the El Niño events

listed by Quinn (1978) and Rasmusson and Carpenter (1981) vis-a-vis (i) summer monsoon rainfall over India, and (ii) frequency of formation of tropical disturbances and their predominant movement over the Bay of Bengal and the Arabian Sea.

Antarctica forms a major area in the Southern Hemisphere and as there are strong evidences that variations in the Southern Hemisphere largely influence the monsoon circulation, we strongly believe that variation of surface temperature over Antarctica can have strong physical linkage with the monsoon circulation. We also cover possible linkage between anomalies of surface temperature over Antarctica and the performance of monsoon in this section. For this purpose the following data was used.

i) Rainfall distribution for various subdivisions of India during summer monsoon for the period 1901-1982.

ii) Frequency of tropical disturbances during the period in the Bay of Bengal and in the Arabian Sea.

iii) El Niño events during the period as listed by Quinn *et al.* (1978) and Rasmusson and Carpenter (1981).

iv) Cold events, other extremes in the SO listed by various authors (e.g., see Bhalme and Jadav, 1984; Van Loon and Shea, 1985) for the years 1901 to 1982.

v) Antarctica monthly mean surface temperature for the years 1960 to 1982.

5.1 El Niño and Indian Weather

5.1.1 *El Niño and Performance of Summer Monsoon*

In this re-examination of the relationship of El Niño with summer monsoon rainfall, we consider a year to be a below normal year, if eight and more subdivisions recorded less than 10 percent of the normal rainfall. This criterion reflects region-wide deficiencies and has been usually considered by the planners in the agriculture sector to describe the monsoon index in India. Using this criterion, we find that there are 44 out of 82 years (1901-1982) which may be termed as deficient years. We have, in Table 5.1 tabulated these years in four different categories, namely i) years of deficit rainfall during the El Niño year, ii) years of deficit when El Niño event was present in the current as well as past year, iii) years

TABLE 5.1 - *Years when deficit rainfall in ⩾ 8 subdivision.*
(June - September)

El Niño event (Current year)		El Niño event (Current & past)		El Niño event (Past year)		No El Niño	
Year	No of subdiv.	Year	No of subdiv.	Year	No of subdiv.	Year	No of subdiv.
1902 (3)	13	1912 (3/4)	12	1901 (3)	19	1904	18
1905 (3)	24	1918 (4/2)	24	1913 (3)	19	1907	13
1911 (4)	20	1930 (3/3)	13	1915 (3)	14	1922	10
1923 (2)	10	1040 (2/2)	12	1920 (3)	21	1928	12
1925 (4)	14	1941 (4/2)	17	1945 (2)	10	1934	8
1929 (3)	15	1976 (3/1)	8	1952 (2)	14	1935	9
1932 (2)	8			1954 (3)	10	1936	8
1939 (3)	17			1959 (4)	8	1937	12
1951 (2)	23			1966 (3)	18	*1938	11
1957 (4)	12			1974 (4)	15	1962	8
1963 (1)	12					1968	16
1965 (3)	16					1971	11
1969 (2)	10					1979	21
1972 (4)	26						
1982 (4)	20						

Note: i) Years marked * are Cold Events.
ii) Figures in parentheses denote category.

of deficit, when El Niño event was in the past year and iv) years of deficit not associated with El Niño. It may be seen that 33 out of 44 deficit years can be associated with either present or past El Niño event and there are 13 (i.e., more than 25 percent of the cases) where the rainfall has been deficit but no El Niño. Years 1904 and 1979 stand out as very spectacular cases when even though these were not El Niño years, still these were significant deficit years when there was deficit in 18 and 21 subdivisions respectively (cases of major droughts).

In Table 5.2 we present similar statistics for 38 years when the monsoon rainfall was deficit in 7 or less than 7 subdivisions. The statistics show that there were 23 years which were associated with El Niño events in the current or the past year or both when the general

performance of the monsoon was good. This also includes cases of 1917, 1926, 1933, 1964, 1970 and 1975 when deficit was only in 2 or less than two subdivisions. Out of these 23 cases, there were a number of years which followed one or two consecutive deficit rainfall years. Although physical reasons are not understood, long term statistics of rainfall data show that there is no case when more than two consecutive years had deficit monsoon rainfall and a few cases when one deficit year was followed by another deficit year. Thus if we consider the combined effect of El Niño which is a planetary scale feature and regional phenomenon, exact physics not known, but which inhibits existence of consecutively two

TABLE 5.2 - *Years when deficit of rainfall* $\leqslant$ 7 *sub-division.*

(June - September)

El Niño event (current year)		El Niño event (current & past)		El Niño event (past year)		No El Niño	
Year	No of sub-div.	Year	No of sub-div.	Year	No of sub-div.	Year	No of sub-div.
1914* (3)	5	1919* (3/3)	3	**1903*	6	**1908	6
1917 (2)	0	1926* (4/4)	1	**1906	6	1909	2
1943 (2)	5	1944 (2/2)	6	**1924*	6	1910	1
1946* (1)	5	1958 (4/4)	5	1927	7	**1916	0
1948 (1)	5	**1973 (4/4)	3	**1931*	7	1921	5
1953* (5)	3			1933*	2	1950	3
1975* (1)	1			**1942*	4	1955	6
				1947	6	1956	3
				**1949	6	1960	6
				**1964*	2	1961	5
				**1970	2	1967	7
						1977	7
						**1978	3
						1980	6
						1981	6

Note: i) Years marked * follow deficit years
Years marked ** are Cold Events.
ii) Figures in parenthesis denote category.

or more deficit years, we can conclude that most of the El Niño events are associated with years of deficit rainfall over India.

Thus establishment or knowledge of likely occurrence of El Niño can provide a useful guidance for long range forecasting of the monsoon rainfall, but its existence or otherwise cannot be used as a foolproof tool for long range forecasting. To prove this we note that there have been cases of large-scale deficit (1904 and 1979) which were not associated with El Niño and there were cases of good monsoon years in the El Niño years (1917, 1926).

5.1.2 *Cold Event and Summer Monsoon Rainfall*

As given by Van Loon (1985), the other extreme of El Niño or warm events (WE) are termed as Cold Events (CE). He observed that during the period 1901-1982, there had been 16 CE (1903, 1906, 1908, 1916, 1920, 1924, 1931, 1938, 1942, 1949, 1954, 1964, 1966, 1970, 1973 and 1978). Taking the analogy that WE are related to deficit monsoon rainfall, the CE can be positively related to normal rainfall. Out of the 16 CE years, there are four years, 1920, 1938, 1954, 1966, which experienced deficit rainfall in 21, 11, 10 and 18 subdivisions respectively; the rest of the 12 CE years were associated with good performance of monsoon rainfall (when the deficit was in 7 or less than 7 subdivisions).

5.1.3 *El Niño and Tropical Disturbances in the Bay of Bengal and the Arabian Sea*

We also examined if El Niño event has any relationship with the frequency of the formation of the tropical disturbance over the Indian Sea. For this purpose, we took the data for the period 1901-1980 to compute the mean annual frequency. The deviation of each year from the mean was then calculated. These deviations in two categories have been presented in the table 5.3 and 5.4 in the same way as in the tables 5.1 and 5.2. In table 5.3 we present the case of the years when the deviation was positive and greater than 20 percent and table 5.4 contains the same information when the percentage departure is negative below -20.

Table 5.3 shows that the years of higher frequency of tropical disturbances are also El Niño years, but table 5.4 provides contradictory

TABLE 5.3 - *Frequency of Tropical disturbances. Percentage departure* > 20.

El Niño event (Current year)		El Niño event (Current & past)		El Niño event (Past year)		No El Niño	
Year	Departure	Year	Departure	Year	Departure	Year	Departure
1925 (4)	49	1973 (4/4)	27	1947 (1)	34	1937	43
1939 (3)	42			1952 (2)	27	1961	32
1941 (4)	42			1966 (3)	34		
1944 (2)	42						
1946 (1)	27						
1948 (1)	34						
1963 (1)	27						
1975 (1)	42						

Note: Figures in parentheses denote category.

TABLE 5.4 - *Frequency of Tropical disturbances vs El Niño percentage departure* < -20.

El Niño event (Current year)		El Niño event (Current & past)		El Niño event (Past year)		No El Niño	
Year	Departure	Year	Departure	Year	Departure	Year	Departure
1905 (3)	−25	1912 (3/4)	−33	1901 (3)	−55	1904	−33
1911 (4)	−48			1913 (3)	−25	1908	−33
1914 (3)	−40			1914 (3)	−33	1909	−40
1953 (3)	−25			1920 (3)	−33	1910	−55
1957 (4)	−48			1983 (4)	−40	1913	−25
						1921	−25
						1938	−25
						1978	−25
						1980	−25

Note: Figures in parentheses denote category.

information, i.e., El Niño years are also associated with decrease in frequency. In conclusion, it may be stated that the frequency of formation of tropical disturbances over Indian seas is not related to the existence or the non-existence of El Niño.

Similar analysis for the direction of the movement, recurvature, etc., shows that there does not seem to be any change in the direction regime of movement of tropical disturbances with El Niño.

The salient results of this analysis may be summarized as follows:

i) El Niño or warm events in the majority of cases are associated with poor performance of the summer monsoon.

ii) Cold events, related to the other extreme of El Niño are commonly related to the good performance of summer monsoon.

iii) Information on establishment of El Niño/cold event clubbed with the regional information (i.e., long term rainfall records show two consecutive years are rarely deficit years and there are never more than two such consecutive years) can be used as good guidance for long range forecasting of monsoon rainfall.

iv) Existence of El Niño/cold event can be used only for guidance purposes but not as a foolproof long range forecasting tool, as India has experienced droughts during non El Niño years (1904, 1979) and good monsoon performance during some El Niño years (1917, 1926, 1942). Similarly there were years associated with cold events which had large-scale deficit (1920, 1966).

5.2 Temperature Anomaly over Antarctica and Indian Summer Monsoon

It is generally believed that the southern hemispheric circulation features play a significant role in the onset and various other phases of monsoon activity (Kumar *et al.*, 1983). The basic concept of Sir George Simpson (1921), that the monsoon is a continuation of southeasterly trade winds of the Indian Ocean, which, after crossing the equator, attain southwesterly direction due to the turning effect of coriolis force, is still valid. A conventional forecaster looks for cross equatorial flow as an important signal for the onset of monsoon over the Indian sub-continent. Datta *et al.* (1981) have also shown a northward shift for the equatorial trough as well as penetration of flow from the southern hemisphere associated with the progress of monsoon over India. The intensity and

location of the well known Mascerene high, a part of the southern hemispheric subtropical anticyclonic belt is also observed to have a great influence on the onset processes and activity of monsoon. Thus there is evidently a linkage between anomalies in the circulation features over the southern hemisphere and performance of monsoon over the Indian sub-continent. Antarctica covers a significant portion of the southern hemisphere. Moreover, compared to the Arctic, where the surface temperatures are of the order of −40°C, the temperatures over Antarctica fall below −70°C. The temperatures over and near the equatorial region remaining the same, of the order of 28°C, the temperature gradients in the southern hemisphere are much steeper. As a result the exchanges taking place between poles and equator are more marked in the southern hemisphere compared to the northern hemisphere. Anomalies in surface temperature (which is to great degree related to ice cover) and other circulation features over Antarctica could, we believe, considerably influence the circulation features over the southern hemisphere and, in turn, the monsoon circulation. The study of Antarctica is thus very interesting for understanding its possible relationship with the anomalies in monsoon circulation.

While seeking the distant relationships, Sir Gilbert Walker (1924) also observed that the December-February pressure of Mcmurdo sound (77.5S, 166.4E) in Antarctica has a positive correlation coefficient of 0.8 with the pressure over northwest India during the following March-May period and a correlation coefficient of 0.6 with the rainfall over peninsular India during the subsequent June-August period.

5.2.1 *Analysis of Temperature Field and Results*

In fig. 5.1, we show from Das and Datta (1985) temperature anomalies over SANE (70.19S, 2.21W) in Antarctica for the years 1971-1980. Qualitatively it can be seen that all the poor monsoon years in the decade (viz. 1972, 1974 and 1979) followed warm anomalies and the rest of the years which had normal or above normal monsoon rainfall followed cold epochs.

Datta (1986) further examined detailed temperature anomaly patterns for the years 1971 to 1980 and specially compared the pattern for the two sets of extreme years, 1972 and 1979, two drought years, and 1977 and 1978, good monsoon years. (Figs. 5.2 to 5.5).

It is interesting to note that the evolution of anomaly patterns during 1972, 1979 (years of poor monsoon) is distinctly different from

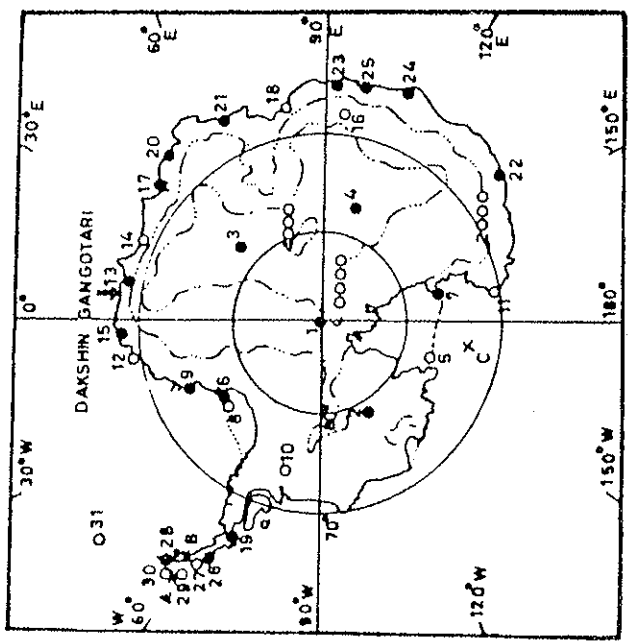

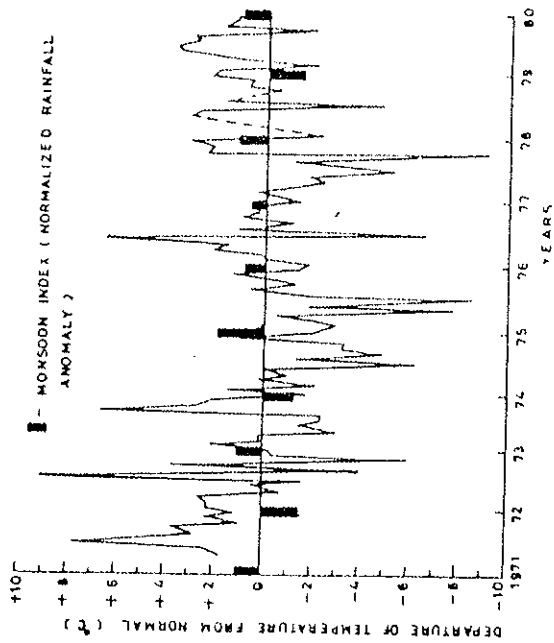

FIG. 5.1. Variation of surface temperature (departure from normal) at SANE (70.19°S, 02.21°W). Antarctica represented in thin line. Monsoon index has been plotted as normalized rainfall anomaly in black bars (dotted line shows missing data).

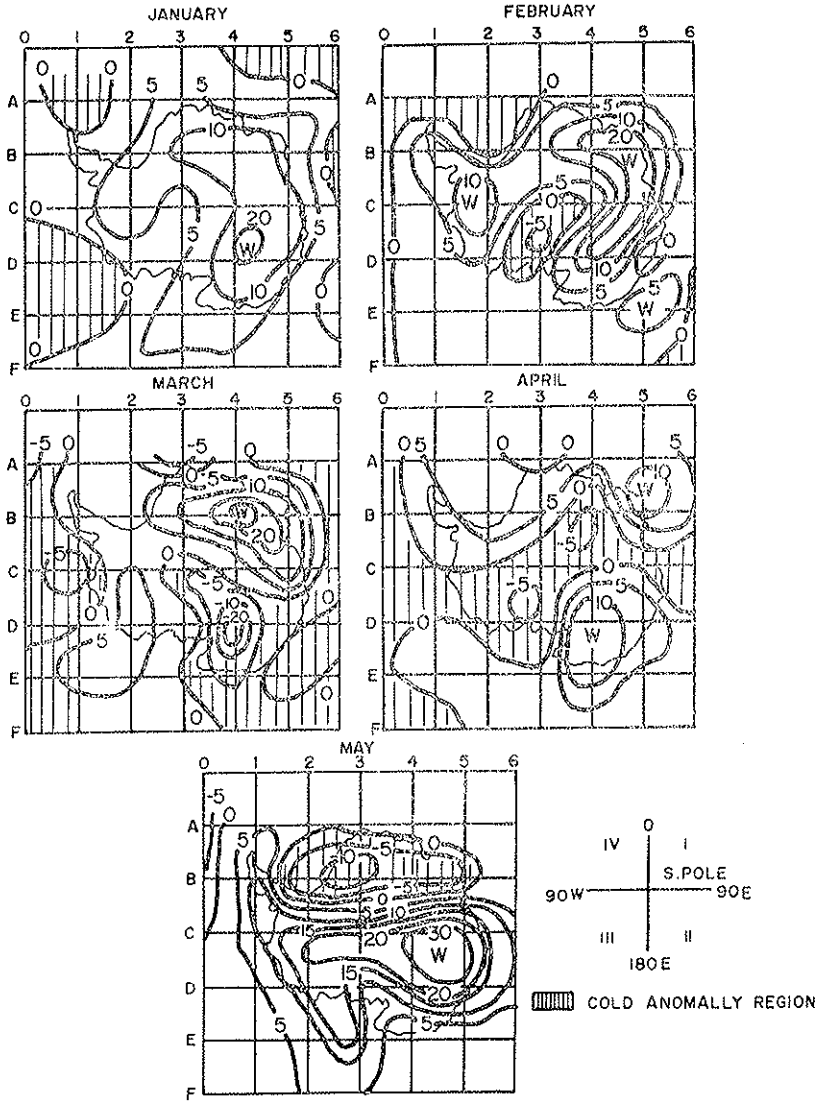

FIG. 5.2. Monthly mean surface temperature anomalies for January, February, March, April, May 1972.

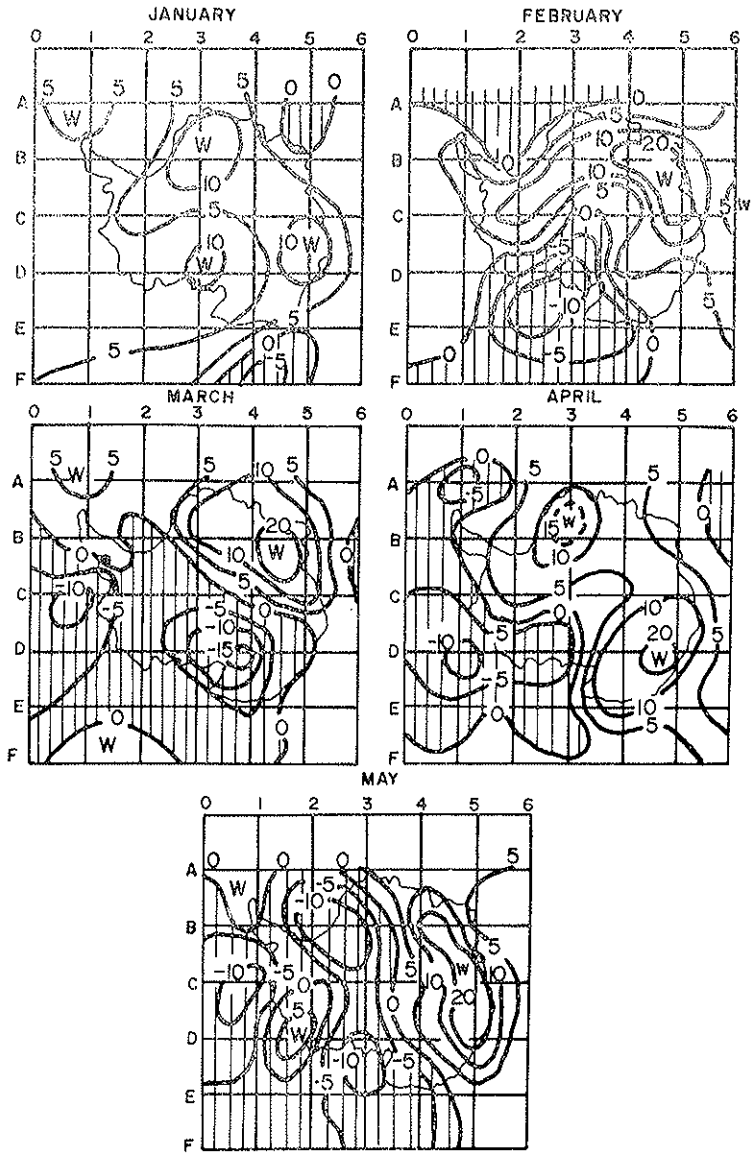

FIG. 5.3. Monthly mean surface temperature anomalies for January, February, March, April, May 1979.

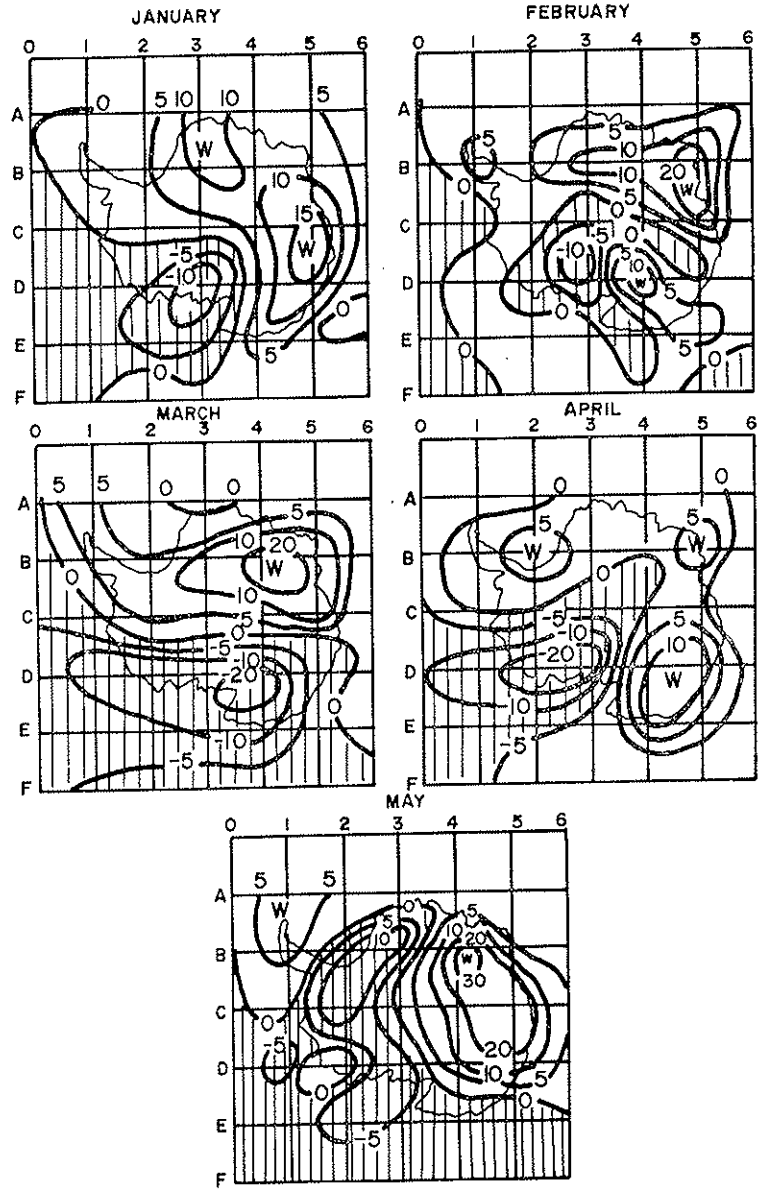

FIG. 5.4. Monthly mean surface temperature anomalies for January, February, March, April, May 1977.

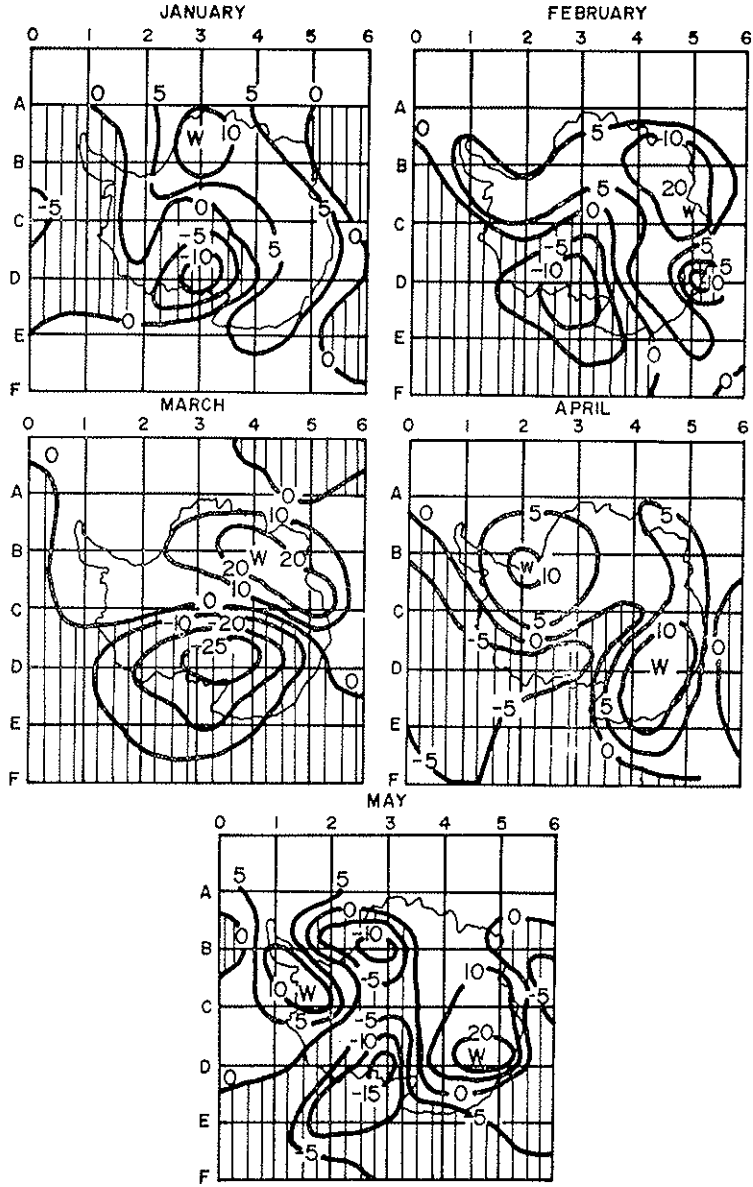

FIG. 5.5. Monthly mean surface temperature anomalies for January, February, March, April, May 1978.

that during 1977 and 1978 (good monsoon years). But between themselves, i.e., 1972, 1979 on one side, and 1977, 1978 on the other side, there is a great similarity of patterns. Salient characteristics of these patterns are summarised below. As the presentation of the patterns are on polar stereographic projection with south pole at the centre, it is convenient to consider the location of anomalies with respect to the quadrants. For simplicity we call the region of Antarctica between 0-90E quadrant I, between 90-180E quadrant II, between 180E-90W quadrant III and between 90W and E quadrant IV.

i) During January 1972, marked positive temperature anomalies (10-20°C) are shown in quadrants I and II with central portion in the quadrant II and a warm anomaly tongue in the western parts of the Antarctica. Mild negative anomaly exists in quadrants III and IV. As the season advances, there is a gradual evolution of the pattern so that most of the Antarctica is covered by positive anomaly pattern except small portions of quadrants I and IV.

ii) During 1979, the evolution of anomaly pattern is broadly similar to that of 1972, especially during January to April, except negative anomaly regions are slightly more prominent than in 1972. During May 1979, the complete Antarctica is divided alternately into the regions of positive and negative anomalies, but positive anomalies being more marked and covering most of the region.

iii) The evolution of anomaly patterns during 1977 and 1978 are very similar. Major centres of negative anomaly are located in quadrant III and adjoining quadrant IV. This gradually becomes more intense covering most of the quadrant III and parts of other quadrants with tongues of warm anomalies.

Significant contrasting patterns being gradual dominance of negative/cold anomaly over most of the Antarctica (especially over most of quadrant III and to lesser degree over adjoining quadrants II and IV) preceding good monsoon, i.e., January to May 1977 and 1978 compared to dominance of positive anomaly in the same region of Antarctica preceding droughts/deficit monsoon years of 1972 and 1979.

Similarly, examination of mean temperature anomaly over the whole Antarctica region, derived by analysis of the temperature field, is presented in fig. 5.6. It may be noticed that out of the years 1960 to 1982, the negative relationship between January to May temperature anomaly over

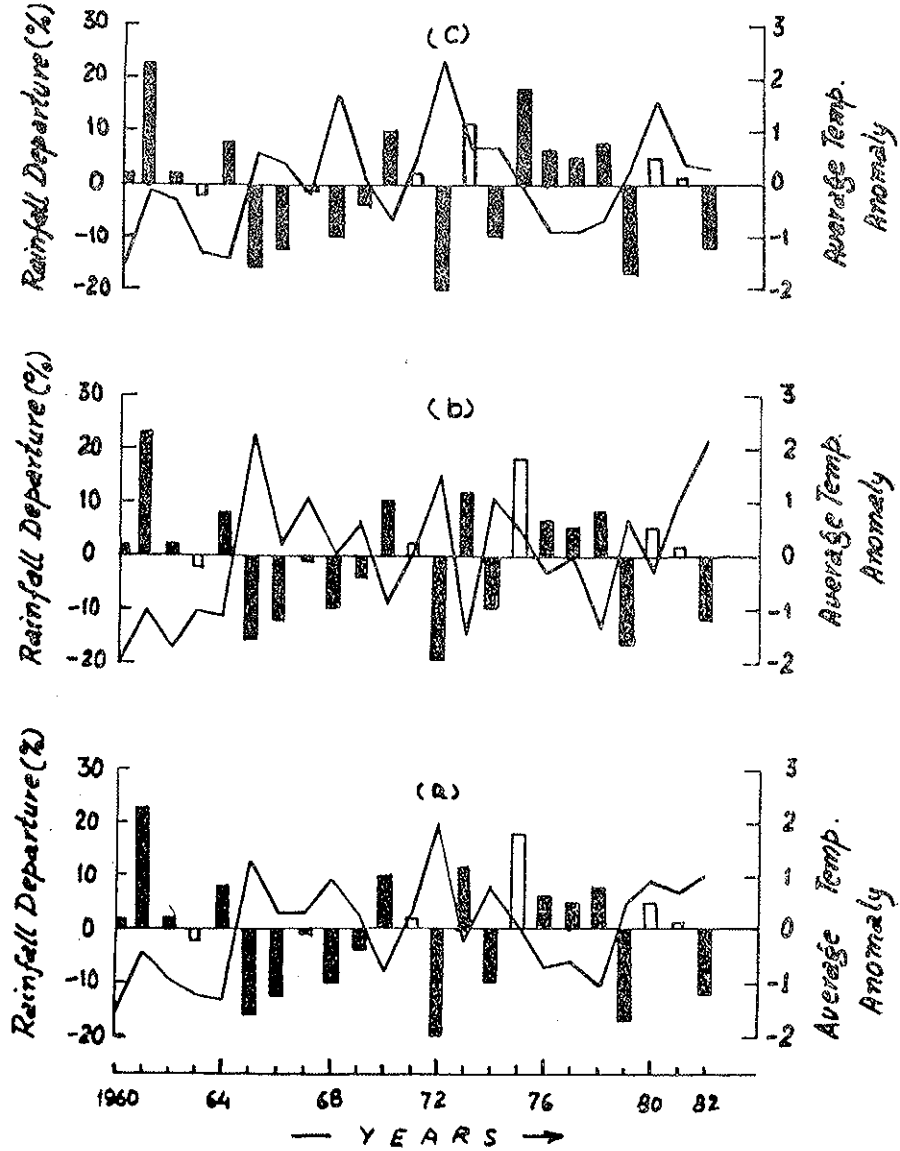

FIG. 5.6. (a) January to May; (b) January and February; (c) March to May.

——— Average Temperature Anomaly.
▬▬▬ Rainfall Departure (%).

Antarctica and performance of monsoon (June to Sept.) over India is valid in most of the years except 6 years.

These contrasting features of temperature anomaly over Antarctica leads one to hypothesize that intense negative anomaly causes steep temperature gradient between the equator and Antarctica, thereby stronger subtropical westerlies in the lower levels over the Southern Hemisphere. This could cause greater momentum transfer from the equator.

Krauss (1977) also observed that during 1972 (a general drought year) 700 mb surface over Antarctica was abnormally warm and height of 700 mb and 500 mb higher than the normal. The similar situation was reflected in the mean 500 mb height over Antarctica, where for the group of two contrasting years 1958-1964 (generally good monsoon years) and 1968-74 (a number of drought years), the mean 500 mb height during dry years was higher than the other years. The difference between these groups was significant and almost double the standard error. Meridional slope from tropic to Antarctica of 500 mb surface is therefore reduced in the case of dry years compared to other years (1958-1964). This observation when combined with surface temperature anomaly patterns presented above, may show that these teleconnections are not accidental. No doubt, more theoretical and simulation studies are necessary to bring up these linkages on the same level as ENSO.

Thus there are a number of distant circulation features and their anomalies which seem to have significant linkages with the performance of monsoon. Prominent among these are ENSO, snow cover anomalies over Asiatic land and temperature anomaly over Antarctica, etc. It is now well understood that the tropical circulation is controlled by the combined effect of meridional and zonal overturnings of Hadley and Walker cells respectively. It would be interesting to understand the influence of ENSO, snow cover anomaly, anomalies over Antarctica and other similar features of the Hadley and Walker circulation in a quantitative manner. Such an understanding is expected to improve long range forecasting techniques.

REFERENCES

ANANTHAKRISHNAN R. and BHATIAL K.L., Proc. Symp. on Monsoon of the World, New Delhi, pp. 157-172 (1958).

ANANTHAKRISHNAN R. and RAMAKRISHNAN A.R., Proc. Symp. Met. results IIOE, pp. 415-419 (1965).

ANANTHAKRISHNAN R. *et al.*, IMD FMU, report No. IV, 18-1-1967.

ANANTHAKRISHNAN R. *et al.*, IMD FMU, report No. IV, 18-2-1968.

ANANTHAKRISHNAN R., Proc. Symp. Monsoon Indian Inst. Trop. Met. Pune, pp. 254-324 (1976).

BANSAL R.K. and DATTA R.K., « IJMG », *23*, 503-506 (1972).

BEDEKAR V.C. and BANERJEE A.K., « IJMG », *20*, 23-30 (1969).

BEDI H.S. and BINDRA M.M.S., « Tellus », *32*, 296-298 (1980).

BERLAGE H.P., K. Ned, Meteorol. Inst. Meded Verh, 88, 152 pp. (1966).

BJERKNES J., « Tellus », *18*, 820-829 (1966).

BJERKNES J., « Mon. Wea. Rev. », *97*, 163-172 (1969).

BJERKNES J., « J. Phy. Oceanogr. », *2*, 212-217 (1972).

BOOGARD H.V., *The mean circulation of the tropical and sub-tropical Atmosphere*. NCAR Tech. Note, 118 pp. (1977).

CARR F., *Monsoon Dynamics*. Edited by T. N. Krishnamurti (1978).

CHARNEY J.G. and DE VORE J.G., « JAS », *36*, 1205-1216 (1979).

CHAUDHARY A. and RAO G.A., Proc. Symp. on Trop. Monsoon, IITM Pune (1976).

CHIU W.C. and LO A., « Mon. Wea. Rev. », *107*, 18-25 (1979).

DAGGUPATTY S.M., Ph. D. Thesis, Pune Univ. (1967).

DAS P.K., « Tellus », *14*, 212-220 (1962).

DAS P.K., DATTA R.K. and CHHABRA B.M. « IJMG », *22*, 331-336 (1971).

DAS S.K. and DATTA R.K., « Mausam », *36*, 525-26 (1985).

DATTA R.K. and GEORGE C.J., « IJMG », *17*, 157-162 (1966).

DATTA R.K., « Proc. Symp. Indian Ocean, NISI », *38*, 943-952 (1967).

DATTA R.K., « IJMG », *26*, 405-409 (1975).

DATTA R.K. and MUKHERJI T.K., « IJMG », *26*, 399-404 (1975).

DATTA R.K. *et al.*, Proc. Symp. Monsoon Dynamics IIT, New Delhi (1978).

DATTA R.K., Monsoon Dynamics, Cambridge University Press, pp. 333-349 (1980).

DATTA R.K., RAO A.V.R.K., PURI S.R. and LAL M., Proc. Int. conf. on scientific results of MONEX, Despar Bali, Indonesia, WMO, Geneva, Oct. 1981, pp. 6-35.

DATTA R.K., RAO A.V.R.K., LAL B., PURI S.R. and LAL M., International Conf. on Early results of FGGE and large scale aspects of Monsoon Exp., Tallahassee, USA, WMO, Geneva, 13-4, 13-8-1981.

DATTA R.K., IMD Prepublished scientific report 86/3, Aug. (1986).

DEBOIS M. and CADET D., Personal communication (1979).

DHAR O.N. and BHATTACHARYA B.K., « Vayu Mandal », *3*, 76-79 (1973).

DOBERITZ R., « Bonner Meteor Abhand », *8*, 61 pp. (1968).

ELIOT J., « Mem of IMD », *2*, 217-448 (1884).

ESTOQUE M.A. and JING J.G., University of Miami T.R., pp. 81 (1981).

FINDLATER J., « QJRMS », *95*, 362-380 (1969a).

FINDLATER J., « QJRMS », *95*, 400-403 (1969b).

FLOHN H., Proc. Symp. Monsoon of the World, New Delhi, pp. 75-88 (1960).

FLOHN H., « Bonner Meteor Abhand », *4*, 83 (1964).

FLOHN H., WMO Tech. Note No. 69, pp. 245-252 (1965).

FROST R. and STEPHENSON P.M., Geophysics Mem., No. 109, London H.M.S.O. (1965).

GEORGE P.A., « IJMG », *7*, 225 (1956).

GEORGE C.J. and DATTA R.K. « IJMG », *16*, 213-230 (1965).

GODBOLE R.T., « Tellus », *29*, 25-41 (1977).

GRAY W.M., Rep Tropical Oceans, UK (1979).

HILDERBRANDSSON H.H., *Quelqes recherches sur les entrés d'action de l'atmosphère.* Kon. Vetens. A Kad Handl., 29, 33 pp. (1897).

IYER DORAISWAMY V., « Mem of IMD », *26*, 6 (1938).

JOSEPH P.V., Proc. of International Conference on Scientific results of Monsoon Experiment, Denspar Bali, Indonesia, Oct., 1981. WMO, Geneva.

JOSEPH P.V. and RAMAN P.L., « IJMG », *17*, spl., 163-182 (1966).

KESHAVAMURTY R.N., « J.A.S. », *39*, 1241-59 (1982).

KOTESWARAM P., « IJMG », *1*, 162-164 (1950).

KOTESWARAM P. and GEORGE C.A., « IJMG », *9*, 9-22 (1958).

KOTESWARAM P., « Tellus », *10*, 43-57 (1958).

KOTESWARAM P., Proc. Symp. Monsoons of the World, New Delhi, India, pp. 105-110 (1960).

KOTESWARAM P. and GEORGE C.A., Proc. Symp. Monsoons of the World, New Delhi, pp. 145-150 (1960).

KOTESWARAM P. and BHASKARA RAO N.S., « Aust. Met. Mag. », *42*, 35-55 (1963).

KOTESWARAM P., RAO C.P. and KRISHNAMURTY M., Being published in Mausam (1986).

KRISHNAMURTI T.N. and HAWKINS R.S., « J. App. Met. », *9*, 442-458 (1970).

KRISHNAMURTI T.N. and BHALME H.N., « J. Atmospheric Sci. », *33*, 1937-1954 (1976).

KRISHNAMURTI T.N. *et al.*, FGGE operational report, series 9, part B, 115, 166 (1980).

KRISHNAMURTI T.N. and SUBRAHMANYAM D., Prepublished report of FSU, Tallahassee, Florida (1982).

LOCKYER N. and LOCKYER W.J.S., *On the similarity of the short period pressure variations over large areas.* « Proc. Roy. Soc. London », *73*, 457-470 (1902).

MADDEN R.A. and JULIAN P.R., « J. Atmos. Sci. », *28*, 702-708 (1971).

MADDEN R.A. and JULIAN P.R., « J. Atmos. Sci. », *29*, 1109-1123 (1972).

MALURKAR S.L., « Mem. of IMD », *28* (IV), 139-170 (1950).

MANDAL G.S. *et al.*, Proc. Symp. Monsoon Dynamics IIT. New Delhi (1979).

MCBRIDE J.L., Dept. of Atmos. Sciences, State Univ. USA, paper No. 308 (1979).

MILLER F.R. and KESHAVAMURTY K.N., Atmospheric response to heat sources during July UH Met, 74-04, Dept. of Met. Univ. of Hawaii (1974).

MISHRA S.K. and SALVAKAR P.S., « JAS », *37*, 383 (1980).

MONEX, *Stands for Monsoon Experiment of 1979* (1979).

MUKERJEE B.K. *et al.*, « Mon. Wea. Rev. », *107*, 1581-88 (1979).

MUKHERJEE A.K. and SHAH K.C., International Conf. on early results of FGGE and large scale aspects of Monsoon Expt, Tallahassee Florida, USA, WMO Geneva, pp. 12-34 (1981).

MUKHERJI T.K., « IJMG », *13*, 571 (1962).

MULKI G. and BANERJEE A.K., « IJMG », *17*, 8-14 (1960).

MULL S. and RAO Y.P., « Ind. J. Phy. », *23*, 371-377 (1949).

MURAKAMI M., « J. Met. Soc. of Japan », *54*, 175 (1976).

MURAKAMI M., « J. Met. Soc. of Japan », *55*, 442-448 (1977).

NATARAJA PILLAI M., Proc. IIOE Symp., pp. 413-414 (1965).

O'BRIEN J.J., « J. App. Met. », *9*, 197-203 (1970).

PALMEN E., « J. Met. », *13*, 313-315 (1956).

PANT P.S. and VERNEKAR A.D., « Proc. IGY Symp. », *2*, 20 (1963).

PISHAROTY P.R. and ASNANI G.C., « IJMG », *8*, 15-20 (1957).

PISHAROTY P.R. and ASNANI G.C., Proc. Symp. Monsoon of the World, New Delhi, pp. 112 (1960).

PRASAD K. and KRISHNA RAO D., « IJMG », *25*, 265-268 (1974).

QUINN W.H., *Monitoring and predicting El Niño inversion.* « J. App. Met. », *13*, 825-830 (1974).

QUINN W.H., ZOPF D.O., SHORT K.S. and YANG R.T.W.K., *Historical trends and statistics of the southern oscillation El Niño and Indonesian droughts.* « Fish. Bull. », *76*, 663-678 (1978).

RAMAGE C.S., Monsoon Meteorology, Academic Press, N.Y. (1971).

RAMAGE C.S., *Preliminary discussion of the meteorology of* 1972-73 *El Niño.* « Bull. Am. Met. Soc. », *56*, 234-242 (1975).

RAMAMURTHI K.M. and JAMBUNATHAN R., Proc. Symp. Met. results IIOE, pp. 371 (1965).

RAMAMURTHY K., IMD, FMU report, IV, 18-3-1969.

RAMAN C.R.V. and RAMANATHAN Y., « Nature », *204*, 31-35 (1964).

RAMAN C.R.V. *et al.*, « Weather », *34*, 252-257 (1979).

RAMAN C.R.V. and MALJEKAL J.A., « Nature », *314*, 430-432 (1985).

RAMANNA G.R., « IJMG », *20*, 148-150 (1965).

RAMASWAMY C., « Tellus », *8*, 26-60 (1956).

RAMASWAMY C., « Tellus », *14*, 337 (1962).

RAMASWAMY C., Prince, Mukarram Jah Lectures (1967).

RAO Y.P., « QJRMS », *90*, 190-194 (1964).

RAO K.V. and RAJAMANI S., « IJMG », *23*, 247-248 (1972).

RAO D.K. and DATTA R.K., « IJMG », *26*, 405-409 (1975).

RAO Y.P., Meteorological monograph of India Meteorological Departmen, India (1976).

RASMUSSON E.M. and CARPENTER T.H., *Variations in tropical sea surface temperature and surface wind fields associated with SO/El Niño.* « Mon. Wea. Rev. », *8*, 354-384 (1981).

RIEHL H., *Tropical Meteorology.* McGraw Hill Publ., New York (1954).

ROWNTREE P.R., *The influence of tropical east Pacific Ocean temperature on the atmosphere.* « Quar. J. Roy Met. Soc. », *98*, 290-321 (1972).

ROY A.K., IMD Tech., Note No. 16 (1946).

ROY S.C. and ROY A.K., « Bettr. Phy. Frei. Atmos. Leipzig », *26*, 224-234 (1930).

SANDERS F., Proc. Int. Conf. on Early results of FGGE and large scale aspects of MONEX Tallahassee, USA (WMO Publ.), II-8 to II-15 (1981). (MONEX, *Monsoon Experiment*).

SHUKLA J., D. Sc. thesis, MIT, Cambridge, USA (1976).

SHUKLA J., *Monsoon Dynamics* (Ed. Krishnamurti T.N.), pp. 1440-1462 (1977-78).

SHUKLA J. and PAOLINO D.A., *The southern oscillation and long range forecasting of the summer monsoon rainfall over India.* « Mon. Wea. Rev. », *111*, 1830-1837 (1983).

SIKKA D.R., *Monsoon Dynamics* (Ed. Krishnamurti T.N.), pp. 1501-1529 (1978).

SIKKA D.R., « Proc. Ind. Acad. Sci. (Earth and Planet. Science) », *89*, 179-195 (1980).

SIKKA D.R. and GADGIL S., « Mon. Wea. Rev. », *108*, 1840-1853 (1980).

SIMPSON C.G., « QJRMS », *47*, 151-172 (1921).

SRINIVASAN V. *et al.*, IMD FMU, Report III, 2-2-1970.

SUD A.M. and DATTA R.K., FGGE operations report series 9, part B, pp. 43-50 (1980).

SUTCLIFFE R.C. and BANNON J.K., Proc. Int. Assn. Met. IUGG, Rome, pp. 322-334 (1954).

VAN LOON H. and SHEA D.J., « Mon. Wea. Rev. », *113* (1985).

WAGNER A., « Beitr. Geophysics », *30*, 196-233 (1931).

YASUNARI T., « J. Met. Soc. of Japan », *58*, 225-229 (1980).

YASUNARI T., « J. Met. Soc. of Japan », *59*, 336-354 (1981).

YIN M.T., « J. Meteor. », *6*, 393-400 (1949).

SAHEL RAINFALL, N. HEMISPHERE CIRCULATION ANOMALIES AND WORLDWIDE SEA TEMPERATURE CHANGES

C.K. FOLLAND, D.E. PARKER, N. WARD and A. COLMAN
Meteorological Office, Bracknell, UK

ABSTRACT

We present observational evidence of decadal time scale fluctuations of worldwide SST anomalies in all seasons of the year during this century. The most prominent fluctuation on this time scale since 1950 has included a relative fluctuation of SST between the oceanic hemispheres. This fluctuation has been accompanied by significantly changed circulation patterns over most of the N. Hemisphere in most months of the year; the details of these changes vary only slowly with season. Northwestern Europe, for example, has been quite strongly affected, especially in summer. An even more compelling association is that with Sahel rainfall. Model experiments confirm that summer Sahel rainfall is almost certainly affected by large scale SST patterns. The model results are presented in detail in a companion paper by Palmer (1986b); only the most salient results are reproduced here.

Interannual as well as interdecadal variations of large scale SST are used to design two statistical forecasting models that attempt to predict summer Sahel rainfall from SST anomaly patterns (referred to as SSTA below) observed in previous months. The likely longer-term skill of the forecasting models is discussed. In June 1986, the first experimental rainfall forecast for the Sahel was issued to African countries (WMO Region I) by the UK Meteorological Office for the summer 1986 season; the performance of this forecast is briefly reviewed to date.

Finally, we summarise ongoing observational and modelling studies

in the Meteorological Office which are designed to explore the consequences of observed large scale SST changes for Sahel rainfall and other climate fluctuations in more detail.

1. Introduction

The Meteorological Office possesses one of the best quality-controlled sea surface temperature (SST) data sets at present available (Minhinick and Folland, 1984; Parker *et al.*, 1987). The SST data set, formerly known as MOHSST (Meteorological Office Historical Sea Surface Temperature data set) is now a component of MOST (Meteorological Office Surface Temperature data sets) which includes several marine air temperature sets; MOST is continuously updated in near real time (Parker *et al.*, 1987). The data sets form a central component of a wide-ranging research program into the physical basis of low-frequency weather and climate variation and into practical monthly and seasonal forecasting using general circulation models and globally distributed observations. The instrumental corrections used in this paper for SST prior to 1942 are those published in Folland, Parker and Kates (1984).

Anomalies of atmospheric circulation, especially in the N. Atlantic sector, are known to have been large at certain seasons over epochs as long as decades and to have been accompanied by large scale SST variations. Examples include changes of atmospheric circulation over the N. Atlantic in winter, especially between early twentieth century decades and recent decades (Lamb, 1972; Makrogiannis *et al.*, 1982; Folland, Parker and Newman (FPN), 1985); changes in Central England temperature in October (warmer) and April (colder) in recent decades (Gilchrist, 1982; FPN, 1985); and a tendency for reduced rainfall over UK in July and August since about 1965. Fig. 1 shows graphs of Central England Temperature (Manley, 1974) for April and October plotted in the form of a 20 year running average (the series has been updated by Storey, Folland and Parker, 1985).

The interannual variability of atmospheric circulation patterns is certainly accompanied by interannual SST changes (although the extent of a direct influence is uncertain). Best known are the interactive effects of El Niño and the atmosphere (e.g., Palmer and Mansfield, 1986; Gill and Rasmusson, 1983). These interactions, (most prominent in the Pacific), are likely to have a near global scale component if only because the SST changes sometimes develop on this scale (Hsiung and Newell, 1983;

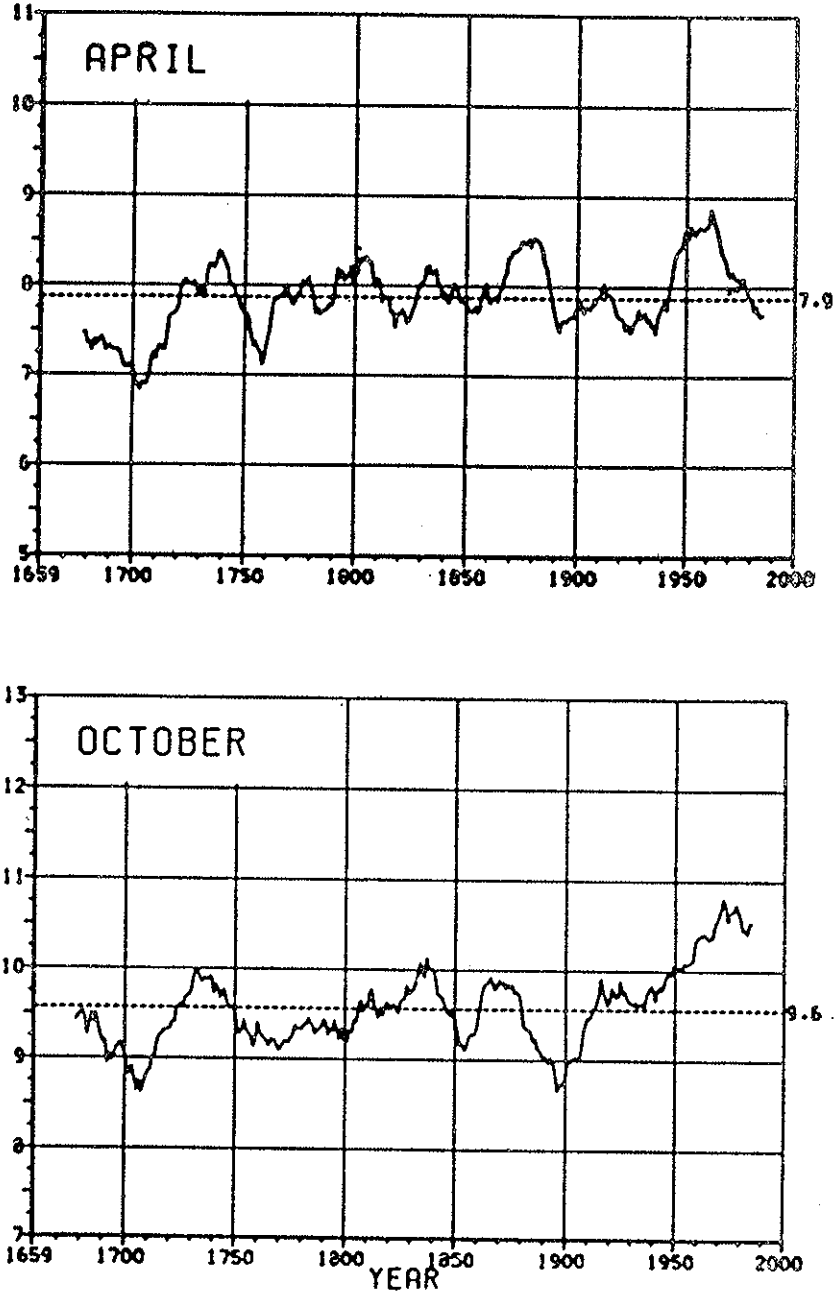

FIG. 1. Long-term changes in Central England Temperature in April and October.

Pan and Oort, 1983; FPN, 1985). On the regional scale fluctuations in the interface between the Gulf Stream and the Labrador Current have been convincingly shown to influence circulation in winter over the N. Atlantic and Europe via a positive ocean-atmosphere feedback (Palmer and Sun, 1985; Ratcliffe and Murray, 1970).

We can gain a "feel" for the worldwide effects of SST anomalies on the atmosphere using the simple physical arguments of Sawyer (1965) about the likely magnitude of the effects of SST anomalies on the atmosphere. For example, imagine a truly worldwide pattern of SST changes to be suddently "switched on" whose regional scales of anomalies having a similar sign are approximately those of the largest scale features of the atmosphere. Let the mean modulus of the anomalies be 0.3 °C. Assuming that the atmosphere is initially in its "climatological mean state", this pattern of SSTA would provide anomalous heating of these atmospheric scales with a mean modulus of about 10 Wm^{-2} over the 70% of the globe that is ocean. The local magnitude of the heating change would vary from zero to substantially larger values.

No change in average heating is necessarily implied here, only a change in its spatial distribution. 10 Wm^{-2} is about 10% of the change in the large-scale heating of the atmosphere by the oceans during the seasonal cycle; (we can imagine changes in ice cover are included). So worldwide changes of SST of this magnitude, which may not involve a globally averaged SST change, or regional changes of considerably larger magnitude (such as those associated with El Niño), can be seen as potentially large enough to affect the global atmospheric circulation.

Using MOST data, Fig. 2 shows a time-sreies of the areal-mean modulus of the changes between successive years of July and August combined SST anomaly between 1951 and 1980 on the 20×20 degree (approximately 3×10^6 km^2) space scale over about 70% of the world ocean (there are few data south of 45°S). The two-month time scale is of special interest because models run in a perpetual single-season mode indicate that the atmosphere tends to come into a near equilibrium with large-scale SST changes, certainly in the tropics, in about two months (example in Folland *et al.*, 1987). The downward trends in Fig. 2 may be the result of gradually improving data. An interannual change with a mean magnitude of 0.48 °C is large enough to affect the atmosphere, and therefore the SSTA changes may be large enough to affect regional scale climate on the interannual time scale in most years. This value may be compared with the value of 0.46 °C that corresponds

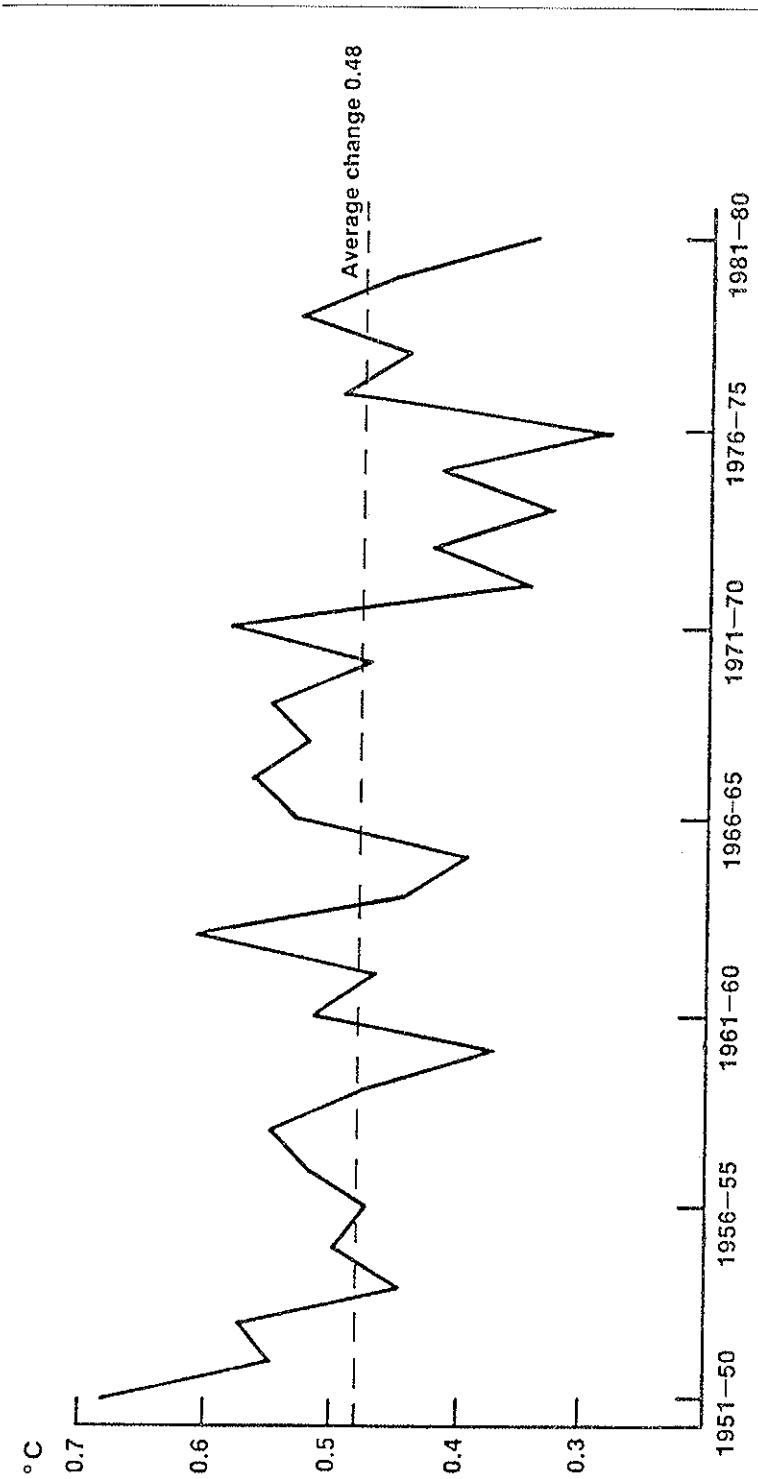

FIG. 2. Mean modulus of interannual changes in combined July and August SST anomaly. (Calculated on a $20° \times 20°$ spatial scale).

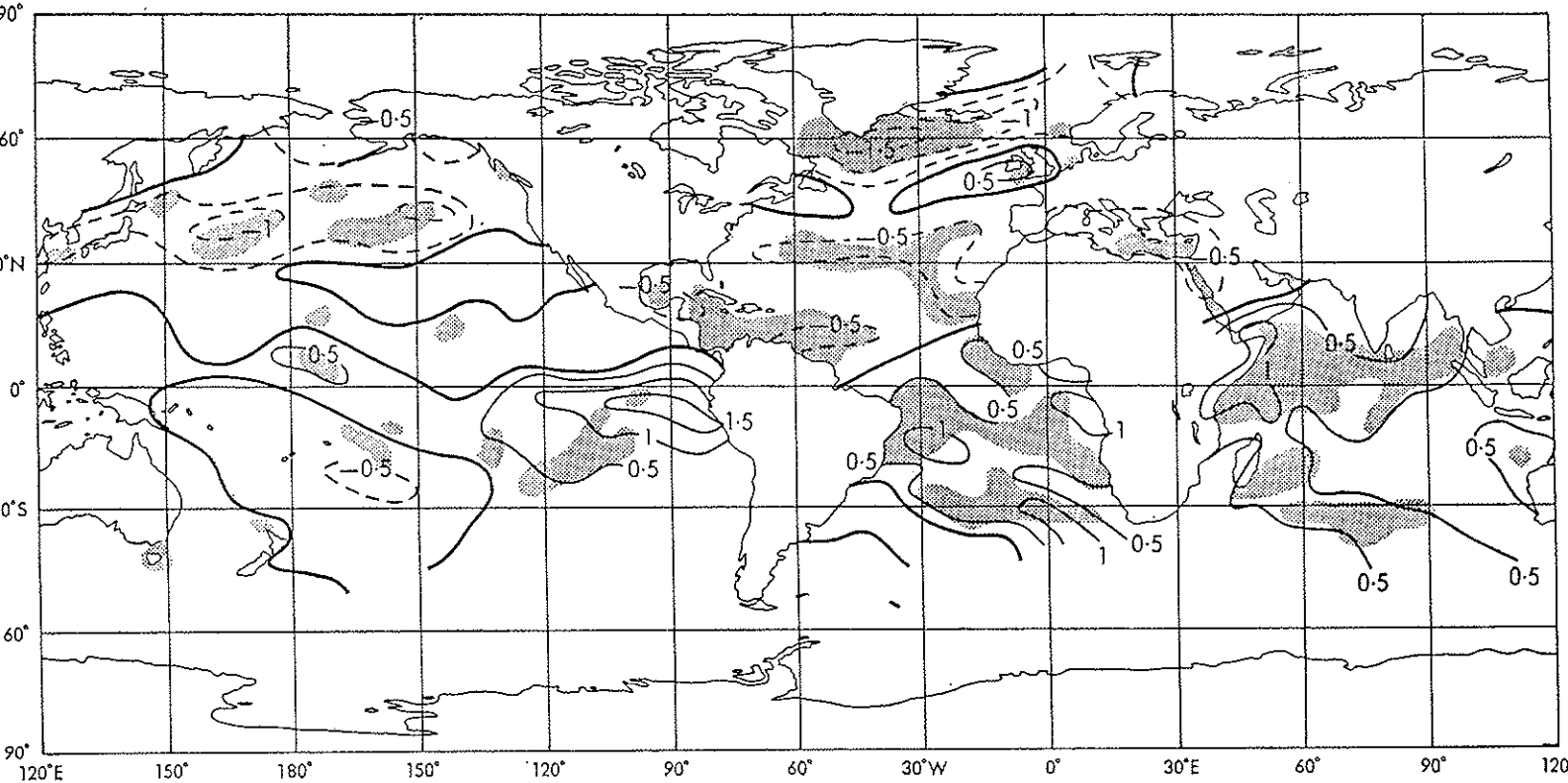

FIG. 3. Difference in July to September SST between five driest and five wettest Sahel wet seasons (1950-1984).

to the SST difference field for July to September on a 5×5 degree space scale (Fig. 3) used in the Sahel modelling experiments of Folland, Palmer and Parker (FPP) (1986).

Table 1 shows the values of two decadally averaged indices (a) the anomalies in global mean SST (July to Sept), (b) those of the Southern Hemisphere with the Northern Indian Ocean SST (SHNI) minus remainder of the N Hemisphere SST (RHN) (July to Sept.). These "slow" global scale SST changes (note their differing relative importance in different epochs) are thus about as important as the interannual two-month time scale changes on a twenty year time scale. Both appear to be of sufficient magnitude to affect the atmosphere. Therefore we suggest that the effects of observed interannual and interdecadal SST variations on regional atmospheric circulation may have been of comparable importance over the last century or so. Because the atmospheric mean flow is different in different seasons (and often in different calendar months) then it might be expected that the atmosphere would respond to these boundary value variations in a manner that varies with season. In transition seasons the atmospheric response may change appreciably from one calendar month to another. Changes in the mean circulation may be easy to discover but accompanying changes in the probability of regional circulation and surface weather extremes are more likely to be of practical importance. Section 5 describes forecasts of summer Sahel rainfall and an attempt is made to predict the probabilities of possible rainfall outcomes.

TABLE 1 - *Decadal mean July to September SST anomalies (wrt 1951-80) for the globe and for Southern Hemisphere with N. Indian Ocean, minus the rest of the N. Hemisphere.*

	Globe	SHNI-RNH
1901-10	−0.37	+0.03
1911-20	−0.33	+0.17
1921-30	−0.24	−0.08
1931-40	−0.11	−0.09
1941-50	−0.03	−0.07
1951-60	+0.04	−0.14
1961-70	−0.02	−0.08
1971-80	−0.01	+0.20

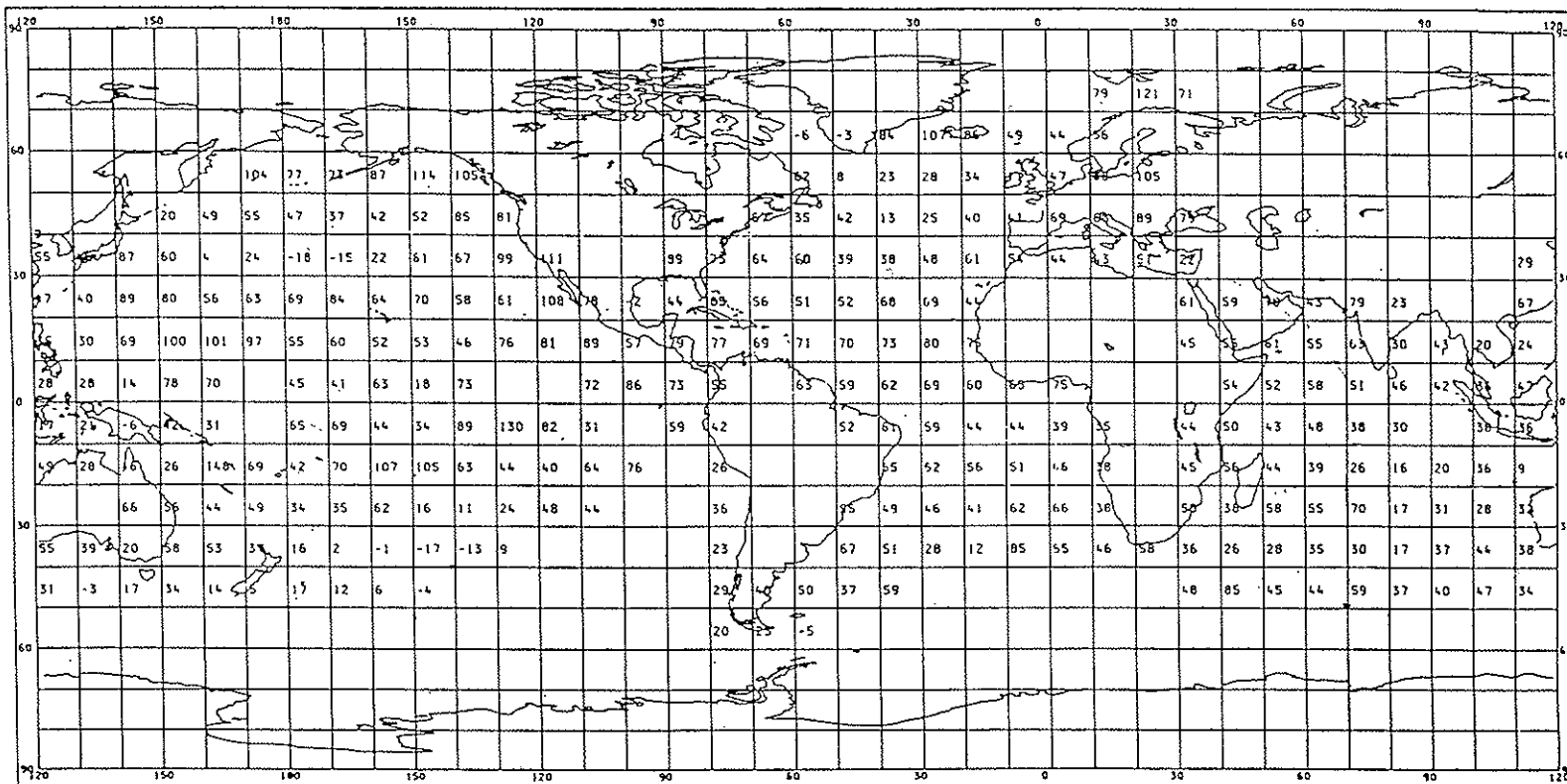

FIG. 4a. First eigenvector of worldwide SST anomaly variation, 1901-1980.

2. Worldwide patterns of SST change since 1901

Figs. 4a, 5a, 6a show the first three covariance eigenvectors of seasonal mean worldwide SST anomalies (from a 1951-80 average) calculated over all available 10×10 degree areas for 1901-80, and Figs. 4b, 5b, 6b (dotted lines) show time series of the eigenvector coefficients from 1901-1986. The EOF's were constructed using data for all seasons together. Season 1 is December-February, season 2 March to May, etc. Missing data have been "filled in" using Chebychev polynomials to interpolate in time. A 10×10 degree anomaly in a given season is regarded as being present if at least one constituent 5×5 degree anomaly is available. A full description of the technique will appear in a later paper. To show that these EOF's represent real physical properties, Figs. 4b, 5b and 6b also show time series (1901-85) of (4b) global mean in all

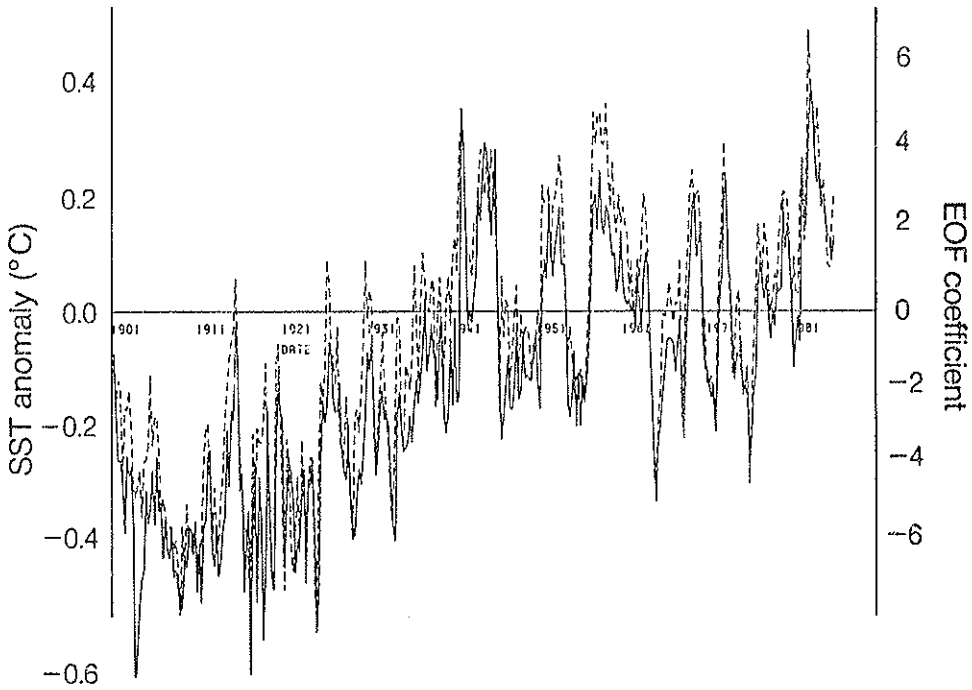

Fig. 4b. Coefficient of the first eigenvector of worldwide SST anomaly variation in Fig. 4a (dashed line), and global average SST anomaly (solid line). Values are for successive seasons (Dec.-Feb. etc.). Correlation between the two series: 0.91 (t-value, 13.8: significance $\ll 10^{-8}\%$).

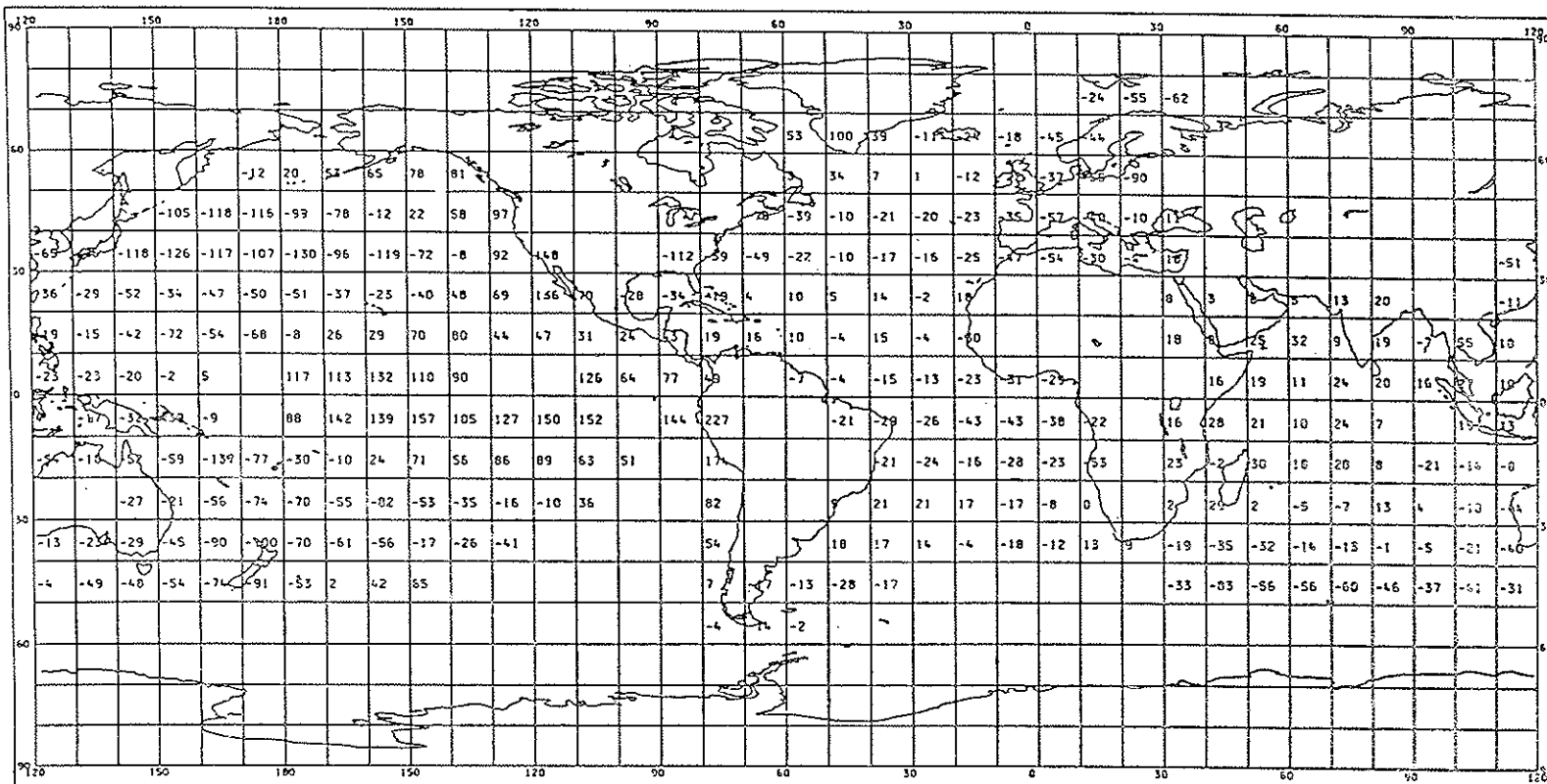

FIG. 5a. Second eigenvector of worldwide SST anomaly variation, 1901-1980.

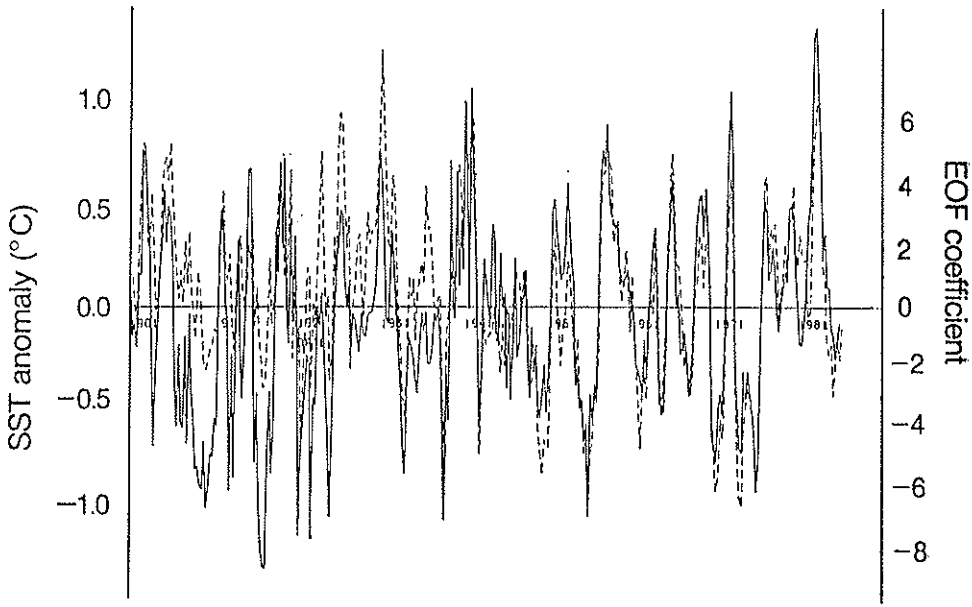

FIG. 5b. Coefficient of the second eigenvector of worldwide SST anomaly variation in Figure 5a (dashed line), and average SST anomaly in the E. Tropical Pacific (20° N-20° S), east of 170° W (solid line). Values are for successive seasons (Dec.-Feb. etc.). Correlation between the two series: 0.65 (t-value, 5.4: significance 2×10^{-4}%). (EOF leads by one season).

seasons, (5b) mean SST for tropical E. Pacific (SST is plotted one season prior to that of EOF2), and (6b) Sahel rainfall (Nicholson, 1985) plotted against the values of EOF3 in June to August. The correlations of the EOF series with the series chosen for comparison are highly significant (significance values shown on diagrams are highly significant assuming 40 degrees of freedom). In fact EOF1 is an excellent representation of the relative importance of worldwide SST changes since 1901, EOF2 is a good representation of the worldwide effects of El Niño (FNP, 1985), and EOF3 "represents" the interhemispheric SST anomalies simultaneously associated with those of Sahel rainfall on the interannual (to some extent) as well as interdecadal time scales (FPP, 1986). EOF3 is fairly similar to the SST difference field (Fig. 3) used by FPP in their modelling experiments (described in more detail in the companion paper by Palmer, 1986b) which show a prima facie case for the physical reality of a connection between Sahel rainfall and worldwide SST. So we may regard

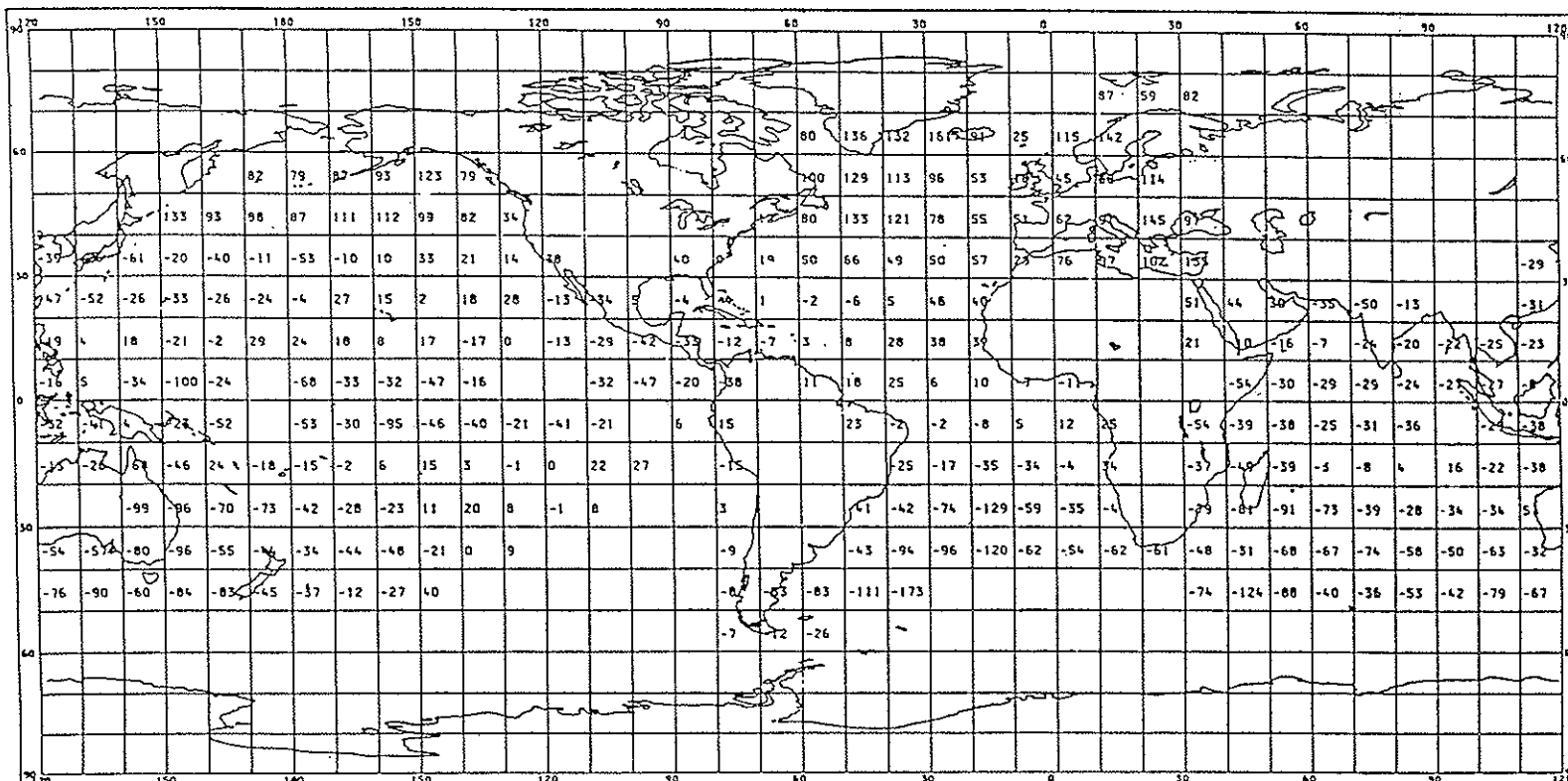

FIG. 6a. Third eigenvector of worldwide SST anomaly variation 1901-1980.

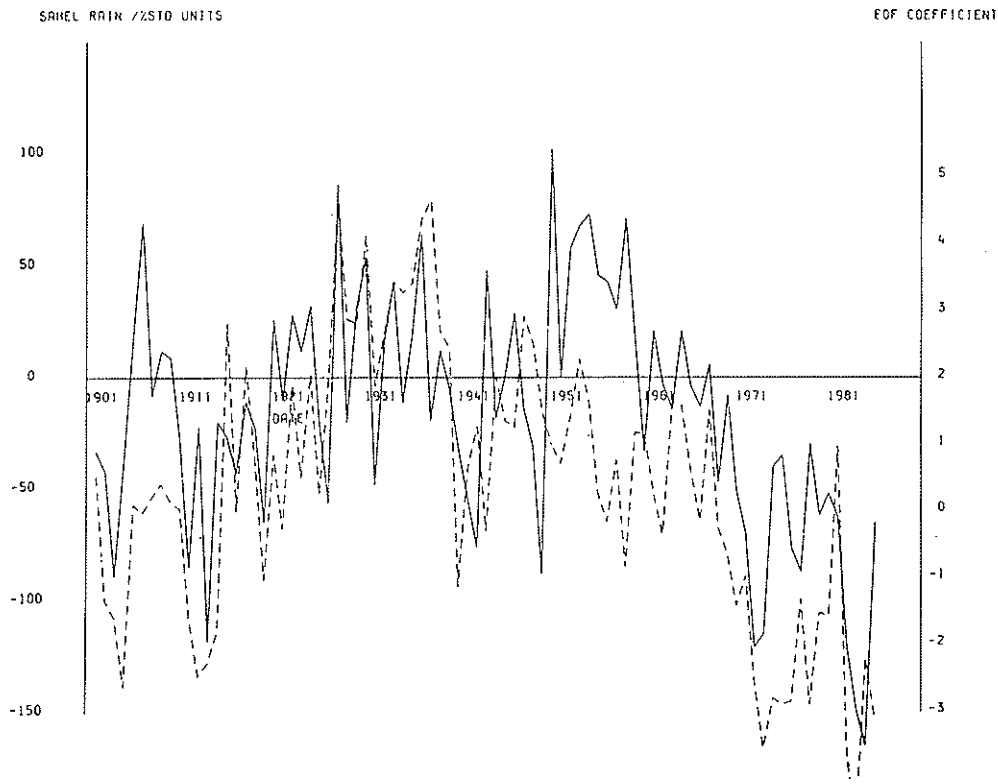

FIG. 6b. Coefficient in June to August of the third eigenvector of worldwide SST anomaly variation in Fig. 6a (dashed line), and Sahel rainfall (which falls mainly in July to September) (solid line). Correlation between the two series: 0.60 (t-value, 4.75: significance, 2×10^{-3}%).

EOF3 as one of the principal patterns of SSTA that influence Sahel rainfall. We now discuss the problem of Sahel rainfall from an observational viewpoint in more detail.

3. SAHEL RAINFALL AND WORLDWIDE SST VARIATIONS

Rainfall records for sub-Saharan North Africa have been collated and normalized by many authors. We have used an updated version of Nicholson's (1980, 1985) annual Sahel series for 1901-84 (Fig. 7a) supplemented by CLIMAT reports for 1985. Fig. 7b gives a map of

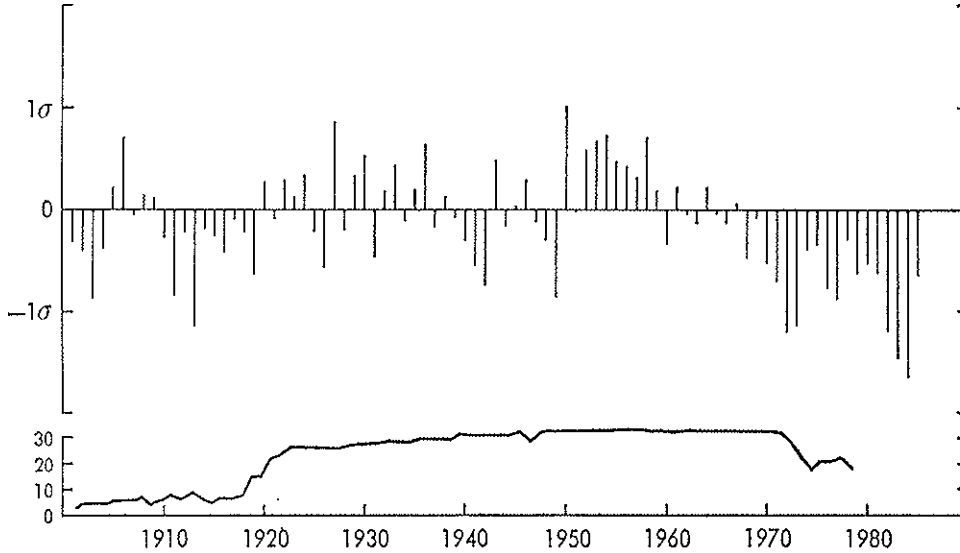

FIG. 7a. Standardized annual rainfall anomalies for the Sahel, 1901-1985 (upper panel). Values to 1984 are after Nicholson (1985): 1985 values are from CLIMAT reports. The lower panel gives the number of stations used.

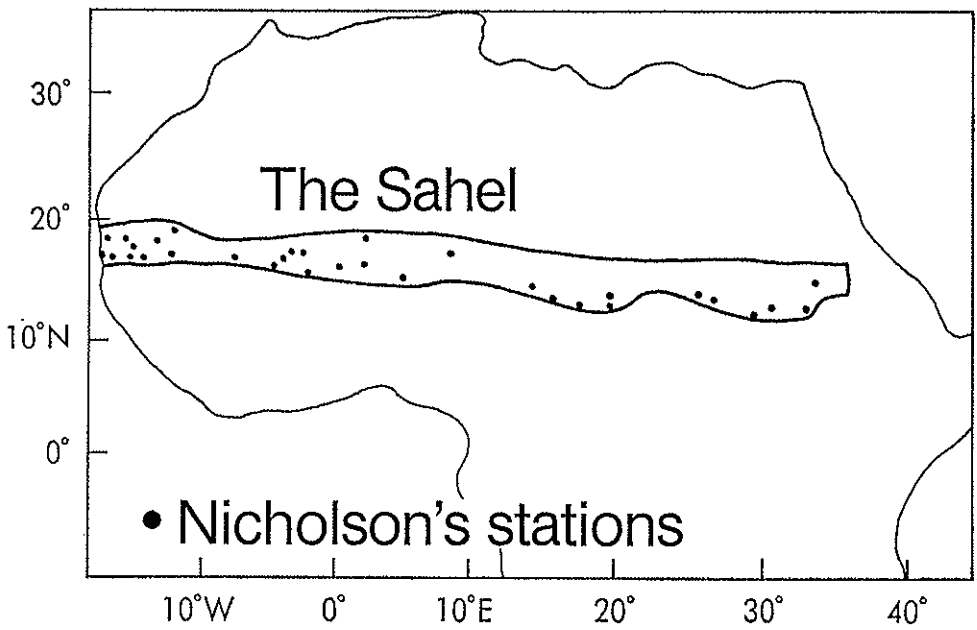

FIG. 7b. Sahel rainfall stations used by Nicholson.

the area, which stretches from Senegal to Soudan at approximately 14-18 N. Nicholson tried to homogenize her rainfall data to allow for the use of widely differing numbers of stations through time; the least reliable estimates are likely to be before 1919 and very recent ones.

Most rain falls in June or July to September or October and is associated with the seasonal movement of the Intertropical Convergence Zone (ITCZ). FPP and Palmer (1986a) suggest that the worldwide patter of SST anomalies represented by Fig. 6a (EOF3) modulates the intensity of the moisture flux convergence into the Intertropical Convergence Zone and to a limited extent modulates the latitude of the convectively active region of that zone. It is probable that the surprising sensitivity of the Sahel rainfall climate to SST is the result of a strong local positive feedback from soil moisture during the wet season (Walker and Rowntree, 1977) (high moisture flux convergence — wetter soil — more evaporation — more local precipitation, etc.) and even from seasonal variations in albedo (wetter soil gives darker soil and/or greener vegetation, etc.), though there is no direct proof of the latter effect. An important question is: could summer Sahel rainfall be predicted in advance from SSTA observed in the previous months?

FPP indicated that the spatial scale of SSTA that simultaneously affects the Sahel is considerably larger than that of the tropical N. and S. Atlantic anomalies as originally discussed by Hastenrath (1984) Lamb (1978) and Lough (1981). This is well illustrated by Table 2. Although large-scale SSTA cannot be the only controlling factor, the type of SSTA pattern represented by EOF3 has probably had (see Fig. 6b) quite a strong influence on Sahel rainfall throughout the period 1901-85. The suggestions by Lough (1981, 1986) that different factors influenced Sahel rainfall (and areas further south) prior to 1940 compared with the postwar period may be correct but Lough's arguments only referred to the influence of the tropical Atlantic. However it is unlikely that the SSTA pattern of Fig. 6a (EOF3) is the only large-scale SSTA pattern that influences Sahel rainfall.

In the current state of knowledge early progress in predicting Sahel rainfall may depend on the extent to which the many degrees of freedom in worldwide SSTA can be represented by a few important worldwide SST patterns which can occur prior to the Sahel wet season and modulate Sahel rainfall. This possibility is suggested by a statistically significant correlation ($r = 0.58$, significant at 99.9% level assuming 40 degrees of

TABLE 2 - *Correlation of July to September SST time series and Sahel rainfall, 1901-84.*

	No. Ocean SST series	r	S	σ_0 (°C)	c	m
1	Southern minus Northern hemisphere	−0.56	**	0.18	−0.15	−1.69
2	SHNI-RNH	−0.62	***	0.19	−0.15	−1.78
3	South−North Atlantic (0-30° S, 0-30° N)	−0.36		0.32	−0.19	−0.60
4	South−North Atlantic	−0.44	*	0.32	−0.24	−0.75
5	As 4 but with division at 5° N	−0.46	*	0.32	−0.25	−0.77
6	South Atlantic+S. Indian+N. Indian+ East Tropical Pacific−N. Atlantic− N. Pacific−Mediterranean	−0.67	***	0.96	−0.23	−0.38
7	As 6 but ocean areas weighted according to size	−0.62	***	0.26	−0.09	−1.26
8	As 6 but with Atlantic split at 5° N	−0.69	***	0.96	−0.23	−0.39

r, Correlation coefficient; S, significance of r (assuming only 32 degrees of freedom because of lag-autocorrelation; *=95%, **=99%, ***=99.9%; σ_0, Standard deviation of SST series (°C); c, regression constant (units are standardized Sahel rainfall); m, regression slope.

freedom), between the coefficients of EOF3 measured in March-May and the subsequent "summer" rainfall in the Sahel measured over the period 1901-85. Fig. 8 shows Nicholson's Sahel series plotted against the March-May coefficients of EOF3 for the period 1901-85. The good correlation may be a result of the persistence of this and perhaps other worldwide SSTA patterns between seasons (though exact persistence is not required, only that a characteristic SSTA pattern in, say, March-May precedes a given, perhaps different, SSTA pattern in July-September).

4. CHANGES OF N. HEMISPHERIC ATMOSPHERIC CIRCULATION SINCE 1950

Inspection of Fig. 7a shows that, in the last few decades, interdecadal fluctuations in Sahel rainfall have been especially large. We now believe that an important reason for the clear increase in the interdecadal component of Sahel rainfall fluctuations is a pattern of relative changes in

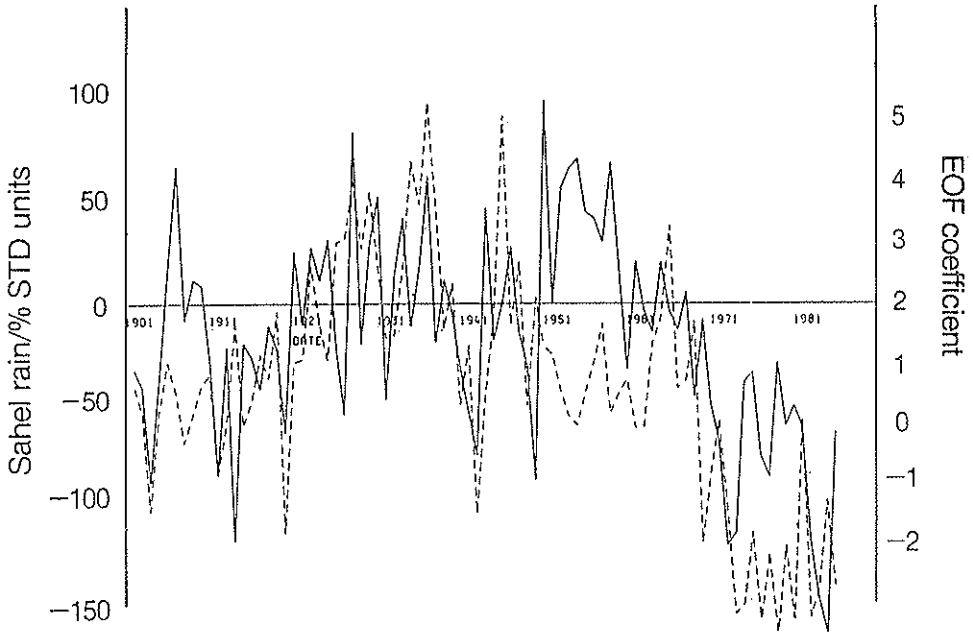

FIG. 8. Coefficient in March to May of the third eigenvector of worldwide SST anomaly variation in Fig. 6a (dashed line), and Sahel rainfall (solid line). Correlation between the two series: 0.58 (t-value, 4.50; significance, 3×10^{-3}%).

SST between the hemispheres which commenced about 1955 and appears in all seasons. This is illustrated by Figs. 9a-9d which show the SST changes (1968-84) minus (1950-59) for (i) January, (ii) April, (iii) July, and (iv) October. It is extremely difficult to estimate the statistical significance of the changes but an attempt has been made using the conservative Fisher Behrens "t" test. The "significant" areas (at the 5% level) are indicated by boxing. These cover 11-19% of the area (Table 3). The mean modulus of the difference in SST between these two periods (20 × 20 degree areas) in July is 0.31°C. Following the arguments of Section 1, this is likely to correspond (approximately) to a change of the pattern of atmospheric heating in July of mean modulus 10 Wm^{-2} in 1968-84 when applied to an atmosphere in "equilibrium" with the 1950-59 SST field. This is about 10% of that due to the annual cycle of worldwide SST between February and August. Other months show broadly similar results.

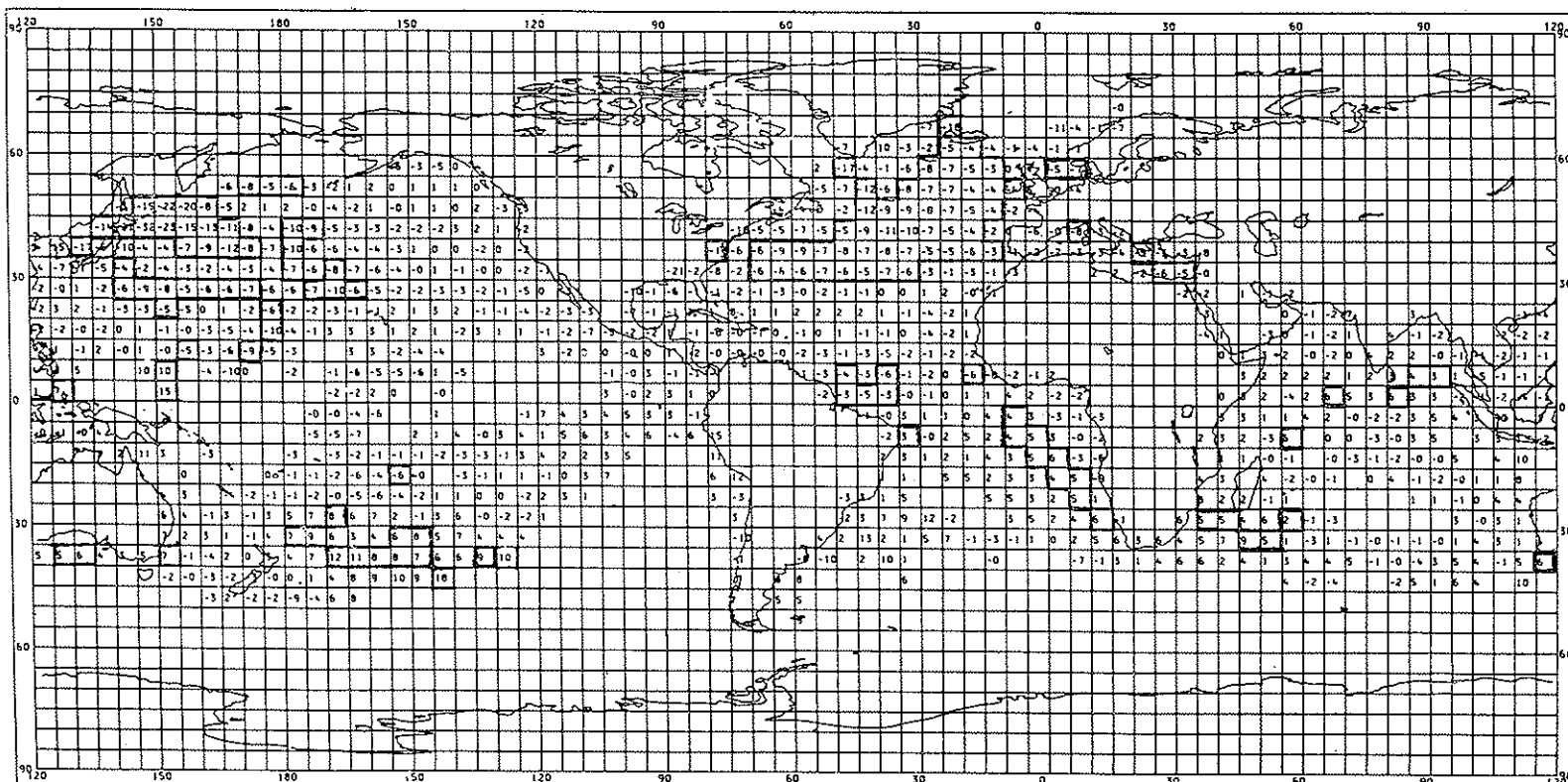

FIG. 9a. Sea surface temperature, 1968-84 minus 1950-59, January. Regions of statistical significante (5% level) are boxed.

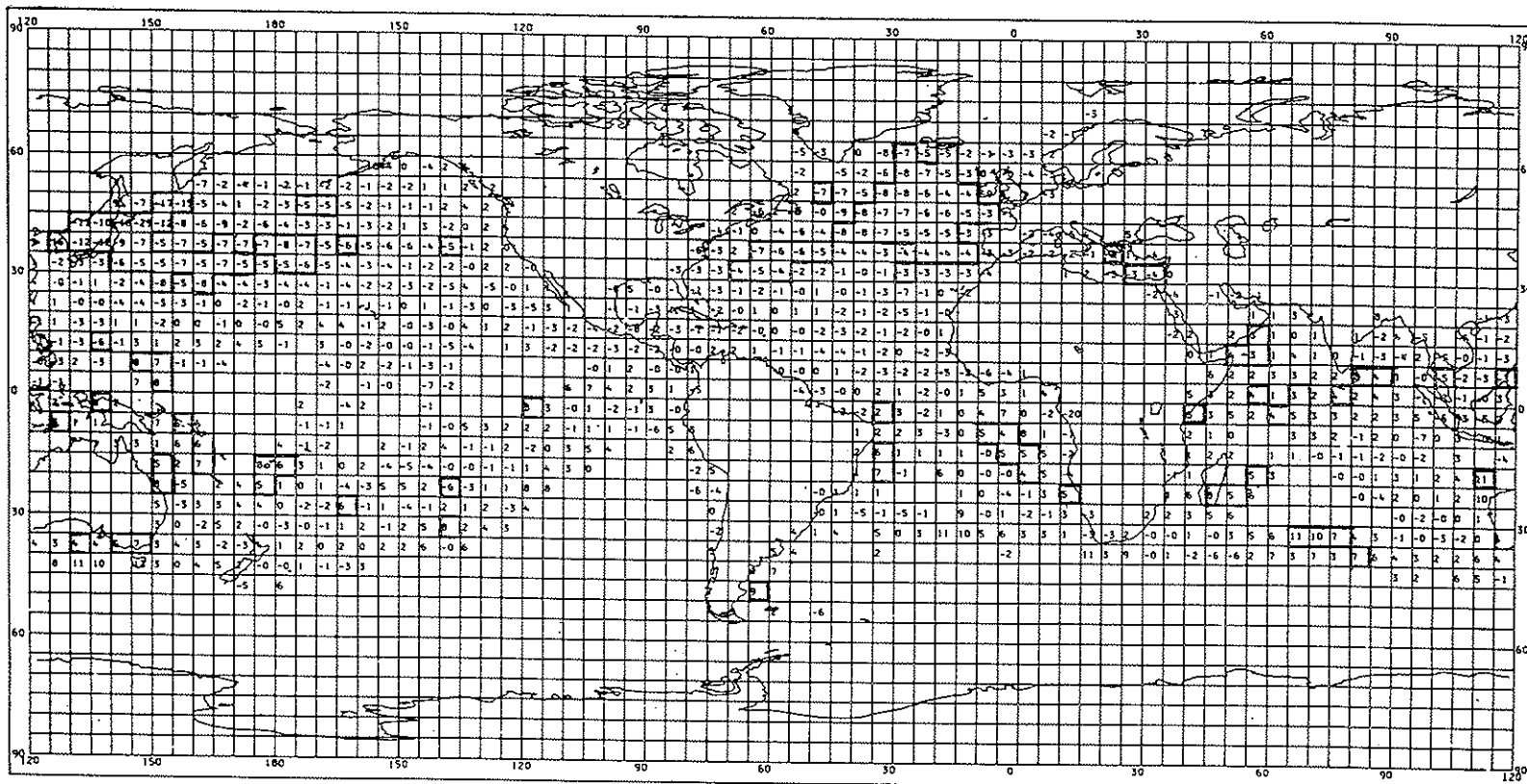

FIG. 9b. Sea surface temperature, 1968-84 minus 1950-59, April. Regions of statistical significante (5% level) are boxed.

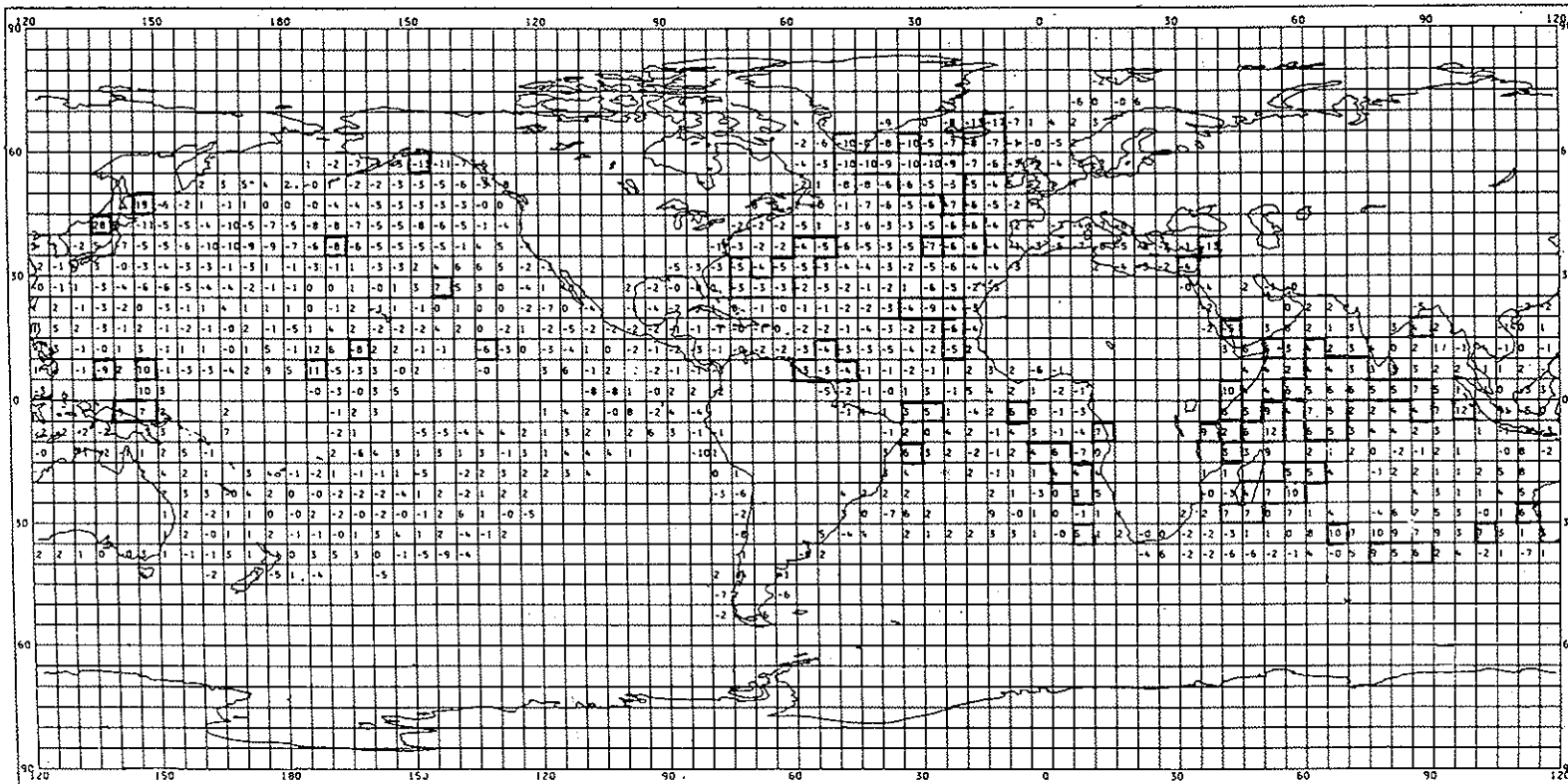

FIG. 9c. Sea surface temperature, 1968-84 minus 1950-59, July. Regions of statistical significance (5% level) are boxed.

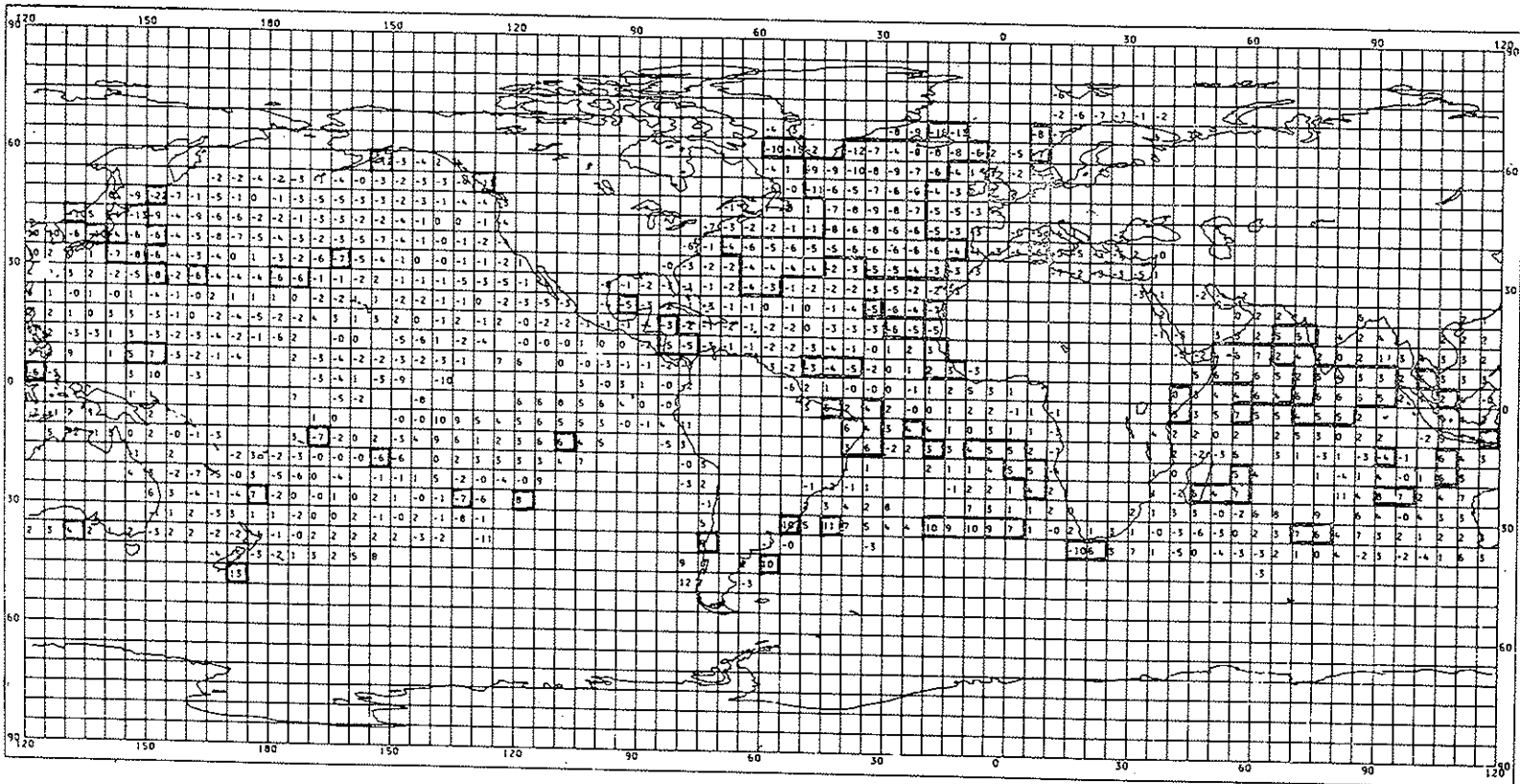

FIG. 9d. Sea surface temperature, 1968-84 minus 1950-59, October. Regions of statistical significance (5% level) are boxed.

Figs. 10a-f show, not unexpectedly, that this change may have been sufficient to affect much of the extratropical N. Hemisphere atmospheric circulation. Here the difference in pressure at mean sea level (PMSL) between 1968-84 and 1950-59 is drawn for March, April, May, July, August and October. Strongly significant changes are also shown in 500 mb height, though the changes tend not to be "equivalent barotropic" in the subtropics over the continents in summer.

Table 3 indicates the spatial extent of statistically significant areas on the PMSL and 500 mb difference maps. Lack of homogeneity of the PMSL data may have influenced the results, especially over the Southern Rocky Mountains and over Tibet (Williams and van Loon, 1976). Nevertheless a fairly coherent picture emerges of changes from month to month in the PMSL patterns, which tend to be largest and often significant in the best observed region — the mid latitude N. Atlantic/European sector. The SST changes are clearly even more coherent (Fig. 9). Fig. 11 shows the mean PMSL changes for the winter (December-March), and for the remainder of the year; these monthly variations have had very

TABLE 3 - *Percentage of data points which are significant when mean 1950-59 PMSL, SST or 500 mb Height data is subtracted from mean 1968-84 data for the month shown. See Figs. 9 and 10 for geographical extent of data.*

Month	Percentage of significant points		
	SST	PMSL	500 mb
January	15	18	13
February	13	21	20
March	12	28	20
April	13	30	19
May	12	34	30
June	11	30	29
July	11	25	16
August	19	32	32
September	18	28	14
October	17	33	19
November	18	30	21
December	15	14	13

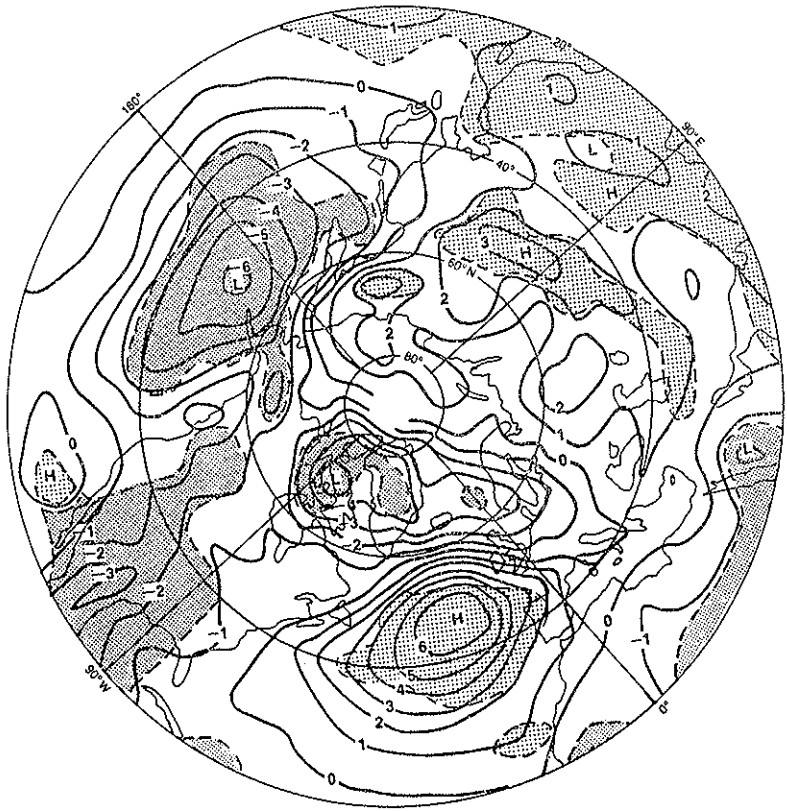

FIG. 10a. MSL Pressure, extratropical N. Hemisphere, 1968-84 minus 1950-59, March. Regions of statistical significance (5% level) are shaded.

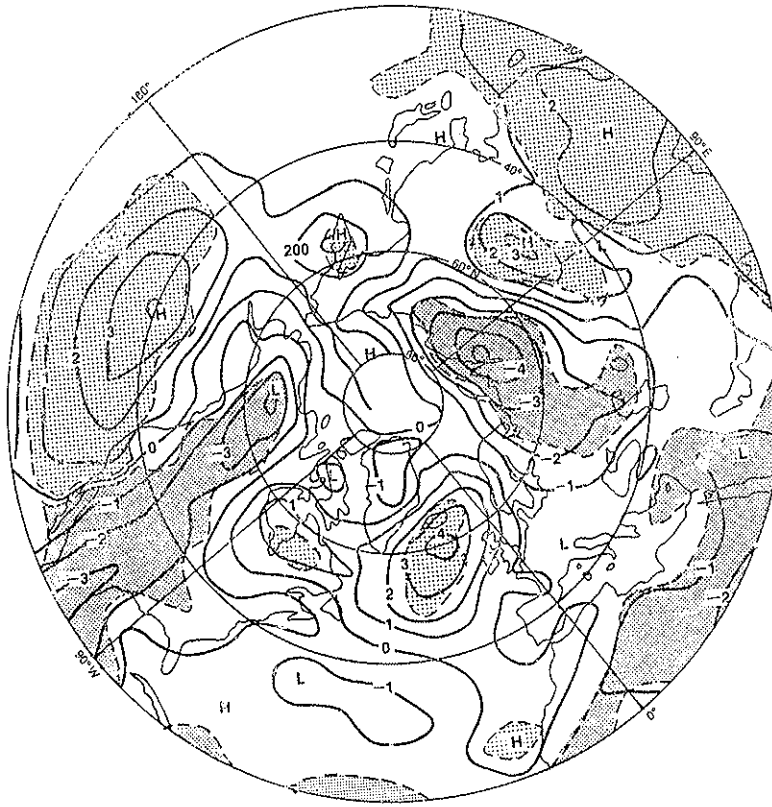

FIG. 10b. MSL Pressure, extratropical N. Hemisphere, 1968-84 minus 1950-59, April.

FIG. 10c. MSL Pressure, extratropical N. Hemisphere, 1968-84 minus 1950-59, May.

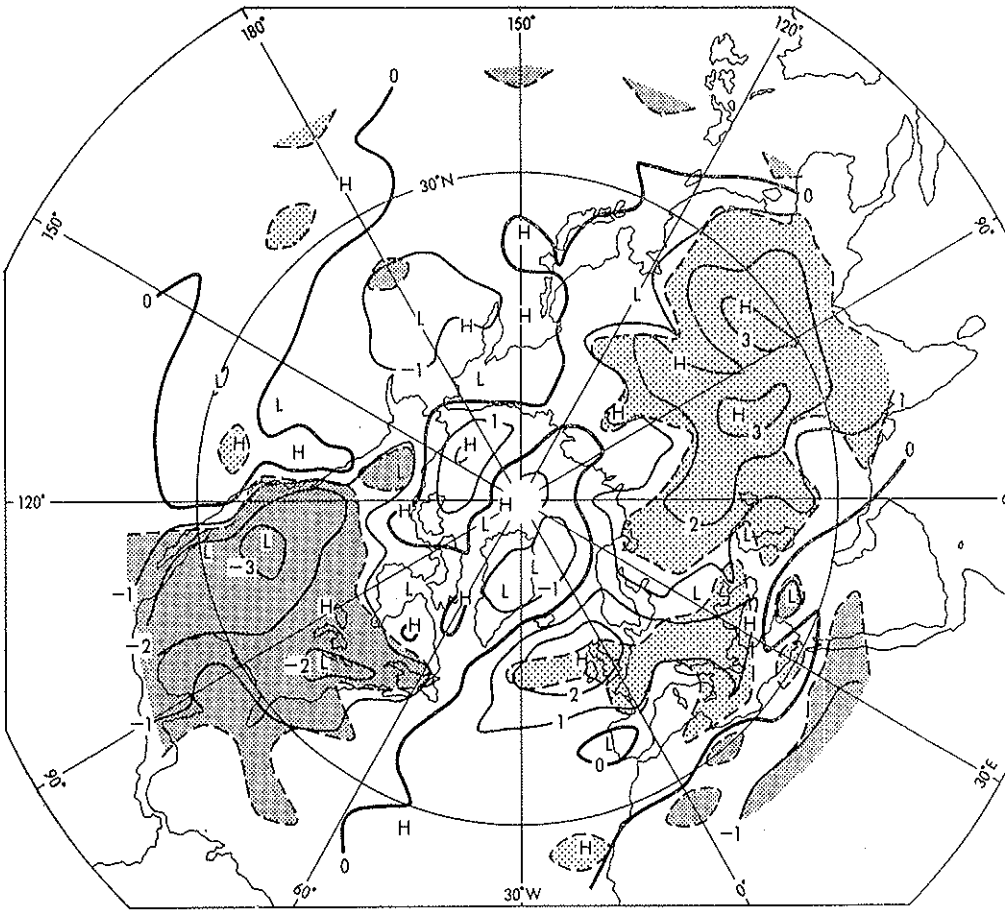

FIG. 10d. MSL Pressure, extratropical N. Hemisphere, 1968-84 minus 1950-59, July.

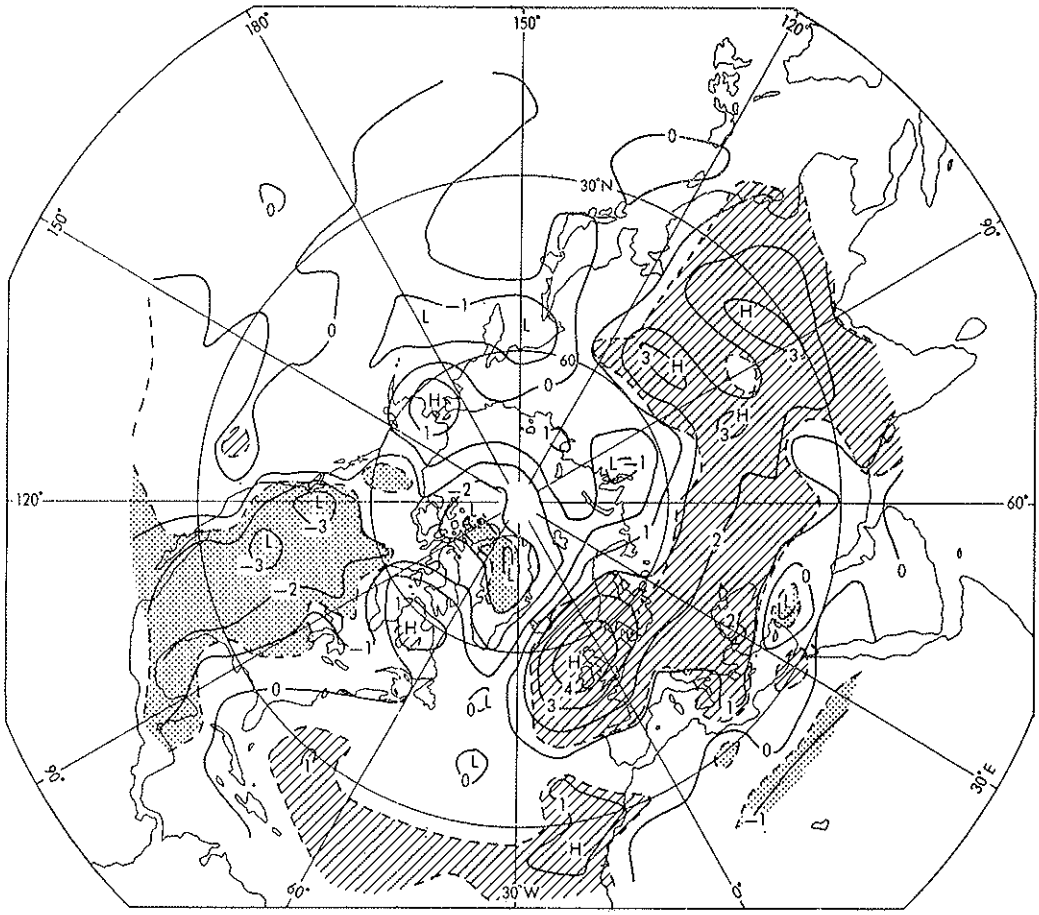

FIG. 10e. MSL Pressure, extratropical N. Hemisphere, 1968-84 minus 1950-59, August.

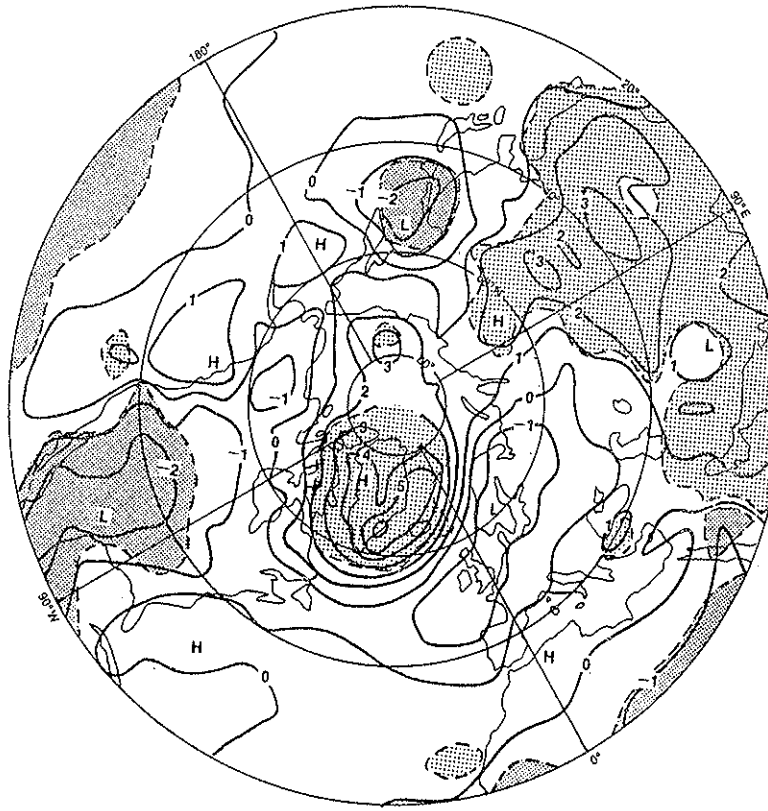

FIG. 10f. MSL Pressure, extratropical N. Hemisphere, 1968-84 minus 1950-59, October.

FIG. 11a. MSL Pressure, extratropical N. Hemisphere, 1958-84 minus 1950-59, December to March.

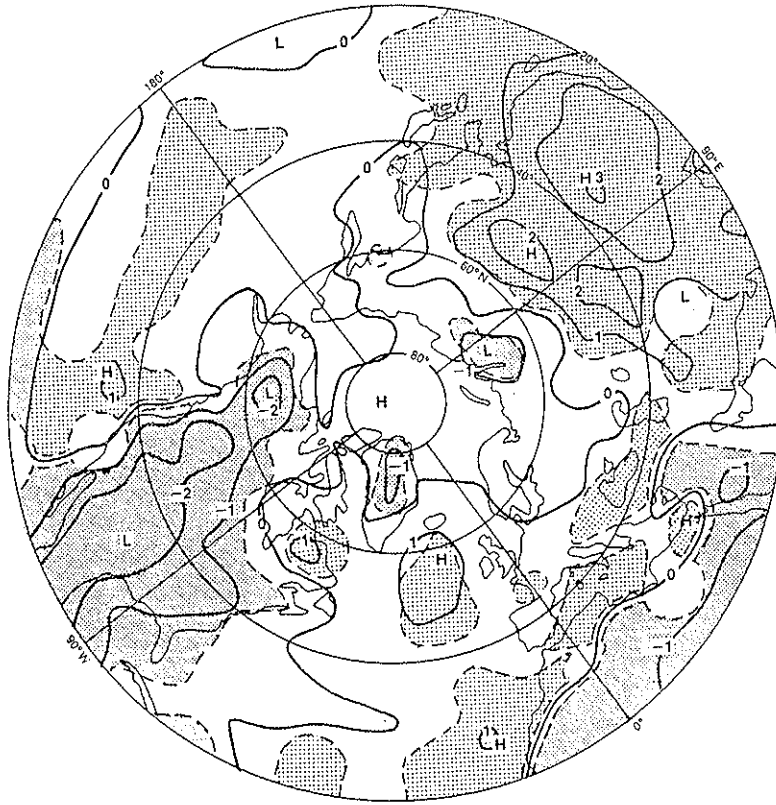

Fig. 11b. MSL Pressure, extratropical N. Hemisphere, 1968-84 minus 1950-59, April to Nov.

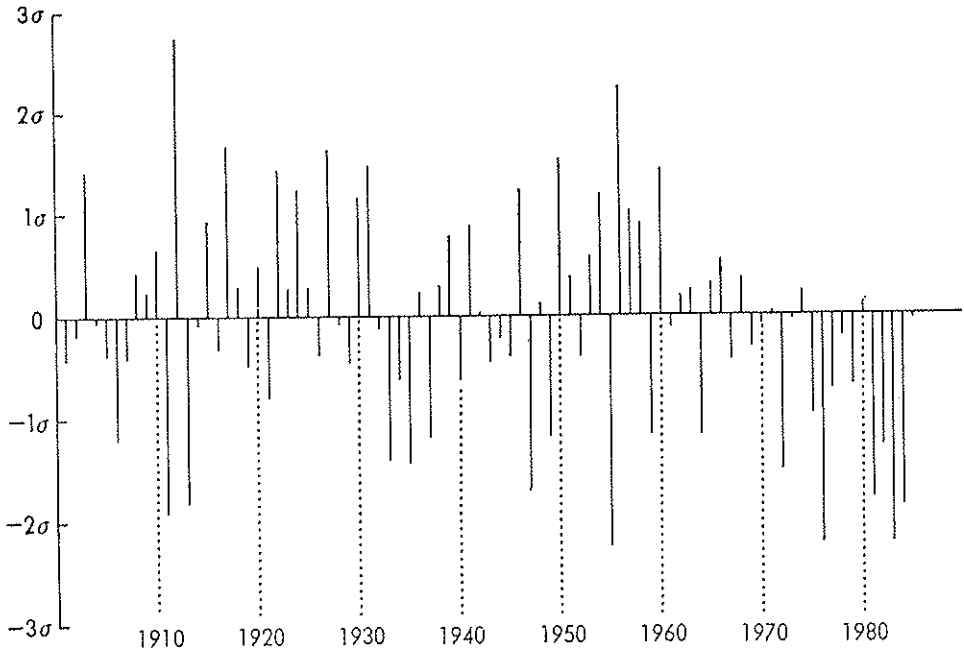

FIG. 12. Standardised England and Wales July and August rainfall, 1901-85.

evident effects on UK weather, especially in April, May, July, August, October and November.

Fig. 12 shows a time-series of rainfall (based on about 200 stations) for England and Wales in July and August; the series was homogenised by Wigley *et al.* (1984) and updated in the Synoptic Climatology Branch of the Meteorological Office. The pattern of SST changes was sufficiently regular that the difference in rainfall over England and Wales between the consecutive periods 1950-67 and 1968-85 was exactly 1 standard deviation (as calculated over the period 1901-80) and significant at at least the 99% level (assuming 10 degrees of freedom in a standard pair "t" test). Fig. 13 shows a time-series of mean July and August PMSL at 55 N 10 W plotted against the SST index SHNI minus RNH (July-Sept) (see Table 1 for definition) and also against Sahel rainfall for 1901-85. The correlation of these series is shown on Fig. 13; all correlations (assuming 40 degrees of freedom) are highly significant. A cross spectral analysis (not shown) indicates that PMSL at 55 N 10 W

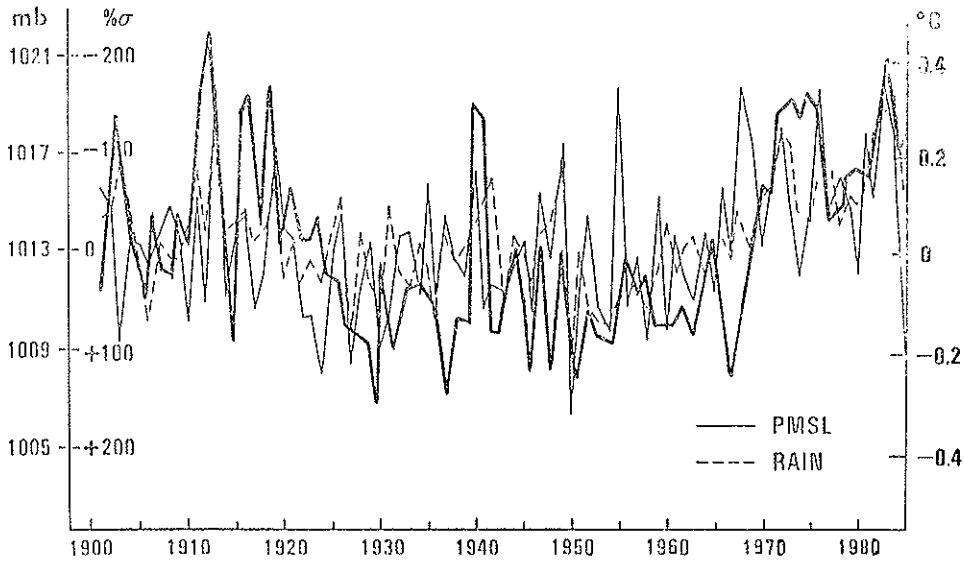

FIG. 13. i) Mean MSL pressure at 55° N 10° W in July and August (———). ii) Annual Sahel rainfall (- - - - - - -). iii) July to September SST, S. Hemisphere with N. Indian Ocean minus rest of N. Hemisphere (———). Correlations between series: i. vs ii): +0.29; i. vs iii): −0.53; ii. vs iii): −0.63.

(corresponding to the high pressure anomaly in Figs. 10d and 10e) is strongly positively correlated with the other time series in Fig. 13 on the interdecadal time scale but rather more weakly on interannual time scales. This is to be expected given the large internal variability of the mid-latitude atmosphere. Further details can be found in Folland, Parker and Palmer (1985).

5. Forecasting Sahel rainfall from Worldwide SST anomalies by empirical models

In June 1986, the Meteorological Office issued an experimental long-range forecast of rainfall over the Sahel for the summer of 1986. This very cautiously worded forecast arose from the research on the relationships between Sahel rainfall and worldwide SST discussed above and the supporting general circulation model results in FPP and in Pal-

mer (1986a). Two techniques of forecasting have been devised and tested on independent data:

(a) A regression technique which relates worldwide SST anomalies in the N. Hemisphere spring to Sahel rainfall in the following summer. The technique provides a "deterministic" forecast whose uncertainty can be fairly readily quantified.

(b) A technique based on the use of linear discriminant prediction. This provides a forecast of the probabiliyt of each of five categories of Sahel rainfall using up to eight predictors. These predictors are (currently) coefficients of covariance eigenvectors of worldwide SSTA of the type described in Section 2: 2 sets of eigenvectors were calculated, using the periods 1901-80 and 1951-80 respectively. A coefficient time series for each eigenvector was calculated over the period 1901-86.

Method (a)

We first calculate the linear regression between Sahel rainfall and locally observed values of SSTA covering much of the globe over some fixed period prior to the Sahel rainfall season. The local SSTA are measured over 5×5 degree or 10×10 degree areas; the regression relationships are calculated from data measured within the period 1901-84. Fig. 14a shows an example of a regression map for 1946-84 that relates March-May SSTA to the following summer's Sahel rainfall; here we show the values of slopes of the regression coefficients that relate Sahel rainfall to the local values of SSTA.

The next stage is to calculate for each year the covariance of the worldwide SSTA field with the regression-slope field for the same calendar period for a set number of years selected as the model's "training period". This provides a measure of the similarity of the SSTA pattern in a given year to the pattern of the regression-slope field. Finally we calculate a new regression equation that relates the values of this covariance factor to Sahel rainfall in the following summer over the training period. This equation can then be used in years subsequent to the training period to forecast the summer Sahel rainfall by measuring the covariance between the observed SSTA field and the fixed regression-slope field in, for example, the spring of the year for which a forecast is required. Fig. 14b shows predictions for 1981 to 1986 made using two versions of this model. A more extensive discussion of the technique, with statistical simulations on independent data, is given in Parker *et al.* (1986).

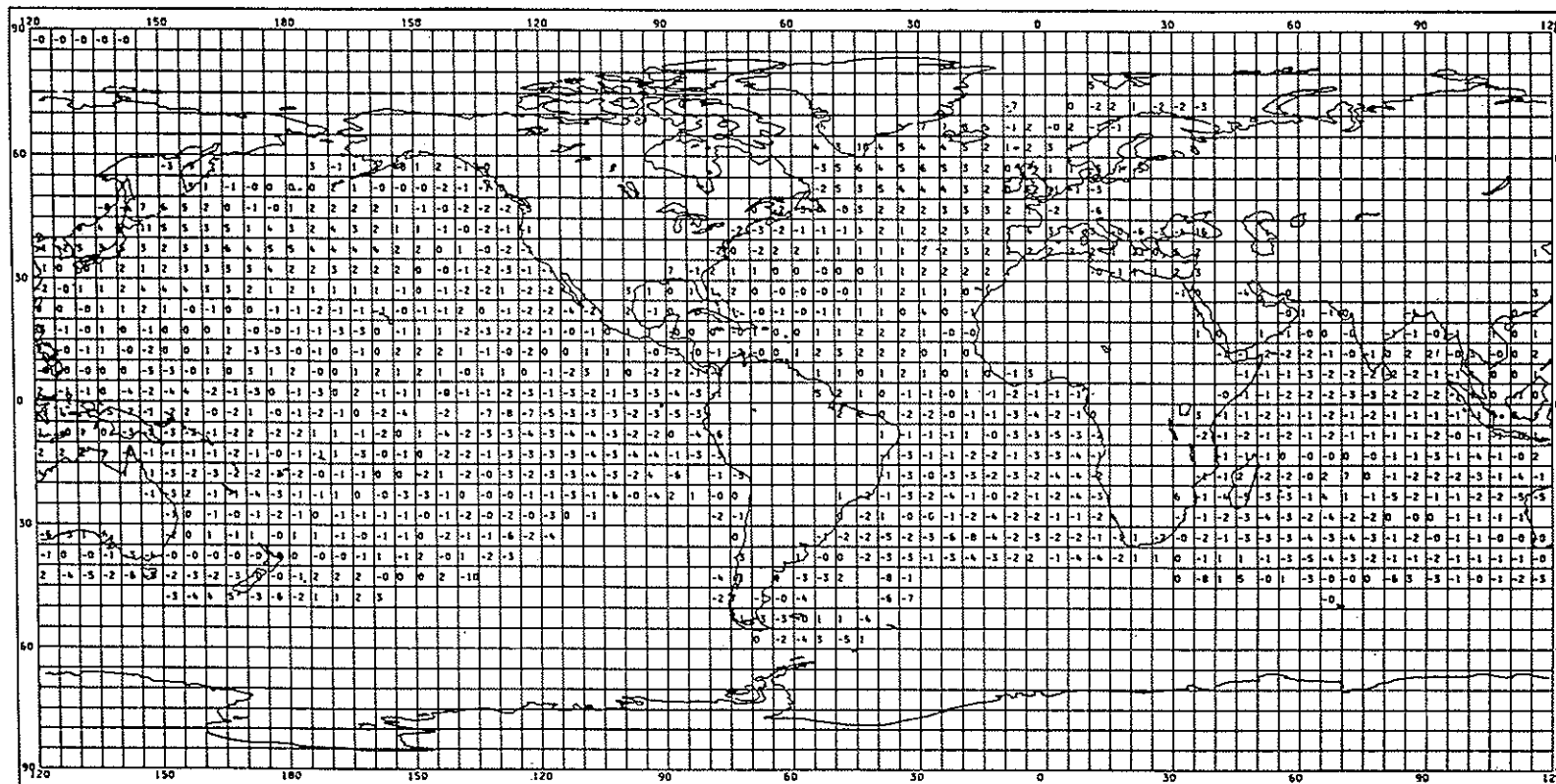

FIG. 14a. Regression slope of March to May SST on Sahel rainfall, 1945-84. Values are in 10ths °C per standard deviation of Sahel rainfall.

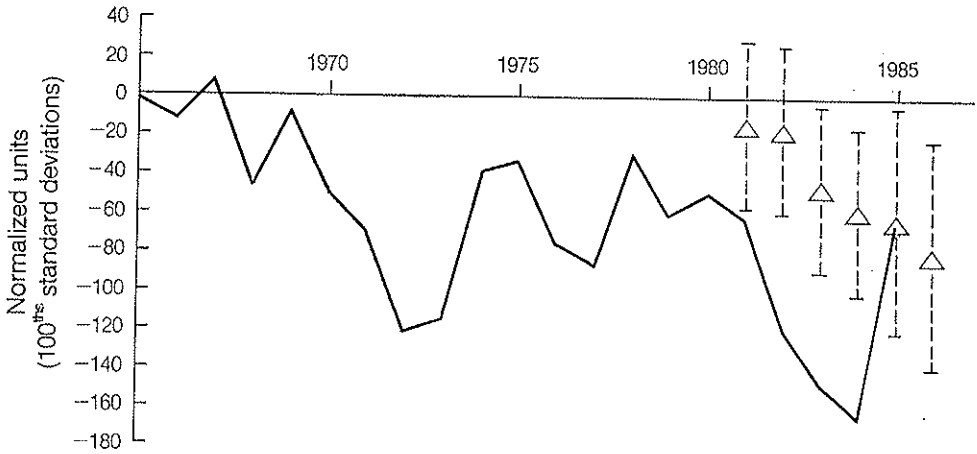

FIG. 14b. Observed Sahel rainfall, 1965-85, and predicted values, 1981-86, using regression technique. The bars on the predictions give the 95% confidence limits.

Method (b)

The linear discriminant prediction technique (see Afifi and Azen, 1979, for a fundamental description of discriminant analysis) also requires that a training period be specified. Sahel summer (July-September) rainfall amounts within the training period are divided (in current models) into equiprobable ranges (« Quints »); their boundaries (quintiles) are derived from the training period. This is necessary as the linear discriminant prediction equations are more stable if equal numbers of observations of the values of each predictor are available in each of the predefined ranges.

Five linear discriminant equations are calculated using a stepwise technique. The equations relate the observed occurrence of each quint in the training period to the values of the coefficients of a set of world-wide SST eigenvectors which are measured over a fixed period in the spring prior to each Sahel rainfall season. The 5 equations forecast the probability of each quint respectively in the coming season using normal distribution theory and Bayes' theorem. This technique is formally similar to but less complex than the multivariate forecasting technique used in monthly long-range forecasting for the UK (Folland and Colman (FC), 1986; Folland and Woodcock, 1986). The "best" a priori model is chosen using a "jackknife test" (see FC, 1986). Quite high jackknife

"hit rates" have been found in some of these models (a "hit" is said to occur when the observed quint category is the same as the quint forecast to have highest probability). One set of models has been based on a 1901-85 training period using eigenvectors based on the period 1951-80. This model gave a hit rate of 40% and an "F" value of 15 for the significance of the 1951-80 EOF2 (quite like the 1901-80 EOF3, Fig. 6a) as a discriminant predictor. Table 4a shows the result of an attempt by a model using the same data as the model described above but with a 1901-67 training period and 1901-80 eigenvectors to "predict" the Sahel

TABLE 4a - *Forecasts of Sahel rainfall (mainly July to September) from 1968 to 1985 using March to May SST EOF coefficients with training data from 1901-1967. The EOFs used were for 1901-80 and 1951-80.*

Year	Observed Quint (1901-67 Quints)	Forecast using 1901-80 EOFs	Forecast using 1951-80 EOFs
1968	1	5	3
1969	3	1	1
1970	1	1	2
1971	1	3	3
1972	1	1	1
1973	1	1	1
1974	1	3	2
1975	1	3	1
1976	1	1	1
1977	1	1	1
1978	2	1	2
1979	1	1	1
1980	1	1	1
1981	1	1	2
1982	1	1	1
1983	1	1	1
1984	1	3	1
1985	1	1	1
% Of correct forecasts (Hits)		61%	67%

drought years from 1968-85. The results are encouraging though "quint 1" based on 1901-67 is not very dry (−0.3 based on Nicholson's measure of Sahel rainfall, Fig. 7a).

Tables 4b and 4c show some predictions for 1981-6 based on shorter training periods but using quint rainfall categories better matched to the present drier Sahel rainfall climate. The predictions are encouragingly successful with most years (1981-85) well predicted. Tables 4a and 4b show occasional gross failures of the models. Indeed these failures underline the need to look more deeply into the statistics of "Sahel rainfall" (rainfall anomalies over the Sahel are not always homogeneous as shown by Nicholson, 1980) as well as other physical processes that affect Sahel rainfall. Nevertheless it is clear that large-scale SST fluctuations have an important controlling influence over rainfall in sub-Saharan Africa. The special importance of regional SST anomalies also requires urgent investigation.

6. Conclusion and Projected Work

We believe we have provided a strong case that coherent large-scale SST changes occur, that they modulate Sahel rainfall and N. Hemisphere atmospheric circulation, and that they have potential for use as predictors in forecasting Sahel rainfall. In addition, worldwide SSTA (measured in limited but widely spread regions) are found to be useful as predictors for the extratropics (for monthly PMSL pattern forecasts in the region of the UK).

We see that the next step is to include a more realistic set of general circulation model experiments which should be designed to study in better detail physical processes which affect Sahel rainfall and involve contrasting worldwide SST anomalies. We have started some "partial annual cycle" experiments running from modelled "Aprils" to "Octobers" using globally complete sequences of observed monthly SST anomalies in those months in selected years. The years will include 1950 and 1984 and are being chosen for their extremes (wet or dry) of Sahel rainfall and for contrasting worldwide SST patterns (Fig. 15). Fig. 16 shows initial results from model experiments representative of 1950, a very wet year in the Sahel. The changes in rainfall, when compared with the model's climatology, are in good qualitative agreement in each month from June to September with observations for these months published by Dennett *et al.* (1985). The model was initialised using atmospheric data

TABLE 4b - *Probability forecasts of Sahel rainfall using a 1946-80 training period: predictors are March to May coefficients of 1951-80 eigenvectors. The average of the best 2 models are shown.*

Year	Forecast Probabilities					Observed
	Quint 1	Quint 2	Quint 3	Quint 4	Quint 5	Quint
1981	0.14	0.24	0.17	0.26	0.14	1
1982	0.51	0.34	0.02	0.06	0.07	1
1983	0.62	0.32	0.02	0.03	0.01	1
1984	0.46	0.35	0.06	0.09	0.04	1

(1946-80 Quints)

TABLE 4c - *Average of 9 forecasts for 1985 and 1986. All models are based on a 1946-84 training period and use predictors formed from 1951-80 EOFS. Models use April to May, March to May and March to April SST's as predictors: each produces a forecast based on 3, 4 and 5 variables, hence a total of 9 forecasts.*

Year	Forecast Probabilities					Observed
	Quint 1	Quint 2	Quint 3	Quint 4	Quint 5	Quint
1985	0.59	0.13	0.12	0.14	0.02	2
1986	0.27	0.53	0.14	0.05	0.01	1?

(1946-84 Quints)

1946-84 *Quint Boundaries*

% standardised Units (1901-80) - (Fig. 7a)

		Normal
Quint 1	Quint 2	−74
Quint 2	Quint 3	−37
Quint 3	Quint 4	− 6
Quint 4	Quint 5	+30

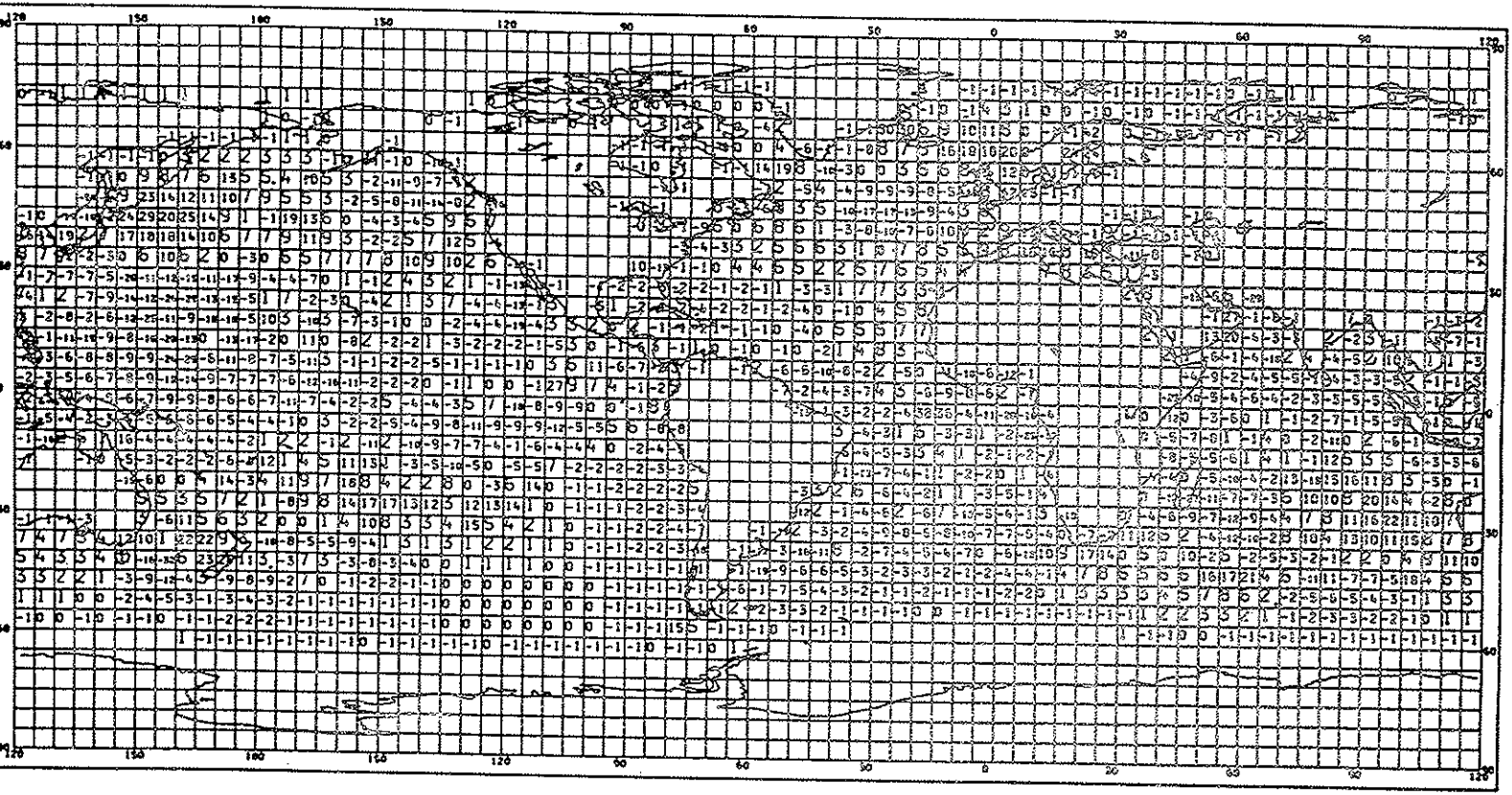

FIG. 15. SST anomalies, August 1950. Values are in 10ths °C.

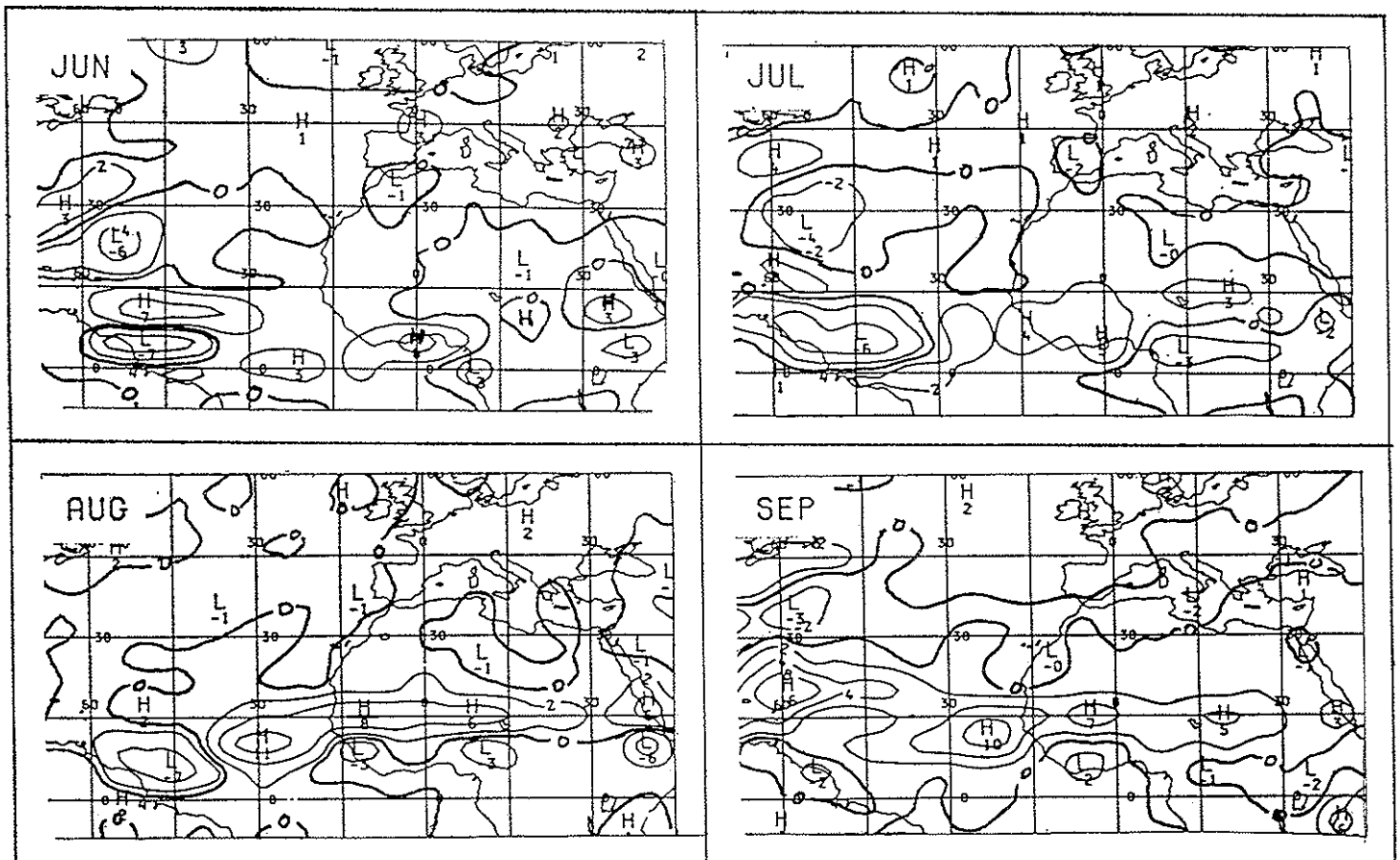

FIG. 16. Monthly deviations of rainfall (mm) from climatology of nu merical general circulation model forced by SST anomalies for 1950.

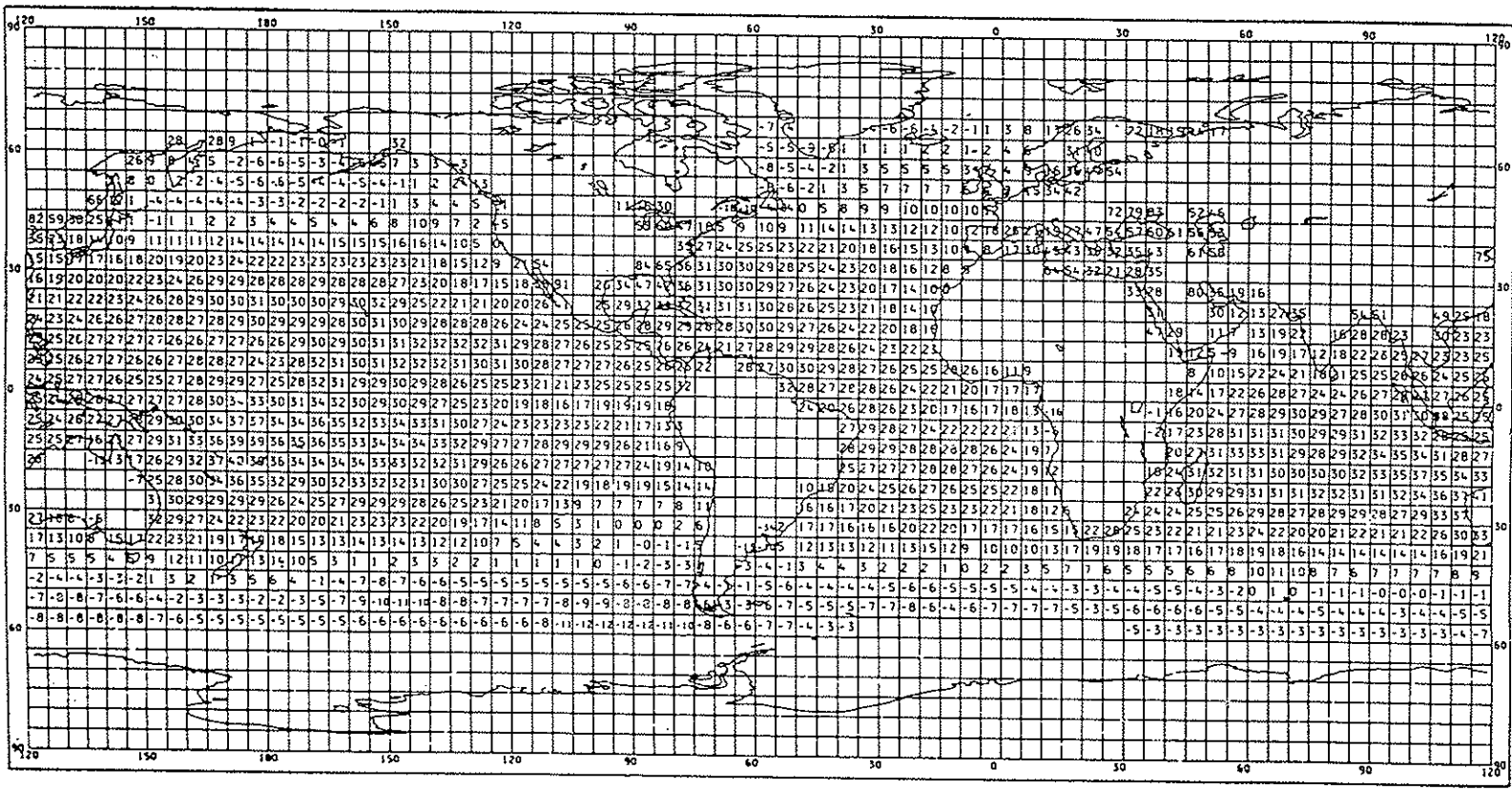

FIG. 17. Corrections to August SST deduced from model of thermodynamics of an uninsulated bucket. Values are in 100ths °C and have been smoothed 1:2:1 east-west then north-south.

for the end of March 1984 and the first two months of the integration have been discarded because at least a month is required for the model to resolve the initial disequilibrium imposed by the SST forcing.

The historical SST data are also being improved. The most immediate activity is the estimation of seasonally and geographically varying corrections for the biases of uninsulated sea temperature buckets using a developed form of the scheme suggested in Folland and Hsiung (1986). An initial picture of the proposed corrections for August is shown in Fig. 17; the average global correction is slightly less than in FPK but what is much more important is a range in the regional values of the corrections of about 0.5°C. Their pattern seems likely to influence the amplitude of EOF3 before 1942 (when the corrections were applied).

We are also carrying out a more detailed study of the atmospheric circulation variations over the extratropical N. Hemisphere (PMSL, 500 mb height and 500 mb-1000 mb thickness). Daily data (1946-1986) are being filtered on several time scales from less than six days to 25-80 days. A rotated eigenvector analysis of some of these data is also planned because Barnston and Livezey (1985) have indicated that this may be a useful way of identifying some of the characteristic patterns associated with low frequency atmospheric variability described by many authors (e.g., Blackmon and Wallace, 1983).

Finally the interhemispheric SST variations discussed in the paper may be the result of cooperative ocean atmosphere interactions on time scales of up to several decades. Initial work on the formulation of hypotheses to explain these changes will be discussed in Folland *et al.* (1987).

REFERENCES

AFIFI A.A. and AZEN S.P., *Statistical analysis — a computer orientated approach.* Second Ed., Academic Press (1979).

BARNSTON A.G. and LIVEZEY R.E., *High Resolution rotated empirical orthogonal function analysis of northern hemisphere 700 mb heights for predictive purposes.* 9th Conf. Prob. Stat. Atmos. Sci., Boston, Mass., pp. 290-297 (1985).

BLACKMON M.L. and WALLACE J.M., *On the structure and time evolution of low frequency atmospheric fluctuations.* Proc. 7th Ann. Clim. Diagn. Workshop, pp. 311-318 (1983).

DENNETT M.D., ELSTON J. and ROBGERS J.A., *A reappraisal of rainfall trends in the Sahel.* « J. Clim. », *5*, 353-361 (1985).

FOLLAND C.K. and COLMAN A., *A multivariante technique for use in long-range forecasting.* « WMO Long-Range Forecast Res. Rep. Ser. », *6* (II), 627-636 (1986).

FOLLAND C.K. and HSIUNG J., *Corrections of seasonally-varying biases in uninsulated bucket sea surface temperature data using a physical model.* Met 0 13 Branch Memorandum No 154, Meteorological Office, Bracknell, England (1986).

FOLLAND C.K., PALMER T.N. and PARKER D.E., *Sahel rainfall and worldwide sea temperatures, 1901-1985.* « Nature », *320*, 602-607 (1986).

FOLLAND C.K., PARKER D.E. and KATES F.E., *Worldwide marine temperature fluctuations 1856-1981.* « Nature », *310*, 670-673 (1984).

FOLLAND C.K., PARKER D.E. and NEWMAN M.R., *Worldwide marine temperature fluctuations on the season to century time scale.* Proc. 9th Climate Diagnostics Conference, Corvallis, Oregan, 22-26 Oct. 1984, pp. 70-85 (1985).

FOLLAND C.K., PARKER D.E. and PALMER T.N., *Sahel drought and worldwide sea surface temperature.* MRSCP/12 Meteorological Office, Bracknell, England (1985).

FOLLAND C.K., PARKER D.E., WIGLEY T.M.L., JONES P.D. and PALMER T.N., *Warming of the southern hemisphere in recent decades.* For Proc. WCRP conf. on Mech. of interannual and longer-term climate variation. Melbourne, 8-12 Dec. 86 (1987).

FOLLAND C.K. and WOODCOCK A., *Experimental monthly long-range forecasts for the United Kingdom.* « Met. Mag. », *115*, 301-318 (1986).

GILCHRIST A., *Long-Range forecasting in the Meteorological Office*, Part I, II, ECMWF Semin. Probl. Prospect. Long Med. Range Weather Forecast, 1981, pp. 21-54 (1982).

GILL A.E. and RASMUSSON E.M., *The 1982-82 climate anomaly in the equatorial Pacific.* « Nature », *306*, 229-234 (1983).

HASTENRATH S., *Interannual variability and annual cycle: mechanisms of circulation and climate in the Tropical Atlantic sector.* « Mon. Weath. Rev. », *112*, 1097-1107 (1984).

HSIUNG J. and NEWELL R.E., *The principal non-seasonal modes of variations of global sea surface temperatures.* « J. Phys. Ocean. », *13*, 1957-1967 (1983).

LAMB H.H., *Climate: Present, Past and Future.* Vol. I. Methuen (1972).

LAMB P.J., *Large-scale tropical Atlantic surface circulation patterns associated with sub-Saharan weather anomalies.* « Tellus », *30*, 240-251 (1978).

LOUGH J.M., *Atlantic sea surface temperatures and weather in Africa.* Ph. D. thesis, Univ. East Anglia (1981).

LOUGH J.M., *Tropical Atlantic sea surface temperatures and rainfall variations in Sub-Saharan Africa.* « Mon. Weath. Rev. », *114*, 561-570 (1986).

MAKROGIANNIS T.J., BLOUTSOS A.A. and GILES B.D., *Zonal index and circulation change in the North Atlantic area, 1873-1972.* « J. Clim. », *2*, 159-169 (1982).

MANLEY G., *Central England temperatures: monthly means 1659 to 1973.* « Q. J. R. Met. Soc. », *100*, 389-405 (1974).

MINHINICK J.M. and FOLLAND C.K., *The Meteorological Office historical sea surface temperature data set.* Met O 13 Branch Memorandum No. 137, Meteorological Office, Bracknell, England (1984).

NICHOLSON S.E., *The nature of rainfall fluctuations in subtropical West Africa.* « Mon. Weath. Rev. », *108*, 473-487 (1980).

NICHOLSON S.E., *Rainfall and atmospheric circulation during drought periods and wetter years in West Africa.* « Mon. Weath. Rev. », *109*, 2191-2208 (1981).

NICHOLSON S.E., *Sub-Saharan rainfall 1981-84.* « J. Clim. App. Met. », *24*, 1388-1391 (1985).

PALMER T.N., *Influence of the Atlantic, Pacific and Indian Oceans on Sahel rainfall.* « Nature », *322*, 251-253 (1986a).

PALMER T.N., *Drought, sea surface temperatures and atmospheric teleconnections.* Proc. Study Week on persistent meteo-oceanographic anom. and telecon. 23-27 Sept. 1986, Vatican City (1986b).

PALMER T.N. and MANSFIELD D.A., *A study of winter time circulation anomalies during past El Niño events using a high resolution general circulation model.* II: *Variability of seasonal mean response.* « Q.J.R. Met. Soc. », *112*, 613-638 (1986).

PALMER T.N. and SUN Z., *A modelling and observational study of the relationship between sea surface temperature in the north-west Atlantic and the atmosphere general circulation.* « Q.J.R. Met. Soc. », *111*, 947-975 (1985).

PAN Y.H. and OORT A.H., *Global climate variations connected with sea surface temperature anomalies in the eastern equatorial Pacific Ocean for the* 1958-73 *period.* « Mon. Weath. Rev. », *111*, 1244-1258 (1983).

PARKER D.E., GREENSLADE R. and FOLLAND C.K., *The stability of statistical relationships between sub-Saharan rainfall and worldwide sea surface temperature.* Met O 13 Branch Memorandum No. 166, Meteorological Office, Bracknell, England (1986).

PARKER D.E., HSIUNG J., FOLLAND C.K., BOTTOMLEY M. and NEWELL R.E., *Climatological atlas of world sea surface temperature.* HMSO/MIT. In preparation (1987).

RATCLIFFE R.A.S. and MURRAY R., *New lag associations between North Atlantic sea temperature and European pressure applied to long-range weather forecasting.* « Quart. J.R. Met. Soc. », *96*, 226-246 (1970).

SAWYER J.S., *Notes on the possible physical causes of long-term weather anomalies.* WMO No. 162 T P 79, Tech. Note No. 66, pp. 227-248 (1965).

STOREY A., FOLLAND C.K. and PARKER D.E., *A homogeneous archive of daily central England temperature* 1772 *to* 1985 *and new monthly average values* 1974 *to* 1985. Met O 13 Branch Memorandum No. 107, Meteorological Office, Bracknell, England (1985).

WALKER J. and ROWNTREE P.R., *The effect of soil moisture on circulation and rainfall in a tropical model.* « Q. J. R. Met. Soc. », *103*, 29-46 (1977).

WIGLEY T.M.L., LOUGH J.M. and JONES P.D., *Spatial patterns of precipitation in England and Wales and a revised, homogeneous England and Wales precipitation series.* « J. Clim. », *4*, 1-25 (1984).

WILLIAMS J. and VAN LOON H., *An examination of the Northern Hemisphere sea-level pressure data set.* « Mon. Weath. Rev. », *104*, 1354-1361 (1976).

BAROTROPIC INSTABILITY, AND ANOMALIES OF THE EXTRATROPICAL NORTHERN HEMISPHERE WINTER CIRCULATION

A. J. SIMMONS
European Centre for Medium Range Weather Forecasts
Shinfield Park, Reading, Berkshire, U.K.

ABSTRACT

A summary is given of results relating to the nature of low-frequency anomalies of the extratropical Northern Hemisphere winter circulation obtained by Simmons (1982) and Simmons, Wallace and Branstator (1983) in studies of wave propagation and instability in a barotropic model incorporating a forced climatological-mean January background flow. Some subsequent related idealized and general-circulation modelling studies, and observational results, are briefly reviewed. The barotropic model is also applied to study the stability of four monthly-mean circulations characterized by large deviations from climatology. These anomalous circulations are shown to be substantially more stable than circulations in which the sign of the observed anomaly is reversed. Some variation in stability from month to month is found, but the number of cases studied is insufficient to determine whether this variation can be related to the observed degree of stability of the anomalies.

1. INTRODUCTION

Maps of the temporal variability of the Northern Hemisphere winter circulation on time scales longer than about ten days exhibit distinct maxima over the northern Pacific and Atlantic Oceans, and over the

Siberian Arctic. Particularly for scales of a month or more, this variability is characterized by geographically-fixed "teleconnection patterns" comprising, over the oceans, zonally elongated dipoles straddling the exit regions of the mean Pacific and Atlantic jet streams, with a more meridional elongation to the anomalous low and high pressure cells which develop to the east or south-east of the region of maximum amplitude. The strongest of these patterns occurs over the Pacific and extends downstream over North America, and is commonly referred to as the "Pacific/North American" (PNA) pattern (Blackmon *et al.*, 1984a, and references).

A possible explanation for the existence of such geographically-fixed anomaly patterns is that they are the atmospheric response to a localized, slowly-changing, anomalous surface forcing. Tropical sea-surface temperature anomalies are a prime candidate, supported for example by the similarity of the PNA pattern with that arising in anomaly maps for Northern Hemisphere winters in which equatorial Pacific surface temperatures are unusually warm (Horel and Wallace, 1981). However, apparently realistic teleconnection patterns are also found in extended integrations of general circulation models using climatological sea-surface temperatures (e.g., Lau, 1981), and (as will be seen later) strong anomalies resembling those occurring at times of extreme equatorial Pacific temperatures are evident in monthly means at other times. Moreover, the extratropical response to anomalous forcing may itself appear preferentially in certain locations due to the substantial longitudinal as well as latitudinal variations that occur in the climatological upper tropospheric flow in winter.

Investigation of this topic using what is perhaps the simplest relevant model was undertaken in studies reported by Simmons (1982) and Simmons *et al.* (1983). Calculations of forced wave motion, dispersion and instability were performed for a barotropic model in which a fixed, steady forcing was applied in order to maintain as a background flow the climatological 300 mb state for January. The principal results and conclusions from these studies are presented in the following section of this paper, and section 3 contains a brief review of related work by a number of other investigators. Some novel results of applying the barotropic model to flows derived from actual monthly-means in cases of significant anomalies are presented in section 4.

2. Barotropic Wave Propagation and Instability

Figure 1 shows the steady, non-linear, anomaly pattern in streamfunction forced by a localized anticyclonic vorticity source centred close to 10°N for various longitudes of maximum forcing. It is clear from the range of amplitudes of the response that longitudinal variations of the background flow have had a significant effect on the extratropical response to the tropical forcing. The strong pattern forced from 120°E bears a striking resemblance to the PNA; forcing centred on the dateline excites a very similar pattern, though of opposite sign and smaller amplitude. The North Pacific is evidently a preferred region of maximum response, and a tendency for a north-south dipole pattern over the North Atlantic may also be discerned.

The role of the longitudinal variations of the basic state in amplifying the response as well as leading to preferred locations can be seen by comparing the amplitudes in Figure 1 with those in the upper plots of Figure 2, which show similar calculations but with the corresponding climatological zonal-average flow and solid-body rotation used as basic states. In these cases only the position of the wave train depends on the longitude of maximum forcing, which is chosen to be 120°E for purpose of illustration. Amplitudes are at most comparable with the weakest of the responses shown in Figure 1. Figure 2 also compares, for the zonally-varying basic state, the responses to cyclonic as well as anticyclonic forcing at the longitude giving maximum response. Some sensitivity in the structure and amplitude of the response is evident. The north-south dipole pattern is located further east for cyclonic forcing; for this case the sign of the dipole corresponds to an eastward extension of the Pacific jet.

The preferential response over the Pacific is also seen in problems involving dispersion of an initially localized perturbation. Six examples showing the disturbance streamfunction at day 10 for perturbations originally centred at 40°N and various longitudes are presented in Figure 3. The most prominent pattern is again that resembling the PNA.

A more extensive series of forced and initial value problems confirms the tendency of structures similar to the PNA pattern, and to a lesser extent to the "East Atlantic" teleconnection pattern (Wallace and Gutzler, 1981), to recur in the responses. Linear calculations with only weak dissipation included also reveal that the basic 300 mb climatological state is barotropically unstable, with a number of growing modes.

In the absence of damping the most unstable mode has an e-folding

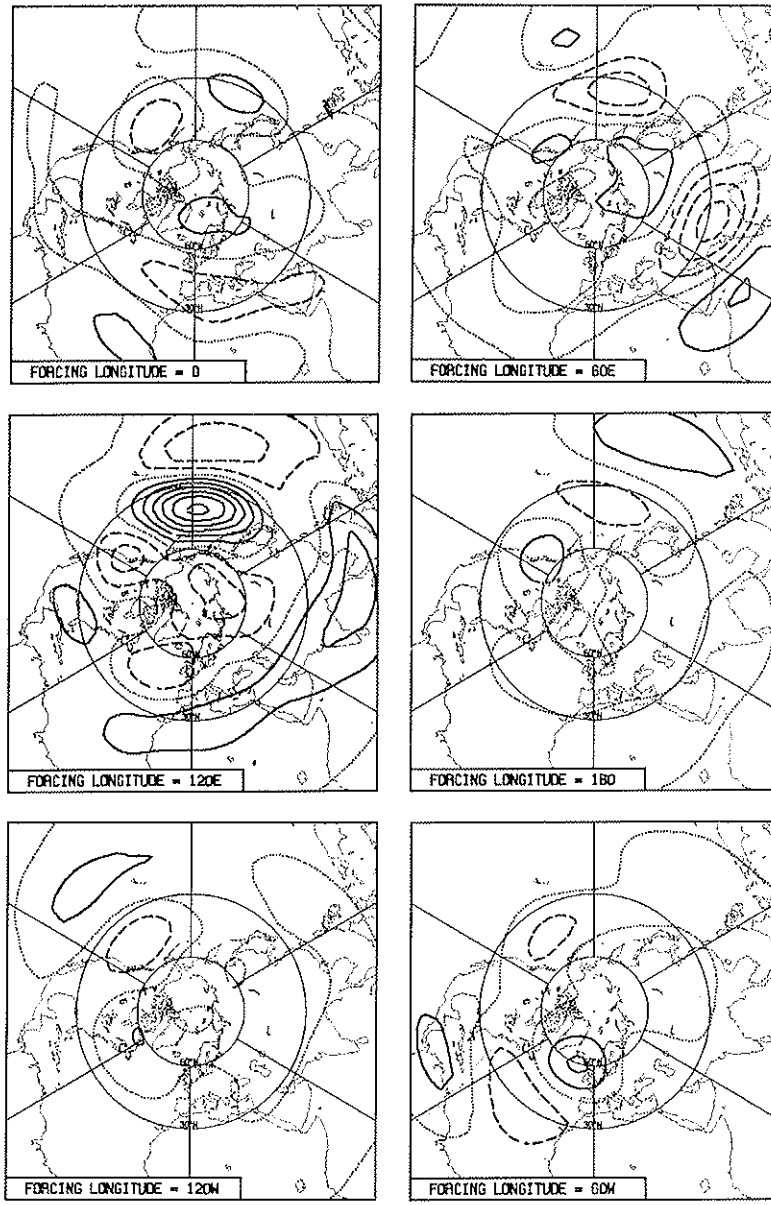

FIG. 1. The steady nonlinear responses in streamfunction to localized anticyclonic forcing centred at 10°N and at six different longitudes indicated on the individual panels. A linear drag with 5-day decay time is included in the model; other details and unspecified parameter values for this and subsequent figures are as given by Simmons *et al.* (1983). The contour interval is equivalent to a 40 m interval for geostrophic geopotential height at 45°N, and is similarly expressed for subsequent figures. Positive contours are drawn with solid lines and negative contours are dashed.

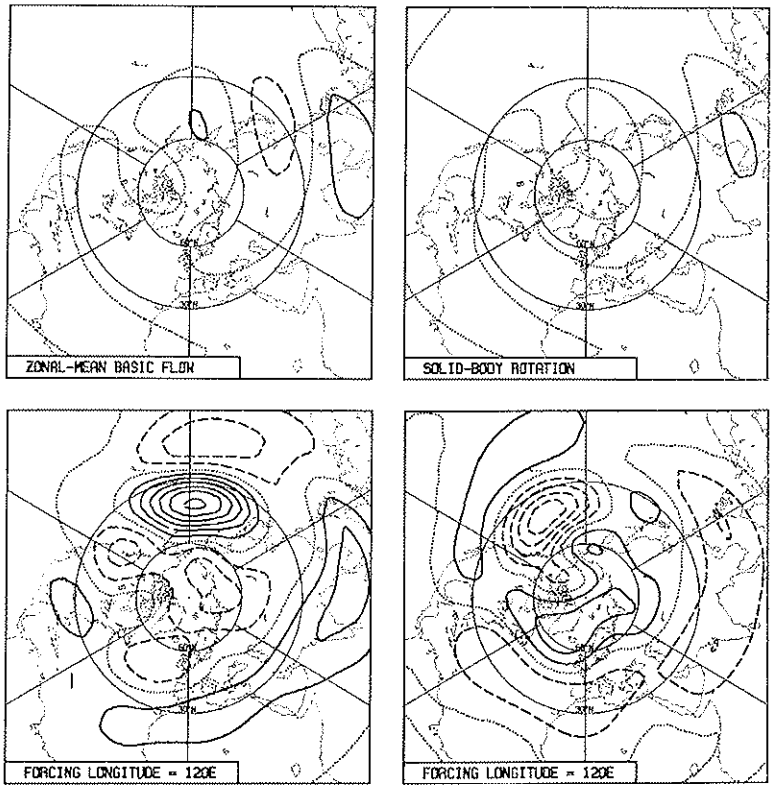

FIG. 2. The steady response to forcing centred at 10°N, 120°E. (Upper left): Anticyclonic forcing, zonal-mean background flow; (Upper right): Anticyclonic forcing, uniformly rotating background flow; (Lower left): Anticyclonic forcing, zonally-varying background flow; (Lower right): Cyclonic forcing, zonally-varying background flow.

time of a little under a week and a period close to 45 days. In localized regions the instantaneous growth rates approach more closely those of baroclinic instability. Episodes of rapid local barotropic growth are interspersed with intervals in which the local perturbation relaxes as energy disperses throughout the hemisphere. This is illustrated in Figure 4, which shows the structure of the mode (with the exponential growth factor suppressed) over one half period. Over the first week or so illustrated, the zonally-elongated dipole grows over the North Pacific with only a very small eastward drift. Subsequently, the mode forms what it is tempting to refer to as the "North American" part of the model's

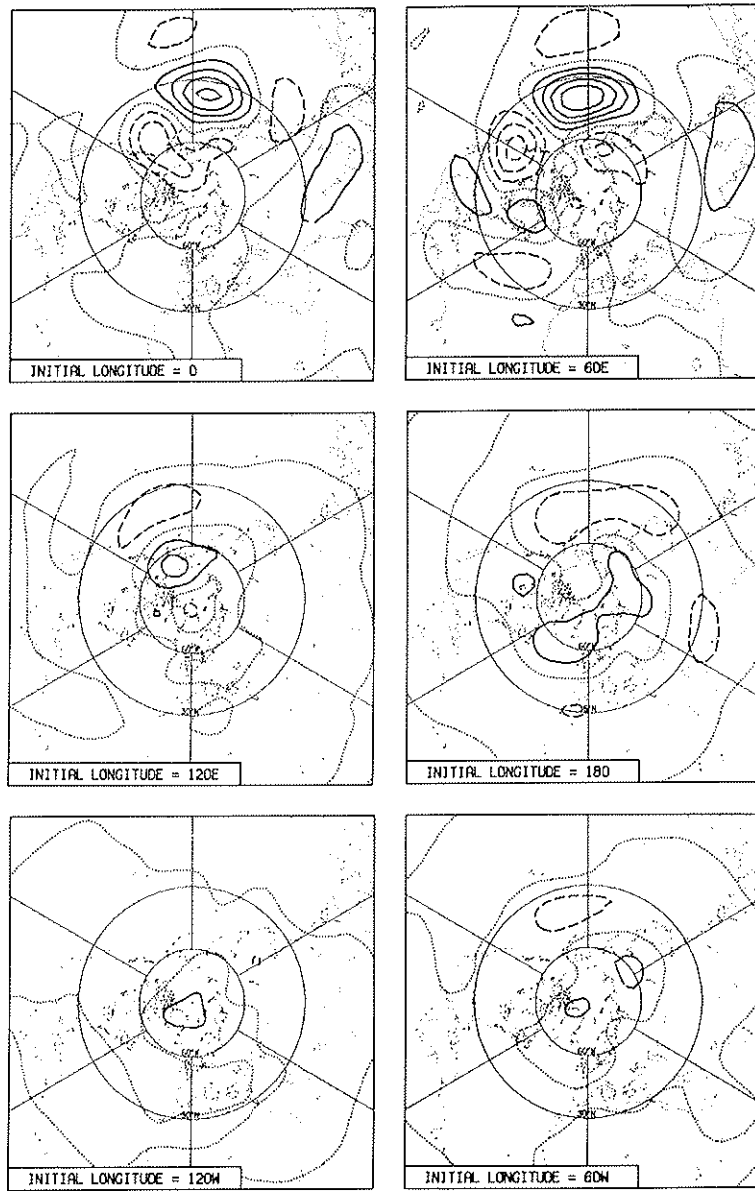

FIG. 3. The streamfunction perturbations at day 10 resulting from nonlinear dispersion of initial disturbances centred at 40°N and six different longitudes. The maximum initial amplitude of the perturbation is 200 m, and the contour interval is 40 m. A 10-day decay time is used for the drag.

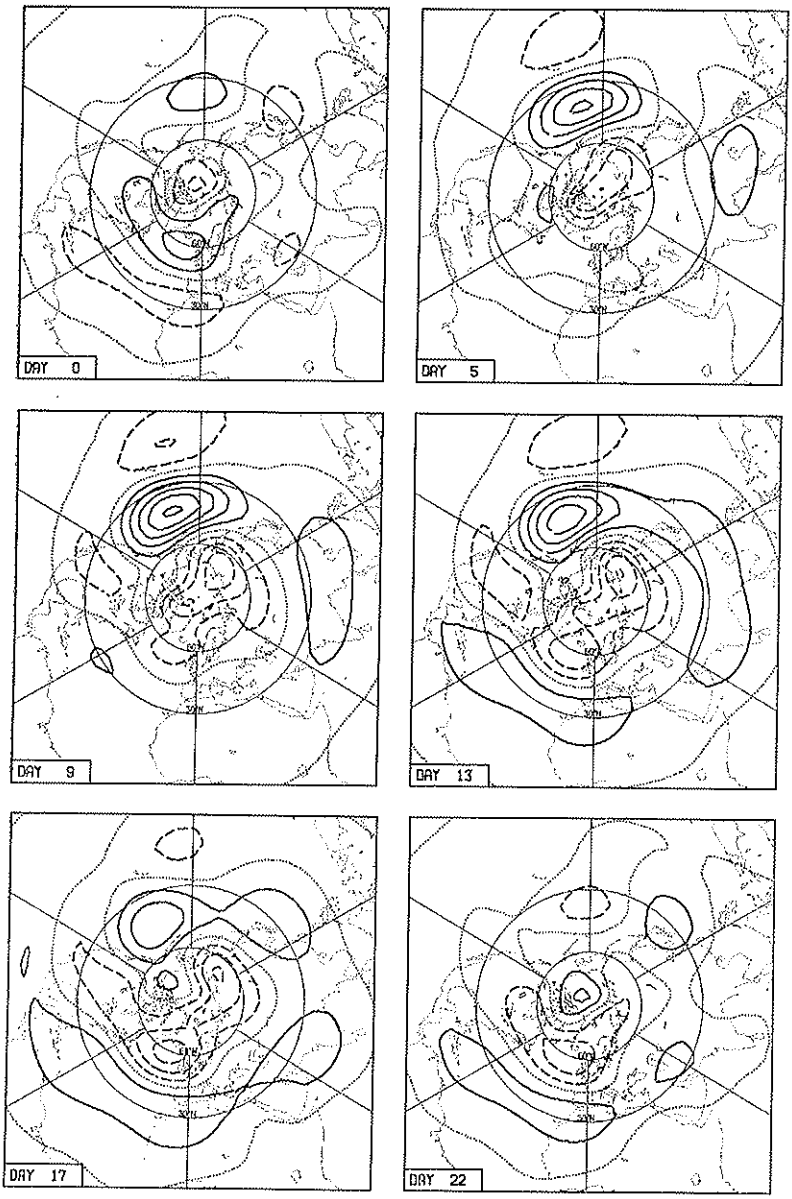

FIG. 4. The streamfunction of the most unstable mode at selected days within one half cycle of its oscillation, for the climatological January background flow. The exponential growth factor is suppressed, and the contour interval is arbitrary.

PNA pattern. As this pattern weakens, the corresponding Atlantic pattern develops.

The dominant processes by which the growing disturbance extracts kinetic energy from the basic state can be described by two conversion terms: $u'v' \partial\bar{u}/\partial y$ and $(v'^2 - u'^2)\partial\bar{u}/\partial x$, where u and v are the velocity components in the zonal (x) and meridional (y) directions respectively, primes refer to the perturbations and overbars to the basic state. For this fastest growing mode the dominant process contributing to the growth is found to be the second term, which is largest in the Pacific jet exit region where the zonally-elongated perturbation is such that $u'^2 \gg v'^2$. This term is also of significant amplitude near the Atlantic jet exit. The first term, representing the energy conversion which arises in barotropic instability of a zonally-uniform basic flow, is of significant magnitude on the northern flank of the strong jet stream over the northeastern Pacific.

The major conclusion derived from these results, and others discussed by Simmons *et al.* (1983), is that certain observed teleconnection patterns may be associated with a preferred barotropic response of the time-mean atmospheric state which can be excited in a variety of ways, including not only forcing due to an anomalous tropical heating, but also the dispersion of eddy energy excited by baroclinic instability, or anomalous extratropical forcing. This view is in accord with the observed occurrence of teleconnection patterns in GCMs with climatological boundary conditions. A consequence is that the observation of wave trains following approximate "great circle" routes does not necessarily imply a tropical source for the perturbation, and even in the case of tropical forcing the position of the wavetrain does not directly imply the position of the source.

Although tropical forcing is not the only way of exciting the preferred wave patterns, it can nevertheless be an effective source of excitation for them. Just as the barotropic model exhibits preferred regions of response in the extratropics, there are regions of the tropics which may excite a particularly large mid-latitude response. One of the most effective of these regions, and one where there is normally a substantial amount of convective activity, is Southeast Asia and the tropical western Pacific. Forcing from this region can readily excite a large response over the extratropical northeast Pacific, and a similar, though weaker, response may be excited by forcing of opposite sign over the tropical central Pacific, as discussed for Figure 1. Thus a tropical anomaly comprising an eastward or westward shift of convective heating between the dateline region and regions lying further to the west, near 120°E, may be a particularly

efficient way of triggering a response which resembles the PNA pattern. Just such a redistribution of convective heating is implied by rainfall and surface-pressure anomalies associated with the Southern Oscillation (Kidson, 1975; Quinn *et al.*, 1978; Liebmann and Hartmann, 1982).

A second major conclusion is that the normal modes associated with the barotropic instability of the zonally varying time mean state may account for an appreciable fraction of the observed low-frequency variability of the geopotential height field during the winter season and, in particular, for the large variability over the Pacific and Atlantic sectors. Whether such perturbations are actually unstable, neutral or damped in the real atmosphere is difficult to determine, but in any case, it seems reasonable to expect that structures resembling the normal modes should be present with disproportionately large amplitudes in comparison to other structures which have no energy source to offset the continuous "spin-down" by boundary layer processes and thermal damping. The same barotropic instability process could conceivably play an important role in restricting the amplitude of the stationary waves to the observed range of values and in limiting the sharpness of the jetstreams.

If barotropic instability is indeed an important source of low frequency variability, it follows that it should make a significant contribution to error growth during the course of medium range numerical prediction. In support of this argument, it can be noted that beyond day 5, forecast error maps from the ECMWF model often show evidence of equivalent barotropic features with horizontal structures qualitatively similar to those derived from initial-value calculations with the barotropic model, particularly when they are averaged over sequences of consecutive days. Examples are presented by Wallace *et al.* (1983).

Other implications of relevance to the design of numerical forecast and general circulation models are suggested by these results. Insofar as inaccurate orographic and thermal forcing in such models may be regarded as a perturbation of the true climatological forcing of the stationary waves, the barotropic model indicates that systematic errors will tend to be largest over the north-eastern Pacific and Atlantic. Such is indeed the case in the operational ECMWF forecast model (e.g., Bengtsson and Simmons, 1983) and in a number of other models. A further consequence is that if the systematic error in a model climatology is such as to give an underestimation of the stationary wave pattern then this model is also likely to underestimate the response to anomalous boundary conditions, for example, anomalies in sea-surface temperature.

3. Some Related Studies

(i) *Idealized modelling*

As in any study involving a relatively simple model, the conclusions discussed in the preceding section must be tempered by recognition of the limitations of the model employed to deduce them. Two particular concerns noted by Simmons *et al.* (1983) were the barotropic nature of the model and the fixed nature of the forcing of the climatological mean state. Subsequent studies have provided evidence which reduces these concerns.

Previously, Frederiksen (1982) had examined the stability of a zonally-varying 8-year mean winter state using a two-layer quasi geostrophic model. Attention was concentrated on the faster growing modes, although the existence of slower growing low frequency (and stationary) modes was also noted. The four most unstable of these latter modes were examined by Frederiksen (1983), and shown to possess upper-level structures resembling the modes discussed by Simmons *et al.* Some westward phase tilt with height was found, and although this was significantly less than was the case for the faster growing baroclinic waves, growth rates were some 20-50% larger than that of the most unstable mode of a barotropic model applied to the upper-level (300 mb) flow. Subsequently, Frederiksen and Puri (1985) studied the non-linear evolution of the most unstable normal mode of the January 1978 mean state, and noted the eventual evolution of a pronounced equivalent-barotropic structure over the north-eastern Pacific. The agreement with the observed PNA pattern was far less striking than shown in the preceding section, but it will be seen in section 4 that the principal modes of barotropic instability for particular monthly means can be quite different from those of the climatological basic state.

Concerning the modelling of the forcing of the basic state, Andrews (1984) drew attention to the fact that the stability properties of zonally-varying flows will in general depend not only on the flow configuration, but also on the forcing mechanism. A specific calculation by Zhang (personal communication) in which a term describing the flux of vorticity by the divergent component of the climatological flow was included in the barotropic model, thereby altering the fixed component of the forcing, has shown that the most unstable mode illustrated in section 2 is little changed. However, the slower growing modes discussed by Simmons *et al.* (1983) were significantly altered, and their significance is thus open to question.

Further support for the relevance of the most unstable mode is

provided by a study by Hendon (1986a) of a highly idealized general circulation model in which a zonally-varying time-mean flow is forced by an isolated orographic feature. Hendon found a maximum of low-frequency variability downstream of the jet maximum that occurred in the lee of the orography. Correlation maps revealed the tendency for a geographically-fixed anomaly pattern to develop, and the temporal evolution and barotropic energy source for this pattern was similar to that over the Pacific/North American region discussed in the preceding section. The pattern was distinctly different from any seen in the absence of the orographic forcing (Hendon and Hartmann, 1985), even with the inclusion of a localized tropical diabatic heating (Hendon, 1986b).

(ii) *General circulation modelling*

Results from a number of integrations of general circulation models including anomalous sea-surface temperatures in the tropical Pacific (Blackmon *et al.*, 1983; Geisler *et al.*, 1985; Palmer and Mansfield, 1986a,b) are also worthy of discussion here, as are further barotropic modelling studies of the type presented in section 2 (Branstator, 1985a,b). The latter were aimed at furthering understanding of the specific results obtained by Blackmon, Geisler and their collaborators.

In the study by Blackmon *et al.* (1983), extratropical anomalies agreeing closely with the observed PNA pattern were excited in 90-day mean fields by the anomalous surface forcing. Branstator (1985a) achieved success in reproducing the extratropical perturbation pattern when the zonally-varying climatological mean 300 mb flow of the general circulation model was used as the background state and anomalous forcing was modelled on the anomalous simulated rainfall of the GCM. Amplitudes were, however, significantly weaker than found by Blackmon *et al.* Branstator (loc. cit.) also found that similar calculations could not directly explain a result of simulations by Geisler *et al.* (1985) which showed the pattern (but not the amplitude) of the long-term extratropical response to be sensitive to forcing over the East Indies, so that small anomalies in vorticity However, as discussed in section 2, the barotropic model is particularly sensitive to forcing over the East Indies, so that small anomalies in vorticity forcing over this region may be of more significance than the major forcing anomaly near the region of anomalous surface temperature.

Branstator (1985b) moreover showed that the long-term mean state of the general circulation model in question exhibited a maximum growth

rate for barotropic instability about half that of the observed mean atmospheric state, suggesting that the model might underestimate the importance of the barotropic instability mechanism. The most unstable mode had a structure similar to that of the recurring anomaly patterns of the general circulation model, although a clear identification of the relevance of any one mode or group of modes could not be obtained.

Palmer and Mansfield (1986a) examined the response to anomalous tropical forcing in two versions of a general circulation model. One had a higher orography, and possessed a flow with a significantly stronger jet stream over the western Pacific and a larger diffluence in the vicinity of the dateline. Only this version exhibited an anomaly pattern close to the observed PNA. This is in accord with expectations based on the barotropic modelling studies, although Palmer and Mansfield identify a different (and perhaps complementary) mechanism involving differences in forcing by high-frequency eddy activity (related to jet-stream differences) over the Pacific, together with a direct orographic influence over North America, arising from the representation of the Rockies.

In a companion paper, Palmer and Mansfield (1986b) examined sensitivity to different patterns and intensity of sea surface temperature anomalies. A strong response over the PNA area was found for a relatively weak anomaly over the West Pacific, in agreement with the conclusion drawn from the barotropic model. Insofar as the further west the El Niño temperature anomalies extended the larger was the response, Palmer and Mansfield's results were also in accord with those of Geisler *et al.* (1985), although the former authors found more variation in the position of the extratropical anomaly.

(iii) *Observational studies*

Studies of composite observed anomalies by Dole (1983) and of time-lagged one-point correlation maps by Blackmon *et al.* (1984b) reveal growth more or less in situ of the Pacific dipole of the PNA pattern, accompanied by the formation of anomaly centres in sequence downstream. In this respect the development closely resembles the appropriate stage in the life cycle of the barotropic normal mode shown in Figure 4. Examining only low-frequency components does not yield a clear picture of a characteristic initial trigger of the anomaly pattern. However, Dole (loc. cit.) displays unfiltered 15-case composites for days prior to the development of a strong mean positive anomaly over the northern Pacific, and these

indicate that the main centre evolves from a propagating, intensifying disturbance moving from Japan to the dateline over a three-day period, a result emphasized by Frederiksen in discussion of his idealized modelling studies summarized previously.

In the pure normal mode form presented in Figure 4, dispersion away from the barotropically unstable source region in the North Pacific acts to trigger the onset of the Atlantic dipole pattern, and the subtropical residual of the Pacific dipole drifts north to amplify as the main perturbation of opposite sign during the second half of the period of the normal mode. With the presence in reality of higher-frequency baroclinic eddies and of various surface forcings, it is perhaps not surprising that the regular oscillatory nature of the normal mode is not obvious in the observational record (Blackmon *et al.*, 1984b). However, the barotropic energy source of the mode has a clear counterpart in both reality and general circulation model statistics, as reviewed by Wallace and Lau (1985).

In a study of intra-seasonal variability based on correlations of 5- and 10-day means of 500 mb heights with tropical outgoing infrared radiation, Liebmann and Hartmann (1984) showed a predominant influence of middle latitudes on the tropics rather than vice-versa. However, an indication of possible forcing of middle-latitude anomalies from the tropics was found in association with radiative anomalies over the far western Pacific, the most likely region suggested by the barotropic model. The extratropical structure was similar to that produced by localized tropical forcing of this model. The observed correlations did not, however, support the modelling result that a sharp phase reversal occurs in the mid-latitude response as the forcing region is moved eastward, although as with the GCM results, uncertainty exists as to the location of the effective tropical vorticity source in such studies (Hoskins, personal communication). It should also be noted that the absence of a marked tropical influence on mid-latitude anomalies in Liebmann and Hartmann's results may also reflect the predominant timescales studied. Blackmon *et al.* (1984a) show that on intermediate time scales (with 10-30 day periods) the dominant patterns of atmospheric variability consist of wavetrains which originate in jet entrance regions and curve southeastward into the tropics; only on longer timescales do the teleconnection patterns on which our attention is concentrated predominate.

4. The Stability of Monthly-Mean Anomaly Patterns

(i) *Choice of cases*

As a further test of the relevance of the barotropic model, calculations of the type carried out by Simmons *et al.* (1983) have been repeated for flows derived from actual monthly-mean circulations computed using the regular operational analyses produced by ECMWF. Four particular 30-day means were chosen, with starting dates 1 January 1981, 11 January 1983, 1 January 1984 and 1 December 1985. Deviations of mean 500 mb heights from climatology are shown in Figure 5.

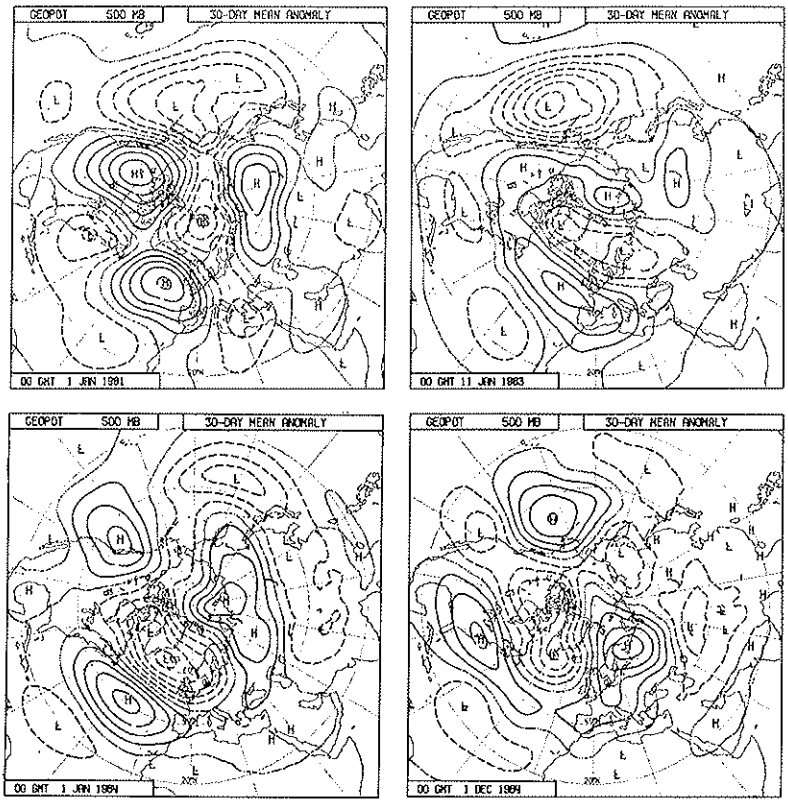

Fig. 5. Deviations from climatology of 30-day mean 500 mb height analyses starting from 1 Jan 1981 (upper left), 11 Jan 1983 (upper right), 1 Jan 1984 (lower left) and 1 Dec 1984 (lower right). The contour interval is 40 m.

The first two spells were chosen because they were known to exhibit a pronounced low-pressure anomaly over the North Pacific, with high pressure to the south in the subtropics. Moreover, in both cases the anomalies were quite stable in the sense that broadly similar patterns are seen in the Pacific/North American sector in individual 10-day means within the period (Figure 6). The second two cases were chosen from a search of monthly-mean anomalies for the December to February period, starting from December 1980. The aim was to choose two cases with pronounced stable high-pressure anomalies over the North Pacific. In the event, it was found that low-pressure anomalies tended to predominate during the period under study, and the monthly-mean anomalies for the chosen months of January and December 1984 shown in Figure 5 are (for the January case in particular) less reproducible in the 10-day means within each period (Figure 7) than shown in Figure 6 for the first two cases. Moreover, means for the subsequent monthly periods presented in Figure 8 show that the anomalies approximately reversed in sign over the Pacific for the latter two cases, whereas for the former two a similar Pacific anomaly was present in the following month, particularly in the 1983 case, which coincided with exceptionally warm sea-surface temperatures in the tropical eastern Pacific.

An incidental consequence of the predominance of low-pressure anomalies is that short-term ECMWF climatologies exhibit a less marked diffluence in the central North Pacific than in the longer term climatologies (Crutcher and Meserve, 1970) used here and for the earlier barotropic studies. This results in a most unstable barotropic mode for the short-term climatology that has a growth rate about half that computed using the longer term mean (Zhang, personal communication).

(ii) *Normal mode instability*

Barotropic stability calculations have been carried out for each of the four 30-day means, and also for four basic states computed by simply reversing the signs of the anomalies observed in each of the four spells in question. Plots of e-folding time and period for all modes with e-folding times of 10 days or less are presented in Figure 9, in which the open circles denote modes for the observed states, closed circles denote the modes for the anomaly of opposite sign, and open triangles the modes for the January climatological state determined as described by Simmons *et al.* (1983).

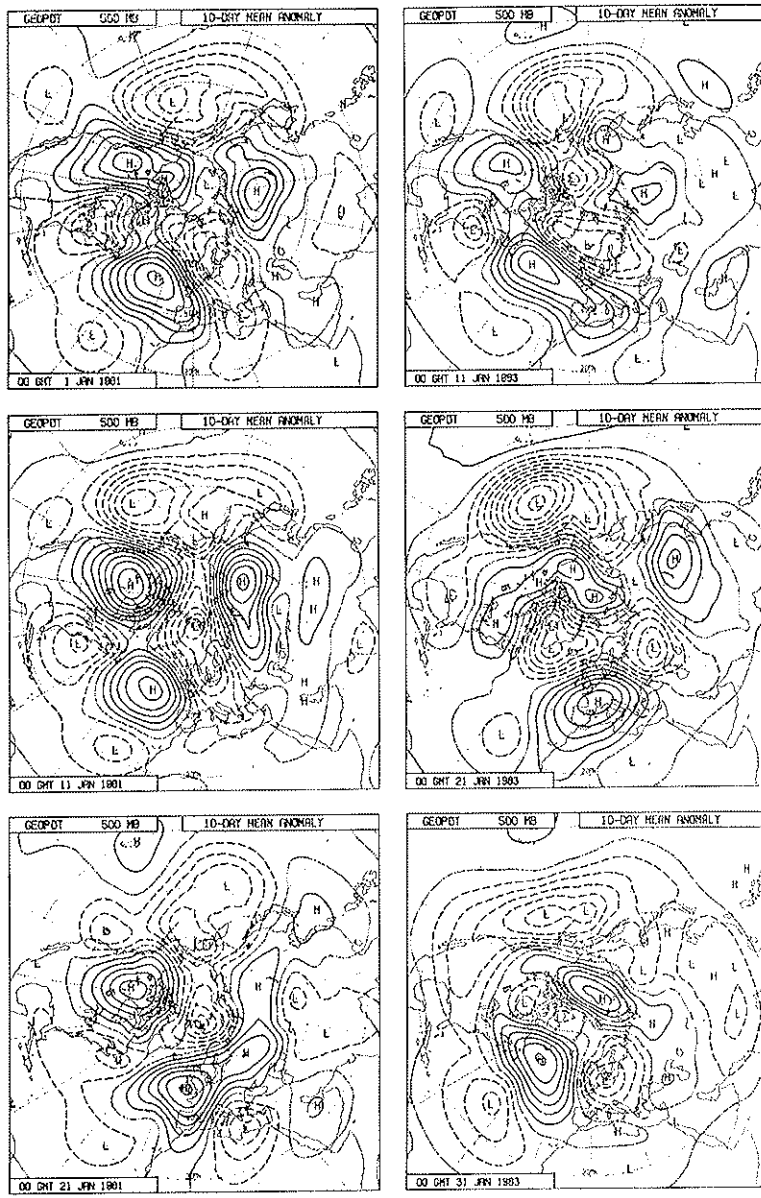

FIG. 6. Deviation from climatology of three consecutive 10-day means of 500 mb height beginning 1 Jan 1981 (left) and 11 Jan 1983 (right). The contour interval is 40 m.

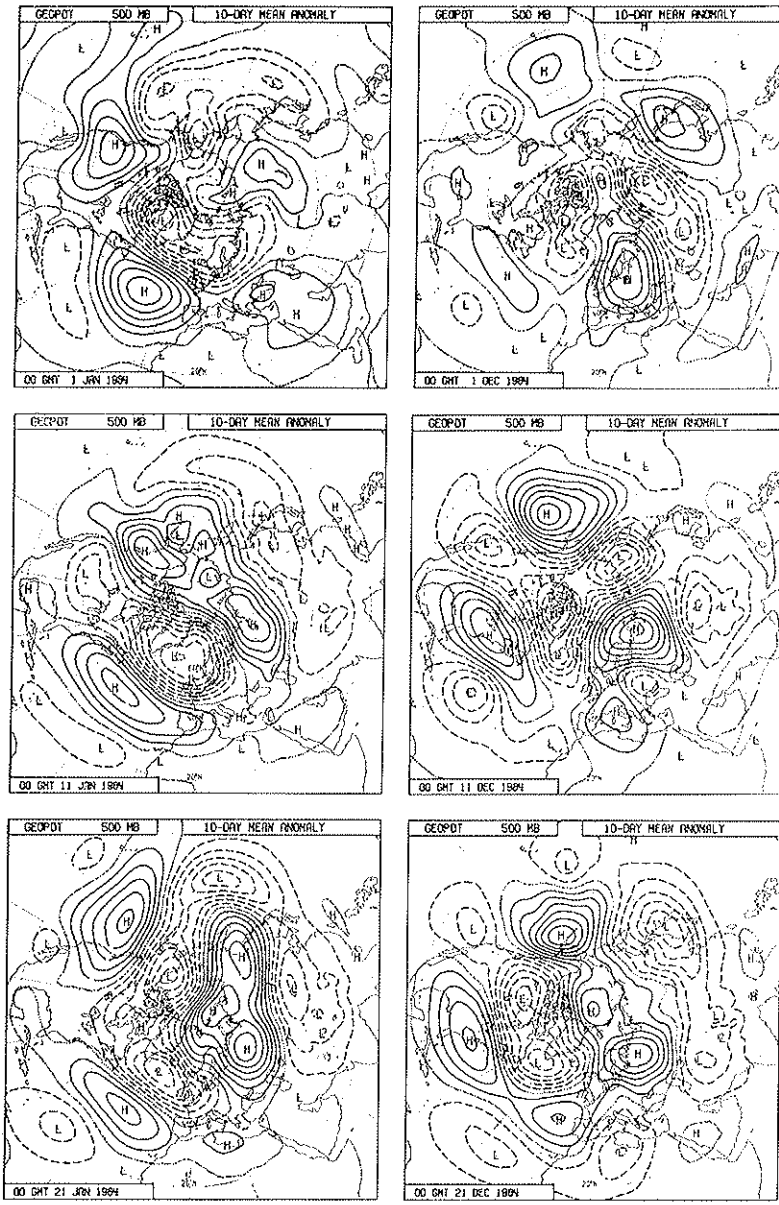

FIG. 7. Deviations from climatology of three consecutive 10-day means of 500 mb height beginning 1 Jan 1984 (left) and 1 Dec 1984 (right). The contour interval is 40 m.

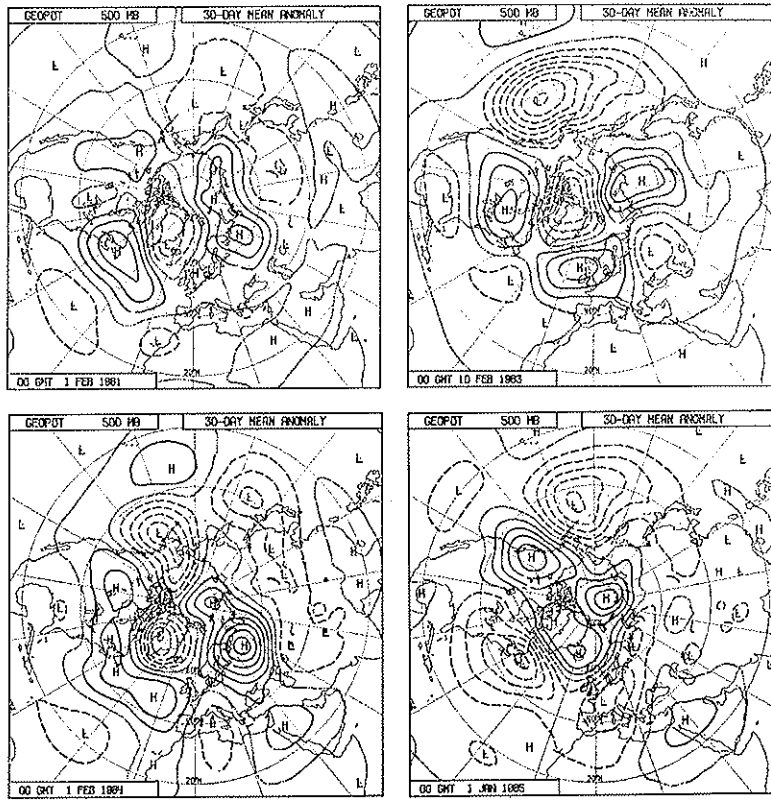

FIG. 8. Deviations from climatology of 30-day mean 500 mb heights starting from 1 Feb 1981 (upper left), 10 Feb 1983 (upper right), 1 Feb 1984 (lower left) and 1 Jan 1985 (lower right). The contour interval is 40 m.

The barotropic instability calculation evidently distinguishes the observed anomalies from those of opposite sign. The latter give rise to faster growth rates, with one or more modes with e-folding times under 4 days in each case. A stationary pattern is found for one such mode in three of the cases. Conversely, two of the observed monthly-mean states yield no modes with e-folding times shorter than the 7 days of the most unstable mode of the climatological state.

The separation between observed and reversed anomalies becomes even clearer when the structures of the more unstable modes are examined. Considering first January 1981, for which two modes of the observed

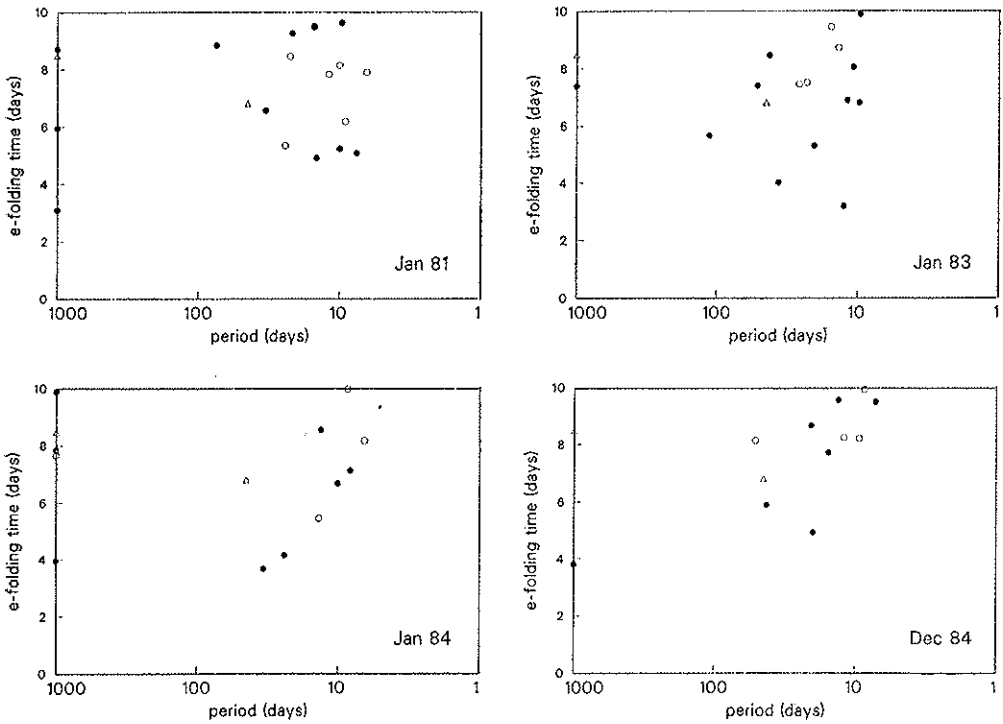

FIG. 9. E-folding times and periods (days) of unstable modes computed for basic states based on 30-day means for Jan 1981 (upper left), Jan 1983 (upper right), Jan 1984 (lower left) and Dec 1984 (lower right). The open circles denote modes for the actual observed mean states, and the solid circles modes for basic states in which the signs of the observed anomalies were reversed. Triangles denote modes for the climatological January basic state. Only modes with e-folding times below 10 days are shown, and stationary modes are plotted at the 1000-day period point of the logarithmically-scaled abscissa.

state grow faster than climatology, the structures in the Northern Hemisphere of the four most unstable modes are presented in Figure 10 for the observed circulation. The absence of amplitude in the upper-left plot shows that the most unstable mode for the observed state is confined to the Southern Hemisphere, and can be discounted for the purposes of this study. The other modes illustrated in Figure 10 have relatively short periods. Over the Pacific, the second and third most unstable modes have significant amplitude only around 140°W near the jet exit region for the month in question (as may be seen by reference

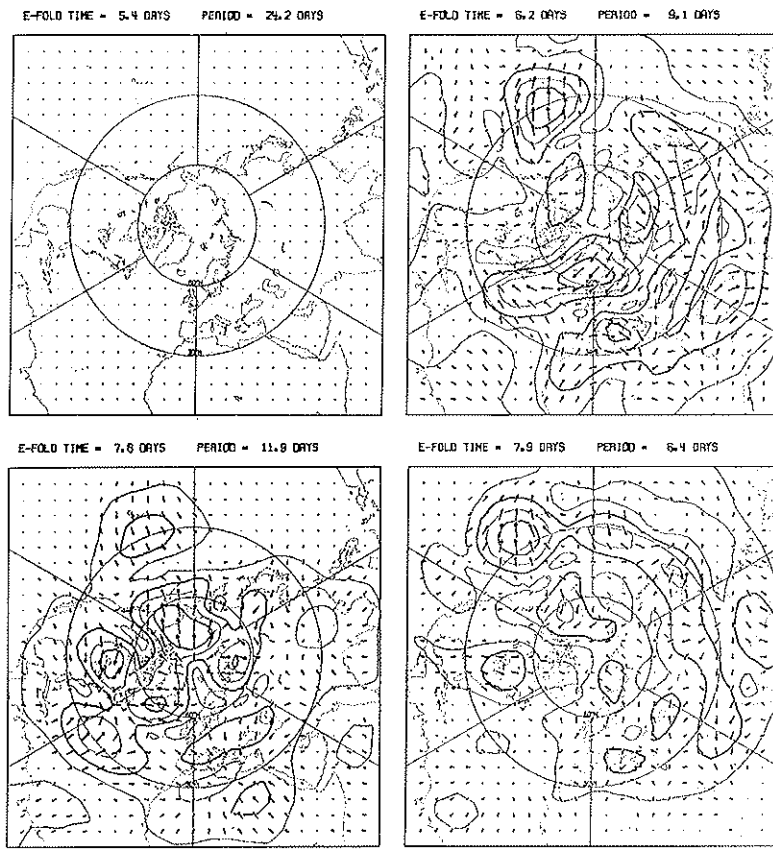

FIG. 10. The structure in the Northern Hemisphere of the four most unstable normal modes for the observed Jan 1981 basic state. Contours and arrow lengths denote amplitude, and the contour interval is 1/5 of the maximum global value. The direction of the arrows denotes phase, with a clockwise rotation representing a passing of time.

to Figure 14), and the higher-frequency fourth mode also has maximum amplitude in this region. One half period of the second mode is illustrated synoptically (with the exponential growth factor again removed) in Figure 11. The perturbation in the exit region of the Pacific jet is seen to develop rapidly, and subsequently disperse. Wave trains directed eastward and equatorward from a growth region in the North Atlantic can also be seen, and patterns bear some similarity to the observed "intermediate time-scale" variability, as identified by Blackmon *et al.* (1984a).

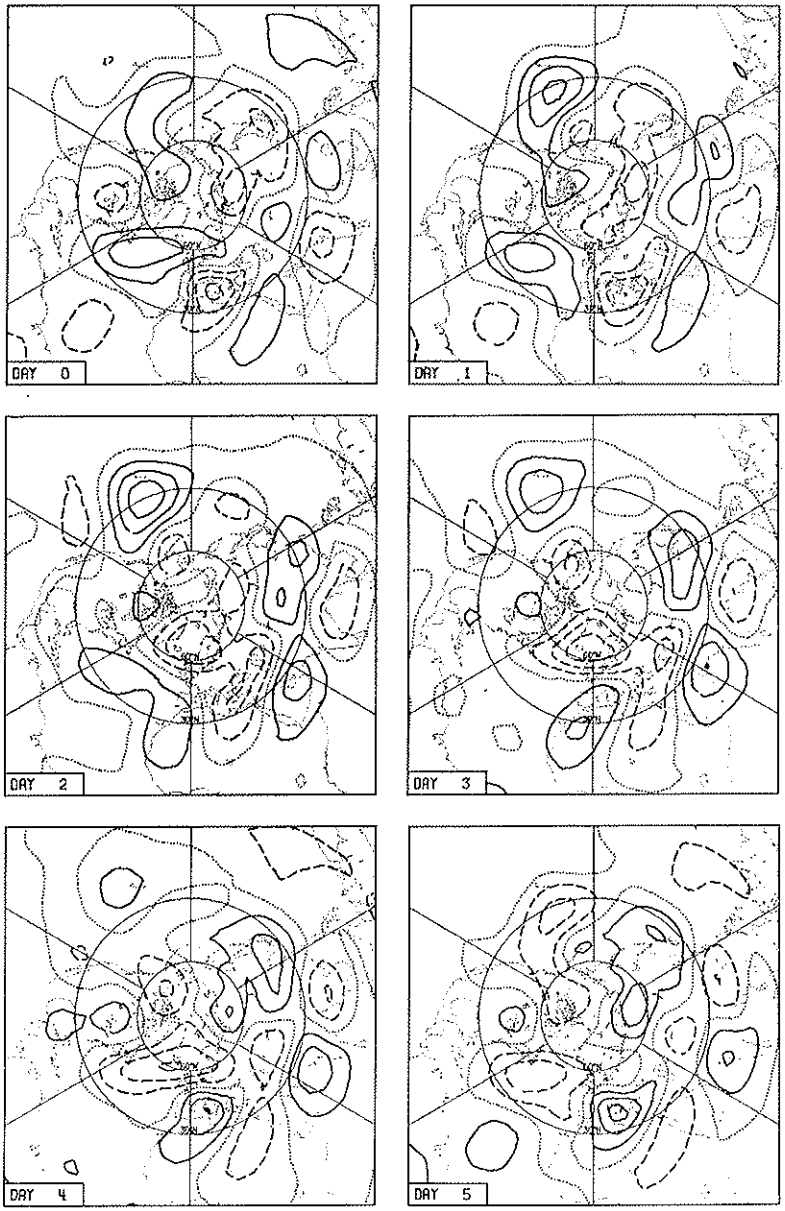

FIG. 11. The streamfunction of the second most unstable mode of the observed Jan 1981 basic state at daily intervals. The exponential growth factor is suppressed.

Three of the four most unstable modes shown in Figure 12 for the reverse of the January 1981 anomaly exhibit substantial amplitude over the North Pacific and northeastern Asia. The regions of maximum amplitude of these modes are broadly similar, although periods differ. Zonally-elongated perturbations and a change in sign of the mode between middle latitudes and the subtropics are evident over the Central Pacific, in a region of diffluence of the forced basic state (which is shown in Figure 15, upper left panel).

Of the other unstable modes of the four observed mean states, only

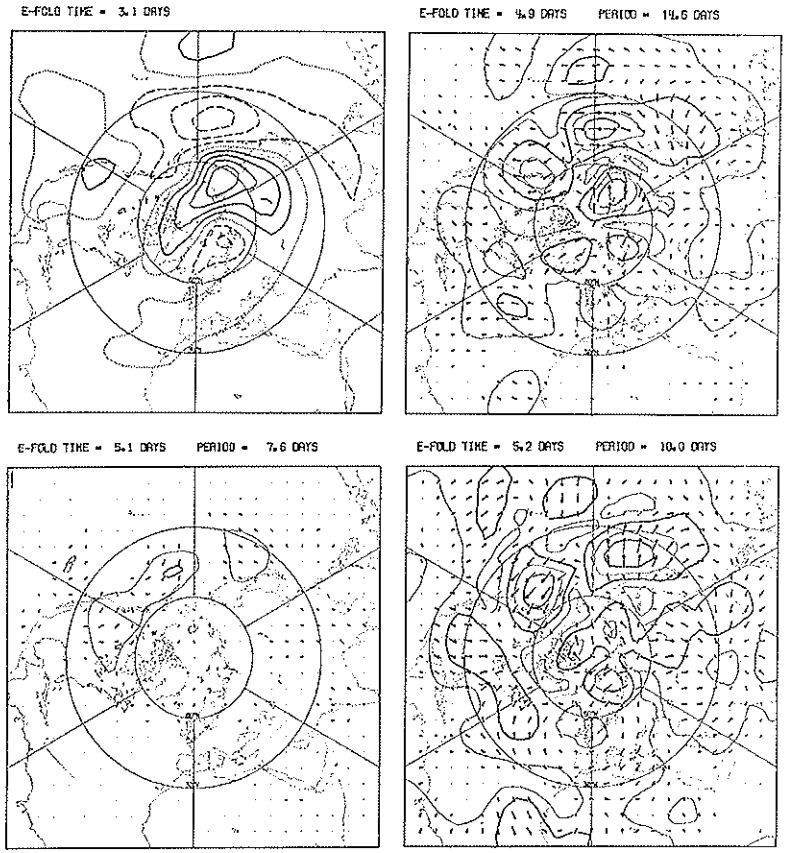

FIG. 12. Normal-mode structures corresponding to those shown in Fig. 10, but for the basic state in which the observed Jan 1981 anomaly is reversed in sign. The fastest growing mode is stationary, and is plotted using positive and negative contours rather than phase arrows.

one (for January 1984) grows faster than the most unstable mode for the climatological-mean January state, and its evolution over half a period is shown in Figure 13. This mode has a relatively simple structure, with growth in situ of an isolated, zonally elongated perturbation in the Pacific jet exit (see Figure 16, centre left panel) followed by dispersion downstream over North America and the western Atlantic. The mode shows only weak evidence of a secondary energy source over the North Atlantic.

(iii) *Initial-value problems*

Non-linear initial value problems generally confirm the results of the stability analyses, but indicate that some modes may be more effective than others of similar growth rate in bringing about change in the forced wave pattern. In particular, results for the observed January 1984 basic state reveal a more unstable pattern than for January 1983 and December 1984, as suggested by the distribution of growth rates shown in Figure 9, but those for January 1981 show only a slight increase in variance over the two months associated with lower normal-mode growth rates. Thus the mode illustrated in Figure 11 for January 1981 appears to be less disruptive than its counterpart for January 1984 shown in Figure 13, although its linear growth rate is not substantially smaller. In each case, reversing the sign of the anomaly is found to result in a much larger time-mean change and temporal variability.

This behaviour is illustrated in a set of results in which the forced state is perturbed by an isolated initial disturbance centred at 40°N on the Greenwich Meridian. Figure 14 shows the evolution of the total field over 50 days for the January 1981 mean state, and Figure 15 presents the corresponding maps for the reverse anomaly. The stability of the flow pattern in the first case, and the substantial change in the second, are evident. Figure 16 shows the initial and day-50 maps for the three other observed states. The stability of the patterns for January 1983 (upper) and December 1984 (lower), and the large change for January 1984 (middle) can be clearly seen.

Extending these integrations beyond 50 days reveals some increase in variability for the observed states, but the general conclusions are unchanged. Figure 17 shows means and standard deviations computed for days 101 to 300 for the January 1981 state (upper) and the corresponding reverse anomaly (lower), and Figure 18 contains similar plots for the three other observed states. The higher variability of the January 84 state is again apparent.

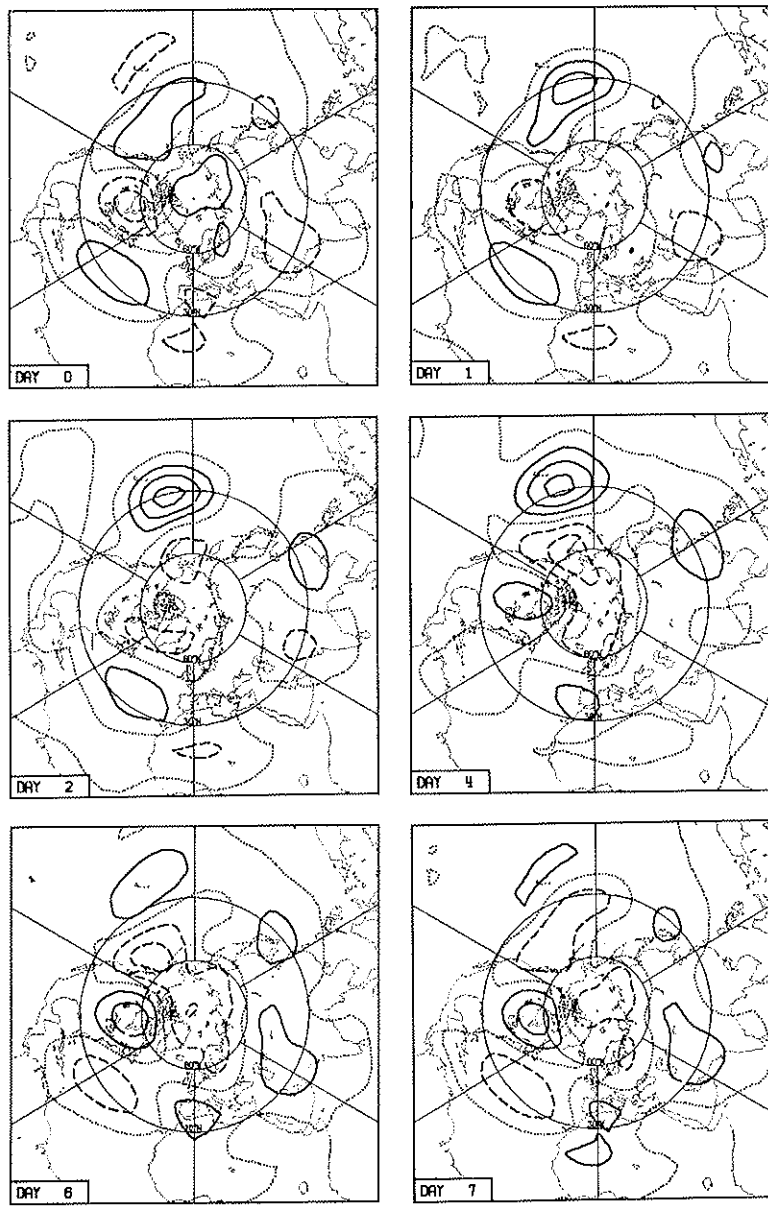

FIG. 13. The streamfunction of the most unstable mode of the observed Jan 1984 basic state at selected days within one half cycle of its oscillation, with the exponential growth factor suppressed.

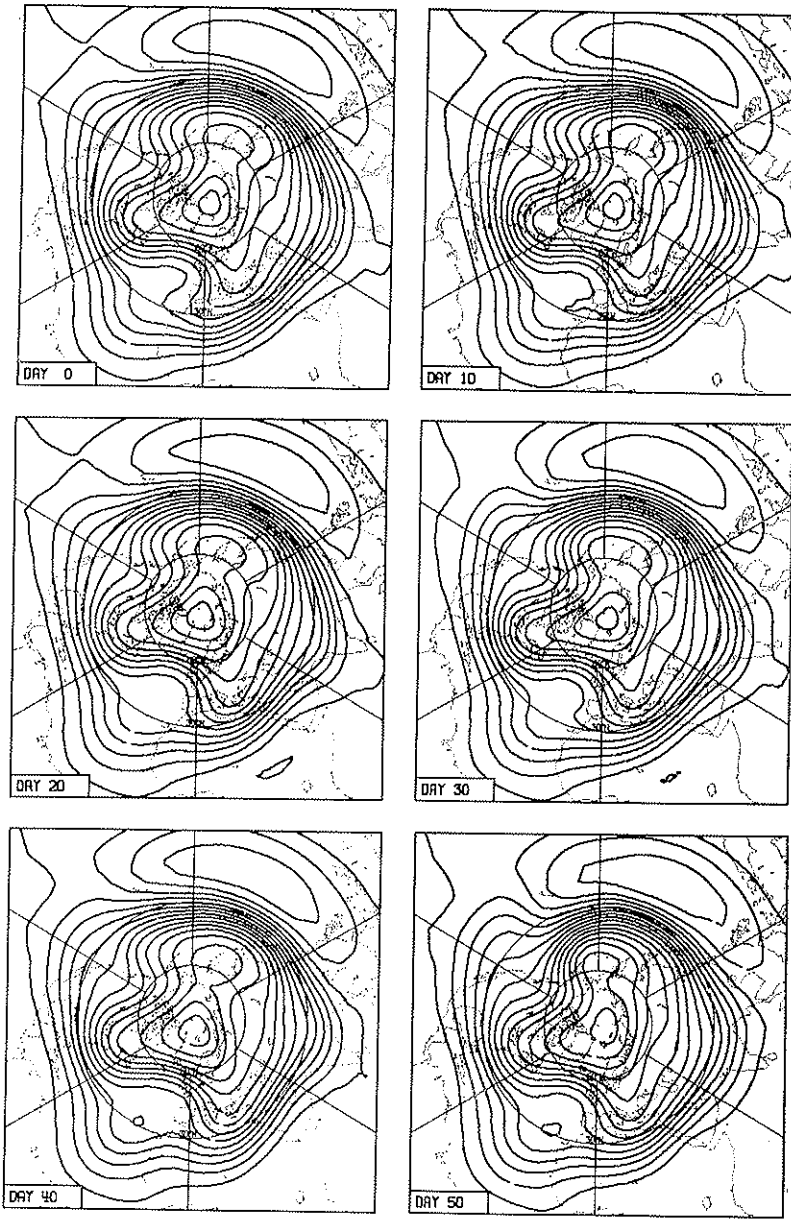

FIG. 14. Total streamfunction at 10-day intervals when the Jan 1981 basic state is initially perturbed locally around 40°N and the Greenwich Meridian. A 10-day decay time is used for the drag. The contour interval is 120 m.

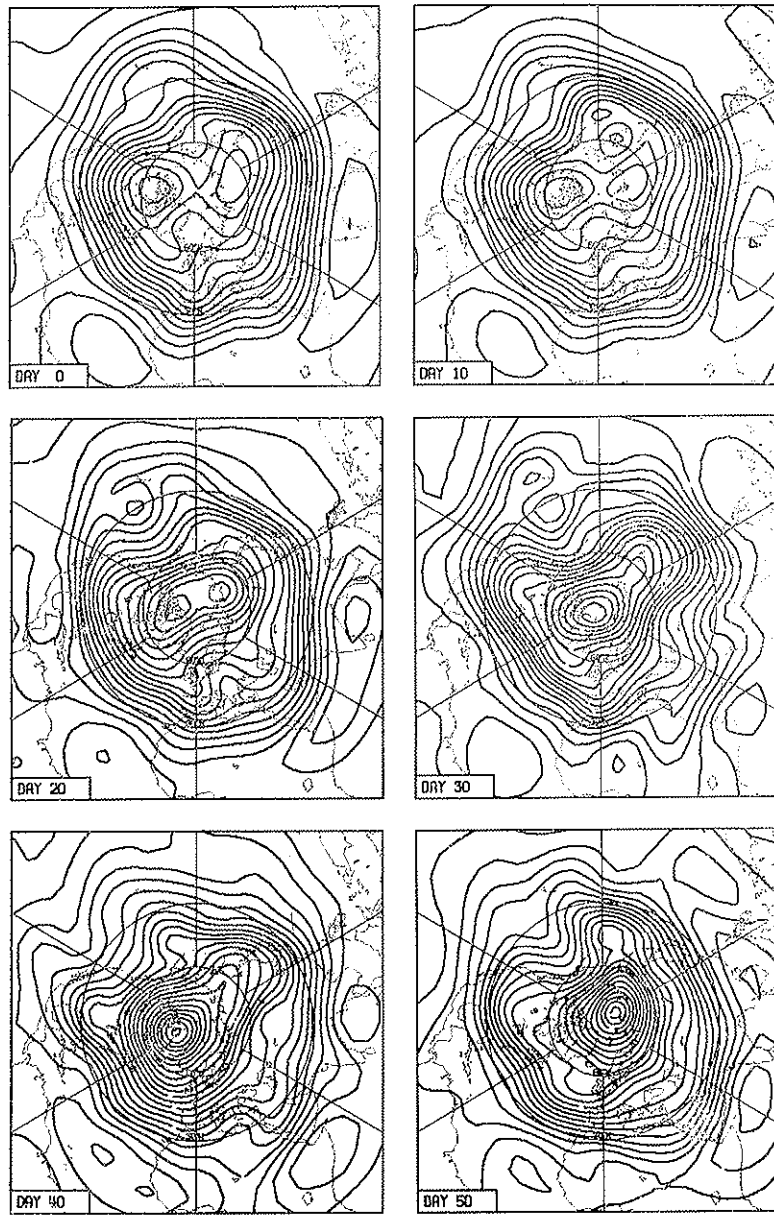

FIG. 15. As Fig. 14, but for the basic state in which the Jan 1981 anomaly is reversed.

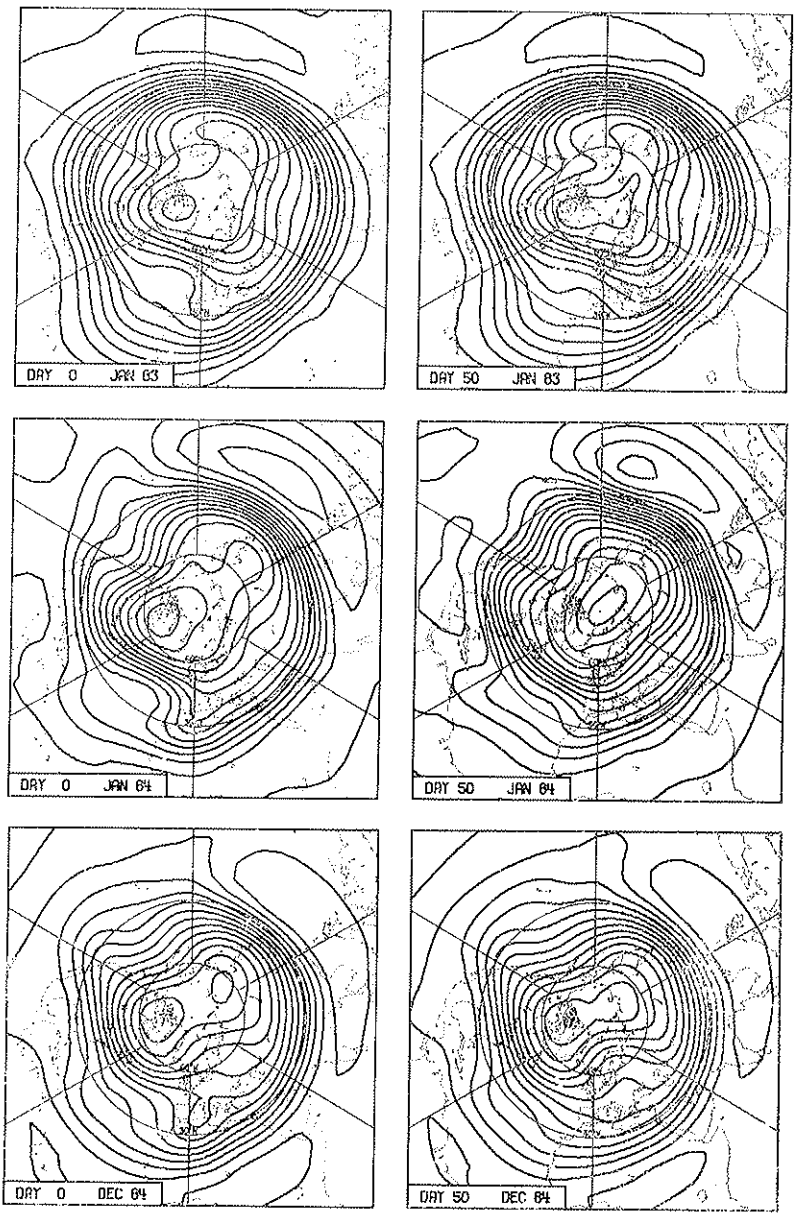

FIG. 16. Total streamfunction at days 0 and 50 for initial value problems as shown in Figures 14, but for the observed Jan 1983 (upper), Jan 1984 (middle) and Dec 1984 (lower) basic states.

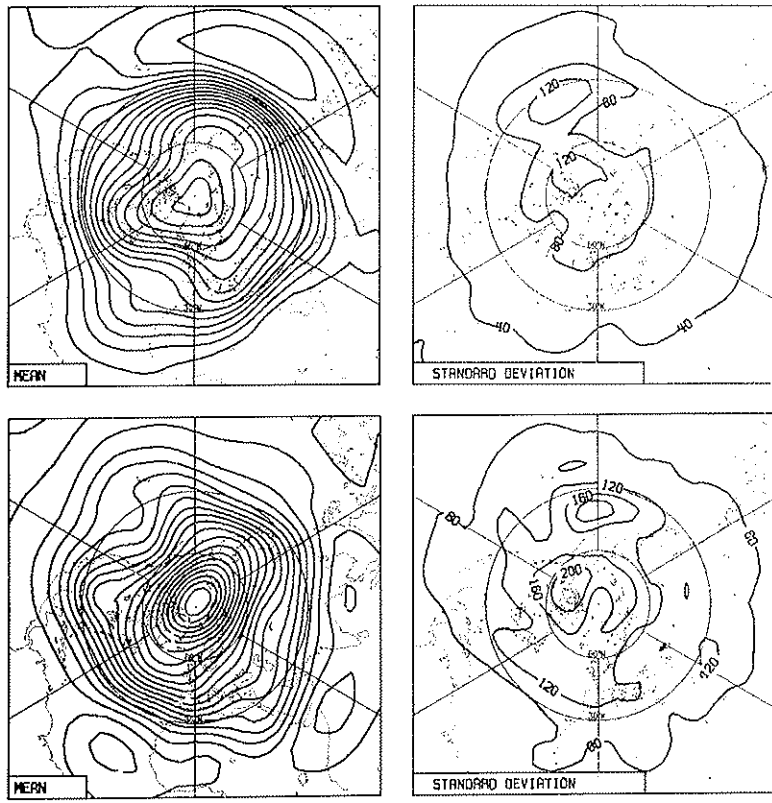

FIG. 17. Mean streamfunctions (contour interval 120 m) and standard deviations (units m) from days 101 to 300 of the integrations shown for days 0 to 50 in Figures 14 and 15. Upper plots are for the observed mean (Jan 1981) state, and the lower plots for the reverse-anomaly case.

5. CONCLUSIONS

A summary has been given of the nature of perturbations to a barotropic model in which the climatological upper tropospheric flow for January is maintained by a fixed forcing. Structures which clearly resemble observed persistent anomaly patterns with amplitude maxima over the North Pacific and Atlantic have been identified. The model gives virtually no indication of the third observed region of large low-frequency variability over the Siberian Arctic.

Subsequent idealized modelling studies have confirmed the principal

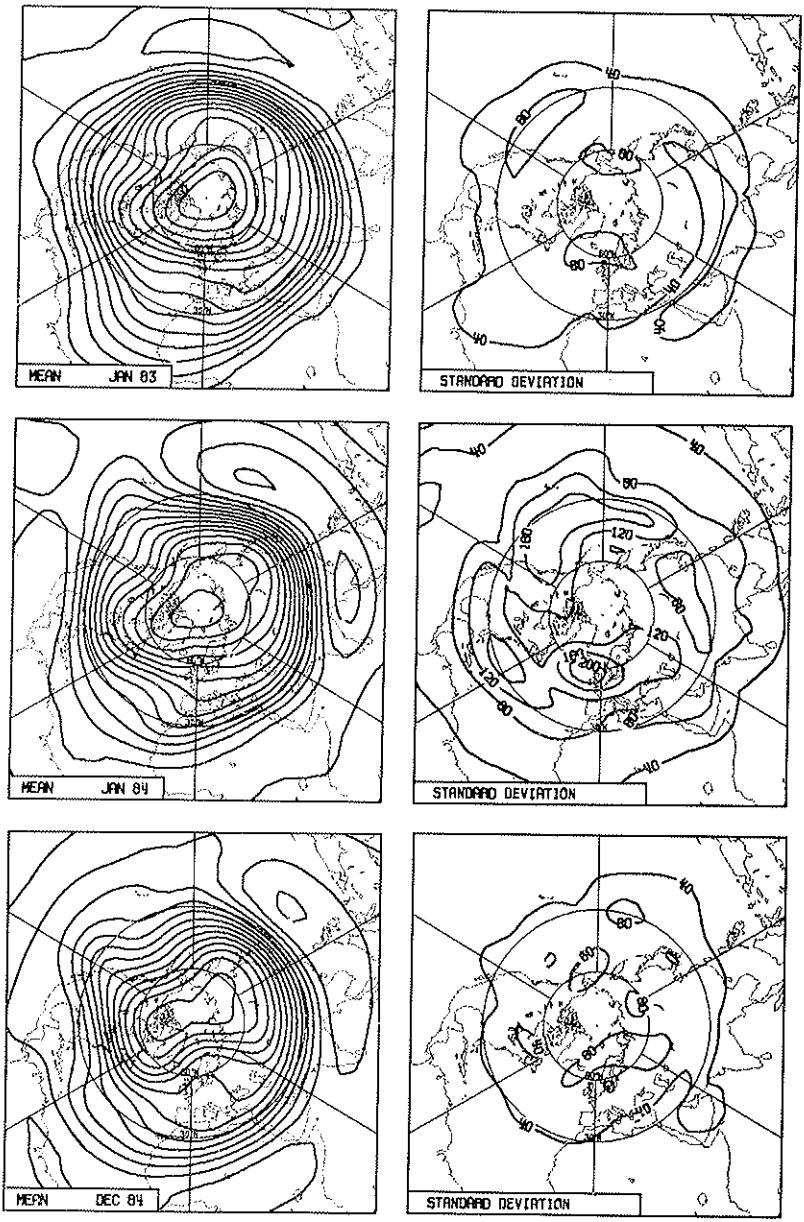

FIG. 18. Means and standard deviations as in Figure 17, but for observed mean states for Jan 1983 (upper), Jan 1984 (middle) and Dec 1984 (lower).

results obtained with the basic barotropic model. Conclusions appear generally to have been borne out by diagnosis of the behaviour of general circulation models and by some observational studies. Since variations in tropical forcing in key regions can excite a disproportionately large extra-tropical response in the barotropic model, detailed comparison with certain GCM or observational results requires a precise picture of the effective vorticity source associated with tropical heating anomalies. In view of the simplicity of the model, it is perhaps anyway only the broader qualitative conclusions that can at best be expected to withstand future scrutiny.

Applying the model to basic states derived from observed monthly mean analyses shows that it is capable of distinguishing between the stability of actual monthly means and the much more unstable nature of artificial basic states constructed by simply reversing the sign of the observed anomalies. These calculations provide further interesting examples of the structure of barotropically unstable modes of zonally varying basic states. The model indicates that one of the four observed mean states studied was more unstable than the other three. In reality, this and (perhaps to a lesser extent) one other state exhibited more variability than the other two.

The idealized modelling results discussed here are sufficiently encouraging to justify further effort along these lines. There is scope for a much more extensive examination of the relevance of the barotropic model as an indicator of the stability of actual time-mean anomalies. Additional investigations might enhance understanding of the predictability (either potential or that achieved by comprehensive forecasting systems) of medium and longer time ranges. Development and application of more realistic baroclinic models is a further challenging task, bringing with it the question of how to deal with the faster developing baroclinic instabilities that arise if the type of approach followed here is directly transferred to a baroclinic model.

Acknowledgements

It is a pleasure to acknowledge the input of collaborators J.M. Wallace and G.W. Branstator to much of the work reviewed here, and B.J. Hoskins for helpful conversations on several aspects.

REFERENCES

ANDREWS D.G., *On the stability of forced non-zonal flows.* « Quart. J. Roy. Meteor. Soc. », *110*, 657-662 (1984).

BENGTSSON L. and SIMMONS A.J., *Medium-range weather prediction — operational experience at ECMWF.* In: « Large-Scale Dynamical Processes in the Atmosphere ». Eds. B.J. Hoskins and R.P. Pearce, Academic Press, pp. 337-363 (1983).

BLACKMON M.L., GEISLER J.E. and PITCHER E.J., *A general circulation model study of January climate anomaly patterns associated with interannual variation of equatorial Pacific sea surface temperatures.* « J. Atmos. Sci. », *40*, 1410-1425 (1983).

BLACKMON M.L., LEE Y.-H. and WALLACE J.M., *Horizontal structure of 500 mb height fluctuations with long, intermediate and short time scales.* « J. Atmos. Sci. », *41*, 961-979 (1984a).

BLACKMON M.L., LEE Y.-H., WALLACE J.M. and HSU H.-H., *Time variation of 500 mb height fluctuations with long, intermediate and short time scales as deduced from lag-correlation statistics.* « J. Atmos. Sci. », *41*, 981-991 (1984b).

BRANSTATOR G., *Analysis of general circulation model sea-surface temperature anomaly simulations using a linear model.* Part I: *Forced solutions.* « J. Atmos. Sci. », *42*, 2225-2241 (1985a).

BRANSTATOR G., *Analysis of general circulation model sea-surface temperature anomaly simulations using a linear model.* Part II: *Eigenanalysis.* « J. Atmos. Sci. », *42*, 2242-2254 (1985b).

CRUTCHER H.L. and MESERVE J.M., *Selected level heights, temperatures and dew points for the Northern Hemisphere.* NAVAIR ATLAS 50-IC-52, Chief Naval Operations, Washington, DC, 132 pp. (1970).

DOLE R.M., *Persistent anomalies of the extratropical Northern Hemisphere wintertime circulation.* In: « Large-Scale Dynamical Processes in the Atmosphere ». Eds. B.J. Hoskins and R.P. Pearce, Academic Press, pp. 95-109 (1983).

FREDERIKSEN J.S., *A unified three-dimensional instability theory of the onset of blocking and cyclogenesis.* « J. Atmos. Sci. », *39*, 969-982 (1982).

FREDERIKSEN J.S., *A unified three-dimensional instability theory of the onset of blocking and cyclogenesis.* II: *Teleconnection patterns.* « J. Atmos. Sci. », *40*, 2593-2609 (1983).

FREDERIKSEN J.S. and PURI K., *Nonlinear instability and error growth in Northern Hemisphere three-dimensional flows: Cyclogenesis, onset-of-blocking and mature anomalies.* « J. Atmos. Sci. », *42*, 1374-1397 (1985).

GEISLER J.E., BLACKMON M.L., BATES G.T. and MUNOZ S., *Sensitivity of January climate response to the magnitude and position of equatorial Pacific sea-surface temperature anomalies.* « J. Atmos. Sci. », *42*, 1037-1049 (1985).

HENDON H.E., *Time-mean flow and variability in a nonlinear model of the atmosphere with orographic forcing.* « J. Atmos. Sci. », *43*, 433-448 (1986a).

HENDON H.E., *Time-mean flow and variability in a nonlinear model of the atmosphere with tropical diabatic forcing.* « J. Atmos. Sci. », *43*, 72-88 (1986b).

HENDON H.E. and HARTMANN D.L., *Variability in a nonlinear model of the atmosphere with zonally symmetric forcing.* « J. Atmos. Sci. », *42*, 2783-2797 (1985).

HOREL J.D. and WALLACE J.M., *Planetary scale atmospheric phenomena associated with the Southern Oscillation.* « Mon. Wea. Rev. », *109*, 813-829 (1981).

KIDSON J.W., *Tropical eigenvector analysis and the Southern Oscillation.* « Mon. Wea. Rev. », *103*, 187-196 (1975).

LAU N.-C., *A diagnostic study of recurrent meteorological anomalies appearing in a 15-year simulation with a GFDL general circulation model.* « Mon. Wea. Rev. », *109*, 2287-2311 (1981).

LIEBMANN B. and HARTMANN D.L., *Interannual variations of outgoing IR associated with tropical circulation changes during 1974-78.* « J. Atmos. Sci. », *39*, 1153-1162 (1982).

LIEBMANN B. and HARTMANN D.L., *An observational study of tropical midlatitude interaction on intraseasonal time scales during winter.* « J. Atmos. Sci. », *41*, 3333-3350 (1984).

PALMER T.N. and MANSFIELD D.A., *A study of wintertime circulation anomalies during past El Niño events, using a high resolution general circulation model.* I: *Influence of model climatology.* « Quart. J. Roy. Meteor. Soc. », *112*, 613-638 (1986a).

PALMER T.N. and MANSFIELD D.A., *A study of wintertime circulation anomalies during past El Niño events, using a high resolution general circulation model.* II: *Variability of the seasonal mean response.* « Quart. J. Roy. Meteor. Soc. », *112*, 639-660 (1986b).

QUINN W.A., ZOPF D.O., SHORT K.S. and KUO YANG R.T.W., *Historical trends and statistics of the Southern Oscillation. El Niño and Indonesian droughts.* « Fish. Bull. », *76*, 663-678 (1978).

SIMMONS A.J., *The forcing of stationary wave motion by tropical diabatic heating.* « Quart. J. Roy. Meteor. Soc. », *108*, 503-534 (1982).

SIMMONS A.J., WALLACE J.M. and BRANSTATOR G.W., *Barotropic wave propagation and instability, and atmospheric teleconnection patterns.* « J. Atmos. Sci. », *40*, 1363-1392 (1983).

WALLACE J.M. and GUTZLER D.S., *Teleconnection in the geopotential height field during the Northern Hemisphere winter.* « Mon. Wea. Rev. », *109*, 785-812 (1981).

WALLACE J.M. and LAU N.-C., *On the role of barotropic energy conversions in the general circulation.* « Advances in Geophysics », *28a*, 33-74 (1985).

WALLACE J.M., TIBALDI S. and SIMMONS A.J., *Reduction of systematic forecast errors in the ECMWF model through the introduction of an envelope orography.* « Quart. J. Roy. Meteor. Soc. », *109*, 683-718 (1983).

SOME STATISTICAL PROPERTIES OF MID-LATITUDE LARGE-SCALE ATMOSPHERIC FLOW ON INTRASEASONAL TIME SCALES

A. SUTERA

CEM Research Group, St. Joseph College
West Hartford, CT 06117

and

Department of Geology and Geophysics, Yale University
New Haven, CT 06520

ABSTRACT

In this paper we consider a variety of large-scale flow indicators and analyze their probability density distributions on time scales longer than the life cycle of typical baroclinic disturbances but shorter than the season. We will show that indicators describing large-scale eddies exhibit a bimodal probability density distribution, while others connected with the zonal structure of the flow typically show a normal probability density distribution. A few speculations about the modeling of these processes are offered.

1. INTRODUCTION

The severity of the winter season or the dryness of a summer has been commonly ascribed to a displacement and/or amplification of the large-scale action centers which show a persistent time behavior. For example, the severity of a winter in the east coast of the United States may be associated with a prolongated amplification of the eastern Pacific climatological high as winters like 1963 and 1976 have shown. Understanding the physical nature of these anomalies represents a challenge to

meteorology for both theoretical and practical reasons. The latter because recently it has been felt by various forecast centers that prediction on monthly time scales by means of numerical models has been more within reach, given the increased and still increasing power of the computational technology. In this perspective, it is a good starting point to examine whether the observed anomalies (for example, the ones associated with the intraseasonal variability) depart significantly from the climatological means. In this case, it could be that the hypothesis requiring the anomaly as a small perturbation of these means might be dynamically inconsistent with the observations. To study this question, we can study the probability density distribution (PDD) induced by samples of selected indicators of the atmospheric behavior. If it is found that a particular indicator shows a Gaussian-like PDD, then the description of the behavior of its mean and variance is sufficient in modeling such a variable. If the PDD shows a significant departure from a Gaussian PDD, then knowledge and hence modeling of the PDD's movements is required. The situation is rather different in the case in which the PDD shows more than one mode. In fact, the minima of the PDD signal that the physical process described by this indicator may arise from an instability which requires it to be properly modeled. The present paper, which reviews recent efforts of the author and few other colleagues, is devoted to the analysis of the question whether winter anomalies such as blocking events can be ascribed to a large-scale instability similar to the one considered by Charney and DeVore (1979). It accounts for the main body of observational evidence so far accumulated, while the contributions in this volume by Benzi and Speranza discuss efforts in modeling the observational results. Along our studies we have encountered difficulties connected with the problem of estimating a PDD. How we have constructed a probability density estimated (PDE) and their statistical significance is discussed.

2. Statistical Techniques

As discussed in the introduction, we will determine the PDD of a set of indicators connected with the large-scale atmospheric behavior during the northern winter. We define winter as the set of days of the year beginning 1 December and extending through 28 February. This data will be a subset of a record encompassing, say, N_y, years; and will be affected by obvious periodicities such as the annual cycle and its sub-harmonics. Since we wish to determine that part of the variability of the

indicators not associated with these periodicities, we will remove from the data these undesired periodicities. We will achieve this aim by different techniques which will be explained later.

Moreover, because we are interested in the variance of the atmospheric field explaining variability on time scales longer than a baroclinic life cycle, a high frequency cut-off will also be applied. In what follows, all indicators will be deprived of frequencies shorter than five days. This choice, though reasonable, is arbitrary, but it can be shown that our results are insensitive to this high frequency cut-off. Once these operations are performed, we are left with a data sample which possesses $N_w N_y$ data, where N_w is the number of observations in each winter. PDEs will be calculated for this data set. Of course, all these data are not independent sample points, hence when we try to establish the statistical confidence of the obtained PDEs, some hypothesis on the number of independent sample points has to be formulated. There is no convincing objective technique to determine the number of independent samples in a time series, and in its absence we considered one observation every five days as independent. In some calculations, we changed this interval to convince ourselves of the lack of sensitivity of the results on it. Before proceeding with the presentation of the results, we will describe the techniques that we have employed in calculating PDEs and their statistical significance.

3. Determination of the PDE

As has been already discussed, the probability density distribution of our sample is unknown. In estimating the true probability density distribution, we have to consider nonparametric statistical techniques. Among nonparametric estimates, the oldest one (probably first employed by Moses in apportioning quotas of draftees among different tribes) is the histogram. At this stage, it is worth mentioning how a histogram is constructed. Suppose that the range of the sample's variable is the interval $[a, b]$. First the interval is divided into equal subintervals (bins); then an estimate of the unknown probability density at each subinterval is obtained by considering the frequency of occurrence of the sample in the subinterval. It appears obvious that the resulting estimation is critically dependent both on the choice of the mesh size (i.e., the number of subintervals) and on the position of the mesh central points, since the PDE estimate at these points does not depend on the density at neighboring central points. Moreover, the estimate is subjected to increasingly large

errors when the mesh size is made smaller. To illustrate a few of these drawbacks, we have constructed the following example (Hansen and Sutera, 1986a). Consider 90 numbers drawn at random from the PDD shown in Fig. 1a. We want to estimate a PDE generated by the sample by using the histogram method. The width of the class interval (i.e., the mesh points) used in the histogram is chosen according to a "rule of thumb" found in Panofsky and Brier (1958): the number of subintervals equals the square root of the number of independent sample points. (A point worth mentioning is that this "rule of thumb" is not unique; i.e., probably there are as many "rules of thumb" as there are applied statistical text books consulted by us. They are similar only in the property that the number of bins tends to zero in the case of no data points and to infinity in the case of infinite data points). The resulting PDE is shown in Fig. 1b. In this realization, the histogram failed to capture the nature of the parent distribution. Of course, by increasing the number of bins and/or changing the bins' center values, the bimodal nature of the parent PDD could be found. However, increasing the number of mesh points would tend to produce a noisy PDE (i.e., it would add spurious modes because of the finiteness of our sample), while the strategy of varying the bins' center values is difficult to implement unless all the possible combinations are tested. Along this line, Rosenblatt (1956) proposed a modification of the histogram by considering the PDE at a point to be the average density of the two subintervals contiguous at that point. This modification improves the quality of the estimate because of the smaller dependence of the estimate on the position of the bins' centers.

Rosenblatt's modification was generalized essentially along two directions known respectively as Kernel estimators (Scott *et al.*, 1978), and maximum penalized likelihood techniques (MPL) (Good and Gaskins, 1980). Both techniques will be used in this paper. Let us consider first MPL estimates. Given a data set $\{X_i\}$, an MPL estimate of the unknown probability density distribution is obtained by solving the following variational problem:

$$\max \{L(w)\} = \prod_i X_i \exp \left\{ -\alpha \int \frac{d^2 w}{d_t^2} \, dt \right\} \tag{1}$$

with the contraints

$$\int w \, dt = 1 \tag{2}$$

Here α denotes a smoothness parameter and w is any probability density.

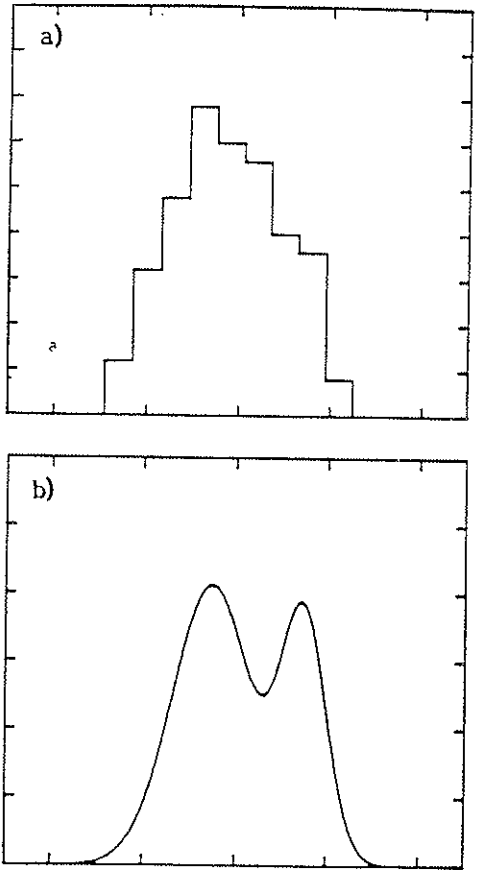

FIG. 1. a) The PDE using the histogram method. b) The parent PDD of the sample.

The discrete version of this principle is obtained by discretization of $L(w)$ in the given range of $\{X_i\}$. It appears that any MPL estimate depends on two parameters — i.e., the mesh size and the smoothness parameter α. In case of real data, we can remove the uncertainty of the mesh size by using a grid interval approximately equal to the experimental error of the sample point measurement. The optimal choice of the parameter α cannot be derived from the data and must be derived empirically. We will discuss this point in Section 3.1.

A Gaussian Kernel estimation is an approximation of the probability density distribution of $\{X_i\}$, and is obtained as follows:

$$P(X) = \sum_{1}^{N} \exp\ [-(X - X_n)^2/2\,\delta^2]/N\sqrt{2} \tag{3}$$

This PDE assumes that the contribution of each observation to the probability density distribution is a scaled Gaussian centered on the particular datum itself. The parameter δ is arbitrary and it will be determined for our data empirically in Section 5.

3.1 *The statistical distribution of large-scale flow in Fourier space: ECMWF data*

In Sutera (1986) there was considered the case in which the large-scale behavior was represented by a global indicator deduced from a latitudinal average of the 500-mb height field. To be more precise, if $Z(\lambda, \varphi, t)$ is the geopotential height at time t and geographical position (λ, φ) (φ longitude and λ latitude), the following average was considered:

$$\bar{Z}(\varphi, t) = \int_{\lambda_1}^{\lambda_2} Z(\lambda, \varphi, t)\ d\lambda \tag{4}$$

By calculating the Fourier transform of $\bar{Z}(\varphi, t)$,

$$\bar{Z}(\varphi, t) = \sum_{k} A_k(t)\, e^{ikX} \tag{5}$$

the following indicator was formed:

$$\Gamma(t) = (\sum_{i} A^2_i)^{1/2} \quad i = 2,3,4 \tag{6}$$

The choice of a spectral band around wave-number 3 was motivated on the theoretical ground that if a multiple-equilibrium theory such as the one proposed by Charney and DeVore (1979) has to be checked, this wave-number band is appropriate (see Benzi *et al.*, 1986a for details). From the definition of Γ, it appears that any conclusions drawn from its properties especially concern the global aspects of the circulation (the Fourier transform smears out any hypothetical local nature of the circulation). In Section 5 we will try to remove this constraint. Of course the indicator Γ is affected by short-term as well as long-term fluctuations. Since, as has been discussed in the introduction, we will restrict our study

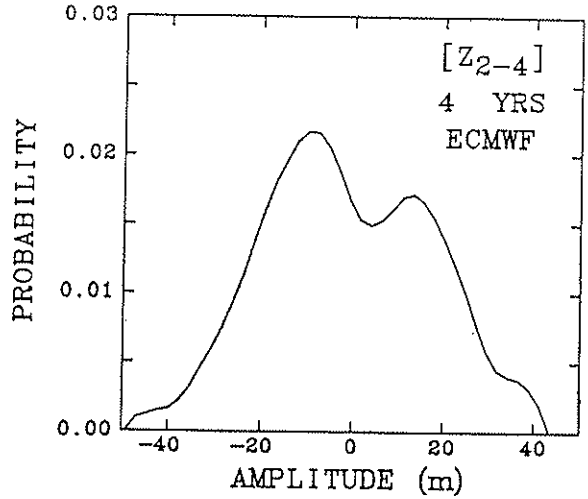

FIG. 2. PDE of Γ for ECMWF 4-winter data.

to periods longer than five days and shorter than a season, the other frequencies have to be removed. The shorter frequencies were removed by cutting off the time Fourier transform of Γ at periods shorter than five days and resynthesizing the Fourier transform. The results to be shown do not depend on the details of this operation; i.e., if other filtering techniques were employed, no significant changes were noted. The long-term fluctuations required more care. We begin by considering the annual cycle. It must be removed because otherwise a bimodal PDE may be the result of the phase of the annual cycle. A way to remove the significant spectral peaks due to the annual cycle is again by computing the Fourier transform and removing the annual frequency. This possibility was analyzed in comparison to other more sophisticated filters and proved to be adequate. When these operations were performed on a sample of Γ containing four years of winter data (1980-84), we obtained the PDE shown in Fig. 2. In this case, the latitude band λ_1, λ_2 extends from 20° to 80°N. The PDE was calculated using the MPL technique. The mesh size was taken to be one meter on the assumption that $\bar{Z}$ is affected by an observational error of the same size. The optimal choice of α was determined as follows. Let us consider a PDE of $\{X_i\}$ with a given value of α: $p(x, \alpha)$. We can test $p(x, \alpha)$ against the sample distribution by

employing a standard method of goodness of fit such as the Kolmogorov-Smirnov text,

$$K = \underset{X_i}{\text{Sup}} \mid S(X_i) - p(X_i, \alpha) \mid , \tag{7}$$

where Sup is the supremum, X_i are the data samples, and S is the sample probability distribution. The variable K is Kolmogorov-Smirnov distributed and we can determine the probability that K is greater than any random choice with the same distribution. This establishes a confidence level. The technique applied to our data determines α as that value which gives a 95 percent confidence level. Figure 2 is obtained for the value of α so determined and by assuming that for the four winters the sample set contains 72 independent observations. A limitation of this technique is that it tacitly employs the data twice — i.e., in determining the PDE and in calculating $S(X_i)$. To avoid this problem, we can proceed as follows. Let us suppose that our sample contains N_I independent observation, and let $p(X, \alpha)$ be an estimate of the true PDD showing a marginally bimodal nature. We can test the confidence of the bimodality of $p(X, \alpha)$ by randomly extracting N_I samples from a known PDD which is not bimodal, calculating a PDE with the same value of α (and of course of the mesh size), and inspecting the corresponding PDE for a bimodal nature.

If we repeat this operation N_s times, we can establish a percent confidence level for our $p(X, \alpha)$. Applying this technique to our data, we always tested a PDE calculated from the data against a Gaussian, and with a value of α being the lowest for which the sign of the derivative for the PDE did not change more than n_m where n_m is the number of modes that we want tested to be significant.

3.2 *NMC Data*

It is obvious from the previous discussion that the major limitation of the Sutera (1986) study is the lack of a substantial number of independent observations. This constraint can be alleviated if we extend our analysis to a longer record. In Hansen and Sutera (1986a) 500-mb height NMC final analyses were considered for the period 1 January 1964 to 31 December 1980. In this case, 500 mb heights were interpolated onto a 5×5 latitude-longitude grid from the NMC octagon grid at 0000 GMT of each day. Missing analyses were filled in by linear inter-

polation from adjacent map times. Of about 6210 days, only 80 analyses were missing. In this second study, a departure from the procedure of Sutera (1986) was in the choice of the latitude zone over which the geopotential height was averaged; i.e., λ_1 and λ_2 in (3.1) are 45°N and 75°N, respectively.

The choice is based on several reasons, the most significant of which is the fact that in the Northern Hemisphere winter the planetary wave amplitudes are largest in this zone. The annual period was filtered from the data as before, but the interannual variability was left in the data. This operation is justified by the following argument. If we assume that each winter has a bimodal distribution, the mean of each individual distribution depends on the relative amount of time spent on either side of the minimum in the distribution. On the other hand, the position of the minimum in the absence of any other physical mechanism is independent of the mean. The effect of removing periods longer than the annual cycle is to constrain the data to have the same mean in each winter. This would displace the position of the minima as a function of the relative probability of residing in each mode during a given winter. In this case, when we estimate the density of the composite, we would be estimating the probability density of a mixture of bimodal distributions in which the positions of the respective minima are randomly placed with respect to the mean of the composite. It is easy to demonstrate that in the limit of a large number of individual bimodal distributions with their minima randomly placed with respect to the mean, the composite density would tend to be normally distributed. As a demonstration of this concept, two bimodal distributions are illustrated in Fig. 3a and 3b that differ in their mean because of the relative probability of residing in one more versus the other. In Fig. 3c, a composite obtained by combining these two samples after removal of their individual means is shown. Clearly, the bimodal nature of the original samples is obscured in the composite. On the other hand, by simply combining the two samples, the distribution in Fig. 3d is obtained. This distribution captures the nature of the individual sample distributions because their minima occur at the same value of the variable.

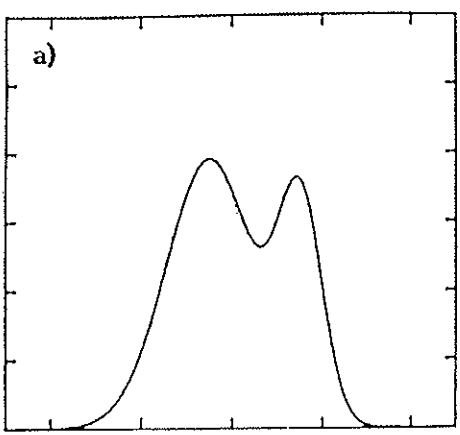

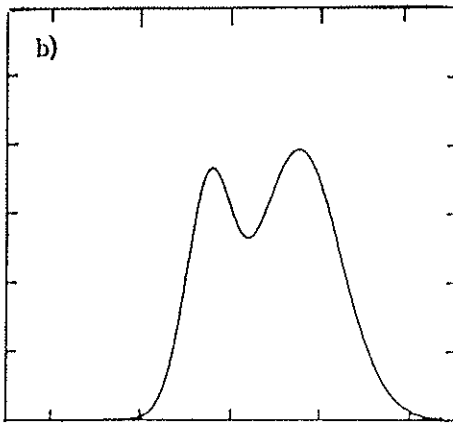

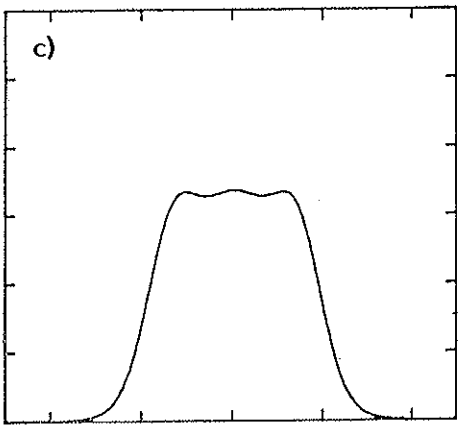

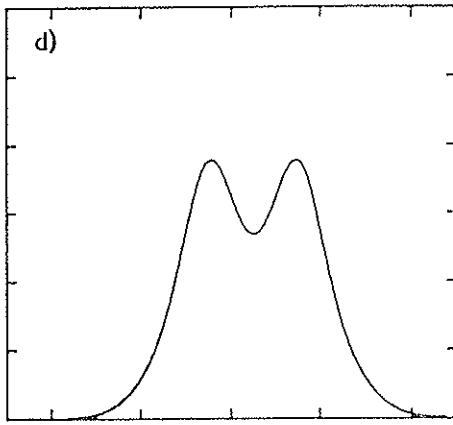

FIG. 3. a-b) Bimodal PDDs with different mean values. c) Composite of 3 a-b by moving the mean values. d) Composite of 3 a-b.

4. RESULTS

4.1 *Composite 16-year results*

After constructing the time series of Γ from 1 January 1964 through 31 December 1980, and filtering it to remove the annual cycle and high frequency variations, a composite data sample was formed, consisting of 90 observations from each of the 16 winters (1 December through 28 February) included in the data set (viz., 1964-65 through 1979-80).

MPL estimations were then made of the probability density of Γ. As the value of the smoothness parameter, α, was made progressively smaller, a minimum in the estimate first became evident at $\alpha = 10^7$ (Fig. 4a). As α was made progressively smaller, the depth of the minimum increased and the two modes surrounding it became better defined (Fig. 4b, $\alpha = 5 \times 10^6$). The two modes are separated by $\sim$ 21 m. This is a slightly wider separation than exhibited in the ECMWF data, where a 20° to 80°N channel was used; the wavenumbers 2 to 4 have the largest amplitude in the 45° to 70°N zone, hence a wider contrast between the two modes could be anticipated. The ECMWF data, when reanalyzed in the 45° to 70° zone, also achieved a wider separation between the modes. The probability of residing on the lower amplitude side of the minimum (Mode 1) in Fig. 4b is 62 percent (891 days out of the 1440 total) and the probability of residing on the higher amplitude side (Mode 2) is 38 percent (549 days). This compares with 54 percent and 46 percent, respectively, found in the 1980-84 ECMWF data.

4.2 *Simulations*

To determine if the appearance of two modes in the composite density estimation could have been obtained by random chance, simulated data were produced by generating random numbers from a normal distribution with the same mean and variance as the estimate. For this test to be useful, the randomly sampled data should include the same number of independent samples as the observational data used to construct the wave amplitude density estimate. However, estimation of the number of independent samples in each winter season's data and thus in the entire observational data set, is not straightforward.

As has been already stated, to be conservative and consistent with the high frequency filter, we assume only 20 independent observations per winter or a total of 320 independent observations in the 16-winter dataset. Therefore, 100 different sets (realizations) of 320 random numbers were chosen from a normal distribution. For each realization, a probability density estimation was then constructed using the same MPL technique used to analyze the observational data. The value of the smoothness parameter, α, was chosen to be 10^7 to match the value for which the observations first showed a second mode. Of these 100 realizations, only one showed any detectable sign of bimodality (Table 1). Empirically, then, it appears highly unlikely that the bimodal density estimate can be obtained

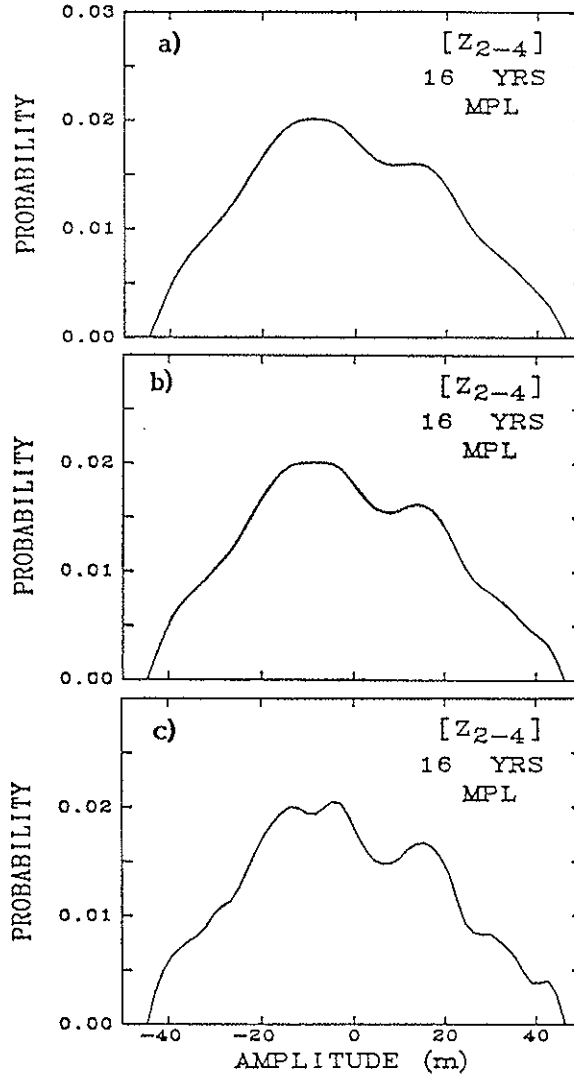

FIG. 4. a) PDE NMC data for $\alpha = 10^7$. b) PDE NMC data for $\alpha = 5 \times 10^6$. c) PDE NMC data for $\alpha = 10^6$.

TABLE 1 - *Summary of Random Sampling Simulations.*

Parent Distribution	Number of Independent Samples/ Realizations	Number of Realizations	α	Percent Unimodal	Percent Bimodal	Percent > 2 Modes
Normal	320	100	10^7	98	1	—
Normal	320	100	10^7	98	2	—
Unimodal (Fig. 6)	320	100	10^7	86	14	—
Bimodal (Fig. 4b)	320	100	10^6	6	36	58

by chance from the observational data with 320 independent observations. Repeating this test with only 240 independent observations per realization (corresponding to one independent observation every six days) reveals only two cases out of 100 with a bimodal estimate obtained by chance (Table 1). Given this result, the hypothesis that the wave amplitude is governed by some process with a normal distribution must be rejected. However, it might be possible that the true probability density is a unimodal but non-normal distribution. To test whether the bimodal distribution obtained from the observations could result by chance from sampling a unimodal distribution, 100 sets of 320 random numbers were drawn from the distribution illustrated in Figure 5. This distribution was obtained from an MPL estimate of the observational data with $\alpha = 10^8$. It might be considered the closest estimate to the data that is still unimodal. Using $\alpha = 10^7$, only 14 of these realizations exhibited a detectably bimodal density estimate, of which only 9 obtained a minimum of comparable depth to that in the observations. Thus, it appears unlikely that the data could have originated from a unimodal distribution. Given the alternative hypothesis that the true probability density of the wave amplitude is either bimodal or unimodal, we should accept the former, based on the random number simulations.

As the value of α is decreased to 5×10^6, the composite distribution remains nearly the same except that the minimum becomes more clearly defined (Fig. 4b). If α is reduced further to 10^6, a second minimum appears near $z = -9$ (Fig. 4c). To determine the lower bound on α

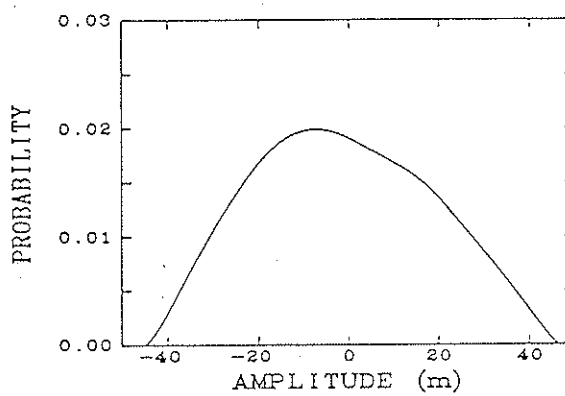

FIG. 5. Unimodal PDD used for the test of PDEs NMC data.

and establish whether the observational density distribution has more than two modes, further simulations were performed.

In this case, the alternative hypotheses are that the distribution is either bimodal or trimodal. Therefore, 100 sets of 320 numbers were chosen randomly from a bimodal parent distribution. The parent population density is the $\alpha = 5 \times 10^6$ estimate shown in Fig. 4b. MPL estimates of the 100 sample distributions were constructed using $\alpha = 10^6$.

We find that over 50 percent of these estimates have more than two modes when $\alpha = 10^6$ (Table 1). Thus, it is quite likely that a trimodal estimate can be obtained by chance from a bimodal parent distribution when this value of α is used. Consequently, we reject the hypothesis that the observational data possesses a density distribution with more than two modes, and conclude that an optimal choice of α for our dataset is approximately $\alpha = 5 \times 10^6$. Notice that there is some small chance of obtaining a unimodal estimate from a bimodal parent distribution (Table 1) even with 320 samples included in the estimate when $\alpha = 10^6$.

4.3 *Density of persistence*

As discussed earlier, the observed bimodality of the indicator might be connected to some periodicity of the time series. The power spectrum of Γ doesn't show any relevant peak for the time scales of interest

($\leq$ 90 days). However, this fact does not preclude the possibility that some hypothetical periodicity is smeared out in the power spectrum because of the superposition of some random process. We can test this possibility by considering the probability density of the duration of the events in each mode. In fact, if some hidden periodicity is generating the observed bimodality at a particular time scale, then this distribution should be Gaussian around this period. In Figure 6 we show the residence density distributions deduced from the data for Mode 1 and Mode 2 events. The distributions in Fig. 6 were made using a Rosenblatt "shifted histogram" technique. As in Sutera (1986), neither residence density shows any sign of a preferred time scale. (Events with durations longer than 20 days are not well sampled in this figure). Visual inspection of these distributions strongly suggests that they resemble those obtained by sampling a Poisson process. So we must reject the hypothesis that the observed bimodal distribution is the consequence of a periodic process.

4.4 *Empirical attempt to remove interannual variations*

In the individual winters, PDE of Γ show year-to-year changes in the position of the minima. It may be assumed that this interannual variability is associated with some physical mechanism that is independent of the process governing the intraseasonal variability of the wave amplitude.

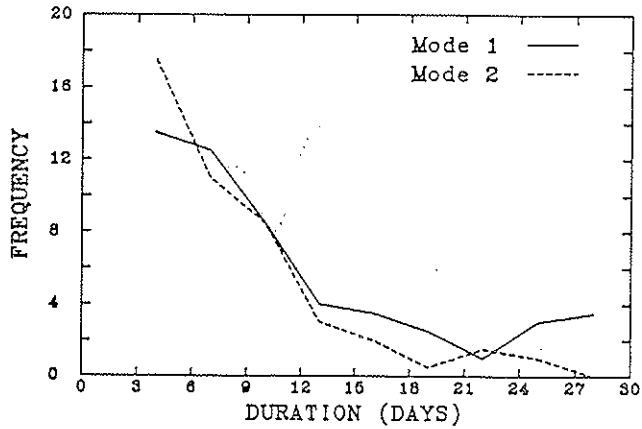

FIG. 6. PDE of the persistence time on the two modes.

Given this hypothesis, we can try to empirically remove the interannual variability by artificially matching the minima in the individual year's results. By so doing, the "best" possible density estimate in terms of bimodality is obtained. Each year's data was shifted by the amount necessary to place its minimum at $z = 0$ and the resulting composite data was used to form an MPL estimate with $\alpha = 5 \times 10^6$. The resulting distribution (Fig. 7) is quite similar to the four winter composite obtained from the ECMWF sample.

We may conclude, therefore, that the true wave-amplitude probability density distribution lies somewhere between this "best" estimate and the "worst" estimate (Fig. 4b) which is obtained without any attempt to remove interannual variations.

4.5 *Signature of the bimodality in physical space*

As in Sutera (1986), we use the density estimate given in Fig. 4b to stratify the data. We then construct mean maps for all days corresponding to the lower amplitude mode (Mode 1) in Fig. 4b (i.e., all days with Γ values less than that of the minimum in Fig. 4b), and mean maps for all days corresponding to the higher amplitude mode (Mode 2) (i.e., those with Γ greater than that of the minimum in Fig. 4b). This is done at 850 mb, 500 mb, and 300 mb (Fig. 8a-f). Certain observations can be made from these figures.

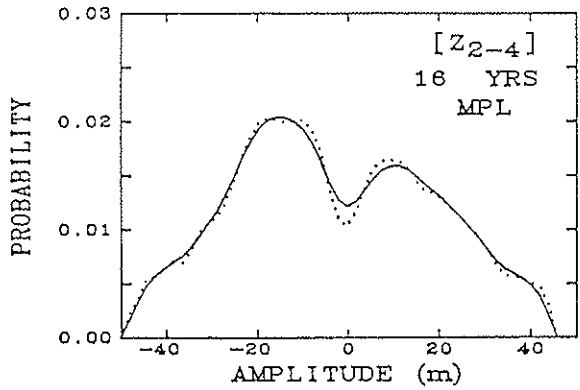

FIG. 7. A PDE for NMC data when individual years have the minimum at $z = 0$ (solid line $\alpha = 5 \times 10^6$, dotted $\alpha = 10^6$).

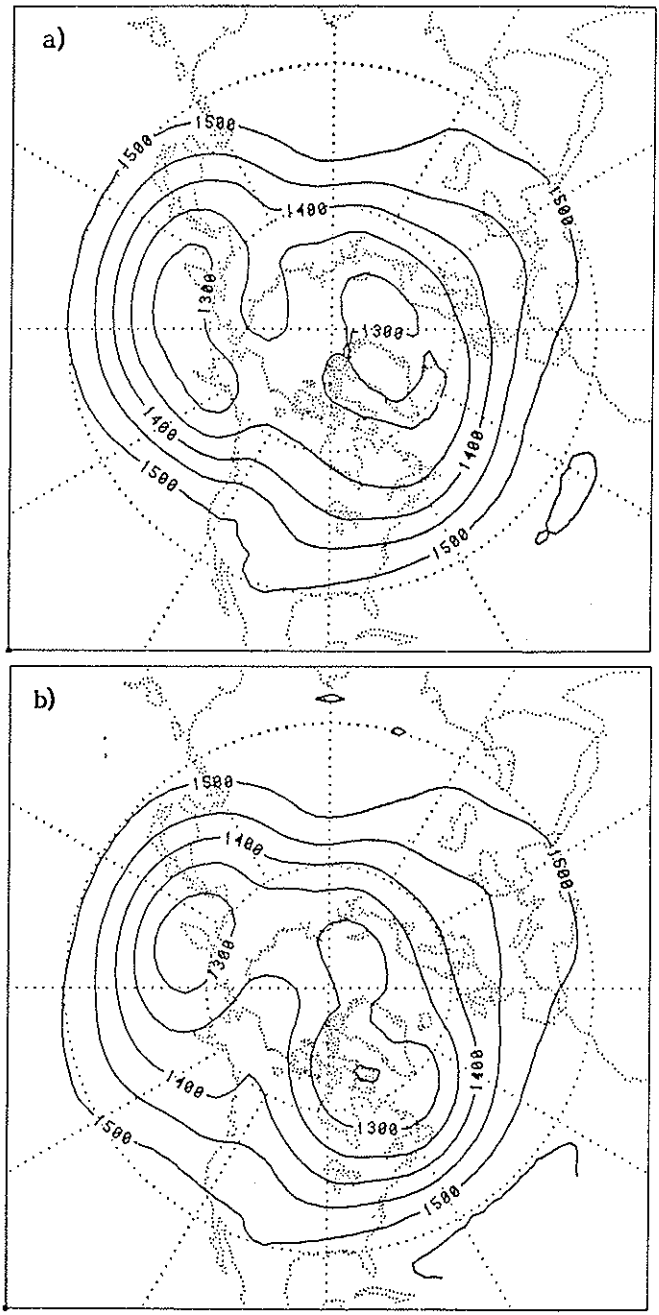

FIG. 8. a) Mean Mode 1 at 850 mb. b) Mean Mode 2 at 850 mb.

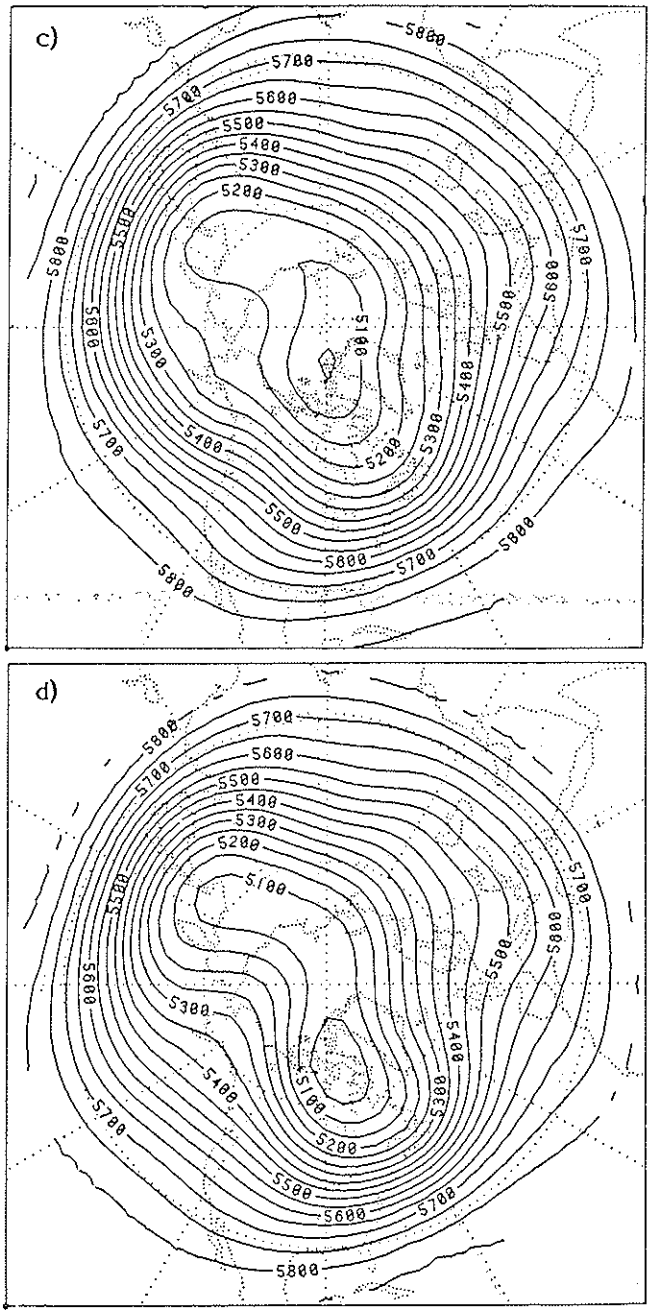

FIG. 8. c) Mean Mode 1 at 500 mb. d) Mean Mode 2 at 500 mb.

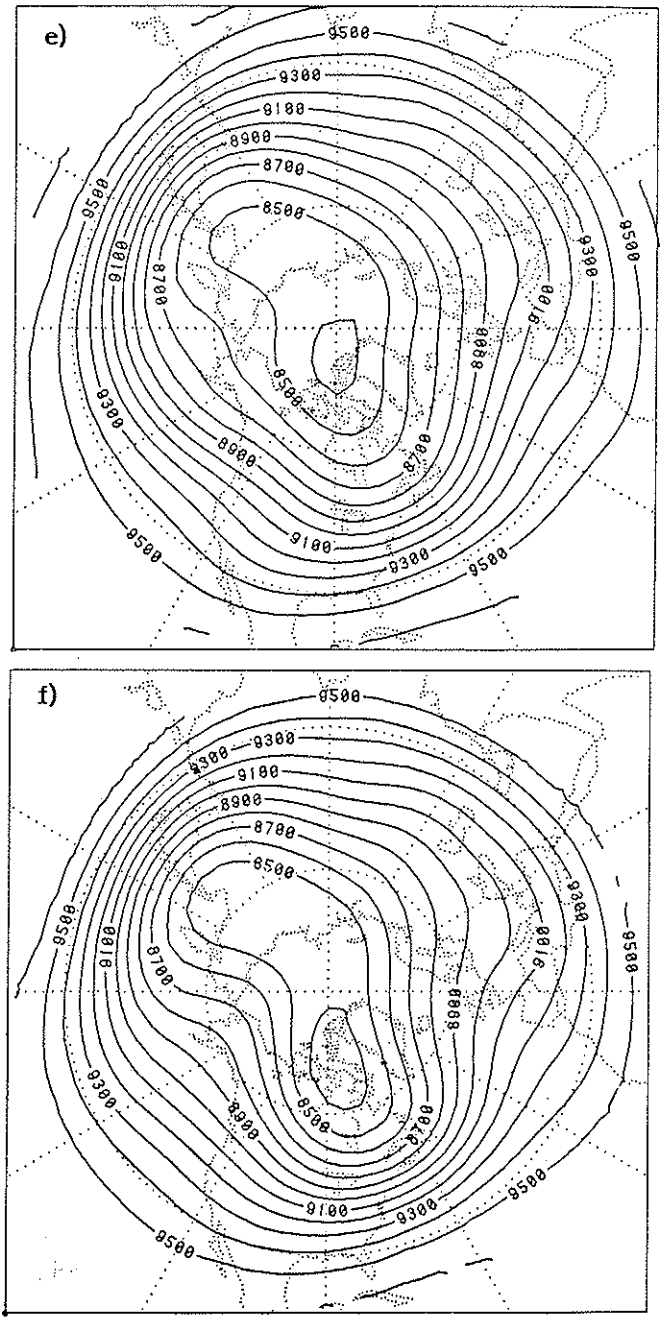

FIG. 8. e) Mean Mode 1 at 300 mb. f) Mean Mode 2 at 300 mb.

1) The overall character of the Mode 1 fields is quite similar at all three levels with a predominantly zonal flow in evidence. For Mode 2, a more amplified wave pattern is present at all levels indicating that the phenomenon inducing the bimodality extends through the depth of the troposphere.

2) For Mode 1, westward vertical tilt of the major trough and ridge axes is quite noticeable between 850 and 500 mb, but little vertical tilt is evident between 500 mb and 300 mb.

3) For Mode 2, vertical tilts very similar to those of Mode 1 are evident. If anything, the vertical tilt between 850 and 500 mb is less for Mode 2 than for Mode 1. Nonetheless, a baroclinic vertical structure is evident in the mean fields for the two modes.

The difference between the Mode 2 height field and the Mode 1 height field is illustrated in Fig. 9a-c, at 850, 500 and 300 mb. The following features are apparent:

1) The differences between the two modes are quite similar at each level, and are dominated by differences at planetary-scale wavelengths, particularly wave number 2.

2) The most prominent features in the difference fields are, in descending order, the east Pacific ridge, Hudson Bay trough, east Atlantic ridge, and east Asian-west Pacific trough. In general, positive (negative) differences at middle and high latitudes are accompanied by negative (positive) differences at lower latitudes.

3) Comparison of the difference fields between the levels reveals that the differences are virtually in phase in the vertical. That is, the structure of the difference field is equivalent barotropic.

4) The difference field is shifted westward compared to the Mode 1 mean field at 850 mb, and eastward or in phase at 500 mb and 300 mb.

In addition, the differences between the NMC height fields based on stratifying the data according to the amplitude indicator reveals results very similar to those found in the ECMWF data (Sutera, 1986; Hansen, 1986).

The net effect of adding the equivalent barotropic difference field onto the underlying baroclinic wave structure, considering the phase relation between the Mode 1 mean field and the difference field will actually be to slightly reduce the vertical tilt of the phase lines of the planetary waves but to significantly intensify the gradients of the height

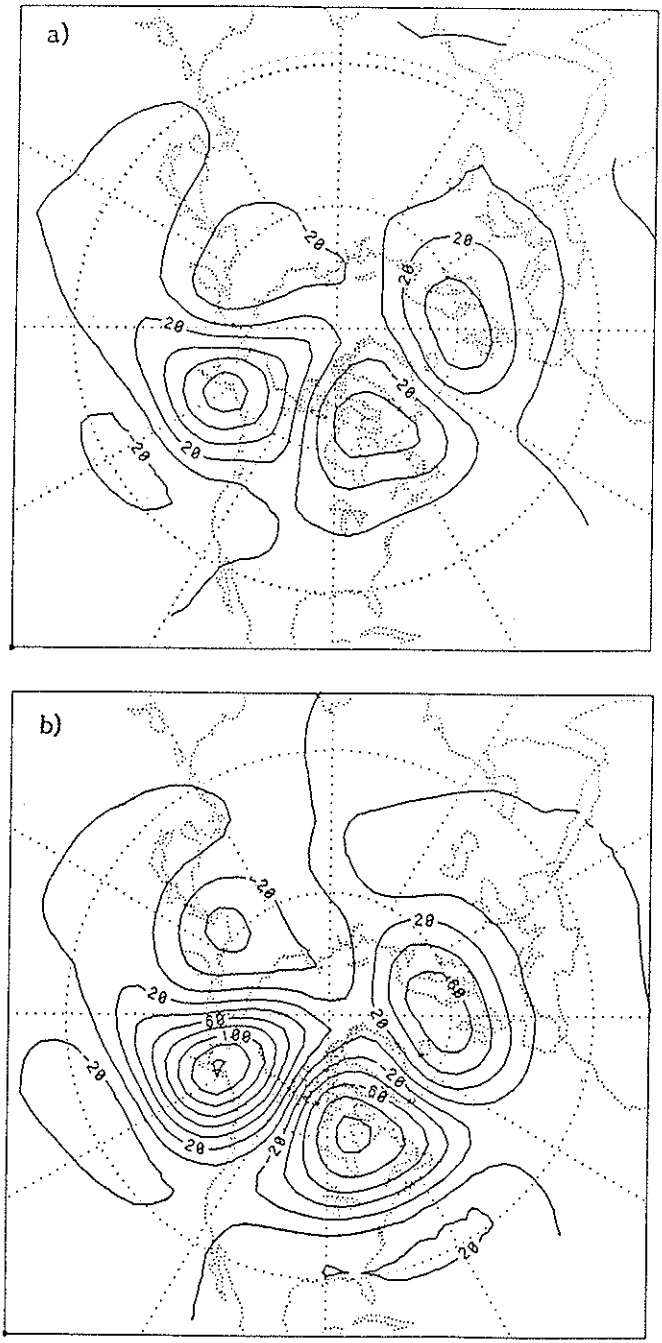

FIG. 9. a) Difference Mode 2 - Mode 1 at 850 mb. b) Difference Mode 2 - Mode 1 at 500 mb.

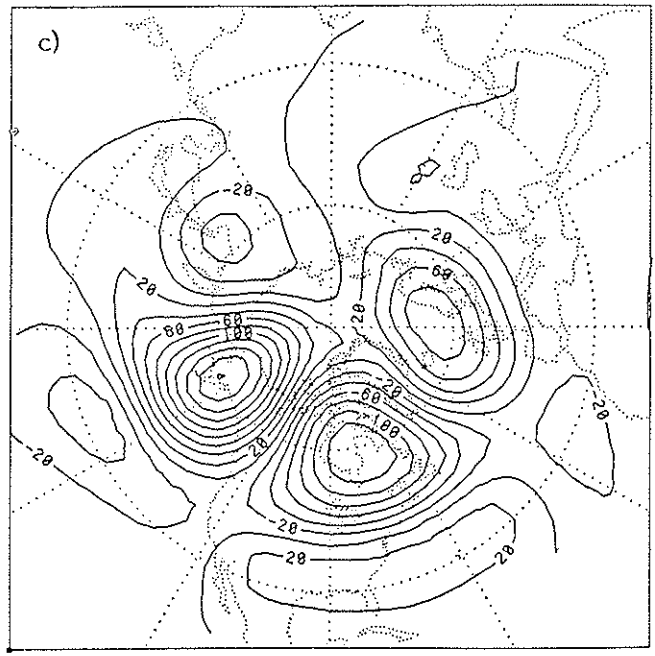

FIG. 9. c) Difference Mode 2 - Mode 1 at 300 mb.

field and the amplitude of the temperature (thickness) field. The net result is an enhanced northward heat transport, and therefore enhanced « baroclinic » energy conversions. This was exactly the situation revealed by the ECMWF data (Hansen, 1986). However, the enhanced baroclinic conversions do not necessarily imply a baroclinic instability. The kinetic energy balance of wavenumbers 2 to 4 for both modes was characterized by a balance between baroclinic conversions and dissipation in the ECMWF data and a similar situation is likely to be found in the current dataset (further investigation of this aspect is planned). The role of the baroclinicity appears to be one of maintaining the flow against dissipation, regardless of its configuration. If this is so, the dynamics underlying the wave amplitude bimodality must have another, nonbaroclinic mechanism in operation. Indeed, the equivalent barotropic nature of the difference field strongly argues against ascribing the bimodality to a purely baroclinic instability. Instead, barotropic mechanisms are likely to be important. Logical candidates include wave-wave nonlinearity, wave-

mean flow nonlinearity, orographic effects or some combination of these. Benzi *et al.*, (1986a,b) have studied some of these possibilities.

5. Bimodality Physical Space

So far, we have shown that a measure of the large-scale waves possesses a bimodal PDD. We have also shown that the stratification of the 500-mb geopotential height in accordance with the PDD of Γ reveals a remarkable difference pattern when we compare events belonging to the two different modes of the PDD. Moreover, this difference appears to be of global nature. However, this last property could be anticipated from the definition of Γ itself. In fact, Γ is a measure of a pattern assumed to be global. To remove this limitation, we shall try to find another indicator which does not depend on this assumption. In particular, we wish to construct PDE of a variable which describes eddy variance, but does so without any assumption on the spatial distribution of these eddies. A way to represent meteorological fields in physical space is to decompose them into empirical orthogorial functions (EOF) (see Wallace and Gutzler, 1981, for a fairly complete description of this operation). In this paper, we depart from the usual way to construct the EOF, by considering the EOF of the eddy field; i.e., we construct the correlation matrix of the "instantaneous" 500-mb geopotential height after we subtract from it the zonal field. Moreover, no long-term mean is considered in determining the anomaly coefficient of the resulting eigenvalue of the correlation matrix. Other details on the construction of this EOF can be found in Molteni *et al.* (1986). In this case, the data set considered is based on operational analysis of the NMC, and described in a four-volume report of the WMO Long Range Forecasting Research Series (Wallace *et al.*, 1983). The data extracted from this archive starts from October 1952 and extends to December 1979. We add data from ECMWF analysis from January 1980 to March 1984. Only non-overlapping 5-day means are considered. In this case, the data should be free from short frequency variability. We consider for this data set the following indicator. Let λ_i be the coefficient of the i^{th} EOF, there

$$\Gamma_{ph}(t) = (\sum \lambda_i^2)^{1/2} \quad i = 1,2, \ldots i_{\max} . \tag{8}$$

A sample of Γ_{ph} can be extracted for the winters by forcing a sample set $\{\Gamma_{ph}\}_w$ by letting t run only for $t \in$ (1 December, 28 February) of each of

the 32 years considered. We have calculated PDE of Γ_{ph} when the series is truncated to different values of i_{max}. There Γ is the time series filtered to remove variability longer than a season (as in ECMWF data for Γ). To illustrate, the robustness of the major finding of this paper (i.e., bimodality of both Γ and Γ_{ph}) we used a Kernal estimator for the PDE of Γ_{ph}. Moreover, we tested the PDE so obtained by a different simulation procedure based on a Monte Carlo approach. In fact, let us assume we know the δ of eq. (3) and we determine a PDE of $\{\Gamma_{ph}\}$ at each sample point. Now we can form, say, a 100 sample set of Γ_{ph} containing the same number of observations as $\{\Gamma_{ph}\}_w$ and randomly extract the sample points from $\{\Gamma_{ph}\}_w$. Each sample differs from $\{\Gamma_{ph}\}_w$ because each of its sample points can be extracted n times, with n arbitrary. For each of the simulated sample sets, we can calculate a PDE with the value δ previously chosen. This would give 100 estimate P_j ($j = 1,100$) of PDD of $\{\Gamma^i_{ph}\}_w$ at each sample point. Then we can order these estimates in increasing order and define a 10 percent confidence based as follows:

$$P'(\Gamma^i_{ph}) = P_{10}(\Gamma^i_{ph}) + P_{11}(\Gamma^i_{ph})/2\,, \tag{9a}$$

$$P''(\Gamma^i_{ph}) = P_{90}(\Gamma^i_{ph}) + P_{91}(\Gamma^i_{ph})/2\,. \tag{9b}$$

This excludes 20 percent of the cases, so it has to be interpreted as a 10 percent confidence, based only for a single-sided test. But this is our case if we want to test for multimodality of the PDE. In fact, because of the normalization constraint, the observed PDE must be lower (greater) than P' (P'') at a minimum (maximum). Therefore, the side of the test is determined. The value of δ can be determined as one that is sufficiently high to cancel most of the insignificant features in comparison to the confidence band, while retaining the relevant ones. In this case, $\delta = 1.5$ was found to be optimal. In Figure 10a-d we show the PDE of $\{\Gamma^i_{ph}\}$ where i_{max} is 1, 4, 5, and 10 respectively. It can be seen that if $i_{max} = 5$, a highly statistically significant bimodal PDD occurs. The bimodal nature of the PDD is obscured if $i_{max} = 10$ (actually it is already statistically insignificant from $i_{max} = 6$ which is not shown). Hence we deduce that the relevant pattern explaining the bimodality of $\{\Gamma^i_{ph}\}$ corresponds to the 5th EOF eigenvector. In Figure 11 we show this pattern. It appears that the pattern is a global one with longitude wave-number 3, with undetectable meridional dispersion. In Figure 12a,b we show the composite fields of the first five EOF when the data are stratified according to each of the

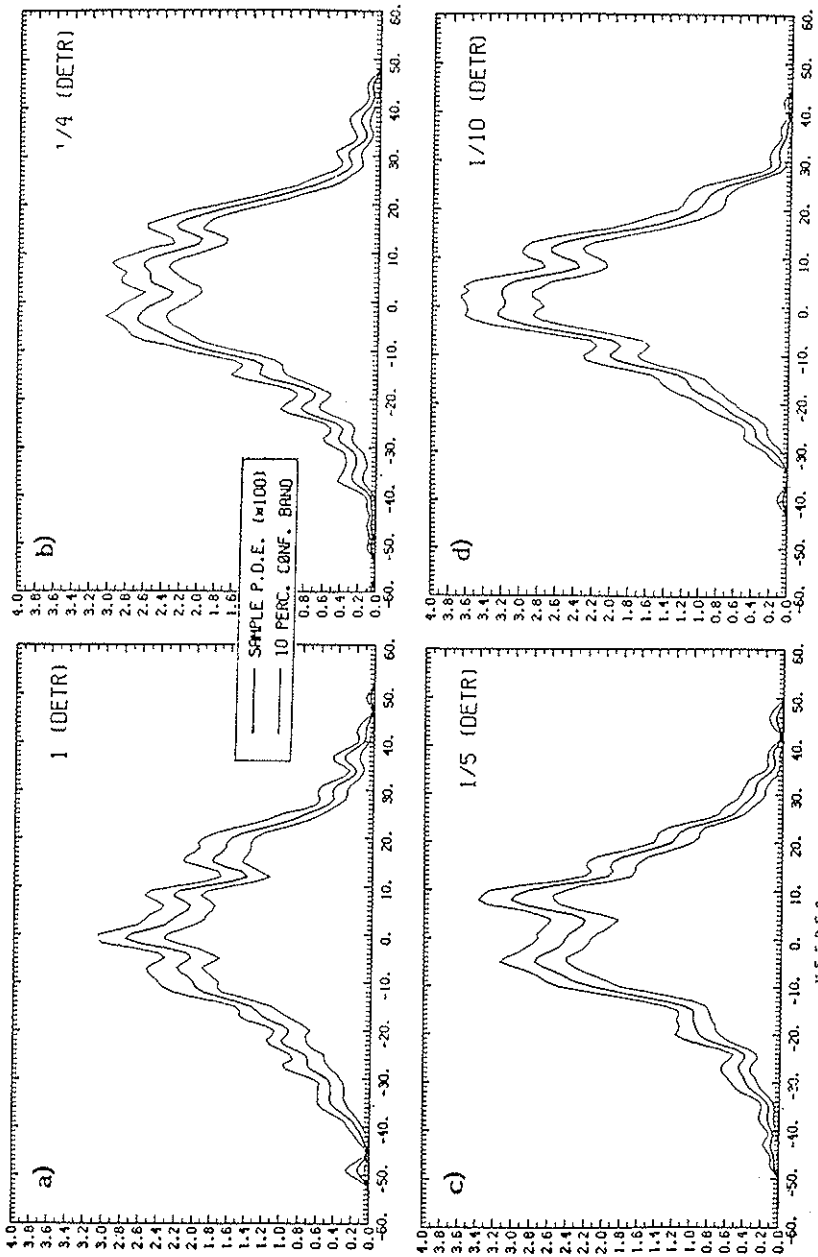

FIG. 10. PDE of the first n EOF, (a) $n = 1$, (b) $n = 4$, (c) $n = 5$, (d) $n = 10$.

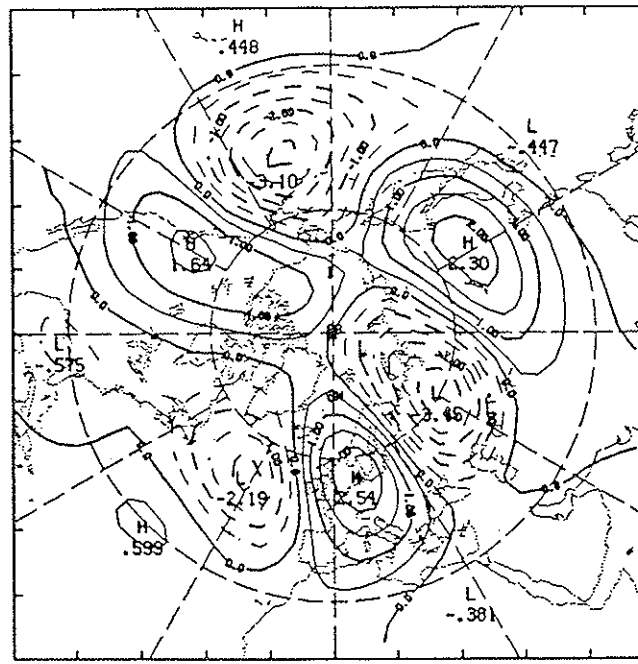

FIG. 11. Pattern of EOF number = 5.

two modes of $\{\Gamma^{i}_{ph}\}$, $i_{max} = 5$ and Figure 12c shows the difference between 12a and 12b. Again we can find high correlation with the analogous composite maps obtained using $\{\Gamma\}$ (see again, Fig. 8a-c). On the basis of this evidence, we conclude that the underlying nature of the physical process determining the bimodal PDD of these indicators must be in both cases of a large-scale global nature. (For more details on the topic considered in this section, see Molteni *et al.*, 1986).

6. PDD OF THE ZONAL QUANTITIES

As was discussed in the introduction, the theoretical motivation of this study lies in considering the observational evidence for the validity of multiple-equilibrium theories of large-scale atmospheric flow (e.g., that of Charney and DeVore, 1979). It appears that these theories are consistent with the data so far analyzed; i.e., the wave field has bimodal PDD

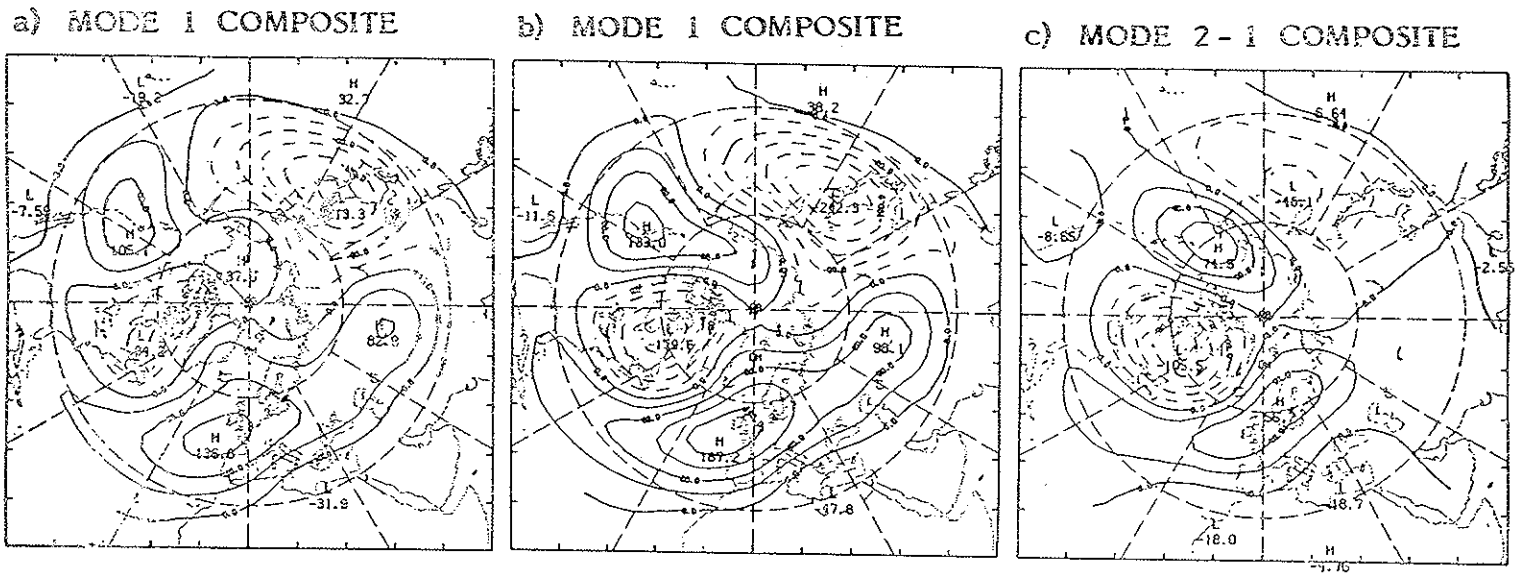

FIG. 12. a) Composite of the 5 EOF fields for Mode 1. b) Composite of the 5 EOF fields for Mode 2. c) Pattern of Mode 2 - Mode 1.

explained by a global pattern. However, it is easy to show that these theories also require a bimodal PDD for the zonal components of the meteorological fields, such as the mean wind, and its latitudinal and vertical shears. To test the extent to which the theories are consistent with observations, we have calculated PDD of these zonal meteorological fields. The data set employed is the NMC analysis as in Hansen and Sutera (1986b). For each day of the data set, we computed zonal wind parameters in a latitudinal band from 45°N to 70°N. Different choices of this band were also considered without any findings of substantial change of the results, hereafter presented.

The parameters were computed as follows: For each day, the grid point 850-, 500-, and 300-mb heights $z(\lambda, \varphi)$ were averaged with respect to longitude, φ, yielding the zonal mean height fields $\bar{z}(\lambda)$. The zonal mean heights were used to compute the zonal mean geostrophic winds. The average speed of the zonal wind, u_z, between latitudes λ_1 and λ_2 was then obtained from

$$u_z = \frac{1}{\sin \lambda_2 - \sin \lambda_1} \int_{\lambda_1}^{\lambda_2} \frac{-g}{f(\lambda)} \frac{\partial z(\lambda)}{\partial \lambda} \cos \lambda \, d\lambda \tag{10}$$

where $f(\lambda)$ is the coriolis force, λ_1, λ_2 are 45°N and 70°N 75°N, respectively. Other notation is conventional. u_z was computed at 850 mb, 500 mb, and 300 mb. The values of u_z at 500 mb were used to form the probability density estimates of the wind speed, and the value at 850 mb and 300 mb were used to compute the vertical shear,

$$u_p = \frac{u_z(300) - u_z(850)}{\Delta p} \tag{11}$$

where $\Delta p = 550$ mb $\cdot$ u_p was computed for the 45° to 70°N zone.

The horizontal shear of the zonal wind $u\varphi$, was computed from

$$u_\varphi = \frac{1}{a} \frac{u_z(\lambda_2) - u_z(\lambda_1)}{\varphi_2 - \varphi_1} \tag{12}$$

where λ_1 and λ_2 equal 45°N and 70°N. The high frequency and low frequency variability of these parameters was removed as in the case of Γ. PDE were obtained by using MPL estimates and the optimal choice of α was determined through simulation.

6.1 *Zonal wind speed*

After constructing the time series of u_z from 1 January 1964 through 31 December 1980 and filtering it to remove the annual and semiannual cycles and high frequency variations, a composite data sample was formed, consisting of 90 observations from each of 16 winters (1 December through 28 February) included in the data set (e.g., 1964-65 through 1979-80). The variance of the composite data was normalized to correspond to that of the wave amplitude indicator studied by Hansen and Sutera (1986a) so that values of α in the range of 10^7 to 10^6 could be used.

The number of mesh points used in making the MPL estimate should be based on the accuracy of the data used to make the estimate. For example, in Sutera (1986) and Hansen and Sutera (1986a), 41 mesh points were used which corresponded to an estimated accuracy in the measurement of planetary wave amplitude of $\pm$ 1 m at 500 mb. In the present case, if we assume that the zonal mean 500-mb geostrophic wind has a typical value of 10 m s^{-1}, and that it is measured to an accuracy of roughly 5 percent, the mesh spacing in the estimate should correspond to roughly 50 cm s^{-1}. This corresponds to zonal mean 500-mb height accuracy of roughly 10 m. Given the variance of the u_z data, 17 mesh points will provide roughly this space. Larger numbers of mesh points were also used in making estimates, but the results were identical. The danger with using more mesh points is that minor modes may appear spuriously at spacings not resolvable by the data.

MPL estimations were then made of the probability density of u_z beginning with a value of the smoothness parameter $\alpha = 10^7$. This value of α was the largest value for which the wave amplitude indicator exhibited bimodality (Hansen and Sutera, 1986). The probability density estimate for u_z in the 45°N to 70°N zone at $\alpha = 10^7$ is a slightly skewed unimodal distribution (Fig. 13a). As the value of α was made progressively smaller, the unimodal nature of the estimate persisted until a second mode first appeared at $\alpha = 10^6$ by random chance; when 17 mesh points are used, 100 sets of 320 random numbers (as we did for Γ) were chosen from a normally distributed parent population with the same variance as the data.

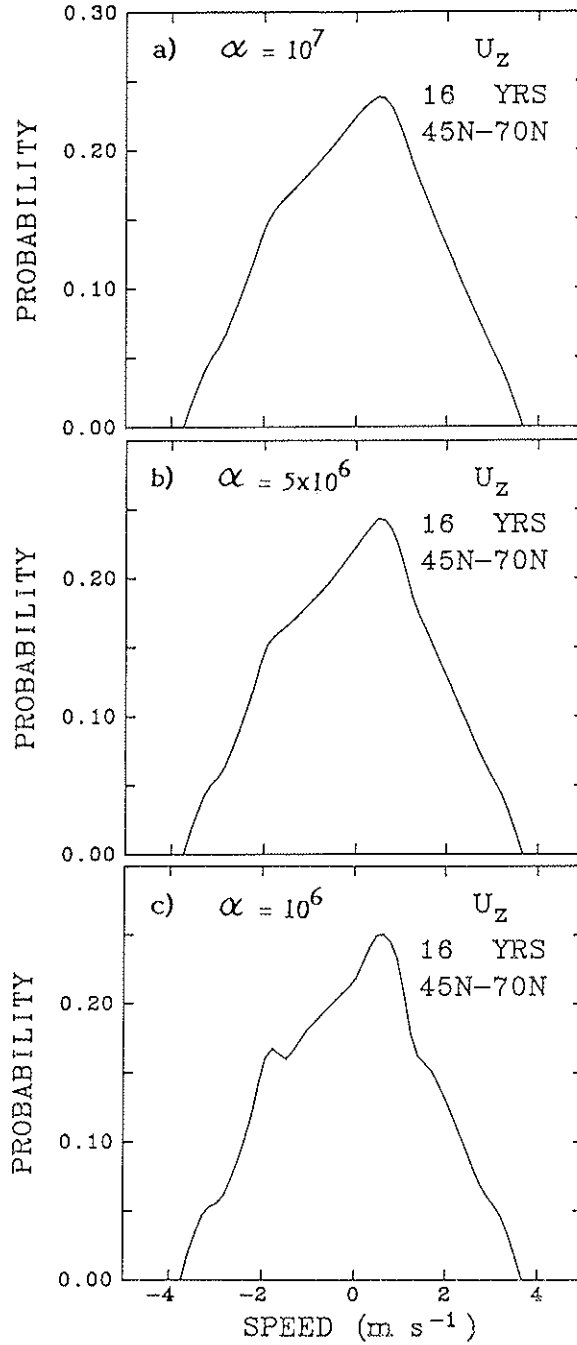

FIG. 13. PDE for the zonal wind speed u_z, (a) $\alpha = 10^7$, (b) $\alpha = 5 \times 10^6$, (c) $\alpha = 10^6$.

With $\alpha = 10^6$, 49 of the 100 realizations exhibited multiple modes (Table 2). Therefore, the bimodality of u_z at $\alpha = 10^6$ is very likely to be the result of random chance. If the u_z data sample has fewer than 320 independent observations, the probability of obtaining multiple modes by random chance is even greater.

Comparison of the u_z estimates at higher values of α to those obtained from randomly sampling a normal population implies that the most likely probability density estimate for u_z in this zone is a normal distribution with a variance $\sigma^2 = (1.76 \text{ m s}^{-1})^2$. Very similar results were also obtained in the wider, 25°N to 70°N zone in which the estimates are unimodal to values of α as small as 10^6. The only difference is that the mean value of u_z in the wider zone is larger (10 m s^{-1} compared to 6 m s^{-1}) and the variance is smaller, $\sigma^2 = (.57 \text{ m s}^{-1})^2$.

These results are in agreement with those obtained by Sutera (1986) from a different, smaller data set. The absence of bimodality in the zonal wind speed argues against theories of low frequency variability that predict this feature, such as that of Charney and DeVore (1979).

6.2 *Horizontal shear of the zonal mean wind*

The probability density distribution of the north-south shear of the zonal mean wind at 500 mb, u_λ, was estimated in a manner analogous to that used for the wind speed. 17 mesh points were also used in these estimates, although use of a finer mesh spacing yielded identical results. The variance of u_λ was normalized in the same way as that of u_z.

The density estimates of u_λ is the 45°N to 70°N zone for $\alpha = 10^7$, 5×10^{-6} and 10^6 are given in Figure 14a-c. u_λ exhibits a slightly skewed unimodal distribution for all values of α until $\alpha = 1 \times 10^6$. As discussed

TABLE 2 - *Random Sampling Results.*

Parent Distribution	Number of Independent Samples/ Realizations	Number of Realizations	α	Number of Mesh Points in Estimate	Percent Unimodal	Percent Bimodal
Normal	320	100	10^6	17	51	49
Normal	320	100	16^6	11	59	41

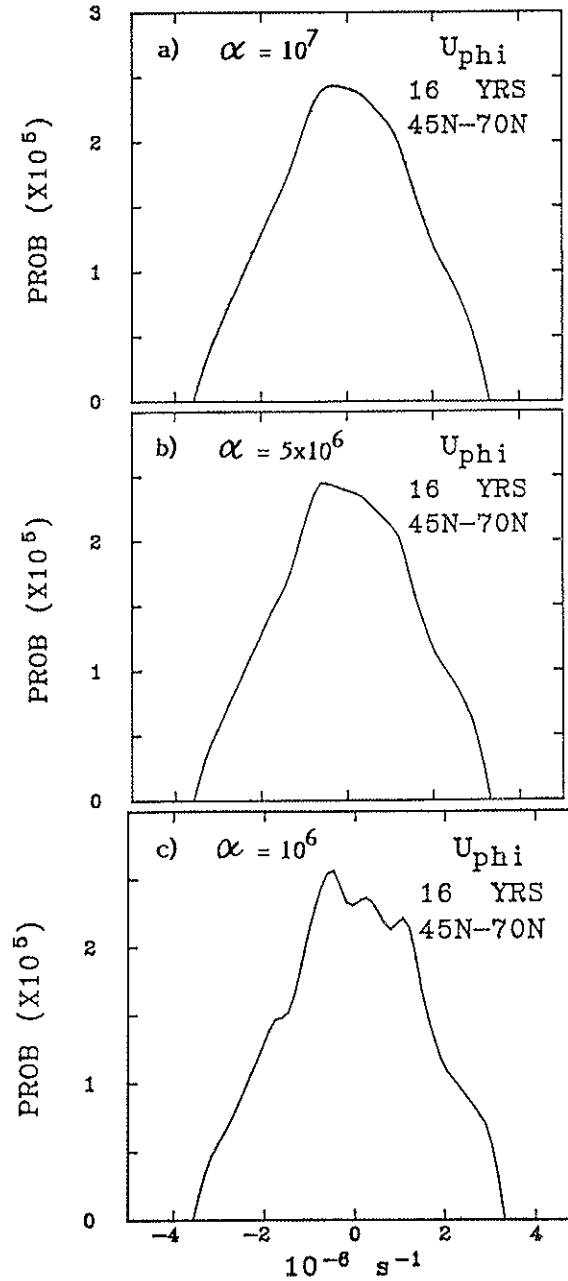

FIG. 14. PDE for the horizontal shear of the zonal mean wind, (a) $\alpha = 10^7$, (b) $\alpha = 5 \times 10^6$, (c) $\alpha = 10^6$.

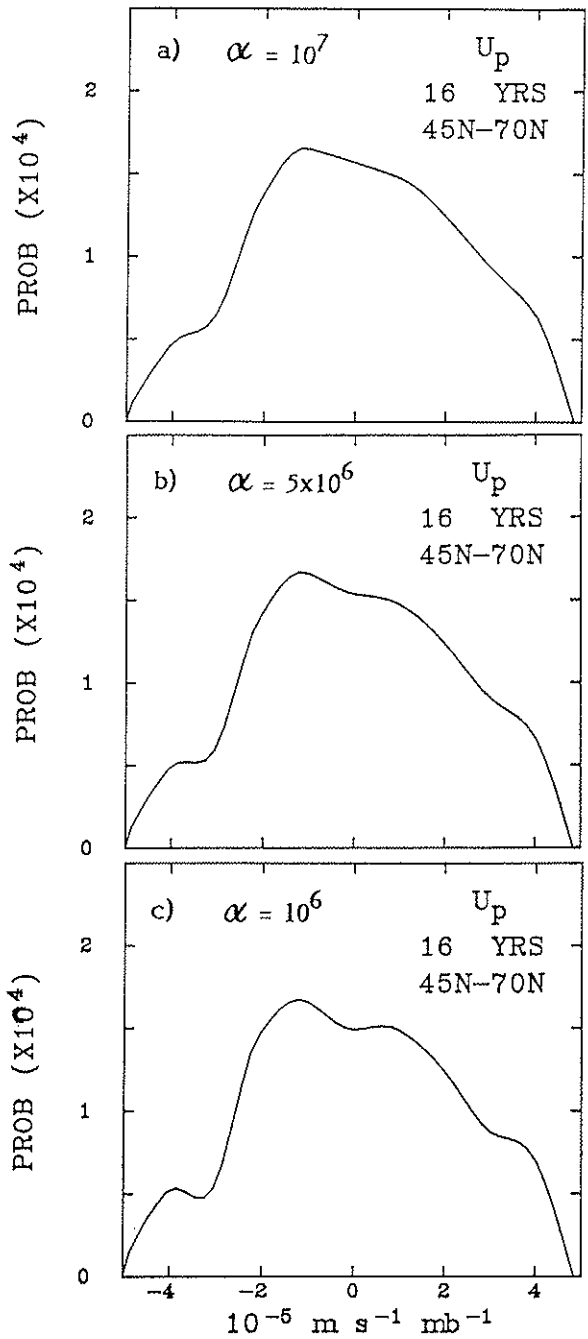

FIG. 15. PDE for the horizontal shear in the 45°N to 70°N 20 m, (a) $\alpha = 10^7$, (b) $\alpha = 5 \times 10^6$, (c) $\alpha = 10^6$.

in the previous section, there is a high probability of obtaining a bimodal estimate from data with this normalized variance by chance from a normal distribution when $\alpha = 10^6$ is used. Therefore, we conclude that the best estimate of the probability density distribution of u_λ is a normal distribution with a variance of $(1.7 \times 10^{-6}$ m sec$^{-1})^2$. If u_λ is computed between 30°N and 70°N, similar results are obtained.

6.3 *Vertical shear of the zonal mean wind*

The vertical wind shear between 300 mb and 850 mb was computed and density estimates were formed. In the case of u_p, if we assume the geostrophic wind speed at 850 mb and 300 mb are also measurable to an accuracy of 50 cm s^{-1}, and given the variance in u_p, only 11 mesh points are justified when making the estimates. For u_p in the 25°N to 70°N zone, the estimates are unimodal and approximately normal down through $\alpha = 10^6$ (not shown). This result is identical even if a much larger number of mesh points is used.

In the 45°N to 70°N zone, estimates for $\alpha = 10^7$, 5×10^{-6} and 10^6 are presented in Fig. 15. A second, nearly undetectable mode first appears at $\alpha = 10^6$. Random sampling simulations analyzed with $\alpha = 10^6$ and with 1 mesh point reveal a high probability of obtaining this result by random change (Table 1) so we again conclude the u_p is a normally distributed variable. For more detail on the topics considered in this section, see Hansen and Sutera (1986b).

Conclusions

From our observational studies, we can conclude that asymmetric perturbations of the large-scale atmospheric flow have a bimodal PDD. The low amplitude mode contains events in which the flow is characterized by a zonal circulation, while the large amplitude mode contains events which can be described as blocking events. These events seem global and not affected by a particularly noticeable latitudinal dispersion. Indicators describing the zonal-mean circulation appear to be unimodally distributed. This picture disagrees with the Charney-DeVore (1979) theory. How-

ever, as discussed by Benzi *et al.* (1986a,b), it is possible in the Charney-DeVore theoretical framework to restore consistency. For further discussion of this point, see Benzi and Speranza contributions.

ACKNOWLEDGMENT

This work was sponsored by the National Science Foundation under NSF Contract No. ATM-8507496.

REFERENCES

BENZI R., MALGUZZI P., SPERANZA A. and SUTERA A., *The statistical properties of the general atmospheric circulation: Observational evidence and a minimal theory of bimodality.* « Quart. J. Roy. Meteorol. Soc. », Iuly (1986a).

BENZI R., SPERANZA A. and SUTERA A., *A minimal baroclinic model for the statistical properties of low frequency variability.* « J. Atmos. Sci. », to appear (1986b).

BENZI R., see this Volume (1986).

CHARNEY J.G. and DEVORE J.G., *Multiple equilibria in the atmosphere and blocking.* « J. Atmos. Sci. », *36*, 1205-1216 (1979).

GOOD I.J. and GASKINS R.A., *Density estimation and bump hunting by the penalized likelihood method exemplified by scattering and meteorite data.* « J. Amer. Stat. Soc. », *75*, 42-56 (1980).

HANSEN A.R., *Observational characteristics of atmospheric planetary waves with bimodal distribution.* « Adv. i Geophys. », *29*, in press (1986).

HANSEN A.R. and SUTERA A., *On the probability density distribution of planetary-scale atmospheric wave-amplitude.* « J. Atmos. Sci. », to appear (1986a).

HANSEN A.R. and SUTERA A., *On the probability density distributions of the speed, horizontal and vertical shear of the zonal mean flow.* « J. Atmos. Sci. », submitted (1986b).

MOLTENI F., SUTERA A. and TRONCI N., *EOF analysis of the geopotential eddies at 500mb in winter and their probability density distributions.* To be submitted (1986).

PANOFSKY H.A. and BRIER G.W., *Some Applications of Statistics to Meteorology*, Pennsylvania State University Press, 224 pp. (1958).

ROSENBLATT M., *Remarks on some non parametric estimates of a density function.* « Ann. Math. Stat. », *27*, 832-835 (1956).

SCOTT D.W., TAPIA P.A. and THOMPSON J.R., *Kernel density estimation revisited.* « Nonlinear Analysis, Theory, Methods and Applications », *1*, 339-372 (1978).

SPERANZA A., see this Volume (1986).

SUTERA A., *Probability density distribution of the large-scale atmospheric flow.* « Adv. in Geophys. », *29*, in press (1986).

WALLACE J.M., AMBROZY J.H., BRONKOVIC C., EDMON H., JENNY R., ORIOL E. and PRICE P., *Five-day Mean 500m Heights and Sea Level Pressure Fields for the Northern Hemisphere (1946-1977).* Long-Range Forecasting Research Project Publ., World Meteorological Organization, Geneva (1983).

WALLACE J.M. and GUTZLER D.S., *Teleconnections in the geopotential height field during the northern hemisphere winter.* « Mon. Wea. Rev. », *109*, 784-812 (1981).

30- AND 60-DAY FORECAST EXPERIMENTS WITH THE ECMWF SPECTRAL MODELS

F. MOLTENI, U. CUBASCH and S. TIBALDI
European Centre for Medium Range Weather Forecasts
Shinfield Park, Reading, Berkshire RG2 9AX, U.K.

ABSTRACT

During the last five years, the feasibility of dynamical extended-range forecasts by means of atmospheric general circulation models (GCMs) has received support from a number of experimental studies. However, despite the encouraging results obtained in some case studies, two main factors still prevent the skill of dynamical forecasts from reaching a level acceptable for practical applications: the intrinsic instability of the atmospheric flow and the presence of systematic errors in the fields predicted by almost all the large GCMs. It has however been shown that both time-averaging and ensemble averaging can effectively reduce the impact of initial uncertainties and model-generated random errors on the quality of the forecast. On the other hand, if really systematic features appear in the error fields produced by a GCM, it should be possible to remove them from the output of a prediction experiment by subtracting the mean error computed from a (possibly) large sample of independent forecasts. The main purpose of the experiments described here has been the evaluation of the impact of i) ensemble forecasting, ii) correction of the systematic error and iii) increased resolution of the model on the forecast skill. Two versions of the ECMWF operational spectral model were used, adopting a triangular truncation at total wavenumber 21 (T21) and 42 (T42) for the expansion of the horizontal fields. The Lagged-Average Forecasting method was used to generate the ensemble of predictions described in the first part of the work. Nine forecasts,

starting from initial conditions separated by 6-hour intervals, were averaged at the corresponding verification times up to 30 days after the last initial analysis; the single, purely deterministic forecasts starting from the last analysis were used, together with persistence, for a comparative assessment of the results. Statistically corrected Lagged-Average and deterministic forecasts were also obtained by subtracting from the predicted fields an estimate of the systematic error, deduced for each experiment from a sample of 10 forecasts starting from analyses separated by 10-day intervals in the same and the following month of the previous two years. The T42 corrected Lagged-Average forecast appears to have the highest skill among all the combinations of resolution/error filtering methods explored. For the 850 mb temperature the forecasts are, on average, more skillful than either climate or persistence.

Finally, a series of 38, purely deterministic, thirty and sixty-day forecasts run from randomly selected winter initial conditions with the ECMWF spectral model using the same two resolutions (T21, T42) have been examined. The purpose of this further study was to assess objectively the skill of purely deterministic extended-range forecasts in a quasi-operational environment. The large ensemble of forecasts allows, furthermore, an estimate of the spread in the forecast quality. It appears again that the higher resolution model (T42) is more skillful than the lower resolution version (T21) and has a higher reliability. The T42 model is better than a persistence forecast of 10-day means up to the first half of the 30-day period. The T42 30-day mean forecast is almost consistently better than persistence. The skill of the T42 model forecast appears to be uncorrelated with the skill of the persistence forecast which undergoes large case-to-case and interannual variations.

1. Introduction

During the last twenty years, extended and long-range weather forecasting (defined as forecasts from 10-15 days to one month and from 1 month to 3 months respectively) has progressed from an empirical stage, dominated by purely statistical approaches with only qualitative physical bases, to the level of an important branch of dynamical meteorology. At present, observational studies and theoretical and numerical models allow the evaluation of the structure and physical causes of the low-frequency components of the atmospheric circulation and, at least partially, to predict their temporal evolution (see Nicholls *et al.*, 1984).

As pointed out in an earlier work by Nicholls (1980), statistical forecasting methods have generally failed to produce reliable operational monthly or seasonal forecasts. However, when used as diagnostic tools, statistical methods have provided plenty of observational evidence on the existence of some modes of low-frequency atmospheric variability that should be dynamically predictable: see, among others, Namias (1969), Ratcliffe and Murray (1970), Horel and Wallace (1981) on the influence of sea-surface temperature anomalies, or the work by Wallace and Gutzler (1981) on the existence of preferred patterns of variability connected to "centres of action". It has also been demonstrated that potential long-range predictability is characterised by a strong seasonal and geographical dependence (e.g., Madden, 1976 and Walsh and Richman, 1981).

Meanwhile, the continuous progress in the numerical simulation of the atmospheric general circulation and in medium-range weather forecasting has shown that, for some situations, it is possible to obtain skillful dynamical monthly forecasts of the larger scale features (Miyakoda and Chao, 1982; Miyakoda *et al.*, 1983).

However, the skill of a deterministic prediction carried out with a numerical model is bounded by two factors. The first factor, the intrinsic instability of the atmosphere with respect to small perturbations, has been discussed in the fundamental works of Lorenz (1963, 1969a, 1969b, 1982). Even with a perfect model, analysis errors as small as the current 24-hour forecast error of a state-of-the-art General Circulation Model (GCM) would double in about two days. However, the smaller the characteristic spatial scale of the initial error, the smaller is its doubling time; so, even if analysis errors are increasingly confined to smaller scales, the time at which the largest scales become unpredictable (that is, when a prediction of their instantaneous state becomes as good as a random forecast) cannot be increased indefinitely. This time limit was determined by Lorenz (1969a) to be about 15 days and this value is now commonly accepted as a good estimate of the limit of deterministic predictability.

The second factor which sets a limit to the forecasting of instantaneous weather patterns is the imperfections and inadequacies of even the best GCMs currently available. This adds further sources of error that, in practice, limit the usefulness of numerical weather predictions (NWPs) to about one week. An important part of this error is not random and causes a gradual drift with time of the mean state of the model atmosphere from the actual climate towards the model's own climate (as deduced from very long integrations). Also von Storch *et al.* (1985) have shown that many

features of the systematic errors are common to different GCMs: examples are the excessive westerlies (Arpe *et al.*, 1985; Arpe and Klinker, 1986 and Palmer *et al.*, 1986) and the tendency in winter to produce a lower ratio of eddy to zonal kinetic energy than that observed, and in particular to underestimate the amplitude of the planetary-scale stationary eddies in the northern extratropics (Hollingsworth *et al.*, 1980 and Wallace *et al.*, 1983).

Despite these limitations, the hope for useful dynamical predictions up to one month or more is supported by the following considerations:

(a) Even though the instantaneous state of the atmosphere cannot be predicted after about 15 days, some statistical properties of the atmospheric variables (for example, the mean fields over periods from 10 days to one month) may "remember" the influence of the initial conditions beyond this limit. This was illustrated by Shukla (1981) who showed that the differences between predicted monthly means computed from initial fields observed on the same date of different years are significantly greater than those obtained by superimposing random perturbations to the same initial fields (all forecasts used climatological boundary conditions). Shukla calls "dynamical predictability" that which derives from the influence of the initial conditions.

(b) As suggested by observational and theoretical studies and confirmed by a number of numerical experiments (e.g., Rasmusson, 1983; Walsh, 1983; Shukla and Wallace, 1983; Shukla, 1984), the forcing generated by the surface boundary conditions (namely, the sea surface temperature (SST), soil moisture, snow cover and sea ice) can significantly affect the general circulation and play an important role in determining the large scale anomalies of the atmospheric fields. Since most of the anomalies in the surface conditions have a typical time of variation of weeks or months, a correct initial analysis of these components of the climatic system and a good model representation of their influence upon atmospheric motion can increase the predictability of the atmospheric anomalies up to forecast times of comparable duration.

(c) Even if a deterministic prediction is subject to the continuous growth of the initial error, which ultimately masks the signal in the forecast, the mostly random nature of this error due to imperfections in the initial conditions suggests that the valuable signal may be more clearly detected by averaging the results of a number of forecasts that start from slightly different initial states. As shown by Epstein (1969), this procedure

of "ensemble forecasting" can be seen as the practical realisation of the theoretical approach of Gleeson (1968, 1970), who suggested that the observed initial state and its uncertainty can be characterised by a probability density function in phase space, and that the temporal evolution of this function gives a probabilistic estimate of the future state of the atmosphere. The theoretical and practical developments of these ideas are known as stochastic-dynamic prediction methods and the Lagged-Average Forecasting (LAF) technique proposed by Miyakoda and Talagrand (1971) and Hoffmann and Kalnay (1983) is based upon such ideas.

(d) A part of the error generated by numerical models is systematic. This suggests that, if the systematic error (SE) is computed from a large sample of integrations in the same period of the year, the subtraction of the SE can reduce the root mean square error of a comparable ENSEMBLE of independent forecasts (see, e.g., Arpe, 1983). The effectiveness of the application of this subtraction to a SINGLE forecast obviously depends on the statistical significance of the SE, that is, on the ratio between mean and standard deviation of the error. Besides, the correction will probably not be suitable for a prediction performed with boundary conditions significantly different from those used in the computation of the SE.

On the basis of these arguments, four sets of experimental monthly forecasts were carried out with the following characteristics:

— the predicted fields were 10-day mean and 30-day mean anomalies of geopotential height and temperature at various pressure levels in the northern hemisphere;

— observed SSTs (analysed operationally by NMC) were used as boundary conditions;

— a stochastic-dynamic method, namely the LAF technique, was chosen in order to reduce the random part of the error, and its performance was assessed against purely dynamical integrations;

— an estimate of the model SE, deduced from a sample of ten independent monthly integrations, (appropriate for the season of year and started from random initial conditions during the previous two years) was subtracted from the LAF output to produce (statistically) corrected anomalies.

— the integrations were performed at two different horizontal resolutions.

Due to the large number of long integrations required for this study, two low-resolution versions of the ECMWF operational spectral model (Louis, 1984) were used. The expansion of the horizontal atmospheric fields in spherical harmonics was limited by a triangular truncation at wavenumber 21 (T21) and 42 (T42). Consequently, the horizontal resolution is, in both cases, isotropic and the length of the smallest wave resolved with these truncations is about 2000 and 1000 km respectively.

This report presents the results of the experiments, and is organised as follows: section 2 is devoted to the problem of the SE of the ECMWF T21 and T42 models. Section 3 describes the results of four LAF 30-day experimental forecasts, discusses a further experiment devised to test the impact of SSTs on the forecast skill and assesses the correlation between the spread of the forecast ensembles and the forecast skill. Section 4 presents some overall results on purely deterministic extended range forecasts by analysing separately the comparatively larger database of 30-day (and some 60-day) integrations used previously to estimate the model systematic error. The conclusions are summarized in Section 5.

2. The Systematic Errors of the T21 and T42 Spectral Model

Before discussing the results of the forecasting experiments, it is worthwhile describing the main characteristics of the SE of the model employed. Emphasis will be placed on the mean 500 mb height and 850 mb temperature (referred to as Z500 and T850) over days 21-30. These parameters are chosen because they are most often used to characterize model behaviour and are widely used as forecasting tools; the period chosen is taken to be the best available to infer the model asymptotic behaviour for longer integrations. The January-February period (used later to correct the LAF forecast started from 17 January 1984) was chosen and the ensemble of ten 30 day integrations had initial dates 1, 11 and 21 January, 1 and 11 February 1982 and 1983.

2.1 *500 mb height*

Fig. 2.1 shows the mean observed Z500 (labelled OBS MEAN), the corresponding mean forecast (labelled FOR MEAN) for the two model resolutions and their SE (labelled SYS ERROR). Apart from a common tendency to underestimate the amplitude of planetary scale

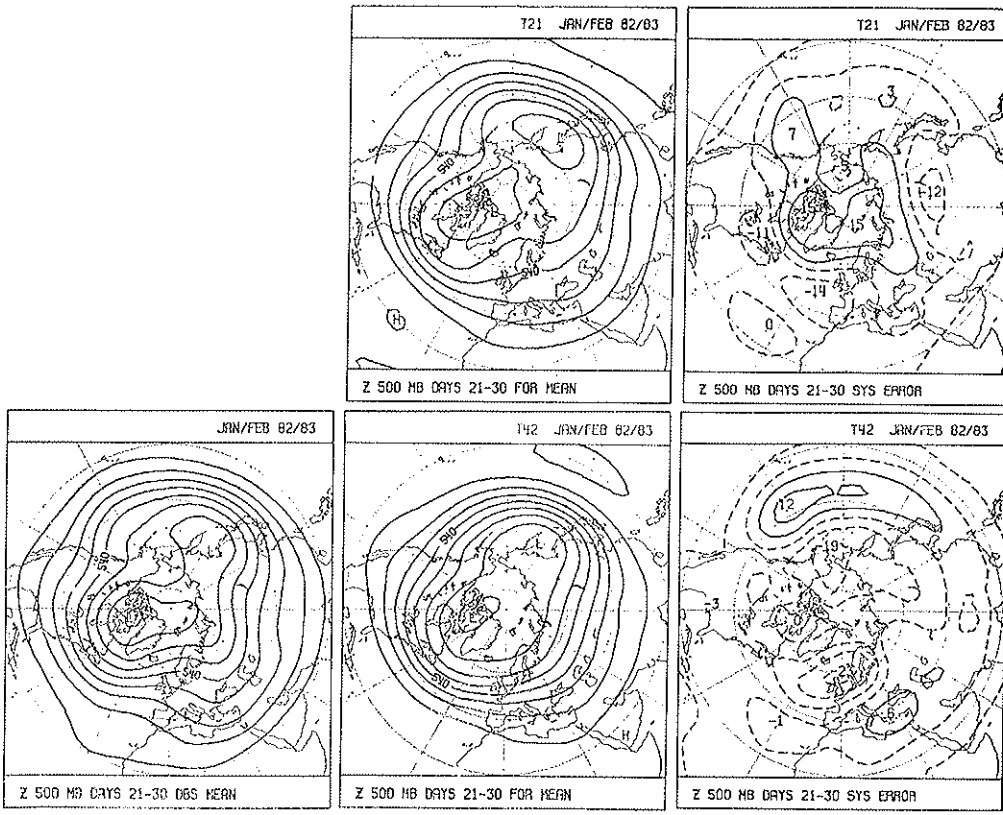

FIG. 2.1. Mean analyses (left), forecasts (centre) and systematic error (right) of northern hemispheric 500 mb height in the 21-30 day range for a sample of ten T21 (top) and T42 (bottom) monthly forecasts started in January and February 1982 and 1983.

waves (see Hollingsworth *et al.*, 1980; Wallace *et al.*, 1983 and Tibaldi, 1986), the structure of the SE field appears to be substantially different for the two resolutions. The T21 clearly tends to reduce the latitudinal height gradient and, hence, the strength of the mean (geostrophic) zonal wind, with the maximum reduction taking place over the Atlantic and Western Europe area; here the jet diffluence is exaggerated and the anticyclonic curvature typical of this area during winter months is lost. On the contrary, the T42 model tends to increase the north-south height gradient and therefore the strength of the jet between 40° and 60°N over the Northern Pacific and over Europe. Also the jet diffluence over

Western Europe is almost completely lost, together with the anticyclonic curvature. Another feature of the T42 forecasts is the damping of the Rocky Mountains and Alaskan ridge; hence the wavenumber 3 signature on the planetary scale eddy field is weakened substantially while wavenumber 2 is wrongly enhanced. South of about 40°N for the T21 and 30°N for the T42, the SE is everywhere negative for both models.

The ability of the two models to reproduce the time variability of Z500 is shown in Fig. 2.2, where the standard deviations of the observed (OBS S.DEV) and forecast fields (FOR S.DEV), and the ratio of the forecast and observed values (FOR S.DEV/OBS S.DEV) are depicted.

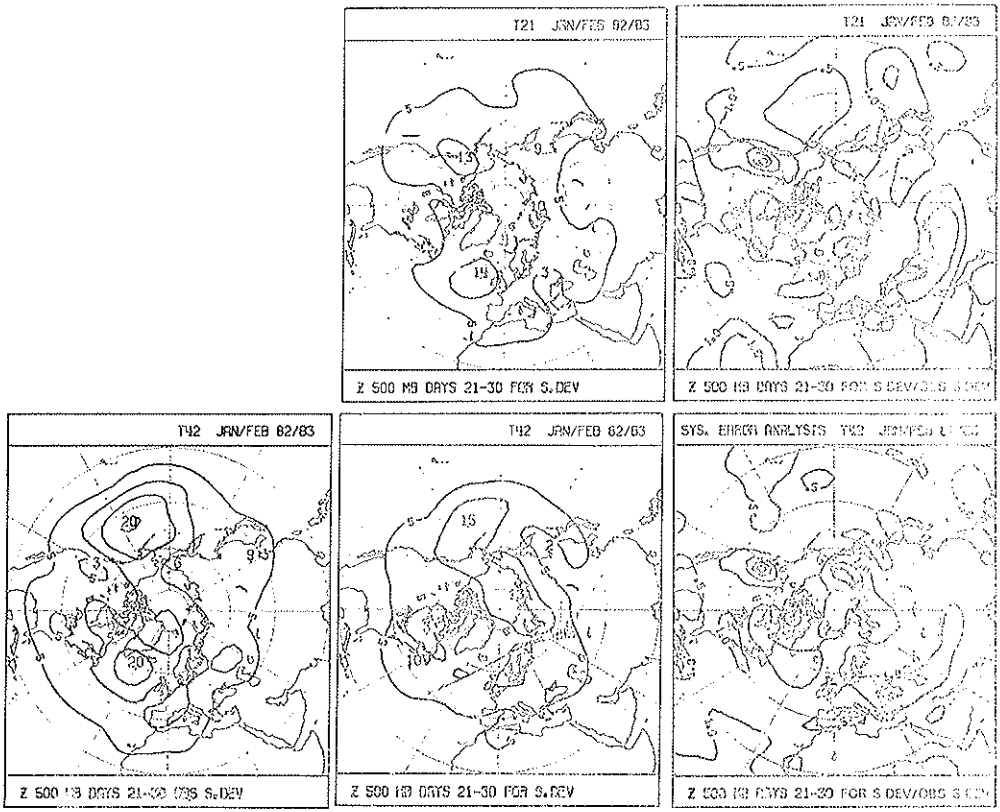

FIG. 2.2. Standard deviation of the analyses (left), of forecasts (centre) and their ratio (forecast/observed, right) of the northern hemispheric 500 mb height in the 21-30 day range for a sample of ten T21 (top) and T42 (bottom) monthly forecasts started in January and February 1982 and 1983.

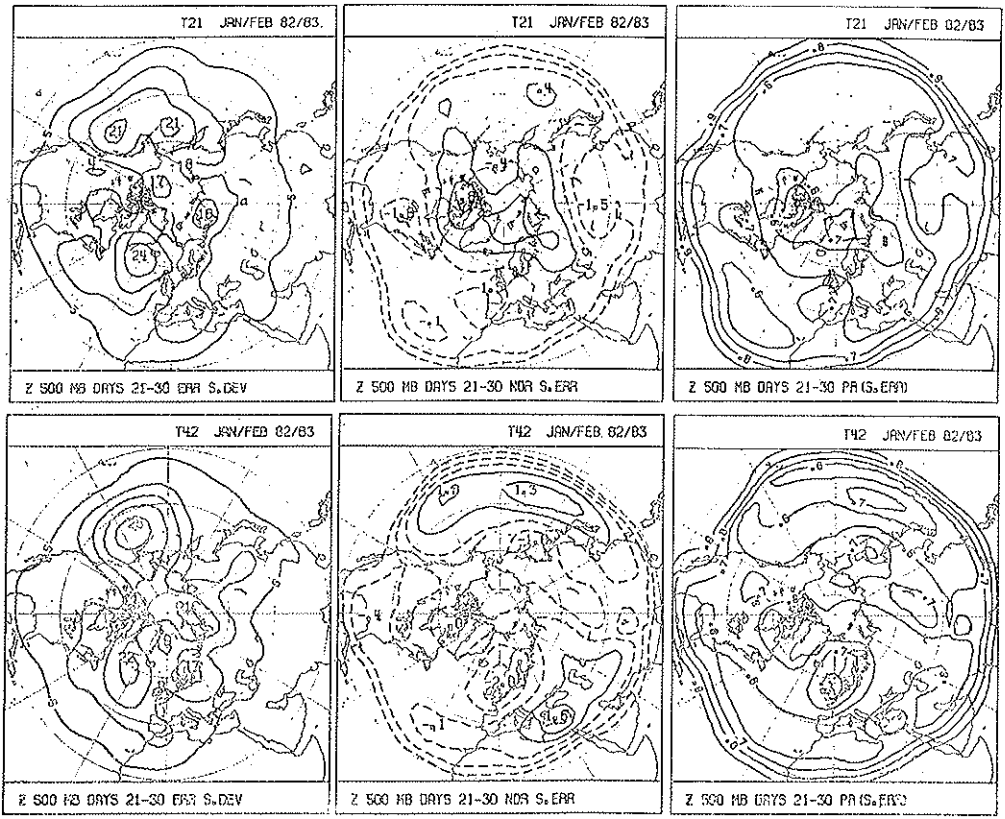

FIG. 2.3. Standard deviation of forecast error (left), ratio between mean and standard deviation (normalised SE, centre) and probability of SE (right). T21, top, and T42, bottom. For more explanations see text, Section 2.

It is evident that both models tend to underestimate such variability, particularly the T21 model over the Pacific area and the T42 model over the Atlantic. The models' standard deviation of Z500 is smoother than the observed and it appears that the influence of orography is not well reproduced (note in particular the Rocky Mountains region).

Fig. 2.3 allows to evaluate the ratio of the random and mean error for the two model resolutions, and therefore the significance of the latter. First consider the standard deviation error (ERR S.DEV) — it is fairly high for both models and, in many areas, greater than the natural variability; this indicates that the correlation between forecast and observed

fields in the period 21-30 days is likely to be very low. The higher standard deviation of the T42 model with respect to the T21 over the Pacific area is most likely due to the higher variability of the higher resolution model, rather than to a worse performance in terms of forecasting skill (as we will see later).

The ratios between mean and standard deviations of the model error, the normalised SE (NOR S.ERR) given in the centre panels of Fig. 2.3, show that for both model resolutions the most noteworthy structures of the SE are statistically significant (for a sample of 10 elements the confidence level of 95% corresponds to a ratio higher than approximately .7); over wide areas the SE is comparable to or greater than the random error. This implies that, on average, we should expect improvements by using this estimate of the SE to correct our forecasts. However, as it will be shown later, on individual cases the results can be very variable.

By assuming that the probability distribution of the error around its own mean is gaussian, it is possible to evaluate, for every point, the probability (PR(S.ERR)) that the error is nearer to its mean value than to zero, that is the probability that a SE correction reduces the total error of a forecast rather than increasing it. This probability is shown in the right panels of Fig. 2.3 and has a minimum value of 50% where the SE is zero. It can be seen how, in the northern hemisphere extratropical latitudes, for both models the term "systematic" it not always appropriate, since only in some areas is the subtraction of the SE advantageous in at least 70% of the cases. A completely different picture is true for tropical regions, where the variability of the error is much smaller than its mean value.

2.2 *850 mb temperature*

The fields shown in Figs. 2.1, 2.2 and 2.3 for the Z500 are reproduced in Figs. 2.4, 2.5 and 2.6 for the T850. The general tendency for both models to cooling the troposphere, already deducible from 500 mb height fields, is evident. Negative peaks of SE are obviously connected to underlying orographic features and the positive areas (larger for T21 than for T42) are confined to arctic regions. For the higher resolution model, noteworthy is the positive centre over the central and east Mediterranean region, including parts of East Europe and Western Asia, due to an excessive zonalisation of the model flow. The T21 error

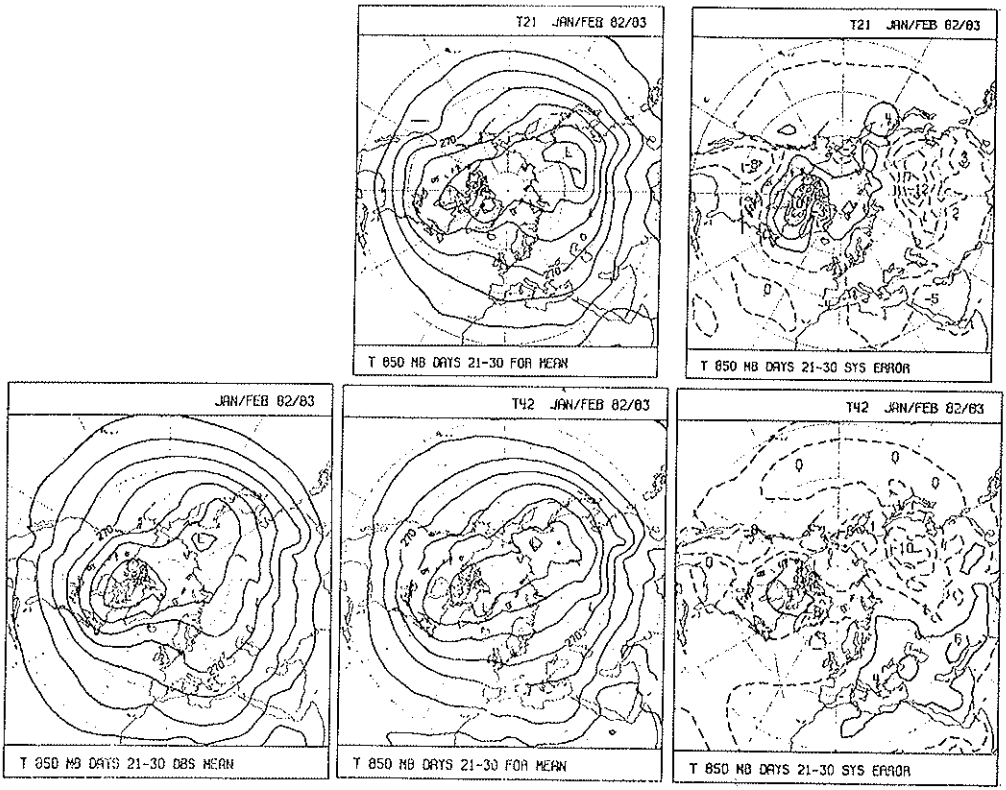

FIG. 2.4. As Fig. 2.1, but for T850.

seems to display a vertical structure of the SE more equivalent barotropic than the T42.

The variability of the model's T850 (Fig. 2.5) is on the whole more similar to the observed field than was found for Z500 (Fig. 2.2), with the T42 model appearing better than the T21. South of 40°N, there are large areas where the model variability appears larger than that observed, while north of this latitude the opposite occurs. It should be noted that the maximum observed variability takes place over continental masses (Alaska, Canada, Eastern Siberia) and that, with the exception of Alaska, in these areas the models display a large SE and a clear lack of variability. Even allowing for some errors due to subterranean extrapolation of the 850 mb temperature in some of those areas, these facts underline the

need for a more appropriate modelling of the thermal interactions between the lower troposphere and the underlying surface.

As for Z500, Fig. 2.6 shows that for T850 the important structures of the SE are also statistically significant; however in middle and high latitudes the mean error is only really "systematic" in limited areas, so that the correction for the SE should give, on average, positive results, but with negative effects in some cases.

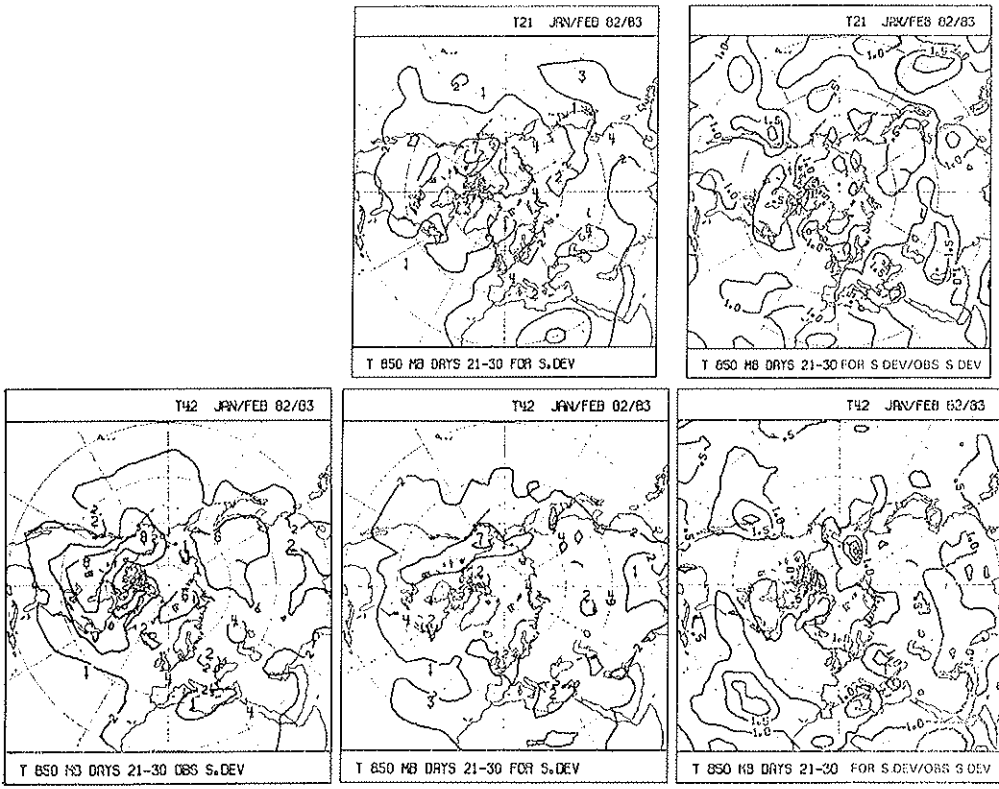

FIG. 2.5. As Fig. 2.2, but for T850.

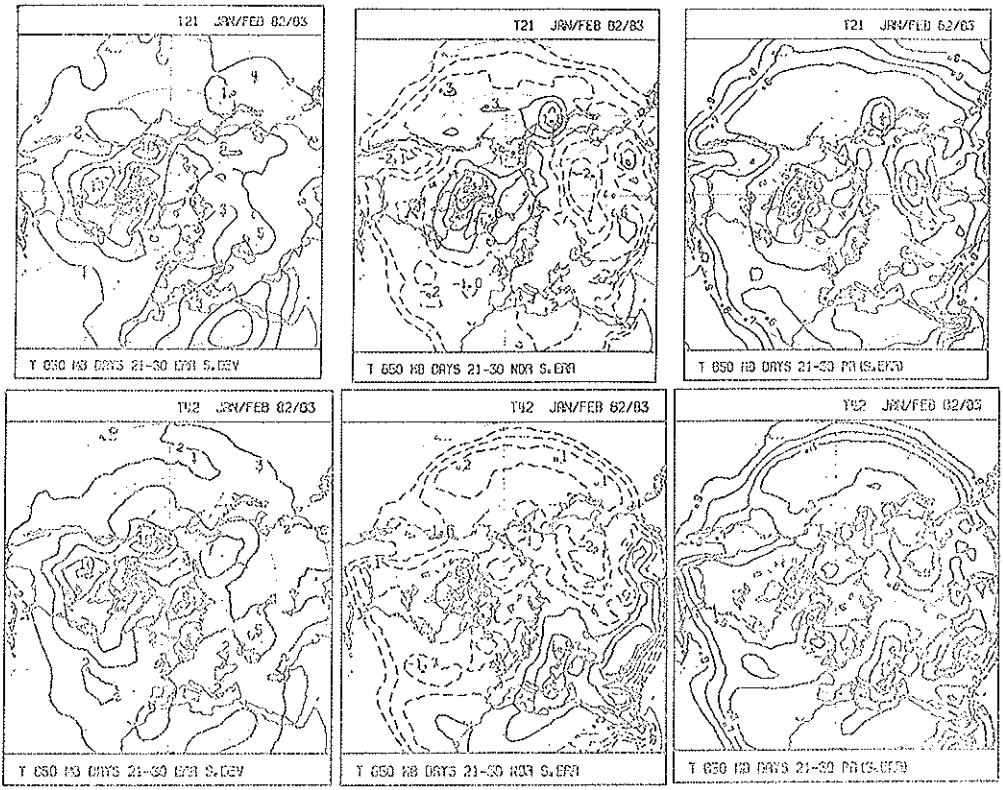

FIG. 2.6. As Fig. 2.3, but for T850.

3. THE LAGGED-AVERAGE FORECASTS

3.1 *Description of the experiments*

The Lagged Average Forecasting (LAF) technique gives an estimate of the predicted fields by averaging the results of n integrations starting from initial times separated by a time δt. If t_o is the initial time of the most recent integration, the ensemble of forecasts start from times t_o, $t_o - \delta t \ldots t_o - (n-1)\ \delta t$. The construction of a LAF ensemble is illustrated in Fig. 3.1. For our experimental 30-day forecasts $n = 9$ and $\delta t = 6$h were used, and the initial times t_o were 12 GMT on 15 December 1983, 17 January 1984, 19 February 1984 and 23 March 1984. The 17 January and 19 February cases were chosen essentially because they had

produced, operationally, a very good and very bad medium-range forecast respectively. The other two were chosen with the sole purpose of spanning a four-month, non-overlapping period and can therefore be considered as chosen at random.

For each of the four initial conditions and each of the two model resolutions the following operations were performed:

(a) Nine forecasts were integrated from progressively lagged initial conditions (see Fig. 3.1). The LAF was then defined as the arithmetic mean of the nine forecasts verifying at the same time. All forecasts had the same weight in such a mean (unlike, for example, in Hoffmann and Kalnay, 1983) because the main interest was on forecast times longer than ten days, for which all weights would have been practically identical.

(b) A purely dynamical deterministic forecast (DET) was obtained by spectrally truncating at T10 and T21 respectively the T21 and T42 integrations that started from the most recent initial conditions amongst the nine. The spatial truncation of the output fields was performed to remove from the DET forecasts all those scales that are filtered out by the ensemble averaging in the LAF experiments. This avoided the LAF experiments appearing objectively more skillful than the DET integrations because less variance was contained in the smaller scales.

(c) An estimate of the SE appropriate for the month of the year of each experiment was computed as the average of the forecast errors of ten independent integrations started from 1, 11 and 21 of the same month

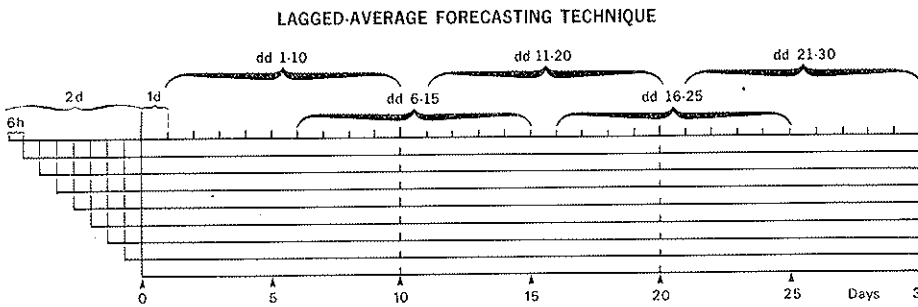

FIG. 3.1. Schematic of the construction of a LAF forecast composed of an ensemble of nine individual deterministic forecasts starting from adjacent initial analyses, progressively lagged of 6 hours. Periods of time-average are also shown.

as the initial conditions and from 1 and 11 of the following month, for the two preceding winters (1981/82 and 1982/83). This SE estimate was then used to produce statistically corrected versions of both LAF and DET forecasts, referred to as SCL and SCD, respectively.

(d) For each forecast objective skill scores (against observed fields) of 10-day running means (days 1-10, 6-15, 11-20, 16-25, 21-30) and of monthly means (days 1-30) for 1000, 500 and 300 mb height and 850, 500 and 300 mb temperature were evaluated. This was done in order to select only the low-frequency components of the atmospheric variability which are suspected of possessing a longer predictability (Smagorinsky, 1969; Gilchrist, 1977; Shukla, 1984). The objective measures used are the anomaly correlation coefficient between forecast and analysed fields (ACC) and the root mean square (RMS) error, both computed over the extra-tropical hemisphere (20°N to 90°N).

(e) Objective skill scores were also computed for two types of persistence forecasts based on the persistence of anomalies, taking therefore the seasonal cycle into account. The first, referred to as simple persistence (PER), assumes that the forecast anomaly at the verification time (10 days or a month) is the observed anomaly averaged over the corresponding period before the initial time of each forecast. The second, referred to as long-term persistence (LTP), is similar to PER, but the observed anomaly is averaged over a period that increases with increasing forecast time. For example, LTP for the anomaly for the forecasting interval 11-20 days is the mean observed anomaly during the previous 20 days. The idea on which this less conventional persistence forecast is based is that those features that appear in a time mean over a period Δt are more likely to persist for the same period of time Δt.

In computing anomaly fields, the climatology used was derived from the ECMWF archives of the five years leading up to December 1983. This climatology is based on a comparatively short period of time and therefore probably contaminated by a degree of interannual variability. However, it was preferred to the NMC-NCAR longer-term climatology, for which there are doubts about the quality of the analysis algorithms employed in constructing the objective analyses on which it is based. Although it is impossible to separate the effects of data availability, analysis quality and interannual variability, the objective scores computed using the NMC-NCAR climate appeared to be consistently biased towards too high values

due to very persistent features of the anomaly fields located over oceanic areas.

3.2 *The skill of the LAF forecasts*

The skill of the LAF forecasts can be compared with the DET forecasts by computing the RMS error and the anomaly correlation coefficient (ACC) between forecast and analysed fields as a function of forecast time, averaged over the four cases.

3.2.1 *RMS error and anomaly correlation coefficient*

Figs. 3.2 and 3.3 show the ACC and RMS error for T850 and Z500 for the Northern Hemisphere, along with the persistence scores.

These results indicate the following:

— T850 is more "forecastable" than Z500 and for the T42 forecasts it outperforms persistence for the entire forecast period. The average ACC for the 30-day mean fields using the T42 SCL (LAF corrected for the systematic model error) has a value of 0.5.

— The most important element affecting objective forecast performance is the model's horizontal resolution rather than the statistical model error correction or the use of the LAF technique. However both techniques have a constant positive impact in reducing RMS errors. For T850 there is a sizeable improvement in ACC going from DET to LAF and, for T21, from LAF to SCL. Taking all the results into account, the T42 SCL gives the overall best forecasts.

— The LAF ACC does not decrease monotonically with forecast time, but shows a minimum for the 11-20 day interval for Z500 and for the 16-25 day interval for T850. For the T21 model in particular, the evidence of such "return" of skill is emphasized by the systematic error correction technique. Similar behaviour in extended range forecasting experiments has been previously reported, e.g., Miyakoda *et al.* (1983), Cubasch and Wiin-Nielsen (1986), but its causes are still very much under debate.

3.2.2 *Variability of forecast skill*

The variability in forecast skill within our limited sample will now briefly be discussed. It has already been seen that the average model skill in forecasting T850 and Z500 is quite different; this is also true for the

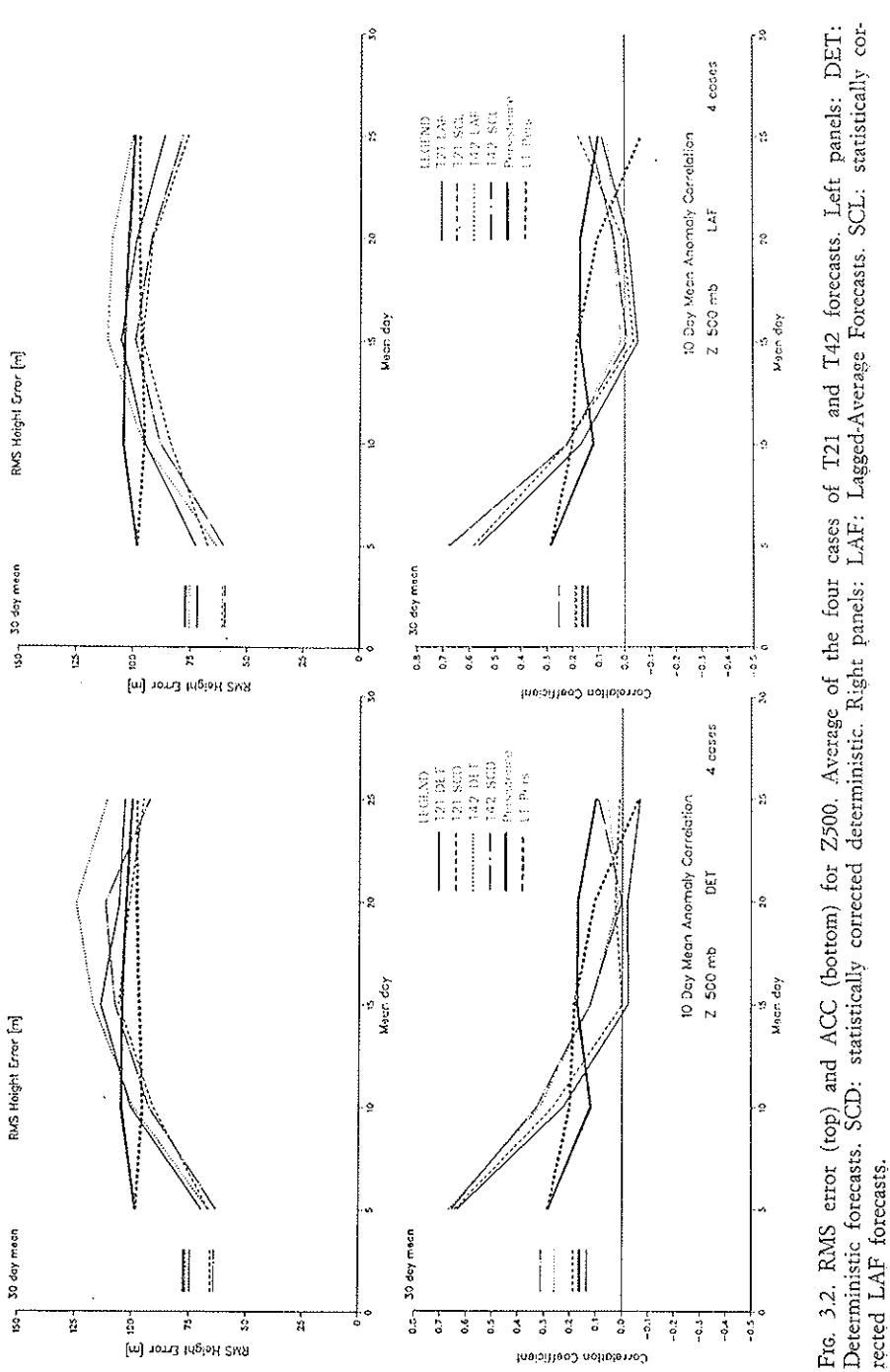

FIG. 3.2. RMS error (top) and ACC (bottom) for Z500. Average of the four cases of T21 and T42 forecasts. Left panels: DET: Deterministic forecasts. SCD: statistically corrected deterministic. Right panels: LAF: Lagged-Average Forecasts. SCL: statistically corrected LAF forecasts.

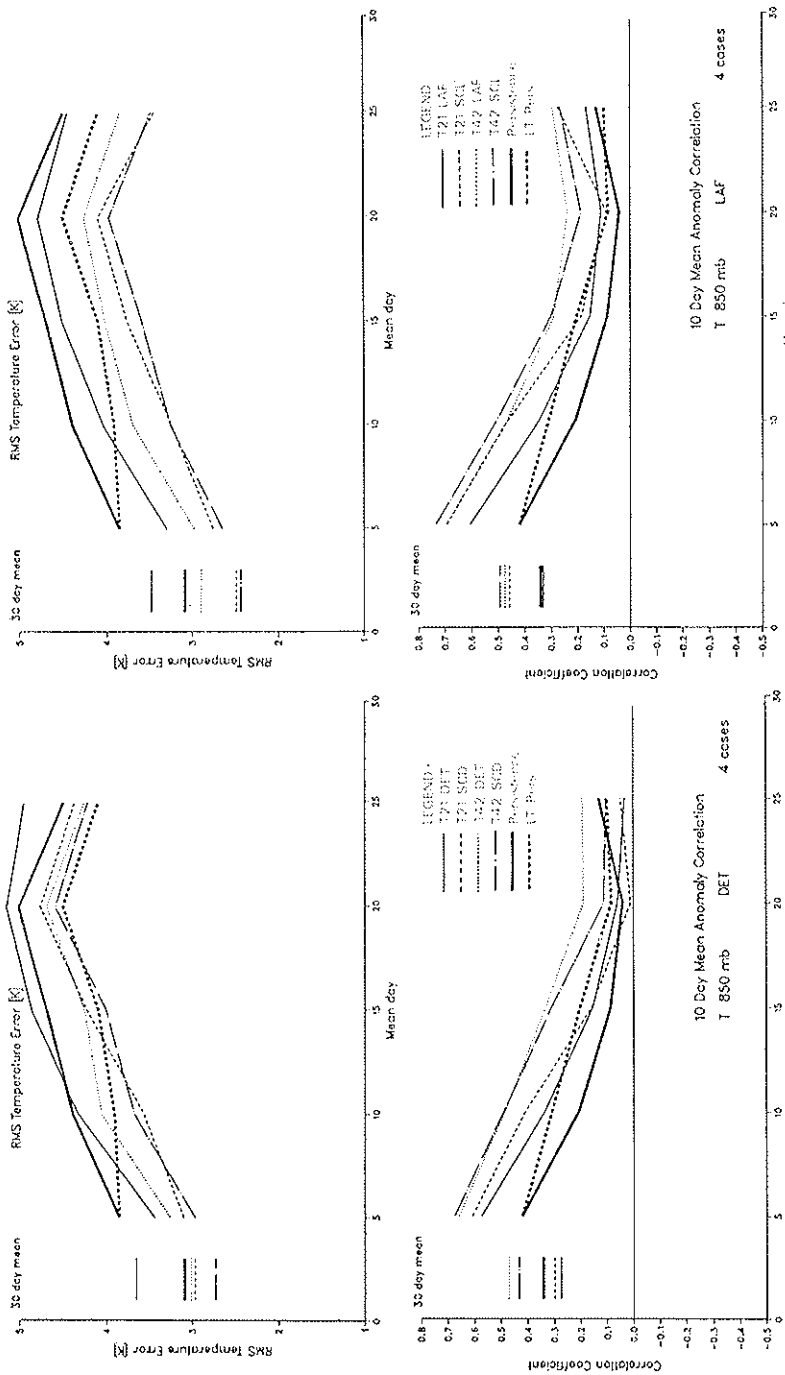

FIG. 3.3. As Fig. 3.2, but for T850.

case-to-case variability. Consider the 30-day mean ACC of the T42 SCL: while for T850 the mean value of .50 comes from the average of four values .43, .57, .44 and .54, the value of .25 for the Z500 is obtained from the four single values of -.05, .58, -.04 and .52. For the (two) high skill cases, therefore, the results for the two variables are quite comparable. However, for the two low skill cases the Z500 skill drops to zero while the T850 skill only partially decreases. A possible explanation for these results is that the higher model skill in forecasting T850 could derive from the model's capability to represent the thermal interaction with the underlying surface (it should be noted however that during the 1983/84 winter there were no substantial SST anomalies). To verify such an idea, the vertical behaviour of the ACC of temperature as a function of forecast time was examined. It was found that the temperature ACC, while almost uniform with height during the first 10 days of the forecast, decreases with height during the last 10 days, going through an intermediate phase (during days 10 to 20) where the ACC has a minimum at 500 mb. This appears to be a clear indication of a positive effect of surface thermal forcing.

Now the question can be posed: is it possible to find, at least *a posteriori*, an indicator of predictability? Although our sample of only four cases cannot provide a proper basis for statistical reliability, it is interesting to compute the RMS variability of the 10-day mean 500 mb height fields with respect to the monthly means and examine the ratio of this to the RMS amplitude of the mean monthly anomaly. The results for observed data and for the two forecast models (after correction for the SE) are shown in Table 3.1. The observed ratio variability/mean appears to be clearly smaller in the two good forecast cases (January and March 1984) than in the two bad cases (December 1983 and February 1984). The mean monthly anomaly appears, therefore, to be more predictable the more persistent it is. This has two consequences. Firstly, it is evident that the (comparatively) low resolution models used for these experiments have difficulties in correctly reproducing the internal dynamic variability of the atmosphere on the monthly time scale. Secondly, since anomalous boundary forcing is usually conducive to increased persistence of atmospheric anomalies, the idea of a positive influence of boundary forcing on atmospheric predictability is strengthened.

Amongst the physical processes that are invoked to explain the low-frequency variability of the atmosphere is (linear and) non-linear resonance. This has been recently found to be (Benzi *et al.*, 1986) a possible source

TABLE 3.1 - Mean and variability of observed and forecast (T21 SCD and T42 SCD) anomalies of Z500 (3.1a, meters) and T850 (3.1b, °K) for the four forecast experiments. The mean is the spatial RMS of the 30-day mean fields. The variability is computed by evaluating the RMS of the departures of the running 10-day means from the 30-day mean. The ratio variability/mean is shown in brackets.

Table 3.1a Z500 (m)

	OBS		T21 SCD		T42 SCD	
Init. date	Mean	Variability	Mean	Variability	Mean	Variability
15/12/83	55	69 (1.25)	42	58 (1.39)	52	51 (.97)
17/ 1/84	71	58 (.82)	41	52 (1.27)	60	57 (.94)
19/ 2/84	52	54 (1.05)	46	45 (.99)	42	55 (1.30)
23/03/84	53	43 (.81)	38	38 (1.00)	47	51 (1.08)

Table 3.1b T850 (°K)

	OBS		T21 SCD		T42 SCD	
Init. date	Mean	Variability	Mean	Variability	Mean	Variability
15/12/83	2.5	2.7 (1.07)	2.3	1.8 (.80)	2.7	2.2 (.81)
17/ 1/84	3.3	2.3 (.70)	2.1	1.9 (.90)	2.7	2.4 (.91)
19/ 2/84	2.3	2.5 (1.09)	2.5	2.0 (.82)	2.2	2.4 (1.08)
23/ 3/84	2.8	1.9 (.68)	2.0	1.8 (.93)	2.2	2.1 (.99)

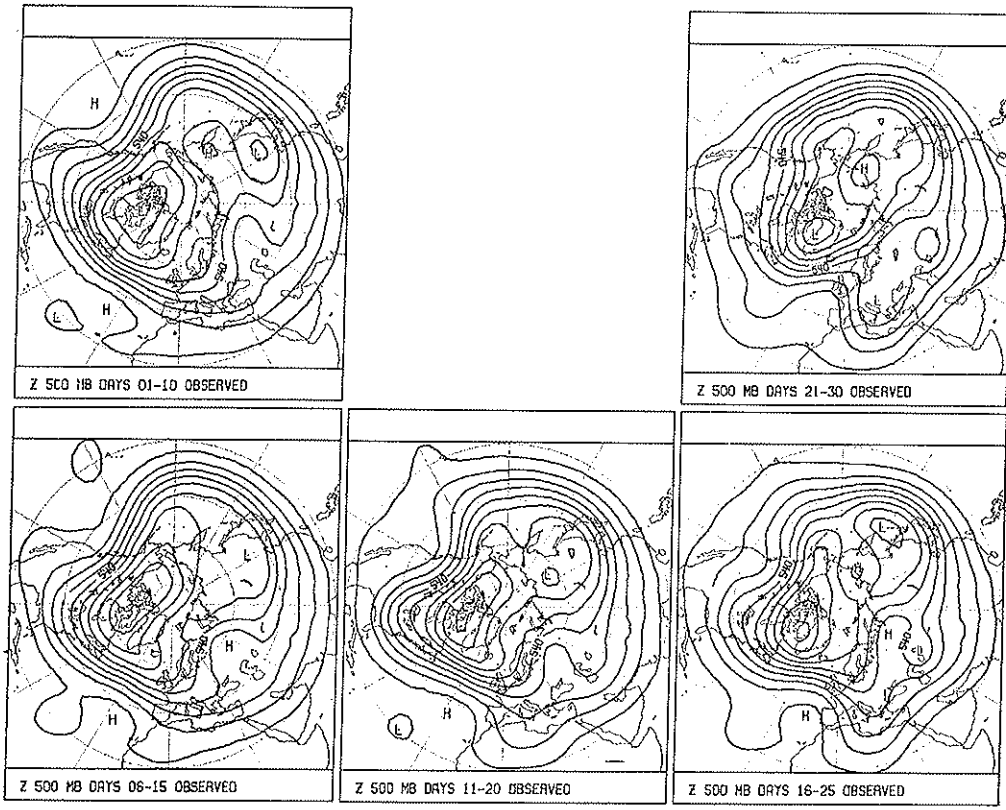

FIG. 3.4. 10-day mean observed Z500 fields at 5 day intervals, corresponding to the verification periods of the 17.1.1984 experiment.

of multiple equilibria states of the Northern Hemisphere extratropical atmosphere as diagnosed, for example, by Sutera (1986) and Hansen and Sutera (1986). Blocked and zonal situations would then be explained as metastable equilibrium states of the extratropics involving a relatively high and low amplitude of the planetary scale waves respectively. Sutera (private communication) has suggested that a substantial proportion of the global models' errors in the medium range might be associated with the inability to represent transitions between zonal states and high planetary wave amplitude states.

Supporting evidence to such ideas comes from comparing the Z500 10-day mean observed fields from the two January and February 1984

cases shown in Figs. 3.4 and 3.5. In the first case (the one with the highest score) the planetary scale waves remained at a high amplitude for almost the entire 30-day period, though they decreased towards the end. However, in the second case, a very poor forecast, the amplitude of the large scale waves was small during the early part of the month but amplified strongly during the central period which coincided with a blocked situation over the Eastern-Atlantic sector and a large amplitude Rockies ridge. Figures 3.6 to 3.9 show, for comparison, the observed and forecast (for DET and SCL) anomalies for the 30-day mean fields for the same two experiments. Their comparatively good and bad (respectively) synoptic value is evident and confirms the results of the objective scores.

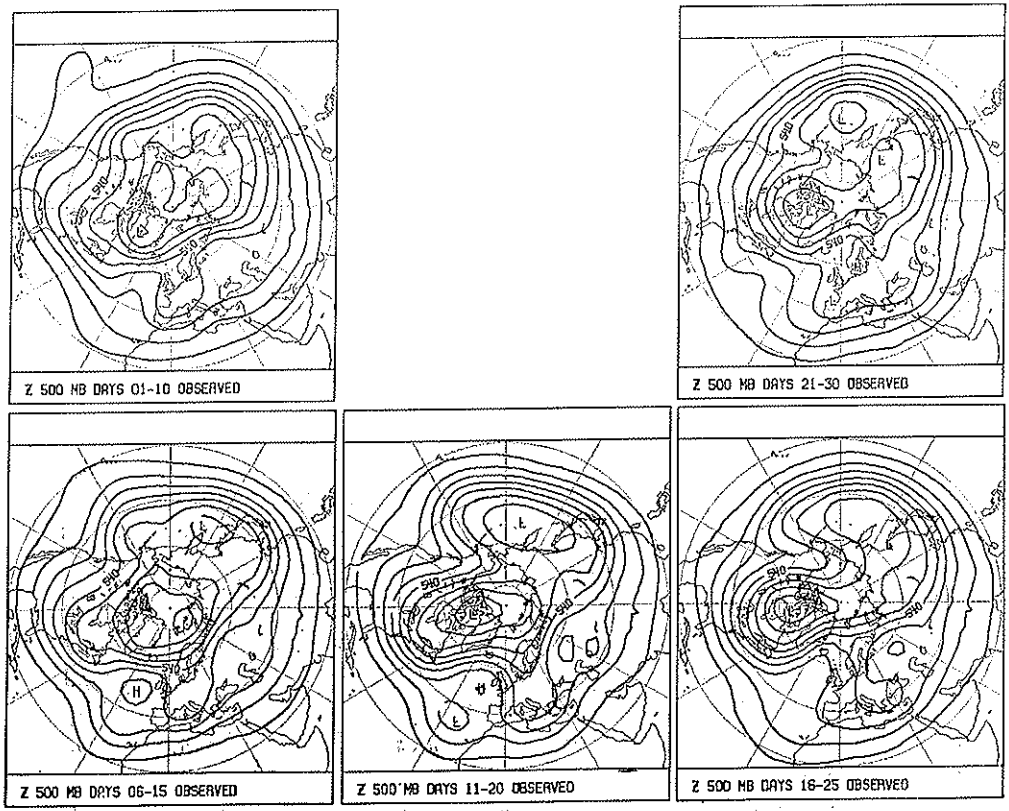

FIG. 3.5. As Fig. 3.4 but for experiment starting 19.2.1984.

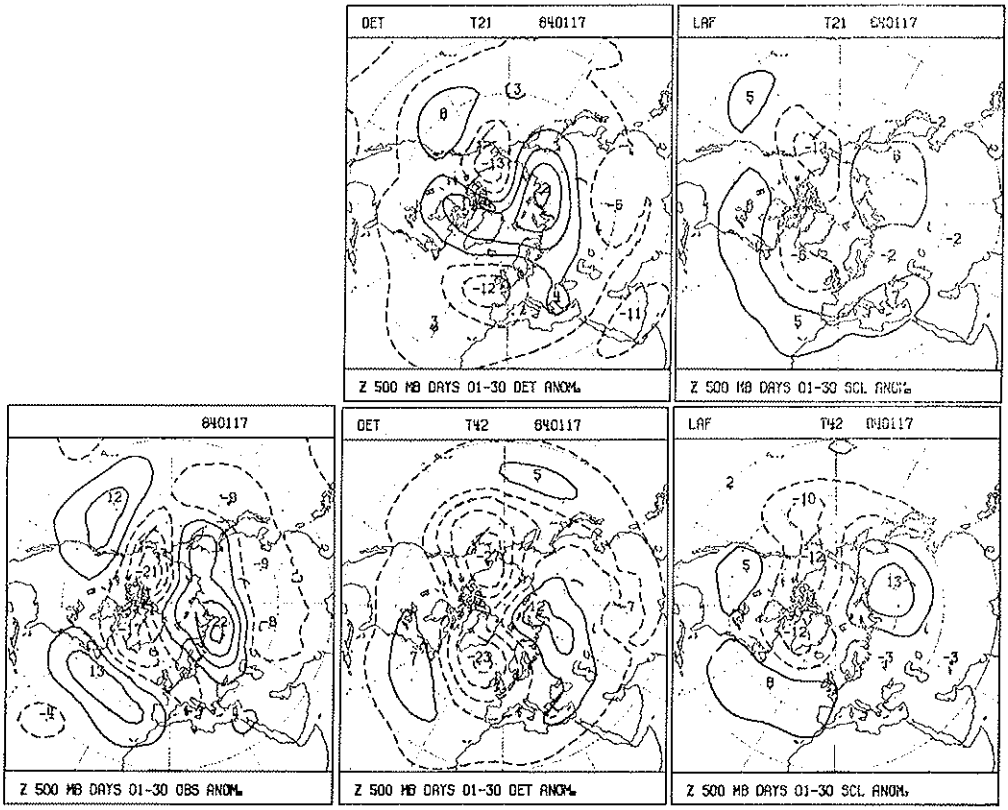

FIG. 3.6. Mean 30-day observed Z500 anomaly (bottom left), DET anomaly (Centre) and SCL anomaly (right) for T21 forecasts (top) and T42 forecasts (bottom). Experiment starting 17.1.1984.

All this pinpoints the need for more systematic studies of the predictability and "forecastability" dependence upon atmospheric large scale regimes, both in the medium and extended range.

3.3 *A test on the impact of SSTs*

The LAF results discussed in the preceding sections did suggest that surface boundary (thermal) forcing might be responsible for increasing the predictability of the atmosphere and, consequently, the model's fore-

casting skill (at least for those large-scale patterns that are expected to be more influenced by the atmosphere's thermal interaction with the underlying surface). Since, however, all the LAF experiments were performed during the 1983/84 winter period, during which the anomalous boundary forcing due to SST anomalies was not particularly strong, it seemed interesting to perform a further experiment for a period in which such forcing was likely to be of importance. The winter 1982/83, characterized by a strong El-Niño event, provided an ideal example on which to test the impact of surface forcing in the ECMWF spectral global model. Two sets of model integrations (both LAF and DET) will be described here; the initial date for all integrations was 19 January 1983, 1200 GMT. One set of model runs (CLI) used climatological SSTs,

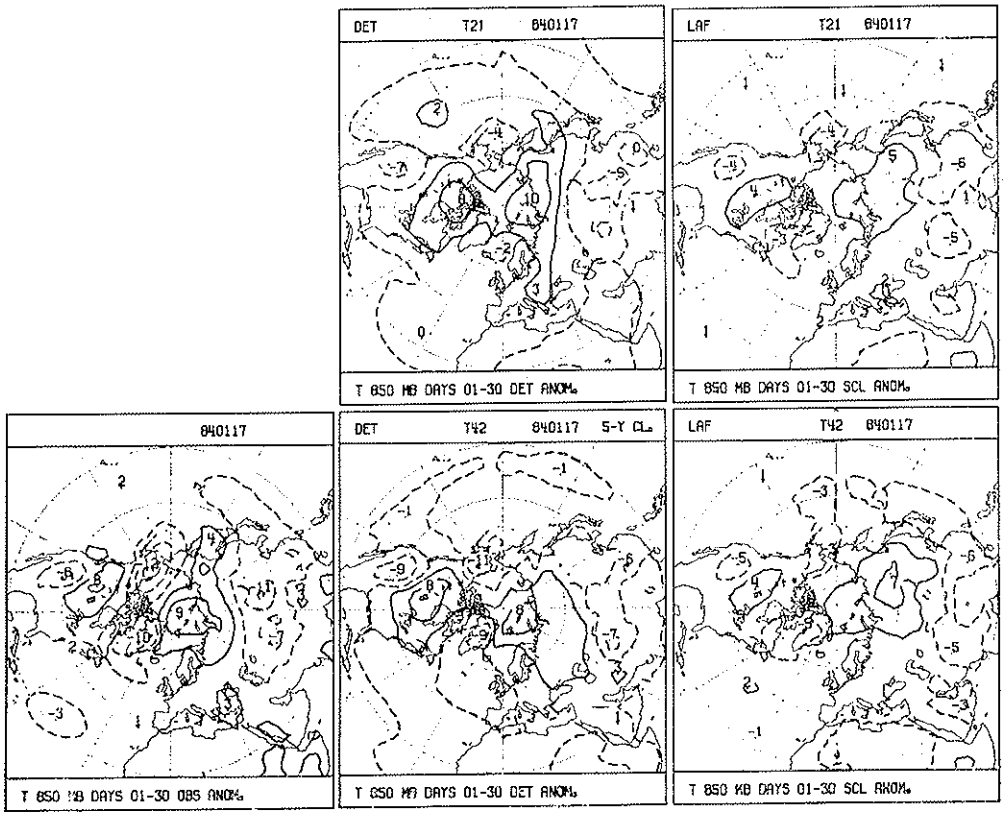

FIG. 3.7. As Fig. 3.6 but for T850.

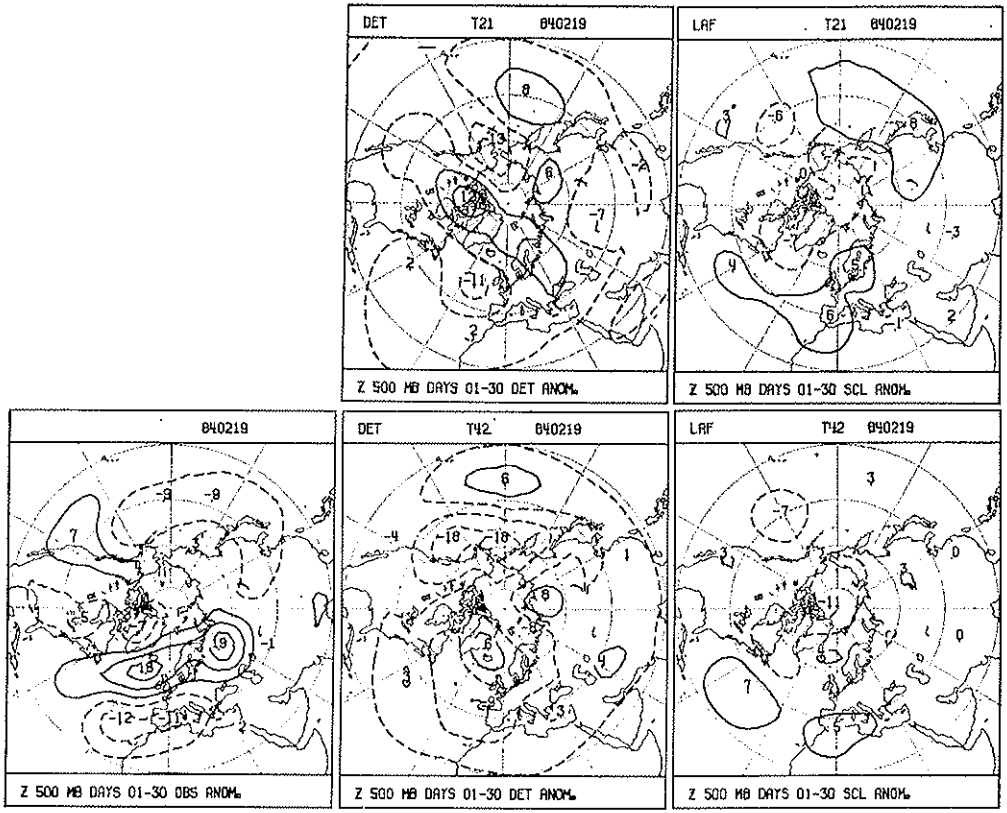

FIG. 3.8. As Fig. 3.6 but for the experiment starting 19.2.1984.

while the other (OBS) was integrated using an SST field constructed by adding to the climatological field the mean anomaly for January 1983, as analysed by the NOAA Climate Analysis Center (Reynolds, 1983). The model used was the ECMWF T42 spectral model and all integrations were carried out to 60 days. In evaluating results, LAF ensembles are compared to the most recent of the nine ensemble elements, referred to as the deterministic forecast (DET). Statistically corrected (SC) versions of all integrations were also produced by subtracting from the forecast fields an estimate of the model's systematic error produced by averaging the forecast error of an independent set of 10 60-day integrations carried out from randomly chosen initial conditions during the 1983/84 and 1984/85 winters with observed SSTs.

Fig. 3.10 shows the correlation coefficients between 500 mb height forecast and observed anomaly fields averaged over running 10-day periods, and the corresponding RMS errors for DET and LAF forecasts, using both OBS and CLI SSTs and for corrected (SC) and uncorrected integrations. These time series can also be compared with the skill of the persistence forecast (PER).

Several interesting points emerge from the analysis of such skill scores. Firstly, there is an anomalously high performance for persistence during this period. The anomaly correlation of persistence reaches the 60% level around day 40. This seems to be fairly characteristic of this El-Niño period, during which the characteristic PNA (Pacific/North American) signature remains a feature of the Northern Hemisphere

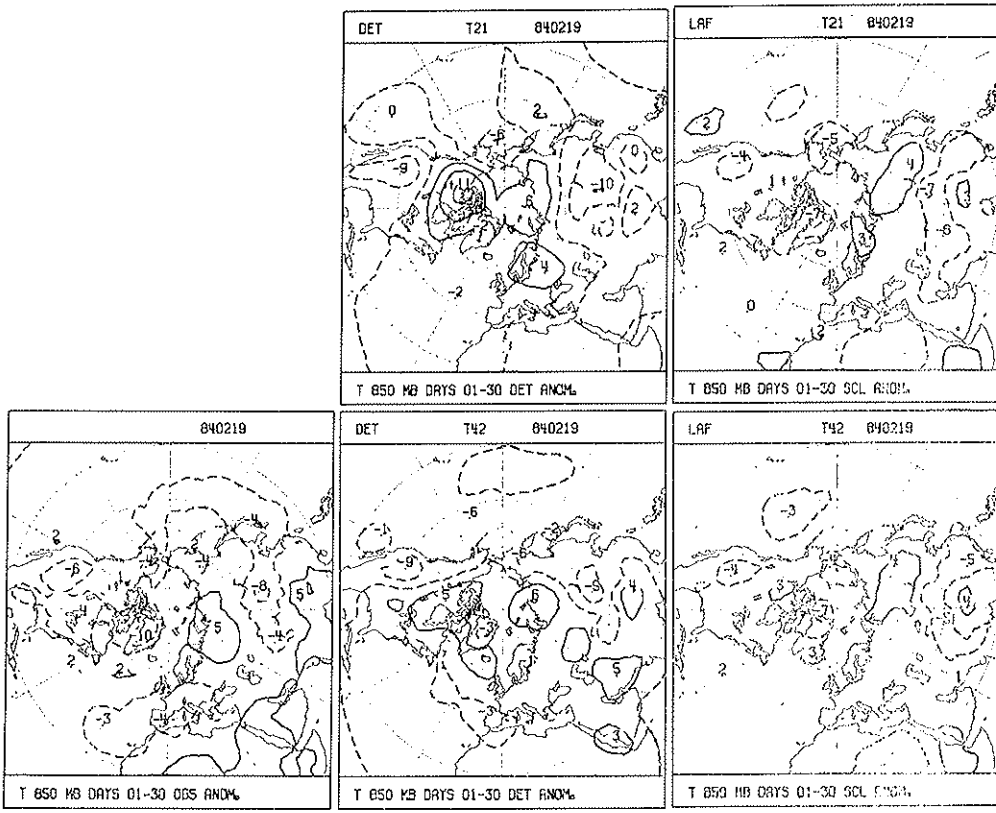

FIG. 3.9. As Fig. 3.7 but for the experiment starting 19.7.1984.

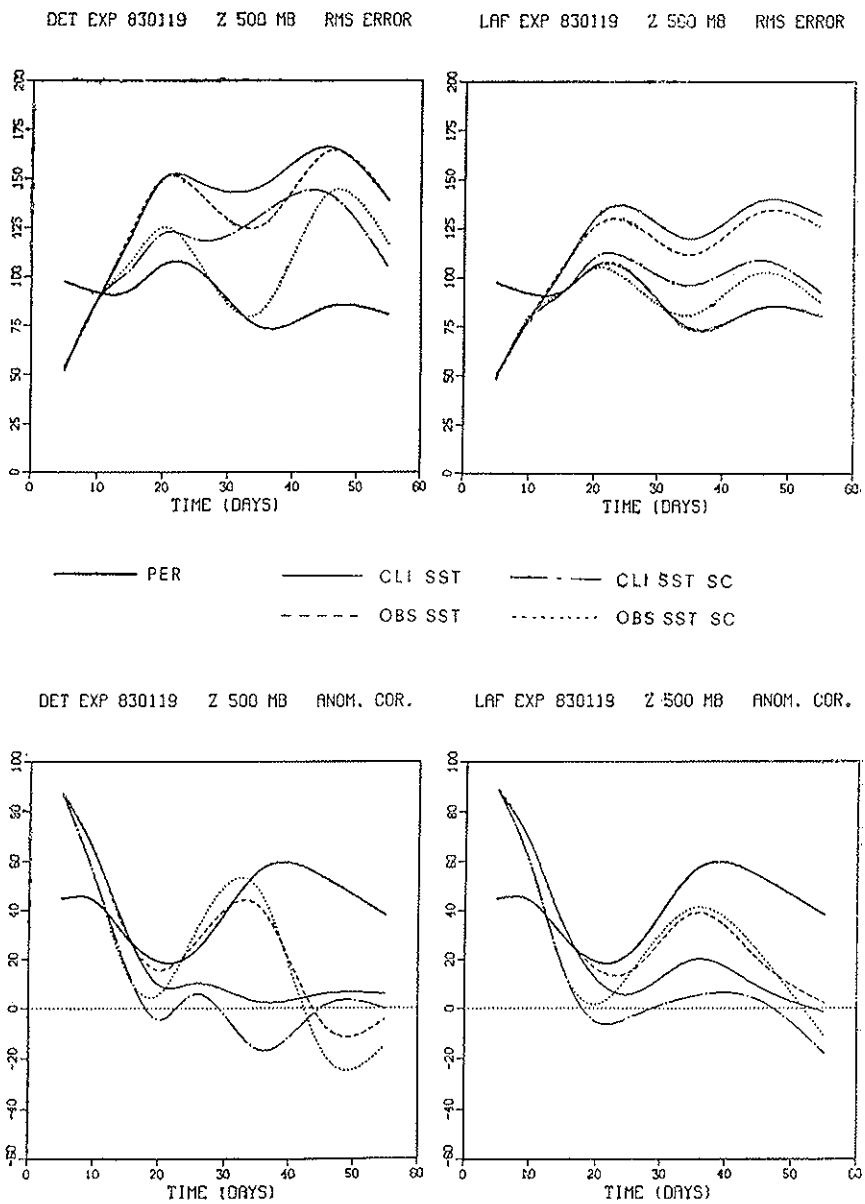

FIG. 3.10. RMS errors (top panels, meters) and anomaly correlation coefficients (bottom panels, %) of 10-day running means of 500 mb height. Deterministic (DET) experiments, left panels. LAF experiments, right panels. The skill scores are shown as a function of forecast time and for persistence forecasts (thick continuous lines), climatological SSTs forecasts (thin continuous lines), observed SSTs forecasts (dashed lines), climatological SSTs statistically corrected forecasts (dashed-dotted lines) and observed SSTs statistically corrected forecasts (dotted lines). All experiments starting on 19.1.1983 1200 GMT.

circulation for a long period of time. Secondly, there is a clear positive impact of the SSTs in the OBS integrations during the day 20 to 50 forecast period. Around the day 30 mark, this improvement is more evident in the DET forecasts than in the LAF, but in the LAF the positive impact of observed SSTs lasts until the end of the integration period.

A further interesting point is the very sizeable "return" of skill again evident in the OBS integrations, suggesting that such a return of skill might in this case be linked to a higher atmospheric predictability induced by surface thermal forcing. It should be noted that the CLI LAF forecast (but not the DET) also shows a return of skill, albeit much weaker. This could be due to the fact that the atmospheric initial conditions "know" about the surface anomalous forcing even if, during the model integration, this knowledge is eliminated. It is plausible, however, that the residual predictability associated with the initial conditions (and their "knowing" about El-Niño) can only be detected after the effects of the smaller scale random forecast errors have been partially eliminated by applying the LAF technique.

The impact of LAF and of the systematic error correction are both clearly positive on the RMS scores, but not so on the ACC. It should be noted that, during the first 20 days of model integration, the growth of the error of the uncorrected LAFs is almost identical to the one shown by the DET forecasts and the impact of the SC is negative on both. This essentially means that, during this interval, the T42 forecast error depends predominantly upon the initial conditions. Thereafter, the beneficial impact of the LAF techniques (and of the SE correction) increases with forecast time, so much so that the SC LAF integrations show the maximum forecast error around day 20.

The amplitude of the "return" in forecast skill taking place in this particular set of experiments, and the fact that it takes place also in the DET forecasts with OBS SSTs, suggest it to be due to the failure of the model to represent a synoptic development of limited lifetime that, in turn, affects little the evolution of the global circulation on a longer ($>$20 days) time scale.

It then becomes interesting to evaluate what proportion of the observed atmospheric anomaly can be thought of as a response to the surface boundary forcing and how much can be explained by internal dynamics. We would then expect internal dynamics to dominate the early, low skill, part of the forecast period and the boundary forcing response to be more

important during the latter part of the 60 days. We can estimate this by comparing the total observed atmospheric anomaly with the difference fields between the two model integrations CLI and OBS, assuming that the latter fields might be representative, albeit approximately, of the atmospheric response to surface forcing. To have more stable and statistically significant fields we will use the difference between the two LAF (sets of 9) integrations. Fig. 3.11 shows this comparison for the Z500 averaged over the two time intervals, day 16-25 and day 31-40, for which the OBS LAF shows, respectively, a relative minimum and a relative maximum of forecast skill. It is evident that, during the first interval, the observed anomaly is dominated by the onset and life-span of an Eastern Atlantic blocking episode. This blocking does not seem to be too influenced by the tropical Pacific thermal forcing, since both LAF integrations fail to model its development: in such conditions, the similarity between the observed anomaly map and the forecast difference (OBS-CLI) map is virtually non-existent over most of the Northern Hemisphere, with the exception of the North Pacific. During the second half of the integration period, on the contrary, the blocking pattern disappears and the observed anomaly and the forecast difference map become highly correlated, suggesting that the atmospheric anomaly is mainly the product of the SST forcing.

In summary, it is arguable that, during the central part of the integration period, the Northern Hemisphere extratropical atmosphere has switched from a regime dominated by internal dynamics variability to a regime driven mainly by anomalous boundary forcing. The model integrations shown seem, furthermore, to be unable to reproduce the former while they show considerable skill in representing the latter.

3.4 *Ensemble spread and forecast skill*

In the previous sections, the results of the lagged-average predictions were evaluated in terms of the skill of the ensemble mean forecast; it was shown that the improvement obtained with the LAF method in comparison with a purely deterministic forecast was much more evident in the RMS errors than in the anomaly correlation coefficients. However, the anomaly correlation improves with increasing horizontal resolution, so that the actual advantage of the LAF technique might be questioned since for a given computational time an extended-range LAF is as expensive, in computer resources, as a deterministic forecast with a model of considerably higher resolution.

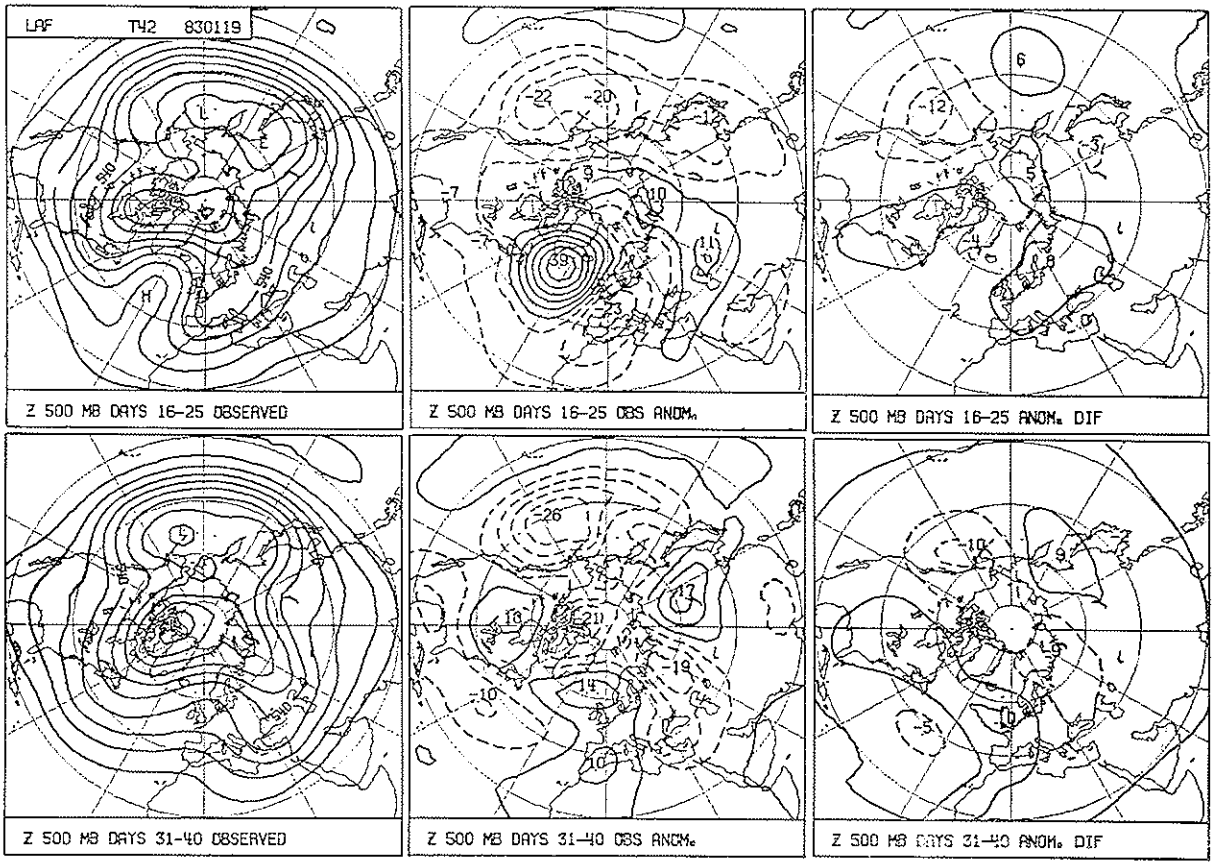

FIG. 3.11. Mean observed 500 mb height fields (left panels), observed anomaly (centre panels) and difference between forecast anomalies (OBS-CLI, right panels) for the two forecast intervals days 16-25 (top panels) and days 31-40 (bottom panels). All experiments are LAF starting on 19.1.1983 1200 GMT.

The perspective would change if it could be proven that the LAF produces not only a marginally better forecast than a deterministic prediction, but can also provide an estimate of the reliability of the forecast that can be deduced from the spread of the ensemble. Theoretically, for a perfect model, the spread of the ensemble could be considered as a measure of the instability of the circulation regime that is present in the initial conditions. A correlation between the spread and the error of the mean forecast should then be expected.

3.4.1 *Effects of systematic errors*

In practice, the effects of the model deficiencies can strongly affect the spread-skill relationship. Rinne and Karhila (1974) and Pitcher (1977) found that the inclusion of a random forcing term (used to parameterize the "external" sources of error) in the equations of the barotropic models used in their stochastic-dynamic experiments was necessary to obtain a reasonable correspondence between the standard deviations of the estimated quantities and their errors. Also Hoffman and Kalnay (1983) had to take into account the existence of model-generated errors in developing a statistical relationship between forecast error and ensemble spread.

The quantitative effects of a model systematic error on the correlation between spread and skill are difficult to evaluate. Once again, very much depends on the actual "systematic" behaviour of this error. If it was simply a superimposed error pattern that depends on forecast time but very little on the initial circulation regime, then a general reduction of the spread (proportionally greater for large forecast times) could be expected; apart from a time-dependent scaling factor, the correlation between skill and spread should be maintained. If, on the other hand, the "systematic" error strongly depends on the initial conditions, then an ensemble of forecasts dominated by the systematic error (whose skill is expected to be very poor) might show a considerably lower spread than another set started from initial conditions that do not give rise to strong biases in the forecasts.

3.4.2 *Evaluation of the local correspondence between forecast spread and forecast skill*

The small number of LAF experiments described here is obviously not sufficient to investigate the correlation between global or hemispheric

measures of spread and errors as shown in Hoffman and Kalnay (1983). However, it is possible to try to test whether there exists a *local* correspondence between these quantities, taking into account that both the errors and the spread are likely to be large over areas where the variability of the predicted fields is large.

For each grid point of a 3.75° × 3.75° regular lat-lon grid covering the Northern Hemisphere (from 22.5°N to 90°N), the RMS values (among the 4 experiments) both of the ensemble error and standard deviation of a given meteorological field were computed. (The ensemble standard deviation is the RMS difference between each of the 9 individual forecasts and their ensemble mean). Then a standardised error ($\hat{E}$) was computed for each grid point and LAF experiment as the ratio between the local error and its RMS value; in this way, $\hat{E}$ reflects only the local variability of the error among the 4 experiments and tends to be independent of the local error variance. In an analogous way, a standardised spread ($\hat{S}$) was defined for each grid point and experiment by dividing each local value of the standard deviation by its RMS value among the 4 experiments.

The range of $\hat{S}$ was divided in 4 classes:

class 1	$0.7 > \hat{S} \geqslant 0$
class 2	$1.0 > \hat{S} \geqslant 0.7$
class 3	$1.3 > \hat{S} \geqslant 1.0$
class 4	$\hat{S} \geqslant 1.3$

and all the values of $\hat{E}$ corresponding to a value of $\hat{S}$ falling in a given class were averaged in an RMS sense (an area weight proportional to the cosine of the latitude of the point was also used for this average).

Instead of comparing 4 spatially averaged values of error and spread, it is possible to compare 4 values of standardised error averaged over all the points and cases in which the value of the standardised spread fell in a given range: such a procedure may be able to reveal a correlation between spread and skill even if it exists only over certain areas.

The results of this computation, for both the LAFs and the SCLs, are shown in Fig. 3.12 for the monthly means of geopotential height at 1000, 500 and 300 mb, and temperature at 850, 500 and 300 mb (obviously the subtraction of the systematic error affected the values of the errors but not those of the standard deviations). In comparing the results of the LAFs with those of the SCLs, it is necessary to take

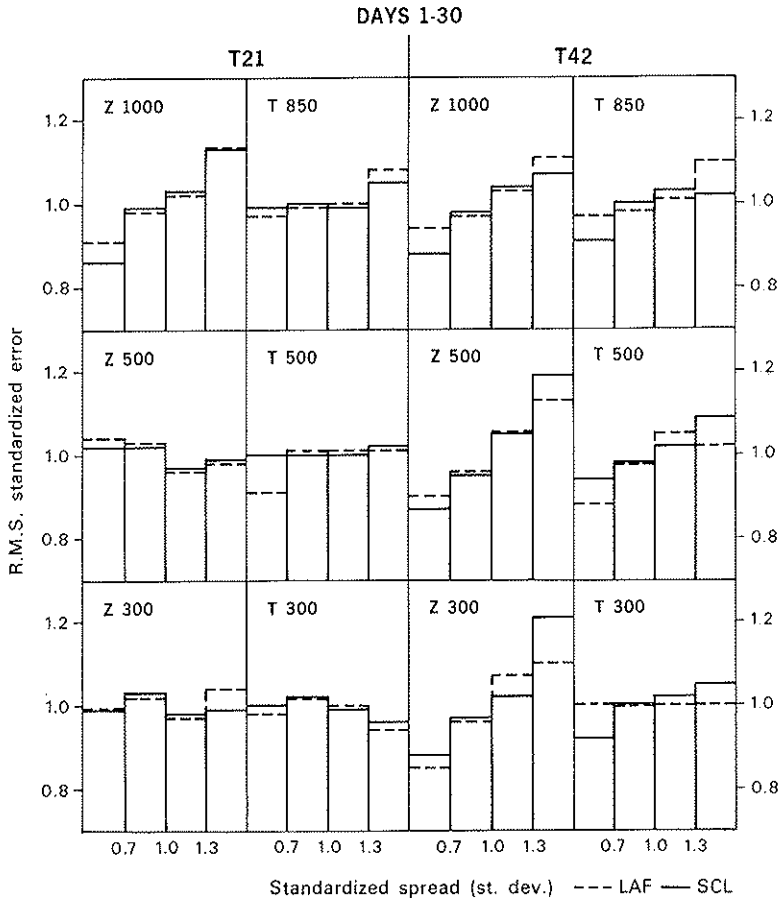

FIG. 3.12. Mean day 1 to 30 spread-error relationship for four classes of standardized spread (standard deviation). Top 1000 (850) mb, centre 500 mb, bottom 300 mb, for both height and temperature. Both LAF experiments (dashed) and SCL experiments (full) are shown. For more explanations see section 3.4.

into account that the central classes of S included more points than the extreme ones.

3.4.3 *Discussion of the results*

The results can be summarised as follows:

— Apart from the Z1000, a correlation between spread and error is not present for any variable or level using the T21 model, even when the systematic error is subtracted.

— A clear correlation can be found for the height fields predicted by the T42 model, especially at 500 and 300 mb; at these levels, a slight correlation also exists for the temperature fields. The removal of the systematic error is in general beneficial: the greatest improvement is found for Z500, while for the T850 only the uncorrected LAF shows a marginal correlation.

It is interesting to see how the correlation evolves with the forecast time: Fig. 3.13 shows the results for the 10-day mean fields (as well as for the monthly mean) of Z1000 and Z500 deduced from the T42 SCL. At both levels, the correlation decreases with forecast time, but it is more stable at 500 mb, even if slightly lower in the beginning of the forecast. At this level, the correlation is stronger for the monthly mean than for any of the 10-day means, while at 1000 mb the results for the 30-day period are very similar to those obtained in the 6-15 day period.

The fact that the correlation is much larger in the T42 results is surprising in some ways, though not in others. It seems obvious that the spread of an ensemble of forecasts can be a good indicator of the probable range of the error only if the variability of the model is comparable with that of the real atmosphere. Therefore, the fact that the T42 shows a larger variability than the T21 can partially explain these results. On the other hand, the mean error of the T42 is less systematic than that of the T21, and on this basis a better correlation for the T21 model should be expected. In these results, the former effect appears to be more important than the latter and the superiority of the T42 model over the T21 is confirmed.

In conclusion, the higher computational cost required by the LAF technique (and to a lesser degree by the correction of the systematic error) appears to be justified not only by a moderate improvement in

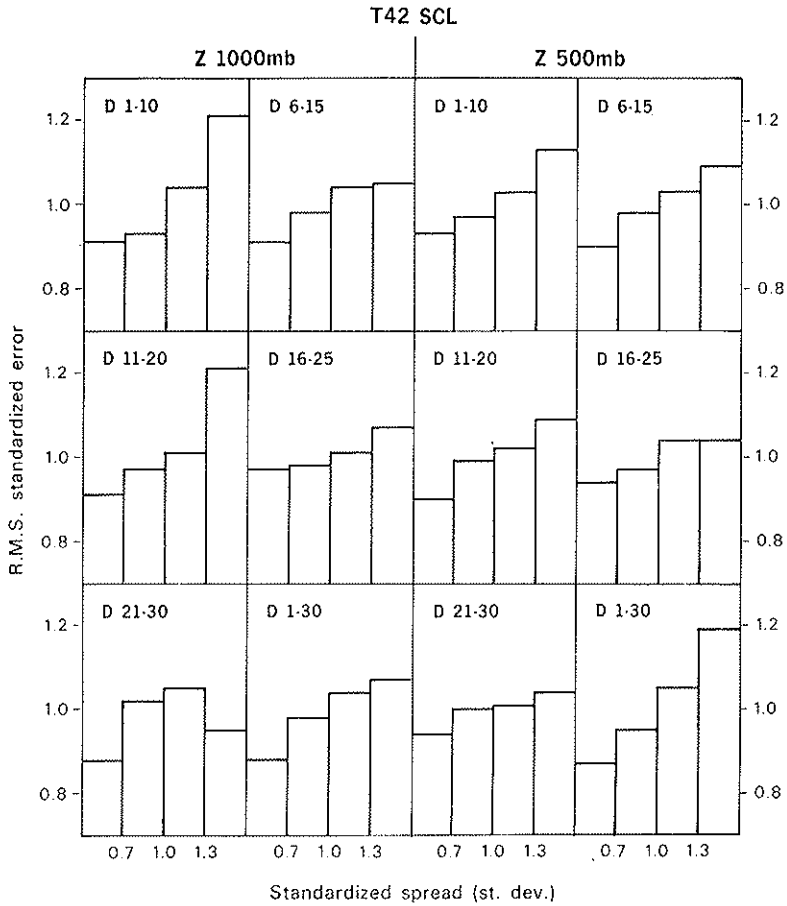

FIG. 3.13. 10-day mean histograms of spread-error relationship for the same four classes of standardized spread for T42 SCL forecasts. Top dd 1-10, centre dd 11-20, bottom dd 21-30. For more explanations see section 3.4.

the forecast skill but also by the existence of a significant correlation between the spread of the ensemble and the error of the mean forecast, at least for some variables and time intervals. The necessary condition for the existence of such a correlation is an internal variability of the forecast model comparable with that of the real atmosphere. The importance that the users of the NWP products attribute to a prediction of the forecast skill is probably the ultimate basis on which to decide if stochastic-dynamic predictions are worth becoming an operational tool, but their superiority over deterministic forecasts is undoubtedly much more than a theoretical speculation.

3.5 *Summary*

An attempt has been made to assess the relative improvements that can be achieved on purely deterministic numerical forecasting by either using the LAF technique and/or by attempting to correct the model's systematic bias by subtracting an estimate of it derived from an independent set of model integrations during a similar seasonal period. The results of this assessment can be summarized as follows.

— The skill of the forecasts, in particular those performed with the LAF technique, does not decrease monotonically with time, but has a minimum in the 11-20 day period for Z500 and in the 16-25 day period for T850. This effect could be partially ascribed to low-frequency periodicity of the atmosphere, as the similar recovery of the persistence forecasts for T850 would suggest.

— Both in an absolute sense and in comparison with persistence, the results for T850 are clearly better than those for Z500. For the former, the T42 SCL is better than persistence in all the verification intervals, both in terms of RMS error and of ACC (in a RMS sense it is also better than climate, apart from the 16-25 day period); for the latter, a consistent improvement over persistence, apart from the first ten days, can be seen only in the monthly mean.

— The LAF technique and the correction of the systematic error lead to a clear and constant improvement of the RMS error; this is most evident for T850 where a positive impact of the LAF method on the ACC can also be detected. The impact of the correction of the systematic error on the ACC is generally positive, but notable exceptions can be found among the deterministic forecasts performed with the T42 model. More

evident, and without exception, is the improvement in the ACC due to the increase of horizontal resolution: the T42 model, even with no correction for its bias, has a consistently higher ACC than the corrected T21.

— Even though for some particular variable or score it is possible to find a forecast method that gives a comparable or slightly better performance than the T42 SCL, but with a lower computational cost, a comprehensive evaluation of the results shows that the T42 SCL has the highest skill among all the combinations of resolution/error filtering methods that we have explored; as pointed out earlier, for T850 the T42 SCL is more skillful than either climate or persistence for the whole monthly range. The SCL also has the advantage of providing an indicator of the reliability of the forecasts, since a considerable correlation between the spread of the forecast ensemble and the skill of the SCL was found for individual geographical locations.

— The results of a further experiment to test the impact of SSTs on the forecast skill during the El-Niño period is consistent with the idea that there is considerable predictability (and "forecastability") coming from the boundaries, but that even in cases of strong forcing this can be easily obscured and overwhelmed if the model fails to represent an important synoptic event whose development is dominated by internal dynamics, e.g., the onset of blocking. When (and if) the effects of such low-frequency transient development fade away, the model seems to be able to recover its capability to represent the effects of boundary forcing.

4. The Deterministic Forecasts

4.1 *Description of the experiments*

This section reports the results of a further study to investigate purely deterministic extended range forecasts which have been selected at regular 10 day intervals in order to simulate operational conditions. The database is the one generated to estimate the T21 and T42 models' systematic error used to correct the LAF experiments described earlier. All initial conditions come, therefore, from the four winters 1981-82 to 1984-85 and give a sample large enough to explore the interannual variability of the forecasting skill. The results of this study should therefore be representative of the typical performance of numerical extended range forecasts to be expected under operational conditions for the winter-spring

period. However, only an estimate of the lower end of the forecasting skill can be obtained, due to the comparatively low resolution of the models employed.

The experiments consisted mainly of 30-day forecasts, though some 60-day forecasts were also carried out. The starting dates of the 38 cases are given in Table 4.1. The initial data have been derived from the operational ECMWF assimilation system by direct spectral truncation to the model resolution. Throughout the integrations the values at the lower boundary of the atmosphere, i.e., SST, deep soil moisture and deep soil temperature, have been kept constant. For 1981 and the first half of 1982, the SSTs have been set to their climatological values, while from winter 1982/83 onwards SSTs analysed by NMC have been used.

Corresponding persistence forecasts have also been evaluated based on either the 10- or 30-day average of the days preceding the initial date. These persistence forecasts provide a baseline against which the dynamical forecast can be compared.

4.2 *Analysis of results*

All experiments have again been evaluated in terms of 10 and 30 day averages. The objective verification has been carried out by calculating the ACC and the RMS errors of 10- and 30-day means for the northern hemisphere between 20°N and 90°N and the ensemble anomaly correlation over the 38 cases using the z-statistics (Seidman, 1981).

4.2.1 *Intra-seasonal variability*

For only two of the winters (1981/82, 1982/83) were enough cases integrated to evaluate the mean monthly forecast scores as a function of the initial date of the forecast. Fig. 4.1 shows the correlation coefficients of 30-day means for the two model resolutions, as well as for persistence, for Z500 in the northern hemisphere. In both winters the persistence forecast scores between 10% and 60% with a smooth transition between periods with good and bad forecasts. The scores of the model forecasts appear to be uncorrelated with those based on persistence. The T42 model simulation nearly always stays above the 25% level and is therefore a more reliable predictor than persistence (at least for the monthly means) whilst the skill of the T21 model undergoes fluctuations which are as large as those found for the persistence forecast. The time evolution of the 10-day mean fore-

TABLE 4.1 - The initial dates of the forecast experiments.

1981	1982	1983	1984*	1985*
	1. 1.	1. 1.	1. 1.	1. 1.
	11. 1.	11. 1.	11. 1.	11. 1.
	21. 1.	21. 1.	21. 1.	21. 1.
	1. 2.	1. 2.	1. 2.	1. 2.
	11. 2.	11. 2.	11. 2.	11. 2.
	21. 2.	21. 2.		
	1. 3.	1. 3.		
	11. 3.	11. 3.		
	21. 3.	21. 3.		
	1. 4.	1. 4.		
	11. 4.	11. 4.		
2.12.	1.12.			
11.12.	11.12.			
21.12.	21.12.			

* 60-day integrations.

cast skill (not shown) exhibits much more variation than for the 30-day mean forecasts, but a correlation between the quality of the persistence and model forecasts could not be found on this shorter timescale either.

4.2.2 *Interannual variability of skill*

The period between 1 January and 11 February is covered for all 4 years. This gives an opportunity to assess the interannual variability of the forecast quality based on a mean of 5 forecasts per year. The T42 model produces the best scores in terms of anomaly correlation and RMS error for the 500 mb height field (Fig. 4.2) during 1985, which is also the worst year for the persistence forecast. The 1982/83 El-Niño winter produces persistence forecasts with considerable skill (particularly in the 30-day mean), but the T42 model forecast quality falls below the average. Conversely, for the T21 model, the 30-day mean scores are quite high. This contradictory result might be explained by the different structure of

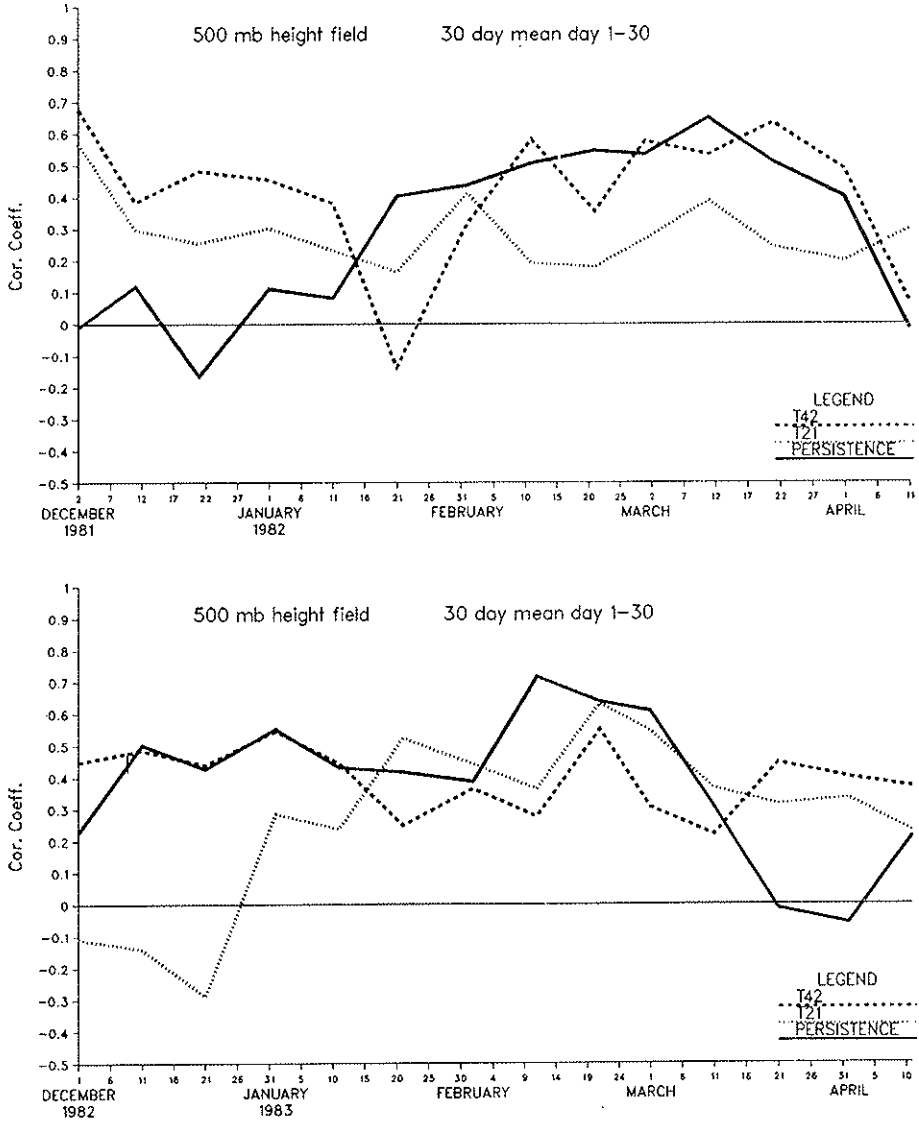

FIG. 4.1. The 30-day mean correlation coefficient for the Z500 as function of the initial day; a) experiments during winter 1981/1982; b) experiments during winter 1982/1983.

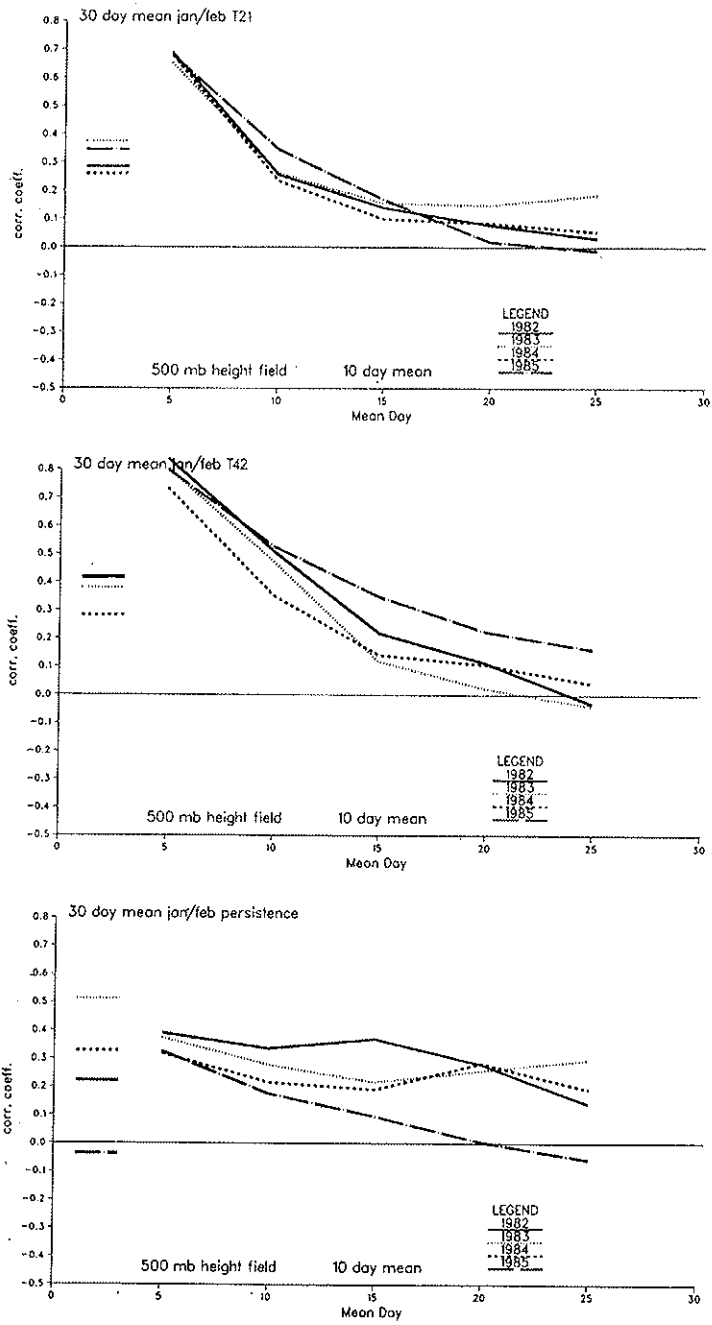

FIG. 4.2. The time evolution of the correlation coefficient for the Z500 averaged over the experiments started during the months of January and February for different years a) for the T21 model forecasts; b) for the T42 model forecasts; c) for the persistence forecast.

the systematic error of the two models (see section 2 and Cubasch and Wiin-Nielsen, 1986). Regarding the better skill attained by the T42 model in the experiments of subsection 3.3, it should be remembered that a different, and more accurate, SST anomaly was used for those integrations. In the experiments described in this section, the El-Niño signature was largely suppressed by the operational NMC SST analysis scheme.

The scores for the 850 mb temperature field confirm the findings for the height field.

4.2.3 *The mean performance of the Z500 forecasts*

To evaluate the mean forecast quality in the extended range, the skill scores have been averaged over all 38 cases (Fig. 4.3). Since this ensemble is dominated by cases from the January/February period, the result is biased towards these months. Additionally the best and the worst scores for every forecast period have been extracted and displayed together with the mean skill in order to give an indication about the spread of the forecast quality. From the standard deviation of the forecasts scores a threshold tube has been calculated which encloses the skill which should be achieved by 95% of the forecasts (assuming a normal distribution). It coincides fairly well with the area of the minimum-maximum spread.

For a persistence forecast in the Northern Hemisphere, the mean Z500 anomaly correlation coefficient shows values between 20 and 30% (Fig. 4.3) and an RMS error of about 1000 m (Fig. 4.4), both of which are quasi-independent of forecast time. On the contrary, the dependency of the model skill on forecast time is very strong at both resolutions: after a sharp drop during the first 10 (T21) and 15 (T42) days, the ACC slowly approaches the zero level. In terms of ACC, the T21 model is less skillful than persistence after days 6 to 15, and the T42 after days 11 to 20. With regard to the RMS error, during the first half of the forecast period the T42 model is more skillful than the T21 model and both models are better than persistence; during the second half, the situation is reversed. The larger RMS error of the T42 model compared to the T21, even in the presence of better ACC scores, can be explained by the higher variability of the T42 forecasts during the second part of the integration period.

The decay of model skill with forecast time is accompanied by an increase of the spread of the forecast skill (see again Fig. 4.3). The slower

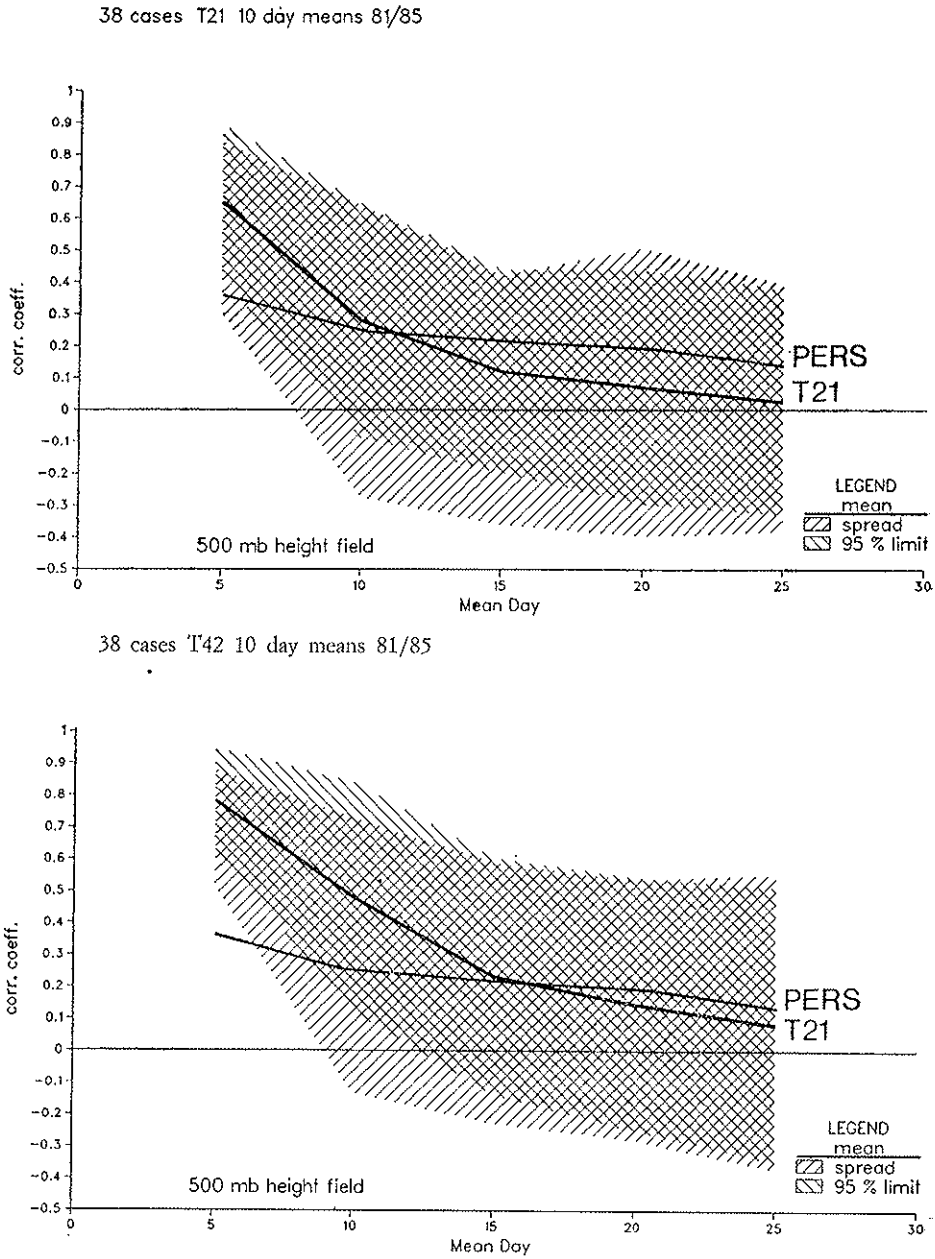

FIG. 4.3. The time evolution of the correlation coefficient and the RMS error for the Z500 averaged over all of the 38 cases; a) for the T21 model forecast; b) for the T42 model forecast. Persistence forecast is also shown in both panels. /// hatching indicates the max-min spread amongst the 38 cases; \\\ hatching indicates the skill variability corresponding to ± 2 standard deviations.

drop of the ACC for the T42 model during the first part of the forecast period has therefore its counterpart in a more contained spread of model skill, particularly at days 1 to 10. This is a further proof of the superior performance of the T42 model in the medium-range.

4.2.4 *60-day forecasts*

Ten experiments have been integrated up to 60 days. These experiments were used to investigate whether there is a recovery of skill during the later part of the forecast, a phenomenon discussed earlier.

The mean behaviour of the 10 cases considered (Fig. 4.5) is similar to the larger ensemble discussed before with a sharp drop in correlation during the first time intervals and a levelling afterwards. The 10-day mean scores for the T42 model stay around the 10% level up to the end of the forecast period. It is interesting to note that, in this limited sample, the performance of the T42 model is always better than persistence, while the skill of the T21 model is about the same as persistence. The recovery in forecasting skill could not be found in the average over the 10 cases; this may indicate that it only occurs in selected cases, for example in cases where the tropical sea surface temperature plays a dominant role or during transitions between flow regimes.

The dynamical forecasts of 30-day means performed with the numerical models are always better than the persistence forecasts, and the skill of the model forecasts improves with resolution.

4.3 *Summary*

Based on the analysis of the objective skill of a set of 38 extended range forecasts starting from independent winter conditions separated by 10 days, the following conclusions can be drawn.

— The T42 model provides a more reliable forecast of 30 day means than persistence. However, the quality of these model forecasts seems to be uncorrelated with the quality of the persistence forecast. This is at variance with the results, obtained on a much smaller sample, described in Section 3.

— There exists a substantial variability in the predictability during different years.

— Up to day 10 the T21 model forecast is better than persistence,

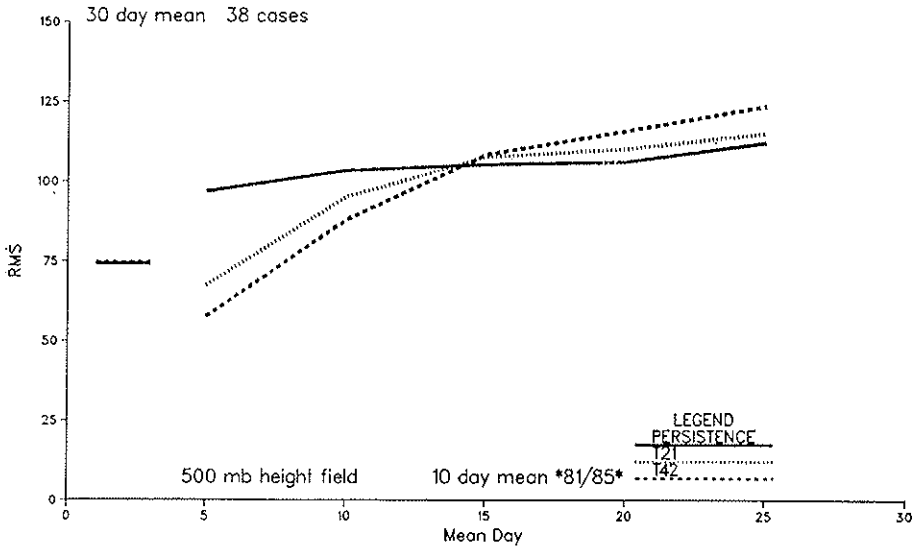

FIG. 4.4. The time evolution of the 500 mb height RMS error averaged over 38 cases: T21, T42 and persistence.

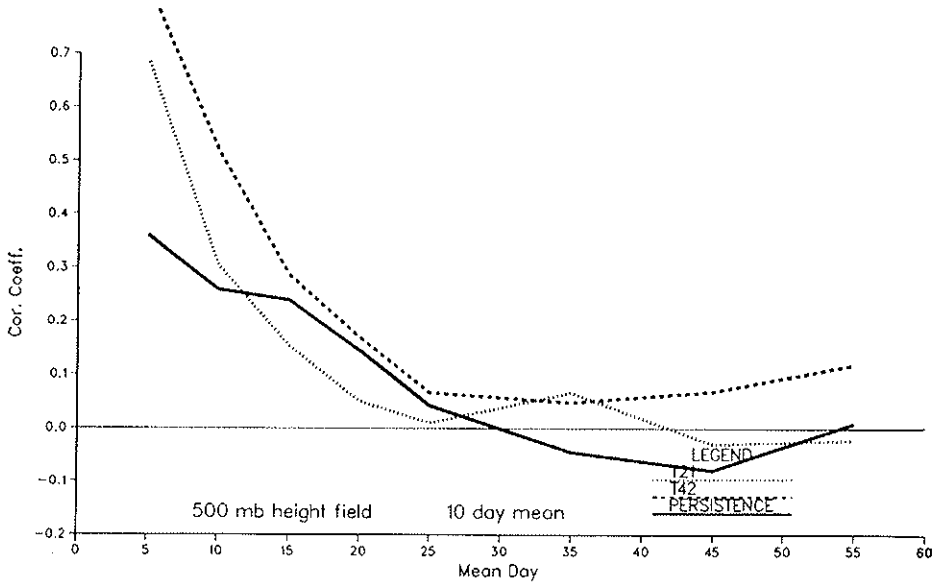

FIG. 4.5. The time evolution of the 10 day mean correlation coefficient for Z500 in a sample of ten 60-day forecasts.

whilst the T42 model forecast stays superior to persistence up to day 15. The higher resolution model outperforms the T21 model in most respects and especially during the earlier part of the forecast period.

— A return of skill in the later part of the forecast period (studied with a subset of the experiments integrated up to 60 days), which had been observed in other forecasting experiments, could not be confirmed as a consistent feature. In these experiments the skill remains low after the drop in the earlier part of the forecast and appears not to recover.

The results indicate that, even using low resolution models, some skill is present on average well beyond the current operational forecast period (10 days at ECMWF).

5. Conclusions

Since summaries of the results of both LAF and deterministic experiments have been given in Sections 3.5 and 4.3, this section will be confined to recalling those points that are either most relevant to future research work or that have possible operational consequences.

Our results have shown that both purely deterministic and Lagged-Average numerical forecasts of 10-day and 30-day means of 500 mb height and 850 mb temperature outperform both persistence and climate forecasts well beyond the currently accepted practical limit for deterministic instantaneous forecasts, estimated around one week to ten days. This happens despite the comparatively low resolution of the models employed in our tests.

It has also been shown how the single most important model characteristic that influences forecast skill is, by far, horizontal resolution, at least in the resolution band examined. Stochastic-dynamic ensemble averaging techniques, although generally beneficial, do not show nearly as much impact as model resolution. However, a word of caution is necessary: it would not be legitimate to export our conclusions on the impact of model resolution to the upper limits of the resolution scale. Further numerical experimentation is needed, with higher resolution models, to estimate if and at what stage resolution ceases to be the most sensitive model characteristic and whether ensemble averaging might assume a much more important role in increasing model skill.

It has been shown that for the LAF technique the use of the spread of forecasts within an ensemble to estimate *a priori* forecast skill is viable

and gives very promising results. Again this conclusion should be tested with higher resolution models and on a much larger statistical basis, encompassing seasons other than winter alone. Another area where more effort is needed.

Systematic error correction techniques have given somewhat inconsistent results. Although they clearly improve the RMS errors of the model, they have little impact on ACC at the highest model resolution tested, for which model internal variability seems to be large enough to make the truly systematic part of the error difficult to estimate from a small sample of independent integrations. Such error correction techniques appear to be more applicable, as theory dictates, to ensemble of forecasts than to single deterministic integrations. When applied to the LAFs, they show the additional advantage of improving the spread-skill correlations.

The "return" of forecast skill found during the latter part of extended range forecasts appears to be a recurrent, but not altogether consistent, feature of such experiments. More work is needed to understand its origin.

The ability of the models used in this set of experiments to represent and forecast the low-frequency variability of the Northern Hemisphere extratropics is itself very variable both on the inter-annual timescale and from case to case. Surface boundary forcings seem to be reasonably well modelled and are very likely to participate in increasing predictability and forecastability, while examples of remarkable model failures in reproducing internal dynamical variability on the 5 to 15 days time scale, e.g., blocking, are common. The understanding of the reasons for such failures is one of the most important topics for future research in dynamical extended-range forecasting.

ACNOWLEDGEMENTS

Large numerical experimentation programmes such as the one presented here are always a collective effort. A large number of individuals, in both the Research and Operations Departments of ECMWF, have in various ways contributed to this project by providing software and assistance, by participating in discussions and exchanging ideas or simply by bearing with us while we were making a nuisance of ourselves in mopping up computer resources. We thank them all. We would like to mention, in particular, R. Riddaway and K. Arpe for carefully reading an earlier version of the manuscript and making many useful suggestions to improve the readability of the text. One of us (FM) participated in this project partly supported by research funds of ENEL, the Italian National Electricity Board, and partly on leave from Istituto di Cosmogeofisica, Italian National Research Council, Turin, Italy.

REFERENCES

ARPE K., *Diagnostic evaluation of analysis and forecasts: Climate of the model.* ECMWF Seminar/Workshop on Interpretation of Numerical Weather Prediction Products, 13-24 September 1982, ECMWF, Reading, U.K., pp. 99-140 (1983).

ARPE K. and KLINKER E., *Systematic errors of the ECMWF operational forecasting model in mid-latitudes.* « Quart. J.R. Met. Soc. », *112*, 181-202 (1986).

ARPE K., HOLLINGSWORTH A., TRACTON M.S., LORENC A.C., UPPALA S. and KALLBERG P., *The response of numerical weather prediction systems to FGGE level IIB data.* Part II. *Forecast verification in implication for predictability.* « Quart. J. Roy. Met. Soc. », *111*, 67-102 (1985).

BENZI R., MALGUZZI P., SPERANZA A. and SUTERA A., *The statistical properties of general atmospheric circulation: observational evidence and a minimal theory of bimodality.* « Quart. J. Roy. Met. Soc. », *112*, 661-674 (1986).

CUBASCH U. and WIIN-NIELSEN A.C., *Predictability studies with the ECMWF spectral model for the extended range: The impact of horizontal resolution and sea surface temperature.* « Tellus », *38A*, 25-41 (1986).

EPSTEIN E.S., *Stochastic dynamic prediction.* « Tellus », *21*, 739-759 (1969).

GILCHRIST A., *An experiment in extended range prediction using a general circulation model and including the influence of sea surface temperature anomalies.* « Beitr. Phys. Atmos. », *50*, 25-40 (1977).

GLEESON T.A., *A modern physical basis for meteorological prediction.* Proceedings First National Conference Statistical Meteorology, Boston, Mass., USA, Amer. Meteor. Soc., pp. 1-10 (1968).

GLEESON T.A., *Statistical-dynamical predictions.* « J. Appl. Meteorol. », *9*, 333-344 (1970).

HANSEN A.R. and SUTERA A., *On the probability density distribution of large-scale atmospheric wave amplitude.* Submitted to JAS (1986).

HOFFMAN R.N. and KALNAY E., *Lagged-average forecasting, an alternative to Monte Carlo forecasting.* « Tellus », *35A*, 100-118 (1983).

HOLLINGSWORTH A., ARPE K., TIEDTKE M., CAPALDO M. and SAVIJÄRVI H., *The performance of a medium-range forecast model in winter - impact of physical parameterizations.* « Mon. Wea. Rev. », *108*, 1736-1773 (1980).

HOREL J.D. and WALLACE J.M., *Planetary-scale atmospheric phenomena associated with the Southern Oscillation.* « Mon. Wea. Rev. », *109*, 813-829 (1981).

LORENZ E.N., *Deterministic nonperiodic flow.* « J. Atmos. Sci. », *20*, 130-141 (1963).

LORENZ E.N., *The predictability of a flow which possesses many scales of motion.* « Tellus », *21*, 289-307 (1969a).

LORENZ E.N., *Atmospheric predictability as revealed by naturally occurring analogues.* « J. Atmos. Sci. », *26*, 636-646 (1969b).

LORENZ E.N., *Atmospheric predictability experiments with a large numerical model.* « Tellus », *34*, 505-513 (1982).

LOUIS J.F. (editor), *The ECMWF forecasting model.* ECMWF Research Manual Vol. 2 and Vol. 3, ECMWF, Shinfield Park, Reading, UK (1984).

MADDEN R.A., *Estimations of the natural variability of time-averaged sea-level pressure.* « Mon. Wea. Rev. », *104*, 942-952 (1976).

MIYAKODA K. and TALAGRAND O., *The assimilation of past data in dynamical analysis.* I. « Tellus », *23*, 310-317 (1971).

MIYAKODA K. and CHAO J.-P., *Essay on dynamical long-range forecasts of atmospheric circulation.* « J. Met. Soc. Japan », *60*, 292-308 (1982).

MIYAKODA K., GORDON T., CAVERLY R., STERN W., SIRUTIS J. and BOURKE W., *Simulation of a blocking even in January 1977.* « Mon. Wea. Rev. », *111*, 846-869 (1983).

MIYAKODA K., SIRUTIS J. and PLOSHAY J., *One-month forecast experiments - without anomaly boundary forcings.* Submitted to « Mon. Wea. Rev. », (1986).

NAMIAS J., *Seasonal interactions between the North Pacific Ocean and the atmosphere during the 1960's.* « Mon. Wea. Rev. », *97*, 173-192 (1969).

NICHOLLS N., *Long-range weather forecasting: Value, status and prospects.* « Rev. Geophys. Space Phys. », *18*, 771-788 (1980).

NICHOLLS N., GRUZA G., KIKUCHI Y. and SOMMERVILLE R., *Long-Range Weather Forecasting: Recent Research.* LRFR Publication Series No. 3, WMO, Geneva (1984).

PALMER T.N., SHUTTS G.J. and SWINBANK R., *Alleviation of a systematic westerly bias in general circulation and numerical weather prediction models through an orographic gravity wave drag parameterization.* « Quart. J. Roy. Met. Soc. », *112*, 1001-1039 (1986).

PITCHER E.J., *Application of stochastic dynamic prediction to real data.* « J. Atmos. Sci. », *34*, 3-21 (1977).

RASMUSSON E.M., *Ocean effects.* Proceedings WMO-CAS/JSC Expert Study Meeting on Long-Range Forecasting, Princeton, 1-4 December 1982, Long-range Forec. Res. Publ. Ser. No. 1, WMO, Geneva, pp. 97-122 (1983).

RATCLIFFE R.A.S. and MURRAY R., *New lag associations between North Atlantic sea temperature and European pressure applied to long-range forecasting.* « Quart. J. Roy. Met. Soc. », *96*, 226-246 (1970).

REYNOLDS R.W., *The sea surface temperatures during the 1982-83 El Niño Event.* Proceedings of the Eighth Annual Climate Diagnostics Workshop, NOAA, US., pp. 86-91 (1983).

RINNE J. and KARHILA V., *Stochastic forecasts computed with an EOF model.* The GARP Programme on Numerical Experimentation, Report of the International Symposium on Spectral Methods in NWP, Copenhagen, 12-16 August 1974. (Report No. 7 of the GARP-WGNE). WMO, Geneva, pp. 333-340 (1974).

SEIDMAN A.N., *Averaging techniques in long range weather forecasting.* « Mon. Wea. Rev. », *109*, 1367-1379 (1981).

SHUKLA J., *Dynamical predictability of monthly means.* « J. Atmos. Sci. », *38*, 2547-2572 (1981).

SHUKLA J., *Predictability of time averages.* Problems and Prospects in Long and Medium Range Weather Forecasting; D.M. Burridge and E. Källén, eds. Springer-Verlag, Berlin and New York, pp. 109-206 (1984).

SHUKLA J. and WALLACE J.M., *Numerical simulation of the atmospheric response to equatorial Pacific sea surface temperature anomalies.* « J. Atmos. Sci. », *40*, 1613-1630 (1983).

SMAGORINSKY J., *Problems and promises of deterministic extended range forecasting.* « Bull. Am. Met. Soc. », *50*, 286-311 (1969).

SUTERA A., *Probability density distribution of large scale atmospheric flow.* Advances in Geophysics, Vol. 29, ed. by B. Saltzman. Ac. Press, Orlando, pp. 227-250 (1986).

TIBALDI S., *Envelope orography and maintenance of the quasi-stationary circulation in the ECMWF global models.* Advances in Geophysics, Vol. 29, ed. by B. Saltzman. Ac. Press, Orlando, pp. 339-374 (1986).

VON STORCH H., ROECKNER E. and CUBASCH U., *Intercomparison of extended-range January simulations with general circulation models: statistical assessment of ensemble properties.* « Beitr. Phys. Atmos. », *58*, 477-497 (1985).

WALLACE J.M. and GUTZLER D.S., *Teleconnections in the geopotential height field during the northern hemisphere winter.* « Mon. Wea. Rev. », *109*, 784-812 (1981).

WALLACE J.M., TIBALDI S. and SIMMONS A.J., *Reductoin of systematic forecast errors in the ECMWF model through the introduction of an envelope orography.* « Quart. J. Roy. Met. Soc. », *109*, 683-717 (1983).

WALSH J.E., *Sea ice, snow cover and soil moisture.* Proceedings of the WMO-CAS/JSC Expert Study Meeting on Long-Range Forecasting, Princeton, 1-4 December 1982, Long-Range Forec. Res. Publ. Series No. 1, WMO, Geneva, pp. 84-96 (1983).

WALSH J.E. and RICHMAN M.B., *Seasonality in the associations between surface temperatures over the United States and the North Pacific Ocean.* « Mon. Wea. Rev. », *109*, 767-783 (1981).

TELECONNECTION STUDIES USING BAROTROPIC MODELS

BRIAN J. HOSKINS and PRASHANT D. SARDESHMUKH
Department of Meteorology
University of Reading, Reading RG6 2AU, U.K.

1. Introduction

Tropical convective heating tends to occur in huge preferred regions which are generally associated with the equatorial continents and with maximum sea surface temperatures. Since, to a large extent, the motion of the atmosphere is driven by this heating it is scarcely surprising that its local nature is important. For the understanding and possible prediction of atmospheric behaviour beyond the time-scale of synoptic weather systems it is crucial that the time-scale for changes in tropical sea surface temperature anomalies is generally from months to years, and that these changes may be predictable. The theory of the linkage between the convective region and the sea surface temperature distribution does not appear to be as simple as might be anticipated, and is the subject of current research. However, if the heating associated with the region of large tropical convection is specified then simple linearised, highly damped models appear to give realistic local low level wind fields (Gill and Rasmussen, 1983). The situation is, however, less simple elsewhere. Observational and model studies (Hoskins, 1983 and references) have suggested that a region of tropical heating leads, on average, to an upper tropospheric source of stationary Rossby waves, a so-called teleconnection pattern. In the extratropics such patterns have an equivalent barotropic structure with the low level wind anomaly generally having the same sign as that at upper levels. If all the linkages in this chain from the SST anomaly to the far field response can be understood there are definite pos-

sibilities of using the knowledge for forecasting significant climatic anomalies.

Simple scaling arguments suggest and observational studies confirm that the thermodynamic balance in the tropics is predominantly one of adiabatic cooling associated with ascent cancelling diabatic heating. Therefore above a region of tropical diabatic heating, at the convective outflow level, which is about the 150 mb level, there will be divergence. The aim of this paper is to consider the Rossby wave source and waves at such a level associated with a region of tropical divergence. Much of the discussion is taken from Sardeshmukh and Hoskins (1986).

2. Upper level vorticity budget and the Rossby wave source

The vorticity equation at an upper tropospheric level may be written

$$\left(\frac{\partial}{\partial t} + \underline{v} \cdot \nabla \right) \zeta = - \zeta D + F . \qquad (1)$$

Here the vertical advection and twisting terms have been neglected since the vertical velocity is relatively small at the level of interest. ζ is the absolute vorticity, D the divergence and F the curl of the body force and frictional terms. Sardeshmukh and Hoskins (1985) found that F is small almost everywhere on planetary length-scales and that above regions of large equatorial heating the absolute vorticity in the anticyclonic cells is almost zero. The local vorticity budget thus reduces to a trivial zero equals zero. It would appear that the divergence above a region of heating creates a region of almost zero absolute vorticity which switches off the local vorticity source.

However, if we are considering the generation of Rossby waves, we are interested in the equation

$$\left(\frac{\partial}{\partial t} + \underline{v}_\psi \cdot \nabla \right) \zeta = S + F . \qquad (2)$$

Here $\underline{v}_\psi$ is the rotational wind associated with ζ, and S is the source for

Rossby waves. Comparing with (1) we see that we should write the total wind in terms of its rotational and divergent components:

$$\underline{v} = \underline{v}_\psi + \underline{v}_\chi ,$$

where

$$\nabla \cdot \underline{v}_\chi = D .$$

Then (1) becomes

$$\left(\frac{\partial}{\partial t} + \underline{v}_\psi \cdot \nabla \right) \zeta = - \underline{v}_\chi \cdot \nabla \zeta - \zeta D + F . \tag{3}$$

Although $|\underline{v}_\chi|$ is a factor of at least 3 smaller than $|\underline{v}_\psi|$ almost everywhere, whereas the latter is in general almost parallel to absolute vorticity contours, the divergent wind is often oriented almost at right angles to these contours. The first two terms on the right hand-side combine to give us the total Rossby wave source:

$$S = - \nabla \cdot (\underline{v}_\chi \zeta) . \tag{4}$$

3. Simple model experiments

A simple experiment will be now described which illustrates important aspects of the source S. A numerical model based on (3) is run with a basic westerly wind field corresponding to a super-rotation of the atmosphere and a circular divergence source indicated in Fig. 1a. The maximum divergence is $8.10^{-6}\,s^{-1}$. F is set to be a linear damping on vorticity perturbations acting on a time-scale of 14.7 days plus a weak biharmonic diffusion. If the model is linearised about the basic zonal flow, the day 30, almost steady state, response is as shown in Fig. 1a. The wave activity emanates from the region of divergence and propagates along almost great circle ray paths in a by now familiar manner. If the model is made non-linear but with the source S fixed with its initial linear structure, the result (Fig. 1b) is dramatically different. The anticyclonic cells generated in the region of the forcing act as a barrier to Rossby wave propagation and there is a negligible extra-tropical response. If the full non-linear equation (3) is used, then the source S changes as

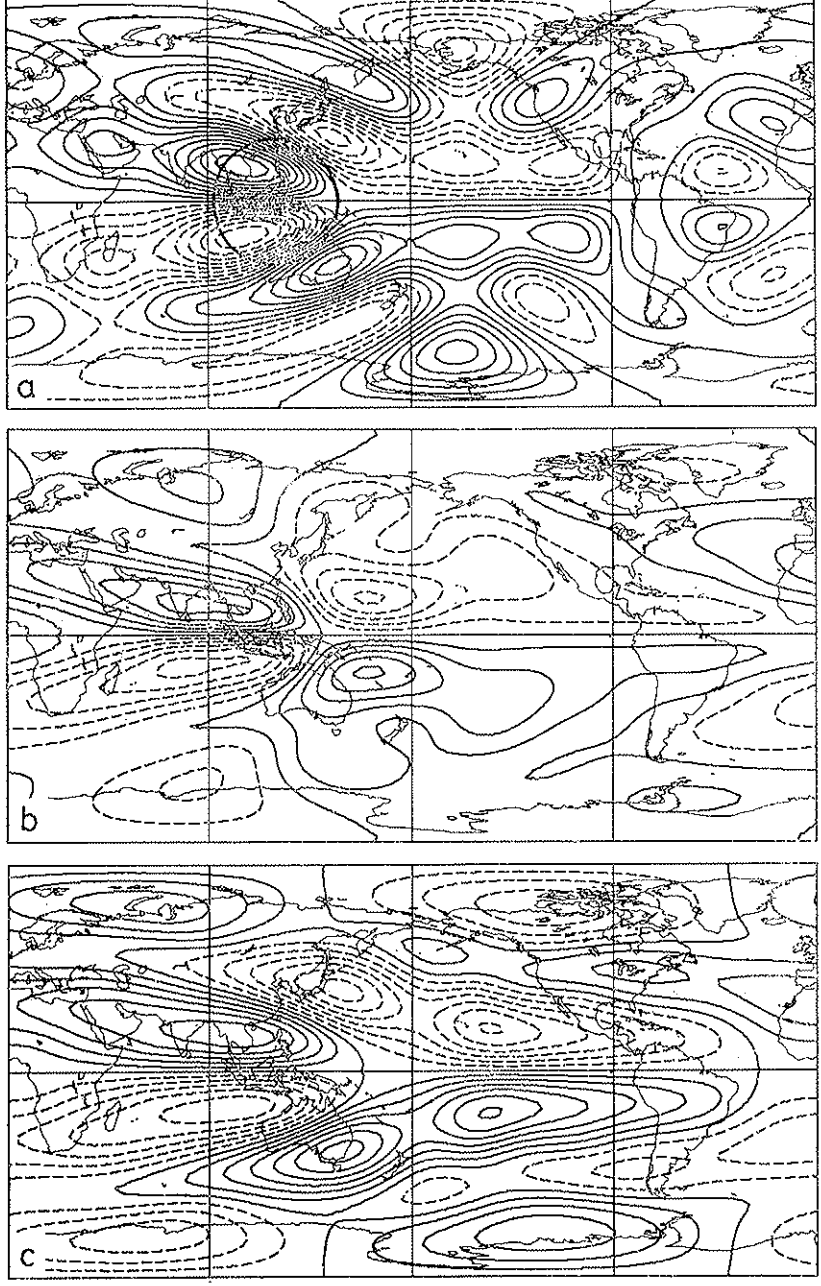

FIG. 1. Streamfunction perturbations for solutions of Eq. 2 for a basic super-rotation corresponding to approximately 15 m s^{-1} at the equator. A circular divergence source of maximum amplitude 8.10^{-6} s^{-1} in the region indicated in (a) is compensated by uniform convergences elsewhere. F is composed of a linear damping on a time-scale of 14.7 days plus a biharmonic diffusion acting on a time-scale of ¼ day at the length scale of the spherical harmonic of degree $n = 42$. The solutions are obtained by time integration over 30 days and the spatial representation is in terms of a series of spherical harmonics truncated at $n = 42$. The streamfunction contour is 5.10^6 m^2 s^{-1} and negative contours are dashed. (a) Linearised problem. (b) nonlinear advection but fixed source, S. (c) Fully nonlinear problem corresponding to Eq. 3.

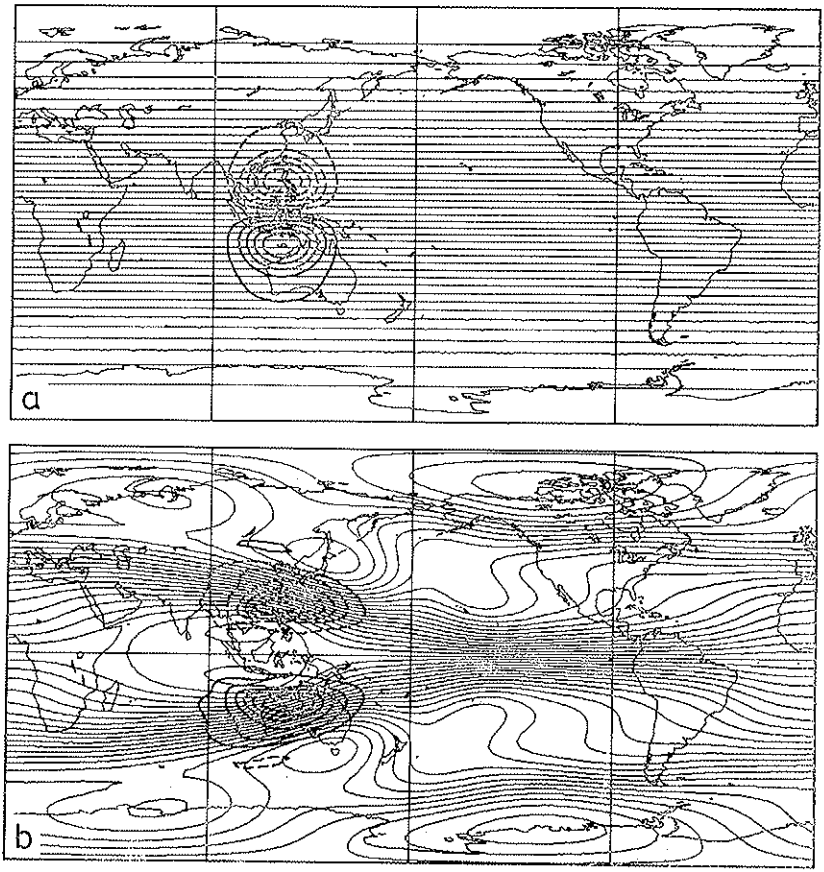

FIG. 2. The source S for the problems whose solutions are shown in Fig. 1. (a) The source for the linearised problem. (b) The day 30 source for the fully nonlinear problem. The contour interval is 5×10^{-11} s^{-2}. The zero contour is not drawn and negative contours are dashed.

the flow evolves. The day 30 response shown in Fig. 1c, compared with Fig. 1a, shows a downstream wave pattern that is quite different. However, given the solution in Fig. 1b, the most important result is that this extratropical response is again strong.

In order to understand this we need to look at the source terms. In Fig. 2a is shown the structure of S in the linear model, which is also the structure used for the result in Fig. 1b and the initial structure for

the fully non-linear interpretation. It is qualitatively similar to the fD type of source often used in simple studies. As the flow develops, the vorticity contours are expelled from the "heating" region and the ζD source becomes smaller. However, at the same time the sub-tropical vorticity gradients become larger and so does the advection of vorticity by the divergent flow. The resulting source at day 30 (Fig. 2b) is similar to the original except that the regions of significant amplitude have moved into the sub-tropics. Here they can act as efficient Rossby wave generators.

Numerous other experiments have confirmed the importance of considering the full form of the source term and that the effective Rossby wave source can be remote from the heating itself. Thus a heating embedded in tropical easterlies can be an efficient generator of an extra-tropical Rossby wave pattern.

When considering perturbations to a non-zonal flow it becomes necessary to consider how that flow is maintained. If the basic flow is a solution of (3) then it must have an associated $\bar{v}_\chi$ or $\bar{F}$ or both. (For a time-averaged basic state, $\bar{F}$ would include the convergence of the vorticity flux due to transients). The perturbation problem will then have the term $-\nabla\cdot(\underline{v}_\chi\,\zeta')$ as well as the fixed source $\nabla\cdot(\underline{v}_\chi'\,\bar{\zeta})$. Even for a zonal flow, it is arguable that the Hadley cell $\bar{v}_\chi$ should be included. Schneider and Watterson (1984) first pointed out the importance of $\bar{v}_\chi\,\partial\zeta'/\partial y$ which is one part of the Hadley cell term. Of course the perturbation problem will also include a forcing F'. This is always taken to have the form of a simple damping, but it is doubtful that this is a good model of the perturbation in the transient vorticity flux convergence.

The maintenance of a typical Northern Hemisphere winter 300 mb flow by $\bar{v}_\chi$ rather than the fixed $\bar{F}$ assumed by Simmons *et al.* (1983) changes the modes found by them (Zhang, Z.-J., pers. comm.). Only modes which have growth rates of the order of a week or less appear to be insensitive.

Fig. 3a shows a basic 150 mb flow which is taken to be maintained by a divergent wind. This is then perturbed by the divergence source indicated. The linearised response is shown in Fig. 3b. Despite the divergence source being totally outside the Northern Hemisphere westerlies, there is a very significant and extensive Northern Hemisphere response. Moving the source 45° to the west gives a broadly similar structured response in the extra-tropical Northern Hemisphere, but with

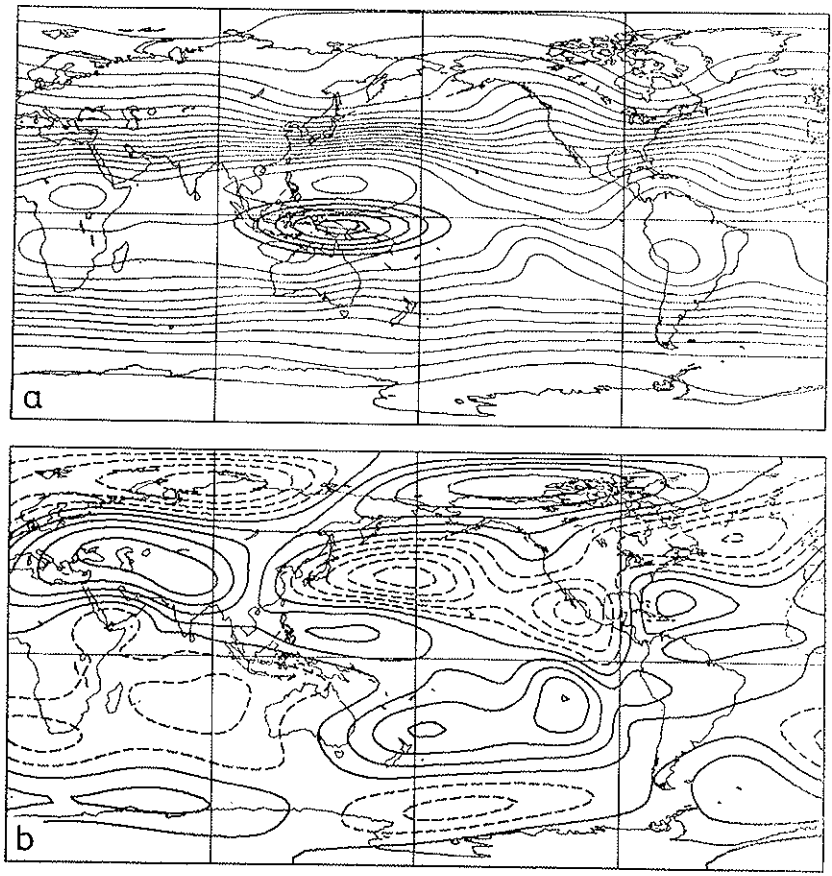

FIG. 3. The full linear problem for a non-zonal basic flow maintained by a divergent wind. (a) Streamfunction of the basic flow and perturbation divergence source. The basic streamfunction corresponds to an observed seasonal mean flow at 150 mb. The contours are light and are drawn at intervals of 10^7 m^2 s^{-1}. The heavy contours are those of the perturbation divergence. (b) The streamfunction perturbation. If the maximum divergence is taken to be 6.10^{-6} s^{-1}, then the contour interval here is 5.10^6 m^2 s^{-1}. Negative contours are dashed.

weaker amplitude. For a source 45° to the east this structure is again similar. Thus a combination of the existence of preferred modes of response in the basic state and the nature of the Rossby wave source leads to relative insensitivity to the longitude of such a heating within the 90° region 100°E-10°W.

4. Concluding comments

The nature of the Rossby wave source associated with tropical heating is clearly important and the barotropic steady state solutions produced are appealing. However it must never be thought that such models will produce simple solutions to the long-range forecasting problem. If they are used with fluctuating sources mimicking the observed 40-50 day oscillation in tropical convective heating, they again produce significant hemispheric responses. If they are used to study a particular season such as in Hoskins and Sardeshmukh (1986), they produce good answers only if the observed vorticity forcing by the synoptic time-scale transients is included. These models are extremely useful for elucidating the important mechanisms.

REFERENCES

GILL A.E. and RASMUSSON E.M.: *The 1982-83 climate anomaly in the equatorial Pacific.* « Nature », *306*, 229-234 (1983).

HOSKINS B.J., *Dynamical processes in the atmosphere and the use of models.* « Quart J. R. Met. Soc. », *109*, 1-21 (1983).

HOSKINS B.J. and SARDESHMUKH P.D., *A diagnostic study of the dynamics of the northern hemisphere winter of 1985-86.* Submitted to « Quart. J. R. Met. Soc. » (1986).

SARDESHMUKH P.D. and HOSKINS B.J., *Vorticity balances in the tropics during the 1982-3 El Niño - Southern Oscillation event.* « Quart. J. R. Met. Soc. », *111*, 261-278 (1985).

SARDESHMUKH P.D. and HOSKINS B.J., *The generation of global rotational flow by idealised tropical divergence.* To be submitted to « J. Atmos. Sci. » (1986).

SCHNEIDER E.K. and WATTERSON I.G., *Stationary Rossby wave propagation through easterly layers.* « J. Atmos. Sci », *41*, 2069-2083 (1984).

SIMMONS A.J., WALLACE J.M. and BRANSTATOR G.W., *Barotropic wave propagation and instability, and atmospheric teleconnection patterns.* « J. Atmos. Sci. », *40*, 1363-1392 (1983).

THE PREDICTABILITY OF MONTHLY MEAN TELECONNECTION PATTERNS

JOSEPH J. TRIBBIA
National Center for Atmospheric Research (*)
Boulder, Colorado 80307

ABSTRACT

This paper presents the results of an ensemble of 20 predictability experiments performed with the NCAR Community Climate Model (CCM). Particular emphasis is placed on the question of the predictability of dynamically driven low-frequency components of the model atmosphere. The conclusion drawn, using time-averaging alone as a means of isolating low-frequency variability, is that in the ensemble mean there is no skill in a 30-day mean forecast. However, further decomposition of the monthly mean anomalies into the empirical orthogonal functions (EOF's) of the monthly mean variability leads to the extraction of two highly predictable teleconnection patterns. The source region for these patterns is examined and a tentative hypothesis as to the nature and stability of these predictable structures is offered.

1. INTRODUCTION

Within the past decade the attention of many dynamical meteorologists has gradually shifted from studies of the dynamics of individual meteorological events, such as cyclone waves and fronts and the statistical equilibria

(*) The National Center for Atmospheric Research is sponsored by the National Science Foundation.

of such events embodied in theories of the general circulation and climate, to studies of atmospheric fluctuations with time scales greater than ten days and less than seasonal. Such fluctuations are often identified by the terms weather regimes, "Grosswetter", or simply low-frequency variability. The tacit hope of many investigators in this area is not only that identifiable dynamical structures associated with this frequency band exist, but furthermore that these structures are predictable signals at extended range within which the largely unpredictable individual weather events are embedded.

Recent studies have given reason for optimism that affirmative answers to both the above-mentioned hopes are likely. The analyses of Wallace and Gutzler (1981) and Blackmon *et al.* (1983) have demonstrated the existence of distinct dynamical structures associated with low-frequency atmospheric variability. Additionally, theoretical studies of Charney and Devore (1979), Charney and Strauss (1980), Källen (1982), Rheinhold and Pierrehumbert (1982) and Legras and Ghil (1985) have suggested that many of the features of observed low-frequency variability are explicable in terms of the nonlinear interaction of planetary-scale waves among themselves, large-scale topography and the statistical residual of synoptic-scale events.

A common element of the above studies is the enhanced predictability of the low-frequency motions as compared to synoptic space and time scale motions. Similarly, many recent studies suggest a large fraction of the power in weather regimes is derived from anomalous boundary forcing of the atmosphere, the strongest of which are associated with anomalous sea-surface temperatures in the equatorial Pacific. The works of Bjerknes (1969), Horel and Wallace (1981), Hoskins and Karoly (1981) and Branstator (1983), demonstrate both the observational evidence for and the dynamical mechanisms which produce the planetary-scale structures forced by these SST anomalies. Insofar as these anomalous boundary conditions can be regarded as known or predictable, the structures which are sustained by this forcing are clearly predictable.

Additionally, a number of numerical prediction/predictability experiments have shown that there is hope that existing numerical models of the atmosphere will be able to produce accurate forecasts of weather regimes. Foremost among these are the investigation by Miyakoda (1986) of the current capability of the GFDL model with regard to forecasting monthly mean anomalies and the demonstration by Shukla (1981) that the divergence of monthly mean forecasts made from slightly different initial conditions does not approach the difference between randomly selected monthly means of the atmosphere, at least for the first 30-day mean.

The above optimistic results lead naturally to the investigation of the frequency of occurrence or probability that the atmosphere be in a configuration allowing an accurate prediction of the low-frequency components of the flow. This question is most straight-forwardly addressed using the model twin, as previously utilized by Shukla (*loc. cit.*). This avoids the problems associated with the imperfect match between the atmosphere and model which necessitates empirical corrections to real-data forecasts, as employed by Miyakoda (*loc. cit.*).

Besides providing a more extensive statistical sample of cases, there are two primary reasons for performing model twin experiments additional to those previously performed. First, the nature of the balances that maintain the low-frequency, large-scale motions in the atmosphere is quite delicate. The slow temporal variations arise typically as the small difference between large terms. Thus, prudence suggests that studies of this nature be performed using several different models so as not to bias the results. Second, no study to date has been internally consistent with regard to the perfect model twin framework, using either atmospheric data for initial conditions, atmospheric climatology for the purpose of determining the level of zero skill, or both. Neither of the above practices used in the investigation of short-range synoptic-scale dominated predictability studies, would alter the results in a significant manner. However, in the study of low-frequency predictability where the differences between the model and the true atmosphere can be substantial, either might lead to erroneous conclusions.

For the above reasons and due to the importance of the results, a comprehensive examination of the question of the predictability of time mean flows was undertaken utilizing the NCAR Community Climate Model (CCM). The results are presented below as follows. First, a recapitulation of the model twin format emphasizing the importance of reasonable model climatological variance within that format is given. Next, a résumé of the relevant climatological aspects of the NCAR CCM simulation is discussed along with the experimental design of the predictability experiments using the climatological integrations as verification. Next, the effects of time averaging and the statistics of the results of the predictability experiments are discussed for various averaging times. Decomposition of the monthly mean heights into the empirical orthogonal functions (EOF's) of the model climatology is performed and the predictability of these patterns is discussed. And, lastly, hypotheses are drawn with regard to the dynamic interpretation of these results.

2. Model Twin Experiments

As noted above, when examining questions relative to the prediction and diagnosis of low-frequency motions, the potential exists for seemingly insignificant details of the analysis or prediction dominating the signal extracted, which is a small residual of larger terms. Thus, care must be taken to ensure that a strict adherence to the tenets of the overall experimental framework is maintained. With regard to model twin experiments then, the implication is that all requisite information and data be taken from the model integrations, not from the known properties of the atmosphere, except in ascertaining the fidelity of the final results. In particular, in predictability experiments this implies that both initial data and the climatological variance against which skill is measured are to be extracted from climatological integrations of the model atmosphere.

One example of the type of erroneous consequences of not strictly adhering to the model twin format which is of particular relevance to the present study lies in the use of atmospheric climatology as opposed to model climatology as a measure of predictive skill. In predictability studies the utility of a forecast is often taken as nil when the transient error variance of a forecast is equal to the transient climatological variance, for beyond this time a forecast of climatology is more skillful. If the model atmosphere's transient climatological variance is less than that of the atmosphere, as is frequently the case, the use of atmospheric climatological variance in this gauge will inappropriately extend the range of useful forecast.

This particular example was chosen for it will be seen below that, as a function of averaging time, the NCAR CCM maintains a decreasing percentage of the transient variance compared to that of the atmosphere. The consequence of this deficiency and its potential causes are discussed in a later section. It is noted here that because of this deficiency, deviations from the model twin framework would amplify their erroneous effects on the results as the averaging time is increased.

3. Experimental Design

The model atmosphere used in this study as ground truth is the 1200-day perpetual January simulation of the NCAR Community Climate Model (CCM0B), a spectral transform model rhomboidally truncated at wavenumber 15, with nine sigma levels in the vertical (Williamson, 1983).

As noted above, the climatological integrations serve a dual purpose, first as a data set from which initial and verifying analyses may be obtained, and second to ascertain the climatological variance of the forecast field in order to gauge forecast skill.

Having already noted the potential difficulties associated with a deficient climatological variance, the transient Northern Hemispheric 500 mb geopotential height variance, as ascertained from the 1200-day climate integration and as estimated by Malone *et al.* (1984) for the atmosphere, is shown in Figs. 1a and 1b respectively. It may be noted that the amplitude and geographical distribution of the model-generated height variance is in general quite realistic. This comparison is not sufficient for the present purpose, however, since not only must the spatial distribution of the model transient variance reproduce that of the atmosphere reasonably well, but also the distribution of that variance in the frequency domain must compare favorably. In order to examine that factor, a comparison is made between the transient time variance of the time-averaged Northern Hemispheric 500 mb height field in the model and the atmosphere as a function of averaging time shown in Fig. 2. The atmospheric values were obtained using eleven Januaries of NMC Northern Hemispheric analyses, removing the 11-sample mean for each date. As can be seen from the figure, the model captures approximately 87% of the (unaveraged) daily variance, near 80% of the 20-day mean variance, and only 67% of the monthly mean variance.

There are at least two reasons for this deficiency in monthly mean variance, the absence of a seasonal cycle in solar declination angle and the absence of external forcing due to boundary anomalies. The addition of a seasonal cycle can excite low-frequency transients which increase the model simulated monthly mean variance to 83% of their January atmospheric magnitude (R. Chervin, personal communication). This implies that with proper seasonal forcing, the model is only slightly less proficient at reproducing monthly mean variance as it is at producing day-to-day variability, i.e., it has excellent low-frequency climatology.

Additional to this free variability is the monthly mean signal due to external variations, such as and in particular those due to sea-surface temperature anomalies. One may conclude from the above that, assuming the NCAR model simulates the partition of atmospheric low-frequency variability into internally and externally caused fractions properly, then the signal-to-noise ratio for boundary-forced low-frequency motions is a meagre 0.2.

Returning once more to the other purpose of the climatological in-

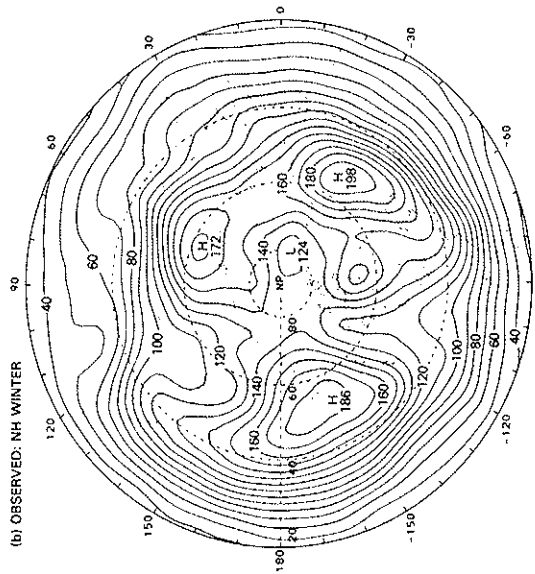

FIG. 1b. Transient 500 mb height variance of CCM from 1200 day perpetual January simulation, after Malone *et al.*, 1984.

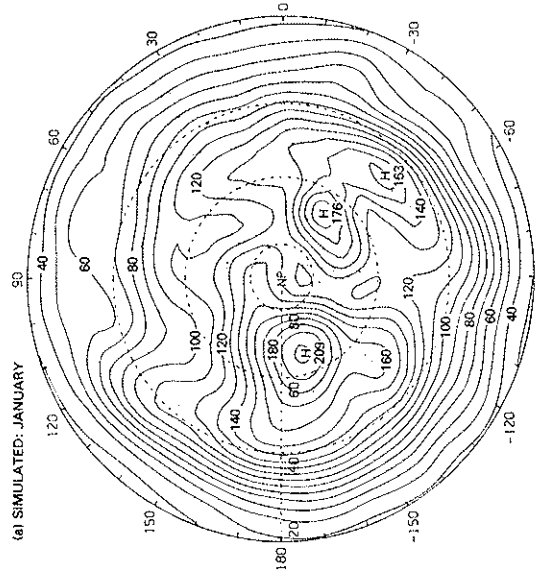

FIG. 1a. Transient 500 mb height variance estimated from NMC analyses, after Malone *et al.*, 1984.

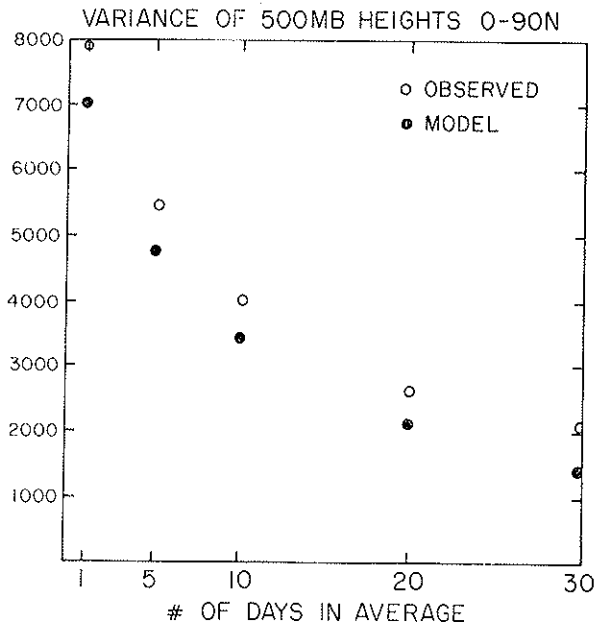

FIG. 2. Transient variance of 500 mb time averaged heights as a function of averaging time for the atmosphere (open dot) and for the NCAR CCM (solid dot).

tegration, serving as a starting point from which initial values for the perturbed predictability forecasts are obtained, the specifics of this process are now described. Every 60 days within the 1200-day climatological integration, the global prognostic fields of velocity and geopotential were sampled and perturbed with small random perturbations in each field. The perturbed fields were initialized using nonlinear normal mode initialization with a 24-hour cut-of period in the gravest four vertical modes consistent with the model climatology (Errico, 1984). The resultant amplitude of the perturbation in the 500 mb geopotential field was 3m global rms. The perturbed iniitalized fields were then integrated forward for 60 days each. Thus, the ensemble of cases consists of twenty 60-day control (climatological) and perturbed integrations.

4. Ensemble Mean Results

Before discussing the results of the ensemble of time average predictability experiments, it is worthwhile to examine the expected consequence of time averaging to these results. The purpose of time averaging, as motivated in the introduction, is to isolate those features of the meteorological fields which might be predictable beyond the range of synoptic day-to-day weather events. This, however, represents a two-edged sword in that while time-averaging (by its very nature) reduces the phase decorrelation rates of the averaged fields and thus eliminates instabilities which propagate with periods less than the averaging time, it also acts as a temporal filter and reduces the climatological variance of the averaged fields. This latter effect is clearly seen in Fig. 2. This variance reduction opposes the tendency for greater predictability of time means and any enhanced predictability of time mean features arises as a trade-off between slower decorrelation rates and variance reduction. Similar comments relate to the efficacy of spatial smoothing and generalized Fourier decomposition.

In order to quantify the results, two standard skill measures are used: the error variance and the anomaly correlation. The error variance measure is defined as mean square difference between the perturbed and control 500 mb height field, i.e.

$$EV \equiv \frac{1}{2\pi a^2} \int_S \left(\overline{z}_p^T - \overline{z}_c^T\right)^2 dS, \tag{1}$$

where $^{-T}$ indicates time average over time T, S is the Northern Hemisphere surface, dS is the differential surface element, and z_p and z_c are the perturbed and control heights respectively. The anomaly correlation is defined following Miyakoda *et al.* (1986):

$$AC \equiv \frac{\int_S \left(\overline{z_c'}^T \overline{z_p'}^T\right) dS}{\left[\int_S \left(\overline{z_c'}^T\right)^2 dS \int_S \left(\overline{z_p'}^T\right)^2 dS\right]^{\frac{1}{2}}} \tag{2}$$

in which $z' = z - \langle z \rangle$ with $\langle z \rangle$ being the 1200-day mean of z and all other notations as in (1). Using these measures, the level of vanishing skill is taken to be error variance equal to the climatological variance (corresponding to the point at which a climatology forecast is as skillful as the numerical forecast and/or anomaly correlation equal to .5 (consistent with the zero skill level for error variance).

As a benchmark calculation, the ensemble mean daily error growth and decorrelation are shown in Figs. 3a and 3b. Figure 3a depicts the ensemble mean error variance as a function of forecast time along with the ensemble mean plus and minus the 20-sample standard deviation of the error variance and the highest and lowest error variance among the 20 cases at each time. Figure 3b shows the same variables mean, mean plus/minus the standard deviation, greatest and least value for the anomaly correlation measure. Both skill measures give the identical result that for the given initial perturbation amplitude the temporally unaveraged forecasts in the ensemble mean loses skill at day 10. This is to be compared with the analogous result of Baumhefner (1985) using the same model with observed initial condition, in which perturbed forecasts lost skill relative to a control at day 11, in the ensemble mean, implying that the perpetual January simulation is slightly more unstable to infinitesimal perturbations than the real atmosphere, as might be anticipated. It may also be noted that there is a wide variation in the error growth across the 20-case ensemble as demonstrated by the plus/minus standard deviation curves and the greatest/least curves, which cross the level of vanishing skill between days 7 and 18. These results are in close agreement with those of Baumhefner, *loc. cit.*

Next the effect of averaging these results for increasingly longer periods of time is shown in Figs. 4a, b, 5a, b, 6a, b, and 7a, b, in which the averaging times are 5 days, 10 days, 20 days, and 30 days, respectively. In each of these figures the error variance and anomaly correlation at day 0 corresponds to the value of the measure for the first N-day average (i.e., the average of days 0 through N), the value at day 1 corresponds to the error in the average of days 1 through N+1, etc. The predictability of 5 and 10 day averages demonstrates clearly the beneficial aspects of time averaging in enhancing the predictability over that of unaveraged fields if one considers the mid-point of the average. Thus, since 5-day averaged forecasts lose their skill in the ensemble mean at day 9 and 10-day averaged forecasts lose their skill at day 8, the mid-points of these averaging intervals lose their skill in the mean at day 11.5 and day 13, respectively, both larger than the unaveraged value of day 10. It may also be noted that the variability in the time at which predictive skill is lost increases as a function of increasing averaging time. As shown, there is a 4, 5 and 7 day difference in the time between the mean minus one standard deviation and mean plus one standard deviation curves for unaveraged, 5-day mean and 10-day mean forecasts, respectively. Note also the greatest/least curves show the same trend in Figs. 4 and 5.

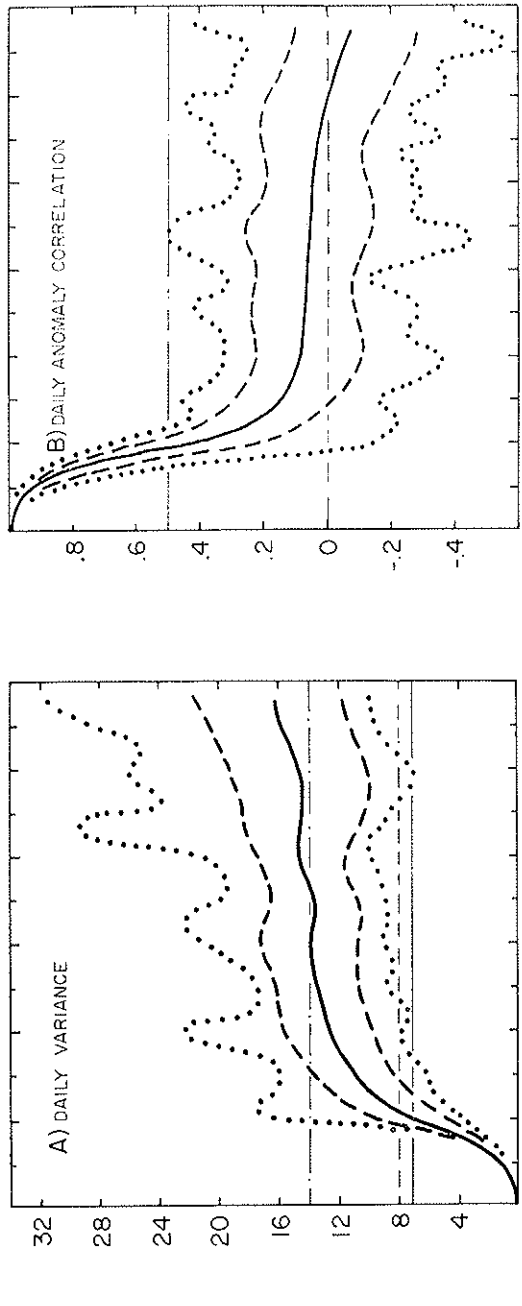

FIG. 3. a) Error variance in $m^2 \times 10^3$ as a function of forecast time in days for unaveraged forecasts. Heavy solid = ensemble mean, dashed = mean plus or minus standard deviation, dotted = best/worst forecast at time, t, light solid = model climatological variance, light dashed = observed climate variance, light dashed, dot = twice model climate variance. b) Anomaly correlation score as a function of forecast time for unaveraged forecast. Heavy solid = ensemble mean, dashed = mean plus or minus standard deviation, dotted = best/worst forecast at time, t, light solid = anomaly correlation of .5, light dashed = anomaly correlation of 0.

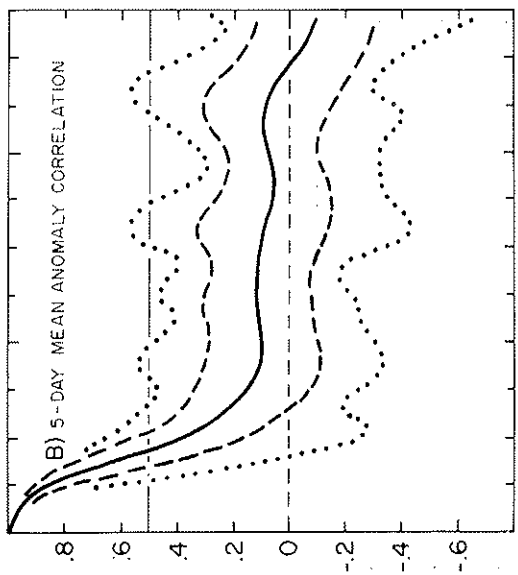

FIG. 4b. As in Fig. 3b for five-day running means. t = 0 score corresponds to average of days 0-5.

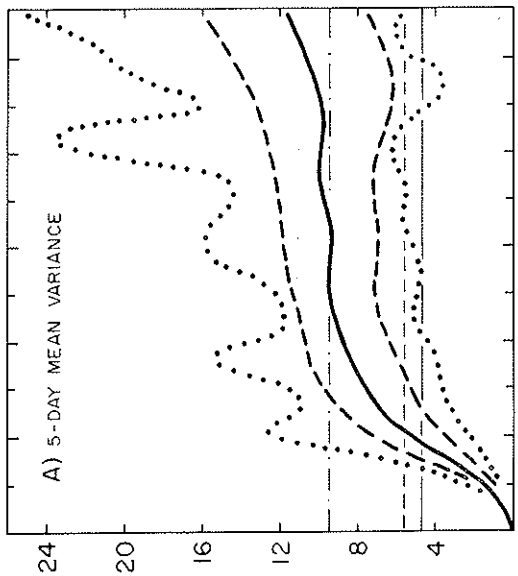

FIG. 4a. As in Fig. 3a for five-day running means. t = 0 corresponds to average of days 0-5.

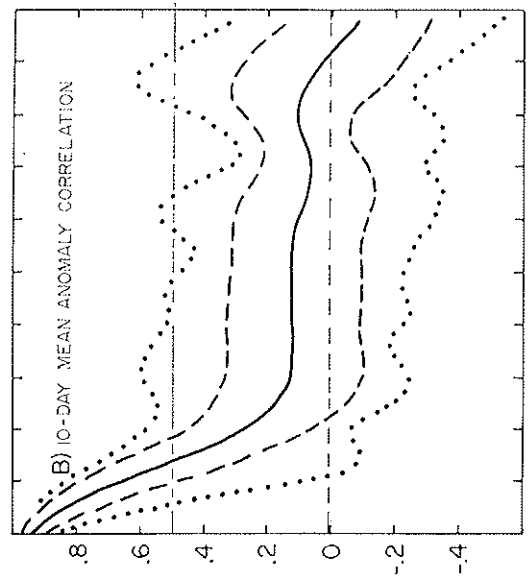

FIG. 5b. As in Fig. 3b for 10-day running means.

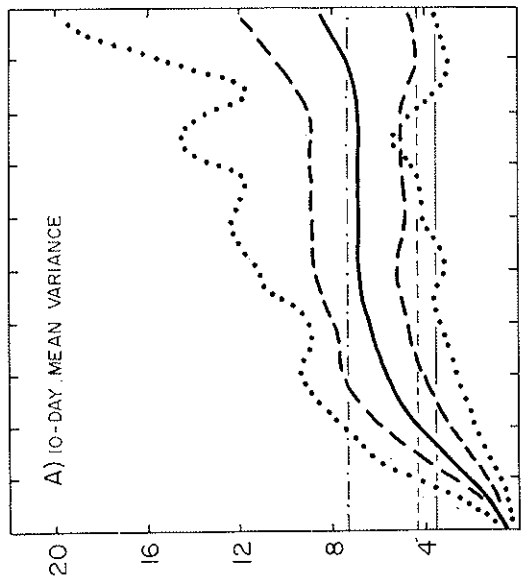

FIG. 5a. As in Fig. 3a for 10-day running means.

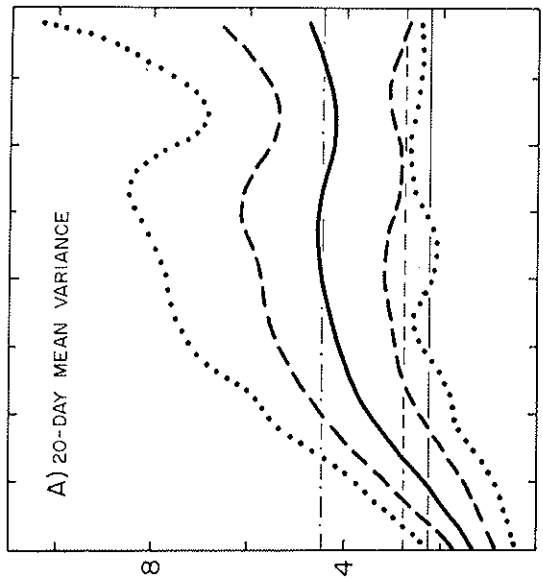

FIG. 6a. As in Fig. 3a for 20-day running means.

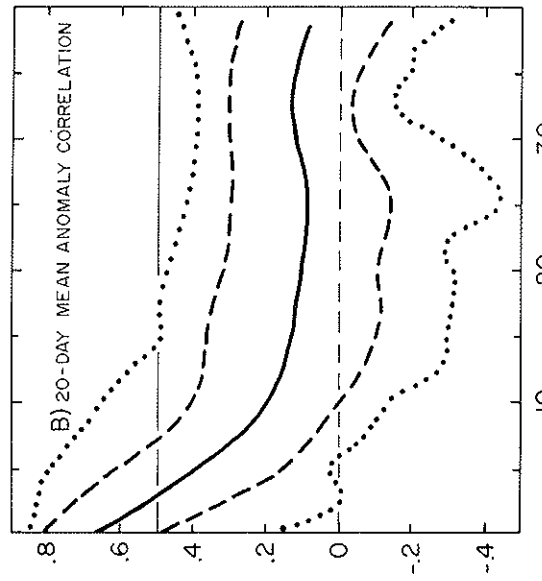

FIG. 6b. As in Fig. 3b for 20-day running means.

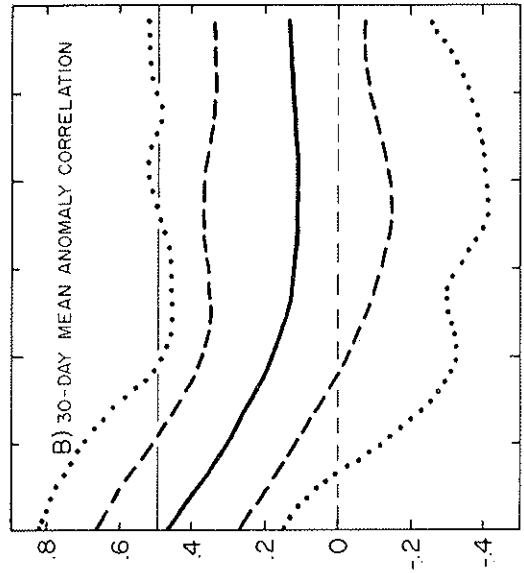

FIG. 7b. As in Fig. 3b for 30-day running means.

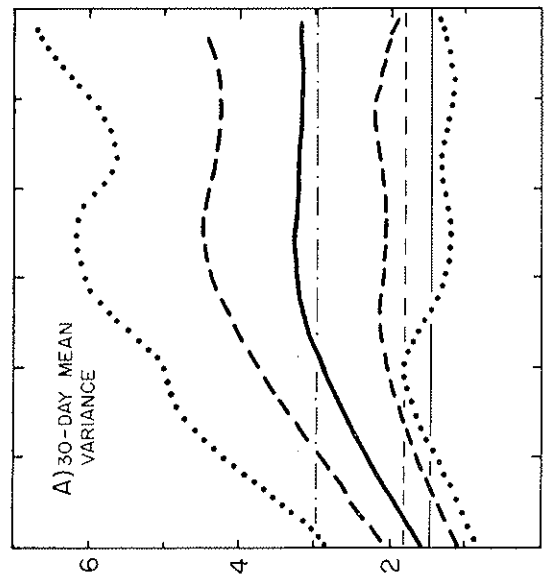

FIG. 7a. As in Fig. 3a for 30-day running means.

Turning next to the 20 and 30-day mean predictability results, the reduction in variance due to temporal filtering becomes more important. This is seen in the 20-day average ensemble mean error growth and decorrelation curves of Figs. 6a and b, which depict loss of skill at day 4, the time average of days 4 through 24, and so the mid-point loses skill at day 14, merely one day later than the corresponding time for 10-day mean running mean forecasts. The mid-point crossing of the level of useful skill then is asymptoting near day 14 and thus it is not surprising, in examining Figs. 7a and b that in the ensemble mean there is no predictive skill in 30-day means using the above-noted skill measures. The ensemble mean error variance in the monthly mean beginning at day 0 is 1620 m^2 while the climatological transient variance is 1440 m^2. Similarly, the ensemble mean anomaly correlation for the monthly mean beginning at day 0 is .47.

In examining the range of skill represented in the 20 cases for both the 20-day averages and 30-day averages, it can be seen that a large fraction of the 20-day mean forecasts are skillful for the forecast of the 0-20 day average since even the mean error plus one standard deviation curve is below the climatological variance for this averaging time (similarly for the anomaly correlation plus one standard deviation). In examining the monthly means, it is noted that somewhat less than 50% of the predictions of the mean of days 0-30 are skillful, since the mean minus one standard deviation error variance curve is below the climatological variance and likewise for the anomaly correlation score. The above statements assume approximate Gaussianity in the distributions of these measures within the ensemble, which has been verified.

5. Predictability of teleconnections

While the results concerning the predictability of monthly means reported in the previous section are somewhat discouraging, they are not totally hopeless. The .47 average anomaly correlation score implies that some components of the verification and forecast monthly mean anomalies are similar. It remains, however, to extract this signal and the most obvious next step in this extraction is spatial filtering. Of the plethora of methods of spatial filtering, that most likely to succeed in the present case is spatial decomposition of the monthly mean fields into the natural modes of low-frequency variation of the model atmosphere. These modes

may be extracted from the climate record using empirical orthogonal function (EOF) analysis.

Performing such an analysis on the 1200-day climate integration results in the 500 mb height anomaly patterns shown in Figs. 8a and 8b, for the two leading EOF's. These two patterns represent respectively 26 and 16 percent of the monthly mean variance of the Northern Hemisphere height anomalies in the climate simulation. These patterns show similarities to the teleconnection patterns obtained by Wallace and Gutzler (1981) showing both a PNA (Pacific North America)-like structure and an EA (Eastern Atlantic) pattern.

In order to investigate the question of the predictability of these structures, the 30-day running mean of the 500 mb Northern Hemispheric height fields for both the perturbed and control integration were projected onto the EOF's. The ensemble mean variance of the difference between the projection coefficients is compared, as a function of time, with the

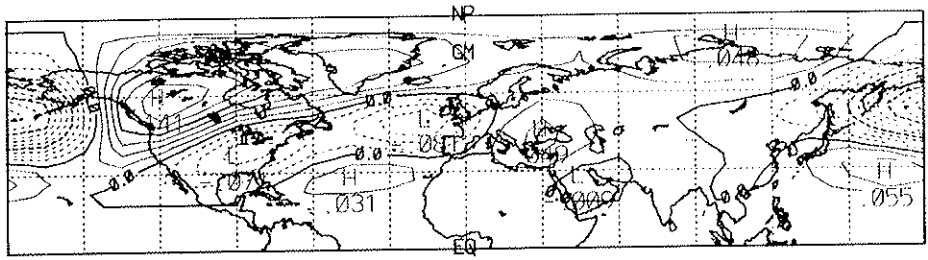

FIG. 8a. Leading EOF of monthly mean 500 mb heights representing 26% of the variance.

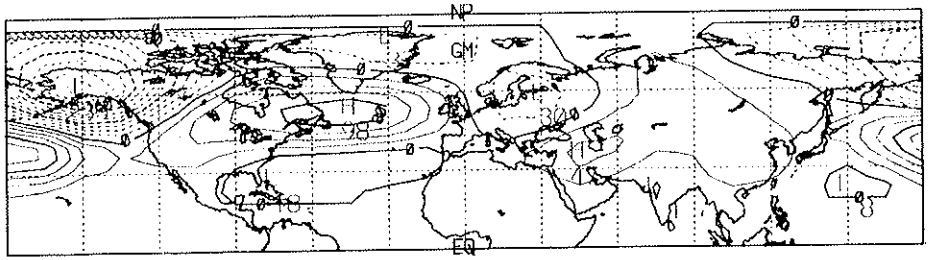

FIG. 8b. Second leading EOF of monthly mean 500 mb heights representing 16% of the variance.

climatological mean value of the variance of each coefficient in order to ascertain predictive skill. As shown in Figs. 9a and 9b, both coefficient amplitudes are predictable, the leading EOF coefficient showing skill for the mean of days 30 through 60 while the prediction of the second leading EOF coefficient retains skill out to the mean of days 9 through 39.

Because of the resemblance of these two EOF patterns to teleconnection structures, it is intriguing to ascertain whether these patterns are stimulated by remote forcing due to naturally occurring anomalous upper level divergence in the tropics. One method by which this may be ascer-

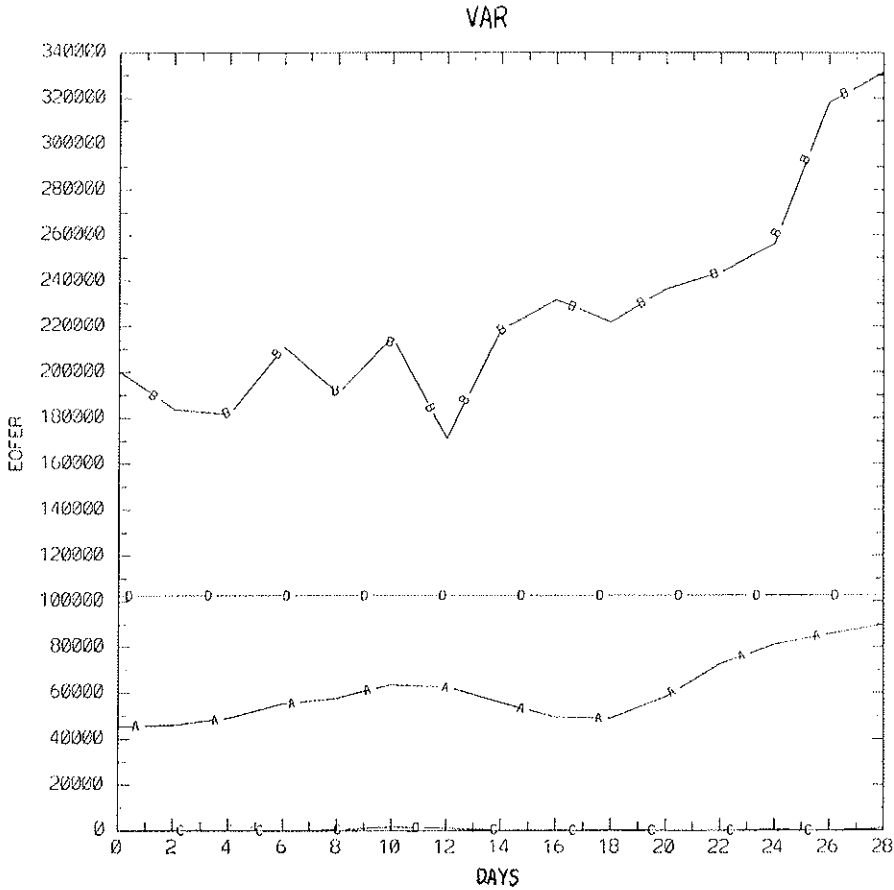

FIG. 9a. Ensemble mean forecast error variance of running 30-means of leading EOF coefficient, A = error variance, B = worst case, D = climatological variance.

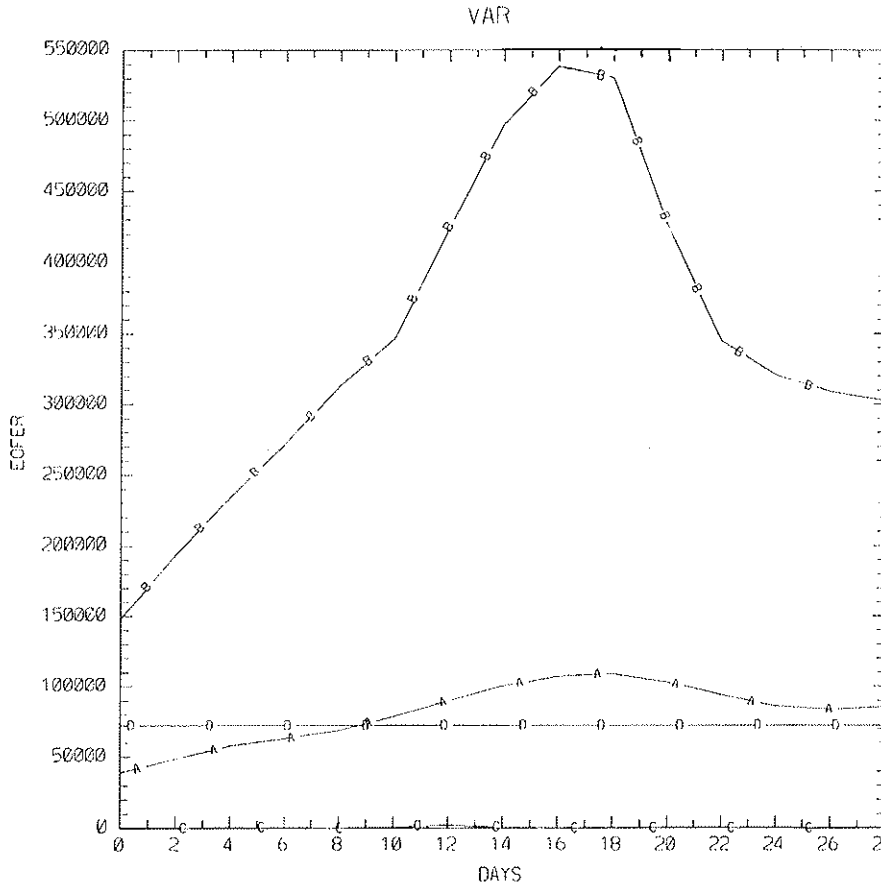

FIG. 9b. As in Fig. 9a for second leading EOF coefficient.

tained is to examine the climatological time record to obtain the 300 mb divergence coexistent with the EOF patterns. This may be accomplished by producing a regression "prediction" of the monthly mean 300 mb divergence anomalies using each EOF amplitude coefficient as the predictor. The predicted divergence anomalies for unit amplitudes in the first and second EOF coefficients are shown in Figs. 10a and 10b respectively. As can be seen, these figures depict a pattern of predominantly tropical divergence. Since the determination of the source/response relationships of these patterns with the EOF structure has not yet been attempted,

one may only safely say that these divergence patterns represent divergence consistent with the height anomalies at middle and high latitudes. Typical values of the correlation coefficients between the EOF coefficients and the tropical low-frequency divergence anomalies are only about 0.4, suggesting non-uniqueness in the sources of these teleconnection patterns.

The reason for the anomalous predictability of these teleconnection patterns is also not yet fully known, but a reasonable working hypothesis has been formulated using the known properties of large-scale teleconnection patterns. First it is noted that the leading and second EOF's have many similarities in structure with the barotropically unstable modes of the climate mean basic state first discussed by Simmons *et al.* (1983). The streamfunction patterns for the two most unstable modes of the CCM perpetual January climatology are shown in Figs. 11a-11d from Branstator (1985). The periods of these modes are 127 days and 22 days and the e-folding times are 15 days and 17 days respectively. The predictable EOF's are likely orthogonalized representations of finite amplitude versions of these two low-frequency modes, which draw their energy from the kinetic energy of the climatic mean state. The most unstable mode is likely to be resistive to unpredictable eddy forcing since the adjoint eigenfunction from this mode shown in Figs. 12a and b has appreciable amplitude only in the tropics. Unfortunately, monthly mean divergent anomalies are highly *un*predictable as shown in Fig. 13, depicting the ensemble mean error variance growth for monthly mean divergence anomalies. This implies that over a monthly mean the perturbed and control forecast should experience different forcings from the divergence anomalies present in each integration.

Two factors tend to mitigate this last effect, however. First the slow growth rate (a factor of two longer than that found by Simmons *et al.* (*loc. cit.*) and the inherent correlation of the time-averaged divergence for short times lead one to suspect a long spin-up time for the deviation in these modes, easily up 30 days. Secondly, the small-scale structure of the adjoint eigenfunction makes it unlikely that a large percentage of the anomalous vorticity generated by the divergence at 300 mb will project on the forcing necessary to excite the SWB mode and thus reduce the effective amplitude of the differential in the monthly mean divergence forcing between the forecast and the control integration.

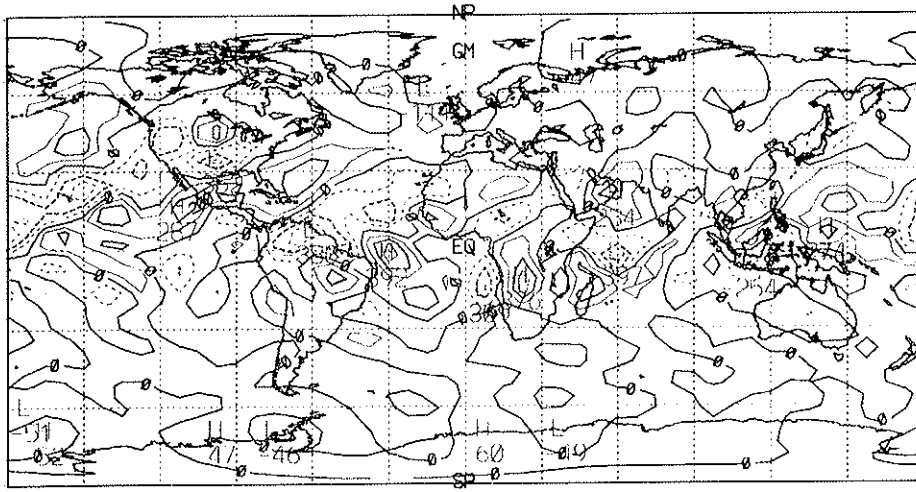

FIG. 10a. Regression coefficient for the 300 mb monthly mean divergence using the leading EOF coefficient as predictor.

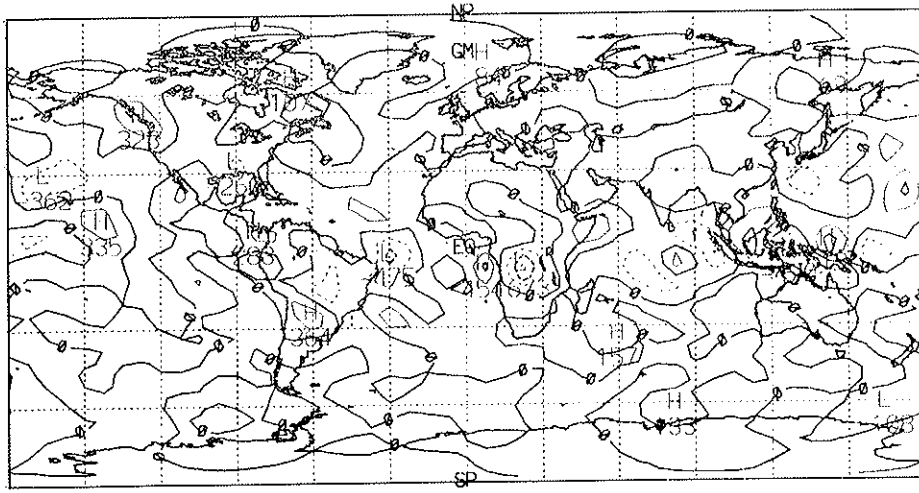

FIG. 10b. As in 10a for the second leading EOF coefficient.

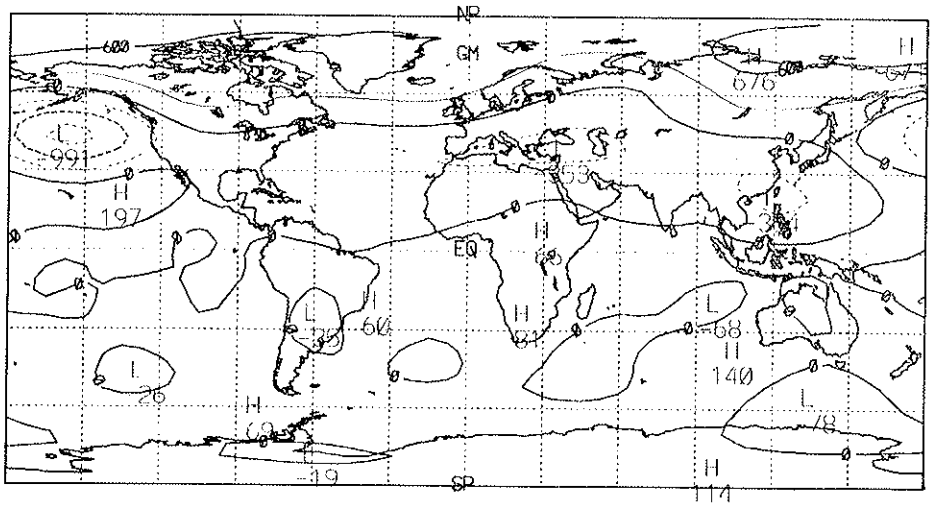

FIG. 11a. Structure of streamfunction associated with the most unstable barotropic mode of the 300 mb climatological flow. Period = 127 days, E-folding time = 15 days. After Branstator, 1985.

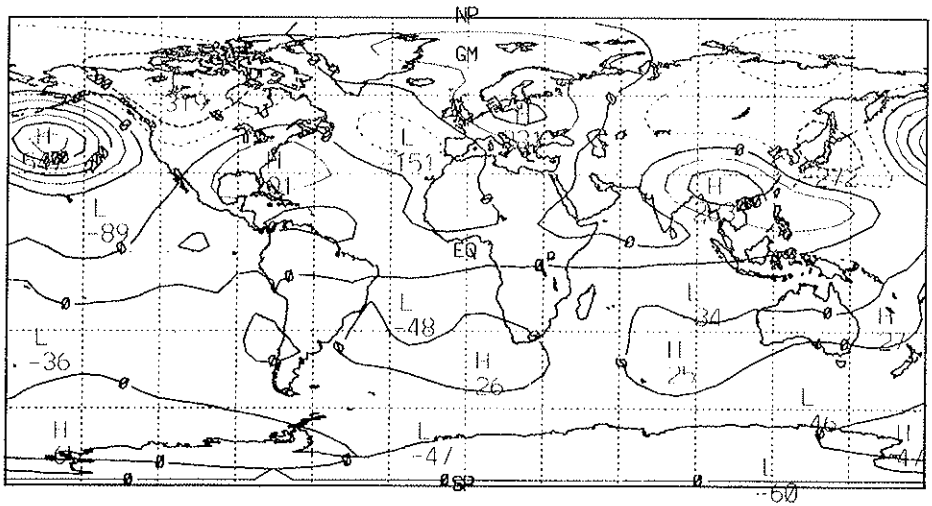

FIG. 11b. As in Fig. 11a, one quarter period later.

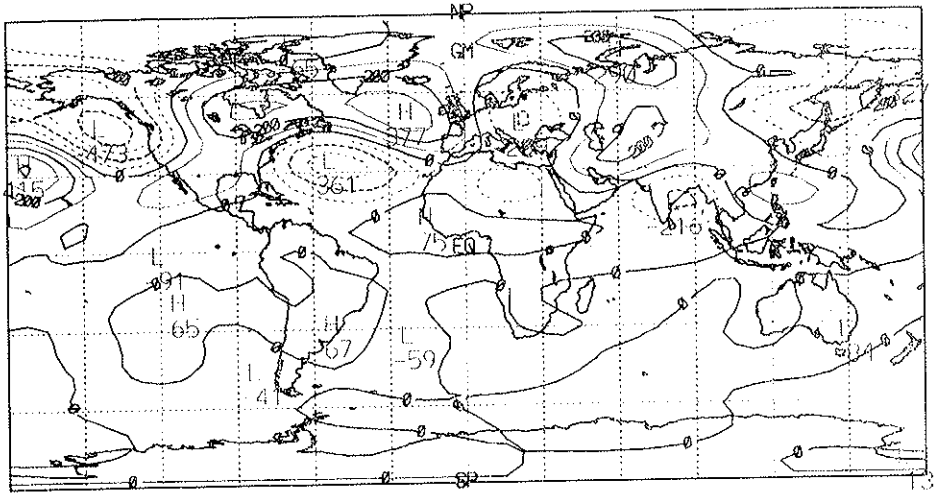

FIG. 11c. As in Fig. 11a for the second most unstable mode. Period = 22 days, E-folding time = 17 days.

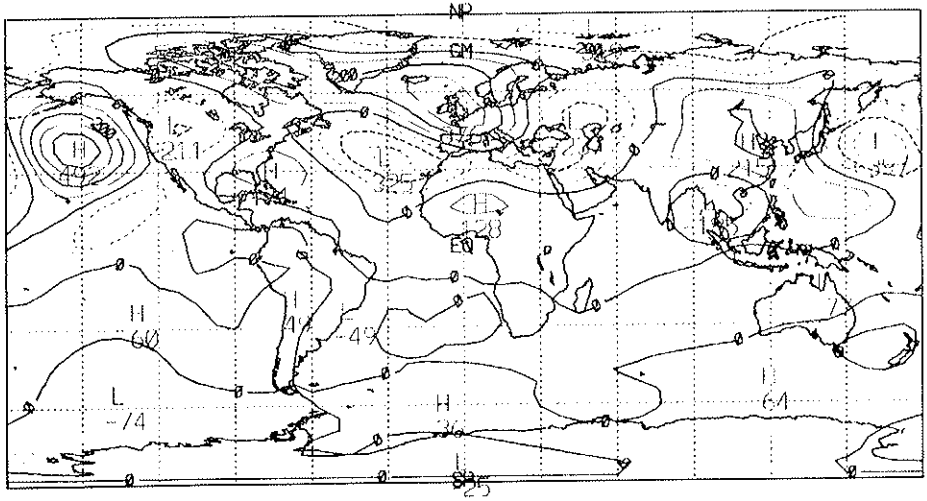

FIG. 11d. As in Fig. 11a one-quarter period later.

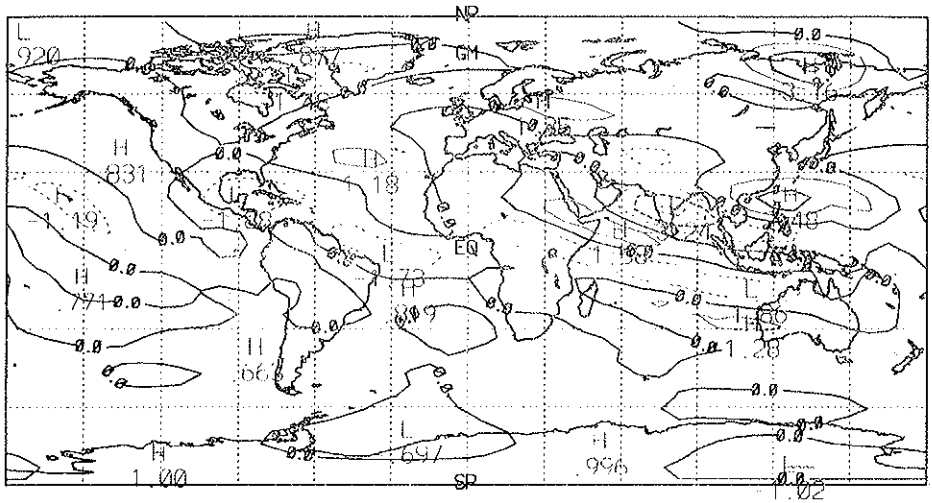

FIG. 12a. Adjoint eigenfunction of mode in Fig. 11a.

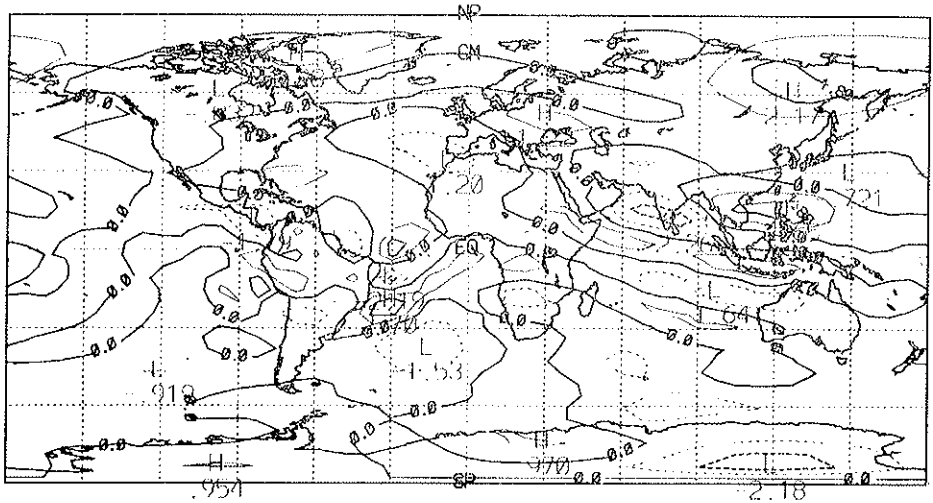

FIG. 12b. Adjoint eigenfunction of mode in Fig. 11b.

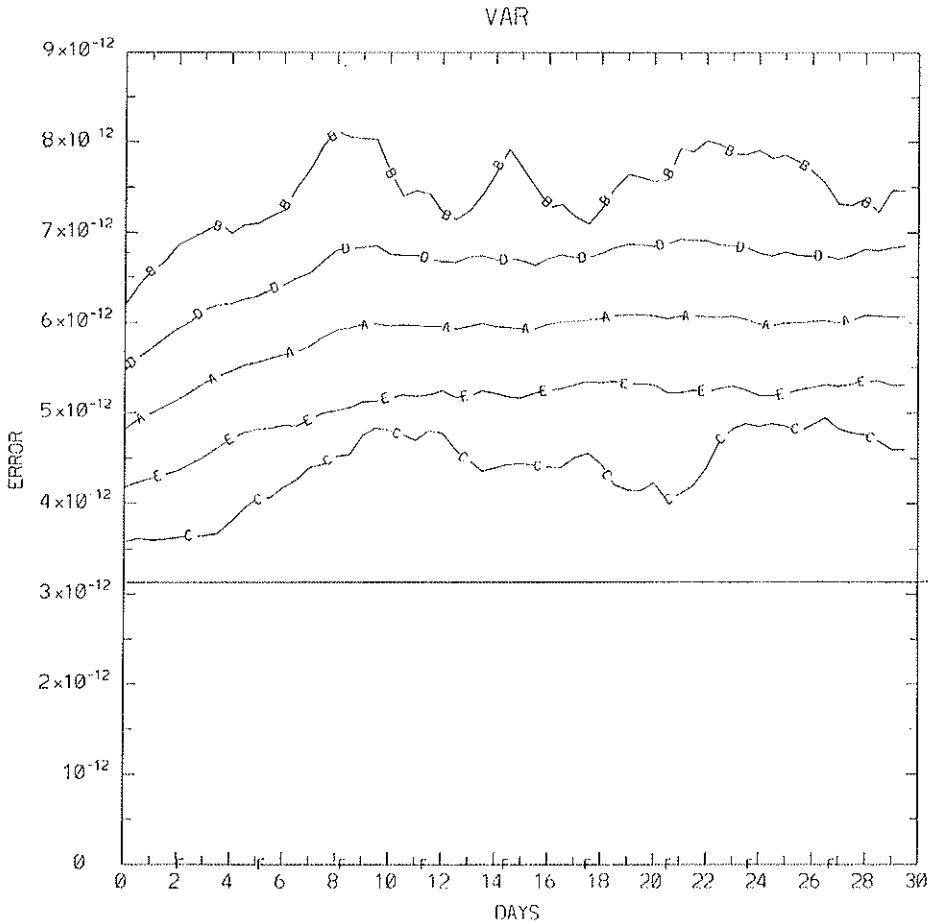

FIG. 13. As in Fig. 7a for the monthly mean divergence anomalies. A = ensemble mean, B = best, C = worst, D = mean plus standard deviation, E = mean minus standard deviation, ——— = climatological variance.

6. Conclusions

A primary purpose of the study reported has been to examine, in a self-consistent model twin experiment, the efficacy of time averaging with regard to extracting a predictable signal, a regime, out of the day-to-day weather fluctuations. It was noted that time averaging and indeed any type of filtering operation is associated with two opposing effects: the elimination of rapid decorrelation rates and propagating instabilities and the reduction of climatological variance against which skill is measured. Thus, the predictability of filtered fields is a trade-off between these two competing effects.

Using the 1200-day perpetual January CCM simulation as the verification and the source of initial conditions which are perturbed to produce "forecasts", a 20-case ensemble of 60-day forecasts was produced. The forecasts were verified against the respective means of the control integration. In the 20-case ensemble mean the results are summarized as follows. If the unaveraged forecast loses skill at day 10, a 5-day running mean will lose skill at day 9 (average of days 9-14), a 10-day running mean will lose skill at day 7 (mean of days 7-17), a 20-day running mean will lose skill at day 4 (average of days 4-24), and a 30-day running mean will be unskillful.

Spatial filtering via EOF projection of the monthly mean flows revealed a predictable signal in the leading and second leading EOF patterns which together represent approximately 40% of the monthly mean variance. These patterns resemble teleconnection patterns and their enhanced stability may be related to their structural similarity to finite amplitude SWB modes. These low-frequency modes extract their energy from the kinetic energy of climate mean state and are structurally insensitive to mid-latitude forcing from unpredictable eddies.

Acknowledgments

The author wishes to thank M. Niemczewski for expert typing and G. Branstator for many helpful discussions during the course of this work.

REFERENCES

BAUMHEFNER D.P., *Analysis and forecast intercomparison using the FGGE SOP-I data base.* « Proc. First National Workshop on the Global Weather Experiment », National Academy Press, pp. 228-246 (1985).

BJERKNES J., *Atmospheric teleconnections from the equatorial Pacific.* « Mon. Wea. Rev. », *97*, 163-172 (1969).

BLACKMON M., LEE Y.-H. and WALLACE J.M., *Horizontal structure of 500 mb height fluctuations with long, intermediate and short periods.* « J. Atmos. Sci. », *41*, 961-979 (1983).

BRANSTATOR G., *Horizontal energy propagation in a barotropic atmosphere with meridional and zonal structure.* « J. Atmos. Sci. », *40*, 1689-1708 (1983).

BRANSTATOR G., *Analysis of general circulation model sea-surface temperature anomaly simulations using a linear model.* II: *Eigenanalysis.* « J. Atmos. Sci. », *42*, 2242-2254 (1985).

CHARNEY J.G. and DEVORE J., *Multiple flow-equilibria in the atmosphere and blocking.* « J. Atmos. Sci. », *36*, 1205-1216 (1979).

CHARNEY J.G. and STRAUSS D.M., *Form-drag instability, multiple equilibria, propagating planetary waves in baroclinically, orographically forced planetary wave systems.* « J. Atmos. Sci. », *37*, 1157-1176 (1980).

ERRICO R.M., *The dynamical balance of a general circulation model.* « Mon. Wea. Rev. », *112*, 2439-2454 (1984).

HOREL J.D. and WALLACE J.M., *Planetary scale atmospheric phenomena associated with the Southern Oscillation.* « Mon. Wea. Rev. », *109*, 813-829 (1981).

HOSKINS B.J. and KAROLY D.J., *The steady linear response to thermal and orographic forcing.* « J. Atmos. Sci. », *38*, 1179-1196 (1981).

KÄLLEN E., *Bifurcation properties of quasi-geostrophic barotropic models and their relation to blocking.* « Tellus », *34*, 258-265 (1982).

LEGRAS B. and GHIL M., *Persistent anomaly blocking and variations in atmospheric predictability.* « J. Atmos. Sci. », *42*, 433-471 (1985).

MALONE R.C., PITCHER E.J., BLACKMON M.L., PURI K. and BOURKE W., *The simulation of stationary and transient geopotential height eddies by a spectral GCM.* « J. Atmos. Sci. », *41*, 1394-1417 (1984).

MIYAKODA K., SIRUTIS J. and PLOSHAY J., *Monthly forecast experiments.* Part I: *Without anomaly boundary forcing.* To appear in « Mon. Wea. Rev. » (1986).

RHEINHOLD B.B. and PIERREHUMBERT R.T., *Dynamics of weather regimes, quasi-stationary waves and blocking.* « Mon. Wea. Rev. », *110*, 1105-1145 (1982).

SHUKLA J., *Dynamic predictability of monthly means.* « J. Atmos. Sci. », *38*, 2547-2572 (1981).

SIMMONS A.J., WALLACE J.M. and BRANSTATOR G.W., *Barotropic wave propagation and instability, and atmospheric teleconnection patterns.* « J. Atmos. Sci. », *40*, 1363-1392 (1983).

WALLACE J.M. and GUTZLER D.S., *Teleconnections in the geopotential height field during the Northern Hemisphere winter.* « Mon. Wea. Rev. », *109*, 784-812 (1981).

WILLIAMSON D., *Description of the NCAR Community Climate Model (CCM0B).* NCAR Technical Note TN-210+STR, 93 pp. (1983).

NON-LINEAR PROSPECTS IN ATMOSPHERIC DYNAMICS

BERNARD LEGRAS
Laboratoire de Météorologie Dynamique
24, rue Lhomond 75231 Paris Cedex 05

Introduction

The quantitative study of the large scale atmospheric flows has been based during the last thirty years on the development of general circulation models. Starting from the simple barotropic equation of vorticity (Charney *et al.*, 1950), they have reached a level of considerable complexity through a continuous process of refinement of the mesh size and the parameterization of physical mechanisms. Short and medium range forecasts are produced operationally on a daily base with skill increasing from year to year. Long range Monte Carlo or lagged average forecasts are now considered which would extend the prediction of some statistical quantities beyond the deterministic predictability limit. In parallel with this effort aiming to simulate as well as possible the atmospheric behavior, more basic theory using simplified models appears still necessary, not only to cure the idiosyncrasies of GCM's through new differentiation schemes, parameterizations or data assimilation processes, but also to build the conceptual tools of our analysis of the observed and the simulated dynamics. Indeed, we have to face the apparent paradox that as one gets closer to the simulation of the real atmosphere, the dynamics of the simulated atmosphere gets closer to the complexity and unintelligibility of the real one. The main advantage of GCM's lies evidently in their ability to generate data in a shorter delay and at a much lower cost than the observation of the real atmosphere.

The theory of atmospheric circulation has been formalized up to a high level but still possesses a special status among physical theories. Unlike many other domains, there is no simplest analytical approach

which would predict even a rough estimate of the atmospheric circulation from the solar input as determined by astronomical positions, the radius of the planet, its rotation speed and the physical characteristics of its atmosphere. The main difficulty lies in the crucial role played by non axisymmetric stationary and transient perturbations in the averaged budget of the atmosphere. Thus, a detailed parameterization of the Reynolds stresses is necessary even at the lowest level of the theory which can hardly be obtained without numerous ad hoc approximations.

On the other hand, there are no major unsolved questions about the mathematical formulation of the problem. Although some important aspects of the atmospheric behavior, like stratospheric chemistry, ocean-atmosphere exchanges of carbon dioxide, or microphysics of clouds, are still imperfectly described, there is little doubt on the adequacy of fluid dynamics equations together with hydrostatic approximation and perfect gas law to describe the dynamics of synoptic and large-scale weather systems. The difficulty comes entirely from the complex chaotic behavior of the observed or simulated dynamics. Such a situation is generic in meteorology but is presently encountered in most domains of physics, due to a general increasing interest in nonlinear phenomena. Numerous developments have been obtained recently in the theory of dynamical systems; they bring considerable light on the transition to chaos and on the character of low-dimensional chaos, but the study of systems with a large number of excited degrees of freedom still relies mainly on empirical and experimental approach, in which computer simulations play a crucial role.

Despite the non linear character of atmospheric motions, linear theories which consider small amplitude perturbations to a basic prescribed flow have been able to furnish an account on a lot of features such as the evolution of planetary scale waves, on the structure of stationary waves, the generation and propagation of synoptic perturbations and more recently the coupling between tropical and mid-latitudes. Starting from the pioneering works of Rossby, Charney and Eady, this approach has so far played a leading role. The study of weakly non linear corrections or of realistic basic states, involving critical layers, leads to sophisticated theories where an arsenal of methods of theorical physics can be deployed, quite often with great mathematical ingenuity. There are however some doubts that the needed approximations can be justified with the same rigour as in other fields of physics. Scale separation between perturbations and mean flow hardly shows up with factors larger than a few units, which are generally insufficient to found an asymptotic expansion. A basic assumption, not

often stated, is that finite amplitude waves like to behave in a similar way as small amplitude waves. Success can be gained from this approach when unresolved nonlinearities and transients act as mixing processes, an approximation commonly used when one has to parameterize their effects. There are however several instances where this is not the case. We are going to give a few insights on two aspects of this problem, the existence of non linear coherent structures and the maintenance of large-scale flows by small-scale transients.

Coherent structures

The development of observations and simulations of turbulent flows, and particularly the use of imaging techniques instead of average measurements, have led to the evidence that a large part of the motion keeps organized, even at very large Reynolds numbers. In two-dimensional turbulence (a topic which originates mainly from geophysical fluid dynamics), the turbulent fields are dominated by the existence of long-lived localized eddies (Fig. 1) which generates spontaneously in a large range of forcing and dissipation mechanisms (Basdevant *et al.*, 1981) and of initial conditions for decay experiments (McWilliams, 1984). Inside these eddies, the vorticity is strongly correlated with the streamfunction, inhibiting the nonlinear interactions. The slope of the energy spectrum is not universal but depends on the forcing and is always steeper than the value -3 predicted by the classical theory ([1]). Although organized eddies block the direct enstrophy cascade in their own domain, the vorticity behaves essentially as a passive scalar in the interstitial fluid, where it can be shown (Babiano *et al.*, 1984) that Kolmogorov theory still applies ([2]). Then the main sources of dynamical unpredictability lie in the irregular motion of the eddies, close enough to the Hamiltonian dynamics of point vortices, in their generation and decay processes which occur on long time scales and in inelastic collisions between eddies. Obviously, theories based only on scale-invariance are too simple to account for the spectral variability

([1]) The attention was focused during many years on the shape of the energy spectrum, which is the sole aspect of the dynamics that statistical closure theories were able to deal with.

([2]) These results, first established with medium resolution numerical experiments have been recently plainly confirmed in high resolution studies conducted by R. Benzi and collaborators.

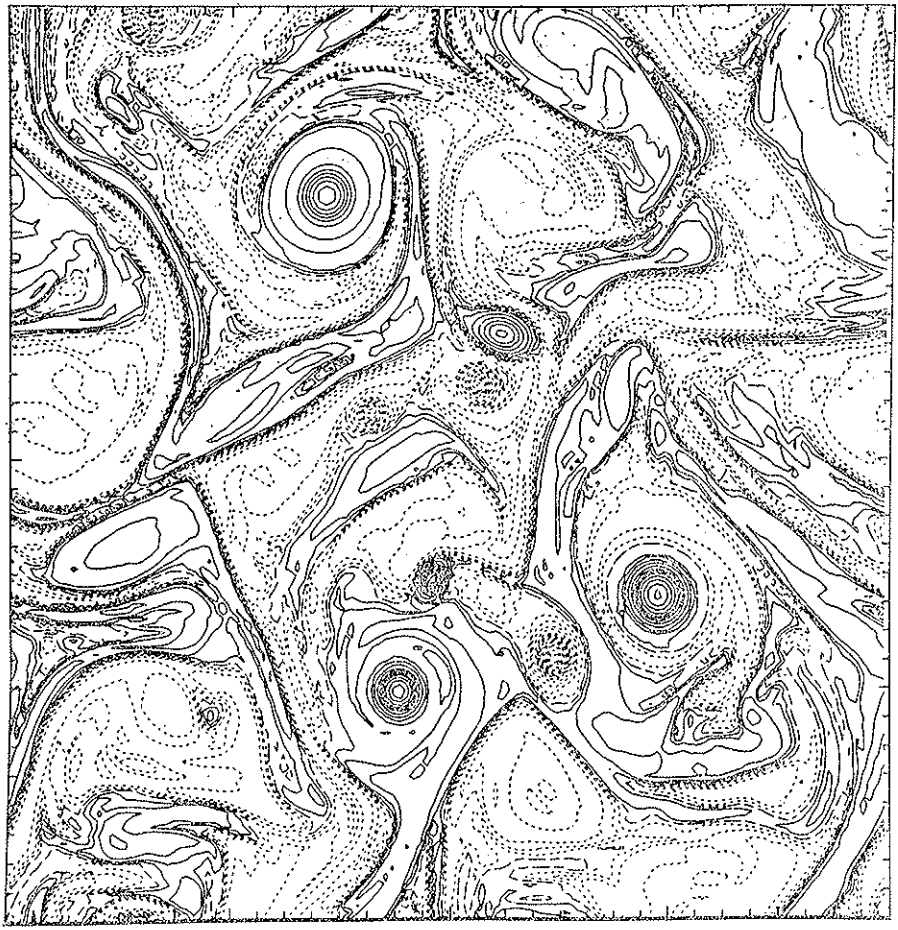

FIG. 1. Vorticity chart taken from a forced experiment in two-dimensional turbulence with resolution 128 × 128. Solid: isolines for positive vorticity. Mixed: isolines for negative vorticity. The interval between contours increases exponentially with the absolute value of the vorticity for small values, then increases linearly for large values. This allows to show details of the vortices and of the interstitial region on the same chart. However, the strong gradients seemingly observed near isoline 0 are not real but only due to this representation.

and the spatial coherence obtained in numerical simulations: what we need is a more extensive understanding based on the multiplicity of actual flow behaviors.

Localized barotropic long-lived eddies are not only produced in numerical experiments. They are observed in the ocean (the Ring Group, 1981) and laboratory experiments (Hopfinger *et al.*, 1982; Couder, 1984). In the atmosphere, the internal Rossby radius of deformation is much larger than in the ocean and does not allow to neglect the planetary advection for any barotropic motion. It is thus unlikely to observe localized axisymmetric barotropic eddies but other forms of local solutions may obtain where the absolute vorticity (instead of the relative vorticity) is correlated with the streamfunction. The modon type of solution (Flierl *et al.*, 1980; Verkley, 1984) is a well-known case and its striking similarities with the blocking dipole has been noticed in several instances (McWilliams, 1980; Pierrehumbert and Malguzzi, 1984). More general types of barotropic solutions have been proposed by Malguzzi and Manalotte-Rizzoli (1982) and extension to baroclinic flows was performed by several authors (see Flierl *et al.*, 1980). These simple theoretical solutions are somewhat idealized with respect to real flows and correspond to some particular situations, nevertheless it is generally observed that persistent organized motion in the atmosphere, such as strong blocking cases, exhibits a high degree of balance between the advection and the auto-deformation of the averaged flow (Holopainen and Fortelius, 1986). It would be extremely interesting to see directly whether this corresponds to a functional relationship between the potential vorticity computed in isentropic coordinates (Hoskins *et al.*, 1985) and the streamfunction.

Although we have been dealing so far with free solutions, the existence of coherent structures is strongly connected with the problem of the atmospheric response to a stationary forcing. In order to explain the temporal variability of quasi-stationary waves, Charney and De Vore (1979) proposed that form-drag instability due to the interaction of the mean zonal flow with the orography might lead to two different regimes, with respectively low and high index, between which transitions are induced by synoptic perturbations. Following this idea Legras and Ghil (1985) studied an hemispherical barotropic T9 model with a simplified orography. We found that nonlinear saturation of the instability leads to multiple unstable stationary solutions with spatial patterns splitting into two families, zonal and blocked regimes, Fig. 2 and 3. The time dependent evolution shows complex chaotic behavior, characterized by the existence of recurrent

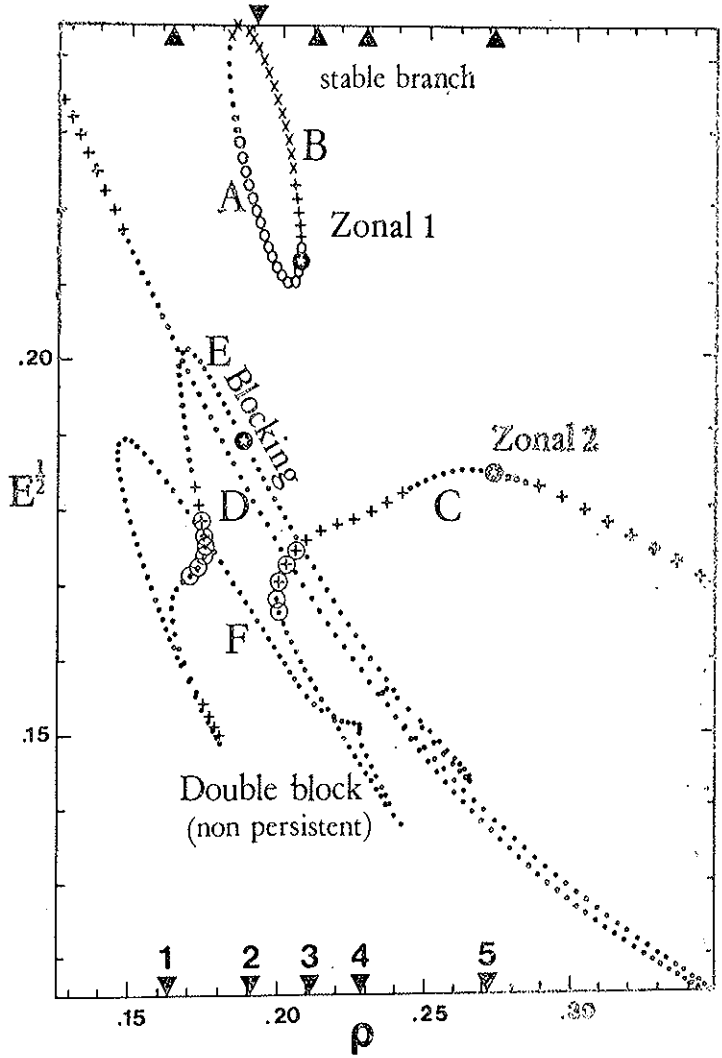

FIG. 2. Stationary solution branches for the barotropic vorticity equation on the sphere with orographic forcing and relaxation towards a prescribed equilibrium for the zonal wind. ρ on the horizontal axis is the amplitude of the forced zonal wind (in arbitrary units) and E is the potential energy of the solution. The solutions are obtained through a Newton's method combined with a continuation algorithm. The various symbols denote the stability of the solution; cross denotes stable solutions, all other solutions are unstable with a small number of eigenvalues with positive real parts. They are however attracting time-dependant solutions in phase space along their stable manifold and thus are correlated with quasi-stationary structures.

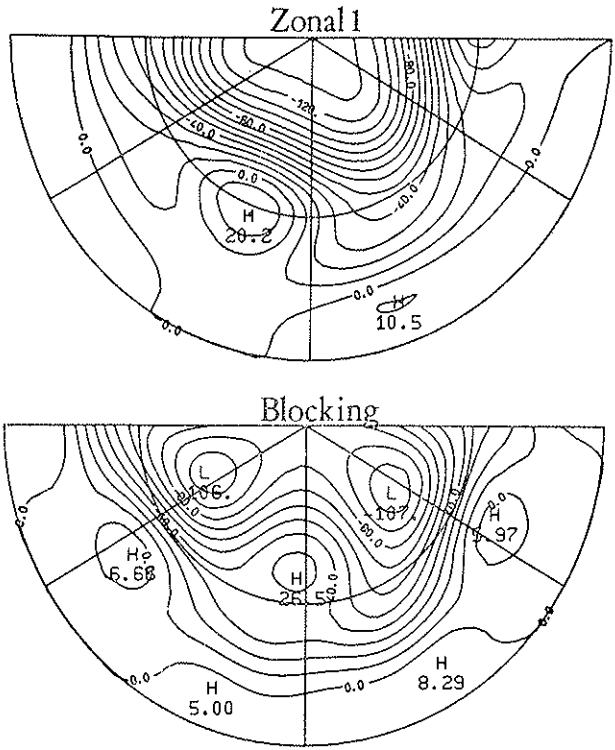

FIG. 3. Flow patterns of the stationary solutions indicated by stars in Fig. 2. This is a conformal conical projection of ratio 2/3. The two half-circles in the figure correspond to the equator and 45°N. Topography high is contained in the first quadrant on the right of the central meridian. a: zonal 1-type solution on branch B; b: blocking-type solution on branch E.

persistent sequences in the vicinity of the unstable equilibria. The statistics of persistence does not show any preferred duration but a characteristic exit time depending on the forcing parameter, so that either blocking or zonal regime may dominate. The pointwise predictability, i.e., the rate of divergence of two nearby trajectories, is also regime dependent. It is found in this model that the conditions of blocking dominance possess increased predictability with respect to the conditions of zonal dominance.

It is interesting to notice that the behaviour of extremely simple models which can be investigated in depth present some striking similarities with the atmosphere. However the mechanism involved and the range of

parameters can only be justified on a heuristic basis. The form-drag instability requires strong driving of the zonal wind coupled with strong orographically induced flux of energy from the zonal flow to the waves, much larger than observed. Indeed there exists no clear way to simulate in a purely barotropic model the barotropic conversion that dominates the generation of eddy kinetic energy in the atmosphere.

The need of form-drag conversion disappears in studies which follow a baroclinic approach. Charney and Strauss (1980) and Benzi *et al.* (1986) found that stationary baroclinic instability can be triggered by orography while involving essentially baroclinic conversion to maintain the waves. Reinhold and Pierrehumbert (1982) showed that a low order baroclinic model with orography exhibits different regimes in the sense that trajectories in phase space seem to be confined in at least two rather separated clouds with transitions between them induced by synoptic scales.

From the observational standpoint, the very existence of multiple regimes is still controversial. There exist indications of such behavior in Dole and Gordon (1983) but it is only recently (Benzi *et al.*, 1986) that clear bimodality was detected in the wave activity ([3]). One may also remark that easily identified strong cases of anomaly account for a relatively small part of the data and that classification of synoptic situations, using purely statistical technics, remains always ambiguous and somewhat subjective (Key and Crane, 1986).

Nonlinear baroclinic equilibration

The most serious difficulty in obtaining a self-consistent baroclinic theory of quasi-stationary waves is how to take in account the effect of non-stationary synoptic waves. If one wishes to end with a closed set of equations on large-scale waves only, a parameterization or computation of the effect of unresolved scales must be provided. Usually, a diffusive approximation is used (White and Green, 1982) but it cannot take in account any positive feedback on the large scales ([4]). The use of the most

([3]) This suggests that even if several regimes can be separated, a large continuum of states lies between them which might be impossible to classify.

([4]) A common but erroneous belief is that all that is small, like transient fluxes of vorticity, does not play a significant role in the dynamics. Scaling arguments must be considered with caution when free non-linear modes are involved. More specifically, in this case the existence of a balance between large-scale advection and auto-deformation

unstable modes with assigned finite amplitude has been also suggested to account for transient effects on the mean flow (Frederiksen, 1982) but clearly the atmospheric energetics does not reduce to this simple linear feature (Gall, 1976; Simmons and Hoskins, 1978). It is the aim of this section to show that a quantitative study of the feedback effect can be performed providing the validity of temporal scale separation between large-scale quasi-stationary waves and synoptic transients.

We concentrate on the problem of Atlantic blocking, for which several recent studies (Illari and Marshall, 1983; Hoskins *et al.*, 1983; Holopainen and Fortelius, 1986) have stressed the importance of synoptic-scale activity in the onset and maintenance of the block. The ability of diffluent jets to be reinforced by travelling disturbances was shown by Shutts (1983) in a purely barotropic framework. His result suggests a baroclinic mechanism of blocking generation, already mentioned by Hoskins *et al.* (1983), which does not involve any dynamical orographic effect. Namely, baroclinic disturbances generated in large shear areas on Eastern margins of the continents mature as they propagate downstream along storm tracks, turning to barotropic profile, and transfer their energy to large-scale barotropic dipoles at the exit of the storm track.

In order to test this idea, we investigate a standard two-layer quasi-geostrophic model in a periodic channel in which a localized baroclinic jet is maintained, Fig. 4 ([5]). The parameters are chosen within the range of realistic values. The mean wind ($U_1 = 14{,}5$ ms^{-1} and $U_2 = 9{,}5$ ms^{-1} in the upper and lower layer respectively) is such that the external mode (3,2) is stationary. The most unstable mode of the basic profile is shown in Fig. 5, for the upper layer; it exhibits a wavenumber 8 structure with a maximum amplitude half a wavelength-downstream of the maximum shear and an e-folding time equal to 5 days.

When integrated in time over a long period, the model exhibits a complex dynamical behavior with an average circulation dominated by a baroclinic jet extending downstream of the forced solution. Through space-time Fourier analysis (Hayashi, 1982), the variance can be shown

does not determine entirely the observed circulation. Thus a weak but coherent forcing is able to select the actual flow among accessible ones. Basically, this is analogous to say that geostrophic balance does not determine by itself the circulation, most of the story is in the "quasi".

([5]) More extensive discussion will be found in Legras and Vautard (1986) and in two forthcoming papers.

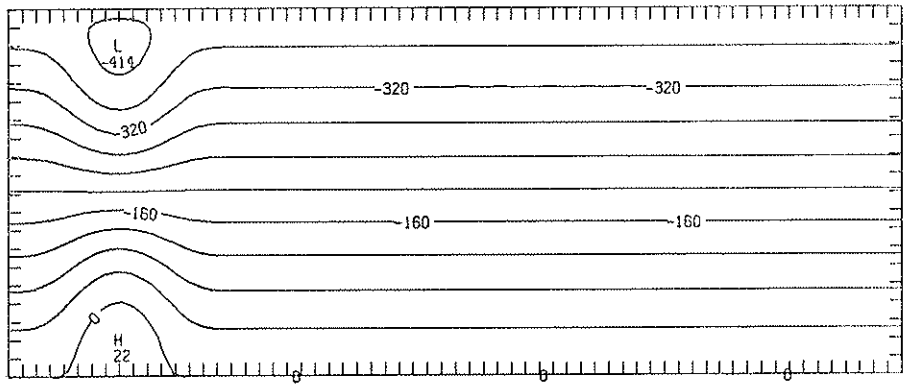

FIG. 4. Streamfunction of the imposed stationary solution in the upper layer.

to split between large-scale quasi-stationary waves ($k \leqslant 3$) and synoptic-scale travelling waves. The latter component is centered in the middle of the channel with a maximum at the exit of the jet; the former has maximum contributions from areas downstream of the jet and off the axis of the channel. Indeed, visual inspection of daily maps reveals alternation of periods during which the perturbations develop and propagate along a storm track downstream of the jet and periods characterized by

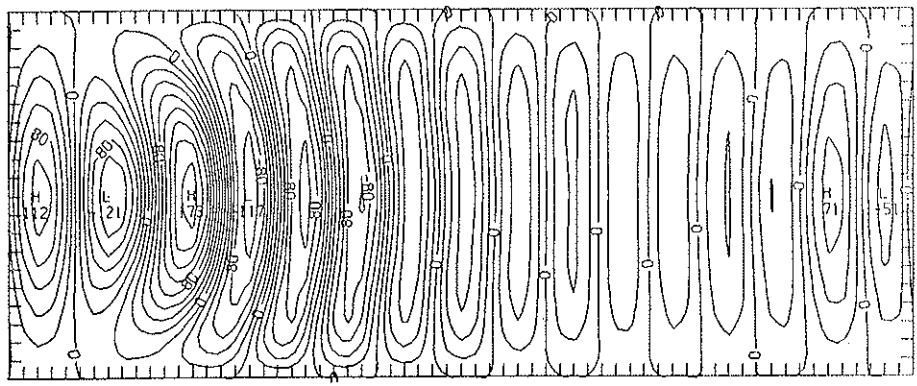

FIG. 5. Instantaneous upper layer streamfunction of the most unstable linear mode for the basic circulation shown in Fig. 4.

strong diffluence of the wind at the exit of the jet which blocks the perturbations.

In order to identify more quantitatively the suggested regimes, we consider the equilibration problem where the large-scale waves are stationary and where the contribution of small-scale waves is evaluated through a suitable time averaging. In shorthand notations, the problem is formulated as

$$O = L = A(L, L) + B(L, \bar{S}) + C(\overline{S, S}) + D(L) \qquad (1)$$

where L stands for the large-scale components of the flow (actually 28 components) and S for the small-scale components. A, B and C are non-linear terms which couple the large-scale components together and with small-scale components. D groups all the linear terms, planetary advection, dissipation and large-scale part of the forcing. The overbar denotes a time average. In order to use minimization procedures and since L is a vector in phase space with 28 components, we define a cost function as

$$J = \langle L, L \rangle$$

where $\langle ., . \rangle$ is a scalar product, actually the energy of the tendency L.

Starting from a given distribution of large-scale components L_0, we want to minimize J and eventually converge to zero. We use a conjugate-gradient algorithm (Gill *et al.*, 1982) which requires knowledge of the gradient of J with respect to the components of L. It is quite straighforward to obtain by formal differentiation the contribution from the terms which depend only on L in the right hand side of (1). The main difficulties arise with the computation of the B and C terms and their gradients. The method used here, in which lies the originality of this study, is to integrate first the model for a very long time and then to use the archived history records as an interactive data base in the optimization process.

$\bar{S}$ and the transients forcing $\overline{C(S, S)}$ are obtained for a given L from a sample of the archived records which satisfy a proximity criterion to L based on the large-scale components only. More precisely, we record the following quantities each five days of a run of 15000 days: the large-scale components L_i the small-scale components $\hat{S}_i$ and transient flux $\hat{C}_i(S, S)$ averaged over five days where i denotes sampling time. Then for a given L, we define

$$\bar{V}(\tilde{L}) = \frac{\sum_i \phi(\|\tilde{L} - L_i\|) \cdot S_i}{\sum_i \phi(\|L - L_i\|)}$$

and

$$\hat{C}(\tilde{L}) = \frac{\sum_i \phi(\|\tilde{L} - L_i\|) \cdot \hat{C}_i}{\sum_i \phi(\|\tilde{L} - L_i\|)}$$

where $\phi(d)$ is a smooth proximity function which verifies $\phi(0) = 1$; $\phi(d) = 0$ for $d > d_0$. The radius d_0 is chosen such that about 200 records are selected among 3000.

From this point and since ϕ is differentiable, there are no considerable difficulties in getting the gradient of V and C through calculation of adjoint operators (Le Dimet and Talagrand, 1986).

As expected from preliminary analysis, the above method is able to distinguish two different regimes, zonal and blocked, displayed in Figs. 6 and 7. Fig. 8 shows the variations of the cost function J as L is interpolated and extrapolated in phase space from the two solutions shown in Figs. 6 and 7. 0 stands here for the zonal solution and 1 for the blocked solution. The two solutions are clearly separated and the residual cost is five orders of magnitude smaller than values obtained for interpolated fields.

It is now important to investigate in which respect the small-scale fluxes are different from one of the two regimes to the other. Figs. 9 and 10 show the contribution due to the $\overline{C(S, S)}$ term in both cases. A first effect is to extend the jet downstream with the strongest tendency in the lower layer, i.e., with damping of the baroclinicity. In the blocked regime this effect extends less downstream than in the zonal case but the mid-channel is occupied by a reverse structure which forces the diffluence of the jet and the generation of blocking dipole. The other terms of the budget can be shown to damp the quasi-stationary wave.

An interesting consistency check is to compute the most unstable mode for both solutions of Figs. 6 and 7. In the blocking case, Fig. 11.b, the perturbations are constrained to split half a wavelength downstream of their maximum amplitude although in the zonal case, Fig. 11.a, they travel straight away, two wavelengths and a half downstream of their maximum.

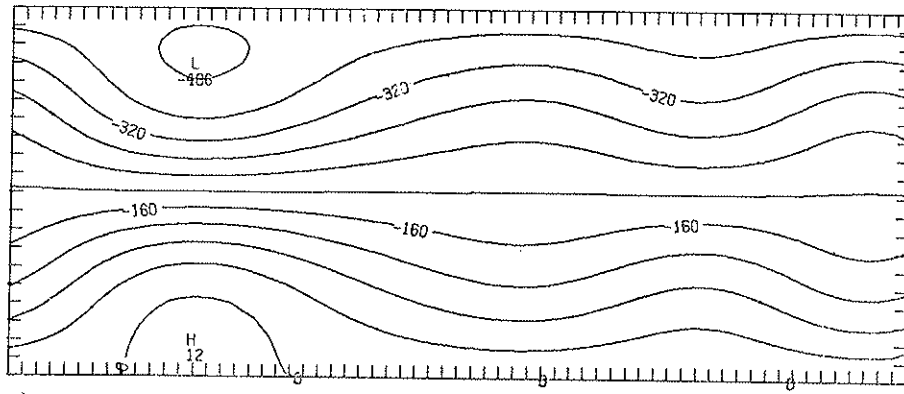

a)

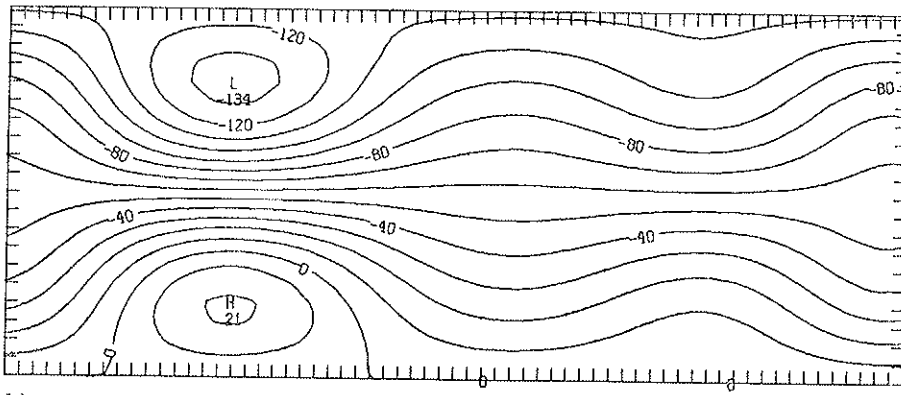

b)

FIG. 6. Streamfunction of the zonal-type equilibrium. a) upper layer; b) lower layer.

Thus, the small-scale transients play an essential role in maintaining the quasi-stationary waves in our model. Although this analysis is based on spatial scale separation and not on time filtering, it is perfectly consistent with the observations of Hoskins *et al.* (1983) on time-filtered high-pass transients. Moreover, if we add our terms A and B we recover a pattern similar to their low-pass forcing of the mean flow. The novelty here is that we are able to distinguish two different flow regimes, with respectively zonal and blocking patterns, which correspond to two different balances of the right hand side of (1).

Discussion and further prospects

Due to the nonlinear character of their dynamics, geophysical flows exhibit a large variety of complex behavior. Far from being purely dissipative, nonlinear interactions generate some organised forms of motion, a few examples of which have been given in this paper. Although such properties are known for many years (e.g., Starr, 1968), it is only recently that intensive use of numerical simulations and advanced diagnostic tools has allowed a quantitative approach to these questions. The use of variational methods combined with estimations of dynamical tendency has been illustrated in the previous section. We showed that this approach allows a precise study of the interactions between large-scale waves and

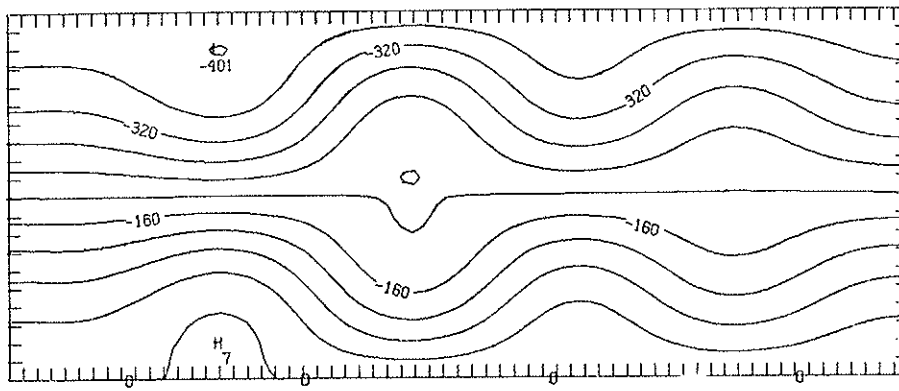

a)

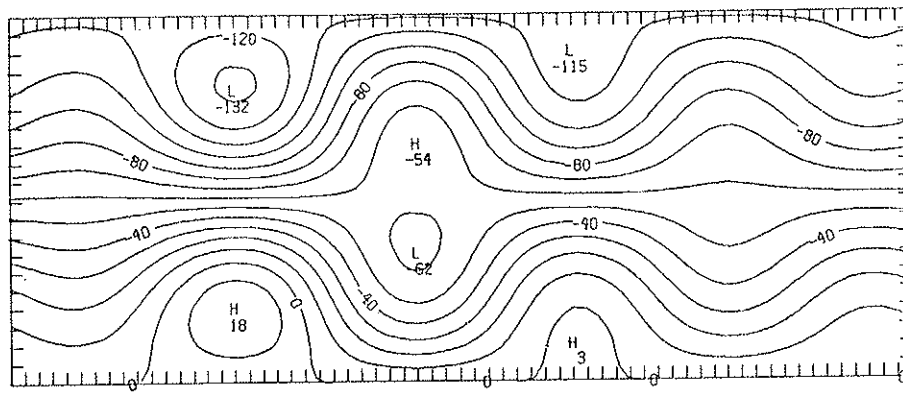

b)

Fig. 7. Same as fig. 7 for the blocking-type equilibrium.

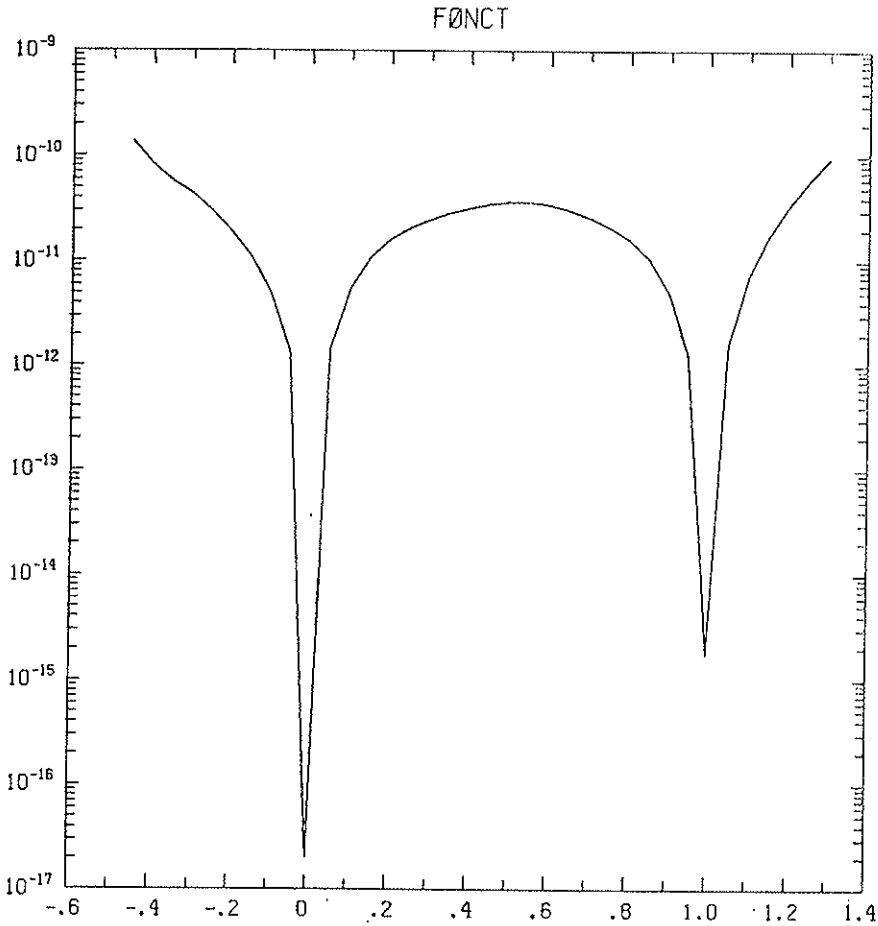

FIG. 8. Variation of the cost function J on the line of phase space which contains the two equilibria shown in Figs. 6 and 7. 0 stands for the zonal solution and 1 for the blocked solution.

small-scale transients and more specially of their respective dependency. It provides also a systematic and efficient mean to identify typical weather regimes from a sufficiently long dataset. In this respect, the advantage over pure statistical approach lies in the incorporation of the dynamical information which avoids the necessity of detailed *a priori* guess on the patterns.

The present study is limited to purely stationary large-scale waves.

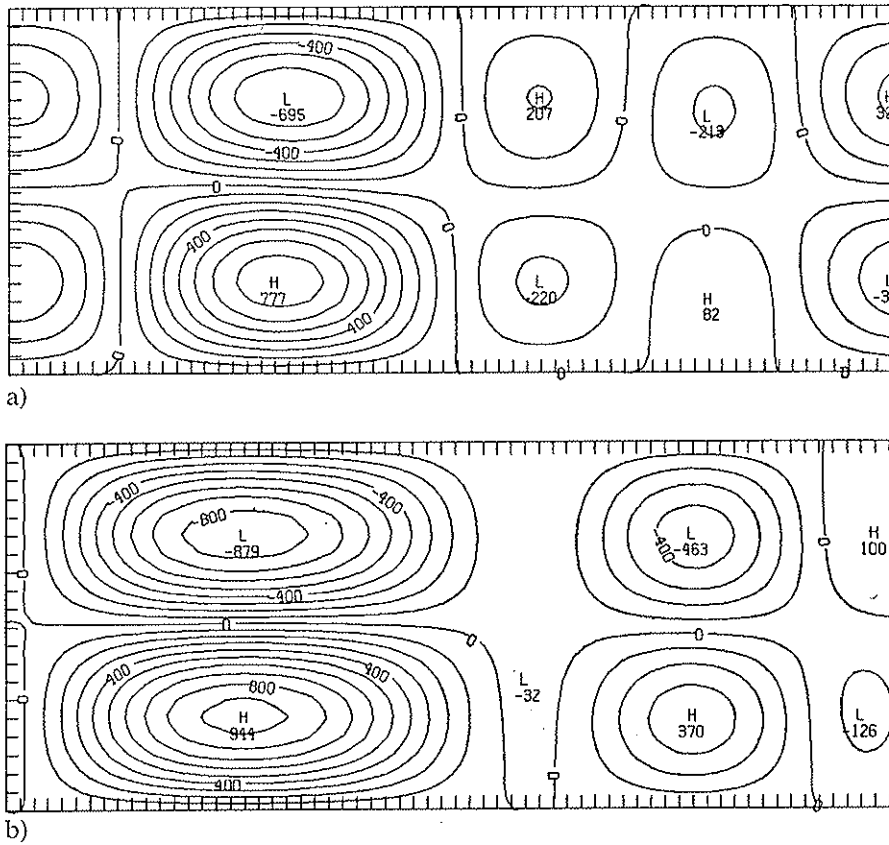

FIG. 9. Contributions of the small-scale term C in (1) to the maintenance of the large-scale equilibrium for the zonal regime. a) upper layer; b) lower layer.

Since a large part of the baroclinic conversion occurs within the large scales, (Chen and Marshall, 1984), it would be desirable to allow for some variability within this domain, with the aim to detect more complicated regularities than quasi-stationary flows. In principle, there is no difficulty in generalizing the method used here to large-scale regular vacillation (limit cycle) but some efforts are still needed to break the involved computational cost.

A second limitation is that as soon as transients are involved there is no easy way to explore the domain of parameters. This question is essential if one wishes to understand the climate response to a variation of external conditions. An interesting method, based on the use of adjoint

equations, was proposed by Cacucci and Hall (1984) to compute the gradient of a given functional with respect to a whole set of climatic parameters. However, their computation is formally identical to the study of sensitivity to a set of initial conditions (Le Dimet and Talagrand, 1986) and this does not lead to convergent gradients for a chaotic system. There are possibilities to cure the deficiency through combination with the Monte Carlo method or the filtering of the diverging part of the climatic propagator, which are presently under investigation.

Finally, we want to stress the fact that the increasing interest for long-range forecasts raises a new series of questions for modelers which differ significantly from the ones posed by short and medium range

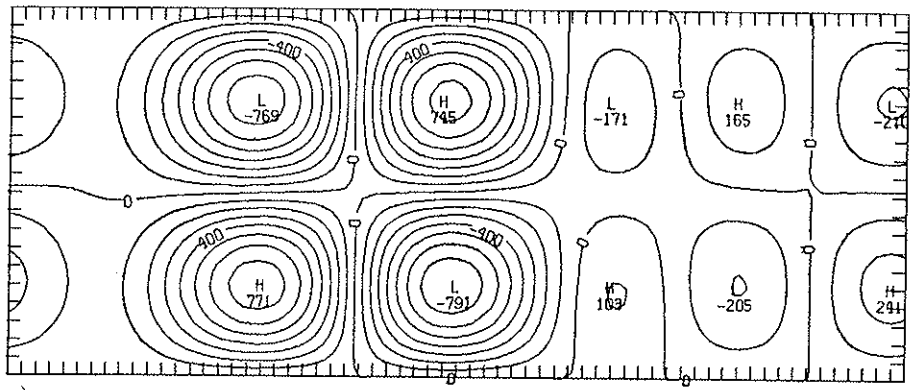

a)

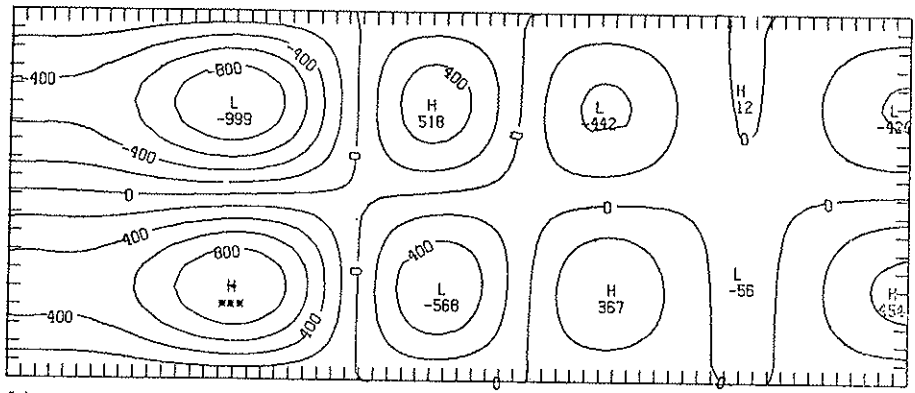

b)

FIG. 10. Same as Fig. 8 for the blocking-type equilibrium.

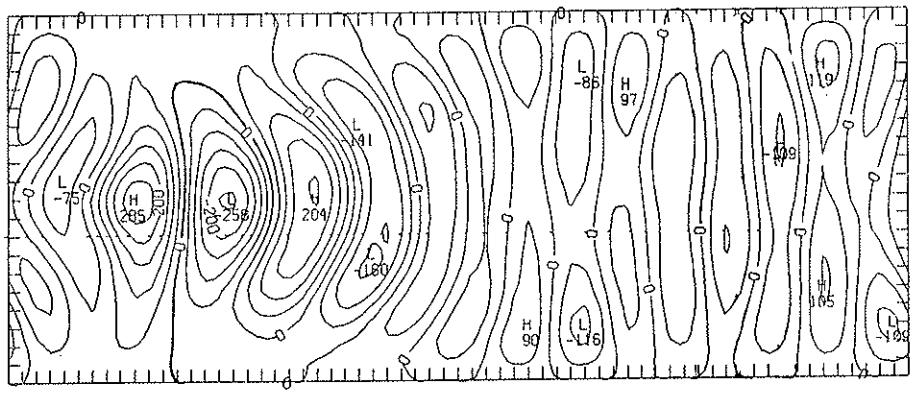

a)

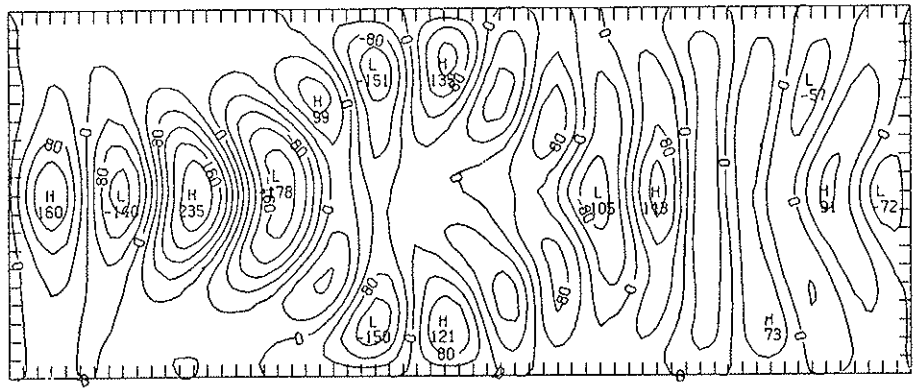

b)

FIG. 11. Instantaneous upper layer streamfunction of the most unstable linear mode. a) for the zonal circulation shown in Fig. 6; b) for the blocked circulation shown in Fig. 7.

forecast. In the latter case, we are dealing essentially with a detailed prediction of what is considered as transients in the former case. Within deterministic predictability limit of a phenomenon, there is no doubt that a detailed representation using precise initial data will always supersede any simpler statistical-dynamical approach. The road to follow does not appear as clear for long-range forecasts. In this case, "the task is seen to be as much one of deciding what best to predict as how to predict" ([6]). We must clearly use the advantages of the best available

([6]) Quoted from Tung and Rosenthal, 1986.

GCM to run long-range forecasts but it is not less clear that the general choice to predict ten-day or one-month averages of global fields is not the best that we can do. A serious limitation to our ability to produce long-range forecast is our lack of knowledge of the low frequency variability. Notable progress was made in the last few years, but still key questions, like the existence of multiple weather regimes or the coupling between tropics and mid-latitudes, remain controversial and far from being operational tools. The detailed study of low-frequency regularities appears as a formidable task if it is directly conducted within the framework of GCM's or observations. In addition, we believe that new tools are necessary for the analysis in order to deal with the full non-linearity of the dynamics. Several approaches like pattern recognition techniques or statistical-dynamical equilibration, as shown here, may prove valuable for the future. However it would be extremely costly to test extensively such ideas with a high resolution GCM.

Simple models (from quasi-geostrophic models to a T21-GCM) provide a framework where perfect experiments can be done easily. Their behaviour differs significantly from the observed atmosphere but is probably realistic enough to test the adequacy of long-range forecast methods, to gain rapidly some experience with them and to improve them. In addition, if one considers a series of imbedded models of increasing complexity, quantitative results obtained at one level may reasonably serve as a first guess at an upper level.

Of course, this does not mean that we must deny ourselves using the best available models to produce long-range forecast but a lot of efforts are still necessary for which using only high resolution GCM might not be the best strategy. The optimal approach will certainly combine extensive case studies with high resolution GCM with theoretical work using simpler models.

REFERENCES

BABIANO A., BASDEVANT C., LEGRAS B. and SADOURNY R., *Dynamiques comparées du tourbillon et d'un scalaire passif en turbulence bi-dimensionnelle.* « C.R. Acad. Sc. Paris », *299*, 601-604 (1984).

BASDEVANT C., LEGRAS B., SADOURNY R. and BELAND M., *A study of barotropic model flows: intermittency, waves and predictability.* « J. Atmos. Sci. », *38*, 2305-2326 (1981).

BENZI M., MALGUZZI P., SPERANZA A. and SUTERA A., *The statistical properties of general atmospheric circulation: observational evidence and a minimal theory of bimodality.* « Quart. J. R. Met. Soc. », *112*, 661-674 (1986).

BENZI R., SPERANZA A. and SUTERA A., *A minimal baroclinic model for the statistical properties of low frequency variability.* Technical Report 6513-4082, IBM-ECSEC (1986).

CACUCCI D.G. and HALL M.C.G., *Efficient estimation of feedback effects with application to climate models.* « J. Atmos. Sci. », *41*, 2063-2068 (1984).

CHARNEY J.G., FJORTOFT R. and VON NEUMANN J., *Numerical integration of the barotropic vorticity equation.* « Tellus », *2*, 237-254 (1950).

CHARNEY J.G. and DEVORE J.G., *Multiple flow equilibria in the atmosphere and blocking.* « J. Atmos. Sci. », *38*, 1205-1216 (1979).

CHARNEY J.G. and STRAUSS D.M., *Form-drag instability, multiple equilibria and propagating planetary waves in baroclinic, orographically forced, planetary waves systems.* « J. Atmos. Sci. », *37*, 1157-1176 (1980).

CHEN T.S. and MARSHALL H.G., *Time variation of atmospheric energetics in the FGGE winter.* « Tellus », *36A*, 251-268 (1984).

COUDER Y., *Two-dimensional grid turbulence in a thin liquid film.* « J. Phys. Lett. », *45*, 353-360 (1984).

DOLE R.M. and GORDON N.D., *Persistent anomalies of the extratropical Northern Hemisphere winter time circulation: Geographical distribution and regional persistence character.* « Mon. Wea. Rev. », *111*, 1567-1586 (1983).

FLIERI G.R., LARICHEV V.D., MCWILLIAMS J.C. and REZNIK G.M., *The dynamics of baroclinic and barotropic solitary eddies.* « Dyn. Atmos. Oceans », *5*, 1-41 (1980).

FREDERIKSEN J.S., *A unified three-dimensional theory of the onset of blocking and cyclogenesis.* « J. Atmos. Sci. », *39*, 969-982 (1982).

GALL R., *A comparison of linear instability theory with the eddy statistics of a general circulation model.* « J. Atmos. Sci. », *33*, 349-373 (1976).

GILL P.E., MURRAY W. and WRIGHT M.H., *Practical optimization.* Academic Press, London, 401 pp. (1982).

HAYASHI Y., *Space-time spectral analysis and its applications to atmospheric waves.* « J. Meteor. Soc. Jap. », *60*, 156-171 (1982).

HOLOPAINEN E. and FORTELIUS C., *On the role of high frequency transient eddies in a blocking-type flow.* Long-Range Forecasting Reports, *6*, WMO/TD N° 87, WMO, Geneva (1986).

HOPFINGER F., BROWAND F.K. and GAGNE Y., *Turbulence and waves in a rotating tank.* « J. Fluid Mech. », *125*, 505-534 (1982).

HOSKINS B.J., JAMES I.N. and WHITE G.H., *The shape, propagation and mean-flow interaction of large scale weather systems.* « J. Atmos. Sci. », *40*, 1595-1612 (1983).

HOSKINS B.J., MC INTYRE M.E. and ROBERTSON A.W., *On the use and significance of isentropic potential vorticity maps.* « Quart. J. R. Met. Soc. », *111*, 877-946 (1985).

ILLARI L. and MARSHALL J.C., *On the interpretation of maps of eddy fluxes during blocking episodes.* « J. Atmos. Sci. », *40*, 2232-2242 (1983).

KEY J. and CRANE R.G., *A comparison of synoptic classification schemes based on "objective" procedures.* « J. Climat. », *6*, 375-388 (1986).

LE DIMET F.X. and TALAGRAND O., *Variational algorithms for analysis and assimilation of meteorological observations: theoretical aspects.* « Tellus », *38A*, 97-110 (1986).

LEGRAS B. and GHIL M., *Persistent anomalies, blocking and variations in atmospheric predictability.* « J. Atmos. Sci. », *42*, 433-471 (1985).

LEGRAS B. and VAUTARD R., *Predictability and baroclinic flow regimes.* ECMWF Workshop on Predictability in the Medium and Extended Range, ECMWF, Reading, UK, in press (1986).

MALGUZZI P. and MANALOTTE-RIZZOLI P., *Nonlinear stationary Rossby waves on nonuniform zonal winds and atmospheric blocking.* Part I: *The analytical theory.* « J. Atmos. Sci. », *41*, 2620-2628 (1984).

MCWILLIAMS J.C., *An application of equivalent modons to atmospheric blocking.* « Dyn. Atmos. Oceans », *5*, 43-66 (1980).

MCWILLIAMS J., *The emergence of isolated, coherent vortices in turbulent flows.* « J. Fluid Mech. », *146*, 21-43 (1984).

PIERREHUMBERT R.T. and MALGUZZI P., *Forced coherent structures and local multiple equilibria in a barotropic atmosphere.* « J. Atmos. Sci. », *41*, 246-257 (1984).

REINHOLD B.B. and PIERREHUMBERT R.T., *Dynamics of weather regimes: Quasi-stationary waves and blocking.* « Mon. Wea. Rev. », *110*, 1105-1115 (1982).

RING GROUP, *Gulf stream cold core rings: their physics, chemistry and biology.* « Science », *212*, 1091-1100 (1981).

SHUTTS G.J., *The propagation of eddies in diffluent jetstreams: eddy vorticity forcing of blocking flow fields.* « Quart. J. R. Met. Soc. », *109*, 737-761 (1983).

SIMMONS A.J. and HOSKINS B.J., *The life cycles of some nonlinear baroclinic waves.* « J. Atmos. Sci. », *37*, 1679-1684 (1978).

STARR V.P., *Physics of negative viscosity phenomena.* McGraw-Hill, New York (1986).

STONE R.H., *A simplified radiative-dynamical model for the static stability of rotating atmospheres.* « J. Atmos. Sci », *29*, 405-426 (1972).

TUNG K.K. and ROSENTHAL A.J., *On the extended-range predictability of large-scale quasi-stationary patterns in the atmosphere.* « Tellus », *38A*, 333-365 (1986).

VERKLEY W.T.M., *The construction of barotropic modons on a sphere.* « J. Atmos. Sci. », *41*, 2492-2504 (1984).

WHITE A.A. and GREEN J.S.A., *A non-linear atmospheric long wave model incorporating parameterizations of transient baroclinic eddies.* « Quart. J.R. Met. Soc. », *108*, 55-85 (1982).

THEORY OF MULTIPLE EQUILIBRIA IN QUASI GEOSTROPHIC FLOWS

R. BENZI
IBM, European Center for Scientific and Engineering Computing
Rome, Italy

ABSTRACT

In this paper we review recent developments of multiple equilibria theory for quasi geostrophic flows. It is shown that in a baroclinic atmosphere wave/wave interaction is able to produce multiple equilibria for the same value of the zonal flow by folding of the orographic resonance. This is in agreement with the observed statistical properties of atmospheric circulation at middle latitudes which show a distinct bimodality of the probability density of planetary waves and a unimodal distribution for all the zonal components. The case of extension of the theory to realistic orography is also discussed.

1. INTRODUCTION

One of the most challenging problems in Dynamic Meteorology is to explain the General Circulation of Earth Atmosphere and its variability on all time scales. As a matter of fact the difficulty we face in trying to solve this problem is a measure of our limited ability in deducing the observed circulation from the equations governing the evolution of the relevant physical quantities (Lorenz, 1967). Our ultimate goal could be to discover a limited number of basic physical processes which can completely explain the General Circulation of the Atmosphere, namely its average flow and the statistical properties of its time fluctuations.

At present it is impossible to foresee if such a goal can ever be achieved. Nevertheless for a well defined space-time domain the task seems to be possible. It is certainly true, for instance, that the dynamics of baroclinic instability dominates the midlatitudes circulation on a time scale of about 2-4 days. The discovery of this basic instability in the atmosphere played a major role in the achievement of numerical weather forecast as we know it today. However, on a longer time scale (about 10 days) the observed atmospheric variability cannot be explained in terms of ordinary baroclinic instability. Although the major source of energy is still available potential energy, on time scales of about 10 days most of the observed variability (hereafter referred to as low frequency variability) is concentrated on ultralong stationary waves of about 10,000 km in wave length (see for example Freidrich and Bottger, 1978). Associated with this stationary variance there are rather well known meteorological phenomena such as "blocking situations" that are usually described in terms of persistent stationary anomalies of the average general circulation.

Any theory of the low frequency variability deals with the dynamics and the statistics of ultralong planetary waves. Many authors have devoted their attention to this topic in the last few years. Among others Charney and DeVore (1979 hereafter CDV) and, independently, Wiin-Nielsen (1979) have introduced the idea that the dynamics of ultralong planetary waves is characterized by a large scale instability with zero phase velocity and rather small growth factor. Hence, large scale flows can grow in place with a time scale within the range of low frequency variability. Nonlinear equilibration of the large scale instability leads to multiple regimes for the atmospheric circulation. One of these regimes can be tentatively identified with a blocking circulation. This theory, as it was formulated initially, suffers of major inadequacies. For instance, in the CDV paper it can be shown that the predicted variance of the zonal flow is unrealistic for any reasonable choice of the model parameters.

After an initial interest, the theory of multiple equilibria was partly disregarded. Probably this was due to systematic inconsistencies revealed by the comparison between predicted and observed circulations: it was not even clear which were the variables to select from observations in order to test the theory. This was very well remarked by Wallace and Blackmon (1983): "..., in absence of a rather specific theoretical guidance, it is difficult to know how to select, from among the myriad of possibilities, the most revealing representations of the state of the general circulation in multi-dimensional phase space". Recently this problem has been

addressed in a series of works by Benzi, Malguzzi, Sutera and Speranza (hereafter BMSS), Sutera (1986), Hansen (1986). On the basis of theoretical considerations, the sum of the square power of the zonal wavenumber 2, 3 and 4 of the Fourier transform of the geopotential height average between 30 and 75 degrees North was selected as indicator of low frequency variability. The probability density estimator of this variable shows a distinct bimodality (see the paper by Sutera in this volume). This observational result strongly suggests that the theory of multiple equilibria can be indeed valid. However the original formulation by CDV and Wiin-Nielsen must be revised in order to fit the observed statistical properties.

In BMSS, Benzi Speranza and Sutera (1986) and Benzi *et al.* (1986) a new theoretical approach to the multiple equilibria theory of the atmospheric circulation has been pursued. The aim of this paper is to review the results so far obtained. We shall be mostly concerned with the physical ideas on which the theory is built, trying to avoid mathematical difficulties and algebraic computations. The readers are referred to the above quoted papers for more technical details.

2. Barotropic theories of multiple equilibria

Let us consider a channel of width D centered at middle latitudes. By x and y we shall denote the zonal and the meridional coordinates in the channel. We intend to study a rather simple model of atmospheric flow at an equivalent barotropic level. In particular we want to understand the dynamics of large scale planetary waves when a smooth orography h is acting on the system.

It is useful to rescale the variables by introducing a characteristic length L and a velocity U_0. Then we can define dimensionless variables in the following way:

$$y', x' = \frac{y}{L}, \frac{x}{L}$$

$$t' = t \frac{U_0}{L}$$

$$\Psi' = \frac{\Psi}{U_0 L}$$

$$h' = \frac{h f_0 L}{H U_0}$$

$$\beta' = \frac{\beta L}{f_0} .$$

Here Ψ is the stream function of the system, $f_0 = 2\Omega \sin \varphi_0$ and $\beta = 2\Omega/a \cos \varphi_0$ where φ_0 is the latitude at the center of the channel, Ω the angular speed of earth's rotation and a the radius of the earth. In the following we shall use $L = 1000$ km and $U_0 = 10$ m/sec. Then a geopotential perturbation of 100 meters corresponds to $\Psi' = 1$ and the time units are expressed in days. Hereafter we shall omit primes on all variables.

The barotropic vorticity equation of the system is:

$$\partial_t \Delta\Psi + J(\Psi, \Delta\Psi + h + \beta y) = -\nu\Delta\Psi + F \tag{1}$$

where $\nu\Delta\Psi$ is an Eckman damping and F is any external forcing acting on the system.

Let us now consider the following decomposition of Ψ

$$\Psi = -\chi(y, t) + \varphi(x, y, t) \tag{2}$$

where χ_y is the zonal wind of the system. We can always assume χ_y split into two main components:

$$\chi_y = U(t) + S(y, t) \tag{3}$$

where U is the angular momentum of the atmosphere in the channel and $S(y, t)$ the latitudinal shear of the zonal wind. Thus:

$$\int_0^D S(y, t)\, dy = 0$$

i.e., $S(y, t)$ does not project onto the mean angular momentum. Until now no assumption has been made on the dynamics of the system. Inserting (2) and (3) into equation (1) we get:

$$\partial_t [\Delta\varphi - S_y] + J(\varphi, \Delta\varphi) + \beta\partial_x \varphi + J(\varphi, h) + \tag{4}$$

$$S_{yy}\partial_x\varphi + S\partial_x\Delta\varphi + S\partial_x h + U\partial_x\Delta\varphi +$$

$$U\partial_x h = -\nu(\Delta\varphi - s_y) + F$$

We can obtain an equation for S by zonally averaging equation (4):

$$\partial_t S_y = \overline{J(\varphi, \Delta\varphi)} + \overline{J(\varphi, h)} - \nu S_y - \bar{F} \tag{5}$$

By subtracting equation (5) from equation (4) we finally get an equation for φ.

To close the system of equation we still need an equation for the angular momentum U. This cannot be derived from the barotropic vorticity equation (1). We shall therefore use the conservation of momentum on the channel. We get:

$$\partial_t U = \overline{\varphi_x h}^{x} - \nu U + FU \tag{6}$$

Equation (6) is the so called form-drag equation. From a physical point of view it is a statement of the conservation of momentum in the atmosphere (a clear derivation of equation (6) can be found in Buzzi *et al.*, 1984). Equations (4), (5) and (6) form a closed system of equation by which we can discuss the dynamics of our model atmosphere. In principle, we can use a numerical integration of these equations and compare the numerical results with the observed circulations in the atmosphere. For our purpose, however, it is better to choose a different strategy. It is a priori clear that the barotropic vorticity equation will not capture all the dynamical features of the atmospheric circulation. Hence with equations (4), (5) and (6) we can only hope to model the long-time large scale dynamics. In particular in the absence of any orography and with time-independent external forcing, the time average circulation described by equations (4), (5) and (6) will share the symmetries of the external forcing F. Orography can break this symmetry and control the amplitude of the stationary waves. This was essentially the idea underlying the work of Charney and Eliassen (1949 hereafter CE). In its simplest formulation the CE approach is as follows. Let us consider a linear version of equation

(4) for a prescribed zonal wind, where no external forcing is acting on the system and

$$\partial_t \Delta\varphi + \beta\partial_x\varphi + J(\varphi, h) + (U + S)\partial_x h + S_{yy}\partial_x\varphi = -\nu\Delta\varphi \tag{7}$$

To simplify further our problem we assume

$$\varphi = A(x, t)$$
$$h = h(x)$$
$$S = 0 \tag{8}$$

where $h(x)$ is a latitudinal average of the real orography. These assumptions look perhaps too drastic, but the model retains all the essential physical ingredients. Inserting (8) into (7) we obtain:

$$A_{xxt} + \beta A_x + UA_{xxx} + Uh_x = -\nu A_{xx} \tag{9}$$

The stationary solution of equation (9) is:

$$\beta A_x + UA_{xxx} + Uh_x = -\nu A_{xx} \tag{10}$$

Integrating once in x we obtain:

$$A_{xx} + \frac{\nu}{U} A_x + \frac{\beta}{U} A + h = 0 \tag{11}$$

Equation (11) can now be interpreted as a harmonic oscillator in x with a dissipative effect ($\frac{\nu}{U} A_x$) and external forcing (h). Hence the amplitude of A is governed by resonances induced by the orography at the natural spatial "frequency" β/U. Given an average value of U we can predict by equation (11) the average value of the geopotential height A.

We cannot use eq. (11) to make any statement on the dynamics of A and in particular on its low frequency variability. A first attempt in this direction was made by Charney and De Vore (CDV), who considered equation (9) coupled with the corresponding form-drag equation (6), namely:

$$\dot{U} = \overline{A_x h}^x - \nu (U - U^*) \tag{12}$$

In (12) U^* represents any kind of external forcing acting on the system in order to maintain a zonal flow U. Equations (9) and (12) are now a closed set of nonlinear differential equations. The nonlinearity in the system is due to the form-drag term. It is an enlightening exercise to solve equations (9) and (12) for a very simple case, namely, the one wave problem:

$$A(x, t) = A_o \cos(kx) + B_o \sin(kx) \tag{13}$$

Correspondently we choose the orography to be of the form:

$$h = h_o \cos(kx) \tag{14}$$

The stationary solution of this simple problem reads:

$$\begin{aligned} &\frac{\nu}{k} A_o + (U - \beta/k^2) B_o = 0 && (a) \\ &\frac{\nu}{k} B_o - (U - \beta/k^2) A_o = -\frac{Uh}{k^2} && (b) \\ &kB_o h - \nu U = -\nu U^* && (c) \end{aligned} \tag{15}$$

We can easily solve equation (15 a,b) for B as a function of U:

$$B_o = -\frac{\nu h U k}{\nu^2 k^2 + (Uk^2 - \beta)^2} \tag{16}$$

It follows that the stationary solution on the $\beta - U$ plane of our problem corresponds to the intersection of the straight line (15c) with the orographic resonance (16). For a given range of value of U^* we can have more than one intersection, namely three. Two of these stationary solutions are always stable, one is unstable. The existence of this instability and the nonlinear equilibration via the form-drag term are responsible for multiple equilibria in this model.

Equations (15) can also be solved analytically for B_o. A simple computation shows that the non-linear term depends on the ratio (h/ν) i.e., the ratio between forcing and dissipation. This is a consequence of the linearity of the equation (9) in the wave field. Because of the over-simplifications introduced in the dynamics in order to set up the CDV model, we cannot hope to obtain a realistic time-dependent dynamics. However, if the mechanism proposed by CDV is acting in the atmospheric circulation there must be two stationary values both of the wave amplitude and of the zonal flow U corresponding to an increased persistence.

Hence a simple way to test the theory is to compute the probability density estimator for A and U. The CDV theory predicts a bimodal density distribution for both. We are coming near the first drawback of the CDV theory. In CDV the value of U is linearly coupled to the value B_o of the component of the wave field out of phase with respect to the orography. If B_o changes by about 100 m then U changes about 20 m/sec. Such changes of U are not observed. The probability density estimator of U is discussed in detail by BMSS and Sutera (1986) (see also the paper by Sutera in this volume). It does not show any evident sign of bimodal distribution and the variance of U is of the order of few meters per second. Hence the CDV theory is completely inadequate in this respect. Since the form-drag is the essential nonlinear feedback in CDV we are forced to doubt this effect even if it expresses the basic momentum conservation in the channel.

The situation does not change if we consider a more complex latitudinal structure of the zonal wind, i.e., if we consider the effect of a zonal shear $S(y)$ previously neglected. This study has been done by Rambaldi and Mo (1985). $S(y)$ acts essentially as U on the wave field. The stationary value of $S(y)$ depends on two terms: the convergence of momentum and again the form drag. If we consider only one wave, as in the CDV case, the convergence of momentum vanishes identically and we are back to the form-drag as the only source of nonlinear feedback in the system. What happens in this case is that this "surplus" of form-drag is able to

bend the resonance, The bending is proportional to h/ν, i.e., to the form-drag effect on the shear of the zonal flow. We can have multiple equilibria for the same value of U but for very different values of $S(y)$. Again this is not observed in the atmosphere circulation (see the paper by Sutera in this volume). From this overview of the CDV theory we learn that any theory of multiple equilibria must be formulated independently of the dynamics of the zonal flow and its latitudinal shear, at least in a barotropic framework.

To this purpose we have to introduce into the theory a non-linear interaction different from the form-drag one. This has been done by BMSS. The idea is to emphasize the role of wave-wave interaction in the wave dynamics. The simplest possible way of doing this consists in assuming a wave self-interaction as the basic nonlinearity.

Let us assume:

$$\varphi = A(x, t)g(y) \quad (a)$$
$$h = hg(y) \quad (b) \tag{17}$$

where g is not the eigenfunction of the Laplace operator (we can think of g as determined by the orographic profile in latitude). Again we shall neglect S because it does not introduce essential physics in our problem. Then, after some straightforward computation we get:

$$A_{xx} - \alpha^2 A + \delta A A_x + \beta A_x + U(A_{xxx} - \alpha^2 A_x) + Uh_x = -\nu(A_{xx} - \alpha^2 A) \tag{18}$$

where:

$$\alpha^2 = \langle g_y^2 \rangle$$
$$\delta = \langle g g_y g_{yy} \rangle \tag{19}$$
$$\langle g^2 \rangle = 1$$

and $\langle \ldots \rangle$ stands for latitudinal average. The effect of wave self-interaction is to bend the resonance towards super-resonant values of U (see BMSS). At variance with the previous theory we now have a nonlinear effect which is not dependent on the form-drag mechanism, i.e., it is independent of the dynamics of the zonal flow. Hence multiple equilibria

can exist for the same value of the zonal flow. Also in this theory the probability density distribution of the wave amplitude must be bimodal, as in the CDV theory. This property has been checked by BMSS and discussed in detail by Sutera in this volume. A bimodal probability distribution is indeed observed in the atmosphere. Thus the theory of multiple equilibria represented by equation (18) is consistent with observations. We can now turn to the problem of the zonal flow.

3. Form-drag equation and baroclinic energetic

It has been mentioned several times in the previous section that the form-drag equation is not consistent with the observed variance of the zonal wind in the framework of barotropic models. However, the form-drag equation is just the angular momentum conservation and it can be included in any other model of the general circulation. We will show in this section that in a baroclinic atmosphere it is possible to find multiple equilibria for almost the same zonal flow maintaining consistence with the form-drag equation.

In a baroclinic model waves can grow at the expense of the available zonal energy instead of the zonal kinetic energy. Recent analyses by Chen and Marshall (1984) and by Hansen (1986) show that this is the case in the low frequency variability spectrum range. Hence it makes sense to investigate whether in a baroclinic atmosphere the form-drag equation gives multiple equilibria for almost the same zonal flow. Of course this is possible only if the resonance is bent; otherwise we would run into the same difficulties of the barotropic case. The bending of the resonance must not be determined by the interaction with the shear of the zonal flow. We already saw that in this case the effective nonlinear parameter is still the form-drag: a significant bending cannot be achieved without taking a significant energy from the zonal kinetic energy. Therefore the assumption of wave self-interaction is again crucial if we want to obtain a realistic energy cycle. Let us consider a two layer baroclinic model:

$$\begin{aligned} \partial_t q_1 + J(\Psi_1, q_1) &= -\nu\Delta\Psi_1 \\ \partial_t q_2 + J(\Psi_2, q_2) &= -\nu\Delta\Psi_2 \end{aligned} \tag{20}$$

where

$$q_1 = \Delta\Psi_1 + F(\Psi_2 - \Psi_1) + \beta y$$
$$q_2 = \Delta\Psi_2 + F(\Psi_1 - \Psi_2) + \beta y \tag{21}$$

As in the previous section, we shall assume:

$$\Psi_1 = -U_1 y + A_1(x, t)g(y)$$
$$\Psi_2 = -U_2 y + A_2(x, t)g(y) \tag{22}$$
$$h = h_0 g(y)$$

Using (22), (21) and (20) we obtain:

$$\partial_t[A_{1xx} - \alpha^2 A_1 + F(A_2 - A_1)] + U_1\partial_x(A_{1xx} - \alpha^2 A_1) + \beta\partial_x A_1 + \delta A_1 A_{1x} \tag{23}$$
$$+ F(U_1 A_{2x} - U_2 A_{1x}) = -\nu_1(A_{1xx} - \alpha^2 A_1)$$
$$\partial_t[A_{2xx} - \alpha^2 A_2 + F(A_1 - A_2)] + U_2\partial_x(A_{2xx} - \alpha^2 A_2) + \beta\partial_x A_2 + \delta A_2 A_{2x}$$
$$+ F(U_2 A_{1x} - U_1 A_{2x}) + U_2 h_x = -\nu_2(A_{2xx} - \alpha^2 A_2)$$

where α^2 and δ are defined as in section 2. Together with equation (23) we shall consider the form-drag equation for the angular momentum $U = 1/2\,(U_1 - U_2)$ and the equation for the time evolution of the average zonal baroclinicity $m = 1/2\,(U_1 - U_2)$:

$$\partial_t U = \overline{A_{2x} h}^{x} - \nu(U - U^*) \tag{24}$$

$$C\partial_t m = 2F\overline{A_2 A_{1x}}^{x} + \overline{A_2 h}^{x} - \nu(m - m^*) \tag{25}$$

Equation (24) is the form-drag equation and it expresses the conservation of the angular momentum. Equation (25) is more subtle. It can be derived from energy closure of the whole system. The constant C represents the thermal inertia of the system. We remark that in equation (24) U^* represents momentum forcing from the boundary. In Benzi, Sutera and Speranza (hereafter BSS) equations (23), (24) and (25) were

studied by perturbative methods. Multiple equilibria were found for realistic value of the parameters, namely, $C = 5$, $\alpha^2 = 0.2$, $F = 1$, $\beta = 1$, $h = 0.1$, $\nu = 0.1$ and $\delta = 0.5$. An illustration of the results obtained by BSS is given in Table I. The first set of values (Table Ia) corresponds to multiple equilibria near the symmetric circulation ($U_2 = 0$): two states (E_1, E_3) are stable and separated by about 100 meters of geopotential. The intermediate state E_2 is unstable with respect to nontravelling baroclinic disturbances of orographic nature. The difference in zonal flow and average baroclinicity between the large and small wave amplitude stable states is confined in a range of few meters per second as required by the observed statistics. The maintenance of the stable equilibria is in agreement with observations (Hansen, 1986), essentially baroclinic as shown by the energetic displayed in Table II.

It is interesting at this point to contrast the above results with those obtained by studying a barotropic nonlinear system computed from the same equations, but setting $m = 0$. We show in Table Ib a second set of equilibrium values computed for the above-defined "barotropic" dynamics. One can immediately see the large differences in the zonal

TABLE Ia

	U	m	A1	A2
E1	2.1	1.7	.73 + i.78	.12 + i.11
E2	2.15	1.72	-.76 + i.61	-.1 + i.1
E3	2.37	1.83	-.15 + i.01	-.01 + i.002

TABLE Ib

	U	m	A1	A2
E1	2.1.	0.	2.08 + i.63	4.16 + i1.21
E2	4.72	0.	-1.53 + i.13	-1.83 + i.17
E3	5.1	0.	-.58 + i.02	-.61 + i.02

TABLE II

	C(Az,Ae)	C(Ae,Ke)	C(Kz,Ke)
E1	0.041.	0.011	0.002
E2	0.033	0.0093	0.002
E3	0.001	0.0002	0.00005

wind of the two extreme (in wave amplitude) equilibria. This difference is due to the balance between zonal and wave kinetic energy, emphasized before as a necessary consequence of barotropy. Morevor the amplitude of the waves is decreasing in the vertical, in contrast with any observed vertical structure of large scale planetary waves. On the other hand the amplitude of the resonant wave in Table Ia is increasing from the lower to the upper layer. This is an essential feature in order to maintain the form-drag term small while the wave amplitude of upper layer is large.

As mentioned previously, the equilibria E1 and E3 of Table Ia are baroclinically stable, which means that the resonant wave (we can think of wave number 3) is baroclinically stable. Ordinary baroclinic instability with respect to larger wave-numbers is systematically eliminated by the perturbative analysis performed in BSS. However non-perturbative numerical analysis (Benzi, Sutera and Speranza, in prep.) shows that this is always the case for the larger amplitude equilibrium (E1) while (E3) becomes baroclinically unstable with respect to short waves. The instability of the intermediate equilibrium E2 is characterized, both in the perturbative and non-perturbative analysis, by zero phase velocity, for the largest growing mode. Baroclinic and barotropic instability could be important to explain the transition mechanism for the multiple equilibria theory. During a transition the system will spend some time near by an unstable equilibrium like E2. It means that large scale planetary waves will grow with zero phase velocity during their amplification. This characteristic is in rather good agreement with observations and can explain the stationary variance of the low frequency variability.

4. Multiple equilibria for realistic orography

One of the interesting features of the CE theory is the rather good agreement between the latitudinal average of the climatological geopotential height and the linear resonant waves for a realistic topography. In the language of section 2 the CE theory corresponds to equation (18), for $\delta = 0$:

$$\dot{A}_{xx} - \alpha^2 \dot{A} + \beta A_x + U(A_{xxx} - \alpha^2 A_x) + U b_x = -\nu(A_{xx} - \alpha^2 A) \tag{26}$$

In (26) b is supposed to be the latitudinal average of earth's orography between 30° and 75° North. An equation similar to (26) was used by Charney, Shukla and Mo (hereafter CSM) to discuss multiple equilibria with realistic topography. Following CDV, CSM studied stationary states of (26) and equation (12), namely, the form-drag equation. The aim of CSM was to compare large amplitude stationary waves with observed positive anomalies as defined by Dole (1982). We want now to pursue the same aim but with the following three modifications:

1. Wave self-interaction must be included to bend the orographic resonance in order to have multiple equilibria for the same value of the zonal flow.

2. The form-drag equation must is disregarded since we consider a barotropic flow for which it is impossible to satisfy observational requirements. A climatological value of U is considered.

3. The large amplitude equilibria is compared with the composite geopotential height obtained from probability density distribution of the observed data.

Let us clarify point (3). Let $\eta(x, y, t)$ be the geopotential height at the 500 mb, where x and y denote zonal and meridional coordinates. By $\Phi(x, t)$ we denote the latitudinal average of $\eta(x, y, t)$. $\Phi(x, t)$ can be decomposed into Fourier modes:

$$\Phi(x, t) = \sum \Phi_n(t) \exp\left(ix \frac{2\pi n}{b} \right) \tag{27}$$

where h is about 30,000 km at the middle latitudes. We then consider the indicator $I(t)$ so defined:

$$I(t) = (|\Phi_2|^2 + |\Phi_3|^2 + |\Phi_4|^2)^{1/2}. \tag{28}$$

BMSS and Sutera (1986) show that the probability density distribution $P(I)$ of $I(t)$ is bimodal, i.e., has two maxima at (I_1, I_3) and a minimum at (I_2), where $I_1 < I_2 < I_3$, while $P(I_3) \cong P(I_1) > P(I_2)$. We can therefore define the composite of Φ for the state I_3 as:

$$A_3(x) = \frac{1}{T} \int \Phi(x, t)\, \Theta\, [I(t) - I_2]\, dt \tag{29}$$

where T is the number of days used in the estimate of $P(I)$ and Θ is the Heaviside function:

$$\begin{aligned} \Theta(x) &= 0 \quad x < 0 \\ \Theta(x) &= 1 \quad x > 0 \end{aligned} \tag{30}$$

We want to compare $A_3(x)$ with the stationary solution of the non linear differential equation (18).

This comparison has been performed by Benzi, Iarlori, Lippolis and Sutera (1986). Here we shall briefly review their results.

In fig. 1 we show $\Phi_3(x)$ obtained by an analysis of 4 winters (80-81, 81-82, 82-83, 83-84). The analysis and the estimate of $P(I)$ can be found in Sutera (1986). Three main ridges can be observed; one near the Rockies, one on the Atlantic and a third one near the Himalayas. We first compare fig. 1 with the linear solution of equation (18).

In fig. 2 we plot $A_M \equiv \mathrm{Sup}_x A(x)$ as a function of U. The parameters of the model are $\nu = 0.1$, h the CSM orography and $\alpha^2 = .5$ which corresponds to a channel width of 5000 km. One can see a clear resonance structure, identical to that of CSM model, with wavenumber 2 dominant at U = 15 m/s. Figures (2) and (3) show $A(x)$ for different values of U, namely for sub and superresonant values of U with respect to the wavenumbers 2 and 3.

Figures 3a and 3b look rather realistic as compared with figure 1. However a more careful inspection reveals that the ridge near the Rockies is westward of the observed ridge and the trough on the Atlantic is too small compared with observations. Of course one can always choose the value of U in such a way that a linear superposition of wave number 2 and 3 looks as realistic as possible. Indeed it is quite clear that the stationary solutions shown in figures 2 and 3 are mostly a linear superposition of wave number 2 and 3. Let us now discuss the results obtained in the nonlinear case, namely, the stationary solutions of equation (18).

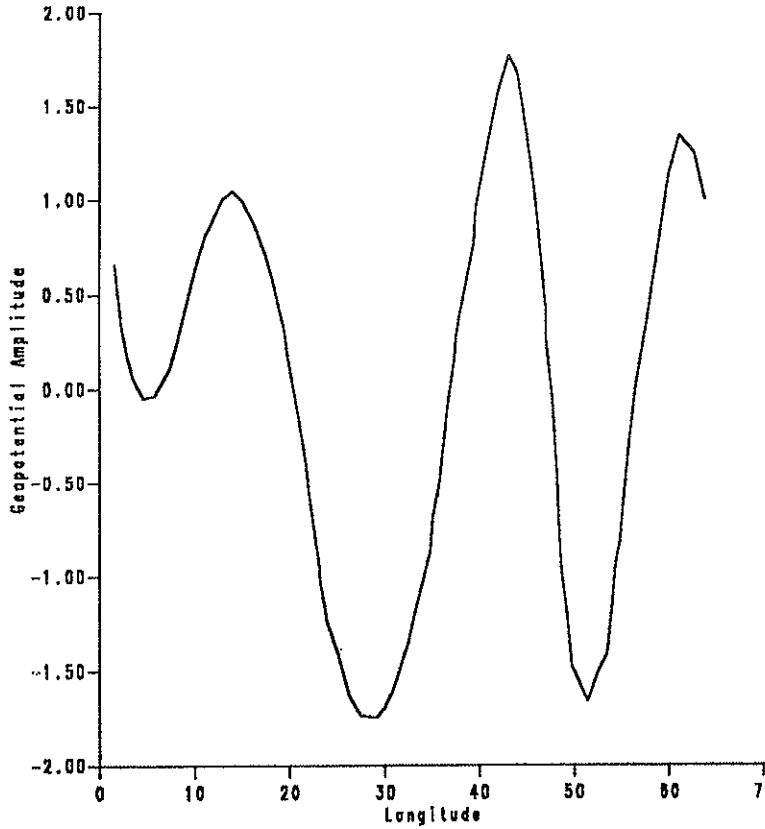

FIG. 1. Profile of the average structure of a persistent anomaly, corresponding to large amplitude mode, selected by the bimodal probability distribution.

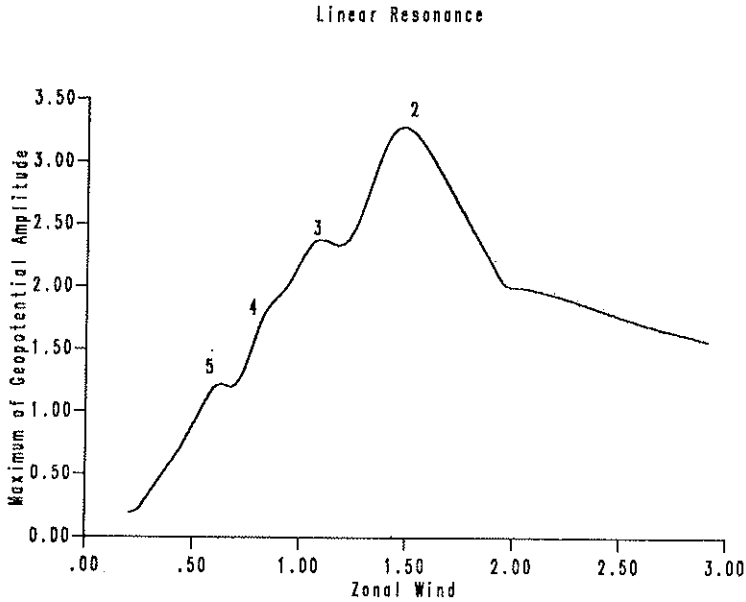

FIG. 2. Maximum of the geopotential amplitude A, computed as a function of the zonal mean wind, for the linear model ($\delta = 0$) unidimensional equation (18). The amplitude is expressed in hundreds of meters and the zonal wind in 10 meters per second; $\alpha = 0.73$, $\nu = 0.1$ and $N = 128$ grid points. The numbers at the peaks indicate the resonant topographic wave numbers.

FIG. 2a. Plot of the subresonant wave number 2 linear solution as a function of longitude, for a value of the wind $U = 13$ m/s. This solution was computed from the linear stationary version of eq. (18). The dashed lines represent the CSM topography.

FIG. 2b. Numerically computed superresonant wave number 2 linear equilibria of the eq. (18) and CSM topography (dashed lines) against the longitude, with a value of the wind U = 17 m/s.

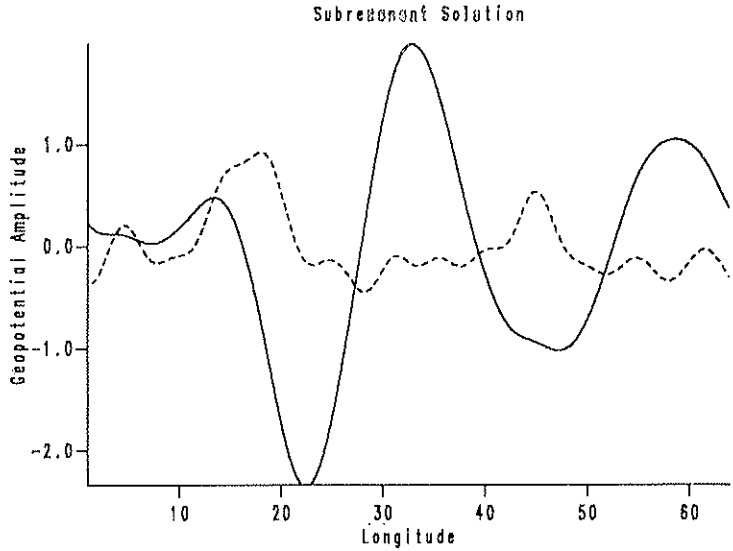

FIG. 3a. Subresonant wave number 3 solution of the resonance curve wind U = 10 m/s. The dashed lines represent the CSM topography.

FIG. 3b. Plot of the numerical superresonant wave number 3 solution corresponding to the case in fig. 1, computed with a value of the zonal flow U = 11.5 m/s. The dashed lines represent the topography (see CSM model) used in the calculation.

Figure 4 is the analogous of fig. 1 for eq. (18) with $\delta = -0.5$. We note the bending of the resonance on wave number 3 and simultaneously a smaller amplitude for wave number 2 resonance.

Figures 5a-b-c show $A(x)$ for $U = 13.5$ m/s. Figure 5a corresponds to the large amplitude equilibrium and must be compared with figure 1. The position of the ridges and troughs of figure 5a corresponds rather well to that of figure 1, better, in fact, than for the linear solution represented in figures 2 and 3. A dominance of wave number 3 can be clearly seen both in fig. 1 and 5a but not in figure 3a or 3b. Moreover the ridge near the Rockies and the trough in the Atlantic region are more realistically predicted in figure 5a than in fig. 3.

However, the main differences between linear and nonlinear solutions do not concern the amplitude and the position of the ridges and the trough, but the dynamical balance of the dispersive terms. For the nonlinear solution of fig. 5a, the dispersive terms are locally balanced by nonlinear terms (see fig. 6). On the other hand, dispersive terms of the linear solution 3a, are balanced by the orography forcing and Eck-

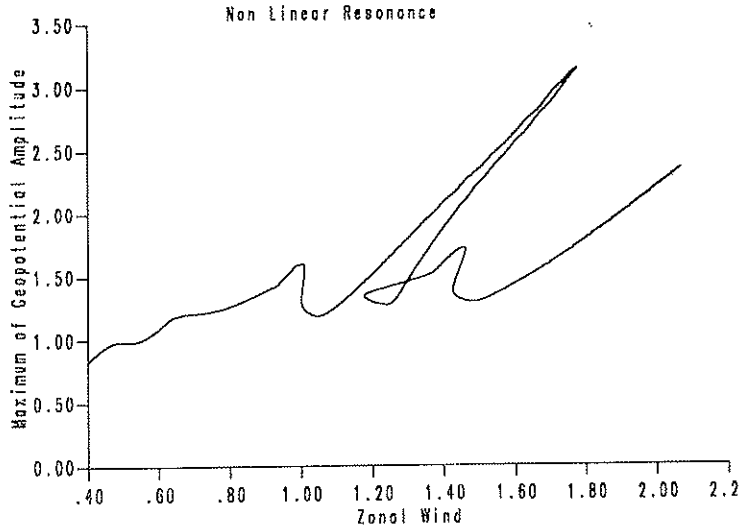

FIG. 4. Plot of the nonlinear resonance of the amplitude A (hundreds of meters) against the zonal wind U (meters per second), computed from the nonlinear equation (18). In this computation $\alpha = 0.73$, $\nu = 0.1$, $\delta = -0.5$ and $N = 128$ grid points. The numbers mark the values of U at which particular zonal wave numbers resonate.

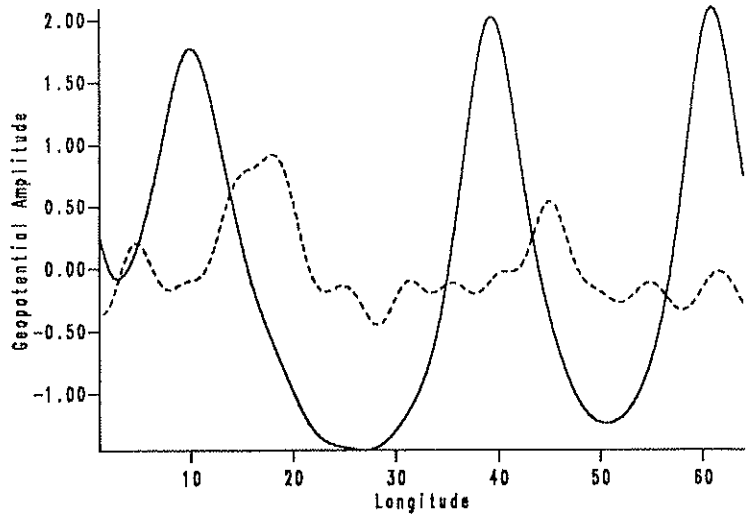

FIG. 5a. Plots of the subresonant numerical solution wave number 3 for a value of zonal wind U = 13.5 m/s and the topography (dashed lines). These solutions correspond to the nonlinear resonance structure, fig. 4.

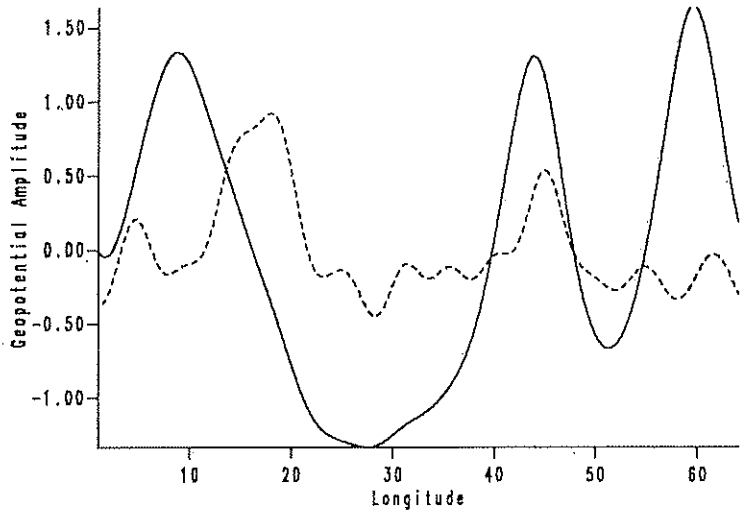

FIG. 5b. Same as in fig. 5a but for the intermediate state.

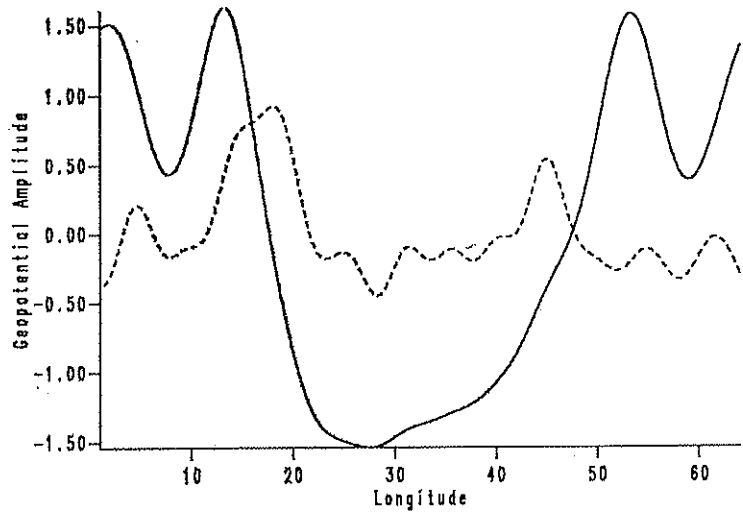

FIG. 5c. Same as in fig. 5a but for the zonal solution.

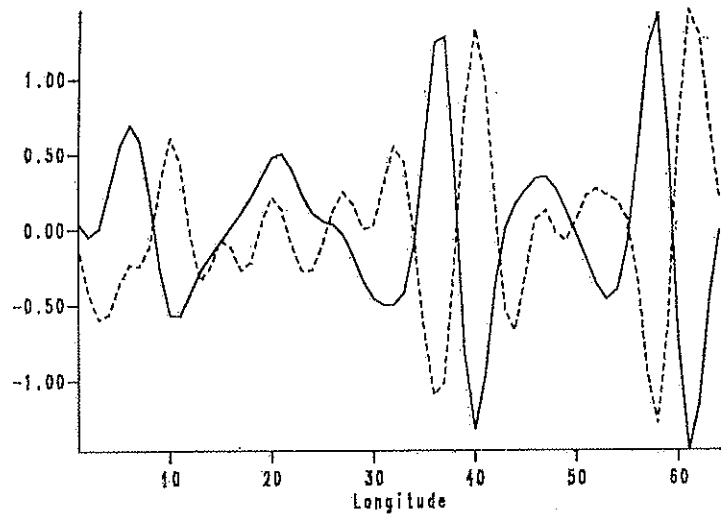

FIG. 6. Plot of δAA_x (dashed line) and the dispersive part of the equation (18), in the nonlinear case, as a function of longitude.

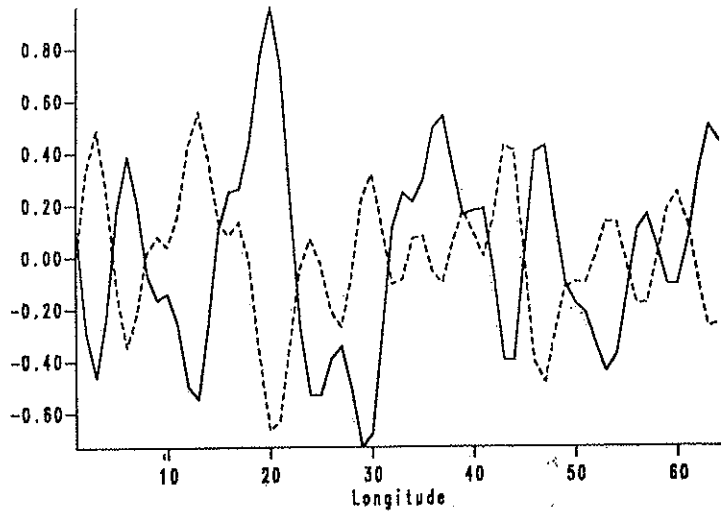

FIG. 7. Plot of Uh_x (dashed line) and the dispersive part of the equation (18), in the linear case, as a function of longitude.

mann dissipation (see fig. 7). This implies that figure 5a can be regarded as a superposition of localized nonlinear solution of the inviscid non-forced stationary equation (18), namely:

$$A_{xxx} + (\beta - \alpha^2 U)A_x + \delta A A_x = 0 \tag{31}$$

This interpretation does agree with some "regional" character of the observed large scale anomalies in the middle latitudes. It is possible to show (Benzi *et al.*, 1986) that the result shown in fig. 5 does not depend on the details of the orography and is weakly dependent on the value of Eckman damping. This is at variance with respect to the linear solutions of figures 2 and 3 which are proportional both to orography forcing and Eckman damping.

5. Conclusions

In this paper we reviewed the theory of multiple equilibria. Non linear resonance, caused by wave self-interaction and orography forcing, produces multiple equilibria in the midlatitude circulation. Most of the predictions of the theory have been confirmed by a theoretically based analysis of the observed atmospheric circulation. The theory of multiple equilibria deeply changes our previous understanding of the general atmospheric circulation. A new time scale is active in the dynamics of the system: the average transition time among equilibria. This time scale is of the order of 7-10 days in agreement with the observed low frequency variability. Transitions between equilibria are the next important problem to be solved. This topic is presently under active investigation.

REFERENCES

BENZI R., MALGUZZI P., SPERANZA A. and SUTERA A., *The Statistical Properties of General Atmospheric Circulation: Observational Evidence and a Minimal Theory of Bimodality.* « Quart. J. R. Met. Soc. », *112*, 661-674 (1986).

BENZI R., SPERANZA A. and SUTERA A., *A minimal baroclinic model for the statistical properties of low frequency atmospheric variability.* « J. Atmos. Sci. », in press (1986).

BENZI R., IARLORI S., LIPPOLIS G. and SUTERA A., *Steady non linear response of a barotropic quasi-unidimensional model to realistic orography.* « J. Atmos. Sci. », submitted (1986).

BUZZI A., TREVISAN A. and SPERANZA A., *Instability of a baroclinic flow related to topography forcing.* « J. Atmos. Sci. », *41*, 637-650 (1984).

CHARNEY J.G. and ELIASSEN A., *A Numerical Method for Predicting the Perturbations of the Middle Latitude Westerlies.* « Tellus », *1*, 38-54 (1949).

CHARNEY J.G. and DEVORE J.G., *Multiple flow equilibria in the atmosphere and blocking.* « J. Atmos. Sci. », *36*, 1205-1216 (1979).

CHARNEY J.G., SHUKLA J. and Mo K. C., *Comparison of a Barotropic Blocking Theory with Observation.* « J. Atmos. Sci. », *38*, 1157-1175 (1981).

CHEN T.C. and MARSHALL H.G., *Time variations of atmospheric energetics.* « Mon. Wea. Rev. », *110*, 947-961 (1984).

DOLE R.H., *Persistent anomalies of the extratropical Northern Hemisphere wintertime circulation.* Ph. D. thesis, M.I.T., Cambridge, Ma (1982).

FREIDERICH K. and BOTTGER H., *A wave number-frequency analysis of the 500 mb geopotential at 50 N.* « J. Atmos. Sci. », *35*, 745-750 (1978).

HANSEN A.R., *Observation characteristics of atmospheric planetary waves with bimodal amplitude distribution.* In « Large scale anomalies and blocking », Advances in Geophysics, 29, edited by B. Saltzman, R. Benzi, A. Wiin-Nielsen, Academic Press (1986).

LORENZ E.N., *The nature and the theory of the general circulation of the atmosphere.* WMO (Publ.) 218, TP 15, 1-161 (1967).

RAMBALDI S. and Mo K.C., *Forced stationary solutions in a barotropic channel: multiple equilibria and theory of non-linear resonance.* « J. Atmos Sci. », *42*, 3135-3146 (1985).

SUTERA A., *Probabilistic distributions of ultra long planetary waves in winter circulations.* In « Large scale anomalies and blocking », Advances in Geophysics, 29, edited by R. Benzi, B. Saltzman and A. Wiin-Nielsen, Academic Press (1986).

WALLACE J.M. and BLACKMON M.L., *Observations of Low-frequency atmospheric variability.* In « Large Scale Dynamical processes in the Atmosphere » *SS-91*, edited by B.J. Hoskins and R.P. Pierce, Academic Press. (1983).

WIIN-NIELSEN A., *Steady states and Stability properties of a low-order, barotropic system with forcing and dissipation.* « Tellus », *31*, 375-386 (1979).

THE RESPONSE OF ATMOSPHERIC CIRCULATION TO ANOMALOUS TROPICAL HEATING: A RE-EXAMINATION OF THE THEORY OF TELECONNECTIONS IN THE CONTEXT OF TURBULENCE THEORY

A. SPERANZA and P. MALGUZZI
CNR FISBAT - Bologna

ABSTRACT

In several studies, information about the dynamics of fully turbulent systems are inferred from the properties of the linear problem around some time-averaged "basic" state; an important example is given by the classical problem of baroclinic instability, where the structures of mid-latitude cyclones and their nonlinear equilibration are often referred to a basic state chosen to fit some average properties of the atmosphere.

A similar methodology is used in the problem of determining the atmospheric response to anomalous tropical heating (teleconnections).

In this work, we show that such procedure leads to incorrect answers in both the above-mentioned cases.

1. INTRODUCTION

The Earth's atmosphere is a complex physical system in turbulent motion. Air flow is ultimately driven by solar heating and dissipated by internal friction together with external drag. Most of solar radiation is not directly absorbed by the atmosphere: its energy is transferred to the atmosphere from the lower boundary. The most mobile part of such boundary, the ocean, is itself in turbulent motion. Heating is variable on decades of space and time scales.

Particular attention has been traditionally paid to changes from season to season (seasonal anomalies) in sea surface temperature (SST). Given the inertia of the ocean, SST anomalies typically develop and evolve on time scales of the order of a month. Since the atmospheric circulation displays itself well marked variations on the monthly time scale, it is conceivable that such variations are coupled (expressions like "caused by" are totally out of place here) with the above oceanic fluctuations.

When dealing with turbulent systems, to answer questions like: "is this specific boundary condition fluctuation coupled with this specific fluctuation in the internal dynamics?" is normally a very difficult task. In fact, unless particular symmetries distinguish fluctuations coupled with the boundary from purely internal ones, the above distinction is often desperate. However, if the external modulation is strong and persistent enough (i.e., averaging many decades of internal turbulence) one can hope to distinguish signs of change in the "régime" of turbulent flow. How to detect and interpret such changes is, in the official literature, a rather confused and confusing topic.

Traditionally, (not only in meteorology) a great deal of attention has been paid to time-averages. It goes without saying that at least other moments of the statistical distribution should be considered. Even if we accept to restrict our attention to the average in time, we must consider its natural and sampling variability (particularly important in numerical experiments). In the atmosphere, seasonal averages have an observed variability around 20% of the average signal. To follow specific fluctuation in such a level of natural "noise" is not easy. As already mentioned, one can try to resort to particular symmetries of the signal, for example by tracing "rays" of wavelike disturbances emitted from the source, or by following other theoretically deduced forms (solitons, etc.). Anyhow, it is clear that the problem cannot be reduced to objective analysis: some theory is necessary in order to detect the discriminant symmetries of the signal.

The classical theory describing the effect of thermal asymmetries (nonzonal heating) on middle latitude tropospheric circulation starts with the well known 1953 paper by Smagorinsky. The idea that signals may propagate from localized vorticity sources (in the form of Rossby waves) goes back to Rossby (1945) (for a review see Dickinson, 1978) and specific application to the long-distance influence of anomalous tropical heating on middle latitude circulation has been performed by many researchers (see, for example, the recent work of Branstator, 1986 a,b).

In essence, the theory is based on the assumption that the effect of anomalies in boundary heating can be modelled as (in most papers on the subject) linear disturbances superimposed on a "basic" state that is either theoretically or empirically prescribed. Almost invariably the basic state is identical with the time-average circulation. Various calculations of signals spreading from localized heat sources indicate a possible long distance influence of anomalous heating. The dynamics described by the equations used in theoretical studies is recognized by the same authors as over-simplified with respect to reality. This is not, however, the point we want to raise here. The subject of the present paper is rather methodological: we will concentrate on the assumption that turbulent fluctuations can be computed as perturbations on a basic state. We will show that this assumption is wrong generally in the theory of atmospheric circulation and specifically in its application to teleconnections between tropical SST anomalies and middle-latitude circulation.

In section 2 we will describe the model of atmospheric circulation used to investigate the above problems. In section 3 we describe the general circulation of such model and interpret its dynamics. In section 4 we discuss experiments with anomalous tropical heating. In section 5 we draw some conclusions.

2. The model

The model used in the numerical experiments discussed throughout this paper is deduced from the two-layer, quasigeostrophic equations:

$$\partial_t \nabla^2\phi + J(\phi, \nabla^2\phi + \beta y) + J(r, \nabla^2 r) = -\frac{\nu_E}{2}\nabla^2(\phi - r) \tag{1}$$

$$\partial_t (\nabla^2 r - 2Fr) + J(r, \nabla^2\phi + \beta y) + J(\phi, \nabla^2 r) =$$

$$\frac{\nu_E}{2}\nabla^2(\phi - r) - \nu_S \nabla^2 r + 2F\nu_H(r - r^*) \tag{2}$$

Here $\phi = (\Psi_1 + \Psi_3)/2$ and $r = (\Psi_1 - \Psi_3)/2$ are respectively the barotropic and the baroclinic (temperature) components of the stream-

function Ψ; J the Jacobian operator, ∇^2 the Laplacian operator, F the Froude number, ν_E ν_S and ν_H are respectively the coefficients of Ekman pumping at the lower surface, friction at the surface separating the two layers, and Newtonian cooling, β the gradient of the Coriolis parameter and r^* the baroclinic generation which forces the fluid motion (see, for instance, Lorenz, 1963). The variables are in the standard nondimensional form of Pedlosky (1979).

After separating the symmetric part:

$$\phi = -\int U(y,t)dy + \phi'(x,y,t) \tag{3}$$

$$r = -\int m(y,t)dy + r'(x,y,t) \tag{4}$$

we introduce a particular form of the solution:

$$\phi' = \sum_n A_n(y,t)\, g_n(x) \qquad + \quad (*) \tag{5}$$

$$r' = \sum_n B_n(y,t)\, g_n(x) \qquad + \quad (*) \tag{6}$$

where the separated x-structure functions $g_n(x)$ are assumed "ad hoc". The main element of convenience of such representations consists in the fact that projection of the equations of motion onto the (complete) g_n-basis gives coefficients of nonlinear interaction that can be made to assume opportune numerical values by properly choosing the g_n's. The general problem is discussed in Malguzzi-Speranza (1986). Here we concentrate on the simplest case:

$$\begin{cases} g_1(x) = e^{ikx} \\ g_n(x) = 0 \quad , \; n > 1 \end{cases} \tag{7}$$

that, as we shall see, describes the essential dynamics of maintenance of the middle latitude jet. With the assumption (7) the equations (3), (4) reduce to:

$$\phi = -\int U dy + A\, e^{ikx} \qquad + \quad (*)$$

$$r = -\int m dy + B\, e^{ikx} \qquad + \quad (*)$$

and, by projection of (1), (2) onto $g_l(x)$:

$$\dot{U} + \frac{\nu_E}{2}(U-m) + 2kI_m\{AA^*_y + BB^*_y\}_y = 0 \tag{8}$$

$$\dot{m}_{yy} - 2F\dot{m} + \nu_S m_{yy} - \frac{\nu_E}{2}(U-m)_{yy} - 2F\nu_H(m-m^*) + \\ + 4kFI_m\{A^*B\}_{yy} + 2kI_m\{AB^*_y + BA^*_y\}_{yyy} = 0 \tag{9}$$

$$\dot{A}_{yy} - k^2\dot{A} + (\nu_E/2 + ikU)A_{yy} - \left[ik^3U + ikU_{yy} - ik\beta + \right. \\ \left. + \frac{\nu_E}{2}k^2\right]A - \left(ikm_{yy} + ik^3m - \nu_E\frac{k^2}{2}\right)B + \left(ikm - \frac{\nu_E}{2}\right)B_{yy} = 0 \tag{10}$$

$$\dot{B}_{yy} - k^2\dot{B} - 2F\dot{B} + \left(\frac{\nu_E}{2} + \nu_S + ikU\right)B_{yy} - \left[ik^3U + ikU_{yy}\right. \\ \left. - ik\beta + \frac{\nu_E}{2}k^2 + \nu_S k^2 + 2F\nu_H + 2ikFU\right]B - \left(ikm_{yy}\right. \\ \left. + ik^3m - \nu_E\frac{k^2}{2} - 2ikFm\right)A + \left(ikm - \frac{\nu_E}{2}\right)A_{yy} = 0 \tag{11}$$

where $r^* = -\int m^*(y)dy$

and where, because of the simple wavelike form of the nonsymmetric disturbances (7), all the wave-wave interaction coefficients vanish and the only nonlinear interactions take place between symmetric and nonsymmetric components (latitudinal convergence of eddy momentum flux and heat flux). A and B coefficients being complex, (8-11) constitute a set of six real field equations in latitude y and time t. We will assume as lateral boundary conditions a rigid wall at $y = 0, L_y$, which implies

$U=m=A=B=0$ at the boundaries. System (8-11) can be transformed into a set of ordinary differential equations by further decomposing U, m, A, B in Fourier series:

$$\begin{Bmatrix} U \\ m \\ A \\ B \end{Bmatrix} = \sum_{J=1}^{JT} \begin{Bmatrix} u_J \\ m_J \\ a_J \\ b_J \end{Bmatrix} \sin \frac{\pi J y}{L_y}$$

The system is driven in the equation for the vertical shear (9) through the term $2F\nu_M (m - m^*)$ which forces a relaxation to the radiative equilibrium $m^*(y)$. In the following, the radiative equilibrium potential temperature profile will be assumed of the form:

$$\theta^* = 2 r^* = \theta_E \cos \frac{\pi y}{L_y}$$

that corresponds to the vertical shear

$$m^* = \theta_E \frac{\pi}{2L_y} \sin \pi y / L_y$$

The parameter θ_E (representing half of the equator-to-pole temperature contrast at the radiative equilibrium) will be determined empirically in such a way as to give a realistic behaviour of our model atmosphere.

System (8-11) describes the nonlinear equilibration of a single baroclinic wave through interactions with the zonal component. In the next section, we shall discuss the statistical properties of such equilibration in the highly supercritical régime. We shall see that a quite realistic zonal jet is maintained by the "turbulent" process modeled by (8-11).

3. Statistical properties: the "general circulation" of the model

We restrict our analysis here to some aspects of the problem that constitute a necessary preliminary for the successive examination of the problem of tropical heating. Full account of our research on general circulation can be found in Malguzzi-Speranza (1986).

Numerical integrations of the system (8-11) have been performed with the spectral scheme discussed in the previous section at different levels of resolution. The experiments discussed here have been run with a leap-frog scheme (time step 1/100 day) for the time derivative and a pseudo spectral representation with 32 Fourier modes in latitude. The integration is carried on for 320,000 time steps (1 hour of CRAY XMP) corresponding to 10 years of real time. Dissipation coefficients are fixed to the values $\nu_E = 0.45$ (that spins down the whole atmosphere with a decay time of 5 days) and $\nu_S = \nu_H = 0.1157$ (decay time 10 days). Other parameters are: $F = 2$, $\beta = 1.6$, $k = 1.3$ (wavelength ~ 4.800 Km), $L_y = 10$ (10,000 Km). The external forcing, acting only on the gravest latitudinal mode, is $\theta_E = 9$ (equator-to-pole temperature difference of 54°K at radiative equilibrium). This value turns out to give (having fixed the other parameters) a super-rotation (mean westerly momentum) of 6.8 m/s that we consider realistic for the winter circulation.

Visual inspection at different fields reveals that the life cycle of non-symmetric disturbances is characterized by rather realistic baroclinic growth and barotropic momentum convergence into the jet. Also, the symmetric component evolves in a rather realistic fashion: all the classical schemes of maintenance of the mid-latitudinal jet are respected, as shown by the energy diagram of Fig. 1.

Fig. 2 displays, for different components, the scatter of states sequentially occupied by the system in time, and Fig. 3 the specific

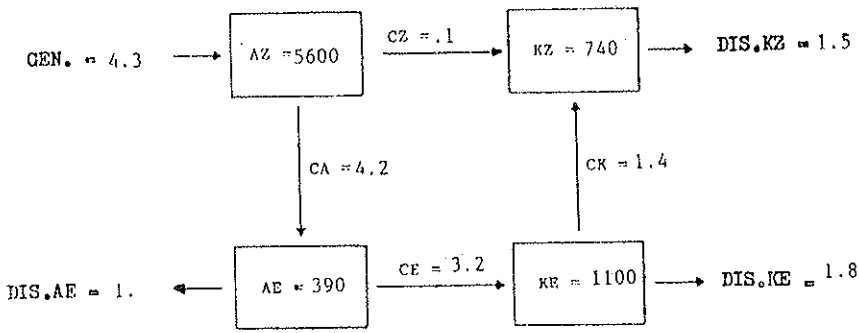

FIG. 1. Energy cycle averaged over 10 years for the experiment described in section 3. Units are w/m² for energy conversions and 10^{-3} J/m² for energy contents. AZ, AE, KZ, KE refer respectively to available energy of the zonal flow, available energy of the eddy part, kinetic energy of the zonal flow, and kinetic energy of the eddies.

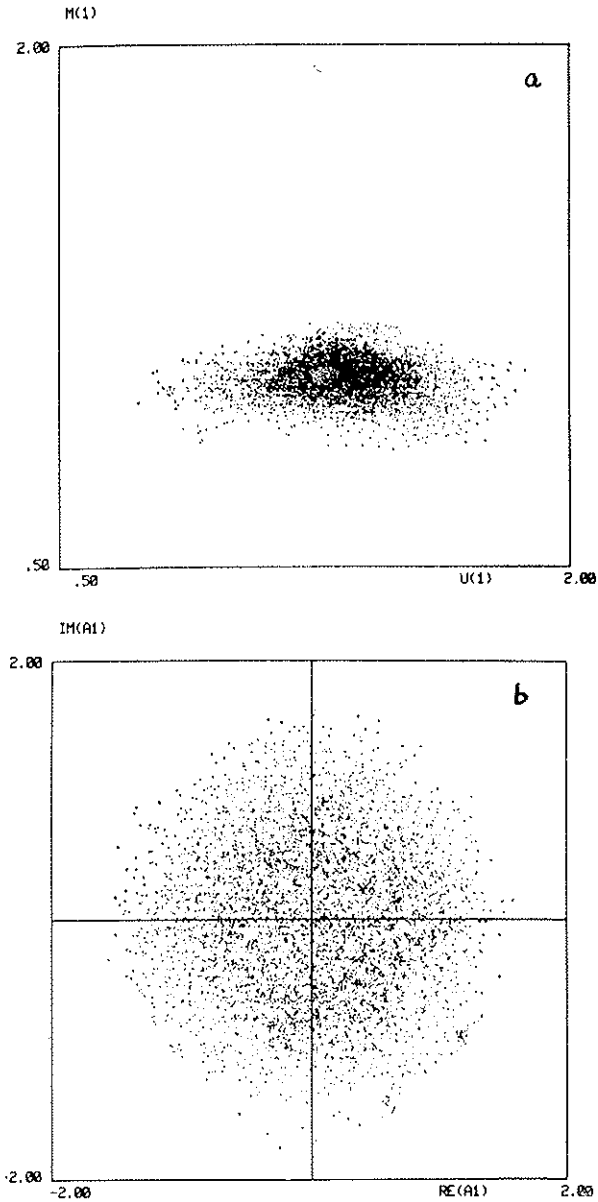

FIG. 2. a) Scatter diagram of the first meridional component of zonal wind shear (m_1) versus the first component of the zonal wind (u_1). Units are dimensionless (one unit corresponds to 10 m/sec for the wind components and 100 m of geopotential for the wave components). The total time of integration is 10 years. b) Same as a) but for the real and imaginary parts of the first barotropic meridional component of the wave-field (A_1).

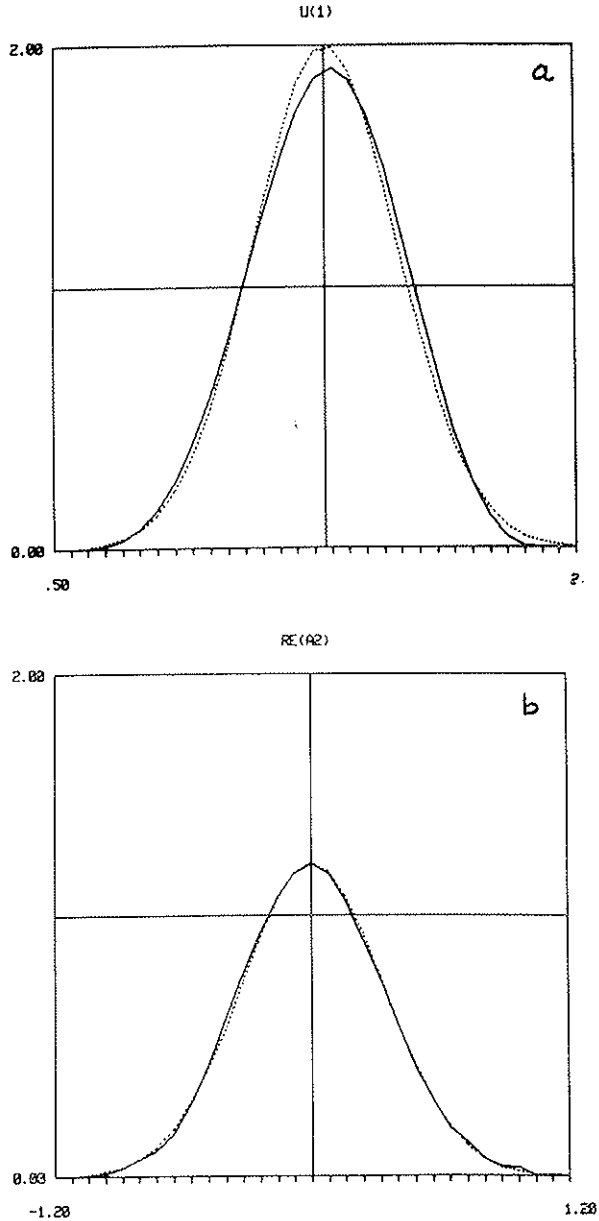

FIG. 3. a) Histograms of u_1 (solid line). The dashed line represents a gaussian having the same mean and variance as the distribution of u_1. b) Same as a) but for the real part of A_2.

probability densities. Fig. 4 shows the average in time (over 10 years) of the zonal flow which is characterized by a high degree of variability from year to year (Fig. 4.b and 4.c). Notice that the 10-year average is not yet symmetric around the center of the channel, indicating variability over very long time scales in these components. The average of wave amplitudes is obviously zero. The wavenumber spectrum is shown in Fig. 5. It should be kept in mind that our dissipation is not scale selective and, therefore, we are not dealing with an inertial range: the exp -3 spectrum is not that of two-dimensional turbulence theory! The power spectra, shown in Fig. 6, confirm the "turbulent" nature of the system. Combined wavenumber-frequency spectra reveal the energetic dominance of the lowest harmonics (Fig. 7). These statistical properties are in reasonable agreement with those of the real atmosphere. For the sake of comparison, we show in Fig. 8 a typical histogram of short baroclinic waves (compare with Fig. 3.b).

Analysis of the dynamic that is at the basis of the statistic described above shows that the classical mechanisms of baroclinic destabilization (with associated heat fluxes) and barotropic stabilization (with associated momentum fluxes) play an important role. The statistical properties of this process cannot be described simply in terms of stability properties of a basic state consisting of a fixed point of the equations of motion chosen to fit the time average of the observed circulation. In order to make this point more clear, it is useful to summarize the bifurcation properties of system (8-11).

A stationary solution is most easily determined as the "Hadley circulation":

$$A = B = 0$$

$$U = m$$

$$\nu_S m_{yy} - 2F\nu_S (m - m^*) = 0$$

that is characterized by zero wind in the lower layer. Linear stability analysis of this solution (a classical topic in meteorology!) gives the results shown in Fig. 9 for the first and second mode. For $k = 1.3$ stability is lost around $\theta_E = 4$. Fig. 10 illustrates the bifurcation sequence. At $\theta_E = 4$ the system is stable; the stable orbit, that at $\theta_E = 4.07$ is winding several times before spiralling down to equilibrium, degenerates

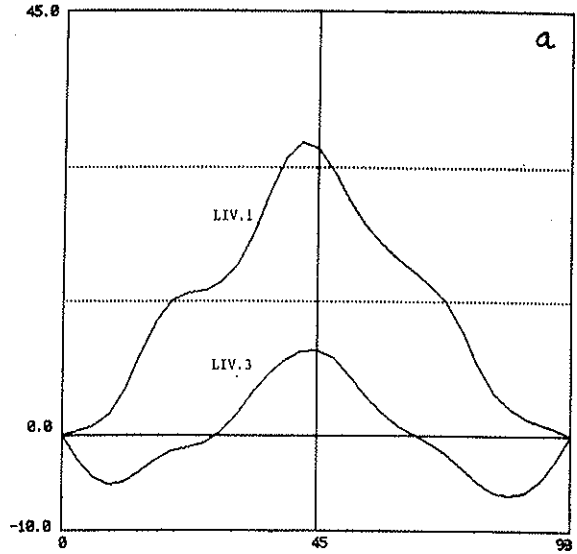

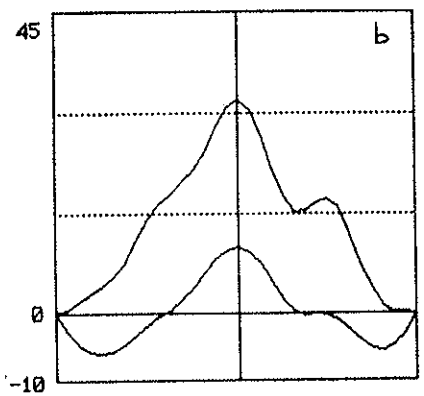

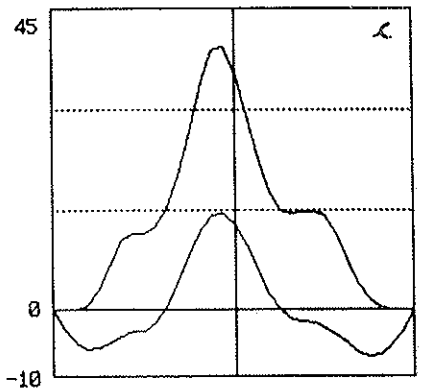

FIG. 4. a) 10-year average of the zonal wind versus latitude at the upper level (liv. 1) and lower level (liv. 3). Units are m/sec. Examples of averages over individual years are shown in b) and c).

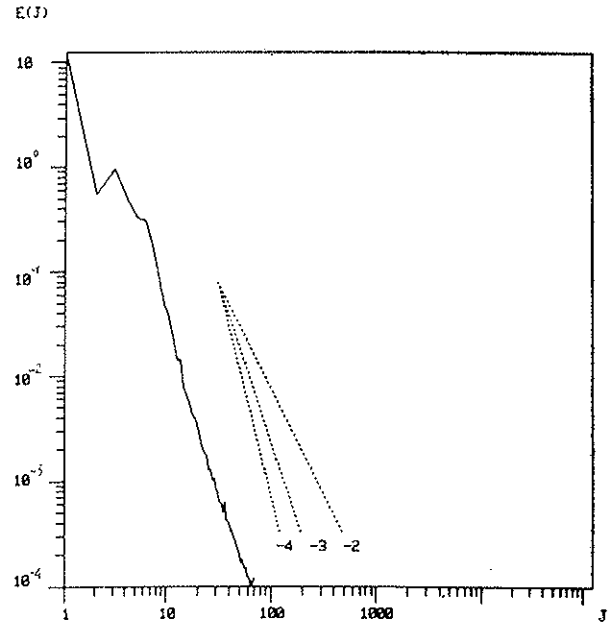

FIG. 5. Fourier spectrum of the total energy (kinetic + available) as a function of the meridional wavenumber $w_j = \pi J/L$ j = 1, 2, 3, . . . The slope of a w_J^{-n} law, $n = 2, 3, 4$, is also plotted for comparison.

at $\theta_E = 4.2$ into a stable Hopf cycle. Between 4.2 and 4.3 another cycle is bifurcated: the motion is quasi-periodic; i.e., the ratio between the period of the new orbit and that of the first Hopf cycle is irrational and the ensuing vacillation is covering its toroidal phase space. At high values of the forcing, the whole space near statistical equilibrium is filled. The sequence seems of the type described by Feigenbaum, Kadanoff and Shenker (1982), who provide also an example of renormalization near the transition to chaos. The chaotic behaviour is generated near the second orbit in a fashion very similar to that described in KAM theory, although the system is here dissipative.

Since the prototype of atmospheric behaviour we are interested in is very far from transition, there is not much quantitative knowledge we can gain from the study of the bifurcation sequence. However, the qualitative understanding of the onset of baroclinic turbulence is crucial for setting up a dynamics of fluctuations in turbulent régime.

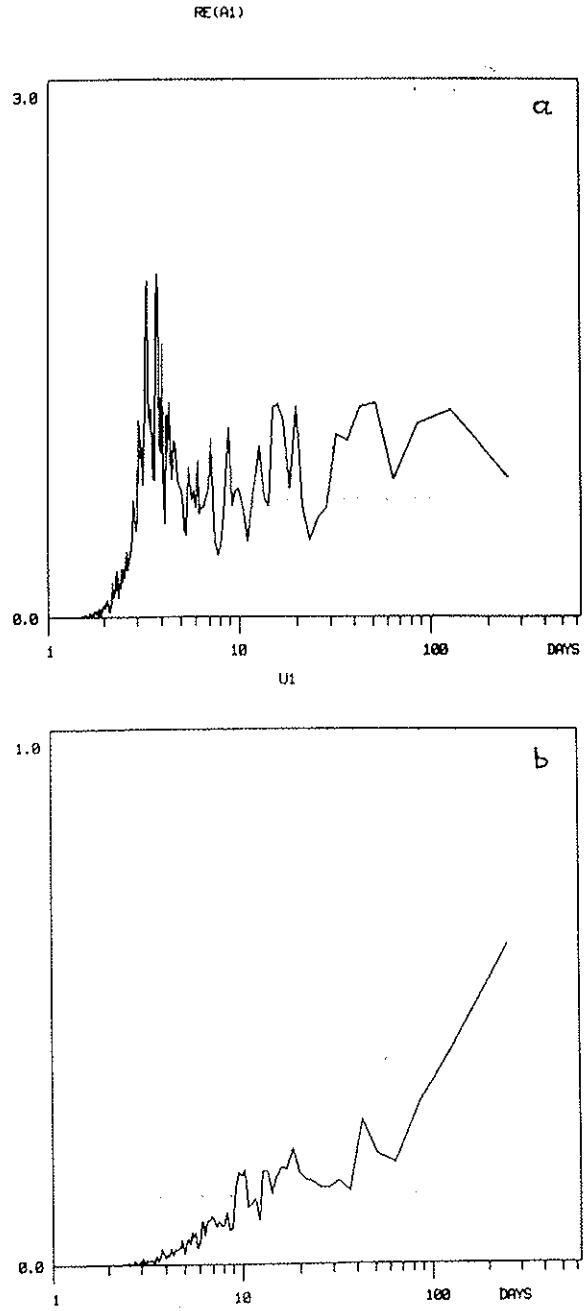

FIG. 6. Power spectrum of a) real part of A_1, and b) first component of the zonal wind u_1 In abscissa is the period (in days) on logarithmic scale.

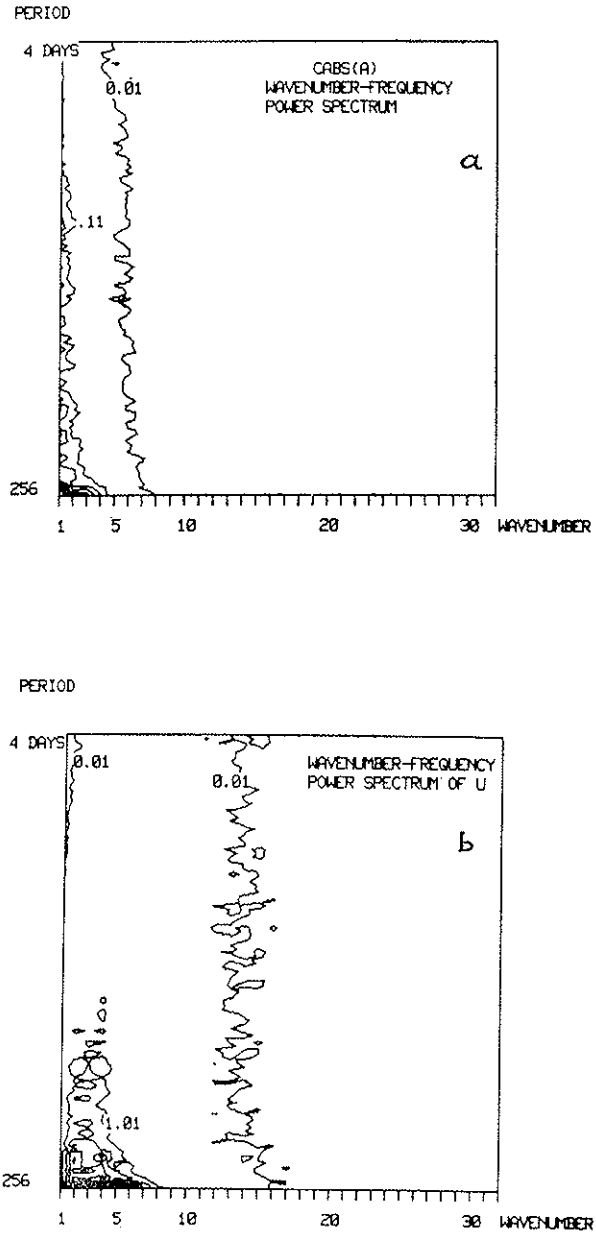

FIG. 7. Wavenumber-frequency power spectrum for a) barotropic wave-component (contour interval .1), and b) zonal wind (contour interval 1.). On the y-axis is the period on logarithmic scale and on the x-axis the meridional wavenumber.

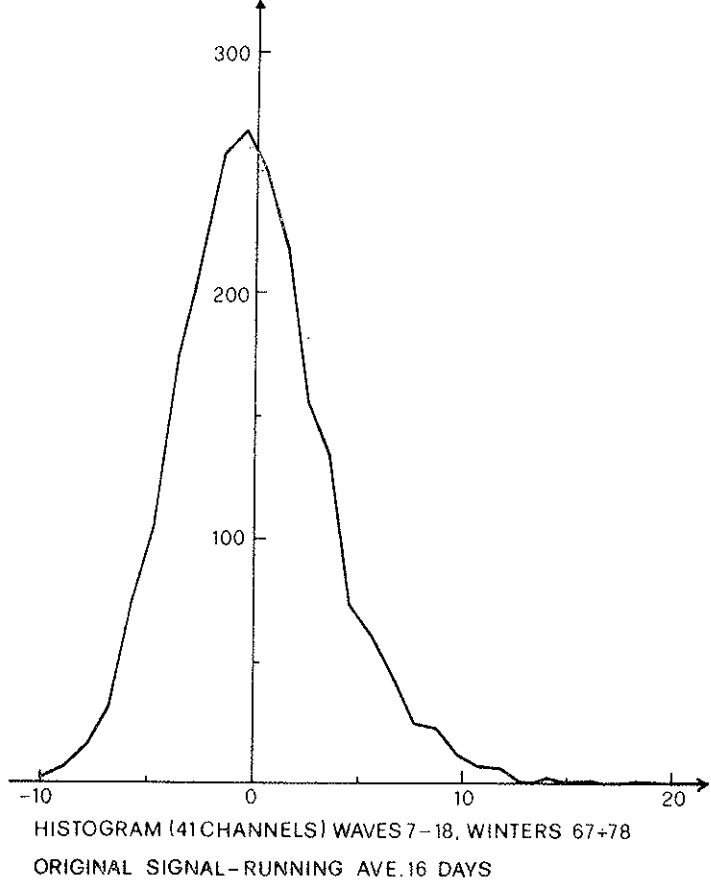

FIG. 8. Histogram of spectral power of short (zonal wavenumbers 7-18) baroclinic waves in the northern hemisphere computed from 500 mb heights of winters 1966-1978. Heights are integrated in latitude between 30 and 75 degrees. The signal is detrended by operating a running average at 16 days. (From Benzi and Speranza, 1986).

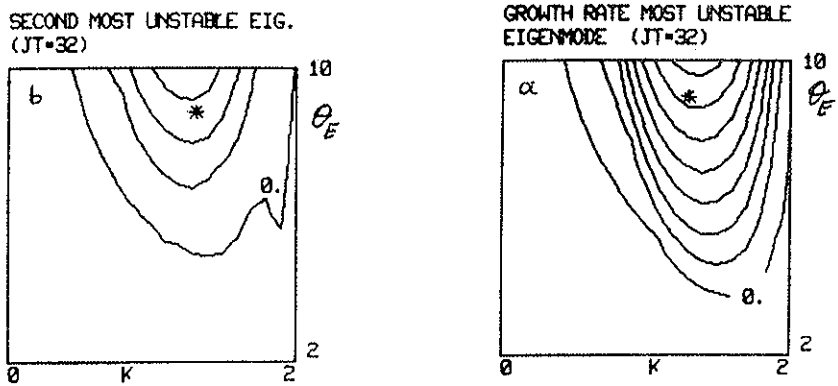

FIG. 9. Growth rates of the most unstable a) symmetric b) anti-symmetric eigenmodes of the linear stability analysis of Hadley circulation versus the zonal wavenumber k and the external forcing θ_E. Contour interval is 1. The star marks the point $k = 1.3$, $\theta_E = 9$.

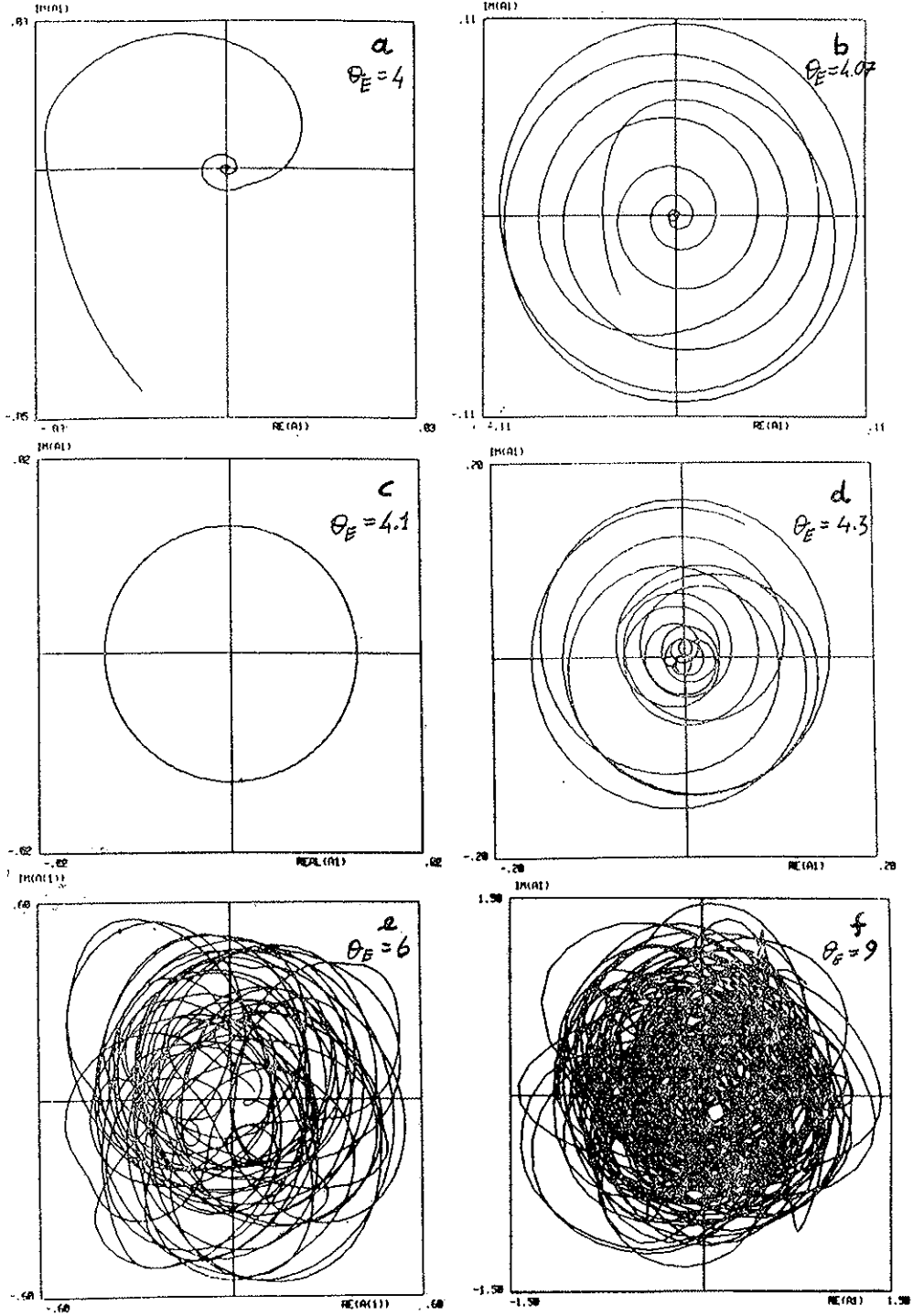

FIG. 10. Projection of the phase-space trajectory on the $(\mathrm{Im}(A_1), \mathrm{Re}(A_1))$ plane for different values of the external forcing. All the trajectories describe a 1-year evolution of the system. a) $\theta_E = 4$. b) $\theta_E = 4.07$ c) $\theta_E = 4.2$ d) $\theta_E = 4.3$ e) $\theta_E = 6$. f) $\theta_E = 9$. The Hadley circulation loses its stability at $\theta_E = 4.158$. Note that the dimension of the attractor is expanding.

We are now in the position of reviewing critically the basic concepts of the classical theory of "general circulation". The theory of general atmospheric circulation revolves around the basic idea that turbulent fluxes maintain an equilibrium circulation (the "stationary flow" determined by time-averaging) conspicuously shifted with respect to the true stationary solution (the Hadley circulation) and that any dynamical theory of fluctuations near statistical equilibrium, e.g., linear stability analysis, should be referred to such state.

We will try here to test the consistency of such a theoretical framework by analyzing our model atmosphere in its context. The statistical equilibrium circulation is well approximated by the average zonal flow of Fig. 4.a. Linear stability analysis of this circulation gives the results shown in Fig. 11. As expected, the system is pushed by turbulent fluxes much nearer to marginal stability than with respect to Hadley circulation (compare with Fig. 9), although still remaining in the unstable range. This result at first sight confirms classical conjectures about baroclinic turbulence in the atmosphere as, for example, those formulated by Stone (1978). However a thorough investigation of nonlinear theory reveals very dangerous inadequacies. In order to avoid the laborious (and boring!) mathematicalities typical of weakly nonlinear expansions, we will try here to give an idea of the nature of the difficulties encountered in the formulation of a consistent theory along the lines that are traditional

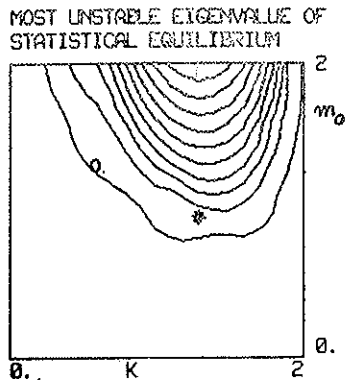

FIG. 11. Growth-rate of the most unstable eigenmode obtained from stability analysis of the time-averaged zonal flow shown in Fig. 4.a. The diagram is constructed by multiplying the vertical shear profile by the constant m_0. Statistical equilibrium corresponds to $k = 1.3$, $m_0 = 1$, and is denoted by a star. Contour interval is .1.

in meteorology by means of a numerical experiment. The experiment consists of a ten-year numerical integration of the system (8-11) for a choice of the external forcing that balances the time-mean state. As a consequence, the new system has a fixed point exactly in the maximum frequency state. The scatter diagrams of various components are reported in Fig. 12. Comparison with the statistics of the original experiment (see again Fig. 2) reveals two conspicuous problems: the variance is too small and the new statistical equilibrium is shifted with respect to the old one. The first problem is associated with the circumstance (previously considered favourable) that the system is very near to marginal stability of the time-mean state. In line of principle, this problem can be handled by carefully reshaping the center manifold near marginal stability. At any rate, the need for an accurate rewriting (renormalization) of the equations emerges already here.

But it is in the second problem that the physical nature of the limitations of classical theory appears most clearly: the shift of the equilibrium is caused by an essential symmetry of the system, namely, that associated with the property of baroclinic instability to transport heat only in one latitudinal direction, so that nothing like an "anti-baroclinic" instability exists. As a consequence, average baroclinicity can only decrease. One can easily convince himself that this difficulty must be faced no matter how one modifies the stability problem; it is not model-dependent and is, therefore, basic.

The existence of a most probable (central) state is due to the existence of several statistically independent processes that produce a centered statistics in the sense of the central limit theorem. The central state has no special dynamical meaning and carries no special information regarding the physics of the fluctuations. The reduction to a minimal system of low dimensionality, if any, must be made by choosing the basic modes in a more elaborate fashion (see again, Malguzzi and Speranza, 1986, for a discussion on this problem).

In conclusion, the foundations of the theory of general circulation appear rather shaky. This perhaps explains why it is so often invoked, but never thoroughly formulated!

4. The influence of anomalous tropical heating

A model like the one described in section 3 is clearly inadequate to describe tropical dynamics. However, as already mentioned, the point

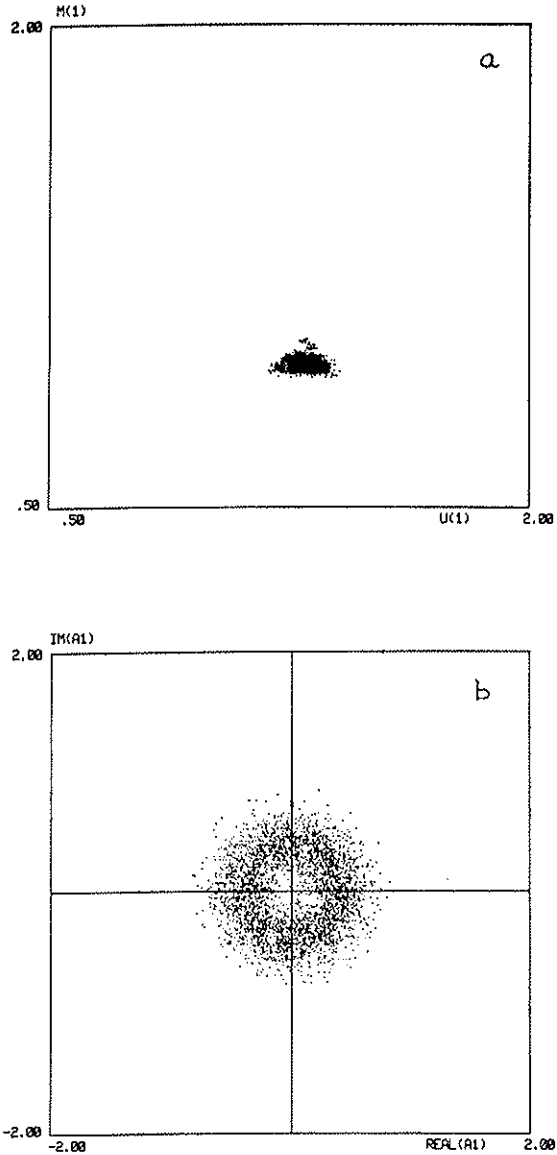

FIG. 12. Scatter diagram of a) zonal wind and b) first barotropic wave-component for the system with external forcing producing a fixed point at the statistical equilibrium. Compare with Fig. 2.

we debate here is methodological: can we compute the response to tropical heating in terms of linear or nonlinear deviations with respect to a "basic state"?

Our answer to this question is negative. The physical motivations of such negative answer have been, in essence, already outlined in section 3: the time mean state is simply the result of a central limit statistical accumulation on a most probable state and is not characterized by any particular dynamical property.

Instead of reporting a long theoretical discussion, we prefer here to provide direct evidence of the significance of our criticism to the classical approach in terms of a numerical experiment performed with the model described in sections 2 and 3.

In order to simulate anomalous tropical heating, we insert in our model a nonsymmetric, stationary heat source $-F \cdot H(x, y)$ in the right hand side of (2) having the structure:

$$H = H_o \, e^{-\left(\frac{y - y_H}{y_o}\right)^2} e^{ikx} \qquad + \quad (*)$$

where

$$H_o = .5$$

(heating rate of $\sim 3°K$/day) (12)

$$y_H = 2.$$

$$y_o = 1.$$

The latitudinal structure of the "tropical" heat source (a localized gaussian) is shown in Fig. 13.

The addition of such source is capable of modifying the climate of our model, although not much. This is shown in Fig. 14 displaying the time-mean flow (14.a) and the time-mean anomaly (14.b); despite the strong internal heat source, the 10-year average anomaly at the ground is about 1 mb. The disturbance is confined to the tropical region; this is not surprising since we are dealing with a quite short wave (zonal wavenumber 6). However, we do not take seriously these details of our

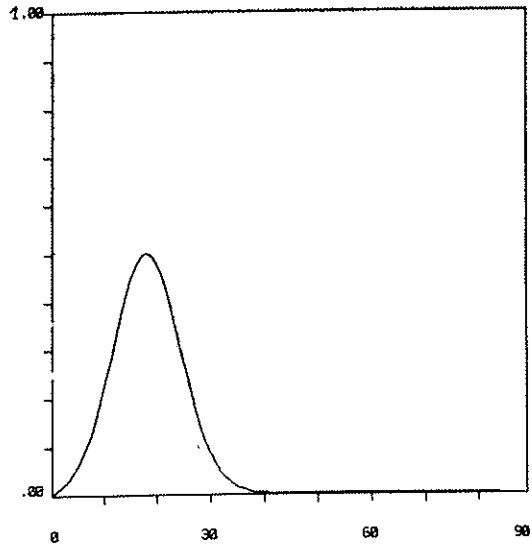

FIG. 13. Latitudinal structure of the heat source used in the numerical experiment described in section 4.

model since it describes anyhow an incorrect tropical dynamics and since we just want to analyze the classical methodology used to face these problems.

Current theories on midlatitude influence (teleconnections) of anomalous tropical heating are based on the computation of flow anomalies with respect to "basic states" almost invariably identified with time-mean flows either of GCM's or of the real atmosphere. In Fig. 15 we show the results of a linear calculation performed along such lines with the same parameters of the numerical simulation described above. The equations of motion are linearized around the time-mean state shown in figure 4.a, and the stationary solution forced by the anomalous heating (12) is computed. Inspection of the linear solution and comparison with the results of direct numerical simulation (Fig. 14) show that the two have nothing in common, except latitudinal confinement (associated with the short longitudinal scale of the heat-source).

The reason for the above differences should at this point be clear: as shown in section 3, the time-mean state in general carries no dynamical information concerning free fluctuations; we have also shown here that the same holds for forced anomalies.

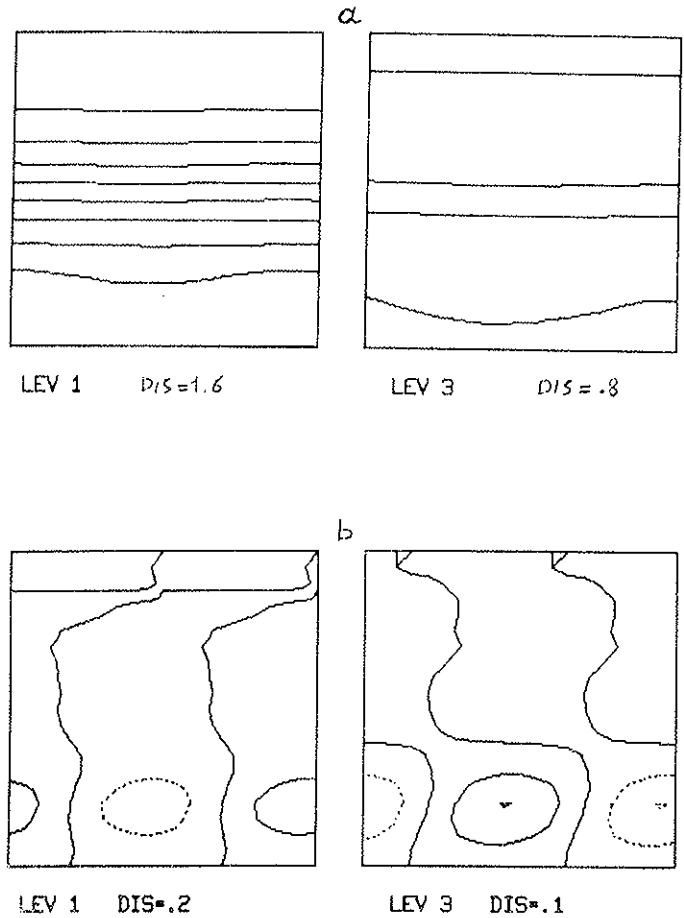

FIG. 14. Ten-year average of a) total streamfunction field and b) deviation from zonal mean (anomaly) plotted at the two levels 1 and 3 (see section 4). Contour intervals are: a) 160 m and 80 m of geopotential height for the total field at level 1 and 3 respectively, b) 20 m and 10 m of geopotential height for the anomaly field at level 1 and 3 respectively.

5. CONCLUSIONS

Critical re-examination of the statistical concepts underlying the classical theory of general circulation shows their inadequacy in providing a sound explanation of the observed atmospheric dynamics. Particularly misleading appears the identification of time-average states with fixed

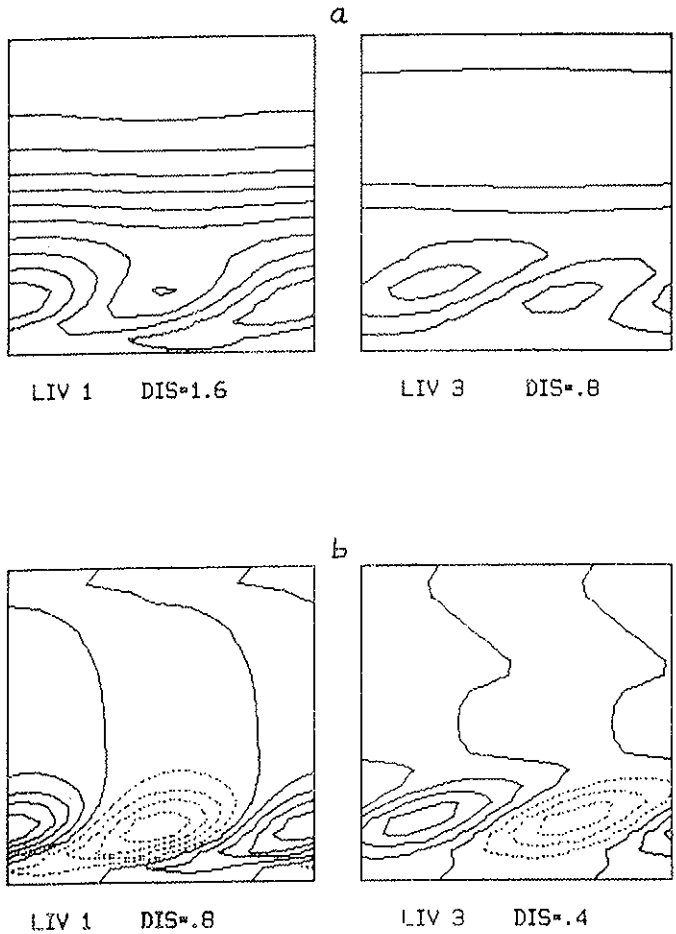

FIG. 15. Stationary, linear response of system (8-11) to the heat source shown in Fig. 13. Same as Fig. 14 but contour interval of anomaly field is 80 m and 40 m of geopotential height at level 1 and 3 respectively. Compare with Fig. 14.

points (stationary solutions) of the basic equations forced by "turbulent stresses". As shown in section 3, the time-mean does not contain sufficient information about the dynamics of turbulent fluctuations.

Many theories based on the above-mentioned statistical concepts suffer for their same inadequacies. In particular, the theory of teleconnections has been mostly developed on the basis of computations of linear,

stationary solutions on a basic state chosen to simulate the time-mean flow. By means of numerical experiments set up along the same lines of Malguzzi and Speranza (1986) we have explicitly shown the fallacy of the classical approach in determining the properties of circulation anomalies forced by tropical heating.

A thorough investigation of the problem of teleconnections between anomalous tropical heating and mid-latitude circulation would require the use of a general circulation model incorporating longer zonal wavelengths than the one allowed here. In fact, due to the relatively short wavelength of the most unstable baroclinic wave, the mid-latitude response to tropical heating is very small here. Furthermore, it is interesting to compute, for such a model, the time-mean of the response obtained by linearizing around each single instantaneous state of the unforced problem. This computation mal suggest a simple statistical model which is capable of providing a better estimation of the real atmospheric response to anomalous external forcing. Work along these lines is in progress.

REFERENCES

BENZI R. and SPERANZA A., *The statistical properties of low frequency variability in the northern hemisphere.* Submitted to « Mon. Wea. Rev. » (1986).

BRANSTATOR G., *Analysis of general circulation model sea-surface temperature anomaly simulation using a linear model.* Part I: *Forced solutions.* « J. Atmos. Sci. », *42*, 2225-2241 (1986a).

BRANSTATOR G., *Analysis of general circulation model sea-surface temperature anomaly simulation using a linear model.* Part. II: *Eigenanalysis.* « J. Atmos. Sci. », *42*, 2242-2254 (1986b).

DICKINSON E.D., *Rossby waves — Long period oscillations of oceans and atmosphere.* « Ann. Rev. Fluid Mech. », *10*, 159-195 (1978).

FEIGENBAUM M.J., KADANOFF L.P. and SHENKER S.J., *Quasi-periodicity in dissipative systems: a renormalization group analysis.* « Physica D », *3*, 370-386 (1982).

LORENZ E.N., *The mechanism of vacillation.* « J. Atmos. Sci. », *20*, 448-464 (1963).

MALGUZZI P. and SPERANZA A., *A re-examination of the classical theory of general circulation.* To be submitted to « J. Atmos. Sci. » (1986).

PEDLOSKY J., *Geophysical fluid dynamics.* New York, Springer (1979).

ROSSBY G.G., *On the propagation of frequencies and energy in certain types of oceanic and atmospheric waves.* « J. Met. », *2*, 187-203 (1945).

SMAGORINSKY J., *The dynamical influences of large-scale heat sources and sinks on the quasi-stationary mean motion of the atmosphere.* « Quart. J. Roy. Meteor. Soc. », *79*, 342-366 (1953).

STONE P.H., *Baroclinic adjustment.* « J. Atmos. Sci. », *35*, 561-571 (1978)